The Mechanism of TRPA1 Activation

Arundhasa Chandrabalan, BSc. (Hons)

Thesis submitted for the Degree of Doctor of Philosophy

The University of Hull and the University of York

Hull York Medical School

September 2017

Abstract

Transient receptor potential ankyrin 1 (TRPA1) is a non-selective cation channel expressed predominantly in the primary afferent sensory neurons, and is a detector of chemical, mechanical and thermal stimuli. TRPA1 is involved in pain, itch, inflammatory and respiratory diseases. The important roles of TRPA1 makes it an exciting target for drug development, but to develop drug-like antagonists it is vital to understand its mechanisms of activation and/or blocking. One known activation mechanism is through covalent modification of either cysteine or lysine residues at the TRPA1 *N*-terminus by reactive electrophilic compounds. However, the mechanism(s) of TRPA1 modulation by non-reactive compounds have not yet been completely resolved.

In this study, it was hypothesised that the functional groups present on the chemicals could be responsible for TRPA1 channel modulation by a non-covalent mechanism. Consequently, to investigate the structure-activity relationship (SAR), and thereby the pharmacology of non-reactive modulators, twenty-two *N*-cinnamoylanthranilate derivatives (CADs) and eighteen aryl sulfonamide derivatives (ASDs) were synthesised, characterised, and screened for agonism and antagonism in HEK293 cells stably transfected with human (h)TRPA1, where the transient elevations of $[Ca^{2+}]_i$ were measured using fluorescence-based calcium signalling assays.

The CADs with different functional groups exhibited different responses, including agonism, partial agonism, antagonism and desensitising effects in hTRPA1, in a concentration-dependent manner. The CADs with inductive electron-withdrawing groups were agonists with desensitising effects (e.g. *p*-Cl CAD-**AC17c**, EC_{50} 10 and IC_{50} 4 µM), and electron-donating groups were either partial agonists or antagonists (e.g. *p*-OH CAD-**AC30d**, IC_{50} 43 µM). The SAR study on the ASDs showed that replacement of the fluoro group in an antagonist (**AC51b**, IC_{50} 10 µM) to a carboxylic acid group (**AC56d**) completely eliminates its antagonism. In addition, site-directed mutagenesis studies revealed that F944 is a key residue involved in the non-covalent modulation of TRPA1 by structurally distinct non-reactive TRPA1 ligands. As hypothesised, minor alterations in the functional groups demonstrated substantial changes in activities. Overall, this would lead to a better understanding of the activation mechanism and potentially aid in the development of TRPA1 specific modulators.

Contents

Abstract 2
Abbreviations 9
List of figures 13
List of schemes 18
List of tables 19
Acknowledgements 20
Author's declaration 21
CHAPTER 1: Introduction 22
1.1 Transient receptor potential (TRP) 22
1.1.1 Transient receptor potential canonical (TRPC) 25
1.1.2 Transient receptor potential vanilloid (TRPV) 26
1.1.3 Transient receptor potential melastatin (TRPM) 26
1.1.4 Transient receptor potential polycystin (TRPP) 27
1.1.5 Transient receptor potential mucolipin (TRPML) 28
1.1.6 Transient receptor potential ankyrin (TRPA) 29
1.1.6.1 TRPA1 in chemosensation 32
1.1.6.2 TRPA1 in thermosensation 39
1.1.6.3 TRPA1 in mechanosensation 39
1.1.6.4 TRPA1 in disorders/diseases 40
1.1.6.5 TRPA1 knockout studies 45
1.1.6.6 TRPA1 species differences 46
1.1.7 Calcium signalling 48
1.1.8 Conclusion 49
1.2 Biological activities of *N*-cinnamoylanthranilates 50
1.2.1 Anti-allergic 51
1.2.2 Anti-collagen, Anti-fibrotic, Anti-proliferative, Anti-cancer and Anti-tubulin 55
1.2.2.1 Fibroblasts 56
1.2.2.2 Diabetic cardiac disease and Gilbert's syndrome 58
1.2.2.3 Mesenteric vascular hypertrophy and Diabetic nephropathy 58
1.2.2.4 Glomerulonephritis 59
1.2.2.5 Restenosis 60

1.2.2.6 Coronary arteriosclerosis 61
1.2.2.7 Nifedipine induced proliferation 62
1.2.2.8 Cancer and Tubulin 62
1.2.3 Anti-inflammatory 64
1.2.4 Anti-oxidant 65
1.2.5 Anti-angiogenesis 65
1.2.6 Anti-microbial 66
1.2.7 Insulin secretion inhibitor 67
1.2.8 Smooth muscle contraction inhibitor 68
1.2.9 Multinucleated giant cell inhibitor 70
1.2.10 Telomerase inhibitor 70
1.2.11 Matrixins inhibitor 71
1.2.12 PLA_2 and TRP channel blocker 72
1.2.13 Niacin receptor agonists 73
1.2.14 Apolipoprotein enhancer 74
1.2.15 B-cell and T-cell modulators 74
1.2.16 Neuroregeneration and neuroprotection 76
1.2.17 Biosynthesis of *N*-cinnamoylanthranilates 76
1.2.18 Conclusion 77
1.3 Biological activities of aryl sulfonamides 78
1.3.1 Probenecid 78
1.3.1.1 Gout 78
1.3.1.2 Depression 79
1.3.1.3 Dye retention 79
1.3.1.4 TRP channel modulator 80
1.3.2 4-Fluoroarylsulfonamides 81
1.3.2.1 TRPA1 channel blocker 81
1.3.3 Conclusion 82
1.4 Research gap, hypothesis and aims 83
CHAPTER 2: Experimental materials and methods 85
2.1 Chemistry 85
2.1.1 General information 85
2.2 General synthetic procedures for *N*-cinnamoylanthranilates 87

2.2.1 Synthesis of *N*-cinnamoylanthranilate derivatives from cinnamic acid derivatives 88
2.2.2 Synthesis of *N*-cinnamoylanthranilate derivatives from aldehyde derivatives 89
2.2.3 Synthesis of *N*-cinnamoyl amino acids 90
2.2.4 Procedures for individual *N*-cinnamoylanthranilate derivative 91
2.2.4.1 *N*-Cinnamoylanthranilic acid (AC18) 91
2.2.4.2 *N*-(4-Fluorocinnamoyl)anthranilic acid (AC14) 92
2.2.4.3 *N*-(2-Chlorocinnamoyl)anthranilic acid (AC15) 93
2.2.4.4 *N*-(4-Bromocinnamoyl)anthranilic acid (AC16) 94
2.2.4.5 *N*-(4-Chlorocinnamoyl)anthranilic acid (AC17) 95
2.2.4.6 *N*-Hydrocinnamoylanthranilic acid (AC21) 97
2.2.4.7 Meldrum's acid 97
2.2.4.8 2-[(Carboxyacetyl)amino]benzoic acid 98
2.2.4.9 *N*-(4-Methoxycinnamoyl)anthranilic acid (AC20) 99
2.2.4.10 *N*-(3,4-Dimethoxycinnamoyl)anthranilic acid (AC24) 99
2.2.4.11 *N*-(2-Methoxycinnamoyl)anthranilic acid (AC26) 100
2.2.4.12 *N*-(3-Ethoxy-4-hydroxycinnamoyl)anthranilic acid (AC27) 101
2.2.4.13 *N*-(3,4-Dihydroxycinnamoyl)anthranilic acid (AC28) 102
2.2.4.14 *N*-(4-Hydroxycinnamoyl)anthranilic acid (AC30) 103
2.2.4.15 *N*-Cinnamoylpipecolinic acid (AC34) 104
2.2.4.16 *N*-Cinnamoylproline (AC36) 105
2.2.4.17 Methyl *N*-(3-phenoxypropionoyl)anthranilate (AC35) 106
2.2.4.18 *N*-(4-Methylcinnamoyl)anthranilic acid (AC39) 106
2.2.4.19 *N*-(4-Trifluoromethylcinnamoyl)anthranilic acid (AC40) .. 107
2.2.4.20 *N*-(4-Nitrocinnamoyl)anthranilic acid (AC41) 108
2.2.4.21 *N*-(α-Phenylcinnamoyl)anthranilic acid (AC42) 110
2.2.4.22 *N*-(α-Methylcinnamoyl)anthranilic acid (AC43) 111
2.2.4.23 *N*-(4-Dimethylaminocinnamoyl)anthranilic acid (AC45) ... 112
2.2.4.24 *N*-(4-Methoxyhydrocinnamoyl)anthranilic acid (AC46) 113
2.3 General synthetic procedures for aryl sulfonamides 115
2.3.1 Synthesis of small aryl sulfonamides 116
2.3.1.1 Aryl sulfonamide derivatives M2 - M14 116

2.3.1.2 4-(Chlorosulfonyl)benzoic acid 122
2.3.2 Synthesis of extended aryl sulfonamides 122
2.3.2.1 (*S*)-*N*-(4-Chlorobenzyl)-1-((4-fluorophenyl)sulfonyl)pyrrolidine-2-carboxamide (AC51) 125
2.3.2.2 2-((4-Fluoro-*N*-methylphenyl)sulfonamido)-*N*-(4-(trifluoromethyl)benzyl)acetamide (AC53) 126
2.3.2.3 2-(*N*-Methylphenylsulfonamido)-*N*-(4-(trifluoromethyl)benzyl) acetamide (AC54) 127
2.3.2.4 (*S*)-4-((2-((4-Chlorobenzyl)carbamoyl)pyrrolidin-1-yl)sulfonyl) benzoic acid (AC56) 128
2.3.2.5 4-(*N*-Methyl-*N*-(2-oxo-2-((4-(trifluoromethyl)benzyl)amino)ethyl)sulfamoyl)benzoic acid (AC57) 129
2.4 Pharmacology 131
2.4.1 HEK293 cell line 131
2.4.2 Calcium signalling 132
2.4.2.1 Cuvette-based system 137
2.4.2.2 Micro-well plate system 138
2.4.2.3 Data analysis 139
2.4.2.4 Statistical analysis 141
2.5 Electrophysiology 141
2.6 Indirect measure of covalent modification 142
2.7 hTRPA1 mutants 143
2.7.1 Primer design 143
2.7.2 Site-directed mutagenesis 143
2.7.2.1 Mutant strand synthesis, *Dpn I* digestion and Bacterial transformation 144
2.7.2.2 hTRPA1 expression in transformed *E. coli* 145
2.7.2.3 Plasmid DNA purification, quantification and sequencing ... 146
2.7.3 Generation of stable hTRPA1 transfected HEK293 cells 148
2.7.3.1 Transfection 148
2.7.3.2 Single cell cloning 148
2.7.4 Gene expression 149

CHAPTER 3: *N*-Cinnamoylanthranilates as modulators of TRPA1 151
3.1 Introduction 151
3.2 Synthetic chemistry 152
3.2.1 *N*-Cinnamoylanthranilates from cinnamic acids 153
3.2.2 *N*-Cinnamoylanthranilates from aldehydes 156
3.2.3 *N*-Cinnamoyl amino acids 158
3.3 Chemical information 158
3.4 Pharmacology of *N*-cinnamoylanthranilates 160
3.4.1 Calcium signalling 160
3.4.1.1 Solubility of compounds 160
3.4.1.2 Suitability of compounds 160
3.4.1.3 Variability in responses with different methods 161
3.4.1.4 Choice of carrier solvent 162
3.4.1.5 Controls 163
3.4.1.6 Fluorescence spectrum 166
3.4.2 Screening of *N*-cinnamoylanthranilates in hTRPA1-HEK293 and structure-activity relationships 167
3.4.2.1 Ring substituted and unsubstituted derivatives 175
3.4.2.2 *Ortho*- and *para*-substituted derivatives 181
3.4.2.3 α,β-Unsaturated and α,β-saturated derivatives 181
3.4.2.4 α-Substituted and α-unsubstituted derivatives 182
3.4.2.5 Planar and non-planar derivatives 182
3.4.2.6 Carboxylic acid and carboxylate ester derivatives 183
3.4.3 Channel specificity 183
3.4.3.1 Screening of *N*-cinnamoylanthranilates in mock-HEK293 ... 183
3.4.3.2 Screening of *N*-cinnamoylanthranilates in hTRPM8-HEK293 184
3.4.4 Reversibility 188
3.4.5 Physicochemical property-activity relationships 189
3.4.6 Electrophysiology 193
3.5 Indirect measure of covalent modification of cysteines 196
3.6 TRP channels could be the reason behind numerous activities of *N*-cinnamoylanthranilates in the literature 200
3.7 Conclusions 200

CHAPTER 4: Aryl sulfonamides as modulators of TRPA1 202
4.1 Introduction 202
4.2 Synthetic chemistry 203
4.2.1 Aryl sulfonamides 204
4.2.2 4-(Chlorosulfonyl)benzoic acid 207
4.3 Chemical information 208
4.4 Pharmacology of aryl sulfonamides 209
4.4.1 Calcium signalling 209
4.4.1.1 Solubility of compounds 209
4.4.1.2 Controls 209
4.4.2 Screening of aryl sulfonamides in hTRPA1-HEK293 and structure-activity relationships 211
4.4.3 Channel specificity 218
4.4.4 Physicochemical property-activity relationships 218
4.5 Conclusions 220
CHAPTER 5: Ligand binding sites in TRPA1 221
5.1 Introduction 221
5.2 Site-directed mutagenesis 224
5.2.1 Screening of TRPA1 ligands in WT-hTRPA1 230
5.2.2 Screening of TRPA1 ligands in S873V/T874L-hTRPA1 237
5.2.3 Screening of TRPA1 ligands in C621A-hTRPA1 240
5.2.4 Screening of TRPA1 ligands in F909A-hTRPA1 245
5.2.5 Screening of TRPA1 ligands in F944A-hTRPA1 246
5.3 Conclusions 247
CHAPTER 6: Summary 249
6.1 Calcium signalling 249
6.2 *N*-Cinnamoylanthranilates as modulators of TRPA1 249
6.3 Aryl sulfonamides as modulators of TRPA1 252
6.4 Ligand binding sites in TRPA1 253
CHAPTER 7: Conclusions and further work 256
References 258
Appendix 279

Abbreviations

AA	Arachidonic acid
ACA	*N*-(*p*-Amylcinnamoyl)anthranilic acid
ACR	Acrolein
AITC	Allyl isothiocyanate
ALK	Activin receptor-like kinase
ALS	Amyotrophic lateral sclerosis
AMTB	*N*-(3-Aminopropyl)-2-((3-methylbenzyl)oxy)-*N*-(thiophen-2-ylmethyl)benzamide
amu	Atomic mass unit
apoA1	Apolipoprotein A1
ASD	Aryl sulfonamide derivative
a.u.	Arbitrary unit
Avn	Avenanthramide
bFGF	Basic fibroblast growth factor
BLAST	Basic local alignment search tool
BMN	Benzylidenemalononitriles
Boc	*Tert*-butyloxycarbonyl
Boc_2O	Di-*tert*-butyl dicarbonate
CA	Cinnamaldehyde
$[Ca^{2+}]_i$	Intracellular calcium ions
CAD	*N*-Cinnamoylanthranilate derivative
CaM	Calmodulin
CAMKII	Ca^{2+}/calmodulin-dependent protein kinase II
cAMP	Cyclic adenosine monophosphate
CD	Cluster of differentiation
$CDCl_3$	Deuterated chloroform
cDNA	Complimentary DNA
CFTR	Cystic fibrosis transmembrane conductance regulator
CHO	Chinese hamster ovary cell line
CIRB	CaM and IP_3R binding site
CNS	Central nervous system
clogD	Calculated distribution coefficient
clogP	Calculated partition coefficient
clogS	Calculated solubility
^{13}C NMR	Carbon nuclear magnetic resonance
COPD	Chronic obstructive pulmonary disease
COX	Cyclooxygenase
c.p.s.	Counts per second
CREB	cAMP response element-binding protein
CTGF	Connective tissue growth factor
CYP450	Cytochrome P450
δ	Chemical shift
DAG	Diacylglycerol
DCF	Diclofenac
DCM	Dichloromethane
ddH_2O	Double distilled water
d_6-DMSO	Deuterated dimethyl sulfoxide
DEPC	Diethyl pyrocarbonate
DIPEA	*N*,*N*-Diisopropylethylamine
DMEM	Dulbecco's Modified Eagle's Medium

DMF	*N*,*N*-Dimethylformamide
DMSO	Dimethyl sulfoxide
dsDNA	Double-stranded DNA
EA	Elemental analysis
EC_{50}	Half-maximal effective concentration
EDAC.HCl	1-(3-Dimethylaminopropyl)-3-ethylcarbodiimide hydrochloride
EDTA	Ethylenediaminetetraacetic acid
EDG	Electron donating group
Edg-1	Endothelial differentiation G-protein coupled receptor-1
5,6-EET	5,6-Epoxyeicosatrienoic acid
EGF	Epidermal growth factor
EI	Electron ionisation
EM	Electron microscopy
ER	Endoplasmic reticulum
ERK	Extracellular-signal regulated kinase
ESI	Electrospray ionisation
EtOH	Ethanol
EWG	Electron withdrawing group
$\lambda_{Ex/Em}$	Excitation and emission wavelengths
FBS	Fetal bovine serum
FEPS	Familial episodic pain syndrome
FFA	Flufenamic acid
FGF	Fibroblast growth factor
Fluo-3AM	Fluo-3 acetoxymethyl ester
Fluo-4AM	Fluo-4 acetoxymethyl ester
FLT3	Feline McDonough sarcoma-like tyrosine kinase 3
FTS	Farnesylthiosalicylic acid
GPCR	G-protein-coupled receptor
HCBT	*N*-Hydroxycinnamoylbenzoyltransferase
HDL	High density lipoproteins
HEK293	Human embryonic kidney 293 cell line
HEK293F	HEK293 cell line adapted to suspension culture in FreeStyle 293 Expression Medium
HEK293T	HEK293 cell line variant containing the SV40 large T-antigen
HEK293T/17	HEK293T cell line / clone 17
HEPES	4-(2-Hydroxyethyl)-1-piperazineethanesulfonic acid
HGF	Hepatocyte growth factor
5-HIAA	5-Hydroxyindoleacetic acid
HM74A	G-protein coupled nicotinic acid receptors
^{1}H NMR	Proton nuclear magnetic resonance
HOBt	1-Hydroxybenzotriazole
5-HPETE	5-Hydroperoxyeicosatetraenoic acid
HSL	Hormone-sensitive triglyceride lipase
HVA	Homovanillic acid
hTRPA1	Human TRPA1
hTRPM8	Human TRPM8
IC_{50}	Half-maximal inhibitory concentration
ICAM-1	Intercellular adhesion molecule-1
IFN-γ	Interferon-γ
IgG	Immunoglobulin G
IgM	Immunoglobulin M
IL	Interleukin
iNOS	Inducible nitric oxide synthase

IP_3	Inositol triphosphate
IP_3R	Inositol triphosphate receptor
J	Coupling constant
JNK	Jun *N*-terminal kinase
K562	Human chronic myelogenous leukaemia cell line
KH	Krebs-Henseleit buffer
LDL	Low density lipoproteins
LOX	Lipoxygenase
M	Molarity
MAP	Mitogen-activated protein
MCP-1	Monocyte chemoattractant protein-1
MFA	Mefenamic acid
$[Mg^{2+}]_i$	Intracellular magnesium ions
MGCs	Multinucleated giant cells
MM2	Molecular mechanics force-field 2
MMPs	Matrix metalloproteases (matrixins)
MS	Mass spectrum
MW	Molecular weight
m/z	Mass to charge ratio
n	Number of repeats within same experiments
N	Number of independent experiments
NADPH	Nicotinamide adenine dinucleotide phosphate
NCBI	National Center for Biotechnology Information
NCI	National Cancer Institute
NDGA	Nordihydroguaiaretic acid
NEFA	Non-esterified fatty acids
NGF	Nerve growth factor
NMR	Nuclear magnetic resonance
NPPB	5-Nitro-2-(3-phenylpropylamino)benzoic acid
NPBA	5-Nitro-2-(phenethylamino)benzamide
NPEB	5-Nitro-2-(phenethylamino)benzoic acid
NSAIDs	Non-steroidal anti-inflammatory drugs
OAT	Organic anion transporter
PAI-1	Plasminogen activator inhibitor 1
PBS	Phosphate buffered saline
pcDNA	Protamine complimentary DNA
PCR	Polymerase chain reaction
P_{Ca}/P_{Na}	Permeability or selectivity ratio for Ca^{2+} relative to Na^+
PDGF	Platelet-derived growth factor
PDL	Poly-D-lysine
PDZ	Post-synaptic density protein, disc-large tumour suppressor, zonula occludens protein
PGE_2	Prostaglandin E_2
PIP_2	Phosphatidylinositol 4,5-biphosphate
PI3K	Phosphoinositide 3-OH kinase
PI3K-SH3	Phosphoinositide 3-OH kinase-SH3-domain proteins
pK_a	($-\log_{10}$) Acid dissociation constant
PKA	Protein kinase A
PKC	Protein kinase C
PKD	Polycystic kidney disease
PLA_2	Phospholipase A_2
PLC	Phospholipase C

PTCA	Percutaneous transluminal coronary angioplasty
PTK	Protein tyrosine kinase
ΔRFU	Change in relative fluorescence unit
ROS	Reactive oxygen species
rpm	Revolutions per minute
RTK	Receptor tyrosine kinase
S1-S6	Transmembrane spanning segments 1 - 6
SAR	Structure-activity relationship
SEM	Standard error of the mean
SD	Standard deviation
α-SMA	α-Smooth muscle actin
SOB	Super optimal broth
SOD	Superoxide dismutase
TAE	Tris-acetate-EDTA
TFA	Trifluoroacetic acid
TGF-β	Transforming growth factor-β
T_H	T-helper cells
Δ^9-THC	Δ^9-Tetrahydrocannabinol
THF	Tetrahydrofuran
TMS	Tetramethylsilane
TNF-α	Tumour necrosis factor-α
TPSA	Topological polar surface area
TRP	Transient receptor potential
TRPA	TRP Ankyrin
TRPC	TRP Canonical
TRPM	TRP Melastatin
TRPML	TRP MucoLipin
TRPN, TRP-NOMPC	TRP No Mechanoreceptor Potential C
TRPP	TRP Polycystin
TRPV	TRP Vanilloid
UGT1A1	Uridine 5′-diphospho-glucuronosyltransferase family 1 member A1
UV	Ultraviolet
VCAM-1	Vascular cell adhesion molecule-1
VEGF	Vascular endothelial growth factor
VLDL	Very low density lipoproteins
VPF	Vascular permeability factor
VR1	Vanilloid receptor 1
VSMC	Vascular smooth muscle cells
WI-38	Human embryonic lung fibroblast cell line
WT	Wild-type
χ	Electronegativity

List of figures

Figure 1.1: *Phylogenetic tree of the mammalian transient receptor potential channels*.....23
Figure 1.2: *The general structure of a TRP channel,* **(a)** *transmembrane topology of a subunit and* **(b)** *tetramer arrangement of four subunits* 23
Figure 1.3: *Topology model and main interaction sites of TRPC1 - 7 channels*.....25
Figure 1.4: *Topology model and main interaction sites of TRPV1 - 6 channels*.....26
Figure 1.5: *Topology model and main interaction sites of TRPM1 - 8 channels*.....27
Figure 1.6: *Topology model and main interaction sites of TRPP2, 3 and 5 channels* 28
Figure 1.7: *Topology model and main interaction sites of TRPML1 - 3 channels*.....28
Figure 1.8: *Topology model of TRPA1 channel* 30
Figure 1.9: **(a)** *Illustration of a mouse TRPA1 dimer in two-dimension, and* **(b)** *three-dimensional electron microscopy density model representing the cysteine residues of TRPA1 involved in disulfide bonding* 30
Figure 1.10: *The structure of hTRPA1 determined using a cryo-EM,* **(a)** *three-dimensional density map showing the side, top and bottom views of hTRPA1 in the presence of a TRPA1 agonist, allyl isothiocyanate, filtered to 3.5 Å resolution,* **(b)** *diagram illustrating the major domains in a single subunit,* **(c)** *ribbon diagrams of a subunit viewed at different angles, and* **(d)** *densities of the domains S4 to coiled-coil showing only two diagonally faced subunits of the tetramer for clarity* 31
Figure 1.11: *Chemical structures of the key TRPA1 activators, which initially revealed the chemosensation property of TRPA1* 33
Figure 1.12: *Spatial distribution of key reactive cysteine and lysine residues located in the cytoplasmic N-terminus of hTRPA1 and the interactions with other domains, determined using a cryo-EM* 34
Figure 1.13: *TRP channel regulation in sensory neurons via phosphorylation*.....36
Figure 1.14: *Cryo-EM density map showing the interactions of the potent TRPA1 specific antagonist A967079 with multiple residues, including S873, T874, F909, F944, T945, V948 and I950, those reside in the pocket formed by S5, pore-helix 1, and S6 in hTRPA1* 37
Figure 1.15: *Chemical structures of TRPA1 modulators* 38
Figure 1.16: *Chemical structures of some species-specific modulators of TRPA1* 47
Figure 1.17: *Chemical structure of calcium ionophore A23187 (calcimycin)* 49
Figure 1.18: *Chemical structures of N-cinnamoylanthranilic acid* (**1**) *and N-(3,4-dimethoxy cinnamoyl)anthranilic acid* (**2**) 51
Figure 1.19: *Structures of anti-allergic compounds* (**3 - 12**).....53
Figure 1.20: *Structure of an anti-fibrotic agent* (**13**) 56
Figure 1.21*: Structure of a collagen synthesis inhibitor* (**14**).....59
Figure 1.22: *Structure of an anti-proliferative compound* (**15**).....61
Figure 1.23: *Compounds* **16a - 16e** *with anti-proliferative activity against cancer cells* 63
Figure 1.24: *Derivatives of compound* **17** *with anti-proliferative activity against cancer cells* 63

Figure 1.25: *N-(4-Amylcinnamoyl)anthranilic acid (ACA,* **18***) - an insulin secretion and* PLA_2 *inhibitor* 67
Figure 1.26: *Smooth muscle relaxants* (**19**, **19a** *and* **19b**)....69
Figure 1.27: *Telomerase inhibitors* (**20** *and* **21**) 71
Figure 1.28: *Matrix metalloproteases inhibitor* (**22**) 71
Figure 1.29: *A* PLA_2 *inhibitor* (**23**)....72
Figure 1.30: *The core structure of TRPV1 modulators* (**24**) 73
Figure 1.31: *Niacin receptor agonists* (**25 - 30**)....74
Figure 1.32: *The core structure of B-cell and T-cell modulators* (**31**)....75
Figure 1.33: *Chemical structures of probenecid and carinamide*....78
Figure 1.34: *Examples of aryl sulfonamide derivatives claimed as potent TRPA1 antagonists by the pharmaceutical companies, Janssen Pharmaceuticals, Orion Corporation, Pharmeste, and Hoffmann-La Roche* 81
Figure 2.1: *Chemical structures of the N-cinnamoylanthranilate derivatives* 87
Figure 2.2: *Chemical structures of the small aryl sulfonamides* **M1 - M14** 115
Figure 2.3: *Chemical structures of the extended aryl sulfonamides* **AC51**, **AC53**, **AC54**, **AC56** *and* **AC57**....115
Figure 2.4: *Vector maps of the mammalian expression vectors,* **(a)** *pcDNA3.1*(+) *and* **(b)** *pcDNA3*....132
Figure 2.5: *Chemical structures and names of the standard agonists and antagonists used in the calcium signalling assays*....135
Figure 2.6: *Chemical structures and names of the ligands characterised in hTRPA1*....136
Figure 2.7: *Traces from a typical* **(a)** *agonist and* **(b)** *antagonist assay, and illustration on calculating a compound's agonism and antagonism as a percentage of calcimycin or standard agonist correspondingly*....140
Figure 2.8: *mRNA sequence of hTRPA1. Letters in blue shows the position of primers used in the mutagenesis study*....147
Figure 3.1: *Chemical structures of the synthesised and screened N-cinnamoylanthranilates* 153
Figure 3.2: *UV-vis absorption and fluorescence spectra of the CAD,* **(a) AC28d** *($\lambda_{Ex/Em}$ 393/461 nm) and* **(b) AC45c** *($\lambda_{Ex/Em}$ 378/502 nm), in isotonic assay buffer*....161
Figure 3.3: *Comparison of the cinnamaldehyde (CA) dose-response curves obtained in two different calcium signalling assay systems with hTRPA1-HEK293 cells either loaded with Fluo-3 or Fluo-4 fluorescent dye* 162
Figure 3.4: *Comparison of the responses obtained in hTRPA1-HEK293 cells for cinnamaldehyde (CA) made in either DMSO or ethanol (0.4 %) solvent* 163
Figure 3.5: *Calcimycin response at different concentrations (1 - 10 µM) in hTRPA1-HEK293 cells* 164

Figure 3.6: *Dose-response curves of the standard TRPA1 agonist and antagonist,* **(a)** *cinnamaldehyde (CA) and* **(b)** *A967079 (against 30 µM CA), respectively, evaluated in hTRPA1-HEK293 cells* 164
Figure 3.7: *Dose-response curves of the standard TRPM8 agonist and antagonist,* **(a)** *WS5 and* **(b)** *AMTB (against 3 µM WS5), respectively, evaluated in hTRPM8-HEK293 cells*.....165
Figure 3.8: *Examples of traces obtained in a calcium signalling assay with a compound at different concentrations* 166
Figure 3.9: *Spectra obtained with seven different cuvettes from the same batch/manufacturer showing the variation in baseline levels with the use of different cuvettes alone* 166
Figure 3.10: *Initial screening results of N-cinnamoylanthranilate derivatives in hTRPA1-HEK293 cells,* **(a)** *agonism and* **(b)** *antagonism*.....169
Figure 3.11: *Initial screening results of methyl N-cinnamoylanthranilate derivatives in hTRPA1-HEK293 cells,* **(a)** *agonism and* **(b)** *antagonism* 169
Figure 3.12: *Dose-response curves* **(a - k)** *of substituted N-cinnamoylanthranilic acid agonists in hTRPA1-HEK293 cells* 170
Figure 3.13: *Dose-response curves* **(a - i)** *of substituted N-cinnamoylanthranilic acid antagonists in hTRPA1-HEK293 cells* 172
Figure 3.14: *Electronic effects of the substituents, EWG - electron withdrawing group and EDG - electron donating group* 175
Figure 3.15: *Colour coded mapping of some analogues of N-cinnamoylanthranilic acid structures highlighting the lipophilicity/hydrophilicity nature of an atom/functional group/substructure*.....177
Figure 3.16: *Real-time spectrum recorded for 10 minutes (incubation period) for the compounds with bimodal activity (potent agonism and desensitisation) in hTRPA1-HEK293 cells,* **(a)** *cinnamaldehyde (CA, 30 µM*), **(b)** *flufenamic acid (FFA, 100 µM*), **(c)** *mefenamic acid (MFA, 10 µM*), **(d)** *diclofenac (DCF, 10 µM*), **(e)** *p-Cl CAD-***AC17c** (*10 µM*), **(f)** *p-Br CAD-***AC16c** (*10 µM*), **(g)** *o-Cl CAD-***AC15c** (*10 µM*) *and* **(h)** *p-F CAD-***AC14c** (*10 µM*) .178
Figure 3.17: *Dose-response curves of cinnamaldehyde (CA) against hTRPA1-HEK293 cells untreated and pre-treated with the inhibitor (p-OH)CAD-***AC30d** *(100 µM). The competitive insurmountable antagonism by* **AC30d** *can be seen by the right-downward shift of the CA curve*.....179
Figure 3.18: *Dose-response curves of the N-cinnamoylanthranilate analogues* **(a)** *ACA and* **(b)** *SB366791 in hTRPA1-HEK293 cells* 180
Figure 3.19: *Optimised geometry of the compounds,* **(a)** *planar N-cinnamoylanthranilic acid* (**AC18b**), *and* **(b)** *non-planar N-cinnamoyl pipecolinic acid* (**AC34**), *determined using the energy minimisation molecular mechanics force-field MM2* 183
Figure 3.20: *An example of the fluorescence spectrum obtained for the compounds* **AC18b-**(*p*-H) *and* **AC14c-**(*p*-F), *when screened in mock-transfected HEK293 cells. Similar responses were obtained for all the tested compounds*.....184

Figure 3.21: *Initial screening results of N-cinnamoylanthranilate derivatives in hTRPM8-HEK293 cells,* **(a)** *agonism, and* **(b)(i)** *antagonism of N-cinnamoylanthranilic acids and* **(b)(ii)** *antagonism of methyl N-cinnamoylanthranilates*.....185
Figure 3.22: *Dose-response curves* **(a - f)** *of N-cinnamoylanthranilate antagonists in hTRPM8-HEK293 cells*.....186
Figure 3.23: (a) *Inhibitory effect shown in cells pre-treated with the compunds and* **(b)** *irreversibility of N-(4-hydroxycinnamoyl)anthranilic acid* (**AC30d**) *on hTRPA1-HEK293 cells* 188
Figure 3.24: (a) *Desensitising effect and* **(b)** *reversibility of halogenated N-cinnamoylanthranilic acids [***AC16b**-*(p-Br),* **AC17b**-*(p-Cl),* **AC15b**-*(o-Cl) and* **AC14b**-*(p-F)] on hTRPA1-HEK293 cells* 189
Figure 3.25: (a - c) *Agonism and* **(d)** *antagonism against acrolein (ACR, 300 µM) induced depolarisation of CADs* **AC40c**-*(p-CF_3),* **AC17c**-*(p-Cl) and* **AC30d**-*(p-OH), on isolated guinea pig vagus nerve preparations*.....194
Figure 3.26: (a) *Dose-response of acrolein (ACR) and* **(b)** *antagonism of* **AC17c**-*(p-Cl) and* **AC30d**-*(p-OH) against acrolein (300 µM), in hTRPA1-HEK293 cells* 194
Figure 3.27: *The sequence alignment of human (Homo sapiens) and guinea pig (Cavia porcellus) TRPA1, aligned using NCBI BLAST, showing 79 % identity*.....195
Figure 3.28: *^{1}H NMR spectra of the reactions carried out to assess, if any, covalent modification of cysteine residues,* **(a)** CAD **AC18a** *in $CDCl_3$,* **(b)** *the CAD with N-acetyl-L-cysteine methyl ester, and* **(c)** *CAD with N-acetyl-L-cysteine, in d_6-DMSO at time intervals* **(i)** *10 minutes,* **(ii)** *1 hour,* **(iii)** *3.5 hours and* **(iv)** *6 hours*.....197
Figure 4.1: *The chemical structure of probenecid* (**M1**), *and observed core structure of the TRPA1 antagonists* (**A1**).....202
Figure 4.2: *Chemical structures of the synthesised and screened aryl sulfonamides* 203
Figure 4.3: *Dose-response curves of the standard TRPA1 agonist and antagonist,* **(a)** *AITC and* **(b)** *A967079 (against 10 µM AITC), respectively, evaluated in hTRPA1-HEK293 cells* 210
Figure 4.4: *Dose-response curves of the standard TRPM8 agonist and antagonist,* **(a)** *WS12 and* **(b)** *AMTB (against 100 nM WS12), respectively, evaluated in hTRPM8-HEK293 cells* 211
Figure 4.5: *Dose-response curve of probenecid* (**M1**) *obtained against hTRPA1-HEK293 cells* 212
Figure 4.6: *Screening results of probenecid derivatives in hTRPA1-HEK293 cells,* **(a)** *agonism and* **(b)** *antagonism*.....213
Figure 4.7: *Colour coded mapping of small aryl sulfonamide derivative structures highlighting the lipophilicity/hydrophilicity nature of an atom/functional group/substructure*.....214
Figure 4.8: *Dose-response curve of* **AC51b** *obtained against hTRPA1-HEK293 cells*.....215
Figure 4.9: *Screening results of aryl sulfonamide derivatives in hTRPA1-HEK293 cells,* **(a)** *agonism and* **(b)** *antagonism*.....216

Figure 4.10: *Optimised geometry of the compounds* **(a) AC51b** *and* **(b) AC53b**, *determined using the energy minimisation molecular mechanics force-field MM2* 217
Figure 5.1: *Locations of hTRPA1 residues (V865 - I950) within segments 5 (S5) and 6 (S6), determined using a single-particle cryo-electron microscopy* 222
Figure 5.2: *Chemical structures, names and codes of the known TRPA1 ligands characterised in wild-type and mutant hTRPA1* 223
Figure 5.3: *UV illumination of the bands obtained in a gel electrophoresis analysis (performed on a 1.3 % agarose gel containing Midori green DNA stain) of the samples from transformed bacterial colonies*.....226
Figure 5.4: *DNA sequencing results of the hTRPA1 DNA constructs extracted from the bacterial clone samples, C621A (1), F909A (5), Y926S (1) and F944A (1)* 227
Figure 5.5: *Spectra obtained from intracellular flow cytometric analysis, to determine the expression levels of hTRPA1 gene in the hTRPA1 mutants* 229
Figure 5.6: *Dose-response curves of the electrophilic compounds, CA, ACR and AITC, in WT-hTRPA1 HEK293 cells*.....230
Figure 5.7: *Dose-response curves of the non-electrophilic compounds, menthol, thymol, carvacrol, eugenol and paracetamol, in WT-hTRPA1 HEK293 cells*.....231
Figure 5.8: *Dose-response curves of the anthranilic acid derivatives,* **(a)** *FFA, MFA and DCF (NSAIDs) and* **(b)** *NPPB, ACA and SB366791, in WT-hTRPA1 HEK293 cells*.....232
Figure 5.9: *Dose-response curves of the TRPA1 activators,* **(a)** *NDGA,* **(b)** *FTS,* **(c)** *URB597 and* **(d)** *(-)-nicotine, in WT-hTRPA1 HEK293 cells*.....233
Figure 5.10: *Dose-response curves of the TRPA1 antagonists,* **(a)** *A967079,* **(b)** *AP18 and* **(c)** *HC030031, in WT-hTRPA1 HEK293 cells* 235
Figure 5.11: *Characterisation of hTRPA1 mutant S873V/T874L with known agonists,* **(a)** *before and* **(b)** *after single cell isolation, and compared against the responses obtained in WT-hTRPA1 HEK293 cells*.....237
Figure 5.12: *Evaluation of CADs for* **(a)** *agonism and* **(b)** *antagonism, in S873V/T874L-hTRPA1 HEK293 cells, and compared against the responses obtained in WT-hTRPA1 HEK293 cells*.....239
Figure 5.13: *Screening results of TRPA1 ligands in the hTRPA1 mutants, F909A, F944A and C621A, and comparison of the responses against WT-hTRPA1 HEK293 cells* **(a - e)** 242
Figure 5.14: *Screening results of CADs in the hTRPA1 mutants, F909A, F944A and C621A, and comparison of the responses against WT-hTRPA1 HEK293 cells,* **(a)** *agonism and* **(b)** *antagonism*.....244
Figure 5.15: *Screening results of ASDs in the hTRPA1 mutants, F909A, F944A and C621A, and comparison of the responses against WT-hTRPA1 HEK293 cells,* **(a)** *agonism and* **(b)** *antagonism*.....245

List of schemes

Scheme 1.1: *Mechanism of the Ca^{2+}-sensitive fluorescent probe, Fluo, in detecting changes in the level of $[Ca^{2+}]_i$* *48*

Scheme 1.2: *Biosynthesis of N-cinnamoylanthranilates* *77*

Scheme 2.1: *Synthesis of N-cinnamoylanthranilate derivatives from cinnamic acid derivatives* *89*

Scheme 2.2: *Synthesis of N-cinnamoylanthranilic acid derivatives from aldehyde derivatives* *90*

Scheme 2.3: *Synthesis of N-cinnamoyl amino acids, rac-***AC34** *and S-***AC36** *90*

Scheme 2.4: *Synthesis of aryl sulfonamides. Conditions and reagents used to synthesise* **M2** - **M9**: *0 °C, then 2 hours at room temperature; and for* **M10** - **M14**: *NaOH (10 % w/v) overnight, then HCl (2 M), at room temperature* *116*

Scheme 2.5: *Synthesis of 4-(chlorosulfonyl)benzoic acid* *122*

Scheme 2.6: *Synthesis of aryl sulfonamides using* **(A)** *4-fluoro or hydro sulfonyl chlorides, or* **(B)** *4-(chlorosulfonyl)benzoic acid* *124*

Scheme 3.1: *Reaction mechanism for the formation of N-cinnamoylanthranilate derivatives from cinnamic acid derivatives,* **(a)** *acylation of cinnamic acid,* **(b)** *coupling of cinnamoyl chloride with methyl anthranilate to form methyl N-cinnamoylanthranilate and* **(c)** *hydrolysis of the ester to produce N-cinnamoylanthranilic acid* *154*

Scheme 3.2: *Reaction mechanism showing that direct coupling of cinnamoyl chloride with anthranilic acid react in 2:1 ratio to produce (E)-2-styryl-4H-benzo[d][1,3]oxazin-4-one via intramolecular cyclisation* *155*

Scheme 3.3: *Reaction mechanism for the formation of α-methylcinnamic acid via Perkin reaction* *155*

Scheme 3.4: *Reaction mechanism for the formation of Meldrum's acid* *156*

Scheme 3.5: *Reaction mechanism for the formation of N-cinnamoylanthranilate derivatives from aldehyde derivatives,* **(a)** *2-[(carboxyacetyl)amino]benzoic acid is produced by reacting Meldrum's acid with anthranilic acid and* **(b)** *2-[(carboxyacetyl)amino]benzoic acid is condensed with a benzaldehyde via Knoevenagel condensation to produce N-cinnamoylanthranilic acid* *157*

Scheme 3.6: *Reaction mechanism for the formation of N-cinnamoyl amino acids* *158*

Scheme 3.7: *Example of a ^1H NMR reaction carried out to assess the possibility of covalent modification of cysteine residues by CADs* *196*

Scheme 4.1: *Reaction mechanism for the formation of aryl sulfonamides,* **(a)** *sulfonylation, and* **(b)** *amide formation* *205*

Scheme 4.2: *Reaction mechanism for the formation of aryl sulfonamides with protection and deprotection steps* *206*

Scheme 4.3: *Reaction mechanism for the formation of 4-(chlorosulfonyl)benzoic acid via modified Sandmeyer reaction* *207*

List of tables

Table 2.1: *Information of the ligands used in the experiments* *135*

Table 2.2: *Information about materials, reagents, media and instruments used in the site-directed mutagenesis* *143*

Table 2.3: *Thermal cycling conditions used for the syntheses of mutants strands* *145*

Table 2.4: *Thermal cycling conditions used to amplify the bacterial plasmids* *145*

Table 3.1: *Chemical data for the synthesised N-cinnamoylanthranilates available in the literature* *159*

Table 3.2: *Comparison of the* EC_{50} *and* IC_{50} *values of the standard TRPA1 and TRPM8 ligands, obtained in hTRPA1- or hTRPM8-HEK293 cells, against the literature values* *166*

Table 3.3: *Screening results of the synthesised N-cinnamoylanthranilic acids in hTRPA1-HEK293 cells* *174*

Table 3.4: *Screening results of the methyl N-cinnamoylanthranilates (3 µM) in hTRPA1-HEK293 cells* *174*

Table 3.5: *Screening results of the synthesised N-cinnamoylanthranilic acids in hTRPM8-HEK293 cells* *187*

Table 3.6: *Screening results of the methyl N-cinnamoylanthranilates (3 µM) in hTRPM8-HEK293 cells.* *187*

Table 3.7: *Physicochemical properties of N-cinnamoylanthranilic acids showing that the compounds obeyed the Lipinski's rule-of-five and the Veber's rules of lead-likeness / oral bioavailability, except* AC42c *191*

Table 3.8: *Physicochemical properties of methyl N-cinnamoylanthranilates showing that the compounds obeyed the Lipinski's rule-of-five and the Veber's rules of lead-likeness / oral bioavailability, except* AC42b *192*

Table 4.1: *Chemical data for the synthesised aryl sulfonamides available in the literature* *208*

Table 4.2: *Comparison of the* EC_{50} *and* IC_{50} *values of the standard TRPA1 and TRPM8 ligands, obtained in hTRPA1- or hTRPM8-HEK293 cells, against the literature values* *210*

Table 4.3: *Physicochemical properties of aryl sulfonamides showing that the compounds obeyed the Lipinski's rule-of-five and the Veber's rules of lead-likeness / oral bioavailability* *219*

Table 5.1: *Information about the designed primer sequences and oligonucleotides containing the mutants C621A, F909A, Y926S and F944A* *224*

Table 5.2: *The* EC_{50} *and* IC_{50} *values of the known ligands obtained in hTRPA1-HEK293 cells using a FlexStation are compared with the literature values of the original findings* *236*

Acknowledgements

I would like to thank my supervisors Dr Laura R Sadofsky, Dr Andrew N Boa and Professor Alyn H Morice for their guidance and for giving me the opportunity to work on this multidisciplinary project. I would also like to thank the thesis advisory panel member Dr Sam Xu, and the panel chair Dr Michael Hird for his advice.

I am also thankful to Dr Kevin Morgan for his initial guidance with the pharmacological work. Thanks are also due to Dr Kevin Welham, Mrs Carol Kennedy, Mr Daniel Mackenzie-Wade and Mr Christopher Crow for their technical support [mass spectra (KW), elemental analysis (CK and DMW) and biological consumables supply (CC)]. I also wish to acknowledge the IR Pharma company for performing the electrophysiological measurements on guinea pig vagus nerves.

Last but not least, I would like to thank my family for their continuous support and encouragement.

Arundhasa Chandrabalan

Author's declaration

I confirm that this work is original and that if any passage(s) or diagram(s) have been copied from academic papers, books, the internet or any other sources these are clearly identified by the use of quotation marks and the reference(s) is fully cited. I certify that, other than where indicated, this is my own work and does not breach the regulations of HYMS, the University of Hull or the University of York regarding plagiarism or academic conduct in examinations. I have read the HYMS Code of Practice on Academic Misconduct, and state that this piece of work is my own and does not contain any unacknowledged work from any other sources.

CHAPTER 1: Introduction

1.1 Transient receptor potential (TRP)

Transient receptor potential (TRP) channels are ligand-gated cation channels, permeable to monovalent and divalent cations. TRP channels act as biological sensors that detect variation in the environment and have a key role in sensing and transmitting physical stimuli. TRP channels were first discovered in a mutant strain (termed *trp*) of *Drosophila melanogaster* while determining the elements of the light-induced current in their photoreceptors, in which, mutation of the gene caused blindness to bright light and was identified as the consequence of a disruption in the calcium entry mediated by TRP channels.[1,2] Since then, various types of TRP channels are found to be expressed in nearly every type of mammalian cells and tissues, and are known to be involved in regulation of numerous cellular functions.[3,4] TRP channels are stimulated by diverse stimuli, including extracellular and intracellular messengers, chemicals, mechanical pressure (osmotic) and to temperature changes, *via* various mechanisms.[5-9]

Based on the amino acid sequence (structural) homology, the mammalian TRP superfamily has been divided into six subfamilies, including TRP Canonical (TRPC), TRP Vanilloid (TRPV), TRP Ankyrin (TRPA), TRP Melastatin (TRPM), TRP Polycystin (TRPP) and TRP MucoLipin (TRPML) (**Figure 1.1**).[8,10,11] There are twenty-eight members of the mammalian TRP channels identified under the six main subfamilies, including TRPC1 - 7, TRPV1 - 6, TRPA1, TRPM1 - 8, TRPP2, 3, 5 and TRPML1 - 3 (**Figure 1.1**),[4] which are briefly described in **Sections 1.1.1 - 1.1.6** with a detailed review on TRPA1 channel. The seventh subfamily, TRP No Mechanoreceptor Potential C (NOMPC, TRPN) consists of only one member, TRPN1, has been detected only in fruit fly (*Drosophila*), zebrafish (*Danio rerio*) and worm (*Caenorhabditis elegans*), and not currently in mammals. TRPN1 is homologous to TRPA1 with twenty-nine ankyrin repeats at the *N*-terminus.[4,12,13]

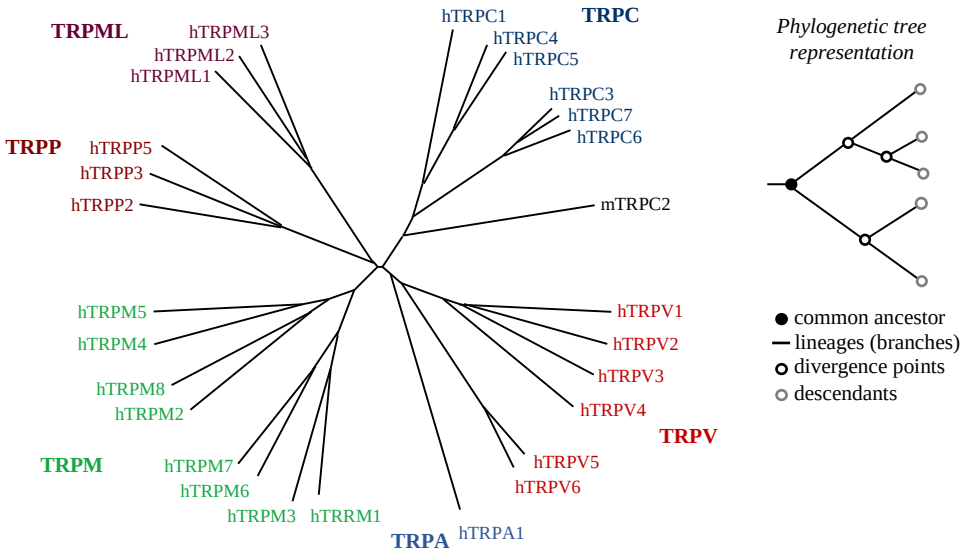

Figure 1.1: *Phylogenetic tree of the mammalian transient receptor potential (TRP) channels. Each superfamily of TRPC, TRPV, TRPA, TRPM, TRPP and TRPML consists of seven, six, one, eight, three and three different mammalian members, respectively.*

Each subunit of a TRP channel contains six putative transmembrane spanning segments, S1 - S6, with -NH_2 and -COOH termini located intracellularly, and a pore loop between S5 and S6 (**Figure 1.2a**). Homo- or hetero-tetramer arrangement of the subunits forms the cation-selective (selectivity filter) channels (**Figure 1.2b**).[4] Despite the fact that there are structural similarities between TRP and voltage-gated channels, TRP channels are grouped as a separate family of channels since several of them are only weakly voltage dependent and do not possess the characteristics of voltage-gated channels.[9] However, mammalian TRP channels are permeable to cations with similar general membrane topology to that of voltage-gated channels.[14]

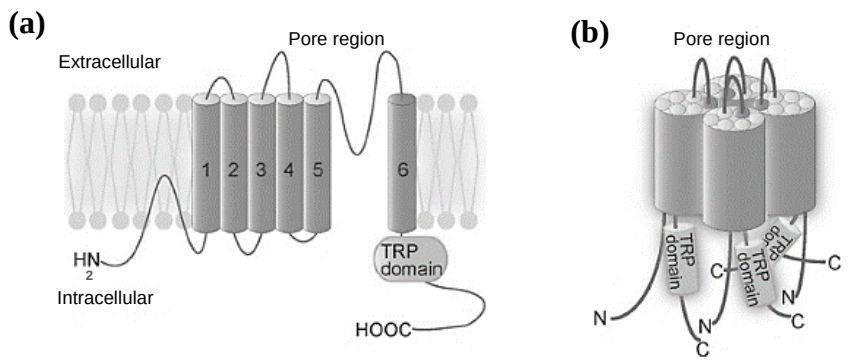

Figure 1.2: *The general structure of a TRP channel,* **(a)** *transmembrane topology of a subunit and* **(b)** *tetramer arrangement of four subunits, adapted from reference 15.*[15]

Almost all TRP channels are non-selectively permeable to Ca^{2+}, and are therefore implicated in numerous Ca^{2+} dependent cellular roles such as gene transcription, transmitter release, muscle contraction, cell proliferation and cell death.[4] However, TRPM4 and TRPM5 are selectively permeable to only singly charged cations. Usually, most TRP channels have poor selectivity for Ca^{2+} relative to Na^{+} (P_{Ca}/P_{Na} = 0.3 - 10), but TRPV5 and TRPV6 are highly Ca^{2+} selective (P_{Ca}/P_{Na} >100). Similarly, TRPM6 and TRPM7 are greatly Mg^{2+} selective, whereas TRPV1, TRPML1 and TRPP3 are vastly H^{+} selective. Hence, TRP channels also function as "gatekeepers" in numerous homeostatic processes such as (re)absorption of Ca^{2+} and Mg^{2+}.[4]

Since most TRP channels have a role in calcium signalling, and as they can function as gatekeepers in homeostatic processes, dysfunction of these channels could have an impact on several cellular and systemic processes. Considering the unique prominence of calcium signalling in all types of cells, malfunction of the Ca^{2+} channels results in pathogenesis of various diseases directly or indirectly.[4] It is also known that the malfunction of TRP channels expressed on intracellular membranes might disrupt organelle function. For instance, mutations in TRPML1 dysregulates the function of the lysosome.[16] As TRP channels have a role in regulating cell growth and proliferation, dysfunctions of these channels could lead to altered growth, cancer and organogenesis. These channels also have the potential to modulate the activity of electrically excitable cells in the heart and the brain.[4] However, the consequences associated with the malfunction of TRP channels remains an important area for future research.

In general, due to the polymodal nature and the diversity of functions the TRP channels participate in, malfunction of TRP channels can lead to complicated pathophysiological mechanisms resulting in development and progression of several diseases in respiratory, cardiovascular, intestinal, renal and urogenital systems, and furthermore in neuronal and neurodegenerative disorders.[4] The participation of TRP channels in diseases have been known from gain- or loss-of-function-, correlation-, chromosomal location- and phenotype-based evidences, and channelopathies (e.g. mutations in TRP channel encoding genes).[4] Genetic defects in TRPC6, TRPM6, TRPML1 and TRPP2 had been

recognised to have a direct link in causing the hereditary diseases focal segmental glomerulosclerosis, hypomagnesemia with secondary hypocalcemia, mucolipidosis type IV and autosomal dominant polycystic kidney disease, respectively. Additionally, variation in TRPM7 has been related to two neurodegenerative diseases; Guamanian amyotrophic lateral sclerosis (ALS) and Guamian Parkinsonism dementia.[4] Though most of the TRP family members are known to be involved in channelopathies, the knowledge on the complete mechanisms of how TRP channels function is yet rudimentary. This hinders the understanding of the roles of TRP channels in diseases and thereby the development of drugs targeting these channels.

1.1.1 Transient receptor potential canonical (TRPC)

Among the mammalian TRP superfamily, TRPC channels are known to be closely related to that of *Drosophila*. The mammalian TRPC channels share a common TRP channel structural motif (**Figure 1.3**), with the invariant sequence EWKFAR in the *C*-terminal tail, and three or four ankyrin repeats at the *N*-terminus.[17,18] TRPC channels are non-selective cation channels, permeable to Ca^{2+}, with significantly different permeability ratios (P_{Ca}/P_{Na}) between different subfamily members.[17,19,20] TRPC channels have also been considered as store-operated channels, and are known to be activated following a stimulation in phospholipase C (PLC) activating receptors. However, the activation mechanism of TRPC allied with PLC is not yet resolved.[21-23] On the other hand, a study reported that TRPC1 is activated directly by membrane stretch.[24]

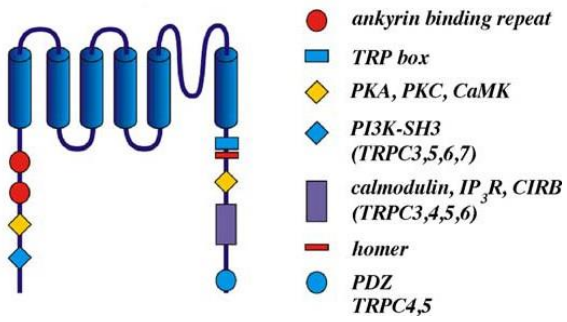

Figure 1.3: *Topology model and main interaction sites of TRPC1 - 7 channels.*[8]

1.1.2 Transient receptor potential vanilloid (TRPV)

Along with the six mammalian TRPV members, there is also Nan from *Drosophila*[25] and Osm-9 from *Caenorhabditis elegans*[26]. TRPV members contain three to five ankyrin repeats at the *N*-terminus and other main interaction sites as in TRPC (**Figure 1.4**). TRPV1 - V4 are non-selective cation channels, sensitive to heat and are activated by a broad range of endogenous and exogenous (natural and synthetic) ligands, functioning as thermo- and chemo-sensors.[27-36] The members, TRPV5 and V6 have distinct properties to TRPV1 - V4. TRPV5 and V6 channels are only Ca^{2+} selective and are strongly controlled by intracellular calcium ions ($[Ca^{2+}]_i$).[37-39] These channels under physiological conditions solely conduct Ca^{2+}, but monovalent cations permeate readily in the absence of extracellular Ca^{2+}, allowing TRPV5 and V6 to function as gatekeepers in epithelial calcium transport, and as selective calcium entry pathways in non-excitable cells.[37-41]

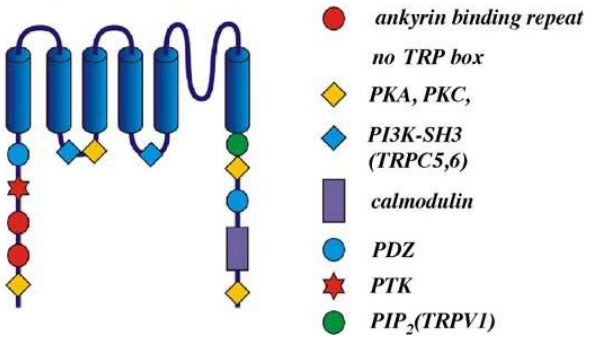

Figure 1.4: *Topology model and main interaction sites of TRPV1 - 6 channels.*[8]

1.1.3 Transient receptor potential melastatin (TRPM)

Based on the sequence homology, the members of TRPM are subdivided into three groups: TRPM1/M3, TRPM4/M5, and TRPM6/M7, where TRPM2 and M8 are structurally distinct channels. TRPM channels do not have ankyrin repeats at the *N*-termini, but some members possess distinctive functional enzymes in their *C*-termini.[4,8] For example, TRPM2 contain NUDT9 domain for ADP-ribose activation,[42,43] and TRPM6 and M7 contain α-kinase[44,45] (**Figure 1.5**). TRPM channels show varying levels of permeability to Ca^{2+} and Mg^{2+}. TRPM4 and M5 are impermeable to Ca^{2+}, whereas TRPM6, M7 and some M3 variants are highly permeable to Ca^{2+} and Mg^{2+}.[46-54] The gating

mechanisms within members of the TRPM channels also vary. For instance, TRPM2 is stimulated by intracellular ADP-ribose,[55] heat and hydrogen peroxide (H_2O_2), whereas TRPM3 is activated by sphingosine[56] and cell swelling. TRPM4 and M5 channels are triggered by a rise in $[Ca^{2+}]_i$[50,57,58] and heat,[59,60] where TRPM6 and M7 gating mechanisms are controlled by the levels of intracellular magnesium ions ($[Mg^{2+}]_i$) and Mg-ATP.[45,54] TRPM8 is activated by cold temperatures and cooling agents like icilin and menthol.[61,62] TRPM1 has not yet been functionally characterised.

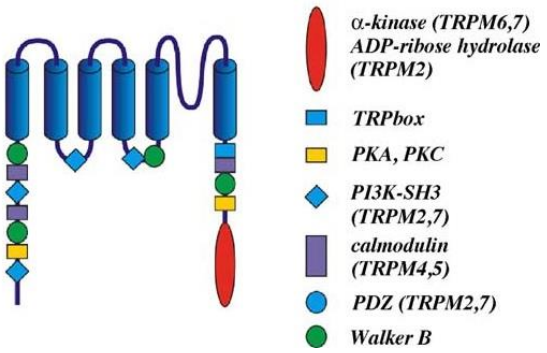

Figure 1.5: *Topology model and main interaction sites of TRPM1 - 8 channels.*[8]

1.1.4 Transient receptor potential polycystin (TRPP)

TRPP2 (PKD2), TRPP3 (PKD2L1) and TRPP5 (PKD2L2) contain a coiled-coil domain, and additionally TRPP2 and TRPP3 possess a Ca^{2+} binding EF-hand motif within the *C*-terminus (**Figure 1.6**).[63-65] TRPP2 and TRPP3 are cation-selective channels permeable to Ca^{2+},[66,67] in which TRPP3 show high selectivity for divalent cations.[68] TRPP1 contains eleven transmembrane domains, a complex lengthy extracellular domain (~3000 amino acid), and an intracellular *C*-terminus interacting with the *C*-termini of TRPP2 *via* a coiled-coil domain.[63-65] However, the last six transmembrane domains of TRPP1 have structural similarity to TRPP2 channel that has structural resemblance to other TRP channels.[68] TRPP1 also contains several structural motifs, including a number of adhesive domains, within the *N*-terminal tail that could participate in cell-matrix and cell-cell interactions. The large intracellular loop between S6 and S7 contains polycystin motifs of undetermined function.[68,69] There is a significant evidence that TRPP1 and TRPP2 together form a signalling complex on the plasma membrane by physically interacting with each other, in

which TRPP2 is employed by TRPP1.[70,71] Recently, TRPP3 has been recognised in mammals as a potential sour taste sensor.[72,73] At present, the inclusion of TRPP1 (also known as PKD1) under the TRP superfamily is being somewhat tentative due to lack of homogeneity between TRPP1 and other TRP channels.[68,69]

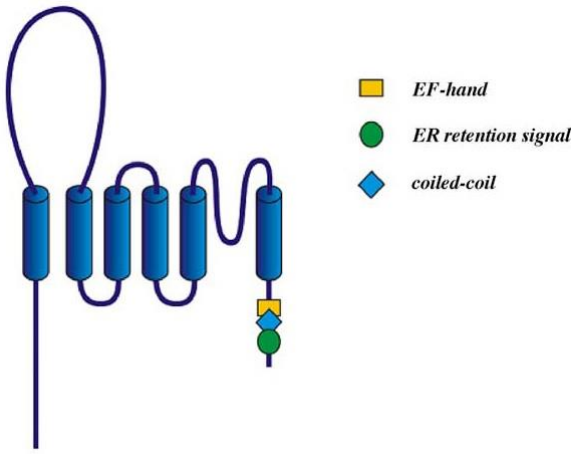

Figure 1.6: *Topology model and main interaction sites of TRPP2, 3 and 5 channels.*[8]

1.1.5 Transient receptor potential mucolipin (TRPML)

In comparison to other TRP channels, TRPML1 - ML3 are small proteins with less than 600 amino acid residues. TRPML1 is predominantly expressed in late endosomes and lysosomes, and it contains a functionally uncharacterised lipase domain between the S1 and S2 loop (**Figure 1.7**).[16,74,75] TRPML1 is reported as a H^+ channel, which could prevent excess acidification by acting as a proton leak in lysosomes.[76,77] TRPML2 and ML3 are not yet been functionally characterised.

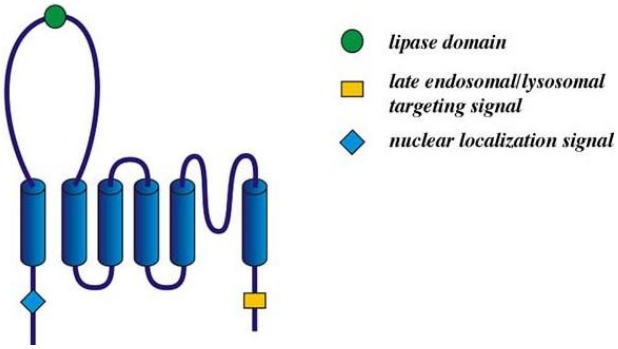

Figure 1.7: *Topology model and main interaction sites of TRPML1 - 3 channels.*[8]

1.1.6 Transient receptor potential ankyrin (TRPA)

Discovery

TRPA1 was first discovered in 1999 in cultured human fibroblasts as an overexpressed protein.[78] It was described as a protein with 1119 amino acids comprising eighteen ankyrin repeats at the *N*-terminal tail and six transmembrane segments in the *C*-terminus similar to TRP-like proteins in overall structure, with a molecular weight of 130 kDa, and the corresponding gene containing twenty-seven exons located on human chromosome 8 (8q13). It also included that this novel protein was expressed at a low level in human fibroblasts, and at a moderate level in liposarcoma cells.[78]

Expression

The TRPA subfamily consists of only one mammalian member, TRPA1 (previously known as ANKTM1).[79] The human TRPA1 (hTRPA1) channel is predominantly expressed in the primary afferent (sensory) neurons[79] including trigeminal[80], dorsal root[81] and nodose[82,83] ganglia. It is also found in epithelial cells (in airway, skin, gastrointestinal tract and bladder), smooth muscle cells, mast cells, islets of Langerhans β-cells, mucosal enterochromaffin cells, epidermal melanocytes, fibroblasts, odontoblasts and in the inner ear.[84-92] In addition, it has been reported that TRPA1 may possibly be present in the central nervous system (CNS).[93]

Structure

One key structural feature of TRPA1 is the presence of fourteen to eighteen ankyrin repeats at the *N*-terminus (**Figure 1.8**). The ankyrin repeats which are of half the size of TRPA1 are thought to play a role as a mechanosensor, and essential for protein-protein interactions and for the insertion of the channel into the plasma membrane.[94,95] The presence of many cysteine residues at the *N*-terminus leads to the formation of disulfide bridges between and within some cysteine monomers (**Figure 1.9**).[94,96,97] The homotetrameric arrangement of the protein monomers forms the cation-selective channel. At physiological membrane potentials, the channel allows Ca^{2+} and Na^{+} to flow into the cell and K^{+} to flow outward through the pore loop between S5 and S6, in which D918 in the pore loop is said to be crucial for the selectivity of Ca^{2+}.[94,95] Also, it has

been suggested that the *N*- and *C*-termini of TRPA1 possess Ca^{2+} binding sites capable of both sensitising and desensitising the channel.[98-102]

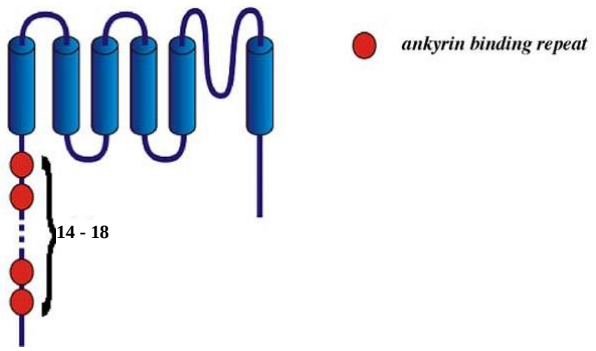

Figure 1.8: *Topology model of TRPA1 channel, adapted from reference 8.*[8]

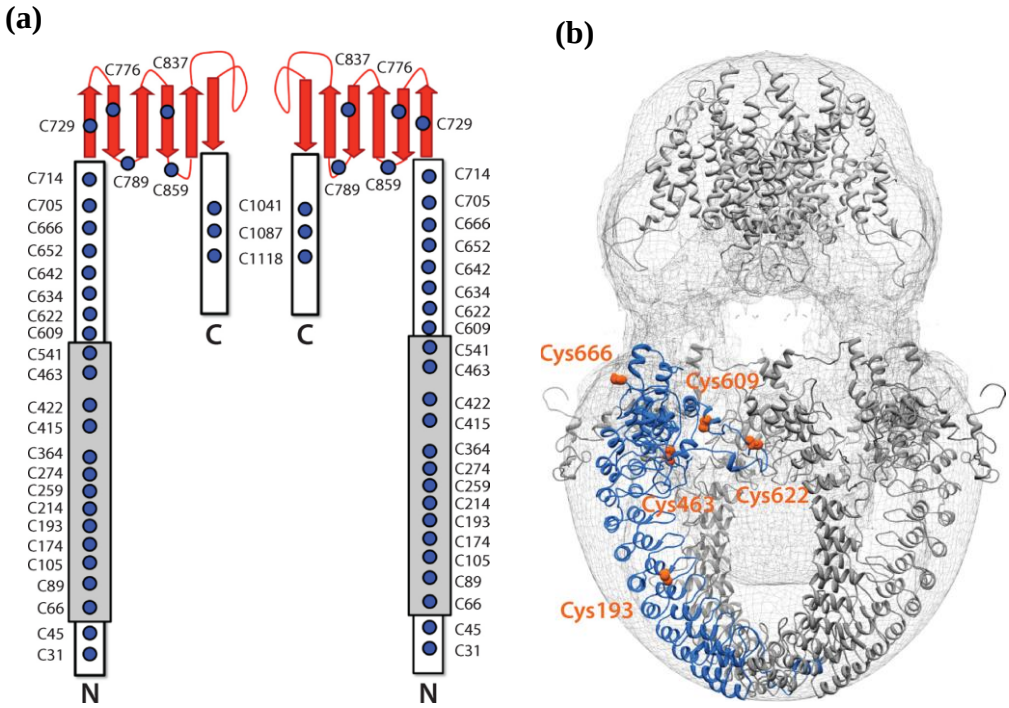

Figure 1.9: (a) *Illustration of a mouse TRPA1 dimer in two-dimension (red arrows denote the six transmembrane helices, blue circles are the cysteine residues and grey box at the N-terminus represents the ankyrin repeats domain), and* **(b)** *three-dimensional electron microscopy density model representing the cysteine residues of TRPA1 involved in disulfide bonding (the cysteines are indicated in orange, and the N-terminus as blue ribbon).*[97]

Recently, the three-dimensional structure of the hTRPA1 was determined to a resolution of ~4 Å using a single-particle cryo-electron microscopy (cryo-EM).[103] The structure of the hTRPA1 homotetramer captured at different views and the key structural features of a TRPA1 subunit are shown in **Figure 1.10**.

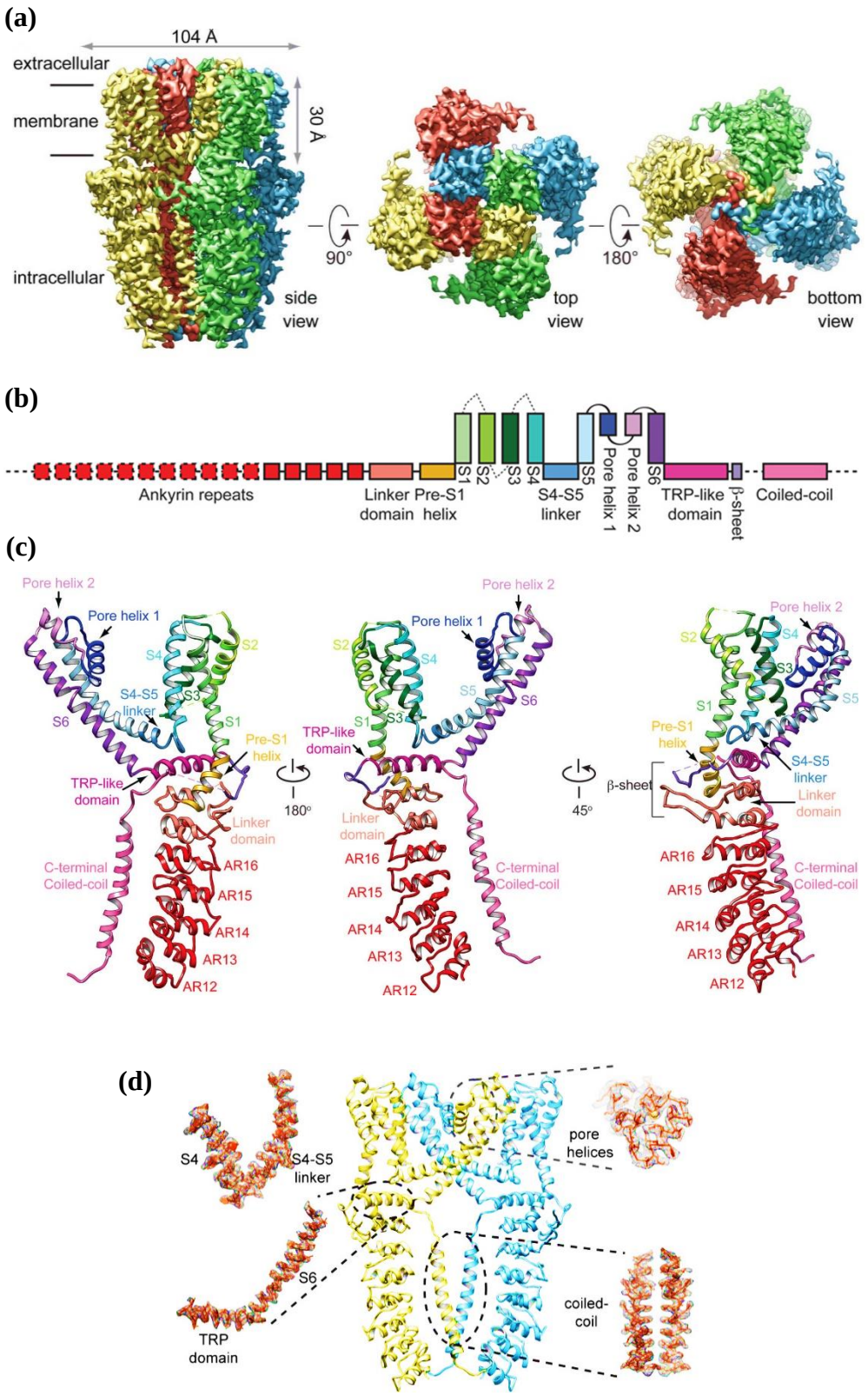

Figure 1.10: *The structure of hTRPA1 determined using a cryo-EM,* **(a)** *three-dimensional density map showing the side, top and bottom views of hTRPA1 in the presence of a TRPA1 agonist, allyl isothiocyanate, filtered to 3.5 Å resolution,* **(b)** *diagram illustrating the major domains in a single subunit,* **(c)** *ribbon diagrams of a subunit viewed at different angles, and* **(d)** *densities of the domains S4 to coiled-coil showing only two diagonally faced subunits of the tetramer for clarity.*[103]

Role

TRPA1 is a non-selective cation channel, permeable to both monovalent (Na^+, K^+) and divalent (Ca^{2+}) cations.[88,95] TRPA1 channels act as a detector of chemical,[104,105] mechanical,[94,106] and thermal stimuli.[79,107,108] This polymodal receptor is known to be involved in pain, itch, inflammatory[109,110] diseases like arthritis,[111] chronic obstructive pulmonary disease (COPD), and other respiratory diseases including chronic cough and asthma.[112-114] Furthermore, TRPA1 present in mast cells, enterochromaffin cells and melanocytes, could perhaps have a crucial role in the innate immunity, gastrointestinal motility regulation and in pigmentation induced by UV radiation, respectively.[83-91] These important roles of TRPA1 in the body have attracted much attention in recent years as a target for drug development, and there are numerous investigations ongoing in understanding the detailed activation and/or blocking mechanisms of TRPA1.

In primary neurons, the flow of Ca^{2+} and Na^+ into cells *via* TPRA1 channels leads to depolarisation of the membrane, action-potential discharge, and release of neurotransmitters at central and peripheral neural projections.[9] At hyperpolarising voltages, TRPA1 channels get inactivated indicating intrinsic voltage dependence for the function of the channel.[8] The property of TRPA1 channel to close in response to hyperpolarisation induced by voltage-dependent Ca^{2+} binding and reopening during depolarisation is known to be an important feature for its function, as it can deactivate the channel during harmless stimulation and activate during painful stimulation.[9]

1.1.6.1 TRPA1 in chemosensation

TRPA1 was initially identified as ionotropic cannabinoid receptors and later as a target for electrophilic and non-electrophilic compounds (**Figure 1.11**).[98,104,115] Further, it has been shown that TRPA1 is activated by certain thiol-reactive compounds (garlic-derived).[116,117] Targeted gene mutation studies revealed cysteine residues (C621, C641 and C665 in human, and C415, C422 and C622 in mouse) located at the *N*-terminus of TRPA1 to be crucial for the activation of TRPA1 by electrophilic compounds.[118,119] The exact locations and spatial distribution of these key cysteine residues in hTRPA1

structure were resolved recently using a cryo-EM (**Figure 1.12**).[103] The residue C621 is shown to be located in the helix-turn-helix 1, C641 in the putative β-strand, and C665 is reported to be in the flexible loop linking the β-strand to the helix-turn-helix 2 (**Figure 1.12**).[103] Nevertheless, lysine residues in the *N*-terminus and cysteine residues in other regions of TRPA1 are also considered as potential targets for electrophiles and oxidants (**Figure 1.11**).[97,120,121] Generally, TRPA1 is described as a channel triggered by endogenous and exogenous cysteine-reactive electrophiles and oxidants, and also by non-electrophilic compounds.

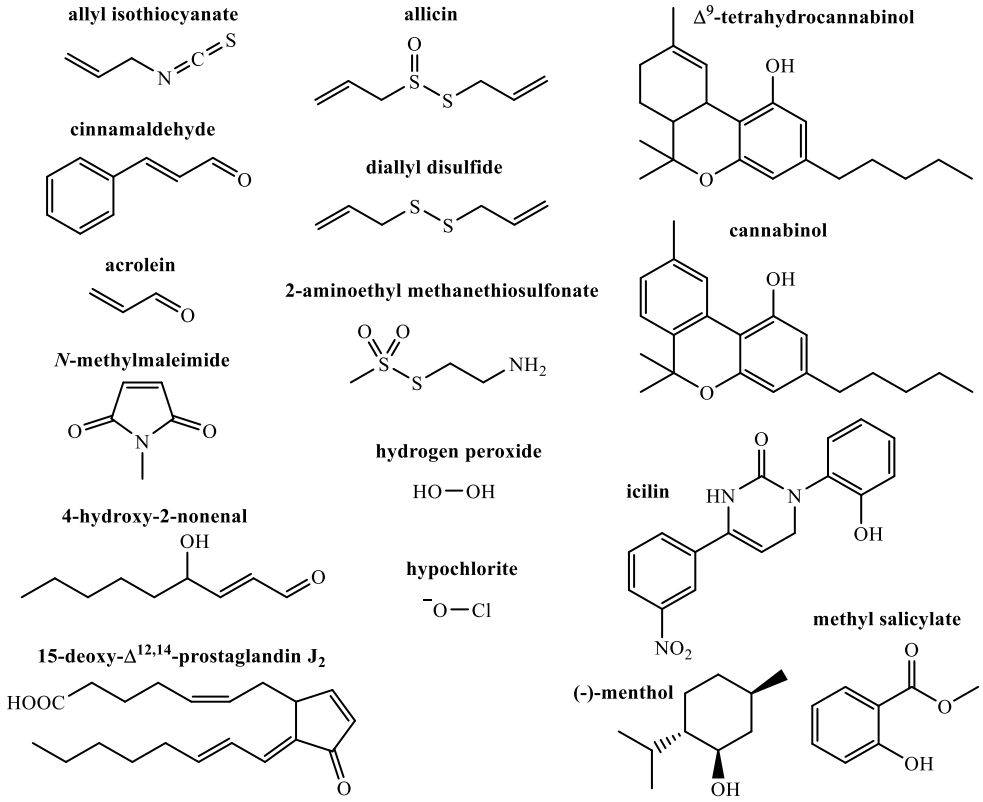

Figure 1.11: *Chemical structures of the key TRPA1 activators, which initially revealed the chemosensation property of TRPA1. The compounds on the left panel are electrophilic compounds those bind to cysteine residues at the N-termini through a covalent mechanism, in the middle panel are weak electrophiles and oxidants that can stimulate the formation of disulfide bonding within TRPA1, and on the right panel are non-electrophilic compounds that could activate the channel via a non-covalent mechanism.*[83]

The covalent mechanism by which electrophilic compounds activate TRPA1 through modification of cysteine residues differs even though the chemical structures of the activators are closely related.[122-124] For instance,

methylglyoxal, an electrophilic ketoaldehyde activates TRPA1 by irreversible binding to the lysine residue K710 located in the pre-S1 helix (**Figure 1.12**) and by promoting disulfide formation of the cysteine residues at the *N*-terminus (**Figure 1.9**).[125] Whereas, umbellulone, a monoterpene ketone activates by reacting covalently with the *N*-termini cysteines, as well as by interacting non-covalently.[126]

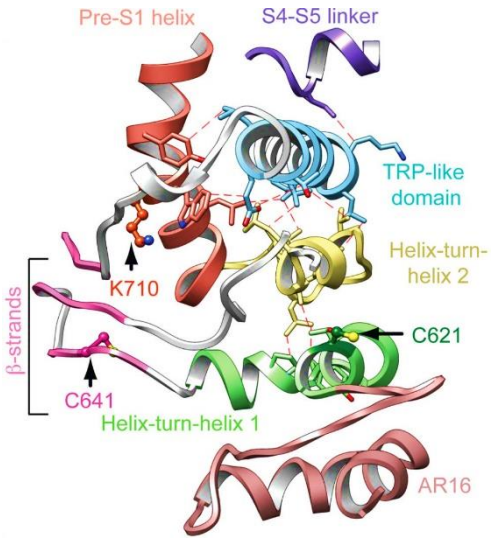

Figure 1.12: *Spatial distribution of key reactive cysteine and lysine residues located in the cytoplasmic N-terminus of hTRPA1 and the interactions with other domains, determined using a cryo-EM. The C621 residue is located in the helix-turn-helix 1, C641 in the putative β-strand, C665 in the flexible loop linking the β-strand to the helix-turn-helix 2, and K710 in the pre-S1 helix.*[103]

Today, there are many natural and synthetic compounds found to activate mammalian TRPA1.[83] In particular, TRPA1 channels can be activated by pungent chemicals like allyl isothiocyanate (AITC, present in wasabi, mustard oil and horse radish),[98,104] allicin (in garlic), diallyl disulfide (in onions and garlic),[116,117] cinnamaldehyde (in cinnamon), eugenol (in clove oil), methyl salicylate (in wintergreen),[104] Δ^9-tetrahydrocannabinol (Δ^9-THC, in marijuana),[98] menthol (in mint),[127] thymol (in thyme),[127,128] carvacrol (in oregano and thyme),[129], acrolein (from cigarette smoke, tear gas and vehicle exhaust fumes),[109] and inflammatory mediators,[87,130] which as a result generates acute painful burning and pricking sensation.[14]

The endogenous TRPA1 activators including inflammatory mediators such as 15-deoxy-Δ12,14-prostaglandin J_2, 4-hydroxy-2-nonenal and H_2O_2 act directly on TRPA1, while bradykinin, histamine, prostaglandins and trypsin act indirectly on TRPA1 by binding to TRPA1 regulating G-protein-coupled receptors (GPCRs) *via* PLC signalling pathway [phosphatidylinositol 4,5-biphosphate (PIP2) depletion, H^+ production, Ca^{2+} release, and protein kinase A (PKA)-mediated phosphorylation, **Figure 1.13**].[87,88,112,131-133] TRP channels can be sensitised or desensitised due to an increase in $[Ca^{2+}]_i$, as a result of Ca^{2+} release from the endoplasmic reticulum (ER) when the inflammatory mediators including bradykinin, serotonin, prostaglandin E_2 (PGE_2), nerve growth factor (NGF) and adenosine triphosphate (ATP) bind to either GPCRs or receptor tyrosine kinases (RTK) to activate PLC, Ca^{2+}/calmodulin-dependent kinase II (CAMKII), P13 kinase (P13K), and protein kinases A and C (PKA and PKC).[14] Since GPCR can activate phospholipase A_2 (PLA_2) too, it triggers the release of arachidonic acid (AA) metabolites, 5,6-epoxyeicosatrienoic acid (5,6-EET) and 5-hydroperoxyeicosatetraenoic acid (HPETE), which are TRP channel agonists **(Figure 1.13)**. The sensitisation by a particular inflammatory mediator differs depending on the type of TRP channels expressed in the sensory neuron.[14]

Zn^{2+} is a potent TRPA1 activator that probably binds to cysteines and histidines at the *C*-terminus.[134,135] Hydrogen sulfide (H_2S), a mild reducing agent, and sodium hydrosulfide, a donor of the H_2S gasotransmitter, have shown to activate TRPA1.[136] A suggested mechanism for the activation of TRPA1 by H_2S is through sulfhydration of thiols directly or indirectly by H_2S.[137-139]

TRPA1 also plays a part in oxygen homeostasis, in which TRPA1 is activated by hyperoxia condition directly and by mild hypoxia condition indirectly, indicating that TRPA1 expressed on perivascular sensory neurons might have an important role in rectifying hypoxia by releasing vasodilator peptides.[83,121] hTRPA1 is also activated at acidic pH (pH below 7).[140,141] Conversely, due to species differences, the sensitivity of TRPA1 to extracellular proton is not seen in TRPA1 orthologues found in rodent and rhesus monkey. It has been reported that the amino acid residues C621 in the *N*-terminus, and V942 and S943 in the transmembrane S6 are responsible for the sensitivity of hTRPA1 to

extracellular acidosis.[140,141] However, the role of C621 residue in proton-sensing role seems to be inscrutable as this residue is present in both rodent and rhesus TRPA1 too.[141] Since extracellular acidification could lead to inflammation, ischaemia, development of cancer, conditions related to pain and nociceptive primary afferents sensitisation, the proton-sensing property of TRPA1 is understood to have a great importance.[83] Though rodent TRPA1 is insensitive to extracellular acidic pH, it has the ability to sense intracellular acid-base environment with a U-shaped link in the pH effect.[142-144] It was also found that mutations of the *N*-termini cysteines, C422 and C622, caused disruption in the activation of the channel stimulated by intracellular alkalisation.[142-144]

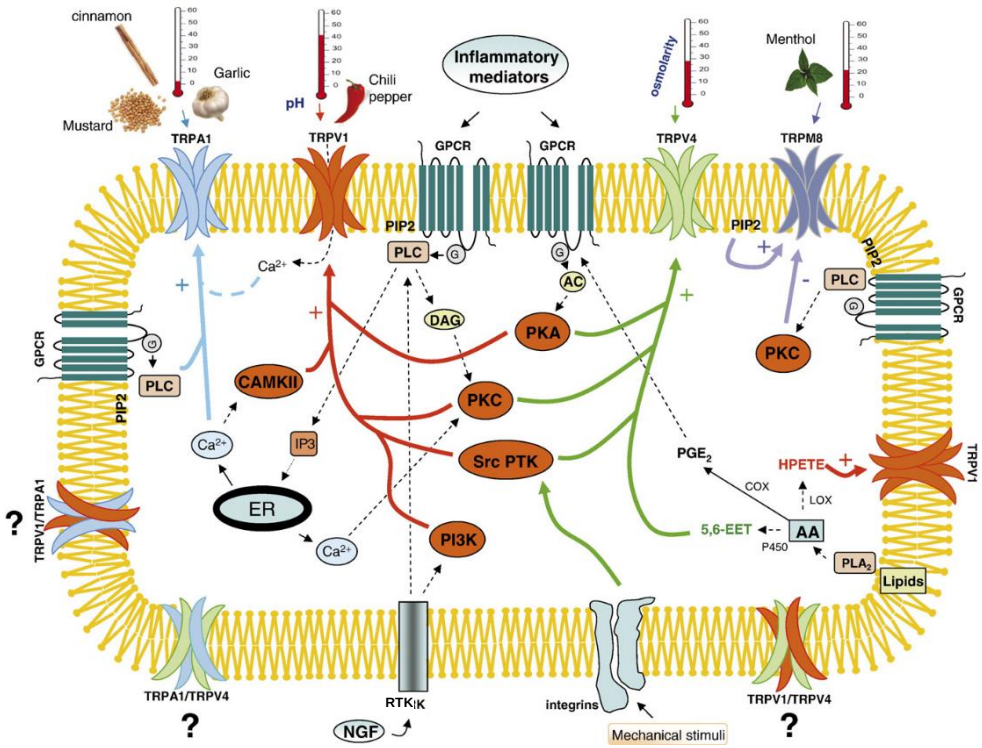

Figure 1.13: *TRP channel regulation in sensory neurons via phosphorylation. Arrow lines in blue, orange, green and purple represent TRPA1, TRPV1, TRPV4 and TRPM8 channel regulation signalling pathways, respectively.*[14]

Activation of TRPA1 by electrophilic paracetamol metabolites (*N*-acetyl-*p*-benzoquinone imine and *p*-benzoquinone) and non-electrophilic cannabinoids leads to spinal anti-nociception.[145] Hence it is suggested that non-tissue-damaging TRPA1 agonists have hope in the treatment of pain.[83,145] It was shown that TRPA1 is also activated by non-steroidal anti-inflammatory drugs

(NSAIDs),[146,147] and other non-covalent activators including clotrimazole and dihydropyridines.[148,149] Thus, it is anticipated that these might serve as prototypes in the development of TRPA1 activating analgesics.[83]

The ability of TRPA1 to respond to several non-electrophilic compounds with a wide range of chemical structures remains interesting. Mutagenesis and chimeric approaches have demonstrated that non-electrophilic activators such as menthol interact directly with TRPA1 by binding to S5 residues S873 and T874.[150] Similarly, multiple binding sites including S873, T874, F909, F944, T945, V948 and I950 residues have been reported in the pore loop of S5 and S6 linker for the potent TRPA1 specific antagonist A967079 [(1*E*,3*E*)-1-(4-fluorophenyl)-2-methylpent-1-en-3-one oxime].[103,151,152] The interaction of A967079 with F909 residue in hTRPA1[103] is shown in a three-dimensional structural view in **Figure 1.14**. Moreover, patch-clamp recordings have indicated that Δ^9-THC also directly interact with TRPA1, signifying that cannabinoids activate TRPA1 in a distinct way to other electrophilic and non-electrophilic TRPA1 activators such as allicin, cinnamaldehyde, AITC, methyl salicylate, trinitrophenol, *N*-ethylmaleimide, 2-aminoethyl methanethiosulfonate, 2-aminoethoxydiphenyl borate and also Ca^{2+}, as these require a cytosolic component to stimulate TRPA1.[132,153]

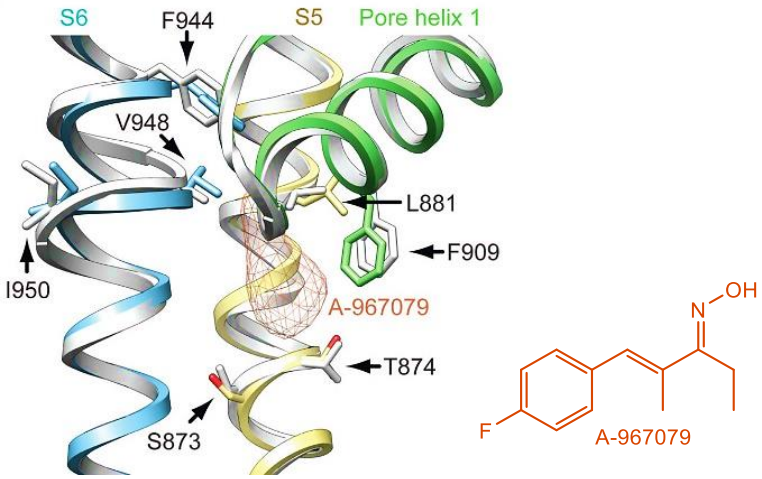

Figure 1.14: *Cryo-EM density map showing the interactions of the potent TRPA1 specific antagonist A967079 with multiple residues, including S873, T874, F909, F944, T945, V948 and I950, those reside in the pocket formed by S5, pore-helix 1, and S6 in hTRPA1.*[103]

Compounds including cinnamaldehyde, camphor,[154] menthol,[127] apomorphine,[155] nicotine,[156] umbellulone[126] and ligustilide[157] (**Figures 1.11** and **1.15**) were found to activate TRPA1 at low concentrations and inactivate at high concentrations, that is, they showed bimodal activity on heterologously expressed TRPA1. Some of these activators were found to be species dependent. Though there is an extensive list of TRPA1 activators, only a few natural inhibitors have been found.[158-161] Resolvin D2 is an example, which inhibits TRPA1 and TRPV1 at nanomolar concentration range. Since the effects of resolvin D2 was pertussis toxin-sensitive, it is thought that resolvin D2 might interact indirectly with the TRP channels.[160]

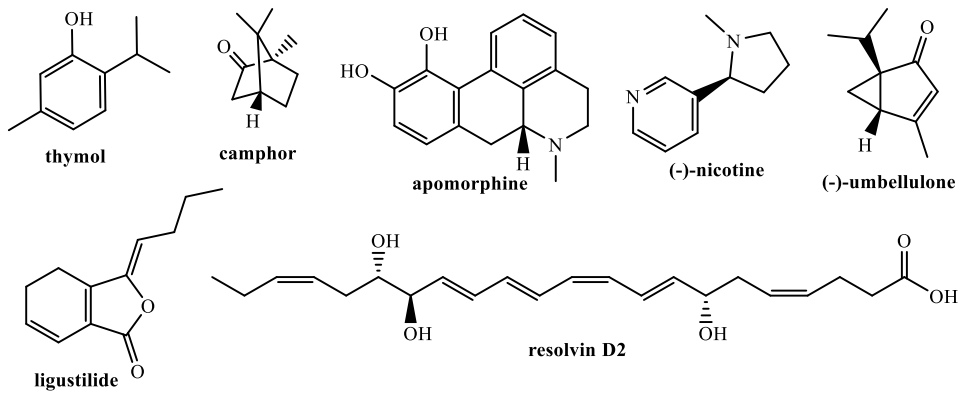

Figure 1.15: *Chemical structures of TRPA1 modulators.*

As most of the TRPA1 activators are known to intervene with other TRP channels and membrane receptors involved in sensory signalling,[162,163] further pharmacological studies on the bimodal action and non-covalent activators against TRPA1 are essential for better understanding of the function of the channel. Moreover, understanding how these compounds have cross channel activity and how they actually bind to the individual receptors could aid in the development of novel TRPA1 activators and inhibitors, which are specific to TRPA1. Though inhibiting the action of TRPA1 seems to be a rational treatment method to relieve pain associated with neuropathic and inflammatory diseases, the intervention of TRPA1 activators in anti-nociceptive signalling is also of interest. Hence based on the action site and intrinsic properties of chemicals, both agonists and antagonists could be useful in treating different conditions of pain, as with TRPV1.

1.1.6.2 TRPA1 in thermosensation

There is an ambiguous statement that noxious cold (<17 °C) could activate TRPA1 channels, but the role of TRPA1 in cold sensation remains debated since it was first suggested.[8,79] However, so far, many *in vitro* and *in vivo* behavioural model studies in mouse and rat species have revealed that TRPA1 is involved in noxious cold sensation and in cold allodynia evoked by peripheral neuropathy, inflammation, nerve injury, diabetic neuropathy, and iatrogenic.[108,164-168] There is a considerable amount of evidence that rodent TRPA1 is involved in cold sensation. However, the absence of the role in hTRPA1 *in vitro* studies is still being reasoned.[98,100,104,169] It has been recently suggested that due to species differences the human variant is unresponsive to cold, contrary to rodent TRPA1.[170] Moreover, the gating mechanism by which cold stimulates TRPA1 is still undetermined.[83]

1.1.6.3 TRPA1 in mechanosensation

Studies have shown that an orthologue form of TRPA1 exists in mechanosensory and nociceptive neurons of the worm (*C. elegans*), suggesting an ancestral form of the method for mechanotransduction.[9,171] Also, there is an unproven prediction that the large ankyrin repeats in TRPA1 could have spring-like mechanical function to enable mechanosensing in the auditory signal transduction function of the inner ear hair cells.[106] Furthermore, it was shown that TRPA1, a mechanogated transduction channel, which functions in response to mechanical forces/stress, is necessary for the auditory response in mammals.[8,9] In later studies performed on TRPA1 gene knockout mice, TRPA1 contribution in hearing could not be observed.[109,164] However, the participation of TRPA1 in noxious mechanosensation such as in hypersensitivity and mechanical allodynia have gained more support with time based on the findings from different behavioural studies using either mouse or rat pain and inflammatory models.[83,134,172] Moreover, TRPA1 has also been shown as a main element in the nociceptive somatosensory neuron mechanotransduction pathway.[165,173-175]

1.1.6.4 TRPA1 in disorders/diseases

Itch and Pain

Itch is an uncomfortable psychophysical sensation that usually leads to scratch. Itch and pain are mediated by different sets of primary afferents.[176] However, mechanical stimulation of pain could inhibit itch response at spinal cord level and result in itch-induced injury.[177] Mechano-sensitive and mechano-insensitive fibres are two sets of primary afferent C-fibres that can be selectively activated by histamine and cowhage spicules (5-hydroxy tryptamine), respectively.[178,179] It has been recently revealed that TRPA1 is essential for itch-induced scratch reaction in response to pruritogens like substance P, leukotriene B4, cowhage spicules, chloroquine and reactive oxygen species (ROS),[89,110,180] but not histamine.[181]

Administration of TRPA1 agonist AITC in mouse cheek was shown to activate pruritogen-sensitive trigeminal second-order neurons.[182] Whereas, administration of AITC or cinnamaldehyde in the skin and nasal mucosa of man resulted in pain sensation, and the observation was regarded as a cross-modality of itch inhibition.[183,184] The cross-modality interaction between pain and itch neural pathways was also observed while testing to silence capsaicin-sensitive nerve fibres using AITC, which produced itch.[179]

It was recently identified that TRPA1 is vital for mediating non-histaminergic itch, and when itch-encoding histamine-insensitive primary afferents are overactive, it could result in atopic and allergic contact dermatitis of chronic itch.[90,110,181,185,186] A dramatic raise in TRPA1 immunoreactivity was observed in biopsies of atopic dermatitis patients, and also surprisingly in keratinocytes and mast cells that barely express TRPA1.[90] Hence, TRPA1 is budding as a hopeful target for novel anti-pruritic drugs targeted for allergic and atopic contact dermatitis. It is suggested that pharmacological inhibition of TRPA1 could break the vicious cycle produced by intense scratching in dermatological diseases, whereas non-inhibition of itch-encoding neurons could possibly increase TRPA1-independent itch pathways.[83]

Inflammatory diseases

As known from animal studies, TRPA1 is involved in inflammation-induced thermal and mechanical sensitisation.[87,187] Endogenous chemicals, including ROS, α,β-unsaturated aldehydes (e.g. 4-hydroxy-2-nonenal and methyl glyoxal) and H_2S, formed during bacterial infection and inflammation, activate and maintain inflammation by activating TRPA1 on non-neuronal cells and sensory nerve fibres.[130,131,138] Moreover, inflammatory mediators, including nerve growth factor, bradykinin and trypsin, can sensitise TRPA1 or increase its expression level and leads to symptoms like itch, hyperalgesia and allodynia.[188-194] TRPA1 was also shown to be involved in sensory hyperactivity, pain perception and progression of inflammatory diseases including dermatitis, pancreatitis, inflammatory bowel disease, asthma and arthritis.[112,131,162,195,196]

Cyclophosphamide-induced haemorrhagic cystitis is a commonly used animal model for the chronic disease interstitial cystitis/bladder pain syndrome. The metabolism of cyclophosphamide and its analogue ifosfamide produces urotoxic acrolein, a TRPA1 activator, which causes mucosal injury on accumulation in the urine.[109] It was found that the overactivity of the bladder triggered by cyclophosphamide in pre-treated rats is effectively reduced through systemic administration of HC030031 [2-(1,3-dimethyl-2,6-dioxo-1,2, 3,6-tetrahydro-7*H*-purin-7-yl)-*N*-(4-isopropylphenyl)acetamide], a TRPA1 blocker.[197]

Respiratory diseases

Chronic respiratory diseases are complex malfunctions that results from airway damage. TRPA1, a chemosensor expressed in the airway primary sensory neurons, is known to be activated by airway irritants, including acrolein, chlorine, tear gas and isothiocyanate. Activation of TRPA1 on the airways by these irritants leads to pain, cough and sneezing, and thereby safeguard the lungs from being exposed to high levels of irritants.[122,198,199] In rodent lungs and guinea pig, activation of TRPA1 led to stimulation of the vagal bronchopulmonary C-fibres.[200,201] It was also shown that isolated guinea pig vagus nerve gets activated and inhibited by the TRPA1 selective agonists

(cinnamaldehyde and acrolein) and antagonists (HC030031 and AP18 (4-(4-chlorophenyl)-3-methylbut-3-en-2-oxime)), respectively.[202] In particular, the antagonists were able to inhibit acrolein-induced activation in a concentration-dependent manner. In isolated human vagus nerve, depolarisation caused by acrolein was inhibited by AP18.[202] Moreover, coughing was induced by cinnamaldehyde and acrolein in human volunteers and guinea pigs, respectively, in which the role of TRPA1 was further confirmed using TRPA1 antagonists.[203] The identification of TRPA1 as a pro-tussive receptor and the ability to selectively block the triggered responses by TRPA1 selective antagonists are considered as important findings, as this link could be utilised to research anti-tussive remedies capable of alleviating normal or chronic cough.[203]

TRPA1 ligands could also be involved in cough hypersensitisation.[114] The environmental toxins, toluene diisocyanate and ozone are TRPA1 activators known to induce wheezing, cough and dyspnea on exposure.[204-207] Reactive airways dysfunction syndrome is caused by excessive amount of exposure to irritant chemicals like aldehydes and chlorine, which are TRPA1 agonists, and is mostly characterised by cough like symptom.[208-210] TRPA1 also has an important role in allergic airway inflammation. In an ovalbumin-induced airway inflammation models, the airway hyperresponsiveness and eosinophilia were shown to be inhibited by the antagonist HC030031, and the role of TRPA1 in this was later confirmed.[211]

An increase in Ca^{2+} influx and increased release of neuropeptide were observed in TRPA1 transfected-human embryonic kidney 293 (HEK293) cells and isolated guinea pig airway tissue, respectively, when exposed to cigarette smoke extract or aldehydes.[198] In addition, it was shown that isolated guinea pig bronchial rings contract on exposure to cigarette smoke extract, acrolein or crotonaldehyde, and the contraction was inhibited by HC030031. These observations suggested that TRPA1 could be used as a target to treat diseases like COPD that is caused by cigarette smoke.[198]

Peripheral neuropathy

Allodynia caused by mechanical and cold stimuli are usually observed in individuals with peripheral neuropathy. It was observed that TRPA1 is usually overexpressed in healthy neurons closer to the site of damage, which could probably indicate neuroinflammatory cues linked to adaptive responses.[188,189,192] Moreover, the symptoms associated with mechanical and cold allodynia were reduced by downregulation of the channel. It has been reported that endogenous electrophilic chemicals could contribute to diabetic neuropathy and related mechanical sensitisation, in which, a potent activator of TRPA1, methylglyoxal generated under hyperglycaemic conditions was shown as a mediator of diabetic neuropathy.[212] The chemicals in tumour microenvironment during neuronal development in cancer could also give rise to TRPA1 expression and activation.[213,214] Thermal and mechanical allodynia are caused by the neurotoxic nature of cancer chemotherapies. In animal models, it was shown that TRPA1, TRPV1 and TRPM8 lead to such allodynic effects in the presence of chemotherapeutic agents such as clioquinol,[134] cisplatin, oxaliplatin,[167] paclitaxel[215,216] and bortezomib[217].

Bladder overactivity is often linked with conditions like diabetes, infections, outflow hindrance, and neurological conditions such as multiple sclerosis and spinal cord injury.[218-220] It was shown that intravesical administration of TRPA1 agonists could mimic bladder overactivity condition.[136,221] Bladder overactivity produced as a result of spinal cord injury in a rat model was found to reduce through downregulation of TRPA1 expression and administration of HC030031.[222] Malfunction of TRPA1 also have a key role in irritable bowel syndrome, a condition diagnosed with symptoms such as pain, diarrhoea and/or obstructive constipation, which is associated with peripheral neuropathy.[223-225]

Central nervous system

TRPA1 can be activated by environmental irritants, mechanical stress and noxious cold in the periphery, but since the CNS is barely exposed to mechanical stress or noxious cold, the physiological role of TRPA1 on primary afferents of the CNS is unclear. However, endogenous molecules such as ROS, cytochrome P450 (CYP450) epoxygenase- and 12-lipoxygenase-derived

metabolites formed in the spinal cord during nerve injury, nociceptive stimulation, and neuroinflammation were known to activate TRPA1.[226-229]

Using immunohistochemistry it had been shown that the outer regions of the dorsal horn are heavily innervated by TRPA1-expressing nerve termini.[145,230] However, in the rat and mouse spinal cords no transcripts encoding TRPA1 were found, thus suggesting nearly all of the TRPA1-containing nerve endings are from the primary sensory neurons.[79,145,230] In addition, TRPA1 was identified at transcriptional and translational levels in the human brain.[93,231] Whole-cell patch-clamp recordings have shown that TRPA1 is present on glutamatergic neurons in the rat supraoptic nucleus.[232] TRPA1 expression was also found in the rodent trigeminal caudal nucleus and hippocampus, where it could possibly regulate long-term potentiation, neuronal survival and interneuron inhibitory synaptic efficacy.[233-235]

The role of TRPA1 on central projections of primary afferents is not completely known. The TRPA1 activators cinnamaldehyde and AITC are known to amplify the rate of spontaneous excitatory and inhibitory postsynaptic currents in substantia gelatinosa neurons from the trigeminal sensory nuclei and the spinal dorsal horn.[236-239] TRPA1 activators administered intrathecally caused tactile allodynia and sometimes heat hyperalgesia.[227,228,240-242] However, electrophilic and non-electrophilic activators of spinal TRPA1 are capable of inhibiting mechanical and acute thermal pain, and therefore the analgesic effects of acetaminophen could be the result of the formation of electrophilic metabolites in the spinal cord.[145] This pharmacological effect was recognised as a Ca^{2+}-dependent presynaptic inhibition of voltage-gated Ca^{2+} and Na^{+} channels,[145] and was in agreement with studies that showed inhibition of the C-fibre- and Aδ-evoked excitatory postsynaptic currents in the spinal cord slices by TRPA1 activators.[238,243,244]

The function of spinal TRPA1 had been shown in several studies *via* intrathecal administration of TRPA1 blockers in neuropathic pain and inflammatory models.[165,172,175,245-247] The findings clearly identified that spinal TRPA1 is involved in mechanical allodynia or hypersensitivity, and administration of AITC or capsaicin at peripherals led to secondary mechanical

hyperalgesia.[165,172,175,245-247] Thus, it is known that spinal TRPA1 plays an important role in central sensitisation. However, when the ion channel is activated pharmacologically it causes interruption to nociceptive neurotransmission in the spine.[145] Additional studies are essential in order to understand this dual action of the channel and its impact on drug development based on TRPA1.

Hereditary disease

It has been shown that topical administration of TRPA1 activators on the skin causes burning sensation, pain, neurogenic inflammation, and thermal and mechanical hypersensitivity.[184,248,249] In addition, an autosomal dominant familial episodic pain syndrome (FEPS) caused by a gain-of-function mutation in TRPA1 emphasised the role of TRPA1 in pain perception.[250] The mutation of transmembrane domain S4 localised N885S residue led to modification of the channel voltage dependency, and at resting membrane potentials made the channel hyperresponsive to cold and electrophilic compounds.[250] Recently, inconsistency in thermosensation was also correlated to a single nucleotide polymorphism, and the cold-sensitive wild-type hTRPA1 was compared against HEK293T/17 cells transfected with hTRPA1 containing the mutant E179K at the *N*-terminus of TRPA1, in which the TRPA1 mutant failed to respond to cold.[169,251]

1.1.6.5 TRPA1 knockout studies

In order to understand the physiological and pathophysiological role of TRPA1 channel, and its potential as a drug target for pain and sensory dysfunction, TRPA1 lacking transgenic mice have been used.[252] In several studies, the role of TRPA1 in chemosensation has been validated using TRPA1 knockout mice.[109,120,164,253] The main concerns in using knockout mice are the resulting functional damages to TRPA1 linked receptors and channels, and the variations between mouse strains,[252] which could be the reason behind disagreement in the role of TRPA1 in mechanosensation and thermosensation.[83] TRPA1 knockout mice based several recent studies have shown that the channel is involved in mechanical hypersensitivity and noxious cold, and was further supported using the TRPA1 antagonists, HC030031 and its analogue

Chembridge-5861528 [2-(1,3-dimethyl-2,6-dioxo-1,2,3,6-tetrahydro-7*H*-purin-7-yl)-*N*-(4-(1-methylpropyl)phenyl)acetamide]. However, HC030031 has off-target effects that need to be considered when using HC030031 and related compounds in the study of their physiological role.[168,254] The use of non-human *in vitro* and *in vivo* TRPA1 models to develop drugs for human is also of a concern due to TRPA1 species differences.[170,255] A review pointed out that knocked out transgenic mouse models were utilised in about 50 % of the hundred high selling molecular target based drugs, and hence, in most cases, knockout models will be useful in validating targets for drug development.[252]

1.1.6.6 TRPA1 species differences

Modulation of TRPA1 by chemical ligands and cold has shown to be species-specific. Originally, the existence of species differences between orthologues of TRPA1 was revealed in a study that reported trichloro(sulfanyl)ethyl benzamides as hTRPA1 antagonists (**Figure 1.16**).[256] Though these compounds were found to potently inhibit hTRPA1, they were found to either activate (AMG5445 and AMG9090) or ineffective (AMG2504 and AMG7160) in rat TRPA1.[256] In another study, analogues of thioaminals which inhibit hTRPA1 (CMP1, CMP2 and CMP3, **Figure 1.16**) were found to activate rat TRPA1.[257] Species-specific effects were also demonstrated by menthol. Menthol, which activates and blocks mouse TRPA1 at lower (0.1 - 100 µM) and higher (10 - 1000 µM) concentrations, respectively, had only agonism in the hTRPA1 (1 - 1000 µM).[150] Moreover, caffeine, an inhibitor of hTRPA1 activates mouse TRPA1.[258] Though there is an ambiguous statement that TRPA1 is involved in thermosenstation,[259-262] there is sufficient evidence that noxious cold (<17 °C) activates mouse TRPA1.[79,108,263] However, hTRPA1 was unaffected by cold.[98] It was then stated that due to species differences, the human variant could be unresponsive to cold contrary to rodent TRPA1.[264] Conversely, TRPA1 of *Drosophila melanogaster* was reported to be activated by heat, and not cold.[265]

In addition, a low sequence homology was found between TRPA1 orthologues that could possibly lead to variation in responses. There was only 79 % identity in sequence homology between human and rodent TRPA1, which was

relatively low compared to the match found in other TRP channels, for example, TRPM8 94 %, TRPV1 86 %, TRPV3 93 %, and TRPV4 94 %.[264] However, chimpanzee and monkey were found to have 99.7 and 97.1 % identical sequence homology with that of hTRPA1, respectively.[264]

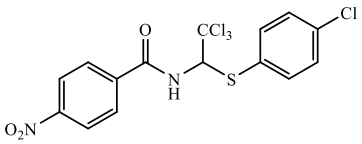

4-Nitro-*N*-(2,2,2-trichloro-1-((4-chlorophenyl) sulfanyl)ethyl)benzamide, **AMG2504**

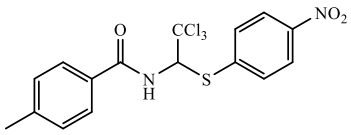

4-Methyl-*N*-(2,2,2-trichloro-1-(4-nitro-phenylsulfanyl)-ethyl)-benzamide, **CMP1**

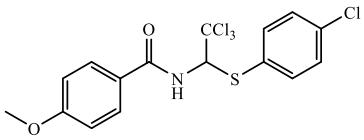

4-Methoxy-*N*-(2,2,2-trichloro-1-((4-chlorophenyl) sulfanyl)ethyl)benzamide, **AMG5445**

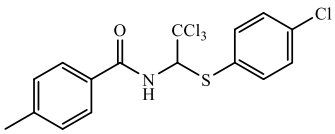

4-Methyl-*N*-(2,2,2-trichloro-1-(4-chlorophenyl sulfanyl)ethyl)benzamide, **CMP2**

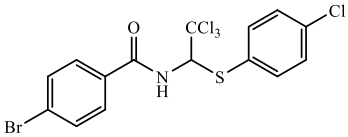

4-Bromo-*N*-(2,2,2-trichloro-1-((4-chlorophenyl) sulfanyl)ethyl)benzamide, **AMG7160**

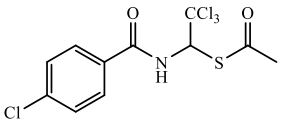

N-(2,2,2-Trichloro-1-(4-chlorophenylsulfanyl) ethyl) acetamide, **CMP3**

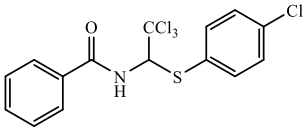

N-(2,2,2-Trichloro-1-((4-chlorophenyl) sulfanyl)ethyl)benzamide, **AMG9090**

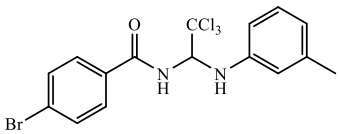

4-Bromo-*N*-(2,2,2-trichloro-1-*m*-tolyamino-ethyl)benzamide, **CMP4**

Figure 1.16: *Chemical structures of some species-specific modulators of TRPA1.*

The species differences remain as a challenge in the field of drug development for TRPA1, as this needs to be considered before extending any findings in a species like a rodent to a human.[264] However, the species-specific effects had been used as a valuable tool in identifying molecular determinants of TRPA1 and thus in understanding TRPA1 modulation.[150,257]

1.1.7 Calcium signalling

TRP channels can cause changes to the concentration of cytosolic free Ca^{2+} either by functioning as calcium entry pathways in the plasma membrane or through membrane polarisation. These channels also form intracellular pathways for the release of Ca^{2+} from various cellular organelles.[266] As TRP channels are involved in calcium signalling, the influx of Ca^{2+} caused *via* stimulation of the channel by an agonist can be measured using Ca^{2+}-sensitive fluorescent probes such as Fluo-3 or Fluo-4 (**Scheme 1.1**), in which changes in fluorescence intensity of the Ca^{2+} indicator corresponds to changes in $[Ca^{2+}]_i$.[266,267] In Ca^{2+}-permeable ion channels targeted drug discovery programs, this type of Ca^{2+} indicators based calcium imaging assays are routinely used for high-throughput screening.[268-270]

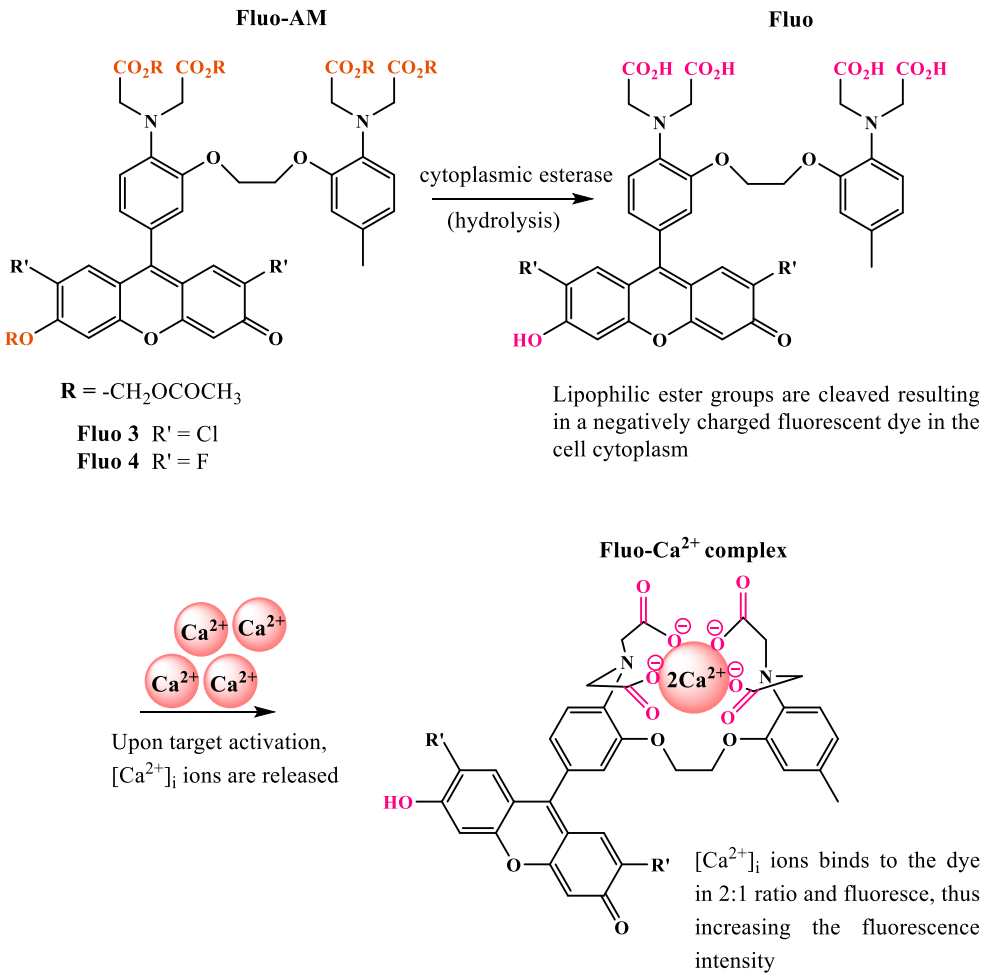

Scheme 1.1: *Mechanism of the Ca^{2+}-sensitive fluorescent probe, Fluo, in detecting changes in the level of $[Ca^{2+}]_i$.*

Calcium ionophore, also known as A23187, calcimycin, or calimycin (**Figure 1.17**), is an antibiotic produced during fermentation of *Streptomyces chartreusensis*.[271] It plays a role as a mobile ion carrier to cross biological membranes, that is, it acts as an ionophore by stably forming complexes with divalent cations such as Ca^{2+}. Hence it is utilised as a tool to study the divalent cations in biological systems.[271]

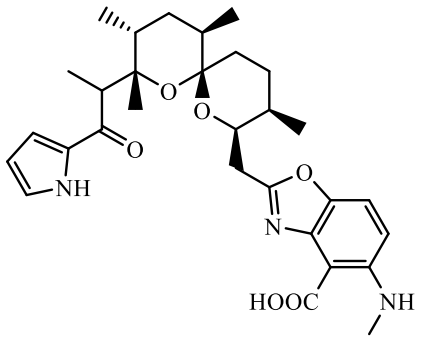

Figure 1.17: *Chemical structure of calcium ionophore A23187 (calcimycin).*

1.1.8 Conclusion

TRP channels are involved in several important cellular functions and in the pathogenesis of various human diseases, and thus have been considered as novel targets for drug development. However, knowledge on the complete mechanisms of how TRP channels function and the link associated with diseases are as yet rudimentary, and this hinders the development of drugs targeting these channels. In addition, certain members of the TRP channels have specific functions, for example, TRPA1, TRPM8 and TRPV1 - V4 expressed in primary afferent neurons, function as thermo-, mechano-, and chemo-receptors. The chemosensing ability of TRPA1 in detecting noxious chemicals, and the covalent activation mechanism, specifically discriminate the receptor from other members of TRP channel superfamily. The therapeutic ability of TRPA1 antagonist in treating itch, pain, inflammatory and respiratory diseases have been supported in various studies, but the capabilities of TRPA1 antagonists to reverse disease development remains to be recognised. There is a clear advancement in the field, but there are several more unknown facts to be understood to utilise the physiological function of TRPA1 in drug development.

1.2 Biological activities of *N*-cinnamoylanthranilates

In numerous studies, derivatives of *N*-cinnamoylanthranilic acid (**1**, **Figure 1.18**) have shown a wide range of biological activities, including anti-allergic, anti-histamine, anti-genotoxic, anti-inflammatory, anti-asthmatic, anti-oxidant, anti-fibrotic, anti-proliferative, anti-neoplastic, anti-cancer, anti-tubulin, anti-apoptotic, anti-platelet and anti-coagulant, and are under several medicinal application studies. The overall aim of this review is to summarise the biological activities of *N*-cinnamoylanthranilate derivatives (CADs) chronologically along with their applications in different experimental models, and wherever possible their structure-activity relationships (SARs) have been correlated.

Natural *N*-cinnamoylanthranilic acid amides are present in certain plants such as *Avena sativa* (oats) and *Nandina domestica* (sacred bamboo). In oats, they are commonly known as avenanthramides (Avn) and act as phytoalexins, which are secondary metabolites synthesised by plants as a measure of defence mechanism against microbial invasion. Oat extracts contain more than thirty Avn, and have been used in traditional medicine to relieve itch and skin reddening reactions.[272]

It has been found that more than twenty-five and twenty different types of Avn are present in the extracts of oat groats and hulls, respectively, where fifteen of them being common in both. The hydroxycinnamic acid phenolics extracted from these grains were structurally dependent in a wide range of biochemical and nutritional processes. Hence, in order to improve the oat based food ingredients, to evaluate nutrition dietary intake data, and to understand the mechanisms involved in resistance against diseases, studies were undertaken to gain knowledge on the types and amounts present, and to determine the structural binding relationships of these phenolics.[273]

The derivative *N*-(3,4-dimethoxycinnamoyl)anthranilic acid (**2**, **Figure 1.18**), which is known by the names Tranilast™ and Rizaben™ is found in *Nandina domestica*.[272,274] The compound **2** is a Kissei Pharmaceutical Co. (Japan) marketed anti-inflammatory drug in South Korea and Japan for more than twenty years, and is used to treat several allergic diseases such as bronchial

asthma, allergic rhinitis, hypertrophic scars and scleroderma.[275-277] However, to optimise the potency and efficacy, and to minimise the toxicity at higher doses of **2**, novel CADs with enhanced biological activities and metabolism were considered to utilise in therapeutic and cosmetic compositions.

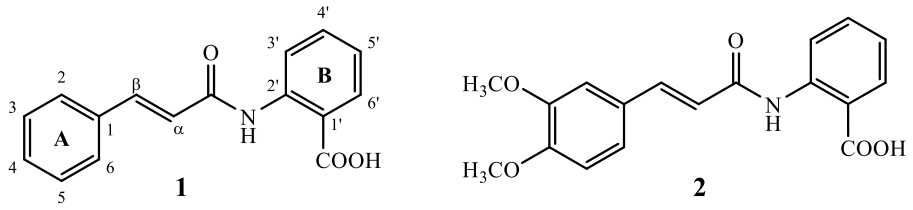

Figure 1.18: *Chemical structures of N-cinnamoylanthranilic acid* (**1**) *and N-(3,4-dimethoxy cinnamoyl)anthranilic acid* (**2**).

The R groups those are not defined in the chemical structures of the compounds provided below in some Sections as examples denote incorporation of a broad range of variable substituents, and the exact details can be found in the corresponding references.

1.2.1 Anti-allergic

Ring **A** and/or **B** (**1**, **Figure 1.18**) substituted cinnamoyl or dihydrocinnamoyl anthranilate derivatives have exhibited strong anti-allergic activity when delivered orally to mammals including human, with a reasonable therapeutic effect. In mammals, on oral administration, the derivatives have shown to antagonise model anaphylaxis such as skin inflammation triggered by an antigen-antibody reaction. As these derivatives had a remarkable impact on antigen-antibody reaction, they were found to be suitable to incorporate in the medicaments for treating allergic diseases such as bronchial asthma, hay fever, urticaria (nettle rash) and atopic dermatitis (eczema).[278-280] The SAR studies have shown that depending on different substituents and substitution patterns on the core compound **1**, there were significant changes to the levels of biological activities observed.[272,278,279,281] Generally, the presence of substituents such as a halogen atom, an alkyl, an alkoxy, an acetoxy or a hydroxyl group on compound **1** showed increased anti-allergic action relative to its unsubstituted form. In particular, the derivatives of compound **1** with halogen atoms (bromine, fluorine or chlorine) or alkoxy groups (e.g. methylenedioxy, **3**, **Figure 1.19**) as their substituents showed strong anti-

allergic effect, whereas the ones with hydrophilic groups like carboxymethoxy and 2,3-dihydroxypropoxy showed considerably weak activity or were inactive.[278,279] Also, increased pharmacological activity was observed either with an increased number of substituents on compound **1** or with their corresponding carboxylate alkali metal salts. However, with ester based derivatives (-COOR instead of -COOH, where R is a small alkyl group) the activity dropped, but still had the ability to inhibit histamine secretion.[278-280,282]

Mast cells are commonly found in mucous membranes of gastrointestinal and respiratory tracts, and in the skin, that is, in the parts of the body which directly interact with the external environment. They have various pathological and physiological roles *via* the release of histamine, immunoregulatory cytokines, mast cell specific proteases such as chymase and tryptase, neutrophil chemoattractants and heparin.[283] These cells can be activated by different mediators like immunoglobulins (IgE) and neuropeptides (substance P).[272,281] Mast cells are well-known to play a crucial role in allergic and inflammatory reactions,[272,281] and further contribute to metabolic syndrome, cardiovascular problems and also known to participate in type 2 diabetes and insulin resistance.[284] Several studies have shown that the neuropeptide substance P released by the nerve terminals in the skin causes mast cells to degranulate, which leads to release of excess mediators including histamine from the storage vessel granula, and results in serious inflammatory and allergic reactions.[272,281] Excess release of histamine leads to several conditions including psoriasis, infections, pruritus, nickel allergy, healing injuries and minor burns. It was also reported that in several kidney diseases, mast cells contribute to the development of tubulointerstitial fibrosis.[283]

Compound **2** at ~10^{-4} M and ~10^{-3} M concentrations have shown to inhibit 50 % of antigen-monoclonal IgE antibody (with 2,4-dinitrophenyl specificity) and substance P induced histamine release from mast cells, respectively. The derivative, *N*-(4-hydroxy-3-methoxycinnamoyl)anthranilic acid (**4**, **Figure 1.19**) also had equivalent anti-allergic effect as compound **2**.[272,281] Hence, the property of CADs to specifically inhibit the release of histamine from mast cells induced by neuropeptide substance P promotes anti-allergic effects. With respect to SAR, derivatives with a free hydroxyl group substituent at position

4 of the cinnamic or dihydrocinnamic, or position 5′ of the anthranilic acid ring have shown considerably high inhibitory effects. Under the same test conditions, oral administration of monosubstituted *N*-(4-hydroxycinnamoyl) anthranilic acid (200 mg/kg, **5**, **Figure 1.19**) inhibited 37 % of antigen-induced histamine release in rat mast cells, whereas disubstituted compound **2** showed relatively higher blocking effect (46 %). CADs **6** and **7** (**Figure 1.19**) with vicinal hydroxyl groups showed the highest activity at 50 ppm by completely inhibiting the release of histamine, whereas compound **2** inhibited only 21 % at the same dose. However, addition of more hydroxyl groups to the anthranilic acid ring did not enhance the activity, and in general, with more substituents there were no significant improvement in the activity.[272,281]

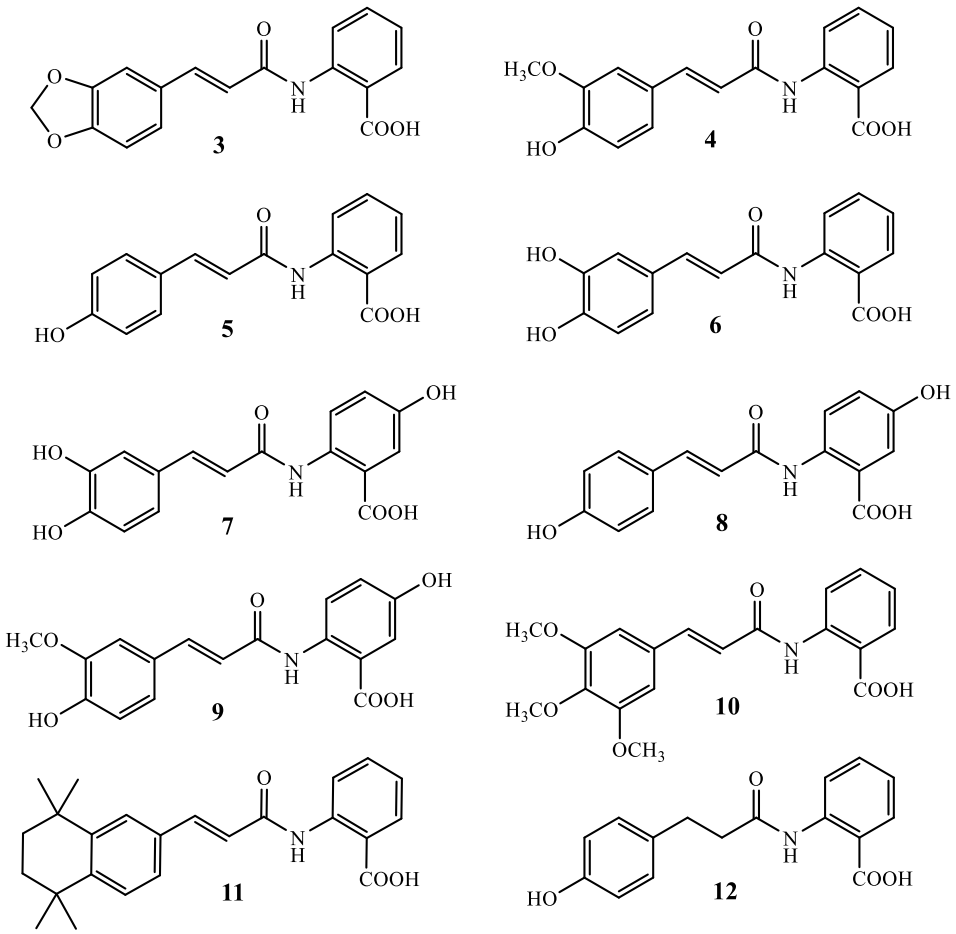

Figure 1.19: *Structures of anti-allergic compounds* (**3 - 12**).

It was found that the derivatives of Avn from oat extract involved in the inhibition of histamine release induced by the neuropeptide substance P from mast cells were *N*-(3,4-dihydroxycinnamoyl)-5′-hydroxyanthranilic acid (**7**),

N-(4-hydroxycinnamoyl)-5′-hydroxyanthranilic acid (**8**) and *N*-(4-hydroxy-3-methoxycinnamoyl)-5′-hydroxyanthranilic acid (**9**), **Figure 1.19**.[272,281]

In addition, *N*-(3,4,5-trimethoxycinnamoyl)anthranilic acid (**10**, **Figure 1.19**) has shown to significantly inhibit passive and reverse cutaneous anaphylaxis, and reduce histamine and serotonin (5-hydroxytryptamine, 5-HT) induced capillary permeability in rats.[285] The derivative at a dose of 80 µl ml^{-1} significantly blocked (78 ± 12 % of $BaCl_2$) antigen-induced contraction in an isolated agonised guinea pig ileum, and at 25 and 50 µg ml^{-1} inhibited degranulation induced by homocytotropic antibody in rat mesentery (48 ± 3 and 36 ± 7 % degranulation) and anaphylactic histamine release from mast cells in rat peritoneal (34 ± 4 and 30 ± 5 % histamine release).[285]

Degranulation of mast cells and release of histamine are also known to be involved in the mediation and regulation of post-operative ileus. The anti-histamine agent and/or mast cell degranulation blocker **2** was utilised as a bioactive constituent in the pharmaceutical composition for preventing or alleviating the post-operative ileus and gastric stasis (paralytic ileus) in mammals following abdominal surgeries, which prevents the decline in gastric emptying and gastrointestinal motility. Derivatives and analogues of **2** have also been suggested as a suitable bioactive constituent for the above. It was anticipated that the effect of compound **2** on post-operative ileus could be *via* inhibition of transforming growth factor-β (TGF-β), cytokines and free radicals produced from inflammatory cells.[286]

Moreover, compound **2** and its salt form were proposed to be used as an active ingredient in the eye and nose drops for treating allergic conjunctivitis and rhinitis.[287] Initially, only oral administration of compound **2** was applied due to its insoluble nature in water, but later as the need arose for topical application to use in the eye or nasal drops, aqueous formulations of **2** were developed.[287,288] Compounds based on the structure **11** (**Figure 1.19**) were also considered as therapeutic agents for treating respiratory, dermatological, rheumatic, ophthalmological (corneopathies) and cardiovascular disorders in human and veterinary, and in cosmetic products as hair and body hygienic agents.[289]

As there are chances for allergic reactions and minor injuries to arise with the use of cosmetics and after shaving, application of itch relieving formulations in cosmetics provides an optimum condition for skin protection and maintenance. Hence, CADs are under investigation for incorporation in cosmetics and perfumes to prevent histamine release, and thereby the allergic reactions and other related symptoms.[272,281] In addition, CADs were found to be suitable for use in hair and scalp care products for reducing or preventing scalp damages or diseases linked with pruritus (itch). It has been demonstrated that combining anti-dandruff agents with anthranilic acid amides intensifies the itch alleviating property. For example, the itch-relieving compound, *N*-(4-hydroxydihydrocinnamoyl)anthranilic acid (or dihydroavenanthramide D, **12**, **Figure 1.19**) combined with an anti-dandruff agent showed enhanced efficacy against the shampoo formulation contained anti-dandruff agent alone. Furthermore, the essential general characteristics of active substances, including toxicity free concentration range, good skin tolerability, stability, odourless and low cost, were all met.[290]

1.2.2 Anti-collagen, Anti-fibrotic, Anti-proliferative, Anti-cancer and Anti-tubulin

The main element of connective tissue, collagen has an important role in the pathogenesis of fibrotic diseases. The production of collagen is rigorously controlled by several humoral factors, such as TGF-β, epidermal growth factor (EGF), tumour necrosis factor-α (TNF-α), interferon-γ (IFN-γ) and interleukin-1 (IL-1).[291] TGF-β1 is a hormone-like polypeptide that regulates differentiation and proliferation of cells, and triggers the formation of extracellular matrix proteins like fibronectin and collagen.[291] It is known that TGF-β has a major role in fibrosis and may cause malfunction of organs leading to pathological fibrotic diseases like fibrotic skin disorders (keloids, hypertrophic scars, scleroderma), pulmonary fibrosis, heart diseases (ischaemic/valvular/ hypertensive heart disease, diabetic cardiomyopathy and hypertension), kidney disease (progressive kidney disease resulting from diabetic nephropathy and glomerulonephritis), liver disease (cirrhosis)[277] and lung fibrosis.[292] Pro-fibrotic growth factors, including TGF-β, connective tissue growth factor

(CTGF) and platelet-derived growth factor (PDGF) also have a function of stimulating fibrosis in the mesangium leading to development and progression of renal diseases.[276] Angiotensin II, which is linked to left ventricular fibrosis also employs TGF-β1 and attenuation in TGF-β expression reduces the increase in weight of the left ventricle (left ventricular hypertrophy) and collagen accumulation (fibrosis).[293] Therefore, inhibiting TGF-β expression is a crucial therapeutic target, and anti-fibrotic drugs will possibly be an approach for treating disorders linked with pathological fibrosis.[277] It is emphasised that in the developed world 45 % of total death may involve pathology of abnormal fibrosis, and there are no optimised anti-fibrotic drugs in clinical use.[276]

Compound **2** is one of the promising anti-fibrotic agents with the potential to block TGF-β, CTGF and PDGF.[276] In addition, halogenated derivatives of CADs were also considered to be used as novel anti-fibrotic agent, where the majority of the derivatives were based on the chemical structure **13** (**Figure 1.20**).[274] CADs are also being studied to use in the prophylaxis of connective tissue degenerative diseases, chronological skin ageing or ageing induced by light, and in cicatrisation (scar formation) disorders.[289]

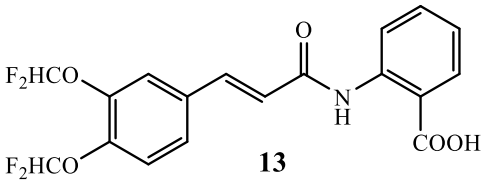

Figure 1.20: *Structure of an anti-fibrotic agent* (**13**).

1.2.2.1 Fibroblasts

Inflammatory cells, including mast cells, lymphocytes, macrophages and monocytes, are known to produce several chemical mediators such as cytokines, which mainly contribute to the progression of hypertrophic scars and keloids, caused by excess collagen deposition and proliferation of connective tissue.[294] As compound **2** is free of toxicity, non-specificity and cellular uptake obstacles, and being a clinically accepted anti-allergic drug with reduced side effects, it is considered to be a useful clinical drug in the treatment of keloids.[291]

In cultured human skin fibroblasts, compound **2** (3 - 300 µM) has shown to block lipopolysaccharide (1 mg ml^{-1}) induced monocytes-macrophages producing chemical mediators, including TGF-β1 and PGE_2 responsible for collagen synthesis, and IL-1β contributing in the proliferation of fibroblasts. Likewise, compound **2** is also known to inhibit the release of IL-1 and IL-2 from human T-cells and macrophages, and the chemical mediators released from antigen-antibody reactions in mast cells and basophils, including histamine, prostaglandins, platelet-activating factor and leukotrienes.[294] Compound **2** (300 µM) also inhibited 55 % of type I and type III collagen synthesis in pre-treated (48 hours) cultured human skin fibroblasts, and selectively reduced the effect of collagen synthesis triggering factor (TGF-β1, 2.5 ng ml^{-1}), at a pre-translational level and had no effect on other non-collagen protein synthesis. Collagen synthesis in scleroderma and keloid fibroblasts was inhibited to an equal and higher level, correspondingly, in comparison to normal skin fibroblasts. It was reported that compound **2** at 300 µM showed no signs of toxicity and did not affect the non-collagen protein synthesis or the β-actin mRNA content under the conditions tested, and the synthesis of collagen was reinstated to its normal level on removal of the drug.[291]

Importantly, selective inhibition of the synthesis of collagen by CAD **2** was observed only in high passages (8 to 10) of normal, keloid and scleroderma skin fibroblasts. Whereas, with initial passages (1 to 2) there were no significant influence and were resistant to compound **2**. The result suggested that collagen inhibition was dependent on cellular ageing, and as the number of passages increased compound **2** resistant cell phenotype was lost. *In vitro*, cells lose several phenotypes during ageing, for example, superoxide dismutase (SOD) enzyme is linked with cellular ageing. Compound **2** (100 µg ml^{-1}) has also been reported to inhibit generation of ROS. Hence from these evidences, it was theorised that anti-fibrotic activity of **2** is *via* its anti-oxidant property, since the high-passaged fibroblasts those lacking anti-oxidant properties turned out to be responsive to the drug. Synthesis of collagen in hepatocytes and skin fibroblasts is stimulated two-three fold by the superoxide anion produced by dihydroxyfumarate.[292] CAD **2** has also been described to inhibit proliferation of several other fibroblasts, including oral squamous cell carcinoma in mice

fibrous tissue, gastric fibroblasts in mouse, pterygium-derived fibroblasts in human and dermal fibroblasts in rabbits.[295]

1.2.2.2 Diabetic cardiac disease and Gilbert's syndrome

In an experimental model it was shown that CAD **2** attenuates collagen synthesis induced by TGF-β in cardiac fibroblasts in diabetic cardiac disease. Compound **2** and its metabolite N3 (4-desmethyl-tranilast) inhibits uridine 5′-diphospho-glucuronosyltransferase family 1 member A1 (UGT1A1, a gene related to Gilbert's syndrome) that results in abnormal metabolism of bilirubin and its deposition.[274,277] Even though the exact mechanisms and action of **2** are not completely known, its capability to block the major intermediate, extracellular-signal regulated kinase (ERK) phosphorylation in the TGF-β signalling pathway is probably due to its anti-fibrotic activity, which is known from its ability to inhibit extracellular matrix production induced by TGF-β in various types of cells.[277]

1.2.2.3 Mesenteric vascular hypertrophy and Diabetic nephropathy

In diabetic rats, CAD **2** (200 mg/kg per day) has shown to prevent mesenteric vascular hypertrophy.[296] Diabetic rats administered with CAD **2** (400 mg/kg per day) have also shown to significantly lessen the mesenteric vessel fibrosis and chymase mast cells, induced by diabetes. A mechanism accompanying the action of compound **2**, in this case was by stabilisation of mast cells that results in reduction of TGF-β and proteases (tryptase and chymase proteolytic enzymes). It has been stated that there are correlations between the number of mast cells and the development of vascular hypertrophy and diabetic nephropathy.[297] CAD **2** possesses potential therapeutic value for treating advanced and possibly early-stage diabetic nephropathy by reducing collagen deposition in renal tissues.[298]

It has been found that, reducing fibrosis in kidneys of diabetes patients by intake of **2** could delay and/or prevent kidney dysfunction. Various novel derivatives of **2** with higher potency and lower toxicity were examined for TGF-β inhibition properties in renal mesangial cells. Among several CADs evaluated, *N*-(3-methoxy-4-propargyloxycinnamoyl)anthranilic acid (**14**,

Figure 1.21) has shown to significantly reduce albuminuria in rats with hypertensive diabetes, and hence this derivative was considered as a lead compound in anti-fibrotic drug discovery for the treatment of diabetic nephropathy. This compound also had exceptional metabolic stability and enhanced *in vivo* activity relative to compound **2**. The compound **14** at 30 and 100 μM inhibited collagen synthesis induced by TGF-β by 55-70 % and 80-100 %, whereas only inhibitions of 40 and 70 % were observed with compound **2**, respectively.[276] With respect to SAR, the carboxylic acid and α,β-unsaturated bond were identified as essential functional groups required to exhibit increased inhibition activity. The activity was reduced in the absence of carboxylic acid group or in the presence of alternative groups such as a primary amide (-$CONH_2$), and similarly compounds without an α,β-unsaturated bond were inactive in the study.[276]

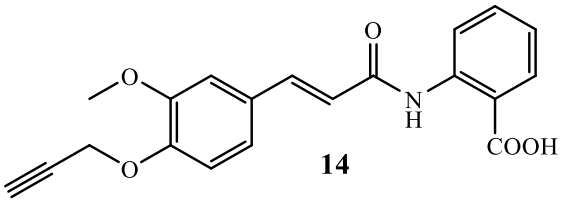

Figure 1.21: *Structure of a collagen synthesis inhibitor* (**14**).

Among several CADs tested, compound **14** was also found to possess strong therapeutic effect for treating or preventing fibrotic diseases characterised by neoplastic (benign or malignant) and inflammatory diseases or conditions such as bronchial asthma, rheumatoid arthritis, allergic rhinitis, multiple sclerosis, inflammatory bowel syndrome, type I and type II diabetes, transplant rejection and systemic lupus erythematosus.[277]

1.2.2.4 Glomerulonephritis

Monocyte chemoattractant protein-1 (MCP-1) mainly stimulates and employs macrophages and monocytes at the inflammatory sites, and plays an important part in glomerulonephritis progression. Jun *N*-terminal kinase (JNK), p38 kinase and ERK are the three subgroups of mitogen-activated protein (MAP) kinases. In mesangial cells, IL-1β stimulates MAP kinases, and only p38 kinase is said to be essential for the expression of MCP-1, whereas in other types of

cells all three MAP kinases participate in the stimulation of the transcriptional regulator nuclear factor-κB (NF-κB) of MCP-1.[299] Compound **2** (30 - 300 μM) attenuated IL-1β cytokine mediated (0.2 nM) NF-κB dependent transcription and inhibited JNK stimulation specifically among other MAP kinases, in a dose-dependent manner, and thereby led to partial inhibition of MCP-1 in rat mesangial cells. This study concluded that the anti-chemokine property of compound **2** may lead it to act as a potential glomerulonephritis therapeutic agent.[299]

1.2.2.5 Restenosis

It has been reported that CAD **2** is likely to prevent the occurrence of angiographic restenosis following percutaneous transluminal coronary angioplasty (PTCA) revascularisation, based on the findings that it has significantly reduced the restenosis after coronary stenting, directional coronary atherectomy and conventional balloon-angioplasty. Clinical trials are ongoing in order to measure the clinical activity of the compound on angiographic and intravascular ultrasound results of restenosis.[300-302]

It was revealed from an *in vitro* study conducted on vascular smooth muscle cells (VSMC) of spontaneously hypertensive rats that compound **2** (30 - 300 μM) inhibits proliferation provoked by fetal bovine serum (FBS) and the growth factors PDGF-BB and TGF-β1. It also inhibited spontaneous and TGF-β1 induced collagen synthesis, and the synthesis of glycosaminoglycan. Overall, these findings proposed that occurrence of restenosis followed by PTCA could be prevented with the use of compound **2**.[303]

PTCA is a treatment given to patients with coronary artery disease/disorder. Within three to six months following PTCA, restenosis develop from VSMC proliferation and excess production of extracellular matrix. Several cytokines and growth factors, mainly TGF-β1 and PDGF, are known to participate in the mechanism of restenosis development.[303] As proposed, in a double blind trial CAD **2** (600 mg per day for three months) has proven to be effective (potent) in blocking occurrence of restenosis following PTCA.[304] Compound **2** decreased the occurrence of restenosis following angioplasty in human clinical trials.[305]

It has been demonstrated on a rat carotid artery after balloon injury, that the injury-induced rise in mRNAs encoding (transcriptional mechanisms) TGF-β isoforms (TGF-β1, TGF-β3), its receptors (type I: activin receptor-like kinases ALK-2 and ALK-5; and type II: TβRII) and integrins (α_v and β_3) linked upregulation can be inhibited by compound **2** in a dose-dependent manner and the effect of the compound was found to be reversible.[305]

In restenosis and development of atherosclerosis, migration and proliferation of smooth muscle cells play a crucial role. Following an arterial injury, smooth muscle cells migrate into the innermost layer (intima) of the arterial wall, and proliferate and produce extracellular matrix constituents. Since selective inhibitions of smooth muscle and endothelial cells proliferation are necessary to treat restenosis, CADs with anti-proliferative activity were evaluated against proliferation induced by PDGF-BB (20 ng ml^{-1}) and FBS (5 %) in human coronary artery endothelial and smooth muscle cells, correspondingly. Among a series of derivatives, compound **15** (**Figure 1.22**) had greater potency and cell selectivity compared to **2**. The IC_{50} values obtained for smooth muscle cells and endothelial cells with **15** were 1 and 4 µM, whereas with **2** the values were 25 and 19 µM, respectively.[306] CAD **2** also inhibits intimal hyperplasia on femoral artery following endothelial injury induced photochemically in spontaneously hypertensive rats,[303] and significantly antagonised the formation of neointimal hyperplasia at 300 mg/kg per day.[300]

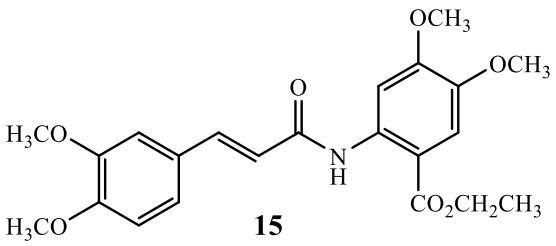

Figure 1.22: *Structure of an anti-proliferative compound* (**15**).

1.2.2.6 Coronary arteriosclerosis

CAD **2**, on oral administration, significantly attenuated the progression of coronary arteriosclerosis in a cardiac transplanted mouse model. In the model pre-treated with **2**, the cyclin-dependent kinase inhibitor p21 was observed to be upregulated in cardiac allografts along with a decrease in the number of cells

proliferated. It also inhibited the expression of TGF-β on cardiac allografts of murine and demonstrated its anti-inflammatory property. These findings suggested that the anti-proliferative and anti-inflammatory properties of **2** could prevent arteriosclerosis resulting from transplantation, and thereby be useful in the prophylaxis of allograft vasculopathy.[300]

1.2.2.7 Nifedipine induced proliferation

Nifedipine is a Ca^{2+} channel antagonist. It causes excess growth of gingival cells as a side effect due to increased $[Ca^{2+}]_i$ levels, excess formation of type 1 collagen and secretion of basic fibroblast growth factor (bFGF) cytokine. Nifedipine (10 μM) triggered proliferation of human gingival fibroblasts *in vitro* was significantly inhibited by compound **2** (100 μM) through antagonising the secretion of bFGF.[295]

1.2.2.8 Cancer and Tubulin

Reduction of TGF-β expression in glioma cells together with inhibition of chemotactic responses, invasiveness and migration by compound **2** revealed its therapeutic benefits for treating human malignant glioma.[307] CADs have been reported to be of potent antagonists of FMS-like tyrosine kinase 3 (FLT3), which is expected to participate in the maintenance of haematopoietic progenitor cell proliferation and survival. Stimulation or unusual expression of FLT3 is known to be linked with various haematopoietic conditions like myelogenous leukaemia, for which CADs could be therapeutically beneficial.[288,308]

A new series of CADs have been discovered as anti-tubulin agents from the anti-proliferative activity exhibited on various types of cancer cells, *in vitro*. From a series of compounds evaluated initially in human chronic myelogenous leukaemia K562 cell line for anti-leukaemic activity, compounds **16a - 16e** (**Figure 1.23**) showed effective anti-proliferative activity. Further, these compounds were particularly chosen and evaluated by the National Cancer Institute (NCI) in approximately sixty different human cancer cell lines from seven different types of cancer: leukaemia, melanoma, brain, colon, ovarian, renal and lung. In all cell lines, compounds **16a - 16e** inhibited 50 % growth at

micromolar concentrations (**Figure 1.23**). Among the substituents (R^1) at 5′ position on benzamido of **16**, iodo-substituted derivative (**16d**) was found to be the most potent (IC_{50} 0.57 μM).[309]

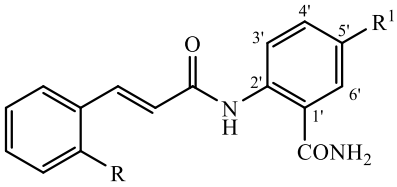

16a - 16e

	R	R^1	Proliferation inhibition (10 μM) / (%)	IC_{50} / (μM)
16a	H	CH_3	65.4	5.5
16b	H	Cl	64.0	2.5
16c	H	Br	62.4	5.0
16d	H	I	74.5	0.57
16e	Cl	I	74.1	1.2

Figure 1.23: *Compounds* **16a - 16e** *with anti-proliferative activity against cancer cells.*

In a further study to understand the SAR, new classes of CADs of structures **17** (**Figure 1.24**) were evaluated *in vitro* for anti-proliferative activity in five different human tumour cell lines of four cancer types: human chronic myelogenous leukaemia (K562), colon (HT29 and HCT116), non-small cell lung (NCI H460) and breast (MCF-7). Among which, compound **17a** (**Figure 1.24**) showed the greatest anti-proliferative activity in all five cell lines (K562 80.0 ± 0.2, HT29 85.0 ± 0.3, HCT116 49.9 ± 0.6, NCI H460 40 ± 4 and MCF-7 45 ± 4 % growth inhibition). In general, substituting the α,β-double bond with a single or a triple bond had only slight difference in the inhibitory effect, where on average, single bond substitution had the lowest (38 % at 10 μM) and triple bond substitution had the highest (48 % at 10 μM) inhibitions of cell growth (K562 cells). Regardless of the substituent groups, substitution at 4′ position on benzamido of **17** with α,β-double bond lowered the growth of K562 cells. Unsubstituted saturated (single bond) compound **17** showed lowest activity, while derivatives with methoxy or chloro substituent at 5′ position on benzamido ring showed the most inhibition against K562.[310]

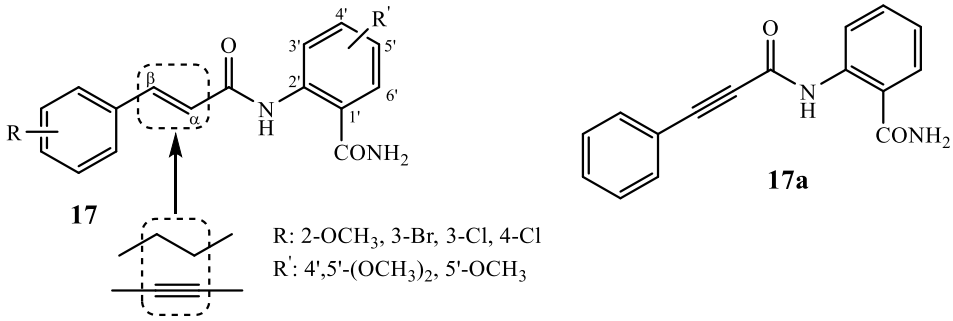

Figure 1.24: *Derivatives of compound* **17** *with anti-proliferative activity against cancer cells.*

1.2.3 Anti-inflammatory

NF-κB is a proinflammatory transcription factor required for the generation of many proinflammatory genes, including cytokines (immunological mediators, viral enhancers, TNF-α, TNF-β, IFN-β, IL-2, IL-6, IL-8, etc.) and endothelial adhesion molecules (vascular cell adhesion molecule-1 (VCAM-1), intercellular adhesion molecule-1 (ICAM-1) and E-selectin). When adhesion molecules are expressed, they induce adhesion of lymphocytes, granulocytes and monocytes onto endothelium.[311]

CAD **2** prevents vascular inflammation by inhibiting NF-κB mediated transcriptional stimulation of endothelial cell adhesion molecules. The compound at a concentration of 100 μg ml^{-1} inhibited the expression of endothelial adhesion molecules (VCAM-1 38 ± 7 %, ICAM-1 32 ± 2 %, and E-selectin 32 ± 2 %) induced by TNF-α, and the activities of ICAM-1-κB and E-selectin-κB reporter genes. Secretion of IL-6 was also blocked by the compound. The expression of cyclic adenosine monophosphate (cAMP) response element-binding protein (CREB) transcriptional coactivator was antagonised by compound **2** (50 μg ml^{-1}), which resulted in suppression of interaction between CREB and NF-κB. Therefore, it was proposed that the anti-inflammatory property of **2** was due to inhibition of endothelial cell adhesion molecules expression and inhibition of IL-6 secretion.[311]

CAD **2** has also shown to significantly decrease post-surgical adhesion formation (post-operative peritoneal adhesions) in rabbit models when applied topically, but was ineffective on oral administration. Whereas, in a double uterine horn model it has shown to be effective on controlled slow intraperitoneal release using biodegradable fibres, in which the efficacy of the compound was improved. Among several delivery systems, this approach was specified as an appropriate method of administration for clinical testing, and was also reported to be free of safety issues. It was reported that the contribution of **2** on the reduction of post-surgical adhesion formations was through the inhibition of TGF-β.[312]

1.2.4 Anti-oxidant

There are suggestions that the inhibitory effects of CAD **2** on fibrosis could possibly be due to suppression of stimulated macrophages which liberate nitric oxide ($^{\bullet}NO$) or alternatively through regulation of inducible nitric oxide synthase (iNOS). Later it was found that the activity and expression of microglial iNOS induced by bacterial endotoxin lipopolysaccharide and IFN-γ were reduced by the compound.[288] Taken together, this shows that compound **2** has a role as a protecting mediator against excess production of ROS including NO.[288,313]

In addition, the anti-oxidant property of CAD **2** was revealed in experimental studies using xanthine-xanthine oxidase system and zymosan-induced polymorphonuclear leukocytes, *in vitro*. In both systems, the compound (100 μg ml^{-1}) significantly reduced the production of ROS such as hydroxyl radical ($^{\bullet}OH$) and H_2O_2. It was anticipated that this newly identified effect of **2** could be through direct inhibitions of xanthine oxidase and/or nicotinamide adenine dinucleotide phosphate (NADPH) oxidase activities.[313]

1.2.5 Anti-angiogenesis

Though the growth factors, TGF-β, FGF and hepatocyte growth factor (HGF) were determined to control angiogenesis, vascular endothelial growth factor (VEGF) has been reported as a specific and potent angiogenic factor.[314] CAD **2** (200 and 400 mg/kg) potently inhibited angiogenesis induced by vascular permeability factor (VPF) or VEGF, and increased the vascular permeability, in a dose-dependent manner in rats. In addition to improving excess angiogenesis, the compound could also participate in antagonising VEGF/VPF-induced excess exudate production and tissue oedema. It is also known to inhibit increases in vascular permeability induced by bradykinin, carrageenin and xanthine oxidase.[315] Hence, CADs could be potentially used in the treatment of diseases linked with angiogenesis such as rheumatoid arthritis, diabetic retinopathy, tumour metaplasia, psoriasis and age-related macular degeneration.[314,315]

Compound **2** non-competitively inhibited the angiotensin II-stimulated contraction in aortic strips of rabbit (IC_{50} 212 μM) and the binding of ^{125}I-

labelled angiotensin II radioligand to the angiotensin AT1 receptor sites in the membranes of rat liver (IC_{50} 289 μM). The compound (100 and 300 μM) antagonised the Ca^{2+} efflux induced by angiotensin II (10^{-8} M) and had no effect on inositol triphosphates (IP_3) formed *via* PDGF inducement that results in increased $[Ca^{2+}]_i$ in human VSMC. These outcomes revealed the non-competitive insurmountable weak antagonism of compound **2** on angiotensin AT1 receptors.[304]

1.2.6 Anti-microbial

Bad breath (foetor oris or halitosis) is produced by the breakdown of food particles and dead cells of mucous membrane, by the normal human oral microflora in the mucous membrane in the mouth and pharynx. The harmless non-pathogenic microorganisms present in the oral cavity protect against pathogenic organisms. However, the anaerobic Gram-negative bacteria are known to be the important cause for halitosis. CADs have been under investigations as anti-microbial agents against Gram-negative and Gram-positive bacteria for potential use in oral hygienic products to inhibit/prevent the growth and/or to destroy such microorganisms, and thereby to cure bad breath.[316]

In particular, CADs were capable of diminishing and/or abolishing the growth of the Gram-negative organisms, which include *Fusobacterium nucleatum*, *Porphyromonas endodontalis*, *Porphyromonas gingivalis*, *Prevotella intermedia*, *Prevotella loeschii*, *Treponema denticola* and *Veillonella parvula*. CADs effectively diminished or abolished the evolution of bad breath or blocked its formation, and were very effective against morning bad breath, probably by inhibiting or preventing the growth of microorganisms in the oral cavity and pharynx. Hence, CADs could be utilised for enhancing dental and oral hygiene, including controlling or preventing formation of plaque, tartar, dental decay and bad breath.[316]

In the study,[316] methoxy- and hydroxy- substituents at different positions on the biaromatic rings of compound **1** were considered. However, the unsubstituted compound **1** on its own showed the highest activity at the lowest minimum effective concentration (10 ppm) at which smell could not be

detected. Physiological oral- and pharynx-microflora were not noticeably harmed by the use of these compounds in the oral hygienic products. The maximum concentration (10000 ppm) at which these compounds were used for the preparation of the oral hygienic products had a neutral taste, and hence did not alter the overall inherent taste of the products, thus making them suitable for the purpose.[316]

1.2.7 Insulin secretion inhibitor

N-(4-Amylcinnamoyl)anthranilic acid (ACA, **18**, **Figure 1.25**) was capable of inhibiting glucose-, glyceraldehyde- and α-ketoisocaproic-induced insulin secretion. CAD **18** completely abolishes glucose-induced accumulation of arachidonate in islets without affecting PLC, and expressing its specificity for PLA_2. Arachidonate is known to regulate voltage-dependent Ca^{2+} channels present in the islet cell membrane. A rise in arachidonate concentration depolarises Ca^{2+} channels and results in an influx of extracellular Ca^{2+}. The compound dose-dependently inhibited glucose-induced secretion of insulin without any signs of toxicity. The effective concentrations of **18** to antagonise insulin secretion induced by glucose (28 mM) was 100 µM, and glyceraldehyde (15 mM) and α-ketoisocaproic (15 mM) were 75 µM.[317] It was reported that **18** blocks glucose-induced insulin secretion in islets *via* stimulation of K^+ efflux resulting in opening of ATP-sensitive K^+ channels.[318]

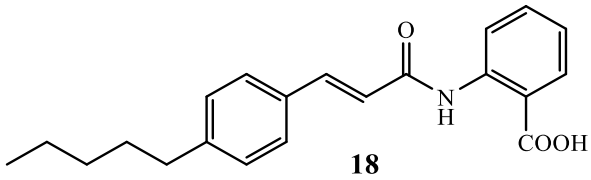

Figure 1.25: *N-(4-Amylcinnamoyl)anthranilic acid (ACA,* **18***) - an insulin secretion and PLA_2 inhibitor.*

In addition, the anti-angiogenesis and anti-inflammatory activities *via* inhibition of inflammatory cytokines, and the anti-oxidant activity of compound **2** are considered to be a possible therapeutic agent for inhibiting insulin resistance, as overexpression of inflammatory markers (TGF-β, TNF-α, IL-2, IL-6, IL-1β, MCP-1 and plasminogen activator inhibitor 1 (PAI-1)) and oxidative stress are known to be involved in insulin resistance inflammatory disease.[319]

1.2.8 Smooth muscle contraction inhibitor

CADs having pharmacological properties are under investigation for treating disorders linked with contraction of smooth muscle, including contraction of the urinary tract, gastrointestinal tract, congestive heart failure, peripheral vascular disease, cerebrovascular disease, neurodegenerative disease, etc., *via* modulation of K^+ and Cl^- channels. K^+ channel modulators are essential in treating cardiovascular, metabolic and the CNS disorders. Diseases such as bronchial asthma, cystic fibrosis, renal disease and cardiac dysrhythmia, however, can be controlled by modulating the Cl^- channels.[320]

The effect of CAD **2** on the mobilisation of Ca^{2+} and contraction of the coronary arteries and vascular smooth muscles were investigated on coronary artery strips of porcine smooth muscle and on aortic strips of rat, *in vitro*, respectively. Compound **2** (0 - 500 µM) significantly antagonised the contraction of coronary artery smooth muscle mediated by the vasoactive agent histamine (300 mM) and increased K^+ (30 mM). Similarly, the compound antagonised the elevated Ca^{2+} and thereby the contraction (increased tension) of vascular smooth muscle induced by endothelin-1 and increased K^+, in a dose-dependent manner.[321,322] The tonic and phasic rises in $[Ca^{2+}]_i$ mediated by histamine, and the tonic rise in $[Ca^{2+}]_i$ caused by elevated levels of K^+ in smooth muscle were significantly inhibited by compound **2**.[321]

At 100 and 500 µM doses of compound **2**, histamine (1 mM) induced contraction was reduced by 25 and 65 %, and the increase in K^+ induced contraction was reduced to 68 ± 7 and 10 ± 2 %, respectively.[321] Aortic strips pre-treated with 100 µM of compound **2** significantly attenuated, the endothelin-1 (300 µM) induced contraction by 34 %, and the increased K^+ (KCl, 50 mM) induced tension caused by direct depolarisation of smooth muscle.[322] The normal state of the coronary artery was regained once the compound was removed, and the effect was proven to be a specific pharmacological activity and not due to cytotoxic effects. These findings demonstrated that inhibition of both influx and efflux of Ca^{2+} from extracellular environment and intracellular Ca^{2+} stores by compound **2** prevents contraction of coronary arteries, and which may also be linked to the prevention of restenosis after PTCA.[321,322]

The compounds of formula **19** (**Figure 1.26**) and their corresponding salts were reported to act as smooth muscle relaxants by activating the K^+ channels and blocking the Cl^- channels. Among several compounds tested, compound **19a** (30 mg/kg, **Figure 1.26**) was identified to be more effective in decreasing spontaneous contractions in a rat bladder hypertrophy *in vivo* model. The IC_{50} values obtained with compound **19a** in bladder and aorta were 0.5 ± 0.2 and 3 ± 2 µM, whereas compound **2** was neither potent nor a selective muscle relaxant and its IC_{50} were 14 ± 5 and 16 ± 9 µM, correspondingly.[320] Though the compounds were characterised to be of potent smooth muscle relaxants *in vitro*, it was postulated that some of the modulators to be active *in vivo* too from the activity seen in a rat bladder hypertrophy model. This series of distinctive compounds were selective for bladder than vascular tissue. It was also found that compound **19b** (**Figure 1.26**) had the ability to activate the maxi K^+ channel in rat bladder cells along with the capability to block the contractions induced by potassium chloride (KCl) on tissues, *in vitro*. Thereby these compounds have shown a pronounced effect on inducing smooth muscle relaxation.[320]

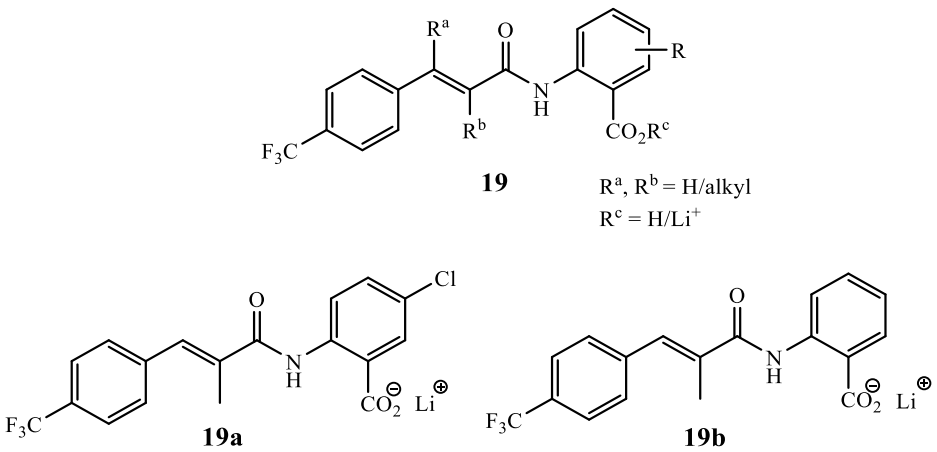

Figure 1.26: *Smooth muscle relaxants* (**19**, **19a** *and* **19b**).

In order to evaluate the blocking effects on cystic fibrosis transregulatory (CFTR) chloride channel and swelling, derivatives of compound **19** were also screened in normal human bronchiolar epithelial cells and in guinea pig bladder cells, from which compound **19b** was identified to have 85 and 71 % inhibitions at 20 µM, respectively, and the effects were reversible.[320]

1.2.9 Multinucleated giant cell inhibitor

Histologically multinucleated giant cells (MGCs) are a cell type generated in granulomatous lesions. Granulomatous diseases include cutaneous sarcoidosis, granuloma annulare and cheilitis granulomatosis. *In vitro* studies were undertaken to examine the activity of CAD **2** on the formation of MGCs from human peripheral monocytes. Compound **2** (10 and 100 μg ml^{-1}) significantly reduced the formation of total MGCs (fusion index = 86 ± 3 and 65 ± 6 %) and the foreign body-type MGCs (fusion index = 56 ± 4 and 29 ± 8 %), and slightly increased the Langhans-type MGCs (fusion index = 30 ± 6 and 37 ± 6 %) from human mononuclear cells activated by concanavalin A-stimulated lymphocyte supernatants. The compound raised the number of MGCs with three-five nuclei and lowered the MGCs with more than sixteen nuclei. Also monocytes treated with the compound showed reduced expressions of ICAM-1, which is known to play a pivotal role in the generation of MGCs. These results indicated compound **2** to have a direct effect on monocyte macrophage-lineage cells.[323]

1.2.10 Telomerase inhibitor

Telomers are the endings of the eukaryotic chromosomes that have repetitive nucleotide sequences, which is required for the structure and function of chromosomes. During each turn of DNA replication, a definite length of telomers is lost from linear chromosomes. As a cell undergoes several cell divisions there will be an abundant reduction in telomeric DNA, which limits the replication of somatic cells. However, in greater than 85 % of human tumours, the telomerase enzyme is reactivated to compensate the telomers loss, which results in infinite replication. The carboxylic acid amides **20** and **21** (**Figure 1.27**) are some examples of telomerase inhibitors being useful as a therapeutic agent for treating diseases characterised with increased telomerase levels, for example, sarcomas, leukaemia and carcinomas.[324] The derivatives **20** and **21** were also suitable for treating diseases caused by parasites (worm and fungal) and protozoan (*Ciliata*, *Rhizopoda*, *Sporozoa*, *Zooflagellata*, etc.) pathogens in human and animals.[324]

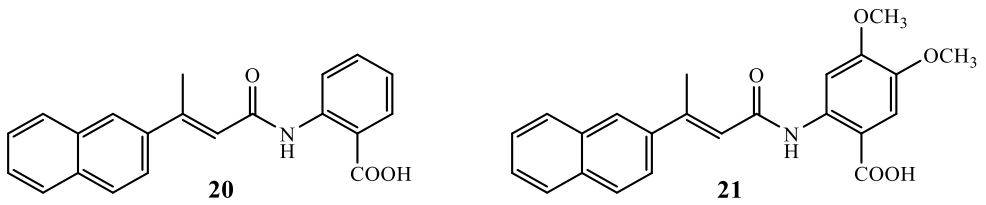

Figure 1.27: *Telomerase inhibitors* (**20** *and* **21**).

1.2.11 Matrixins inhibitor

Matrix metalloproteases (matrixins or MMPs) are zinc-dependent proteases involved in the degradation/regulation of extracellular matrix, and matrix metalloprotease 13 (MMP-13) is a collagenase. These enzymes are overexpressed in cancer cells and are believed to participate in metastasis and proliferation. In rheumatoid arthritis and osteoarthritis, the imbalance between MMP and endogenous metalloproteases tissue inhibitor results in excess MMP causing damage to cartilage and bone. Hence it is anticipated that inhibiting excess MMPs may prevent progression of diseases such as cancer, rheumatoid arthritis and osteoarthritis. In osteoarthritis, the levels of IL-1 and TNF-α also rise, and cause degradation of the extracellular matrix. On the other hand, the production of MMP is increased by type II collagen and fibronectin degradation products resulting in progressive matrix degradation in the joints. It is known that MMP-13 plays an important part in the type II collagen cleavage. Derivatives of compound **22** (**Figure 1.28**) possess antagonising effect on MMP-13 production and are under investigation for use in the treatment of diseases, such as osteoarthritis, articular rheumatism, cancer, etc., those related to MMP-13 production.[325]

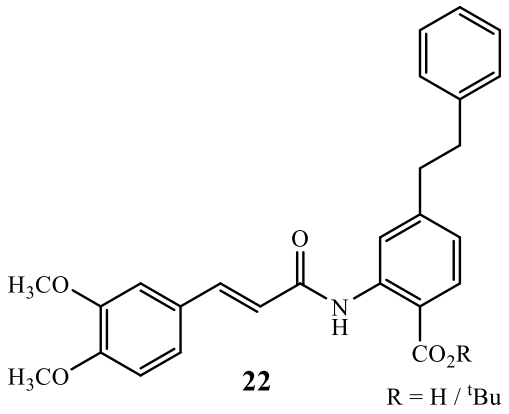

Figure 1.28: *Matrix metalloproteases inhibitor* (**22**).

1.2.12 PLA_2 and TRP channel blocker

TRP channels are involved in cellular calcium signalling, and thus participate in contraction of smooth muscle, release of transmitters, cell proliferation and gene transcription. Compound **23** (ONO-RS-082, **Figure 1.29**) was utilised as a PLA_2 inhibitor to examine the signalling cascades triggered by epinephrine in human platelets,[326] where a rise in thromboxane B_2 and phosphatidic acid production was attenuated by the compound (3.5 μM). The compound also attenuated the receptor-induced $[Ca^{2+}]_i$ and the resulting myosin light chains phosphorylation in vascular smooth muscle cells.

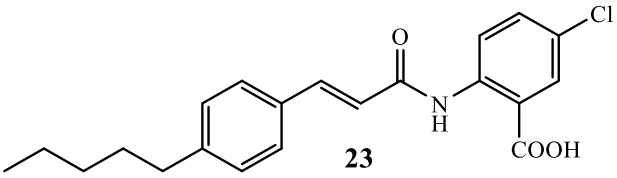

Figure 1.29: *A PLA_2 inhibitor* (**23**).

Compound **18** is also used as a broad-spectrum PLA_2 blocker to study AA mediated modulation of the TRPM2 cation channel and was characterised as a novel TRPM2 inhibitor (IC_{50} 4.5 μM) from electrophysiological measurements. Compound **18** not only inhibited TRPM2, but also directly blocked other TRP channels, including TRPM8 (IC_{50} 3.9 μM), TRPC3 (IC 20 μM), TRPC6 (IC_{50} 2.3 μM) and TRPV1 (IC >20 μM).[327]

AA is an omnipresent cellular mediator released by PLA_2 enzymes from phospholipids. The activities of a range of proteins including GPCRs are modulated by AA and the resulting metabolites from cyclooxygenase (COX), lipoxygenase (LOX) or CYP450 enzyme reactions. PLA_2 enzymes are categorised by their intra- (cytosolic) and extra- (secreted) forms, their specificity to PLA_2 blockers, and calcium-dependent regulation.

As compounds **18** and **23** were characterised as PLA_2 antagonist, the observed biological effects of the compounds were deduced to be the responses triggered by PLA_2. It was suggested that the effects of these two compounds were the result of blocking TRP channels, as both TRPC6 and TRPM4 channels are known to be involved in smooth muscle contraction and since compound **18** had shown to inhibit TRP channels. Compounds **18** and **23** also antagonised histamine release induced by substance P from mast cells,[328] PGE_2 production

induced by endothelin 1 in mesangial cells,[329] and secretion of lung surfactant[327,330]

It is known that vanilloid receptor 1 (VR1 or TRPV1) maintain efferent and afferent functions of sensory nerves, and therefore it is anticipated that diseases involving sensory nerves in the pain pathway can be treated by modulating TRPV1. The majority of derivatives based on the compound structure **24** (**Figure 1.30**) were tested as TRPV1 modulators (ligands) for treating TRPV1 triggered disorders. These TRPV1 modulators (agonists and antagonists) could be used as anaesthetics and anti-inflammatory agents for treating neuropathic/inflammatory/acute pain (allodynia and hyperalgesia) and chronic inflammatory disorders.[331]

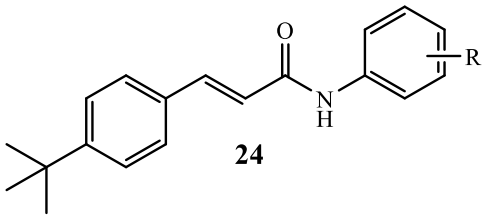

Figure 1.30: *The core structure of TRPV1 modulators* (**24**).

1.2.13 Niacin receptor agonists

Nicotinic acid (niacin, vitamin B3) is a drug used clinically for more than 40 years for the treatment of various dyslipidaemia. Nicotinic acid alters lipoprotein levels in a favourable way by inhibiting the hormone-sensitive triglyceride lipase (HSL) that lowers the non-esterified fatty acids (NEFA) in plasma, thereby reducing the very low- and low density lipoproteins (VLDL and LDL) while increasing the high density lipoproteins (HDL).

CADs **3** and **25 - 28** (**Figure 1.31**) are used as active compounds in pharmaceutical compositions for treating diseases associated with deactivation of the activity of G-protein coupled nicotinic acid receptors HM74A, where activation of receptors is advantageous. These HM74A agonists were reported to be useful in both veterinary and human medicaments.[332] In further studies, the majority of derivatives possessing the core structures **29**[333] and **30**[334] (**Figure 1.31**) were revealed to be of effective serum lipid levels regulating niacin receptor agonists.

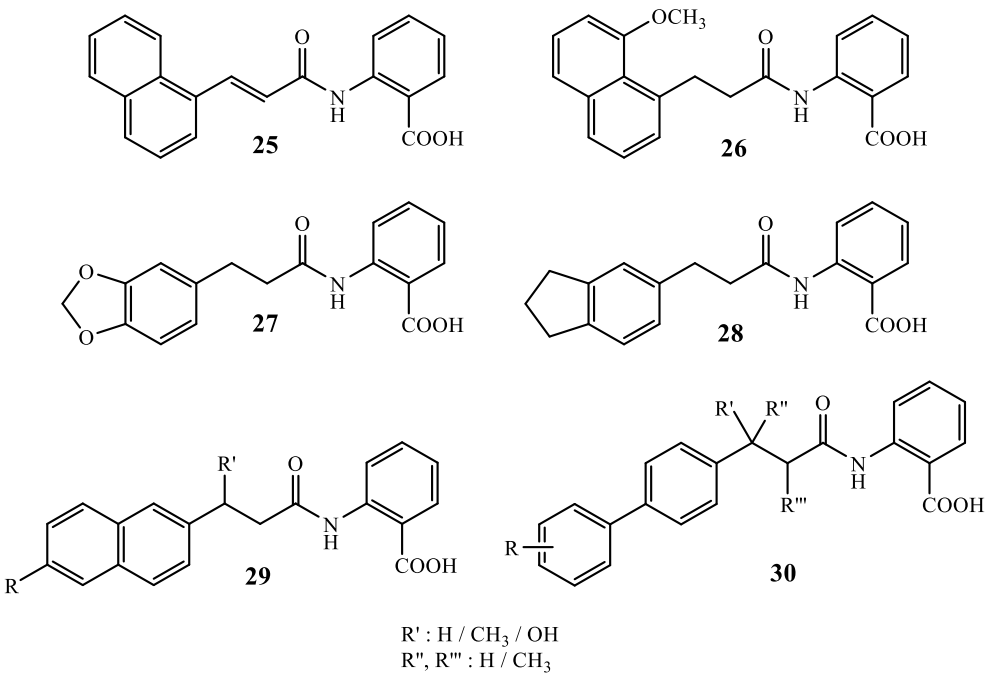

Figure 1.31: *Niacin receptor agonists* (**25 - 30**).

1.2.14 Apolipoprotein enhancer

Lipoproteins contain predominantly lipids and proteins known as apoprotein. Apolipoprotein A1 (apoA1) is an apoprotein of HDL. The level of good cholesterol, HDL, in plasma increases with increase in apoA1 production in serum by enhanced expression of the apoA1 gene. In an experimental study, CADs were shown to be effective in improving apoA1 expression, which stimulates the activity of HDL reverse cholesterol transport system, and the anti-inflammatory and anti-coagulant activities. Hence, CADs have pharmaceutical benefits in compositions of medicaments for treating or preventing various diseases related to HDL such as dyslipidaemia (lower level of serum HDL, hypertriglyceridemia and hypocholesteraemia) and arteriosclerotic diseases (arteriosclerosis, cardiac incompetence, myocardial infarction and several other cardiovascular diseases).[335]

1.2.15 B-cell and T-cell modulators

Rheumatoid arthritis is an inflammatory disease classified by the attack of immune response/complexes, which triggers and intensifies the inflammatory response. As a result, damages to the synovial membrane and connective tissues mostly in the joints occur. Inflammation is known to be the consequence

of accumulation of immune molecules and cells at a target site. Hence as inflammation exacerbates, B cells and T cells are detected at the site, where they interact and produce immunoglobulins, persisting the immune-complex syndrome.[336] T_H1 and T_H2 cells are immune cells those express T cell receptor along with CD4. T_H cells those produce particularly TNF-α, IFN-γ, IL-2 and triggers cell induced/inflammatory immune responses are known as T_H1, and those particularly produce IL-4, IL-5, IL-10 and triggers humoral responses are known as T_H2.[337]

CAD **2** and derivatives of general formula **31** (**Figure 1.32**) were reported to downregulate the harmful B cell (B lymphocyte) functioning particularly in autoimmune conditions like rheumatoid arthritis (synovial inflammation) and B cell proliferation, and the T_H1 cell functioning. Compound **2** effectively downregulates the response of T_H1 by skewing the T_H1 autoimmune responses to T_H2 response by upregulating the production of T_H2 cytokine. These findings appear to be of great importance, as CADs provides selective controlling towards the immune responses of B cells and T_H1 cells, where the conventional immunosuppression related side-effects that downregulate the function of all immune cells can be avoided.[336,337]

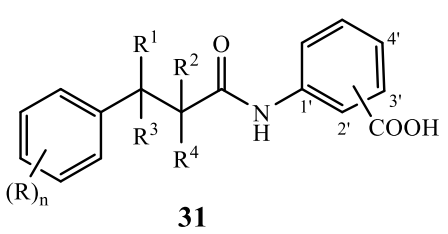

R^1, R^2: H
R^3, R^4: H / C_1-C_4 alkyl
R: OH / halogen / C_1-C_4 alkyl / C_1-C_4 alkoxy / alkyl, alkoxy

n = 1-3
CO_2H in position 2' / 3' / 4'

Figure 1.32: *The core structure of B-cell and T-cell modulators* (**31**).

Compound **2** (100 - 400 mg/kg per day given for 10 days) has attenuated type II collagen-induced arthritis in a mouse model (swelling of mice paw) in a concentration-dependent manner, by reducing synovitis level, loss of cartilage and erosion of bone. Compound **2** (100 µg ml^{-1}) has also revealed its potent anti-proliferative activity *in vitro* by inhibiting the B cell proliferation induced by lipopolysaccharide, anti-CD40 or anti-IgM antibody. *In vitro,* it has shown to inhibit the anti-CD40 and anti-CD3/CD28 induced proliferation of B cells

(IC_{50} 73 μM) and T cells (IC_{50} 28 μM), and the production of anti-type II collagen IgG_1 antibody in mice.[336]

1.2.16 Neuroregeneration and neuroprotection

Analogues of *N*-cinnamoylanthranilates have been considered as therapeutic agents in the treatment or prevention of motor neuron and neurodegenerative diseases, including ALS and Parkinson's disease, that is caused by the loss of motoneurons and/or dopaminergic neurons, or due to general tissue loss from the *substantia nigra*.[338] CADs were also considered for use in the prophylaxis of neuroregeneration and neuroprotection by improving or stimulating neurogenesis, and moreover in stem cell therapy using *in vitro* treated differentiated stem cells.[288]

Surprisingly, the derivatives **1 - 3** and analogues of CADs have shown to improve or trigger neurogenesis by producing new neurons from neuronal stem cells and by preventing neurodegeneration. These derivatives have also revealed their valuable anti-apoptotic neuroprotective action in treating progressive neuronal loss at later stage, by reversing the loss that has already happened and thereby improving the survival of neurons. All these compounds have also shown to significantly activate the differentiation of neuronal stem cells and anti-apoptotic effects, and were found to be of valuable in the treatment of neurological conditions.[288]

1.2.17 Biosynthesis of *N*-cinnamoylanthranilates

Biosynthesis of medicaments using microbes is an alternative eco-friendly synthetic approach to the common conventional chemical synthesis. It is known that in plants like oats, a few analogues of *N*-cinnamoylanthranilates are made naturally *via* amine condensation on coupling of anthranilic acid with different hydroxycinnamoyl-coenzyme A conjugates. With this knowledge, potential biosynthesis strategy for producing CADs by enzymatic reactions in engineered yeast strain has been demonstrated, by which natural and non-natural compounds could be synthesised as shown in **Scheme 1.2**.[339-342]

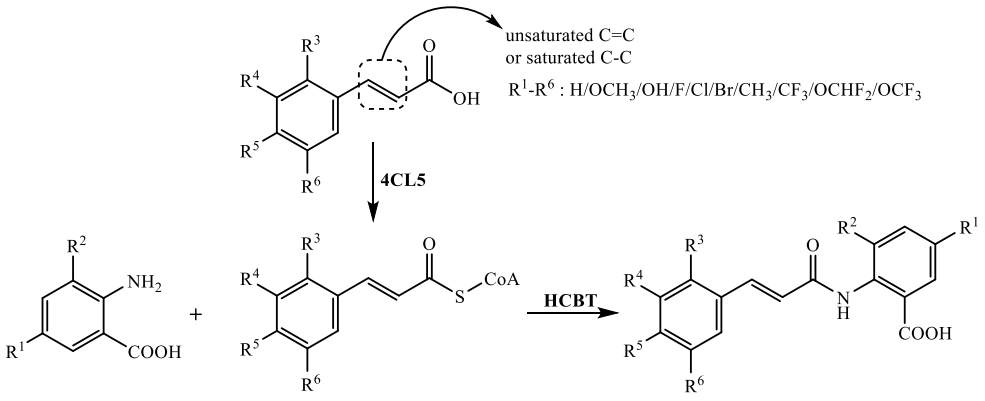

Scheme 1.2: *Biosynthesis of N-cinnamoylanthranilates. The genes encoding enzymes 4-coumaroyl:CoA ligase 5 (4CL5) and hydroxycinnamoyl/benzoyl-CoA/anthranilate N-hydroxycinnamoylbenzoyltransferase (HCBT) from plant species, Arabidopsis thaliana and Dianthus caryophyllus were engineered into the microbial yeast, Saccharomyces cerevisiae, and various mixtures of anthranilates and cinnamic acid derivatives were supplied exogenously, and incubated at 30 °C with agitation (200 rpm) for 24 hours to produce different defined CADs. During the incubation period, cinnamic acids (donors) are converted into coumaryl-CoA thioesters by 4CL5 and coupled to anthranilic acids (acceptors) by HCBT. Using this approach more than seventy cinnamoyl and dihydrocinnamoyl anthranilate derivatives have been reported to be synthesised.*[339-342]

On the other hand, biosynthetic pathway for producing hydroxycinnamoyl anthranilates (Avn) and possibly other derivatives, from glucose in *Escherichia coli* (*E. coli*) microbes was reported. In this case, 4-hydroxycinnamoyl and 3,4-dihydroxycinnamoyl anthranilic acid (Avn D and Avn F) were synthesised when a pre-characterised anthranilate-accumulating *E. coli* strain coexpressing *N*-hydroxycinnamoylbenzoyltransferase (HCBT) and Nt4CL1 (from tobacco) grown in the culture medium was added with *p*-coumarate and caffeate, correspondingly.[340]

1.2.18 Conclusion

In various experimental studies undertaken both *in vivo* and *in vitro*, several promising compounds as potential lead have been identified at concentrations suitable for clinical use specific to the diseases. Overall, these small organic molecules have shown a wide range of biological activities in several studies as described, and it is revealed that they have several potential therapeutic applications in treating and/or preventing numerous disorders/diseases, and thereby being a great value in the field of medicinal chemistry. As CADs have shown to inhibit TRP channels, for example compound **18** (ACA)[330] was

characterised as a novel TRPM2 (IC_{50} 4.5 μM), TRPM8 (IC_{50} 3.9 μM), TRPC3 (IC 20 μM), TRPC6 (IC_{50} 2.3 μM) and TRPV1 (IC >20 μM) channel blocker,[327] it is anticipated that TRPA1 cation channel specific modulators could be attained by incorporating different substituents and substitution patterns in the *N*-cinnamoylanthranilic acid core structure (**1**).

1.3 Biological activities of aryl sulfonamides

1.3.1 Probenecid

Probenecid [*p*-(dipropylsulfamyl)benzoic acid] was first synthesised in 1949[343] based on the chemical structure (**Figure 1.33**) of the compound carinamide[344,345] [*p*-(benzylsulfonamido)benzoic acid], and initially it was recognised by its brand name as Benemid.[345] The compound was originally introduced for the purpose of reducing renal excretion of the antibiotic penicillin.[345] In later studies, its effectiveness to improve withholding of other antibiotics was also identified.[346,347] Over the past years, probenecid had been utilised in several fundamental and clinical researches, such as in the prevention of calcium-sensitive dye (e.g. Fura-2) leakage in Ca^{2+} transient studies,[348,349] and its potential use to treat depression.[347,350,351] Recently, probenecid has been reported as a potent TRPV1 agonist (EC_{50} 31.9 μM),[352] pannexin 1 inhibitor (IC_{50} ~150 μM),[353] and also as a TRPA1 agonist (EC_{50} 4.2 mM).[354]

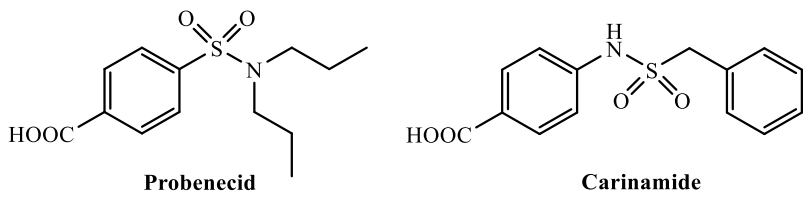

Figure 1.33: *Chemical structures of probenecid and carinamide*.

1.3.1.1 Gout

Gout is a type of inflammatory arthritis that develops as a result of increased uric acid or urate in the bloodstream, which crystallises at high concentrations (uric acid stones) due to its partial water solubility. While studying probenecid's activity to reduce excretion of antibiotics, it was recognised by chance that probenecid inhibits tubular reabsorption of urate and thereby

improves its renal excretion, and hence it was used to treat gout.[355,356] Particularly, probenecid is known to inhibit the organic anion transporter (OAT)-mediated reabsorption of uric acid from urine by acting as a competitive blocker of OAT.[357] The effectiveness of probenecid in lowering the levels of serum uric acid and improving gout symptoms had been tested clinically.[358] Though the toxicity of the compound was considered to be insignificant, several side-effects including fever, nausea, abdominal cramps, headaches, vomiting, shortness of breath and gastrointestinal symptoms had been reported with the use of probenecid in treatments. These regular side effects were observed only at a dose of 3 g per day, and when the dose was decreased to 2 g per day several symptoms declined.[358] The uricosuric properties of the compound was utilised to treat gout only for some time, and it is no longer used to treat both renal excretion of antibiotics and gout due to the availability of more advanced treatments nowadays.[359]

1.3.1.2 Depression

Probenecid had shown to block the release of serotonin and dopamine metabolites, 5-hydroxyindoleacetic acid (5-HIAA) and homovanillic acid (HVA), from the CNS.[350,360] Therefore, it has been suggested that probenecid could be used as a tool to study the levels of neurotransmitters in the brain and cerebrospinal fluid.[347,351] Similarly, it was found that probenecid has an effect on other monoamine metabolites, such as norepinephrine, that are associated with neuropsychiatric diseases.[361] Administration of probenecid led to increased level of norepinephrine in the cerebrospinal fluid and plasma,[361] and reduced levels of tyrosine and tryptophan in the serum.[362] A decrease in dopamine levels causes Parkinson's disease, and since probenecid can block the acid metabolites of dopamine, the compound has a new consideration in the neurology field. In addition, probenecid administered in conjunction with L-kynurenine have shown protective effects on the dopaminergic affected areas.[363]

1.3.1.3 Dye retention

Fluorescent indicators, such as Fura-2, are being used in $[Ca^{2+}]_i$ *in vitro* studies for more than 25 years.[364,365] When Fura-2 was initially used, dye leaking

through cell membrane was observed. However, with the use of probenecid at a concentration of 2.5 mM in the cell culture medium, it was shown that the leaking is blocked *via* competitive inhibition of the OAT.[366] Since then, probenecid has been regularly used with Ca^{2+} fluorescent dyes in various types of cells,[367] including astrocytoma[349], macrophages[348] and smooth muscle cells[368]. In isolated cardiac myocytes, Fura-2 or Fluo-4 with probenecid had been utilised to measure Ca^{2+} transients and sparks. However, it was found that probenecid leads to an increased contractility and calcium sparks in isolated myocytes.[359]

1.3.1.4 TRP channel modulator

Probenecid has been used in several TRPV2 studies with dyes,[369-371] without knowing that it has an agonistic effect on the channel. Probenecid selectivity for the channel was revealed by a dose-dependent increase in $[Ca^{2+}]_i$ influx in exogenous TRPV2 expressing HEK293T cells (EC_{50} 31.9 µM).[352] In their study, TRPA1, TRPM8, TRPV1, TRPV3 and TRPV4 examined under similar sets of conditions did not show any responses to probenecid.[352] Since TRPV channels are involved in diseases, it is anticipated that probenecid could be utilised within the research fields of cardiology and neurology as a useful pharmacological tool.[359]

In contrast to the above observation that probenecid was inactive in TRPA1 channels, in a more recent study, activation of TRPA1 (EC_{50} 4.2 mM) had been observed.[354] In addition, it has been shown that prolonged incubation of probenecid together with fluorescent indicators during dye-loading process desensitises TRPA1 channels, and consequently decreases the potency of other agonists evaluated in the study.[354] For instance, when hTRPA1 expressing Chinese Hamster Ovary (CHO) cells were dye-loaded with probenecid (2 mM), the EC_{50} obtained for the TRPA1 agonist AITC significantly ($p < 0.01$) increased from 1.5 to 7.3 µM.[354]

1.3.2 4-Fluoroarylsulfonamides

1.3.2.1 TRPA1 channel blocker

Several pharmaceutical companies have claimed aryl sulfonamide derivatives containing a 4-fluoroarylsulfonamide motif as potent TRPA1 antagonists (**Figure 1.34**). In 2010, the company Janssen Pharmaceuticals reported a series of heterocyclic amides as TRPA1 modulators, among which the aryl sulfonamide moiety containing compounds, **A** (IC_{50} 2 nM) and **B** (IC_{50} 7 nM) shown in **Figure 1.34** were found as potent TRPA1 antagonists.[372] In 2012, Orion Corporation disclosed a series of compounds analogous to the reported

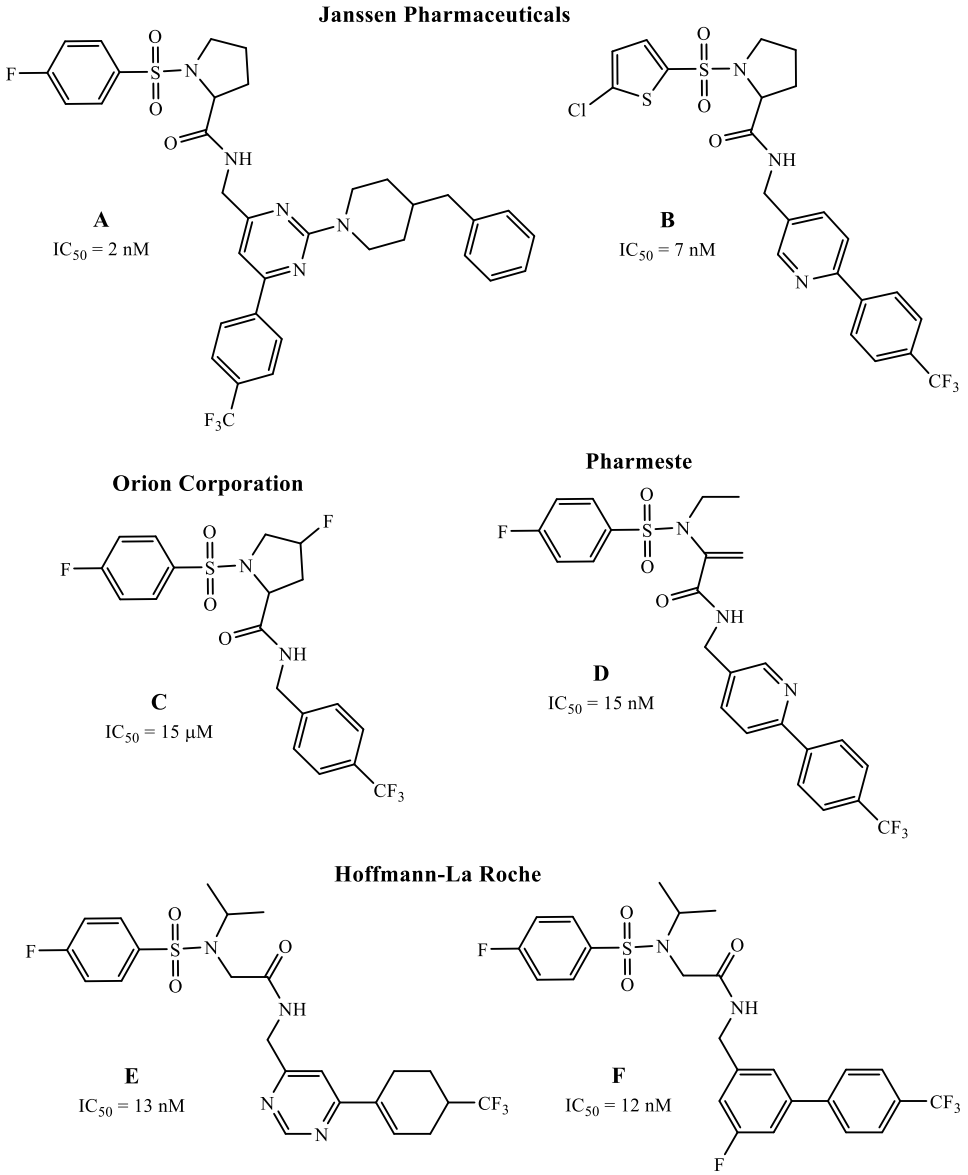

Figure 1.34: *Examples of aryl sulfonamide derivatives claimed as potent TRPA1 antagonists by the pharmaceutical companies, Janssen Pharmaceuticals,*[372] *Orion Corporation,*[373] *Pharmeste,*[374] *and Hoffmann-La Roche*[375,376].

Janssen Pharmaceuticals' sulfonamides as TRPA1 antagonists.[373] For example, derivative **C** (**Figure 1.34**) was shown to antagonise the agonism of AITC in human (IC_{50} 15 μM) and rat (IC_{50} 22 μM) TRPA1,[373] but it was less potent compared to the Janssen's sulfonamides. Recently, in 2014, Pharmeste[374] and Hoffmann-La Roche[375,376] have also claimed novel aryl sulfonamides similar to the Janssen Pharmaceuticals' compounds as antagonists of TRPA1. An example of a derivative disclosed by Pharmeste, **D** (**Figure 1.34**) was shown to block both human (IC_{50} 15 nM) and rat TRPA1 (IC_{50} 14 nM) with similar potency.[374] Similarly, the compounds **E** (IC_{50} 13 nM) and **F** (IC_{50} 12 nM) with 2-(4-fluoro-*N*-isopropylphenylsulfonamido)acetamide moiety (**Figure 1.34**) were found as potent TRPA1 antagonists from the Hoffmann-La Roche series.[375,376]

1.3.3 Conclusion

Probenecid, a competitive inhibitor of OAT, was recently found to activate TRPA1 and desensitise the channel on prolonged incubation during dye-loading process, when it was used to prevent leakage of Ca^{2+} sensitive fluorescent dyes from cells. In addition, several aryl sulfonamide derivatives with 4-fluorobenzenesulfonamide motif claimed by different pharmaceutical companies were found to inhibit the channel. Therefore, it is anticipated that the fluoro group on the benzenesulfonamide is important for the antagonistic effect on TRPA1.

1.4 Research gap, hypothesis and aims

The non-selective cation channel TRPA1 expressed predominantly in primary sensory neurons, including trigeminal, dorsal root and nodose ganglia, is known to be involved in pain, itch, inflammatory diseases including arthritis, asthma, chronic cough and COPD, peripheral neuropathy, and hereditary diseases.[83,109-114] These important roles of TRPA1 makes it an exciting target for drug development, but to develop drug-like antagonists it is vital to understand the mechanisms of modulation (activation/blocking) of TRPA1.

There are many natural and synthetic compounds found to modulate TRPA1, among them the compounds containing reactive electrophilic groups or oxidants are known to activate the channel through covalent modification of either cysteine or lysine residues at the *N*-terminus of the protein.[83,118,119] However, TRPA1 is also stimulated by non-reactive compounds which are not capable of undergoing covalent attachment to TRPA1. In a few studies,[83,103,119,150-152,377] mutagenesis and chimeric approaches have been utilised to elucidate the interactions of some non-reactive chemicals with the channel. However, the non-covalent mechanism(s) of modulation by compounds with distinct structures are currently much less well determined, and this lack of knowledge hinders the understanding of the role of TRPA1 channel in diseases and thereby in the development of drugs targeting the channel.

In this study, it was hypothesised that the functional groups present on the chemicals could be responsible for the modulation of TRPA1 channel non-covalently. Consequently, the aims were to:

- synthesise series of compounds with different functional groups as TRPA1 modulators.
- evaluate the synthesised compounds in a TRPA1 expressing cell line.
- investigate the structure-activity relationships and the pharmacology of the TRPA1 active modulators.
- use site-directed mutagenesis to produce TRPA1 mutants, and evaluate TRPA1 modulators in the mutants expressing cell lines to determine the binding site(s) of non-reactive TRPA1 ligands.

Outline

The background information, including the literature review, research gap, hypothesis and aims of the study are covered in this **Chapter 1**. The experimental materials and methods utilised in the chemical syntheses and pharmacological studies are provided in **Chapter 2**. The structure characterisation data of the synthesised chemical compounds are also given in **Chapter 2** along with the synthesis procedures. **Chapter 3** covers the results and discussions of the synthesis and screening of *N*-cinnamoylanthranilic acid derivatives in TRPA1 expressing cell line, and the study of their structure-activity relationships and pharmacological properties. **Chapter 4** covers the results and discussions of the synthesis and evaluation of aryl sulfonamide derivatives in TRPA1, and the study of their structure-activity relationships. The results and discussions of the TRPA1 ligand binding sites studied through a site-directed mutagenesis approach are given in **Chapter 5**. The overall research work including the key findings are summarised in **Chapter 6**, and the general conclusions with further work are given in **Chapter 7**.

CHAPTER 2: Experimental materials and methods

2.1 Chemistry

2.1.1 General information

The chemicals, including cinnamic acid derivatives, methyl anthranilate, anthranilic acid, aldehydes, sulfonyl chloride derivatives, 4-aminobenzoic acid, secondary amines, bases, acids, salts and solvents were from commercial suppliers, including Sigma-Aldrich (Aldrich Chemical), Alfa Aesar, Acros, Fluorochem, Lancaster Synthesis, Fisher Scientific and VWR Chemicals, and were used without further purification unless stated otherwise. The structure and purity of the synthesised compounds were confirmed by ^{1}H and ^{13}C NMR, mass spectra (MS), CHN elemental microanalysis (EA) and melting point (m.p.).

NMR spectra were recorded using either a JEOL JNM ECP400 or JEOL JNM LA-400 spectrometer with tetramethylsilane (TMS, δ_H = 0) as the internal standard, and deuterated chloroform ($CDCl_3$, δ_H = 7.27, δ_C = 77.0 ppm) and/or deuterated dimethyl sulfoxide (*d*$_6$-DMSO, δ_H = 2.56, δ_C = 39.0 ppm) as the solvents. ^{1}H NMR and ^{13}C NMR were recorded at 400 MHz and 100 MHz, respectively. In the NMR data, $CDCl_3$--*d*$_6$-DMSO represents the use of $CDCl_3$ and a few drops of *d*$_6$-DMSO solvent mixture for dissolution; s, singlet; d, doublet; dd, double doublet; t, triplet; dt, double triplet; q, quartet; m, multiplet; br, broad. The coupling constant (*J*) values of the olefinic protons (J_{H^5} and J_{H^6}) obtained for some of the compounds contained ± 0.2 Hz experimental error, and hence the average values of the two coupling constants were reported in the ^{1}H NMR data.

Electron ionisation (EI, 70 eV positive mode) MS were recorded on a Perkin Elmer Turbomass interfaced to a Quadrupole mass spectrometer with Perkin Elmer Autosystem XL GC [carrier gas: helium at 1 ml min^{-1}; column: Thames Restek Rxi-1ms (fused silica), 30 m × 0.25 mm × 0.25 µm; temperatures: ion source 180 °C, injector 250 °C, MS interface 250 °C; GC oven programme: 40 °C initial temperature for 3 min, ramp to 280 °C (20 °C increase per min), hold 280 °C for 10 min; split injection ratio: 50:1; mass scan range: 30 - 550 amu]. Electrospray ionisation (ESI, positive mode) MS were recorded on a Bruker

HCT Ultra Ion Trap MS [solvent flow: 250 µl min^{-1}, 0.1 % HCOOH (70 % CH_3CN + 30 % H_2O); nebulizer pressure: 35.0 psi; dry gas flow: 9.0 l min^{-1}; drying temperature: 300 °C; scan range: 75 - 2000 amu; maximum acquisition time: 200 ms].

CHN combustion elemental microanalyses were performed on a Fisons CHN Analyzer Carlo-Erba EA1108 with a Mettler T5 microbalance, based on dynamic flash combustion (combustion reactor: made of translucent silica and filled with 40 mm silica wool, 60 mm silvered cobalt oxide, 10 mm silica wool, chromium oxide and 10 mm silica wool; reduction reactor: made of transparent silica and packed with 10 mm silica wool, 50 mm copper oxide wires, 10 mm silica wool, 280 mm copper wires, 10 mm silica wool, 50 mm copper oxide wires and 10 mm silica wool), GC separation (GC column: Porapak QS 50-80 mesh) and thermal conductivity detector. Melting points were determined on a Stuart melting point apparatus SMP10, and were compared against the literature findings, where available.

The physicochemical parameters and the hydrophilicity/lipophilicity colour coded mapping of the compounds were obtained using the online ACD/Labs I-Lab 2.0 (https://ilab.acdlabs.com/iLab2/) software. The optimised geometry of the compounds were determined by the energy minimisation molecular mechanics force-field, MM2, using the molecular modelling software, ChemBio3D Ultra 14.0.

2.2 General synthetic procedures for *N*-cinnamoylanthranilates

Three synthetic routes were followed to synthesise the *N*-cinnamoyl anthranilate derivatives (CADs, **Figure 2.1**). In one approach, the cinnamic acid derivative was converted to its corresponding acid chloride, which was coupled to methyl anthranilate[378] and the resulting methyl *N*-cinnamoyl anthranilate was hydrolysed[379] to yield the corresponding *N*-cinnamoyl anthranilic acid derivative (**Scheme 2.1**, **Section 2.2.1**). In the second approach, Meldrum's acid[380] was reacted with anthranilic acid to produce 2-[(carboxyacetyl)amino]benzoic acid, which was then condensed with a benzaldehyde derivative *via* a piperidine-catalysed Knoevenagel condensation producing *N*-cinnamoylanthranilate as the piperidinium salt, and was acidified to yield the final product (**Scheme 2.2**, **Section 2.2.2**).[381] In the third approach, a secondary amino acid was reacted with cinnamoyl chloride under basic conditions and the resulting salt was acidified to yield the product (**Scheme 2.3**, **Section 2.2.3**).[382]

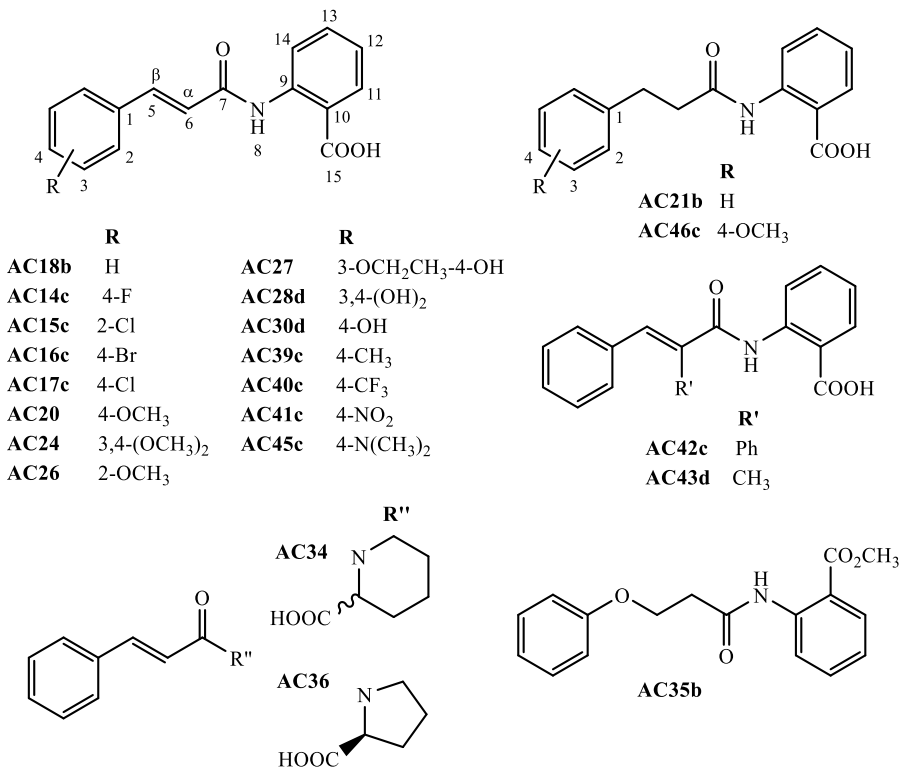

Figure 2.1: *Chemical structures of the N-cinnamoylanthranilate derivatives.*

2.2.1 Synthesis of *N*-cinnamoylanthranilate derivatives from cinnamic acid derivatives

(a) *Cinnamoyl chlorides* - Cinnamic acid derivatives were stirred with oxalyl chloride (5 ml g^{-1}) for up to 4 hours, and the excess reagent was evaporated under reduced pressure. The stirring time differed depending on the dissolution/reaction rate of the starting cinnamic acid derivative. For derivatives with 4-NO_2 or 4-$N(CH_3)_2$ substituents, a drop of dry *N*,*N*-dimethylformamide (DMF) was added to catalyse the reaction.

The hydroxy groups in the hydroxycinnamic acid derivatives were acetylated[281] prior to reaction with oxalyl chloride by stirring the derivative (0.0244 mol) in acetic anhydride (5 ml g^{-1}) and pyridine (0.5 ml) at room temperature (~20 °C) overnight. Cold water (~50 ml) was added to the mixture and stirred for further 5-10 minutes with cooling in an ice-water bath, and the resulting precipitate of acetoxycinnamic acid was obtained by vacuum filtration, washed with cold water and dried.

(b) *Methyl N-cinnamoylanthranilates* - The cinnamoyl chloride (0.014 mol) was added to a solution of excess methyl anthranilate (0.017 mol) in dry pyridine (10 ml g^{-1}), and the mixture was stirred for an hour at room temperature. Cold water (250 ml) was added to the reaction mixture and the resulting precipitate was filtered and washed with cold water until free of pyridine, and was recrystallised from hot ethanol.[378] In contrast, methyl *N*-hydrocinnamoylanthranilate derivatives, with a low melting point, were extracted in diethyl ether (2 × 70 ml), washed with cold water (2 × 50 ml) and solvent evaporated under reduced pressure.

(c) *N-Cinnamoylanthranilic acids* - The methyl *N*-cinnamoylanthranilate (0.01 mol) was stirred in a mixture of tetrahydrofuran (THF, 100 ml) and methanol (20 ml), and aqueous LiOH (~1 M, 0.05 mol) was added to the reaction mixture and stirred at room temperature overnight. The solvents were evaporated under reduced pressure. The crude product was dissolved in water (~350 ml) and acidified slowly to pH 4 using dilute HCl (1 M) with stirring.[379] The precipitate was obtained by vacuum filtration, washed with water and dried, and was recrystallised from hot aqueous ethanol (water-ethanol, 1:4). In the case of *N*-hydroxycinnamoylanthranilate derivatives, water was added to the resulting solution to aid crystallisation.

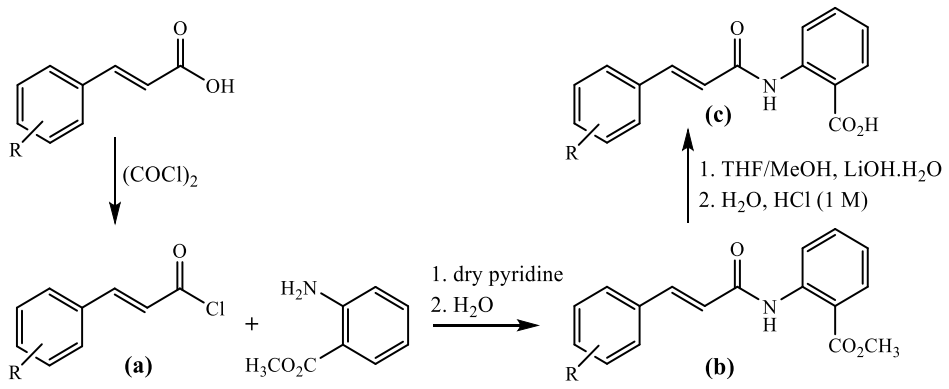

Scheme 2.1: *Synthesis of N-cinnamoylanthranilate derivatives from cinnamic acid derivatives. The derivatives* **AC14 - AC18**, **AC21**, **AC28**, **AC30**, **AC35**, **AC39 - AC43**, **AC45** *and* **AC46** *were synthesised using this approach.*

2.2.2 Synthesis of *N*-cinnamoylanthranilate derivatives from aldehyde derivatives

(i) *2-[(Carboxyacetyl)amino]benzoic acid* - Anthranilic acid (0.145 mol) was added to a solution of Meldrum's acid (0.150 mol) in toluene (165 ml), and the reaction mixture was heated under reflux with a Dean-Stark apparatus for 3 hours with gentle stirring.[381] Meldrum's acid was synthesised by reacting malonic acid, acetic anhydride and acetone as reported in the literature.[380] The reaction mixture was cooled to room temperature and further in an ice-water bath, and the precipitate was obtained by vacuum filtration, washed with toluene (~50 ml) and dried.[381]

(ii) *N-Cinnamoylanthranilic acid* - Piperidine (0.0154 mol) was added to a mixture of a benzaldehyde derivative (0.0154 mol) and 2-[(carboxyacetyl)amino]benzoic acid (0.0148 mol) in toluene (20 ml), and the reaction mixture was heated under reflux with a Dean-Stark apparatus for 4 hours. The reaction mixture was cooled to room temperature and stirred vigorously for an hour. The resulting piperidinium salt was filtered, washed with toluene and dried. The precipitate was dissolved in a mixture of methanol (5 ml g^{-1}) and water (2 ml g^{-1}) at 40 °C, and acidified to pH 4 using dilute HCl (1 M), and the crude product was obtained by vacuum filtration, washed with water and dried.[381] The precipitate was recrystallised from hot aqueous ethanol (water-ethanol, 1:4).

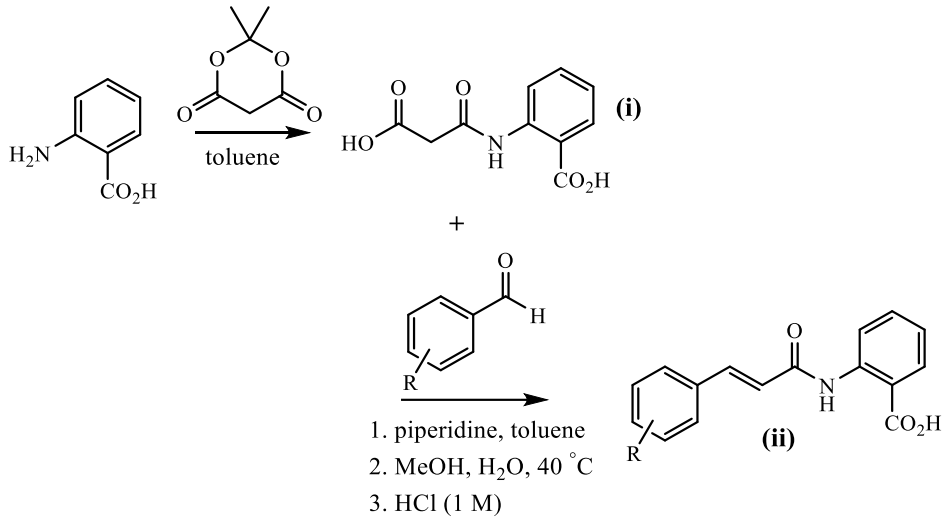

Scheme 2.2: *Synthesis of N-cinnamoylanthranilic acid derivatives from aldehyde derivatives. The derivatives* **AC20**, **AC24**, **AC26** *and* **AC27** *were synthesised using this approach.*

2.2.3 Synthesis of *N*-cinnamoyl amino acids

R,S-Pipecolinic acid or *S*-proline (0.0333 mol) was dissolved in NaOH (1 M, 70 ml) and cooled in an ice-water bath, and cinnamoyl chloride (0.0260 mol) dissolved in diethyl ether (15 ml) was added. The reaction mixture was stirred vigorously for 1.5 hours with cooling, then at room temperature for further 3 hours. The solution was washed with diethyl ether (20 ml) and the aqueous layer was acidified to pH 1 using HCl (6 M). The precipitate was obtained by vacuum filtration and dissolved in dichloromethane (DCM). The filtrate was extracted in more DCM (30 ml). The combined organic solutions were dried over anhydrous sodium sulfate, filtered and solvent evaporated under reduced pressure.[382] The precipitate was recrystallised from hot ethanol to yield the product.

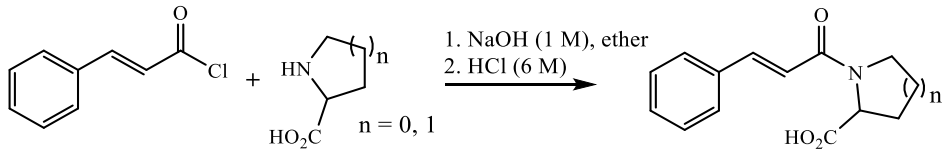

Scheme 2.3: *Synthesis of N-cinnamoyl amino acids, rac-***AC34** *and S-***AC36**.

2.2.4 Procedures for individual *N*-cinnamoylanthranilate derivative

2.2.4.1 *N*-Cinnamoylanthranilic acid (AC18)

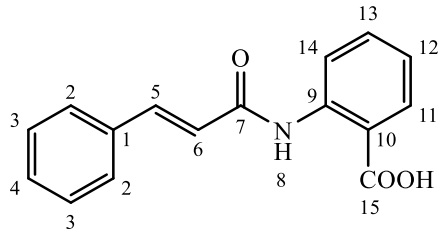

Cinnamoyl chloride - purchased from Aldrich.

Methyl N-cinnamoylanthranilate (**AC18a**) **-** Methyl anthranilate (2.700 g, 0.0165 mol) and dry pyridine (45 ml) were added to cinnamoyl chloride (2.462 g, 0.0148 mol) and stirred for an hour at room temperature. Cold water (200 ml) was added to the mixture and continued stirring for 30 minutes. The precipitate was obtained by vacuum filtration, washed with cold water (300 ml) until the precipitate was free of pyridine and dried. The white precipitate was recrystallised from hot ethanol, cooled down to room temperature, filtered and washed with water to yield pure methyl *N*-cinnamoylanthranilate as a white precipitate (3.494 g, 84 %); m.p. 99-101 °C (lit.[383] 99 °C). ^{1}H NMR (400 MHz, $CDCl_3$) δ 3.97 (s, 3H, CH_3), 6.64 (d, *J* = 15.6 Hz, 1H^{5}), 7.09-7.14 (m, 1H^{12}), 7.37-7.44 (m, 3H$^{3, 4}$), 7.57-7.62 (m, 3H$^{2, 13}$), 7.77 (d, *J* = 15.6 Hz, 1H^{6}), 8.07 (dd, *J* = 8.0, 1.6 Hz, 1H^{14}), 8.89 (dd, *J* = 8.5, 1.1 Hz, 1H^{11}), 11.39 (br s, 1H^{8}); ^{13}C NMR (100 MHz, $CDCl_3$) δ 52.38, 114.85, 120.54, 121.93, 122.54, 128.05, 128.83, 129.97, 130.86, 134.63, 134.76, 141.82, 142.26, 164.48, 168.92. MS (EI): *m/z* 281 $C_{17}H_{15}O_3N^{+\bullet}$ ($M^{+\bullet}$), 266 $C_{17}H_{15}O_3N^{+}$ $(M\text{-}CH_3)^{+}$, 204 $C_{11}H_{10}O_3N^{+}$ $(M\text{-}C_6H_5)^{+}$, 151 $C_8H_8O_2N^{+}$ $(M\text{-}C_9H_7O)^{+}$, 131 $C_9H_7O^{+}$ $(M\text{-}C_8H_8O_2N)^{+}$, 103 $C_8H_7^{+}$ $(M\text{-}C_9H_8O_3N)^{+}$, 77 $C_6H_5^{+}$ $(M\text{-}C_{11}H_{10}O_3N)^{+}$. EA (%) $C_{17}H_{15}O_3N$: calculated C, 72.58: H, 5.37: N, 4.98; found C, 72.42: H, 5.50: N, 4.99.

N-Cinnamoylanthranilic acid (**AC18b**) **-** Methyl *N*-cinnamoylanthranilate (2.176 g, 0.0077 mol) was stirred in a mixture of THF (100 ml) and methanol (20 ml), and aqueous LiOH [~1 M, LiOH (1.392 g) dissolved in H_2O (55 ml)] was added and continuously stirred for 7 hours at room temperature. The solvents were evaporated under reduced pressure, and the resulting white solid was dissolved in water (200 ml) and acidified slowly to pH 4 using HCl (1 M,

40 ml) with stirring. The resulting precipitate was obtained by vacuum filtration, washed with water (350 ml) and dried. The precipitate was recrystallised from hot aqueous ethanol (water-ethanol, 1:4), cooled down to room temperature, filtered and washed with water to yield pure *N*-cinnamoyl anthranilic acid as a white precipitate (1.559 g, 75 %); m.p. 197-199 °C (lit.[381] 188-189 °C). ^{1}H NMR (400 MHz, $CDCl_3$--d_6-DMSO) δ 6.50 (d, *J* = 15.6 Hz, 1H^{5}), 6.96-7.01 (m, 1H^{12}), 7.23-7.31 (m, 3H$^{3, 4}$), 7.41-7.48 (m, 3H$^{2, 13}$), 7.60 (d, *J* = 15.6 Hz, 1H^{6}), 7.99 (dd, *J* = 8.0, 1.6 Hz, 1H^{14}), 8.72 (dd, *J* = 8.6, 1.0 Hz, 1H^{11}), 11.59 (br s, 1H^{8}); ^{13}C NMR (100 MHz, $CDCl_3$--d_6-DMSO) δ 114.88, 119.29, 121.42, 121.70, 127.14, 128.09, 129.18, 130.69, 133.46, 133.75, 140.94, 141.09, 163.42, 169.80. MS (ESI): *m/z* $[M+H]^+$ 268. EA (%) $C_{16}H_{13}NO_3$: calculated C, 71.90: H, 4.90: N, 5.24; found C, 71.68: H, 4.86: N, 5.26.

2.2.4.2 *N*-(4-Fluorocinnamoyl)anthranilic acid (AC14)

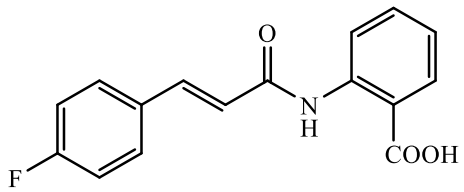

4-Fluorocinnamoyl chloride (**AC14a**) **-** Oxalyl chloride (16 ml; 5 ml g^{-1}) was added to 4-fluorocinnamic acid (3.031 g, 0.0182 mol) and stirred at room temperature for 4 hours with a calcium chloride guard tube. The excess reagent was evaporated under reduced pressure and cooled to room temperature to yield the dark brown hard crystal of 4-fluorocinnamoyl chloride (3.337 g, 99 %); m.p. 44-47 °C. ^{1}H NMR (400 MHz, $CDCl_3$) δ 6.59 (d, *J* = 15.6 Hz, 1H^{6}), 7.10-7.19 (m, 2H^{2}), 7.55-7.64 (m, 2H^{3}), 7.81 (d, *J* = 15.6 Hz, 1H^{5}).

Methyl N-(4-fluorocinnamoyl)anthranilate (**AC14b) -** Quantities: methyl anthranilate (5.236 g, 0.0346 mol), dry pyridine (50 ml) and 4-fluorocinnamoyl chloride (3.039 g, 0.0165 mol). The synthesis procedure was as described for **AC18a**. Product: pale yellow fine crystals (4.205 g, 85 %); m.p. 132-135 °C. ^{1}H NMR (400 MHz, $CDCl_3$) δ 3.96 (s, 3H), 6.55 (d, *J* = 15.5 Hz, 1H), 7.06-7.14 (m, 3H), 7.55-7.62 (m, 3H), 7.72 (d, *J* = 15.5 Hz, 1H), 8.04-8.09 (m, 1H), 8.87 (dd, *J* = 8.6, 1.0 Hz, 1H), 11.38 (br s, 1H); ^{13}C NMR (100 MHz, $CDCl_3$)

δ 52.38, 114.84, 115.95 (d), 120.53, 121.68, 122.57, 129.86 (d), 130.86, 134.77, 140.95, 141.78, 162.45, 164.28, 164.94, 168.93. MS (EI): *m/z* 299 $C_{17}H_{14}O_3NF^{+\bullet}$ ($M^{+\bullet}$), 284 $C_{16}H_{11}O_3NF^{+}$ $(M\text{-}CH_3)^{+}$, 149 $C_9H_6OF^{+}$ $(M\text{-}C_8H_8O_2N)^{+}$, 121 $C_8H_6F^{+}$ $(M\text{-}C_9H_8O_3N)^{+}$. EA (%) $C_{17}H_{14}NO_3F$: calculated C, 68.22: H, 4.71: N, 4.68; found C, 68.12: H, 4.58: N, 4.71.

N-(4-Fluorocinnamoyl)anthranilic acid (**AC14c**) **-** Quantities: methyl *N*-(4-fluorocinnamoyl)anthranilate (2.561 g, 0.00856 mol), THF (100 ml), methanol (20 ml) and aqueous LiOH [~1 M, LiOH (1.694 g) dissolved in H_2O (76 ml)]. The hydrolysis procedure was as described for **AC18b**. Product: white precipitate (2.021 g, 83 %); m.p. 201-203 °C (lit.[282] 200-201.5 °C). ^{1}H NMR (400 MHz, $CDCl_3$--d_6-DMSO) δ 6.56 (d, *J* = 15.4 Hz, 1H), 7.07-7.16 (m, 3H), 7.52-7.63 (m, 3H), 7.68 (d, *J* = 15.4 Hz, 1H), 8.11 (dd, *J* = 8.1, 1.5 Hz, 1H), 8.82 (d, *J* = 8.4 Hz, 1H), 11.72 (br s, 1H); ^{13}C NMR (100 MHz, $CDCl_3$--d_6-DMSO) δ 115.53, 115.62, 115.84, 119.87, 121.82, 122.31, 129.71, 130.73, 131.27, 134.01, 140.25, 141.62, 163.79, 170.31. MS (ESI): *m/z* $[M+H]^+$ 286. EA (%) $C_{16}H_{12}NO_3F$: calculated C, 67.37: H, 4.24: N, 4.91; found C, 67.50: H, 4.05: N, 4.93.

2.2.4.3 *N*-(2-Chlorocinnamoyl)anthranilic acid (AC15)

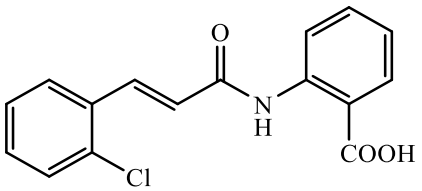

2-Chlorocinnamoyl chloride (**AC15a**) **-** Quantities: oxalyl chloride (16.5 ml) and 2-chlorocinnamic acid (2.777 g, 0.0512 mol). The acylation procedure was as described for **AC14a**, but stirred for 5.5 hours to ensure complete reaction. Product: pale yellow hard crystal (2.973 g, 97 %). ^{1}H NMR (400 MHz, $CDCl_3$) δ 6.66 (d, *J* = 15.6 Hz, 1H), 7.31-7.51 (m, 3H), 7.66 (dd, *J* = 7.8, 1.6 Hz, 1H), 8.30 (d, *J* = 15.6 Hz, 1H).

Methyl N-(2-chlorocinnamoyl)anthranilate (**AC15b**) **-** Quantities: methyl anthranilate (3.376 g, 0.0223 mol), dry pyridine (45 ml) and 2-chlorocinnamoyl chloride (3.189 g, 0.0159 mol). The synthesis procedure was as described for **AC18a**. Product: white fine crystals (4.036 g, 81 %); m.p. 129-131 °C. ^{1}H

NMR (400 MHz, $CDCl_3$) δ 3.96 (s, 3H), 6.62 (d, *J* = 15.7 Hz, 1H), 7.09-7.15 (m, 1H), 7.28-7.34 (m, 2H), 7.41-7.46 (m, 1H), 7.57-7.72 (m, 2H), 8.07 (dd, *J* = 8.0, 1.6 Hz, 1H), 8.17 (d, *J* = 15.7 Hz, 1H), 8.89 (dd, *J* = 8.4, 1.0 Hz, 1H), 11.45 (br s, 1H); ^{13}C NMR (100 MHz, $CDCl_3$) δ 52.39, 114.91, 120.54, 122.67, 124.67, 126.96, 127.60, 130.15, 130.71, 130.86, 132.97, 134.78, 134.97, 138.11, 141.70, 163.95, 168.92. MS (EI): *m/z* 315/317 (3:1) $C_{17}H_{14}O_3NCl^{+\bullet}$ ($M^{+\bullet}$), 280 $C_{17}H_{14}O_3N^+$ $(M\text{-}Cl)^+$, 165 $C_9H_6OCl^+$ $(M\text{-}C_8H_8O_2N)^+$, 137 $C_8H_6Cl^+$ $(M\text{-}C_9H_8O_3N)^+$. EA (%) $C_{17}H_{14}NO_3Cl$: calculated C, 64.67: H, 4.47: N, 4.44; found C, 64.79: H, 4.34: N, 4.47.

N-(2-Chlorocinnamoyl)anthranilic acid (**AC15c**) **-** Quantities: methyl *N*-(2-chlorocinnamoyl)anthranilate (2.590 g, 0.0082 mol), THF (100 ml), methanol (20 ml) and aqueous LiOH [~1 M, LiOH (1.613 g) dissolved in H_2O (72 ml)]. The hydrolysis procedure was as described for **AC18b**. Product: white precipitate (1.935 g, 78 %); m.p. 203-205 °C (lit.[384] 200 °C). ^1H NMR (400 MHz, $CDCl_3$--d_6-DMSO) δ 6.63 (d, *J* = 15.7 Hz, 1H), 7.13 (t, *J* = 7.7 Hz, 1H), 7.29-7.77 (m, 5H), 8.07-8.15 (m, 2H), 8.84 (t, *J* = 8.6 Hz, 1H), 11.83 (br s, 1H); ^{13}C NMR (100 MHz, $CDCl_3$--d_6-DMSO) δ 115.66, 119.98, 122.54, 124.93, 127.10, 127.48, 129.97, 130.74, 131.41, 132.71, 134.20, 134.50, 137.25, 141.67, 163.67, 170.55. MS (ESI): *m/z* $[M+H]^+$ 303. EA (%) $C_{16}H_{12}NO_3Cl$: calculated C, 63.69: H, 4.01: N, 4.64; found C, 63.53: H, 3.84: N, 4.61.

2.2.4.4 *N*-(4-Bromocinnamoyl)anthranilic acid (AC16)

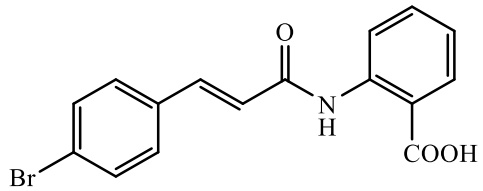

4-Bromocinnamoyl chloride (**AC16a**) **-** Quantities: oxalyl chloride (20 ml) and 4-bromocinnamic acid (3.740 g, 0.0165 mol). The acylation procedure was as described for **AC14a**, but stirred overnight to ensure complete reaction. Product: white precipitate (4.037 g, 100 %). ^1H NMR (400 MHz, $CDCl_3$) δ 6.65 (d, *J* = 15.6 Hz, 1H), 7.45 (dt, *J* = 8.9, 2.1 Hz, 2H), 7.59 (dt, *J* = 8.8, 2.1 Hz, 2H), 7.78 (d, *J* = 15.6 Hz, 1H).

Methyl N-(4-bromocinnamoyl)anthranilate (**AC16b**) **-** Quantities: methyl anthranilate (2.277 g, 0.0151 mol), dry pyridine (40 ml) and 4-bromo cinnamoyl chloride (3.604 g, 0.0147 mol). The synthesis procedure was as described for **AC18a**. Product: white precipitate (4.724 g, 89 %); m.p. 151-154 °C. ^{1}H NMR (400 MHz, $CDCl_3$) δ 3.96 (s, 3H), 6.61 (d, *J* = 15.5 Hz, 1H), 7.09-7.15 (m, 1H), 7.43-7.72 (m, 6H), 8.06 (dd, *J* = 8.0, 1.6 Hz, 1H), 8.86 (dd, *J* = 8.6, 1.0 Hz, 1H), 11.40 (br s, 1H); ^{13}C NMR (100 MHz, $CDCl_3$) δ 52.40, 114.87, 120.54, 122.58, 122.66, 124.14, 129.43, 130.87, 132.05, 133.55, 134.78, 140.88, 141.70, 164.10, 168.93. MS (EI): *m/z* 359/361 (1:1) $C_{17}H_{14}O_3NBr^{+\bullet}$ ($M^{+\bullet}$), 344 $C_{16}H_{11}O_3NBr^{+}$ $(M\text{-}CH_3)^{+}$, 300 $C_{15}H_{11}ONBr^{+}$ $(M\text{-}CO_2CH_3)^{+}$, 209 $C_9H_6OBr^{+}$ $(M\text{-}C_8H_8O_2N)^{+}$, $C_8H_6Br^{+}$ $(M\text{-}C_9H_8O_3N)^{+}$. EA (%) $C_{17}H_{14}NO_3Br$: calculated C, 56.69: H, 3.92: N, 3.89; found C, 56.74: H, 3.70: N, 3.93.

N-(4-Bromocinnamoyl)anthranilic acid (**AC16c**) **-** Quantities: methyl *N*-(4-bromocinnamoyl)anthranilate (2.594 g, 0.0072 mol), THF (100 ml), methanol (20 ml) and aqueous LiOH [~1 M, LiOH (1.475 g) dissolved in H_2O (65 ml)]. The hydrolysis procedure was as described for **AC18b**. Product: pale yellow precipitate (1.919 g, 77 %); m.p. 219-222 °C (lit.[282] 222-225 °C). ^{1}H NMR (400 MHz, $CDCl_3$--d_6-DMSO) δ 6.62 (d, *J* = 15.6 Hz, 1H), 7.12 (t, *J* = 7.7 Hz, 1H), 7.42-7.59 (m, 5H), 7.65 (d, *J* = 15.6 Hz, 1H), 8.11 (dd, *J* = 8.1, 1.5 Hz, 1H), 8.83 (d, *J* = 8.4 Hz, 1H), 11.74 (br s, 1H); ^{13}C NMR (100 MHz, $CDCl_3$--d_6-DMSO) δ 115.62, 119.96, 122.46, 122.83, 123.72, 129.34, 131.35, 131.86, 133.48, 134.11, 140.23, 141.61, 163.73, 170.41. MS (ESI): *m/z* $[M+H]^{+}$ 347. EA (%) $C_{16}H_{12}NO_3Br$: calculated C, 55.51: H, 3.49: N, 4.05; found C, 55.53: H, 3.20: N, 4.09.

2.2.4.5 *N*-(4-Chlorocinnamoyl)anthranilic acid (AC17)

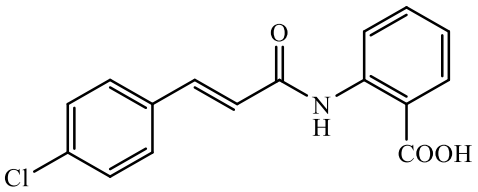

4-Chlorocinnamoyl chloride (**AC17a**) **-** Quantities: oxalyl chloride (16 ml) and 4-chlorocinnamic acid (3.101 g, 0.0170 mol). The acylation procedure was as described for **AC14a**, but stirred for 5 hours to ensure complete reaction.

Product: pale yellow precipitate (3.376 g, 99 %). ^{1}H NMR (400 MHz, $CDCl_3$) δ 6.63 (d, *J* = 15.6 Hz, 1H), 7.43 (dt, *J* = 8.8, 2.1 Hz, 2H), 7.53 (dt, *J* = 8.8, 2.1 Hz, 2H), 7.80 (d, *J* = 15.6 Hz, 1H).

Methyl N-(4-chlorocinnamoyl)anthranilate (**AC17b**) **-** Quantities: methyl anthranilate (2.570 g, 0.0170 mol), dry pyridine (40 ml) and 4-chlorocinnamoyl chloride (3.010 g, 0.0150 mol). The synthesis procedure was as described for **AC18a**. Product: white fine needle-like crystals (4.090 g, 87 %); m.p. 137-140 °C. ^{1}H NMR (400 MHz, $CDCl_3$) δ 3.96 (s, 3H), 6.60 (d, *J* = 15.5 Hz, 1H), 7.09-7.15 (m, 1H), 7.35-7.62 (m, 5H), 7.71 (d, *J* = 15.5 Hz, 1H), 8.06 (dd, *J* = 8.2, 1.6 Hz, 1H), 8.87 (dd, *J* = 8.6, 1.0 Hz, 1H), 11.40 (br s, 1H); ^{13}C NMR (100 MHz, $CDCl_3$) δ 52.39, 114.86, 120.54, 122.48, 122.65, 129.09, 129.20, 130.87, 133.13, 134.78, 135.80, 140.81, 141.72, 164.11, 168.93. MS (EI): *m/z* 315/317 (3:1) $C_{17}H_{14}O_3NCl^{+\bullet}$ ($M^{+\bullet}$), 300 $C_{16}H_{11}O_3NCl^{+}$ $(M-CH_3)^{+}$, 165 $C_9H_6OCl^{+}$ $(M-C_8H_8O_2N)^{+}$, 137 $C_8H_6Cl^{+}$ $(M-C_9H_8O_3N)^{+}$. EA (%) $C_{17}H_{14}NO_3Cl$: calculated C, 64.67: H, 4.47: N, 4.44; found C, 64.76: H, 4.26: N, 4.44.

N-(4-Chlorocinnamoyl)anthranilic acid (**AC17c**) **-** Quantities: methyl *N*-(4-chlorocinnamoylanthranilate (3.131 g, 0.0098 mol), THF (100 ml), methanol (20 ml) and aqueous LiOH [~1 M, LiOH (1.987 g) dissolved in H_2O (90 ml)]. The hydrolysis procedure was as described for **AC18b**. Product: white fine crystals (2.380 g, 80 %); m.p. 218-220 °C (lit.[384] 220 °C). ^{1}H NMR (400 MHz, $CDCl_3$--d_6-DMSO) δ 6.36 (d, *J* = 15.6 Hz, 1H), 6.78-6.85 (m, 1H), 7.03-7.11 (m, 2H), 7.20-7.26 (m, 3H), 7.35 (d, *J* = 15.6 Hz, 1H), 7.84 (dd, *J* = 8.0, 1.4 Hz, 1H), 8.50 (dd, *J* = 8.4, 0.8 Hz, 1H), 11.80 (br s, 1H); ^{13}C NMR (100 MHz, $CDCl_3$--d_6-DMSO) δ 116.50, 118.98, 121.54, 122.28, 128.07, 128.30, 130.64, 132.36, 132.65, 134.38, 139.01, 140.63, 162.93, 170.19. MS (ESI): *m/z* $[M+H]^{+}$ 303. EA (%) $C_{16}H_{12}NO_3Cl$: calculated C, 63.69: H, 4.01: N, 4.64; found C, 63.45: H, 3.95: N, 4.46.

2.2.4.6 *N*-Hydrocinnamoylanthranilic acid (AC21)

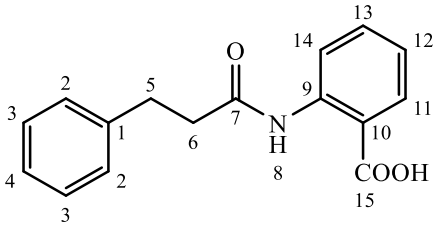

Hydrocinnamoyl chloride - purchased from Aldrich.

Methyl N-hydrocinnamoylanthranilate (**AC21a**) **-** Solution of methyl anthranilate (3.156 g, 0.0209 mol) and dry pyridine (45 ml) was added to hydrocinnamoyl chloride (2.772 g, 0.0164 mol) and stirred for an hour at room temperature. Cold water (250 ml) was added to the mixture and continued stirring for 30 minutes. The viscous brown layer that separated off from water was extracted in diethyl ether (100 ml) and the aqueous layer was washed with more diethyl ether (40 ml). The solvent was evaporated under reduced pressure to yield the brownish-yellow liquid of methyl *N*-hydrocinnamoylanthranilate.

N-Hydrocinnamoylanthranilic acid (**AC21b**) **-** Quantities: methyl *N*-hydro cinnamoylanthranilate (0.0164 mol), THF (100 ml), methanol (20 ml) and aqueous LiOH [~1 M, LiOH (0.987 g) dissolved in H_2O (44 ml)]. The hydrolysis procedure was as described for **AC18b**. Product: white crystals (2.761 g, 63 %); m.p. 138-141 °C (lit.[385] 138.7-139.7 °C). ^{1}H NMR (400 MHz, $CDCl_3$--d_6-DMSO) δ 2.74 (t, J = 7.9 Hz, 2H^5), 3.06 (t, J = 7.9 Hz, 2H^6), 7.07 (t, J = 7.7 Hz, 1H^{12}), 7.16-7.32 (m, 5H^{2,3,4}), 7.51 (t, J = 7.9 Hz, 1H^{13}), 8.06 (d, J = 8.1 Hz, 1H^{14}), 8.69 (d, J = 8.4 Hz, 1H^{11}), 11.44 (br s, 1H^8); ^{13}C NMR (100 MHz, $CDCl_3$--d_6-DMSO) δ 31.21, 39.96, 115.49, 119.91, 122.28, 126.15, 128.27, 128.45, 131.39, 134.20, 140.65, 141.63, 170.47, 170.93. MS (ESI): *m/z* $[M+H]^+$ 270. EA (%) $C_{16}H_{15}NO_3$: calculated C, 71.36: H, 5.61: N, 5.20; found C, 71.56: H, 5.60: N, 5.25.

2.2.4.7 Meldrum's acid

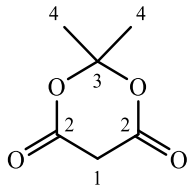

Malonic acid (31.246 g, 0.300 mol) was added to a mixture of acetic anhydride (36.00 ml, 38.283 g, 0.375 mol) and acetone (24.45 ml, 19.166 g, 0.330 mol) with stirring. The mixture was cooled (5-10 °C) in an ice-water bath and concentrated sulfuric acid (0.9 ml, 0.0165 mol) was added. The temperature of the reaction mixture rose to 20 °C and the mixture was left at the temperature for further 10 minutes (during which the malonic acid dissolved completely). The solution was cooled to (-5)-0 °C for 3 hours and during the cooling period the suspension was diluted slowly with water (135 ml) while maintaining the temperature between 0-5 °C, and left further for an hour at 0 °C. The white fine crystals of Meldrum's acid was obtained by vacuum filtration, washed with water and dried.[380] Yield 21.821 g, 50 %. ^{1}H NMR (400 MHz, $CDCl_3$) δ 1.78 (s, 6H^{4}), 3.63 (s, 2H^{1}); ^{13}C NMR (100 MHz, $CDCl_3$) δ 27.65, 36.26, 106.39, 162.87.

2.2.4.8 2-[(Carboxyacetyl)amino]benzoic acid

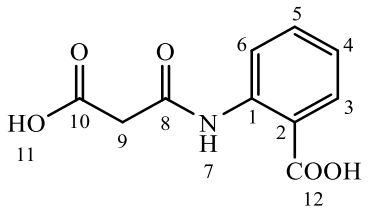

Anthranilic acid (19.890 g, 0.145 mol) was added to a solution of Meldrum's acid (21.821 g, 0.151 mol) in toluene (165 ml), and the reaction mixture was heated under reflux with a Dean-Stark apparatus for 3 hours with gentle stirring. The suspension was cooled to room temperature and the pinkish-white precipitate of 2-[(carboxyacetyl)amino]benzoic acid was collected by vacuum filtration, washed with toluene and dried.[381] Yield 28.357 g, 88 %. ^{1}H NMR (400 MHz, $CDCl_3$--d_6-DMSO) δ 3.41 (s, 2H^{9}), 7.04-7.11 (m, 1H^{4}), 7.46-7.52 (m, 1H^{5}), 8.02 (dd, J = 8.0, 1.6 Hz, 1H^{6}), 8.60 (d, J = 8.4 Hz, 1H^{3}), 11.58 (br s, 1H^{7}); ^{13}C NMR (100 MHz, $CDCl_3$--d_6-DMSO) δ 44.95, 115.99, 119.81, 122.51, 131.04, 133.75, 140.77, 164.36, 168.70, 169.72. MS (ESI): *m/z* $[M+Na]^+$ 246. EA (%) $C_{10}H_9NO_5$: calculated C, 53.82: H, 4.06: N, 6.28; found C, 53.58: H, 3.83: N, 6.17.

2.2.4.9 *N*-(4-Methoxycinnamoyl)anthranilic acid (AC20)

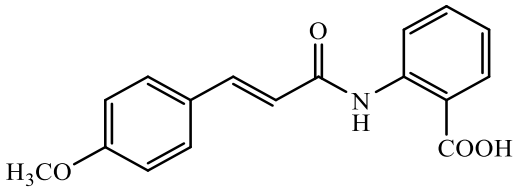

Piperidine (1.56 ml, 0.0156 mol) was added to a mixture of 4-methoxy benzaldehyde (2.119 g, 0.0156 mol) and 2-[(carboxyacetyl)amino]benzoic acid (3.303 g, 0.0148 mol) in toluene (20 ml), and the reaction mixture was heated under reflux with a Dean-Stark apparatus for 4 hours. The solution was cooled to room temperature and stirred for an hour, and the solvent was evaporated under reduced pressure. The viscous, dark brown mixture was dissolved in methanol (5 ml g^{-1}) and water (2 ml g^{-1}) at ~40 °C with stirring. The solution was acidified at room temperature to pH 4 using HCl (1 M, 20 ml) with stirring, and the precipitate was obtained by vacuum filtration, washed with water and dried. The crude product was recrystallised from hot aqueous ethanol (water-ethanol, 1:4) to yield the pale yellow crystals of pure *N*-(4-methoxy cinnamoyl)anthranilic acid (2.460 g, 56 %); m.p. 196-199 °C (lit.[282] 195-198 °C). ^{1}H NMR (400 MHz, $CDCl_3$--d_6-DMSO) δ 3.68 (s, 3H), 6.33 (d, *J* = 15.6 Hz, 1H), 6.73-6.78 (m, 2H), 6.90-6.96 (m, 1H), 7.33-7.42 (m, 3H), 7.51 (d, *J* = 15.6 Hz, 1H), 7.95 (dd, *J* = 8.0, 1.6 Hz, 1H), 8.68 (dd, *J* = 8.5, 0.9 Hz, 1H), 11.48 (br s, 1H); ^{13}C NMR (100 MHz, $CDCl_3$--d_6-DMSO) δ 54.92, 113.85, 115.08, 119.30, 119.70, 121.87, 126.89, 129.14, 131.07, 133.88, 141.07, 141.67, 160.63, 164.31, 170.25. MS (ESI): *m/z* $[M+H]^+$ 298. EA (%) $C_{17}H_{15}NO_4$: calculated C, 68.68: H, 5.09: N, 4.71; found C, 68.40: H, 4.88: N, 4.70.

2.2.4.10 *N*-(3,4-Dimethoxycinnamoyl)anthranilic acid (AC24)

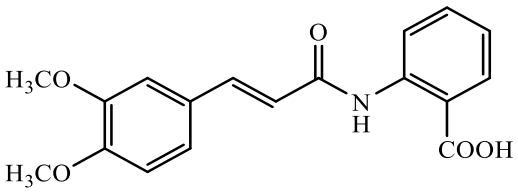

Piperidine (1.53 ml, 0.0153 mol) was added to a mixture of 3,4-dimethoxy benzaldehyde (2.548 g, 0.0153 mol) and 2-[(carboxyacetyl)amino]benzoic acid

(3.303 g, 0.0148 mol) in toluene (20 ml), and the reaction mixture was heated under reflux with a Dean-Stark apparatus for 4 hours. The solution was cooled to room temperature and stirred vigourously for an hour. The precipitate was obtained by vacuum filtration, washed with little toluene and dried. The rest of the synthesis procedure was as described for **AC20**. Product: yellowish-white precipitate (3.035 g, 62 %); m.p. 195-198 °C (lit.[381] 208-209 °C). ^{1}H NMR (400 MHz, $CDCl_3$--d_6-DMSO) δ 3.91 (s, 3H), 3.95 (s, 3H), 6.51 (d, *J* = 15.7 Hz, 1H), 6.91 (d, *J* = 8.1 Hz, 1H), 7.08-7.20 (m, 3H), 7.52-7.67 (m, 2H), 8.09 (dd, *J* = 7.9, 1.3 Hz, 1H), 8.82 (d, *J* = 8.8 Hz, 1H), 11.65 (br s, 1H); ^{13}C NMR (100 MHz, $CDCl_3$--d_6-DMSO) δ 55.74, 55.79, 109.54, 111.05, 115.42, 119.73, 119.89, 122.15, 122.38, 127.36, 131.28, 134.04, 141.58, 141.84, 148.94, 150.62, 164.31, 170.37. MS (ESI): *m/z* $[M+H]^+$ 328. EA (%) $C_{18}H_{17}NO_5.H_2O$: calculated C, 62.60: H, 5.55: N, 4.06; found C, 62.48: H, 5.45: N, 4.04.

2.2.4.11 *N*-(2-Methoxycinnamoyl)anthranilic acid (AC26)

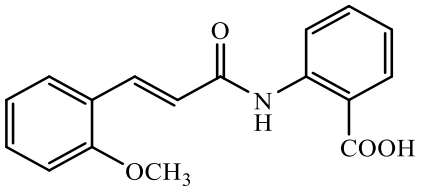

Piperidine (1.54 ml, 0.0154 mol) was added to a mixture of 2-methoxy benzaldehyde (2.104 g, 0.0154 mol) and 2-[(carboxyacetyl)amino]benzoic acid (3.303 g, 0.0148 mol) in toluene (20 ml), and the reaction mixture was heated under reflux with a Dean-Stark apparatus for 4 hours. The solution was cooled to room temperature and stirred vigorously for an hour. The precipitate was obtained by vacuum filtration, washed with little toluene and dried. The obtained piperidinium salt was dissolved in methanol (5 ml g^{-1}) and water (2 ml g^{-1}) at ~40 °C with stirring. The solution was acidified at room temperature to pH 4 using HCl (1 M, 20 ml) with stirring, and the precipitate was obtained by vacuum filtration, washed with water and dried. The crude product was purified by dissolving the precipitate in aqueous NaOH (2 M, 20 ml) at ~40 °C during which the precipitate dissolved completely, and was washed with DCM. The aqueous carboxylate layer was extracted and acidified to pH 4 using HCl (1 M, 16 ml) with stirring. The precipitate was obtained by vacuum filtration,

washed with lots of water and dried to yield the yellowish-white precipitate of pure *N*-(2-methoxycinnamoyl)anthranilic acid (2.744 g, 62 %); m.p. 212-215 °C. ^{1}H NMR (400 MHz, $CDCl_3$--d_6-DMSO) δ 3.92 (s, 3H), 6.69 (d, *J* = 15.7 Hz, 1H), 6.93-7.14 (m, 3H), 7.37 (t, *J* = 7.9 Hz, 1H), 7.51-7.60 (m, 2H), 7.99 (d, *J* = 15.7 Hz, 1H), 8.09 (d, *J* = 7.7 Hz, 1H), 8.82 (d, *J* = 8.4 Hz, 1H), 11.68 (br s, 1H); ^{13}C NMR (100 MHz, $CDCl_3$--d_6-DMSO) δ 55.34, 111.07, 115.55, 119.80, 120.50, 122.12, 122.35, 123.13, 128.28, 131.09, 131.24, 133.93, 136.84, 141.78, 157.89, 164.46, 170.31. MS (ESI): *m/z* $[M+Na]^+$ 320. EA (%) $C_{17}H_{15}NO_4$: calculated C, 68.68: H, 5.09: N, 4.71; found C, 68.42: H, 4.94: N, 4.71.

2.2.4.12 *N*-(3-Ethoxy-4-hydroxycinnamoyl)anthranilic acid (AC27)

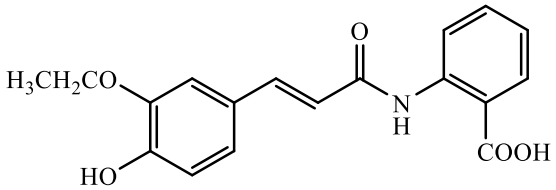

Quantities: piperidine (1.53 ml, 0.0153 mol), 3-ethoxy-4-hydroxy benzaldehyde (2.552 g, 0.0153 mol), 2-[(carboxyacetyl)amino]benzoic acid (3.310 g, 0.0148 mol) and toluene (20 ml). The synthesis procedure was as described for **AC26**. Product: pale yellow precipitate (3.443 g, 71 %); m.p. 193-195 °C. ^{1}H NMR (400 MHz, d_6-DMSO) δ 1.48 (t, *J* = 7.0 Hz, 3H), 4.24 (q, *J* = 7.0 Hz, 2H), 6.78-6.99 (m, 2H), 7.22-7.35 (m, 2H), 7.45 (d, *J* = 1.5 Hz, 1H), 7.62-7.78 (m, 2H), 8.13 (dd, *J* = 8.1, 1.1 Hz, 1H), 8.76 (d, *J* = 8.4 Hz, 1H), 9.63 (br s, 1H), 11.40 (br s, 1H); ^{13}C NMR (100 MHz, d_6-DMSO) δ 15.29, 64.50, 113.11, 126.21, 117.05, 119.37, 120.85, 123.15, 123.32, 126.50, 131.71, 134.57, 141.74, 142.62, 147.63, 149.78, 164.88, 170.07. MS (ESI): *m/z* $[M+Na]^+$ 350. EA (%) $C_{18}H_{17}NO_5.H_2O$: calculated C, 62.60: H, 5.55: N, 4.06; found C, 62.82: H, 5.42: N, 4.02.

2.2.4.13 *N*-(3,4-Dihydroxycinnamoyl)anthranilic acid (AC28)

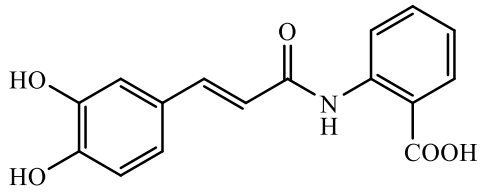

3,4-Diacetoxycinnamic acid (**AC28a**) **-** 3,4-Dihydroxycinnamic acid (2.644 g, 0.0148 mol) was added to a solution of acetic anhydride (40 ml) and pyridine (2.5 ml), and stirred at room temperature overnight. Cold water (~50 ml) was added to the mixture and stirred for 5-10 minutes with cooling. The white precipitate of 3,4-diacetoxycinnamic acid was obtained by vacuum filtration, washed with cold water and dried. Yield 3.472 g, 89 %. ^{1}H NMR (400 MHz, $CDCl_3$--d_6-DMSO) δ 2.31 (s, 6H), 6.38 (d, *J* = 16.1 Hz, 1H), 7.23 (d, *J* = 8.4 Hz, 1H), 7.35-7.47 (m, 2H), 7.54-7.63 (m, 1H); ^{13}C NMR (100 MHz, $CDCl_3$--d_6-DMSO) δ 19.72, 19.74, 119.39, 121.73, 123.07, 125.35, 132.43, 141.41, 141.54, 142.45, 166.99, 167.09, 167.12.

3,4-Diacetoxycinnamoyl chloride (**AC28b**) **-** Quantities: oxalyl chloride (17 ml) and 3,4-diacetoxycinnamic acid (3.205 g, 0.0121 mol). The acylation procedure was as described for **AC14a**. Product: off-white crystals (3.231 g, 94 %). ^{1}H NMR (400 MHz, $CDCl_3$) δ 2.32 (s, 6H), 6.59 (d, *J* = 15.6 Hz, 1H), 7.26-7.31 (m, 1H), 7.41-7.49 (m, 2H), 7.77 (d, *J* = 15.6 Hz, 1H); ^{13}C NMR (100 MHz, $CDCl_3$) δ 20.59, 20.65, 123.39, 123.68, 124.33, 127.42, 131.68, 142.68, 144.84, 148.44, 165.85, 167.75, 167.95.

Methyl N-(3,4-diacetoxycinnamoyl)anthranilate (**AC28c**) **-** Quantities: methyl anthranilate (2.000 g, 0.0132 mol), dry pyridine (45 ml) and 3,4-diacetoxy cinnamoyl chloride (3.100 g, 0.011 mol). The synthesis procedure was as described for **AC18a**. Product: pale yellow fine crystals (2.837 g, 65 %); m.p. 165-167 °C. ^{1}H NMR (400 MHz, $CDCl_3$) δ 2.32 (s, 6H), 3.96 (s, 3H), 6.56 (d, *J* = 15.6 Hz, 1H), 7.07-7.15 (m, 1H), 7.21-7.27 (m, 1H), 7.40-7.48 (m, 2H), 7.54-7.62 (m, 1H), 7.69 (d, *J* = 15.6 Hz, 1H), 8.06 (dd, *J* = 8.2, 1.6 Hz, 1H), 8.86 (dd, *J* = 8.6, 1.0 Hz, 1H), 11.40 (s, 1H); ^{13}C NMR (100 MHz, $CDCl_3$) δ 20.59, 20.64, 52.39, 114.90, 120.54, 122.53, 122.67, 123.04, 123.86, 126.49, 130.86, 133.56, 134.77, 140.34, 141.68, 142.39, 143.24, 163.94, 168.01,

168.10, 168.92. MS (ESI): *m/z* $[M+H]^+$ 398. EA (%) $C_{21}H_{19}NO_5$: calculated C, 63.47: H, 4.82: N, 3.52; found C, 63.69: H, 4.62: N, 3.53.

N-(3,4-Dihydroxycinnamoyl)anthranilic acid (**AC28d**) **-** Quantities: methyl *N*-(3,4-diacetoxycinnamoyl)anthranilate (2.500 g, 0.0063 mol), THF (100 ml), methanol (20 ml) and aqueous LiOH [~1 M, LiOH (3.826 g) dissolved in H_2O (172 ml)]. The hydrolysis procedure was as described for **AC18b**. Product: brownish-white precipitate (1.387 g, 74 %); m.p. 233-235 °C (lit.[386] 221-230 °C). ^{1}H NMR (400 MHz, d_6-DMSO) δ 6.58 (d, *J* = 15.5 Hz, 1H), 6.84 (d, *J* = 8.2 Hz, 1H), 7.07 (d, *J* = 8.2 Hz, 1H), 7.13-7.26 (m, 2H), 7.51 (d, *J* = 15.5 Hz, 1H), 7.66 (t, *J* = 7.9 Hz, 1H), 8.06 (dd, *J* = 7.8 Hz, 1H), 8.66 (d, *J* = 8.4 Hz, 1H), 9.22 (br s, 1H), 9.62 (br s, 1H), 11.32 (br s, 1H); ^{13}C NMR (100 MHz, d_6-DMSO) δ 114.58, 115.79, 116.66, 118.48, 120.29, 121.20, 122.63, 125.89, 131.15, 134.01, 141.10, 141.94, 145.60, 148.02, 164.19, 169.54. MS (ESI): *m/z* $[M+H]^+$ 300. EA (%) $C_{16}H_{13}NO_5.2H_2O$: calculated C, 57.31: H, 5.11: N, 4.18; found C, 57.32: H, 5.00: N, 4.15.

2.2.4.14 *N*-(4-Hydroxycinnamoyl)anthranilic acid (AC30)

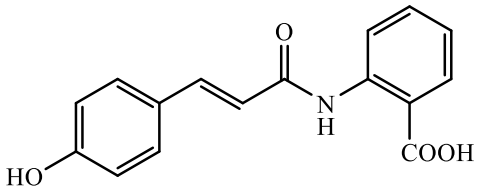

4-Acetoxycinnamic acid (**AC30a**) **-** Quantities: 4-hydroxycinnamic acid (4.000 g, 0.0244 mol), acetic anhydride (25 ml) and pyridine (1 ml). The acetylation procedure was as described for **AC28a**. Product: white precipitate (4.571 g, 91 %). ^{1}H NMR (400 MHz, $CDCl_3$--d_6-DMSO) δ 2.28 (s, 3H), 6.35 (d, *J* = 15.9 Hz, 1H), 7.04-7.18 (m, 2H), 7.46-7.84 (m, 3H).

4-Acetoxycinnamoyl chloride (**AC30b**) **-** Quantities: oxalyl chloride (20 ml) and 4-acetoxycinnamic acid (4.000 g, 0.0194 mol). The acylation procedure was as described for **AC14a**, but stirred for ~4.5 hours to ensure complete reaction. Product: pale yellow precipitate (4.070 g, 93 %). ^{1}H NMR (400 MHz, $CDCl_3$) δ 2.34 (s, 3H), 6.62 (d, *J* = 15.5 Hz, 1H), 7.17-7.23 (m, 2H), 7.58-7.64

(m, 2H), 7.82 (d, J = 15.5 Hz, 1H); ^{13}C NMR (100 MHz, $CDCl_3$) δ 21.12, 122.42, 122.52, 130.29, 130.63, 149.41, 153.39, 166.01, 168.88.

Methyl N-(4-acetoxycinnamoyl)anthranilate (**AC30c**) **-** Quantities: methyl anthranilate (2.419 g, 0.0160 mol), dry pyridine (45 ml) and 4-acetoxycinnamoyl chloride (3.500 g, 0.0156 mol). The synthesis procedure was as described for **AC18a**. Product: orangish-white precipitate (4.459 g, 84 %); m.p. 145-147 °C. ^{1}H NMR (400 MHz, $CDCl_3$) δ 2.33 (s, 3H), 3.97 (s, 3H), 6.59 (d, J = 15.5 Hz, 1H), 7.09-7.17 (m, 3H), 7.57-7.64 (m, 3H), 7.74 (d, J = 15.5 Hz, 1H), 8.07 (dd, J = 8.2, 1.4 Hz, 1H), 8.88 (dd, J = 8.5, 0.9 Hz, 1H), 11.39 (br s, 1H); ^{13}C NMR (100 MHz, $CDCl_3$) δ 21.13, 52.39, 114.88, 120.56, 122.07, 122.10, 122.58, 129.17, 130.87, 132.40, 134.78, 141.15, 141.80, 151.84, 164.30, 168.94, 169.18. MS (ESI): *m/z* $[M+H]^+$ 340. EA (%) $C_{19}H_{17}NO_5$: calculated C, 67.25: H, 5.05: N, 4.13; found C, 67.17: H, 5.02: N, 4.26.

N-(4-Hydroxycinnamoyl)anthranilic acid (**AC30d**) **-** Quantities: methyl *N*-(4-acetoxycinnamoyl)anthranilate (2.518 g, 0.0074 mol), THF (100 ml), methanol (20 ml) and aqueous LiOH [~1 M, LiOH (2.990 g) dissolved in H_2O (134 ml)]. The hydrolysis procedure was as described for **AC18b**. Product: yellowish-white precipitate (1.744 g, 83 %); m.p. 230-232 °C (lit.[282] 220.5-221.5 °C). ^{1}H NMR (400 MHz, $CDCl_3$--d_6-DMSO) δ 6.42 (d, J = 15.5 Hz, 1H), 6.80-6.86 (m, 2H), 7.04-7.11 (m, 1H), 7.39-7.45 (m, 2H), 7.49-7.61 (m, 2H), 8.05 (dd, J = 8.0, 1.6 Hz, 1H), 8.77 (d, J = 7.5 Hz, 1H), 9.56 (br s, 1H), 11.58 (br s, 1H); ^{13}C NMR (100 MHz, $CDCl_3$--d_6-DMSO) δ 114.38, 114.78, 117.31, 118.73, 120.99, 124.43, 128.50, 130.19, 132.90, 140.67, 140.82, 158.41, 163.41, 169.21. MS (ESI): *m/z* $[M+H]^+$ 284. EA (%) $C_{16}H_{13}NO_4$: calculated C, 67.84: H, 4.63: N, 4.94; found C, 67.63: H, 4.83: N, 4.94.

2.2.4.15 *N*-Cinnamoylpipecolinic acid (AC34)

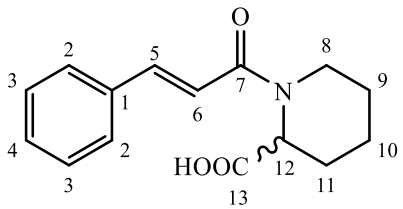

R,S-Pipecolinic acid (4.320 g, 0.0334 mol) was dissolved in NaOH (1 M, 70 ml) and cooled in an ice-water bath, and cinnamoyl chloride (4.284 g, 0.0257 mol) dissolved in diethyl ether (15 ml) was added. The reaction mixture was stirred vigorously for 1.5 hours with cooling, then at room temperature for further 3 hours. The solution was washed with diethyl ether (20 ml) and the aqueous layer was acidified to pH 1 using HCl (6 M). The precipitate was obtained by vacuum filtration and dissolved in DCM. The filtrate was extracted in more DCM (30 ml). The combined organic solutions were dried over anhydrous sodium sulfate, filtered and solvent evaporated under reduced pressure. The precipitate was recrystallised from hot ethanol to yield the product as pale yellow crystals (2.118 g, 31 %); m.p. 186-188 °C. ^{1}H NMR (400 MHz, $CDCl_3$--d_6-DMSO) δ 1.05-1.92 (m, 5H^{9,10,11}), 2.33 (m, 1H^{11}), 2.81, 3.40 (m, 1H^{8}), 4.07, 4.58 (m, 1H^{8}), 4.89, 5.40 (m, 1H^{12}), 6.87-7.13 (m, 1H^{5}), 7.28-7.45 (m, 3H^{3,4}), 7.49-7.73 (m, 3H^{2,6}); ^{13}C NMR (100 MHz, d_6-DMSO) δ 20.00, 24.50, 25.72, 26.36, 42.55, 51.19, 116.73, 126.69, 127.76, 128.53, 134.16, 141.00, 141.29, 165.38, 172.00. MS (ESI): *m/z* $[M+H]^+$ 260. EA (%) $C_{15}H_{17}NO_3$: calculated C, 69.48: H, 6.61: N, 5.40; found C, 69.59: H, 6.83: N, 5.41.

2.2.4.16 *N*-Cinnamoylproline (AC36)

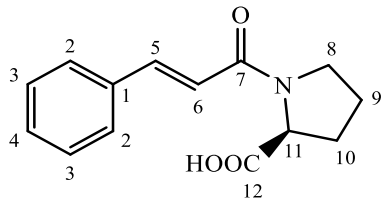

Quantities: *S*-proline (3.456 g, 0.0333 mol) and cinnamoyl chloride (4.284 g, 0.0257 mol). The synthesis procedure was as described for **AC34**. Product: white crystals (2.983 g, 47 %); m.p. 179-181 °C (lit.[382] 178.5-180 °C). ^{1}H NMR (400 MHz, $CDCl_3$--d_6-DMSO) δ 1.91-2.40 (m, 4H^{9,10}), 3.58-3.90 (m, 2H^{8}), 4.58 (m, 1H^{11}), 6.82 (d, J = 15.5 Hz, 1H^{5}), 7.32-7.43 (m, 3H^{3,4}), 7.46-7.58 (m, 2H^{2}), 7.57-7.69 (m, 1H^{6}); ^{13}C NMR (100 MHz, d_6-DMSO) δ 21.68, 23.73, 28.05, 30.28, 45.69, 46.05, 58.15, 58.30, 117.50, 117.79, 126.82, 126.90, 127.86, 128.70, 128.79, 133.98, 134.04, 140.65, 141.20, 163.65, 163.94, 172.83, 173.28. MS (ESI): *m/z* $[M+H]^+$ 246. EA (%) $C_{14}H_{15}NO_3$: calculated C, 68.56: H, 6.16: N, 5.71; found C, 68.82: H, 6.26: N, 5.77.

2.2.4.17 Methyl *N*-(3-phenoxypropionoyl)anthranilate (AC35)

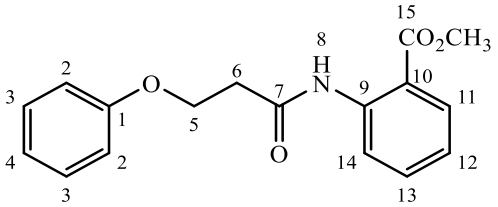

3-Phenoxypropionoyl chloride (**AC35a**) **-** Quantities: oxalyl chloride (15 ml) and 3-phenoxypropionic acid (3.009 g, 0.0181 mol). The acylation procedure was as described for **AC14a**. Product: brownish-yellow liquid (3.340 g, 100 %). ^{1}H NMR (400 MHz, $CDCl_3$--d_6-DMSO) δ 2.70-3.01 (m, 2H^{6}), 4.19-4.29 (m, 2H^{5}), 6.85-6.98 (m, 3H^{3,4}), 7.22-7.31 (m, 2H^{2}).

Methyl N-(3-phenoxypropionoyl)anthranilate (**AC35b**) **-** Quantities: methyl anthranilate (2.563 g, 0.0170 mol), dry pyridine (40 ml) and 3-phenoxy propionoyl chloride (3.004 g, 0.0162 mol). The synthesis procedure was as described for **AC18a**. Product: pale brown fine crystals (3.151 g, 65 %); m.p. 89-91 °C (lit.[387] 88-89 °C). ^{1}H NMR (400 MHz, $CDCl_3$) δ 2.92 (t, *J* = 6.2 Hz, 2H^{6}), 3.93 (s, 3H, CH_3), 4.37 (t, *J* = 6.2 Hz, 2H^{5}), 6.92-6.97 (m, 3H^{3,4}), 7.07-7.12 (m, 1H^{12}), 7.25-7.30 (m, 2H^{2}), 7.52-7.57 (m, 1H^{13}), 8.03 (dd, *J* = 8.1, 1.7 Hz, 1H^{14}), 8.73 (dd, *J* = 8.5, 0.9 Hz, 1H^{11}), 11.26 (br s, 1H^{8}); ^{13}C NMR (100 MHz, $CDCl_3$) δ 38.62, 52.33, 63.68, 114.64, 115.07, 120.53, 120.96, 122.60, 129.39, 130.77, 134.62, 141.31, 158.50, 168.60, 169.30. MS (ESI): *m/z* $[M+H]^+$ 300. EA (%) $C_{17}H_{17}NO_4$: calculated C, 68.22: H, 5.72: N, 4.68; found C, 68.48: H, 5.75: N, 4.78.

2.2.4.18 *N*-(4-Methylcinnamoyl)anthranilic acid (AC39)

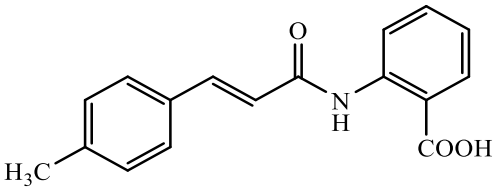

4-Methylcinnamoyl chloride (**AC39a**) **-** Quantities: oxalyl chloride (20 ml) and 4-methylcinnamic acid (4.026 g, 0.0248 mol). The acylation procedure was as described for **AC14a**. Product: white crystals (4.341 g, 97 %). ^{1}H NMR (400 MHz, $CDCl_3$) δ 2.41 (s, 3H), 6.60 (d, *J* = 15.5 Hz, 1H), 7.22-7.27 (m, 2H), 7.45-7.50 (m, 2H), 7.82 (d, *J* = 15.5 Hz, 1H).

Methyl N-(4-methylcinnamoyl)anthranilate (**AC39b**) - Quantities: methyl anthranilate (3.818 g, 0.0253 mol), dry pyridine (70 ml) and 4-methyl cinnamoyl chloride (3.806 g, 0.0211 mol). The synthesis procedure was as described for **AC18a**, but stirred overnight. Product: white crystals (5.552 g, 89 %); m.p. 120-122 °C. ^{1}H NMR (400 MHz, $CDCl_3$) δ 2.38 (s, 3H), 3.95 (s, 3H), 6.58 (d, *J* = 15.5 Hz, 1H), 7.07-7.12 (m, 1H), 7.20 (d, *J* = 8.0 Hz, 2H), 7.49 (d, *J* = 8.2 Hz, 2H), 7.55-7.61 (m, 1H), 7.73 (d, *J* = 15.5 Hz, 1H), 8.05 (dd, *J* = 8.2, 1.4 Hz, 1H), 8.88 (dd, *J* = 8.6, 1.0 Hz, 1H), 11.34 (br s, 1H); ^{13}C NMR (100 MHz, $CDCl_3$) δ 21.43, 52.34, 114.80, 120.54, 120.86, 122.42, 128.04, 129.56, 130.83, 131.89, 134.73, 140.33, 141.92, 142.24, 164.68, 168.91. MS (ESI): *m/z* $[M+H]^+$ 296. EA (%) $C_{18}H_{17}NO_3$: calculated C, 73.20: H, 5.80: N, 4.74; found C, 73.46: H, 6.01: N, 4.86.

N-(4-Methylcinnamoyl)anthranilic acid (**AC39c**) - Quantities: methyl *N*-(4-methylcinnamoyl)anthranilate (4.004 g, 0.0135 mol), THF (100 ml), methanol (20 ml) and aqueous LiOH [~1 M, LiOH (2.746 g) dissolved in H_2O (124 ml)]. The hydrolysis procedure was as described for **AC18b**. Product: white crystals (3.352 g, 88 %); m.p. 220-222 °C (lit.[282] 210.5-213 °C). ^{1}H NMR (400 MHz, $CDCl_3$--d_6-DMSO) δ 2.38 (s, 3H), 6.59 (d, *J* = 15.5 Hz, 1H), 7.07-7.14 (m, 1H), 7.22 (d, *J* = 8.0 Hz, 2H), 7.46-7.67 (m, 4H), 8.07 (dd, *J* = 8.0, 1.4 Hz, 1H), 8.79 (d, *J* = 7.8 Hz, 1H), 11.65 (br s, 1H); ^{13}C NMR (100 MHz, $CDCl_3$--d_6-DMSO) δ 20.03, 114.43, 118.67, 119.80, 121.06, 126.62, 128.26, 130.06, 130.39, 132.78, 138.80, 140.28, 140.51, 162.83, 169.03. MS (ESI): *m/z* $[M+H]^+$ 282. EA (%) $C_{17}H_{15}NO_3$: calculated C, 72.58: H, 5.37: N, 4.98; found C, 72.58: H, 5.49: N, 5.00.

2.2.4.19 *N*-(4-Trifluoromethylcinnamoyl)anthranilic acid (AC40)

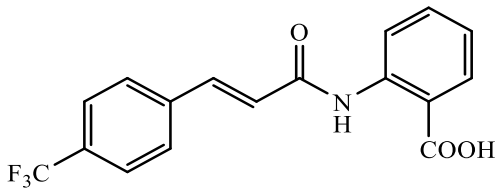

4-Trifluoromethylcinnamoyl chloride (**AC40a**) - Quantities: oxalyl chloride (20 ml) and 4-trifluoromethylcinnamic acid (4.005 g, 0.0185 mol). The acylation procedure was as described for **AC14a**, but stirred overnight.

Product: yellowish-white fine crystals (4.151 g, 96 %). ^{1}H NMR (400 MHz, $CDCl_3$) δ 6.73 (d, *J* = 15.6 Hz, 1H), 7.67-7.73 (m, 4H), 7.85 (d, *J* = 15.6 Hz, 1H).

Methyl N-(4-trifluoromethylcinnamoyl)anthranilate (**AC40b**) - Quantities: methyl anthranilate (3.050 g, 0.0202 mol), dry pyridine (70 ml) and 4-trifluoro methylcinnamoyl chloride (3.710 g, 0.0158 mol). The synthesis procedure was as described for **AC18a**, but stirred overnight. Product: white crystals (4.938 g, 89 %); m.p. 170-172 °C. ^{1}H NMR (400 MHz, $CDCl_3$) δ 3.97 (s, 3H), 6.70 (d, *J* = 15.7 Hz, 1H), 7.10-7.16 (m, 1H), 7.57-7.79 (m, 6H), 8.07 (dd, *J* = 8.1, 1.5 Hz, 1H), 8.87 (dd, *J* = 8.5, 0.9 Hz, 1H), 11.46 (br s, 1H); ^{13}C NMR (100 MHz, $CDCl_3$) δ 52.43, 114.97, 120.59, 122.52, 122.83, 124.43, 125.22, 125.81 (q, CF_3), 128.16, 130.91, 131.29, 131.61, 134.83, 138.05, 140.43, 141.60, 163.75, 168.98. MS (ESI): *m/z* $[M+H]^+$ 350. EA (%) $C_{18}H_{14}NO_3F_3$: calculated C, 61.89: H, 4.04: N, 4.01; found C, 62.09: H, 4.16: N, 3.81.

N-(4-Trifluoromethylcinnamoyl)anthranilic acid (**AC40c**) - Quantities: methyl *N*-(4-trifluoromethylcinnamoyl)anthranilate (3.514 g, 0.01 mol), THF (100 ml), methanol (20 ml) and aqueous LiOH [~1 M, LiOH (2.031 g) dissolved in H_2O (91 ml)]. The hydrolysis procedure was as described for **AC18b**. Product: white fine crystals (2.385 g, 71 %); m.p. 233-235 °C. ^{1}H NMR (400 MHz, $CDCl_3$--d_6-DMSO) δ 6.76 (d, *J* = 15.5 Hz, 1H), 7.10-7.16 (m, 1H), 7.53-7.60 (m, 1H), 7.65-7.78 (m, 5H), 8.09 (dd, *J* = 8.0, 1.6 Hz, 1H), 8.79 (dd, *J* = 8.4, 1.0 Hz, 1H), 11.77 (br s, 1H); ^{13}C NMR (100 MHz, $CDCl_3$--d_6-DMSO) δ 115.04, 119.34, 121.75, 121.93, 124.04, 124.46, 124.93, 127.39, 129.99, 130.31, 130.70, 133.47, 137.38, 139.10, 140.86, 162.73, 169.79. MS (ESI): *m/z* $[M+H]^+$ 336. EA (%) $C_{17}H_{12}NO_3F_3$: calculated C, 60.90: H, 3.61: N, 4.18; found C, 60.51: H, 3.36: N, 4.18.

2.2.4.20 *N*-(4-Nitrocinnamoyl)anthranilic acid (AC41)

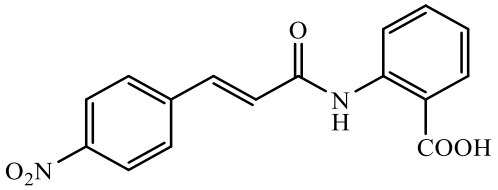

4-Nitrocinnamoyl chloride (**AC41a**) - Quantities: oxalyl chloride (20 ml), 4-nitrocinnamic acid (4.015 g, 0.0208 mol) and dry DMF (a drop). The acylation procedure was as described for **AC14a**, but stirred for 24 hours with slight heating (~50 °C). Product: pale yellow fine crystals (4.227 g, 96 %). ^{1}H NMR (400 MHz, $CDCl_3$) δ 6.78 (d, *J* = 15.6 Hz, 1H), 7.73-7.79 (m, 2H), 7.87 (d, *J* = 15.6 Hz, 1H), 8.27-8.34 (m, 2H); ^{13}C NMR (100 MHz, $CDCl_3$) δ 124.37, 126.36, 129.59, 138.79, 146.91, 149.34, 165.64.

Methyl N-(4-nitrocinnamoyl)anthranilate (**AC41b**) - Quantities: methyl anthranilate (3.050 g, 0.0202 mol), dry pyridine (100 ml) and 4-nitrocinnamoyl chloride (3.557 g, 0.0160 mol). The synthesis procedure was as described for **AC18a**, but stirred overnight with heating (~125 °C) for initial 2 hours. The crude product was recrystallised from a mixture of hot DCM-ethanol (2:1). Product: yellow crystals (4.245 g, 81 %); m.p. 239-241 °C. ^{1}H NMR (400 MHz, $CDCl_3$) δ 3.96 (s, 3H), 6.72 (d, *J* = 15.7 Hz, 1H), 7.10-7.16 (m, 1H), 7.56-7.62 (m, 1H), 7.68-7.80 (m, 3H), 8.07 (dd, *J* = 8.1, 1.5 Hz, 1H), 8.22-8.27 (m, 2H), 8.84 (d, *J* = 8.4 Hz, 1H), 11.44 (br s, 1H); ^{13}C NMR (100 MHz, $CDCl_3$, 55 °C) δ 52.43, 115.17, 120.70, 123.03, 124.17, 126.32, 128.60, 130.97, 134.86, 139.78, 140.97, 141.54, 148.44, 163.29, 169.03. MS (ESI): *m/z* $[M+H]^+$ 327. EA (%) $C_{17}H_{14}N_2O_5$: calculated C, 62.57: H, 4.32: N, 8.59; found C, 62.69: H, 4.34: N, 8.61.

N-(4-Nitrocinnamoyl)anthranilic acid (**AC41c**) - Quantities: methyl *N*-(4-nitrocinnamoyl)anthranilate (3.100 g, 0.0095 mol), THF (100 ml), methanol (20 ml) and aqueous LiOH [~1 M, LiOH (1.926 g) dissolved in H_2O (86 ml)]. The hydrolysis procedure was as described for **AC18b**, but stirred with heating (~100 °C). Product: dark yellow precipitate (2.805 g, 95 %); m.p. >305 °C (decomposed). ^{1}H NMR (400 MHz, d_6-DMSO) δ 6.98-7.09 (m, 2H), 7.35-7.42 (m, 1H), 7.72 (d, *J* = 15.7 Hz, 1H), 8.01-8.11 (m, 3H), 8.30 (d, *J* = 8.4 Hz, 2H), 8.64 (d, *J* = 8.2 Hz, 1H); ^{13}C NMR (100 MHz, d_6-DMSO) δ 118.61, 121.84, 124.00, 125.07, 128.21, 128.98, 130.09, 131.26, 137.13, 140.66, 141.42, 147.55, 162.46, 169.25. EA (%) $C_{16}H_{12}N_2O_5$.1¼H_2O: calculated C, 57.40: H, 4.37: N, 8.37; found C, 57.13: H, 3.87: N, 8.30.

2.2.4.21 *N*-(α-Phenylcinnamoyl)anthranilic acid (AC42)

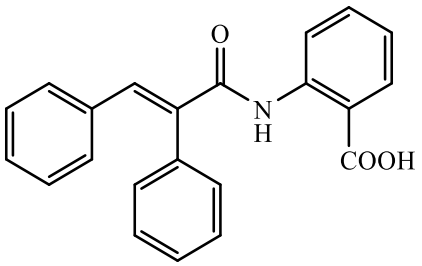

α-Phenylcinnamoyl chloride (**AC42a**) - Quantities: oxalyl chloride (25 ml) and α-phenylcinnamic acid (3.092 g, 0.0138 mol). The acylation procedure was as described for **AC14a**. Product: pale orange hard crystal (3.251 g, 97 %). ^{1}H NMR (400 MHz, $CDCl_3$) δ 7.00-7.13 (m, 2H), 7.16-7.54 (m, 8H), 8.11 (s, 1H).

Methyl N-(α-phenylcinnamoyl)anthranilate (**AC42b**) - Quantities: methyl anthranilate (2.134 g, 0.0141 mol), dry pyridine (50 ml) and α-phenyl cinnamoyl chloride (3.106 g, 0.0128 mol). The synthesis procedure was as described for **AC18a**, but stirred for 2 hours with slight heating (~50 °C). Product: white fine crystals (3.836 g, 84 %); m.p. 129-132 °C. ^{1}H NMR (400 MHz, $CDCl_3$) δ 3.67 (s, 3H), 7.02-7.22 (m, 6H), 7.32-7.38 (m, 2H), 7.46-7.58 (m, 4H), 7.90-7.95 (m, 2H), 8.88 (dd, *J* = 8.6, 1.0 Hz, 1H), 10.75 (br s, 1H); ^{13}C NMR (100 MHz, $CDCl_3$) δ 51.94, 116.08, 120.82, 122.69, 128.15, 128.60, 128.70, 129.48, 130.21, 130.52, 130.76, 134.21, 134.99, 135.30, 136.08, 138.07, 141.09, 166.55, 167.64. MS (ESI): *m/z* $[M+H]^+$ 358. EA (%) $C_{23}H_{19}NO_3$: calculated C, 77.29: H, 5.36: N, 3.92; found C, 77.48: H, 5.33: N, 3.98.

N-(α-Phenylcinnamoyl)anthranilic acid (**AC42c**) - Quantities: methyl *N*-(α-phenylcinnamoyl)anthranilate (2.515 g, 0.0070 mol), THF (100 ml), methanol (20 ml) and aqueous LiOH [~1 M, LiOH (1.419 g) dissolved in H_2O (64 ml)]. The hydrolysis procedure was as described for **AC18b**. Product: white fine crystals (2.244 g, 93 %); m.p. 240-242 °C. ^{1}H NMR (400 MHz, $CDCl_3$--d_6-DMSO) δ 6.96-7.22 (m, 6H), 7.33 (dd, *J* = 7.3, 1.6 Hz, 2H), 7.40-7.58 (m, 4H), 7.84 (s, 1H), 7.97 (dd, *J* = 8.0, 1.6 Hz, 1H), 8.87 (d, *J* = 8.4 Hz, 1H), 11.24 (br s, 1H); ^{13}C NMR (100 MHz, $CDCl_3$--d_6-DMSO) δ 115.13, 119.01, 121.36, 126.98, 127.35, 127.50, 128.13, 128.93, 129.09, 130.07, 132.67, 133.64, 133.98, 135.14, 136.46, 140.33, 164.87, 168.42. MS (ESI): *m/z* $[M+H]^+$ 344.

EA (%) $C_{22}H_{17}NO_3$: calculated C, 76.95: H, 4.99: N, 4.08; found C, 76.72: H, 5.05: N, 4.10.

2.2.4.22 *N*-(α-Methylcinnamoyl)anthranilic acid (AC43)

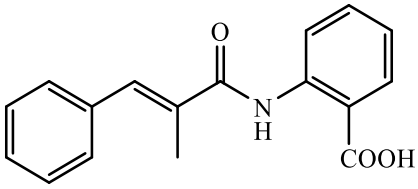

α-Methylcinnamic acid (**AC43a**) - To a mixture of benzaldehyde (5 ml, 0.0492 mol) and propionic anhydride[388] (10 ml, 0.0780 mol), anhydrous sodium acetate (2.5 g) was added and heated under reflux for 4 hours. Once the mixture has cooled down to room temperature, cold water (50 ml) was added and alkalised with saturated aqueous sodium carbonate (85 ml). The resulting solid suspension was heated to dissolve completely. The unreacted benzaldehyde was extracted in DCM (2 × 25 ml), and the aqueous layer was acidified with concentrated HCl (12 M) with cooling. The pale yellowish-white crystals (yield 2.098 g, 26 %) of α-methylcinnamic acid was obtained by vacuum filtration, washed with little cold water (~10 ml) and dried. ^{1}H NMR (400 MHz, d_6-DMSO) δ 2.08 (s, 3H), 7.39-7.55 (m, 5H), 7.62-7.68 (m, 1H).

α-Methylcinnamoyl chloride (**AC43b**) - Quantities: oxalyl chloride (10 ml) and α-methylcinnamic acid (2.009 g, 0.0124 mol). The acylation procedure was as described for **AC14a**. Product: pale yellow hard crystal (2.238 g, 100 %). ^{1}H NMR (400 MHz, $CDCl_3$) δ 2.20 (s, 3H), 7.36-7.62 (m, 5H), 7.99-8.09 (m, 1H); ^{13}C NMR (100 MHz, $CDCl_3$) δ 15.17, 128.67, 129.76, 130.07, 132.42, 134.52, 147.50, 170.15.

Methyl N-(α-methylcinnamoyl)anthranilate (**AC43c**) - Quantities: methyl anthranilate (1.965 g, 0.0130 mol), dry pyridine (40 ml) and α-methyl cinnamoyl chloride (2.012 g, 0.0111 mol). The synthesis procedure was as described for **AC18a**, but stirred for 2 hours. Product: white precipitate (2.728 g, 83 %); m.p. 93-95 °C. ^{1}H NMR (400 MHz, $CDCl_3$) δ 2.28 (s, 3H), 3.94 (s, 3H), 7.08-7.13 (m, 1H), 7.30-7.44 (m, 5H), 7.56-7.64 (m, 2H), 8.07 (dd, J = 8.0, 1.6 Hz, 1H), 8.87 (dd, J = 8.6, 1.0 Hz, 1H), 11.66 (br s, 1H); ^{13}C NMR (100 MHz, $CDCl_3$) δ 14.11, 52.38, 115.17, 120.54, 122.46, 127.95, 128.34,

129.52, 130.89, 132.68, 134.71, 135.60, 136.21, 141.87, 167.98, 168.86. MS (ESI): *m/z* $[M+H]^+$ 296. EA (%) $C_{18}H_{17}NO_3$: calculated C, 73.20: H, 5.80: N, 4.74; found C, 72.90: H, 5.92: N, 4.66.

N-(α-Methylcinnamoyl)anthranilic acid (**AC43d**) - Quantities: methyl *N*-(α-methylcinnamoyl)anthranilate (2.504 g, 0.0085 mol), THF (100 ml), methanol (20 ml) and aqueous LiOH [~1 M, LiOH (1.716 g) dissolved in H_2O (77 ml)]. The hydrolysis procedure was as described for **AC18b**. Product: white crystals (2.204 g, 93 %); m.p. 186-188 °C. ^{1}H NMR (400 MHz, $CDCl_3$--d_6-DMSO) δ 2.26 (s, 3H), 7.08-7.14 (m, 1H), 7.30-7.45 (m, 5H), 7.54-7.60 (m, 2H), 8.11 (dd, *J* = 8.0, 1.6 Hz, 1H), 8.83 (d, *J* = 8.4 Hz, 1H), 12.00 (br s, 1H); ^{13}C NMR (100 MHz, $CDCl_3$--d_6-DMSO) δ 13.41, 115.24, 119.38, 121.71, 127.27, 127.66, 128.72, 130.81, 132.07, 133.55, 134.51, 135.43, 141.26, 167.06, 169.95. MS (ESI): *m/z* $[M+H]^+$ 282. EA (%) $C_{17}H_{15}NO_3$: calculated C, 72.58: H, 5.37: N, 4.98; found C, 72.50: H, 5.49: N, 5.00.

2.2.4.23 *N*-(4-Dimethylaminocinnamoyl)anthranilic acid (AC45)

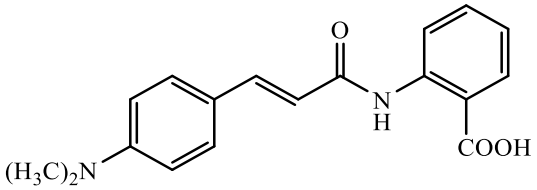

4-Dimethylaminocinnamoyl chloride (**AC45a**) - Quantities: oxalyl chloride (20 ml), 4-dimethylaminocinnamic acid (4.003 g, 0.0209 mol) and dry DMF (a drop). The acylation procedure was as described for **AC14a**, but stirred for 24 hours. Product: dark green precipitate (7.415 g, >100 % due to presence of unevaporated DMF).

Methyl N-(4-dimethylaminocinnamoyl)anthranilate (**AC45b**) - Quantities: methyl anthranilate (6.046 g, 0.040 mol), dry pyridine (70 ml) and 4-dimethyl aminocinnamoyl chloride (0.0209 mol). The synthesis procedure was as described for **AC18a**, but stirred for 2.5 hours with slight heating (~50 °C). Product: dark green precipitate (2.413 g, 36 %); m.p. 164-166 °C. ^{1}H NMR (400 MHz, $CDCl_3$) δ 2.99 (s, 6H), 3.92 (s, 3H), 6.41 (d, *J* = 15.4 Hz, 1H), 6.58-6.71 (m, 2H), 7.06 (t, *J* = 7.6 Hz, 1H), 7.37-7.59 (m, 3H), 7.69 (d, *J* = 15.4 Hz, 1H), 8.04 (d, *J* = 8.0 Hz, 1H), 8.89 (d, *J* = 8.6 Hz, 1H), 11.22 (br s, 1H); ^{13}C

NMR (100 MHz, $CDCl_3$) δ 40.14, 52.26, 111.81, 114.59, 116.43, 120.48, 122.02, 122.48, 129.67, 130.77, 134.65, 142.26, 142.74, 151.55, 165.45, 168.91. MS (ESI): *m/z* $[M+H]^+$ 325. EA (%) $C_{19}H_{20}N_2O_3$: calculated C, 70.35: H, 6.21: N, 8.64; found C, 70.05: H, 6.44: N, 8.60.

N-(4-Dimethylaminocinnamoyl)anthranilic acid (**AC45c**) - Quantities: methyl *N*-(4-dimethylaminocinnamoyl)anthranilate (2.204 g, 0.0068 mol), THF (100 ml), methanol (20 ml) and aqueous LiOH [~1 M, LiOH (1.257 g) dissolved in H_2O (56 ml)]. The hydrolysis procedure was as described for **AC18b**. Product: greenish-yellow fine crystals (1.812 g, 86 %); m.p. 216-218 °C. ^1H NMR (400 MHz, $CDCl_3$--d_6-DMSO) δ 3.04 (s, 6H), 6.38 (d, *J* = 15.5 Hz, 1H), 6.66-6.72 (m, 2H), 7.04-7.11 (m, 1H), 7.42-7.66 (m, 4H), 8.08 (dd, *J* = 8.0, 1.6 Hz, 1H), 8.82 (dd, *J* = 8.5, 0.9 Hz, 1H), 11.56 (br s, 1H); ^{13}C NMR (100 MHz, $CDCl_3$--d_6-DMSO) δ 39.16, 110.21, 110.90, 114.49, 115.56, 119.03, 121.08, 121.20, 128.63, 130.51, 131.37, 133.23, 141.37, 150.63, 164.22, 169.63. MS (ESI): *m/z* $[M+H]^+$ 311. EA (%) $C_{18}H_{18}N_2O_3$: calculated C, 69.66: H, 5.85: N, 9.03; found C, 69.46: H, 5.99: N, 8.95.

2.2.4.24 *N*-(4-Methoxyhydrocinnamoyl)anthranilic acid (AC46)

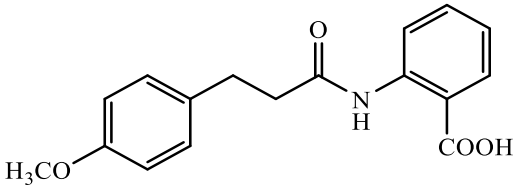

4-Methoxyhydrocinnamoyl chloride (**AC46a**) - Quantities: oxalyl chloride (16 ml) and 4-methoxyhydrocinnamic acid (3.119 g, 0.0173 mol). The acylation procedure was as described for **AC14a**, but stirred for 5 hours. Product: yellow viscous liquid (3.431 g, 100 %). ^1H NMR (400 MHz, $CDCl_3$) δ 2.95 (t, *J* = 7.5 Hz, 2H), 3.17 (t, *J* = 7.5 Hz, 2H), 3.79 (s, 3H), 6.81-6.88 (m, 2H), 7.07-7.14 (m, 2H).

Methyl N-(4-methoxyhydrocinnamoyl)anthranilate (**AC46b**) - Quantities: methyl anthranilate (2.721 g, 0.018 mol), dry pyridine (40 ml) and 4-methoxy hydrocinnamoyl chloride (3.100 g, 0.0156 mol). The synthesis procedure was as described for **AC21a**. Product: yellow liquid with some needle-like crystals (low m.p.).

N-(4-Methoxyhydrocinnamoyl)anthranilic acid (**AC46c**) - Quantities: methyl *N*-(4-methoxyhydrocinnamoyl)anthranilate (0.0156 mol), THF (100 ml), methanol (20 ml) and aqueous LiOH [~1 M, LiOH (3.164 g) dissolved in H_2O (100 ml)]. The hydrolysis procedure was as described for **AC18b**. Product: pale yellow precipitate (3.691 g, 79 %); m.p. 161-163 °C. ^{1}H NMR (400 MHz, $CDCl_3$--d_6-DMSO) δ 2.69 (t, *J* = 7.8 Hz, 2H), 2.99 (t, *J* = 7.8 Hz, 2H), 3.77 (s, 3H), 6.79-6.83 (m, 2H), 7.04-7.18 (m, 3H), 7.48-7.54 (m, 1H), 8.05 (dd, *J* = 7.9, 1.5 Hz, 1H), 8.67 (d, *J* = 7.5 Hz, 1H), 11.41 (br s, 1H); ^{13}C NMR (100 MHz, $CDCl_3$--d_6-DMSO) δ 29.64, 39.55, 54.45, 113.13, 114.83, 119.17, 121.52, 128.51, 130.66, 131.94, 133.44, 140.93, 157.20, 169.73, 170.24. MS (ESI): *m/z* $[M+H]^+$ 300. EA (%) $C_{17}H_{17}NO_4$: calculated C, 68.22: H, 5.72: N, 4.68; found C, 68.23: H, 5.89: N, 4.69.

2.3 General synthetic procedures for aryl sulfonamides

Aryl sulfonamides, **M2 - M14** with Formula 1 (**Figure 2.2**) were produced by sulfonylation between an aryl sulfonyl chloride and a secondary amine as per **Scheme 2.4** and **Section 2.3.1.1**.[389] The 4-(chlorosulfonyl)benzoic acid required for the reaction was synthesised as per **Scheme 2.5** and **Section 2.3.1.2**.[390] The derivatives, **AC51** and **AC56** with Formula 2 (**Figure 2.3**), and **AC53**, **AC54** and **AC57** with Formula 3 (**Figure 2.3**) were synthesised as provided in **Scheme 2.6** and **Section 2.3.2**.[372,373,391,392] Probenecid (**M1**) was purchased from Sigma-Aldrich, whereas the compounds **M2 - M14** were previously synthesised at the University of Hull (unpublished work), but some of them were purified or resynthesised as required.

Formula 1

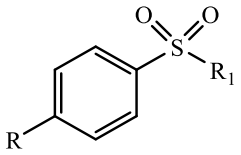

	R	R_1
M1	COOH	dipropylamine
M2	H	diethylamine
M3	OCH_3	diethylamine
M4	OCH_3	pyrrolidine
M5	F	diethylamine
M6	F	pyrrolidine
M7	F	piperidine
M8	F	morpholine
M9	F	indoline
M10	NHAc	diethylamine
M11	COOH	diethylamine
M12	COOH	pyrrolidine
M13	COOH	piperidine
M14	COOH	morpholine

Figure 2.2: *Chemical structures of the small aryl sulfonamides* **M1 - M14**.

Formula 2

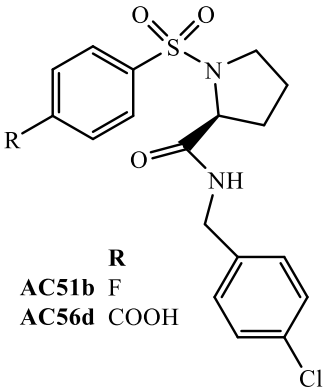

	R
AC51b	F
AC56d	COOH

Formula 3

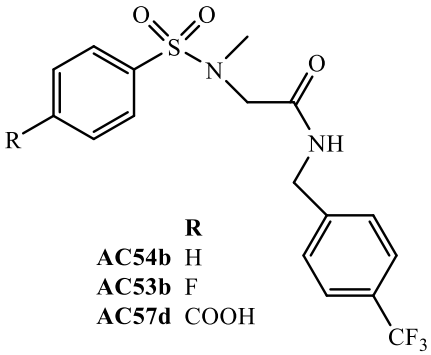

	R
AC54b	H
AC53b	F
AC57d	COOH

Figure 2.3: *Chemical structures of the extended aryl sulfonamides* **AC51**, **AC53**, **AC54**, **AC56** *and* **AC57**.

2.3.1 Synthesis of small aryl sulfonamides

2.3.1.1 Aryl sulfonamide derivatives M2 - M14

M2 - M9

An aryl sulfonyl chloride derivative (1.0 mmol) was dissolved in THF and cooled to 0 °C, and a secondary amine (2.2 mmol) was added dropwise maintaining the reaction temperature between 0-5 °C. The reaction mixture was stirred for 5 minutes at 0 °C, then at room temperature for further 2 hours. The organic layer was diluted with ethyl acetate, washed with water, dried over anhydrous sodium sulfate, filtered and solvent evaporated under reduced pressure. The crude products of **M2 - M5** and **M8** were recrystallised at a sub-zero temperature from a DCM-hexane mixture (1:4), whereas **M6**, **M7** and **M9** were recrystallised at a sub-zero temperature from a mixture of ethanol-water (5:1), and the pure products were obtained by vacuum filtration. The characterisation data for each compound are given under this section.

M10 - M14

An aryl sulfonyl chloride derivative (0.014 mol) was added to a solution of a secondary amine (0.032 mol) in aqueous NaOH (10 % w/v, 30 ml) and stirred at room temperature overnight. The solution was acidified with HCl (6 M) to pH 1 and stirred for further 20 minutes. The resulting precipitate was obtained by vacuum filtration, washed with water or HCl (1 M), and dried.[389] The crude products of **M11 - M14** were recrystallised from hot ethanol, whereas the crude precipitate of **M10** was dissolved in DCM, filtered and solvent evaporated under reduced pressure to yield the pure products. The characterisation data for each compound are given under this section.

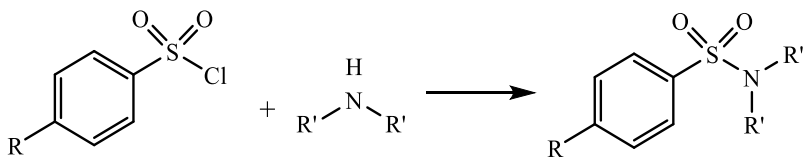

Scheme 2.4: *Synthesis of aryl sulfonamides. Conditions and reagents used to synthesise* **M2 - M9**: *0 °C, then 2 hours at room temperature; and for* **M10 - M14**: *NaOH (10 % w/v) overnight, then HCl (2 M), at room temperature.*

N,N-Diethylbenzenesulfonamide (**M2**)

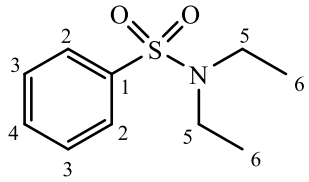

Product: white crystals (20 %); m.p. 46-50 °C (lit.[393] 40 °C). ^{1}H NMR (400 MHz, $CDCl_3$) δ 1.13 (t, *J* = 7.1 Hz, 6H^{6}), 3.25 (q, *J* = 7.2 Hz, 4H^{5}), 7.44-7.59 (m, 3H^{3,4}), 7.77-7.85 (m, 2H^{2}); ^{13}C NMR (100 MHz, $CDCl_3$) δ 14.08, 41.97, 126.92, 128.96, 132.19, 140.35. MS (EI): *m/z* 213 $C_{10}H_{15}NO_2S^{+\bullet}$ ($M^{+\bullet}$), 141 $C_6H_5O_2S^+$ $(M\text{-}C_4H_{10}N)^+$, 77 $C_6H_5^+$ $(M\text{-}C_4H_{10}NO_2S)^+$. EA (%) $C_{10}H_{15}NO_2S$: calculated C, 56.31: H, 7.09: N, 6.57: S, 15.03; found C, 56.52: H, 7.30: N, 6.58: S, 15.10.

N,N-Diethyl-4-methoxybenzenesulfonamide (**M3**)

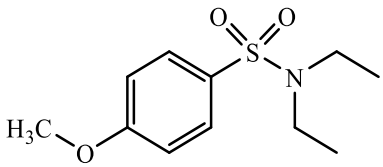

Product: white crystals (72 %); m.p. 43-46 °C (lit.[394] 53-54 °C). ^{1}H NMR (400 MHz, $CDCl_3$) δ 1.12 (t, *J* = 7.1 Hz, 6H), 3.22 (q, *J* = 7.2 Hz, 4H), 3.86 (s, 3H), 6.93-7.00 (m, 2H), 7.69-7.79 (m, 2H); ^{13}C NMR (100 MHz, $CDCl_3$) δ 14.08, 41.90, 55.53, 114.07, 129.03, 132.06, 162.52. MS (EI): *m/z* 243 $C_{11}H_{17}NO_3S^{+\bullet}$ ($M^{+\bullet}$), 228 $C_{10}H_{14}NO_3S^+$ $(M\text{-}CH_3)^+$, 171 $C_7H_7O_3S^+$ $(M\text{-}C_4H_{10}N)^+$, 107 $C_7H_7O^+$ $(M\text{-}C_4H_{10}NO_2S)^+$. EA (%) $C_{11}H_{17}NO_3S$: calculated C, 54.30: H, 7.04: N, 5.76: S, 13.18; found C, 54.47: H, 7.22: N, 5.76: S, 13.35.

1-((4-Methoxyphenyl)sulfonyl)pyrrolidine (**M4**)

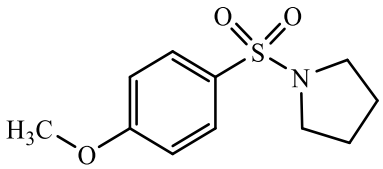

Product: white crystals (58 %); m.p. 93-95 °C (lit.[395] 165-166 °C). ^{1}H NMR (400 MHz, $CDCl_3$) δ 1.70-1.81 (m, 4H), 3.17-3.28 (m, 4H), 3.88 (s, 3H), 6.95-

7.04 (m, 2H), 7.71-7.82 (m, 2H); ^{13}C NMR (100 MHz, $CDCl_3$) δ 25.14, 47.86, 55.55, 114.10, 128.60, 129.58, 162.81. MS (EI): *m/z* 241 $C_{11}H_{15}NO_3S^{+\bullet}$ ($M^{+\bullet}$), 171 $C_7H_7O_3S^+$ $(M-C_4H_8N)^+$, 107 $C_7H_7O^+$ $(M-C_4H_8NO_2S)^+$, 77 $C_6H_5^+$ $(M-C_5H_{11}NO_3S)^+$, 70 $C_4H_8N^+$. EA (%) $C_{11}H_{15}NO_3S$: calculated C, 54.75: H, 6.27: N, 5.80: S, 13.29; found C, 54.98: H, 6.33: N, 5.81: S, 13.24.

N,N-Diethyl-4-fluorobenzenesulfonamide (**M5**)

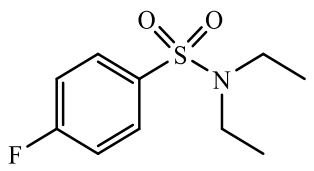

Product: white crystals (70 %); m.p. 53-57 °C (lit.[396] 39-40 °C). ^{1}H NMR (400 MHz, $CDCl_3$) δ 1.14 (t, *J* = 7.1 Hz, 6H), 3.24 (q, *J* = 7.1 Hz, 4H), 7.12-7.23 (m, 2H), 7.75-7.89 (m, 2H); ^{13}C NMR (100 MHz, $CDCl_3$) δ 14.07, 41.97, 116.16 (d), 129.57 (d), 163.55, 166.07. MS (EI): *m/z* 231 $C_{10}H_{14}FNO_2S^{+\bullet}$ ($M^{+\bullet}$), 159 $C_6H_4FO_2S^+$ $(M-C_4H_{10}N)^+$, 95 $C_6H_4F^+$ $(M-C_4H_{10}NO_2S)^+$. EA (%) $C_{10}H_{14}NO_2SF$: calculated C, 51.93: H, 6.10: N, 6.06: S, 13.86; found C, 52.18: H, 6.18: N, 6.07: S, 14.00.

1-((4-Fluorophenyl)sulfonyl)pyrrolidine (**M6**)

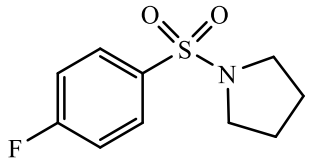

Product: pale yellow crystals (91 %); m.p. 93-95 °C. ^{1}H NMR (400 MHz, $CDCl_3$) δ 2.96-3.04 (m, 4H), 3.72-3.78 (m, 4H), 7.20-7.28 (m, 2H), 7.74-7.82 (m, 2H). EA (%) $C_{10}H_{12}FNO_2S$: calculated C, 52.39: H, 5.28: N, 6.11: S, 13.98; found C, 52.75: H, 5.00: N, 6.39: S, 13.77.

1-((4-Fluorophenyl)sulfonyl)piperidine (**M7**)

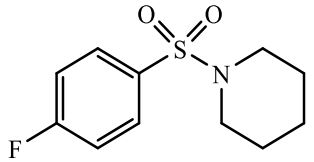

Product: white crystals (65 %); m.p. 95-96 °C (lit.[397] 76-77 °C). ^{1}H NMR (400 MHz, $CDCl_3$) δ 1.38-1.49 (m, 2H), 1.59-1.71 (m, 4H), 2.93-3.03 (m, 4H), 7.15-7.26 (m, 2H), 7.72-7.81 (m, 2H). MS (ESI): *m/z* $[M+H]^+$ 244. EA (%) $C_{11}H_{14}FNO_2S$: calculated C, 54.30: H, 5.80: N, 5.76: S, 13.18; found C, 54.34: H, 6.01: N, 5.72: S, 13.33.

4-((4-Fluorophenyl)sulfonyl)morpholine (**M8**)

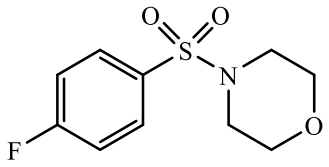

Product: white crystals (59 %); m.p. 110-112 °C (lit.[398] 104-106 °C). ^{1}H NMR (400 MHz, $CDCl_3$) δ 2.96-3.06 (m, 4H), 3.72-3.79 (m, 4H), 7.21-7.28 (m, 2H), 7.72-7.84 (m, 2H); ^{13}C NMR (100 MHz, $CDCl_3$) δ 45.92, 66.02, 116.43 (d), 130.50 (d), 164.09, 166.62. MS (EI): *m/z* 245 $C_{10}H_{12}FNO_3S^{+\bullet}$ ($M^{+\bullet}$), 159 $C_6H_4FO_2S^+$ $(M-C_4H_8NO)^+$, 95 $C_6H_4F^+$ $(M-C_4H_8NO_3S)^+$, 86 $C_4H_8NO^+$. EA (%) $C_{10}H_{12}NO_3SF$: calculated C, 48.97: H, 4.93: N, 5.71: S, 13.07; found C, 49.18: H, 5.00: N, 5.72: S, 13.30.

1-((4-Fluorophenyl)sulfonyl)indoline (**M9**)

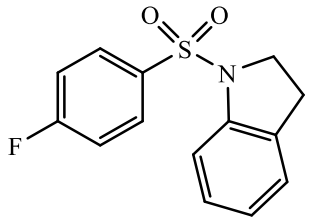

Product: pale brown powder (10 %); m.p. 115-116 °C. ^{1}H NMR (400 MHz, $CDCl_3$) δ 2.90 (t, *J* = 8.5 Hz, 2H), 3.92 (t, *J* = 8.4 Hz, 2H), 6.95-7.24 (m, 5H), 7.63 (d, *J* = 8.0 Hz, 1H), 7.74-7.86 (m, 2H). MS (ESI): *m/z* $[M+Na]^+$ 300. EA (%) $C_{14}H_{12}FNO_2S$: calculated C, 60.64: H, 4.36: N, 5.05: S, 11.56; found C, 60.67: H, 4.58: N, 5.06: S, 11.73.

N-(4-(N,N-Diethylsulfamoyl)phenyl)acetamide (**M10**)

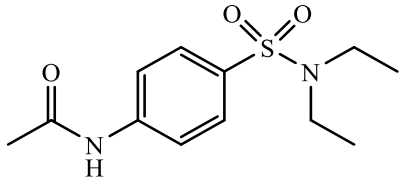

Product: yellowish-white crystals (53 %); m.p. 77-80 °C (lit.[399] 82 °C). ^{1}H NMR (400 MHz, $CDCl_3$) δ 1.12 (t, *J* = 7.1 Hz, 6H), 2.21 (s, 3H), 3.22 (q, *J* = 7.2 Hz, 4H), 7.57-7.78 (m, 4H), 7.97 (br s, 1H); ^{13}C NMR (100 MHz, $CDCl_3$) δ 14.09, 24.62, 42.02, 119.36, 128.08, 134.76, 141.79, 168.98. MS (ESI): *m/z* $[M+H]^+$ 271. EA (%) $C_{12}H_{18}N_2O_3S.¼H_2O$: calculated C, 52.44: H, 6.78: N, 10.19; found C, 52.17: H, 6.94: N, 10.11.

4-(N,N-Diethylsulfamoyl)benzoic acid (**M11**)

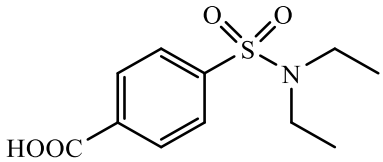

Product: orange crystals (34 %); m.p. 196-199 °C (lit.[400] 194-195 °C). ^{1}H NMR (400 MHz, $CDCl_3$--d_6-DMSO) δ 1.13 (t, *J* = 7.1 Hz, 6H), 3.25 (q, *J* = 7.2 Hz, 4H), 7.80-7.90 (m, 2H), 8.10-8.21 (m, 2H); ^{13}C NMR (100 MHz, $CDCl_3$--d_6-DMSO) δ 13.14, 41.09, 125.74, 129.36, 133.65, 142.78, 165.76. MS (ESI): *m/z* $[M+H]^+$ 258. EA (%) $C_{11}H_{15}NO_4S$: calculated C, 51.35: H, 5.88: N, 5.44; found C, 51.47: H, 5.99: N, 5.38.

4-(Pyrrolidin-1-ylsulfonyl)benzoic acid (**M12**)

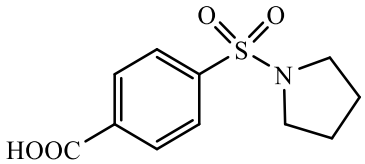

Product: orange crystals (48 %); m.p. 240-243 °C with decomposition. ^{1}H NMR (400 MHz, $CDCl_3$--d_6-DMSO) δ 1.69-1.84 (m, 4H), 3.17-3.32 (m, 4H), 7.82-7.94 (m, 2H), 8.14-8.26 (m, 2H); ^{13}C NMR (100 MHz, $CDCl_3$--d_6-DMSO) δ 24.22, 47.04, 126.29, 129.39, 134.00, 139.26, 165.84. MS (ESI): *m/z*

$[M+H]^+$ 256. EA (%) $C_{11}H_{13}NO_4S$: calculated C, 51.75: H, 5.13: N, 5.49; found C, 51.99: H, 5.21: N, 5.37.

4-(Piperidin-1-ylsulfonyl)benzoic acid (**M13**)

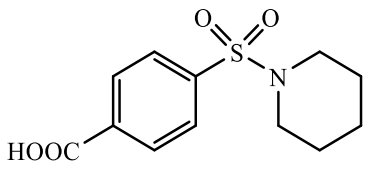

Product: orange precipitate (98 %); m.p. 266-268 °C with decomposition (lit.[400] 263-264 °C). ^{1}H NMR (400 MHz, $CDCl_3$--d_6-DMSO) δ 1.35-1.51 (quintet, *J* = 5.8 Hz, 2H), 1.58-1.71 (quintet, *J* = 5.7 Hz, 4H), 3.00 (t, *J* = 5.4 Hz, 4H), 7.76-7.83 (m, 2H), 8.15-8.23 (m, 2H); ^{13}C NMR (100 MHz, $CDCl_3$--d_6-DMSO) δ 22.74, 24.50, 46.31, 126.83, 129.71, 134.39, 139.20, 166.34. MS (ESI): *m/z* $[M+H]^+$ 270. EA (%) $C_{12}H_{15}NO_4S$: calculated C, 53.52: H, 5.61: N, 5.20: S, 11.90; found C, 53.76: H, 5.70: N, 5.17: S, 11.77.

4-(Morpholinosulfonyl)benzoic acid (**M14**)

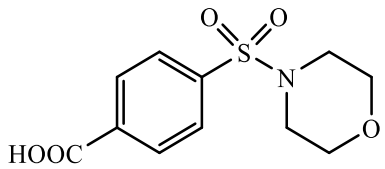

Product: orange precipitate (46 %); m.p. 285-288 °C with decomposition (lit.[400] 282-283 °C). ^{1}H NMR (400 MHz, d_6-DMSO) δ 2.98 (t, *J* = 4.7 Hz, 4H), 3.72 (t, *J* = 4.7 Hz, 4H), 7.90-8.02 (m, 2H), 8.22-8.32 (m, 2H); ^{13}C NMR (100 MHz, d_6-DMSO) δ 45.83, 65.27, 127.93, 130.28, 134.99, 138.19, 166.15. MS (ESI): *m/z* $[M+H]^+$ 272. EA (%) $C_{11}H_{13}NO_5S$: calculated C, 48.70: H, 4.83: N, 5.16: S, 11.82; found C, 49.00: H, 5.00: N, 5.03: S, 11.71.

2.3.1.2 4-(Chlorosulfonyl)benzoic acid

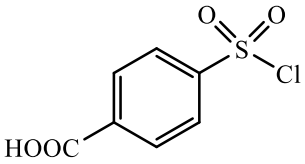

Step I: Thionyl chloride (42 ml) was added dropwise into cold deionised water (250 ml, 0 °C) over an hour period maintaining the reaction temperature between 0-7 °C using an ice-acetone-water bath. The reaction mixture was stood at room temperature overnight. Copper (I) chloride (0.151 g) was added maintaining the reaction temperature between 0-5 °C and the resulting solution was cooled to 0 °C.

Step II: Concentrated HCl (12 M, 65.5 ml) was added to 4-aminobenzoic acid (63.4 mmol) and cooled to 0 °C. Aqueous sodium nitrite (10 g in 40 ml H_2O) was added dropwise to the reaction mixture having the temperature between 0-5 °C, and stirred for further 10 minutes at 0 °C.

The reaction mixture prepared in *Step II* was added slowly to the reaction mixture prepared in *Step I* over a 45 minutes period, maintaining the temperature of both reaction mixtures between 0-5 °C.[390] The resulting suspension was stirred for further 2 hours and stood at 0 °C overnight to precipitate. The pale orange precipitate of 4-(chlorosulfonyl)benzoic acid was obtained by vacuum filtration, washed with water and dried. Yield: 9.458 g, 68 %. ^{1}H NMR (400 MHz, $CDCl_3$--d_6-DMSO) δ 7.69-8.46 (m, 4H), 11.95 (br s, 1H); ^{13}C NMR (100 MHz, $CDCl_3$--d_6-DMSO) δ 125.14, 128.90, 131.91, 147.49, 166.43.

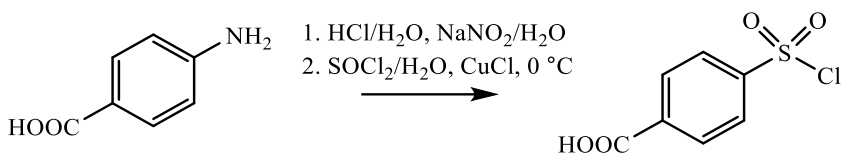

Scheme 2.5: *Synthesis of 4-(chlorosulfonyl)benzoic acid.*

2.3.2 Synthesis of extended aryl sulfonamides

A(i) *Sulfonylation of aryl sulfonyl chloride with a secondary amine* - aryl sulfonyl chloride (0.01 mol) derivative was dissolved in THF (30 ml) and

added to a solution of secondary amine (0.01 mol) in NaOH solution (10 % w/v, 30 ml), and stirred at room temperature overnight. The reaction mixture was acidified with HCl (1 M) to pH 2. The organic phase was extracted in ethyl acetate (3 × 20 ml), washed with brine (2 × 5 ml), dried over anhydrous sodium sulfate, filtered and solvent evaporated under reduced pressure.[372]

A(ii) *Coupling of aryl sulfonamide with a benzylamine* - aryl sulfonamide (5 mmol), benzylamine (5 mmol), 1-hydroxybenzotriazole (HOBt, 5.5 mmol), 1-(3-dimethylaminopropyl)-3-ethylcarbodiimide hydrochloride (EDAC.HCl, 5.5 mmol) and *N*,*N*-diisopropylethylamine (DIPEA, 5.5 mmol) were stirred in DCM (40 ml) for 5 hours at room temperature. The mixture was washed with HCl (1 M, 10 ml) and sodium carbonate (1 M, 10 ml), and the organic portion was extracted. The remaining organic phase was further extracted from the aqueous phase with more DCM (20 ml). The combined organic layer was washed again with sodium carbonate (1 M, 20 ml), dried over anhydrous sodium sulfate, filtered and solvent evaporated under reduced pressure.[373] The crude product was recrystallised from a mixture of hot heptane-ethyl acetate (1:1), and the crystals were obtained by vacuum filtration, washed with heptane and dried.

B(i) *Protection of secondary amines* - di-*tert*-butyl dicarbonate (Boc_2O, 28.4 mmol) in THF (28 ml) was added to a solution of secondary amine (19 mmol) in sodium carbonate (10 %, 47 ml) at 0 °C. The reaction mixture was stirred at room temperature overnight and added into water (100 ml). The mixture was washed with diethyl ether (3 × 20 ml) and the aqueous layer was acidified with HCl (1 M) to pH 2. The suspension was extracted with ethyl acetate (3 × 50 ml), dried over anhydrous magnesium sulfate, filtered and solvent evaporated under reduced pressure. The crude product was recrystallised from hot diethyl ether.[391]

B(ii) *Coupling of N-Boc-amide with a benzylamine* - Coupled as described in **A(ii)**, but carried on to the next step without purification.

B(iii) *Deprotection of N-Boc-amide* - Trifluoroacetic acid (TFA, 20 ml) was added to the *N*-Boc-amide in DCM (20 ml) at 0 °C and stirred at room temperature for 1.5 hours. More DCM (20 ml) was added to the reaction mixture and washed with water (20 ml), neutralised (washed) with saturated

sodium carbonate (~30 ml), and further washed with water (10 ml) and brine (10 ml). The organic extract was dried over anhydrous magnesium sulfate, filtered and solvent evaporated under reduced pressure.[392]

B(iv) *Sulfonylation of aryl sulfonyl chloride with a secondary amine* - Sulfonylated as described in **A(i)**, but precipitated on acidifying and hence extraction was not carried out. The precipitate was obtained by vacuum filtration, washed with HCl (1 M) and dried. The product was purified by stirring it in a mixture of hot heptane-ethyl acetate (1:1, ~25 ml).

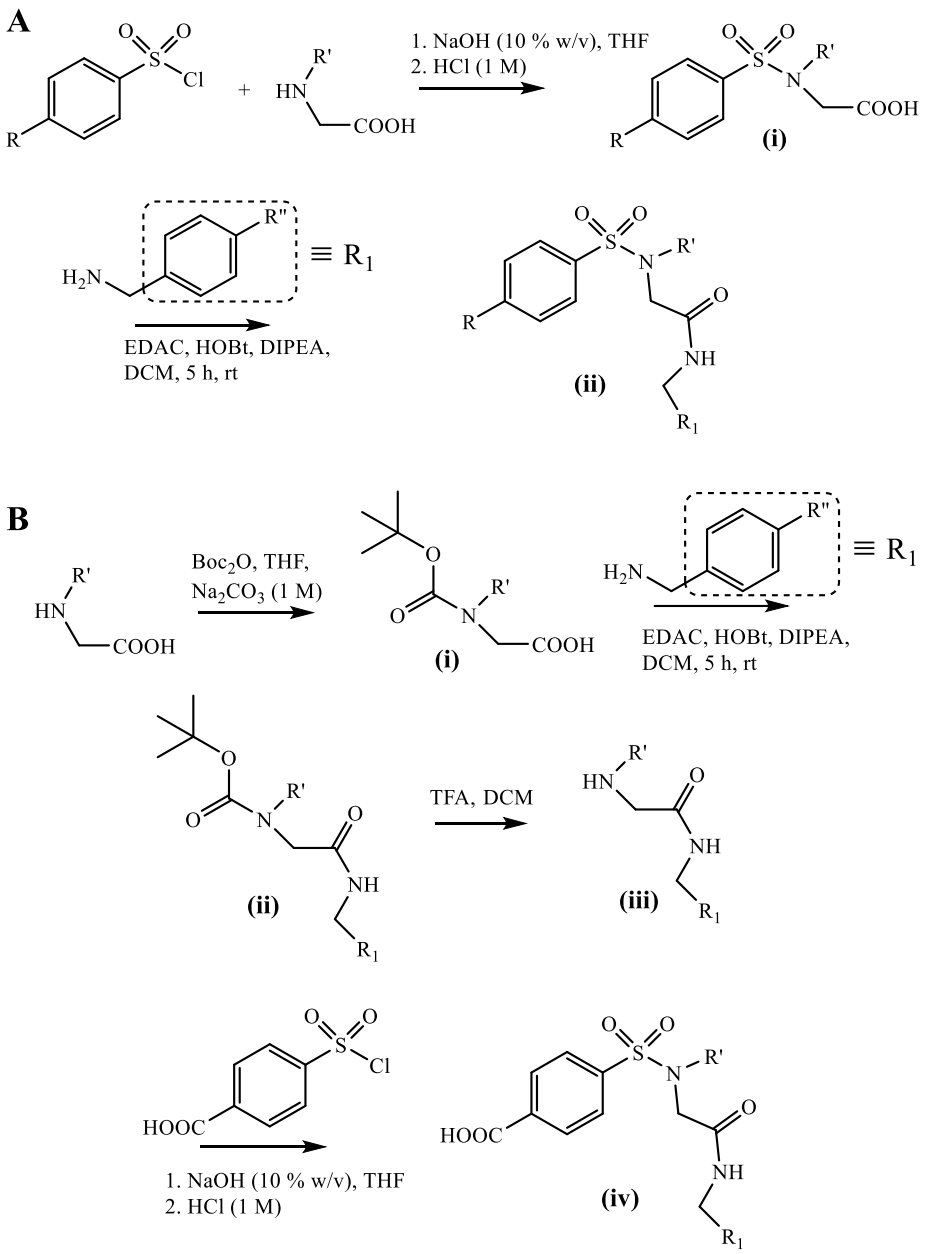

Scheme 2.6: *Synthesis of aryl sulfonamides using* **(A)** *4-fluoro or hydro sulfonyl chlorides, or* **(B)** *4-(chlorosulfonyl)benzoic acid.*

2.3.2.1 (*S*)-*N*-(4-Chlorobenzyl)-1-((4-fluorophenyl)sulfonyl)pyrrolidine-2-carboxamide (AC51)

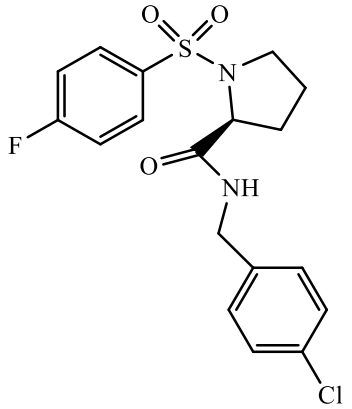

((4-Fluorophenyl)sulfonyl)-L-proline (**AC51a**) - Quantities: 4-fluorobenzene sulfonyl chloride (1.946 g, 0.01 mol) and L-proline (1.152 g, 0.01 mol). The **A(i)** procedure given under **Section 2.3.2** was followed. Product: cream-white crystals (2.105 g, 77 %); m.p. 115-118 °C. ^{1}H NMR (400 MHz, d_6-DMSO) δ 1.54-1.70 (m, 1H), 1.76-2.02 (m, 3H), 3.29-3.43 (m, 2H), 4.14 (dd, J = 8.6, 4.1 Hz, 1H), 7.41-7.54 (m, 2H), 7.86-7.99 (m, 2H); ^{13}C NMR (100 MHz, d_6-DMSO) δ 24.10, 30.31, 48.25, 60.30, 116.28, 116.50, 130.02, 130.12, 134.14, 163.18, 165.69, 172.91. MS (ESI): *m/z* $[M+H]^+$ 274. EA (%) $C_{11}H_{12}FNO_4S$: calculated C, 48.35: H, 4.43: N, 5.13: S, 11.73; found C, 48.44: H, 4.37: N, 5.09: S, 11.50.

(S)-N-(4-Chlorobenzyl)-1-((4-fluorophenyl)sulfonyl)pyrrolidine-2-carboxamide (**AC51b**) - Quantities: 4-chlorobenzylamine (0.708 g, 0.005 mol), **AC51a** (1.366 g, 0.005 mol), HOBt (0.842 g, 0.0055 mol), EDAC.HCl (1.054 g, 0.0055 mol) and DIPEA (0.711 g, 0.0055 mol). Coupled following the **A(ii)** procedure given under **Section 2.3.2**. Product: white fine crystals (1.533 g, 77 %); m.p. 134-135 °C. ^{1}H NMR (400 MHz, $CDCl_3$) δ 1.57-1.85 (m, 3H), 2.14-2.31 (m, 1H), 3.08-3.22 (m, 1H), 3.51-3.63 (m, 1H), 4.10 (dd, J = 8.8, 2.9 Hz, 1H), 4.39-4.55 (m, 2H), 7.19-7.36 (m, 7H), 7.80-7.93 (m, 2H); ^{13}C NMR (100 MHz, $CDCl_3$) δ 24.43, 30.20, 42.92, 49.97, 62.67, 116.61, 116.83, 128.83, 130.51, 130.60, 131.93, 133.28, 136.55, 164.39, 166.94, 170.96. MS (ESI): *m/z* $[M+H]^+$ 398. EA (%) $C_{18}H_{18}ClFN_2O_3S$: calculated C, 54.48: H, 4.57: N, 7.06: S, 8.08; found C, 54.45: H, 4.57: N, 7.08: S, 8.20.

2.3.2.2 2-((4-Fluoro-*N*-methylphenyl)sulfonamido)-*N*-(4-(trifluoromethyl) benzyl)acetamide (AC53)

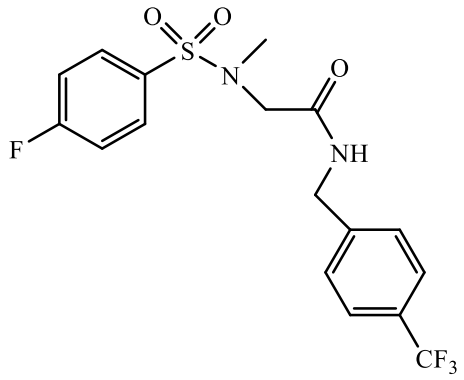

N-((4-Fluorophenyl)sulfonyl)-N-methylglycine (**AC53a**) - Quantities: 4-fluorobenzenesulfonyl chloride (1.946 g, 0.01 mol) and *N*-methylglycine (0.891 g, 0.01 mol). The **A(i)** procedure given under **Section 2.3.2** was followed. Product: white fine crystals (1.606 g, 65 %); m.p. 161-164 °C. ^{1}H NMR (400 MHz, $CDCl_3$--d_6-DMSO) δ 2.88 (s, 3H), 3.91 (s, 2H), 7.18-7.28 (m, 2H), 7.79-7.90 (m, 2H); ^{13}C NMR (100 MHz, $CDCl_3$--d_6-DMSO) δ 34.81, 50.02, 115.30, 115.53, 129.25, 129.35, 133.90, 162.97, 165.49, 169.19. MS (ESI): *m/z* $[M+Na]^+$ 270. EA (%) $C_9H_{10}FNO_4S$: calculated C, 43.72: H, 4.08: N, 5.67: S, 12.97; found C, 43.53: H, 4.00: N, 5.58: S, 13.00.

2-((4-Fluoro-N-methylphenyl)sulfonamido)-N-(4-(trifluoromethyl)benzyl) acetamide (**AC53b**) - Quantities: 4-(trifluoromethyl)benzylamine (0.701 g, 0.004 mol), **AC53a** (0.989 g, 0.004 mol)), HOBt (0.689 g, 0.0045 mol), EDAC.HCl (0.863 g, 0.0045 mol) and DIPEA (0.582 g, 0.0045 mol). Coupled following the **A(ii)** procedure given under **Section 2.3.2**. Product: white fine crystals (1.098, 68 %); m.p. 162-164 °C. ^{1}H NMR (400 MHz, $CDCl_3$) δ 2.81 (s, 3H), 3.67 (s, 2H), 4.56 (d, J = 6.0 Hz, 2H), 7.08 (br s, 1H), 7.21-7.67 (m, 6H), 7.76-7.92 (m, 2H); ^{13}C NMR (100 MHz, $CDCl_3$) δ 36.19, 42.18, 52.91, 115.85, 116.08, 124.84 (q, CF_3), 127.35, 128.60, 128.92, 129.67, 129.77, 132.52, 142.31, 163.50, 166.04, 167.17. MS (ESI): *m/z* $[M+H]^+$ 405. EA (%) $C_{17}H_{16}F_4N_2O_3S$: calculated C, 50.49: H, 3.99: N, 6.93: S, 7.93; found C, 50.29: H, 4.00: N, 6.84: S, 8.00.

2.3.2.3 2-(*N*-Methylphenylsulfonamido)-*N*-(4-(trifluoromethyl)benzyl) acetamide (AC54)

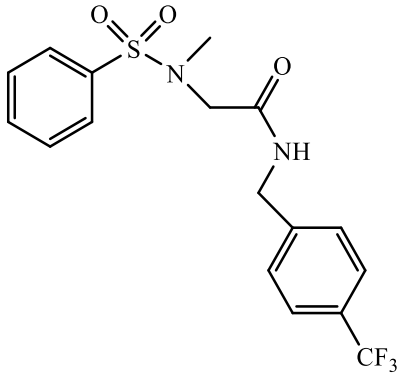

N-Methyl-N-(phenylsulfonyl)glycine (**AC54a**) - Quantities: benzenesulfonyl chloride (2.296 g, 0.013 mol) and *N*-methylglycine (0.891 g, 0.01 mol). The **A(i)** procedure given under **Section 2.3.2** was followed. Product: white crystals (2.031 g, 68 %); m.p. 177-180 °C with decomposition (lit.[401] 179.5-180.5 °C). ^{1}H NMR (400 MHz, $CDCl_3$--d_6-DMSO) δ 2.88 (s, 3H), 3.89 (s, 2H), 7.51-7.65 (m, 3H), 7.77-7.85 (m, 2H); ^{13}C NMR (100 MHz, $CDCl_3$--d_6-DMSO) δ 34.85, 50.01, 126.40, 128.29, 131.97, 137.24, 169.23. MS (ESI): *m/z* $[M+Na]^+$ 252. EA (%) $C_9H_{11}NO_4S$: calculated C, 47.15: H, 4.84: N, 6.11: S, 13.98; found C, 46.81: H, 4.61: N, 5.98: S, 14.05.

2-(N-Methylphenylsulfonamido)-N-(4-(trifluoromethyl)benzyl)acetamide (**AC54b**) - Quantities: 4-(trifluoromethyl)benzylamine (0.876 g, 0.005 mol), **AC54a** (1.146 g, 0.005 mol), HOBt (0.842 g, 0.0055 mol), EDAC.HCl (1.054 g, 0.0055 mol) and DIPEA (0.711 g, 0.0055 mol). Coupled following the **A(ii)** procedure given under **Section 2.3.2**. Product: white fine crystals (1.612 g, 83 %); m.p. 151-153 °C. ^{1}H NMR (400 MHz, $CDCl_3$) δ 2.81 (s, 3H), 3.68 (s, 2H), 4.56 (d, J = 6.1 Hz, 2H), 7.18 (br s, 1H), 7.42 (d, J = 8.2 Hz, 2H), 7.53-7.72 (m, 5H), 7.73-7.85 (m, 2H); ^{13}C NMR (100 MHz, $CDCl_3$) δ 37.22, 42.86, 54.18, 122.68, 125.69 (q, CF_3), 127.50, 127.76, 129.47, 129.97, 133.52, 135.77, 141.84, 167.77. MS (ESI): *m/z* $[M+H]^+$ 387. EA (%) $C_{17}H_{17}F_3N_2O_3S$: calculated C, 52.84: H, 4.43: N, 7.25: S, 8.30; found C, 52.76: H, 4.40: N, 7.29: S, 8.32.

2.3.2.4 (*S*)-4-((2-((4-Chlorobenzyl)carbamoyl)pyrrolidin-1-yl)sulfonyl) benzoic acid (AC56)

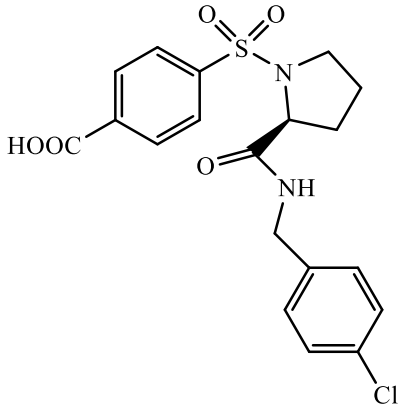

(tert-Butoxycarbonyl)-L-proline (**AC56a**) - Quantities: Boc_2O (6.198 g, 0.0284 mol) and L-proline (2.188 g, 0.019 mol). Protected following the **B(i)** procedure given under **Section 2.3.2**. Product: white crystals (3.370 g, 82 %). ^{1}H NMR (400 MHz, $CDCl_3$) δ 1.22-1.56 (m, 9H), 1.82-2.36 (m, 4H), 3.29-3.64 (m, 2H), 4.15-4.44 (m, 1H), 9.73 (br s, 1H).

tert-Butyl (S)-2-((4-chlorobenzyl)carbamoyl)pyrrolidine-1-carboxylate (**AC56b**) - Quantities: 4-chlorobenzylamine (0.991 g, 0.007 mol), **AC56a** (1.614 g, 0.0075 mol)), HOBt (1.225 g, 0.008 mol), EDAC.HCl (1.534 g, 0.008 mol) and DIPEA (1.034 g, 0.008 mol). Coupled following the **B(ii)** procedure given under **Section 2.3.2**. Product: pale yellow viscous liquid. ^{1}H NMR (400 MHz, $CDCl_3$) δ 0.94-1.56 (m, 9H), 1.62-2.51 (m, 4H), 2.83-3.60 (m, 2H), 4.05-5.35 (m, 3H), 6.89-7.62 (m, 4H).

(S)-N-(4-Chlorobenzyl)pyrrolidine-2-carboxamide (**AC56c**) - **AC56b** (0.007 mol) was deprotected following the **B(iii)** procedure given under **Section 2.3.2**. Product: Pale yellow precipitate (0.709 g, 42 %). ^{1}H NMR (400 MHz, $CDCl_3$) δ 1.61-2.26 (m, 4H), 2.49 (br s, 1H), 2.81-3.12 (m, 2H), 3.82 (dd, J = 9.1, 5.4 Hz, 1H), 4.39 (d, J = 6.1 Hz, 2H), 7.13-7.35 (m, 4H), 8.05 (br s, 1H); ^{13}C NMR (100 MHz, $CDCl_3$) δ 26.13, 30.73, 42.18, 47.19, 60.47, 128.68, 128.88, 133.00, 137.18, 174.94.

(S)-4-((2-((4-Chlorobenzyl)carbamoyl)pyrrolidin-1-yl)sulfonyl)benzoic acid (**AC56d**) - Quantities: 4-(chlorosulfonyl)benzoic acid (0.684 g, 0.0031 mol), THF (5 ml), **AC56c** (0.709 g, 0.0029 mol) and NaOH (10 % w/v, 5 ml). The

B(iv) procedure given under **Section 2.3.2** was followed. Product: white precipitate (0.760 g, 62 %); m.p. 206-208 °C. ^{1}H NMR (400 MHz, d_6-DMSO) δ 1.48-1.64 (m, 1H), 1.73-1.91 (m, 3H), 3.20-3.60 (m, 2H), 4.09-4.19 (m, 1H), 4.27-4.42 (m, 2H), 7.32-7.47 (m, 4H), 7.99-8.08 (m, 2H), 8.15-8.25 (m, 2H), 8.71 (t, J = 6.1 Hz, 1H); ^{13}C NMR (100 MHz, d_6-DMSO) δ 24.16, 30.87, 41.47, 49.21, 61.69, 127.68, 128.17, 128.87, 130.25, 131.26, 134.79, 138.50, 140.28, 166.21, 171.20. MS (ESI): *m/z* $[M+H]^+$ 424. EA (%) $C_{19}H_{19}ClN_2O_5S$: calculated C, 53.97: H, 4.53: N, 6.62: S, 7.58; found C, 53.60: H, 4.38: N, 6.33: S, 7.20.

2.3.2.5 4-(*N*-Methyl-*N*-(2-oxo-2-((4-(trifluoromethyl)benzyl)amino)ethyl) sulfamoyl)benzoic acid (AC57)

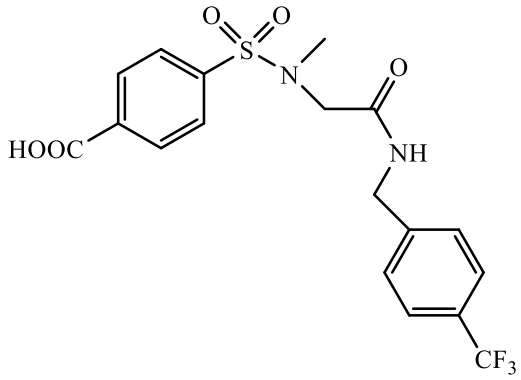

N-(tert-Butoxycarbonyl)-N-methylglycine (**AC57a**) - Quantities: Boc_2O (6.198 g, 0.0284 mol) and *N*-methylglycine (1.693 g, 0.019 mol). Protected following the **B(i)** procedure given under **Section 2.3.2**. Product: white crystals (3.383 g, 94 %). ^{1}H NMR (400 MHz, $CDCl_3$) δ 1.35-1.54 (m, 9H), 2.94 (s, 3H), 3.95 (s, 1H), 4.03 (s, 1H), 8.78 (br s, 1H).

tert-Butyl methyl(2-oxo-2-((4-(trifluoromethyl)benzyl)amino)ethyl)carbamate (**AC57b**) - Quantities: 4-(trifluoromethyl)benzylamine (0.007 mol), **AC57a** (1.419 g, 0.0075 mol)), HOBt (1.225 g, 0.008 mol), EDAC.HCl (1.534 g, 0.008 mol) and DIPEA (1.034 g, 0.008 mol). Coupled following the **B(ii)** procedure given under **Section 2.3.2**. Product: yellowish-white precipitate (2.207 g, 91 %). ^{1}H NMR (400 MHz, $CDCl_3$) δ 1.42 (s, 9H), 2.96 (s, 3H), 3.91 (s, 2H), 4.52 (d, J = 5.9 Hz, 2H), 7.38 (d, J = 8.0 Hz, 2H), 7.58 (d, J = 8.2 Hz, 2H).

2-(Methylamino)-N-(4-(trifluoromethyl)benzyl)acetamide (**AC57c**) - **AC57b** (1.980 g, 0.0057 mol) was deprotected following the **B(iii)** procedure given under **Section 2.3.2**. Product: Pale yellow precipitate (0.508 g, 36 %). ^{1}H NMR (400 MHz, $CDCl_3$) δ 1.88 (br s, 1H), 2.44 (s, 3H), 3.32 (s, 2H), 4.53 (s, 2H), 7.35-7.76 (m, 5H); ^{13}C NMR (100 MHz, $CDCl_3$) δ 36.83, 42.39, 54.48, 125.42, 125.58 (q, CF_3), 127.60, 127.82, 142.56, 171.58.

4-(N-Methyl-N-(2-oxo-2-((4-(trifluoromethyl)benzyl)amino)ethyl)sulfamoyl) benzoic acid (**AC57d**) - Quantities: 4-(chlorosulfonyl)benzoic acid (0.684 g, 0.0031 mol), THF (5 ml), **AC57c** (0.508 g, 0.0021 mol) and NaOH (10 % w/v, 5 ml). The **B(iv)** procedure given under **Section 2.3.2** was followed. Product: white precipitate (0.535 g, 59 %); m.p. 239-241 °C. ^{1}H NMR (400 MHz, d_6-DMSO) δ 2.86 (s, 3H), 3.86 (s, 2H), 4.40 (d, J = 5.9 Hz, 2H), 7.51 (d, J = 8.0 Hz, 2H), 7.74 (d, J = 8.0 Hz, 2H), 7.96 (d, J = 8.6 Hz, 2H), 8.18 (d, J = 8.6 Hz, 2H), 8.75 (t, J = 6.0 Hz, 1H); ^{13}C NMR (100 MHz, d_6-DMSO) δ 36.23, 41.75, 52.05, 125.16 (q, CF_3), 125.69, 127.47, 127.68, 127.86, 130.15, 134.59, 140.93, 144.12, 166.21, 167.25. MS (ESI): *m/z* $[M+H]^+$ 431. EA (%) $C_{18}H_{17}F_3N_2O_5S.H_2O$: calculated C, 48.21: H, 4.27: N, 6.25: S, 7.15; found C, 48.09: H, 3.79: N, 6.09: S, 6.89.

2.4 Pharmacology

2.4.1 HEK293 cell line

The human embryonic kidney 293 (HEK293) cell line that is extensively used as a recombinant protein expression vehicle, due to its amenability to transfection with high efficiency, rapid growth rate (approximate cell-doubling time of 24 hours) and easy maintenance,[402] was utilised in the study for stable transfection with the protein of interest. The HEK293 cell line is also known to be widely used in the study of neurobiology.[402] In preference to native neurons expressing TRP channels, a cell line is used to study the receptor properties having isolated from other receptors of the same family. Furthermore, using the same cell line as the protein expression vehicle to study mutants of the protein of interest provides a similar environment as to the wild-type and thus variability within assays are kept to a minimum.

HEK293 cells stably transfected with either pcDNA3.1(+) constructs containing cDNA for hTRPA1,[403] hTRPM8[404] or hTRPA1 mutants, or pcDNA3 (mock), **Figure 2.4**, were grown in Dulbecco's Modified Eagle's Medium (DMEM), containing 25 mM 4-(2-hydroxyethyl)-1-piperazine ethanesulfonic acid (HEPES) and 4.5 g l^{-1} glucose, supplemented with 2 mM L-glutamine, 100 U ml^{-1} penicillin - 100 U ml^{-1} streptomycin (all from BioWhittaker™ Lonza), 10 % v/v heat inactivated Fetal Bovine Serum (FBS, Gibco® Life technologies™) and 0.25 mg ml^{-1} geneticin (G418 Sulfate, Corning), in a 75 cm^2 tissue culture flask (T75, Greiner Bio-One CELLSTAR® or Corning) in a humidified cell culture incubator (New Brunswick Galaxy 170 S or Sanyo) at 37 °C with 5 % CO_2.

When the cells reached ~90 % confluence, confirmed under an inverted light microscope (Olympus CK2 microscope or Nikon TMS), they were harvested in 10 ml phosphate buffered saline (PBS, Sigma-Aldrich) solution by gently tapping the flask by hand to lift the loosely adherent HEK293 cells. The cells in PBS were centrifuged at 205 × *g* (SciQuip Sigma or MSE Mistral 1000) for 4 minutes in a 25 ml universal tube (Sarstedt) and the supernatant was removed. The cells were passaged and/or diluted in complete DMEM to an appropriate

concentration, as detailed in **Sections 2.4.2.1** and **2.4.2.2**, for calcium signalling experiments (**Section 2.4.2**).

(a) pcDNA3.1(+)

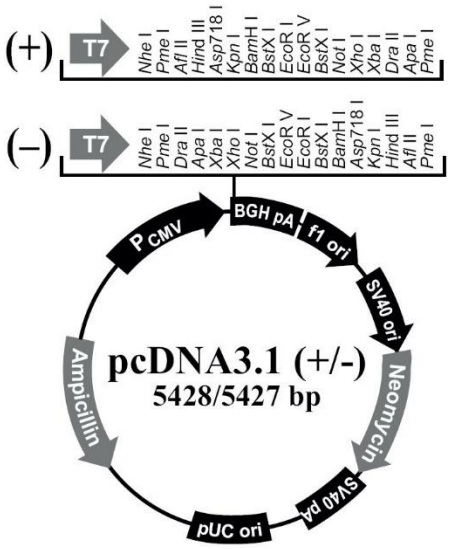

Comments for pcDNA3.1(+)

5428 nucleotides
CMV promoter: bases 232-819
T7 promoter/priming site: bases 863-882
Multiple cloning site: bases 895-1010
pcDNA3.1/BGH reverse priming site: bases 1022-1039
BGH polyadenylation sequence: bases 1028-1252
f1 origin: bases 1298-1726
SV40 early promoter and origin: bases 1731-2074
Neomycin resistance gene (ORF): bases 2136-2930
SV40 early polyadenylation signal: bases 3104-3234
pUC origin: bases 3617-4287 (complementary strand)
Ampicillin resistance gene (*bla*): bases 4432-5428 (complementary strand)
ORF: bases 4432-5292 (complementary strand)
Ribosome binding site: bases 5300-5304 (complementary strand)
bla promoter (P3): bases 5327-5333 (complementary strand)

(b) pcDNA3

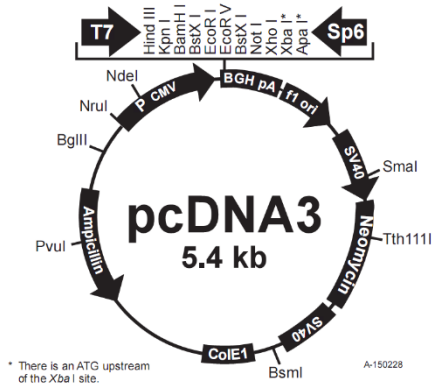

Comments for pcDNA3

5446 nucleotides
CMV promoter: bases 209-863
T7 promoter: bases 864-882
Polylinker: bases 889-994
Sp6 promoter: bases 999-1016
BGH polyadenylation sequence: bases 1018-1249
SV40 promoter: bases 1790-2115
SV40 origin of replication: bases 1984-2069
Neomycin ORF: bases 2151-2945
SV40 polyadenylation: bases 3000-3372
ColE1 origin: bases 3632-4305
Ampicillin ORF: bases 4450-5310

Figure 2.4: *Vector maps of the mammalian expression vectors,* **(a)** *pcDNA3.1*(+) *and* **(b)** *pcDNA3. Abbreviations: CMV, cytomegalovirus; BGH, bovine growth hormone; SV40 Simian virus 40; ORF, open reading frame; pUC, plasmid University of California; ColE1, Colicin E1.*

2.4.2 Calcium signalling

Protein expression level, activity, selectivity, reversibility and binding site

To determine the levels of functional TRPA1 and TRPM8 protein stably expressed in the transfected HEK293 cells, they were characterised with known hTRPA1 and hTRPM8 specific agonists and antagonists (**Figure 2.5**) using a fluorescence-based calcium signalling assay as described in **Sections 2.4.2.1**

and **2.4.2.2**, and the responses obtained were compared within assays and against the literature.

The modulatory effects of the *N*-cinnamoylanthranilates (CADs) and the aryl sulfonamides (ASDs) series were evaluated on hTRPA1, hTRPM8 and pcDNA3 (mock) transfected-HEK293 cells using the fluorescence-based calcium signalling assays (**Sections 2.4.2.1** and **2.4.2.2**). The compounds were initially evaluated at a single concentration to determine if there is any activity, and further, dose-response curves were carried out within the concentration range 0 - 1000 µM to identify if the activities shown by the compounds were concentration-dependent. The efficacy and potency of the compounds were determined from the shape of the dose-response curves and from the obtained half-maximal effective concentration (EC_{50}) or half-maximal inhibitory concentration (IC_{50}) values, respectively.

Agonism of the compounds was measured by assessing the influx of Ca^{2+} in hTRPA1-HEK293 cells upon exposure to the test compounds, and antagonism was measured using the ability of the test compounds to antagonise the standard agonist-evoked calcium response. To determine the channel selectivity of CADs and ASDs, they were assessed in pcDNA3 mock-HEK293 cells for agonism, and in hTRPM8-HEK293 cells for both agonism and antagonism. The reversibility of a compound was assessed by carrying out a wash-out experiment as described in **Sections 2.4.2.1** and **2.4.2.2**. To determine the binding site(s) of hTRPA1 active ligands, including CADs and ASDs, the ligands were functionally characterised in HEK293 cell lines stably transfected with hTRPA1 mutants S873V/T874L[150], F909A, F944A or C621A.

Controls and Sample preparation

The standard agonists used for the hTRPA1 channels were cinnamaldehyde (CA, 30 µM), acrolein (ACR, 30 µM) or allyl isothiocyanate (AITC, 10 µM), and for hTRPM8 were ethyl ((1*R*,2*S*,5*R*)-2-isopropyl-5-methylcyclohexane-1-carbonyl)glycinate (WS5, 1 µM) or (1*R*,2*S*,5*R*)-2-isopropyl-*N*-(4-methoxy phenyl)-5-methylcyclohexane-1-carboxamide (WS12, 100 nM). The standard antagonists used were the potent TRPA1 selective (1*E*,3*E*)-1-(4-fluorophenyl)-2-methylpent-1-en-3-one oxime (A967079, 100 or 300 nM] and TRPM8

selective *N*-(3-aminopropyl)-2-((3-methylbenzyl)oxy)-*N*-(thiophen-2-yl methyl)benzamide hydrochloride (AMTB.HCl, 1 or 3 μM). The chemical structures and suppliers of the standard ligands used in the assays are provided in **Figure 2.5** and **Table 2.1**, respectively.

The TRPA1 ligands characterised in the hTRPA1 mutants were cinnamaldehyde, allyl isothiocyanate, acrolein, menthol, thymol, carvacrol, eugenol, paracetamol, flufenamic acid (FFA), mefenamic acid (MFA), diclofenac (DCF), nordihydroguaiaretic acid (NDGA), cyclohexylcarbamic acid 3′-carbamoyl-biphenyl-3-yl ester (URB597), farnesylthiosalicylic acid (FTS), (-)-nicotine, 5-nitro-2-(3-phenylpropylamino)benzoic acid (NPPB), *N*-(3-methoxyphenyl)-4-chlorocinnamide (SB366791), *N*-(4-amylcinnamoyl) anthranilic acid (ACA), probenecid, 2-(1,3-dimethyl-2,6-dioxo-1,2,3,6-tetrahydro-7*H*-purin-7-yl)-*N*-(4-isopropylphenyl)acetamide (HC030031), 4-(4-chlorophenyl)-3-methylbut-3-en-2-oxime (AP18) and A967079. The chemical structures and suppliers of the ligands are provided in **Figures 2.5** and **2.6**, and **Table 2.1**, respectively.

The stock solutions of the compounds were made and serially diluted to lower half-log scale concentrations in DMSO (100 %, analytical reagent grade, Fisher Scientific), and thus the concentration of DMSO was maintained constant in a given total volume of sample. In each assay, DMSO (0.2 or 0.4 %) was included as the vehicle control, and calcimycin (calcium ionophore A23187, Fisher Scientific, 2 or 8 μM) was added at the end of each spectrum as a maximum response control and to ensure cell viability after the test.

Isotonic assay buffer

Isotonic assay buffer was prepared with 10 mM HEPES (Fisher Scientific), 145 mM NaCl (Fisher Scientific), 5 mM KCl (99 % Sigma-Aldrich or Fisher Scientific), 1 mM $MgCl_2.6H_2O$ (≥ 99 % Sigma-Aldrich or Fisher Scientific), 1 mM $CaCl_2$ (BDH AnalR Volumetric Solution 1 mol l^{-1}) and 10 mM D-(+)-glucose (ACS reagent Sigma or Fisher Scientific) in double distilled water (ddH_2O, Ondeo - Purite Water Purification System or ELGA PURELAB flex 18.2 MΩ), and the pH was adjusted to 7.4 using NaOH (98.8 % ACS reagent Sigma-Aldrich or Fisher Scientific).

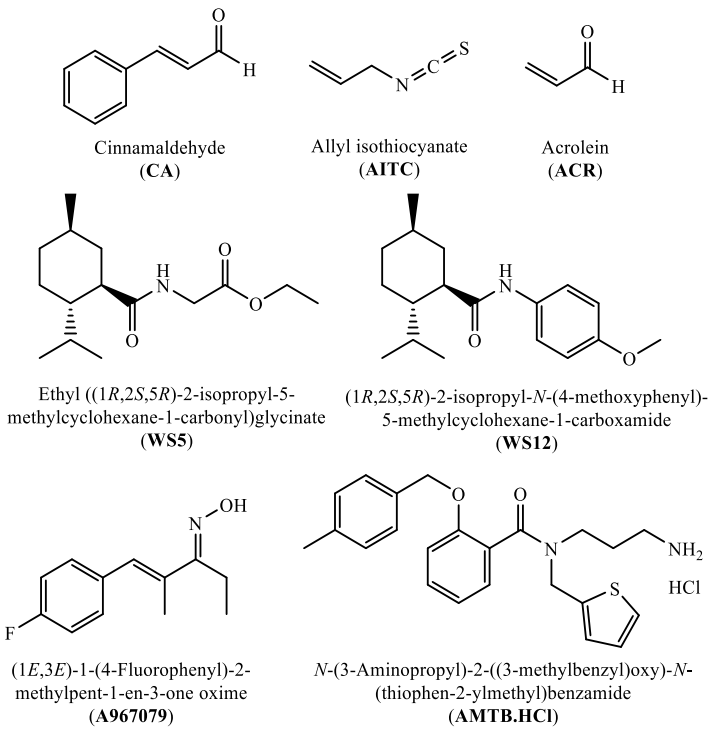

Figure 2.5: *Chemical structures and names of the standard agonists and antagonists used in the calcium signalling assays.*

Table 2.1: *Information of the ligands used in the experiments.*

Ligand	**Vendor**
Cinnamaldehyde	≥ 95 %, natural, Sigma-Aldrich
Allyl isothiocyanate	analytical standard, Sigma-Aldrich
Acrolein	analytical standard, Sigma-Aldrich
WS5	Millennium Specialty Chemicals Inc., Procter & Gamble
WS12	Santa Cruz Biotechnology
A967079	Tocris Bioscience
AMTB.HCl	Tocris Bioscience
Menthol	99 %, Sigma-Aldrich
(-)-Menthol	Sigma-Aldrich
Thymol	≥ 99.5 %, Sigma Life Science
Carvacrol	98 %, Aldrich Chemistry
Eugenol	99 %, Aldrich
Flufenamic acid	analytical standard, Fluka Analytical
Mefenamic acid	98 %, Johnson Matthey Company
Diclofenac	> 98 %, Tokyo Chemical Industry
Nordihydroguaiaretic acid	Santa Cruz Biotechnology
URB597	≥ 98 %, Sigma Life Science
Farnesylthiosalicylic acid	Santa Cruz Biotechnology
(-)-Nicotine	≥ 99 %, Sigma Life Science
NPPB	≥ 98 %, Sigma-Aldrich
SB366791	Tocris Bioscience
N-(*p*-Amylcinnamoyl)anthranilic acid	≥ 98 %, Sigma Life Science
4-Acetamidophenol	98 %, Acros Organics
Probenecid	Sigma Life Science
AP18	≥ 98 %, Sigma Life Science
HC030031	Sigma Life Science

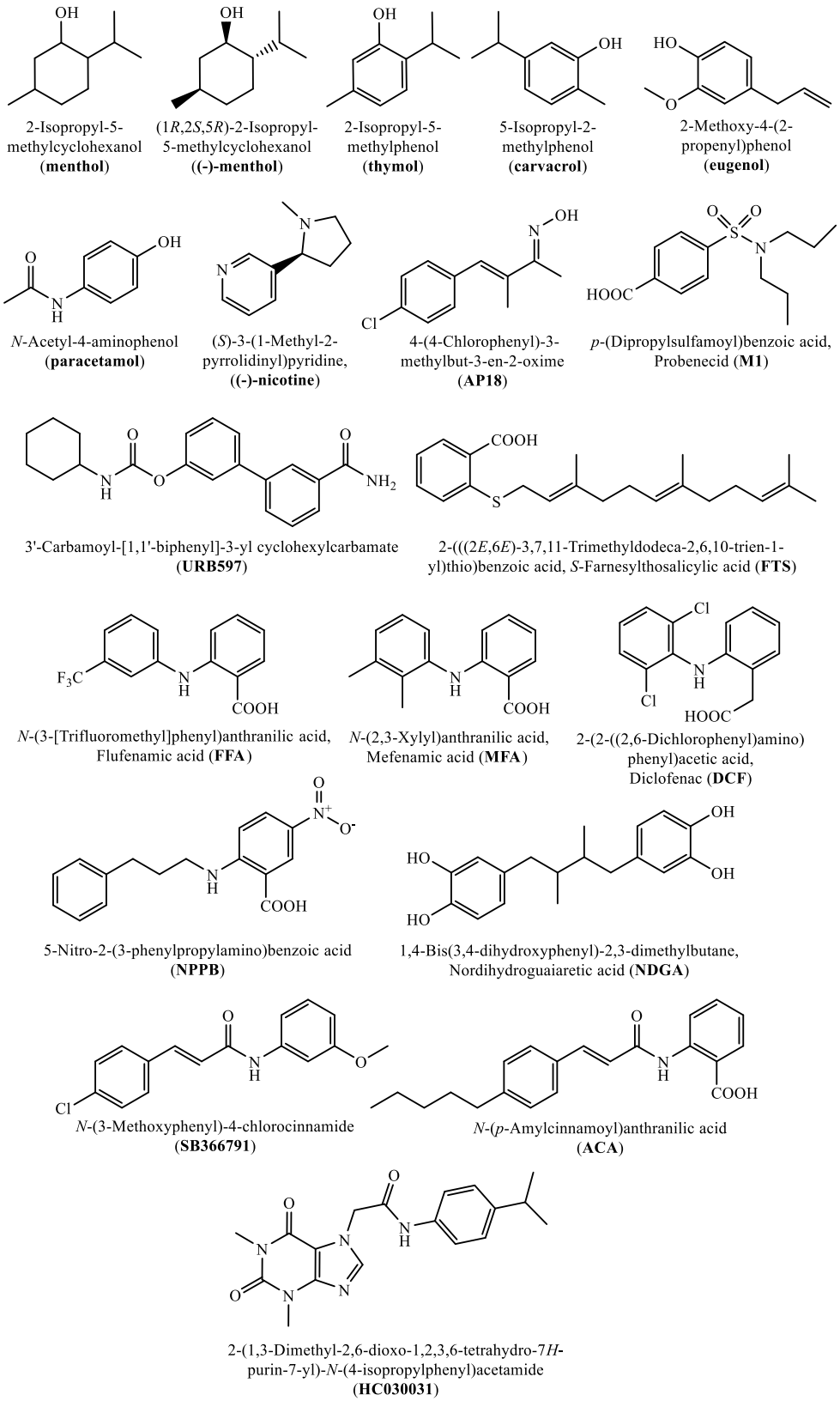

Figure 2.6: *Chemical structures and names of the ligands characterised in hTRPA1.*

2.4.2.1 Cuvette-based system

A previously reported protocol was followed.[404] Briefly, the cell pellet obtained from ~90 % confluence in T75 flask (**Section 2.4.1**) was resuspended in 0.5 ml complete DMEM and incubated with 2.5 µl Fluo-3AM fluorescent dye ($\lambda_{Ex/Em}$ 506/526 nm, Life technologies) of 2.5 µg μl^{-1} (50 µg Fluo-3AM in 20 µl DMSO) for 30 minutes at room temperature with gentle (50 rpm) rotary mixing, during which the Fluo-3AM ester internalise and gets hydrolysed to Fluo-3 by the esterase in the cells. The cells were washed free of excess extracellular dye with 4.5 ml PBS by centrifuging as before, and the pellet was resuspended in isotonic assay buffer (2 ml) at a density of 5×10^6 cells ml^{-1} (determined using a Sigma Bright-Line Hemacytometer). Cell suspension (100 µl) was added to cuvettes (10 × 10 × 45 mm, 4 clear sides UV grade disposable cuvettes, polystyrene, Fisher Scientific) containing a small magnetic stirring flea and the isotonic assay buffer (1.9 ml).

The assays were carried out at room temperature using a PTI™ (Photon Technology International) fluorometer with a photomultiplier tube (814 PMT) detector, interfaced to a computer with FelixGX version 4.2.2 software (PTI Inc.). An excitation and emission wavelengths of 506 and 526 nm were used for measurements, with the excitation and emission, and entrance and exit slit widths set as 5 nm. The stirrer speed was set to gentle stirring to evenly distribute the cells in the cuvette and for immediate mixing of any compound added during an assay. The amount of $[Ca^{2+}]_i$ released upon activation of TRP channels were measured as a real-time-based fluorescence spectrum as the intracellular Fluo-3 dye fluoresce upon formation of Fluo-3-Ca^{2+} complex, as described in **Section 1.1.7** of **Chapter 1**.

The cuvette was placed in the cuvette holder of the PTI instrument and the baseline of the spectrum was recorded for 20 s before the addition [using an autopipette fitted with a disposable long end tip (Sapphire Pipette Tip, 10 µl XL, Greiner Bio-One)] of a test compound (4 µl agonist) and the response was recorded for another 90 s, followed by the addition of calcimycin (2 µM) and recording for further 30 s. In antagonist assays, the standard antagonist, the vehicle control or the test compounds were pre-incubated with cells for 10 minutes prior to the addition of a standard agonist, and the spectrum was

recorded as before. As only 4 µl of a test compound prepared in DMSO is added to 2 ml assay buffer (total cell sample volume in the cuvette), the final concentration of DMSO in a sample was 0.2 %. To determine the reversibility of an antagonist, after pre-incubation for 10 minutes, the cells were washed with 5 ml assay buffer by centrifuging as before and resuspended in 2 ml fresh assay buffer, and the response for the TRPA1 standard agonist cinnamaldehyde (30 µM) was examined. Competitiveness of an antagonist was determined by pre-incubating cells with the test antagonist compound of a known concentration for 10 minutes and performing a dose-response curve for cinnamaldehyde, and considering the shift relative to the curve obtained with untreated cells.

2.4.2.2 Micro-well plate system

96-Well cell culture microplates (black polystyrene, flat µClear bottom, Greiner Bio-One) were coated with poly-D-lysine (PDL, MW 70-150 kDa, Sigma, 50 µg ml^{-1} prepared in sterile PBS and filtered through 0.22 µm filter) as follows: PDL was added to the wells (200 µl cm^{-2}) and incubated for an hour at room temperature, excess PDL solution was aspirated and the wells were washed with PBS (2 × 100 µl per well), and air-dried at room temperature for 2 hours in a safety cabinet. Cell suspension (200 µl of 12500 cells per well in complete DMEM, **Section 2.4.1**) was added to the coated wells and incubated in a cell culture incubator for 48 hours to yield a final concentration of 5×10^4 cells per well. The cell concentration was determined using a haemocytometer (Fuchs-Rosenthal Counting Chamber).

The culture medium was replaced with 100 µl of 2 µM Fluo-4AM [$\lambda_{Ex/Em}$ 494/506 nm, Life technologies, diluted in phenol red-free DMEM (Gibco Life technologies) from 2.5 µg μl^{-1} DMSO stock] and incubated in the dark at room temperature for 45 minutes. The cells were rinsed with PBS (2 × 100 µl per well), and the assay buffer (100 µl per well for agonist assays and 50 µl per well for antagonist assays) was added to the wells. In antagonist assays, the cells in 50 µl assay buffer were incubated with 50 µl test compounds (antagonists) for 10 minutes before assaying. To determine agonism and antagonism, 50 µl of either test agonist or standard agonist, respectively, was

added to 100 µl initial volume, and was followed by the addition of 50 µl calcimycin. The test compound solutions were prepared in DMSO and diluted in assay buffer maintaining the final concentration of DMSO as 0.4 %. To determine the reversibility of an antagonist, after pre-incubation with the compound for 10 minutes, the cells were washed with assay buffer (2 × 100 µl) and the response to a standard agonist was measured as described below.

The assays were carried out using a FlexStation 3 Molecular Devices interfaced to computer with SoftMax® Pro Software version 5. The protocol utilised was adapted from the literature.[270,354] Briefly, the real-time-based fluorescence spectra were recorded using the read-mode/type: Flex fluorescence (RFUs) bottom-read. An excitation and emission wavelengths of 485 and 538 nm were used for measurements with 530 nm as an auto cut-off. Each spectrum was recorded for a total run time of 240 s, where the baseline was recorded for 20 s and at the end of which the first addition (compound) was made followed by the second addition (calcimycin) at 180 s. All assays were carried out at room temperature. FlexStation® Molecular Devices Pipet Tips (96, black) was used in the FlexStation automatic pipetting system.

2.4.2.3 Data analysis

Raw data traces from a typical agonist and antagonist assays carried out using the calcium signalling technique are shown in **Figure 2.7**. The agonism and antagonism responses ($[Ca^{2+}]_i$ released) were calculated and presented either as a percentage of calcimycin or a standard agonist, respectively, using the differences in the maximum and minimum relative fluorescence unit (ΔRFU) values, as illustrated in **Equation 2.1** and **Figure 2.7**. ΔRFU_1 is the agonist compound's ΔRFU (a.u.), and ΔRFU_2 is the calcimycin's or standard agonist's ΔRFU (a.u.). The maximum and minimum RFU values of the fluorescence spectra were obtained manually from the FelixGX software, whereas the raw data from the SoftMax® Pro Software were copied to Microsoft Excel spreadsheet to work out the ΔRFU.

An increase in ΔRFU_1 (**Figure 2.7a**) on addition of a test compound to cells shows that the compound has an *agonising effect*, whereas a compound is considered to have an *antagonising effect* when a decrease in ΔRFU_1, relative

to ΔRFU_2, (**Figure 2.7b**) is observed for the standard agonist on addition to cells pre-treated with the test compound. A compound is said to have a *desensitising effect* when a reduction in response is observed on exposure to an agonist when an agonist is continuously present at the receptor. A compound that has an agonistic effect but cannot reach a maximal response is a *partial agonist*. In a series of compounds, the compound with a low EC_{50} or IC_{50} value is considered to be more *potent*, whereas the compound that could reach a higher response relative to another compound at the same high concentration level is considered to be more *efficacious*.

$$[Ca^{2+}]_i \text{ released} = \frac{\Delta RFU_1}{\Delta RFU_2} \times 100\ \% \quad \textbf{Equation 2.1}$$

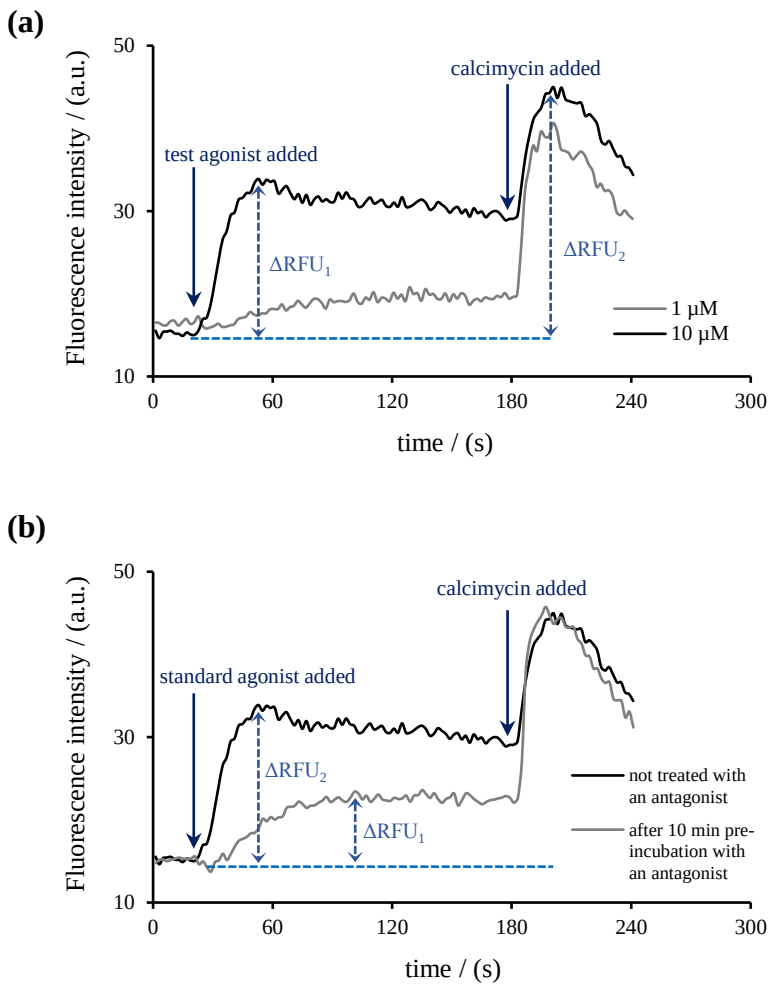

Figure 2.7: *Traces from a typical* **(a)** *agonist and* **(b)** *antagonist assay, and illustration on calculating a compound's agonism and antagonism as a percentage of calcimycin or standard agonist, correspondingly.*

Initial screening results correspond to three independent experiments (N = 3) and the errors reported are the standard error of the mean (SEM). The dose-response curves were plotted and analysed using the standard slope (1.0 for stimulation, -1.0 for inhibition) dose-response stimulation [$Y_{response} = Y_{min\ response} + ((Y_{max} - Y_{min})_{response} / (1 + 10^{(\log EC_{50} - X_{[dose]})}))$] or inhibition [$Y_{response} = Y_{min\ response} + ((Y_{max} - Y_{min})_{response} / (1 + 10^{(X_{[dose]} - \log IC_{50})}))$] three parameters models with a non-linear regression curve fit in GraphPad Prism version 5, and the values of $\log EC_{50}$ and $\log IC_{50}$ were obtained with their SEM. The antilog of $\log EC_{50}$ and $\log IC_{50}$ values will give the corresponding EC_{50} and IC_{50}, respectively. However, the use of antilog for their SEM will considerably shift the symmetry of uncertainty, that is, only when the error values are stated in log scale the uncertainty is symmetrical, and hence antilog of the errors will be inappropriate. Each data point on a dose-response curve corresponds to the mean of three independent experiments (N = 3), performed either in duplicates (n = 6) or triplicates (n = 9), with their SEM. The agonism responses were normalised by subtracting the noise/response obtained for the vehicle control (DMSO). In antagonist assays, the maximum response was obtained by normalising the standard agonist response to 100 %.

2.4.2.4 Statistical analysis

To determine any statistically significant difference between two $\log EC_{50}$ values of the same compound obtained in the same cell line subjected to different treatments, the extra-sum-of-squares F-test at $p < 0.05$ was utilised in the GraphPad Prism version 7. To determine statistical significance between two or more groups, the one-way analysis of variance (ANOVA) at $p < 0.05$ was carried out using Microsoft Excel 2013, and if any significant difference was obtained for more than two groups, Tukey's *post-hoc* test was considered to identify the significantly different group(s).

2.5 Electrophysiology

The electrophysiology measurements on vagus nerves were carried out by the IR Pharma (http://www.irpharma.co.uk/) company using the method outlined here. Vagus nerves of male Dunkin-Hartley guinea pigs were isolated,

characterised and experimented as described previously.[202,405] Compound stock solutions were prepared in DMSO and diluted 1000× in Krebs-Henseleit (KH) buffer. The depolarisation was recorded in mV. To determine if a compound caused activation of the nerve, non-cumulative concentration responses to potential tussive stimuli were carried out. A control response to the TRPV1 agonist capsaicin (1 μM) was carried out to determine nerve viability, following which the nerve was stimulated with single concentrations of a test compound for 2 minutes. After application of each concentration of the compound, the nerve was washed with KH buffer until it returned to baseline, and this was repeated with the full range of concentrations. A similar stimulation was also carried out with the vehicle control (DMSO). A further control response to TRPA1 agonist acrolein (300 μM) was carried out at the end of the experiment to determine nerve viability.

In order to study antagonism in TRPA1, the nerve was exposed to acrolein (300 μM) for 2 minutes and washed with KH buffer until the response returned to baseline. This was repeated to provide two control agonist responses. The nerve was then pre-treated with a test compound for 10 minutes, and then re-stimulated with acrolein (300 μM) for 2 minutes 20 seconds (the additional 20 seconds was to allow for the changeover of stimuli) to assess if the compound was able to affect the magnitude of the depolarisation induced by the acrolein. Following a brief washout, the nerve was exposed to acrolein (300 μM) for 2 minutes to provide a recovery response to ensure nerve viability and that the compound was washed off.

2.6 Indirect measure of covalent modification

To determine if the CADs undergo covalent modification through conjugate addition,[123] compound **AC18a** (4 equiv., 226 mM) and *N*-acetyl-L-cysteine methyl ester (1 equiv., 56 mM) or *N*-acetyl-L-cysteine (1 equiv., 61 mM) in d_6-DMSO were mixed together, and the progress of the reactions, if any, were monitored using ^{1}H NMR spectra recorded at 25 °C and at known time intervals.

2.7 hTRPA1 mutants

2.7.1 Primer design

Primers for the hTRPA1 (sequence ID / accession number: Y10601) mutants (C621A, F909A, Y926S, and F944A) were designed using the online Agilent QuikChange Primer Design Program (http://www.genomics.agilent.com/primerDesignProgram.jsp), and the mutants containing synthetic oligonucleotides were purchased from Eurofins Genomics (MWG Operon).

2.7.2 Site-directed mutagenesis

Information about the reagents and instruments that are not provided in the site-directed mutagenesis methodology description in **Sections 2.7.2.1 - 2.7.2.3** are provided in **Table 2.2**.

Table 2.2: *Information about materials, reagents, media and instruments used in the site-directed mutagenesis.*

Materials	Supplier and Preparation
Nuclease-free ddH_2O	DEPC Water, Omega Bio-tek, Inc.
Primers	(synthetic oligonucleotides) Eurofins Genomics MWG Operon
hTRPA1 dsDNA	100 ng TRPA1 cDNA in pcDNA3.1(+) (**Figure 2.4**)
PCR tubes	0.2 ml Thin-Walled Tubes with Domed Caps, Thermo Scientific
Thermal cycler	Techne® Prime 96 × 0.2 ml Thermal Cycler
Shaker	New Brunswick Scientific Innova® 40 Incubator Shaker Series
Broth	SOB Broth, Biotechnology grade, Amresco® Preparation: Broth (2.55 g) was dissolved in ddH_2O (100 ml) and the pH was adjusted to 7.5 with NaOH. Autoclaved at 120 °C for 20 minutes, and $MgSO_4$ (2 ml of 1 M, Sigma®) was sterile filtered (0.22 µm filter) into the broth.
Agar	LB-Agar (Miller) for Microbiology, VWR Chemicals BDH Prolabo® Preparation: Agar (4 g) was added to ddH_2O (100 ml), and autoclaved at 120 °C for 20 minutes.
Ampicillin	Ampicillin anhydrous, 96.0-100.5 % (anhydrous basis), Sigma-Aldrich
Agar plates	Agar was melted in a microwave oven prior to use and ampicillin (200 µg ml^{-1}) was added. Agar containing ampicillin (15 ml) was added to Petri-dishes (90 mm × 15 mm PE-LD)
Incubator	VWR® INCU-Line Digital Mini Incubator (for bacterial culture)
Glycerol	Glycerol for molecular biology, ≥ 99 %, G5516 Sigma-Aldrich
Agarose	Broad Separation range for DNA/RNA/Genetic Analysis Grade, Fisher BioReagents

Continued…

Continued…

Materials	Supplier and Preparation
PCR master mix (25 µl)	2.5 µl 10× DreamTaqGreen buffer (Thermo Fisher Scientific) 0.5 µl 10 µM hTRPA1 Primer mix (sense): 2D: 5′-CACAGCCATTCATTTTGCTG-3′ (**Figure 2.8**) 0.5 µl of 10 µM hTRPA1 Primer mix (antisense): 3U: 5′-AAGTGCAGTGTTCCCGTCT-3′ (**Figure 2.8**) 0.5 µl 10 mM dNTP mix (Thermo Fisher Scientific) 0.125 µl DreamTaq DNA Polymerase (Thermo Fisher Scientific) 20.875 µl nuclease-free ddH_2O
1× TAE buffer	50× Stock was diluted to 1× working solution in ddH_2O. 50× TAE stock solution was prepared in 1 litre ddH_2O with: 242 g Tris base (BP152-1, Fisher Scientific), 57.1 ml Glacial acetic acid (Sigma-Aldrich), 100 ml 0.5 M EDTA (pH 8.0) (Sigma-Aldrich). 1× TAE buffer contained 40 mM Tris base (pH 7.6), 20 mM acetic acid and 1 mM EDTA.
Midori Green	Midori Green Advance DNA Stain, MG04 Nippon Genetics Europe GmbH
1 kb DNA ladder	Thermo Fisher Scientific
Electrophoresis equipment	Flowgen Bioscience electrophoresis tank with PowerPac™ Basic Bio-Rad power supply
Molecular Imager	VersaDoc™ Imaging System 4000 MP interfaced to a computer with Quality One - 4.6.9 software, Bio-Rad
Microcentrifuge	Heraeus™ Pico 17 Centrifuge ThermoScientific

2.7.2.1 Mutant strand synthesis, *Dpn I* digestion and Bacterial transformation

Site-directed mutagenesis was carried out using a Agilent Technologies QuikChange Lightning Site-Directed Mutagenesis Kit (Catalog # 210518) as instructed in their manual (available from: https://www.agilent.com/cs/library/usermanuals/Public/210518.pdf). Briefly, TRPA1 mutants strands were synthesised by performing thermal cycling (PCR parameters are given in **Table 2.3**), followed by digestion of the parental- and hemi-methylated supercoiled double-stranded (ds)DNA in the amplified products with *Dpn* I (*Diplococcus pneumoniae*) restriction enzyme. The amplified DNA was then transformed into XL10-Gold ultracompetent cells (*E. coli*) treated with β-mercaptoethanol (to increase transformation efficiency) for nick repair. The transformation reaction mixture was added to an agar plate containing ampicillin antibiotic (200 µg ml^{-1}) and was incubated at 37 °C for 16 hours.

Table 2.3: *Thermal cycling conditions used for the syntheses of mutants strands.*

Segment	Steps	Cycles	Temperature / (°C)	Time / (s)
	Preheat lid		105	
1	Initial denaturation	1	95	120
2	Denaturation	18	95	20
	Annealing		60	10
	Extension		68	270 (30 s per kb of plasmid length)
3	Final extension	1	68	300
	Hold		10	∞

2.7.2.2 hTRPA1 expression in transformed *E. coli*

To verify the expression of hTRPA1 DNA in transformed *E. coli*, wherever possible, five single *E. coli* colonies from each agar plates were picked using a 20 µl pipette tip end, and a tiny amount of each colony was amplified in PCR master mix (25 µl, **Table 2.2**) by thermal cycling (PCR parameters are given in **Table 2.4**). A positive control (parental hTRPA1 dsDNA template) and a negative control (just PCR master mix) were also included. The remaining bacterial colony samples in the tips were placed (along with the tip) in broth (SOB, 5 ml) containing ampicillin (100 µg ml^{-1}) in separate 25 ml universal tubes at room temperature.

Table 2.4: *Thermal cycling conditions used to amplify the bacterial plasmids.*

Segment	Steps	Cycles	Temperature / (°C)	Time / (s)
	Preheat lid		105	
1	Initial denaturation	1	95	180
2	Denaturation	27	95	30
	Annealing		55	30
	Extension		72	60
3	Final extension	1	72	600
	Hold		10	∞

The amplified product from PCR was analysed by gel electrophoresis. Agarose solution (1.3 %) prepared in 1× TAE buffer (112.5 ml, **Table 2.2**) was stained with Midori Green DNA stain (5.625 µl), and solidified in an electrophoresis tray (15 × 15 cm) containing combs. Combs were removed and the electrophoresis tank was filled with 1× TAE buffer. Controls and samples (20 µl) were loaded into the wells (made in TAE agarose gel) along with 1 kb DNA ladder in a well. The electrophoresis was run at 110 V for ~45 minutes, and the gel was visualised using a molecular imager (UV illuminator) at 280 nm. Depending on the obtained DNA bands relative to the controls, the universal tubes containing the remaining bacterial samples in SOB were selected and

incubated at 37 °C overnight in an incubator shaker at 230 rpm, to allow expansion of the colonies and thereby to obtain high-copy plasmids.

2.7.2.3 Plasmid DNA purification, quantification and sequencing

Plasmid DNA was isolated from the saturated *E-coli* SOB culture (3 ml) using a NucleoSpin® Plasmid DNA purification miniprep kit (Macherey-Nagel) according to the manufacturer's protocol (available from: https://www.chemie.uni-kl.de/fileadmin/agpierik/Methoden/Nucleospin_Plasmid_no_lid_DNA_purification_Macherey-Nagel.pdf). The purified dsDNA in elution buffer was quantified using a NanoDrop spectrophotometer (NanoDrop Lite Spectrophotometer, Thermo Scientific). The instrument was calibrated to zero with a blank elution buffer (2 µl) before quantifying the samples, where the absorbance of the samples was measured at 260 nm. The samples were prepared for DNA sequencing by adding appropriate hTRPA1 primer (2 µl, 10 pmol μl^{-1}) to the purified DNA (15 µl, 50-100 ng μl^{-1}, diluted in nuclease-free ddH_2O) in a 1.5 ml safe-lock microcentrifuge tube. The primers were designated according to the conditions provided for DNA sequencing by the Eurofins Genomics (available from: https://www.eurofinsgenomics.eu/media/892645/samplesubmissionguide_valuereadtube.pdf). The hTRPA1 primer added to the DNA constructs containing the mutants F909, Y926 and F944 was 4D (5′-TACCAGCTCATCTGCAGTGG-3′), and to C621 was 3D (5′-AAGACGGGAACACTGCACTT-3′). The regions of the primers chosen in hTRPA1 sequence are shown in **Figure 2.8**. Premixed samples were DNA sequenced by the Eurofins Genomics DNA sequencing service (https://www.eurofinsgenomics.com/en/products/dna-sequencing/all-sequencing-options.aspx). The sequenced results were compared to the parent hTRPA1 sequence (sequence ID: Y10601) using the Nucleotide BLAST tool on PubMed (https://blast.ncbi.nlm.nih.gov/Blast.cgi).

```
        1 atgaagtgca gcctgaggaa gatgtggcgc cctggagaaa agaaggagcc ccagggcgtt
       61 gtctatgagg atgtgccgga cgacacggag gatttcaagg aatcgcttaa ggtggttttt
      121 gaaggaagtg catatggatt acaaaacttt aataagcaaa agaaattaaa aacatgtgac
      181 gatatggaca ccttcttctt gcattatgct gcagcagaag gccaaattga gctaatggag
      241 aagatcacca gagattcctc tttggaagtg ctgcatgaaa tggatgatta tggaaatacc
      301 cctctgcatt gtgctgtaga aaaaaaccaa attgaaagcg ttaagtttct tctcagcaga
      361 ggagcaaacc caaacctccg aaacttcaac atgatggctc ctctccacat agctgtgcag
      421 ggcatgaata atgaggtgat gaaggtcttg cttgagcata gaactattga tgttaatttg
      481 gaaggagaaa atggaaacac agctgtgatc attgcgtgca ccacaaataa tagcgaagca
      541 ttgcagattt tgcttaacaa aggagctaag ccatgtaaat caaataaatg gggatgtttc
      601 cctattcacc aagctgcatt ttcaggttcc aaagaatgca tggaaataat actaaggttt
      661 ggtgaagagc atgggtacag tagacagttg cacattaact ttatgaataa tgggaaagcc
      721 acccctctcc acctggctgt gcaaaatggt gacttggaaa tgatcaaaat gtgcctggac
2D    781 aatggtgcac aaatagaccc agtggagaag ggaaggtgca cagccattca ttttgctgcc
      841 acccagggag ccactgagat tgttaaactg atgatatcgt cctattctgg tagcgtggat
      901 attgttaaca caaccgatgg atgtcatgag accatgcttc acagagcttc attgtttgat
      961 caccatgagc tagcagacta tttaatttca gtgggagcag atattaataa gatcgattct
     1021 gaaggacgct ctccacttat attagcaact gcttctgcat cttggaatat tgtaaatttg
     1081 ctactctcta aaggtgccca agtagacata aaagataatt ttggacgtaa ttttctgcat
     1141 ttaactgtac agcaacctta tggattaaaa aatctgcgac ctgaatttat gcagatgcaa
     1201 cagatcaaag agctggtaat ggatgaagac aacgatgggt gtactcctct acattatgca
     1261 tgtagacagg ggggccctgg ttctgtaaat aacctacttg gctttaatgt gtccattcat
     1321 tccaaaagca aagataagaa atcacctctg cattttgcag ccagttatgg gcgtatcaat
     1381 acctgtcaga ggctcctaca agacataagt gatacgaggc ttctgaatga aggtgacctt
     1441 catggaatga ctcctctcca tctggcagca aagaatggac atgataaagt agttcagctt
     1501 cttctgaaaa aaggtgcatt gtttctcagt gaccacaatg gctggacagc tttgcatcat
     1561 gcgtccatgg gcgggtacac tcagaccatg aaggtcattc ttgatactaa tttgaagtgc
3D,3U1621 acagatcgct tggatgaaga cgggaacact gcacttcact ttgctgcaag ggaaggccac
     1681 gccaaagccg ttgcgcttct tctgagccac aatgctgaca tagtcctgaa caagcagcag
     1741 gcctcctttt tgcaccttgc acttcacaat aagaggaagg aggttgttct tacgatcatc
     1801 aggagcaaaa gatgggatga atgtcttaag attttcagtc ataattctcc aggcaataaa
     1861 tgtccaatta cagaaatgat agaatacctc cctgaatgca tgaaggtact tttagatttc
     1921 tgcatgttgc attccacaga agacaagtcc tgccgagact attatatcga gtataatttc
     1981 aaatatcttc aatgtccatt agaattcacc aaaaaaacac ctacacagga tgttatatat
     2041 gaaccgctta cagccctcaa cgcaatggta caaaataacc gcatagagct tctcaatcat
     2101 cctgtgtgta aagaatattt actcatgaaa tggttggctt atggatttag agctcatatg
     2161 atgaatttag gatcttactg tcttggtctc atacctatga ccattctcgt tgtcaatata
     2221 aaaccaggaa tggctttcaa ctcaactggc atcatcaatg aaactagtga tcattcagaa
     2281 atactagata ccacgaattc atatctaata aaaacttgta tgattttagt gtttttatca
     2341 agtatatttg ggtattgcaa agaagcgggg caaattttcc aacagaaaag gaattatttt
     2401 atggatataa gcaatgttct tgaatggatt atctacacga cgggcatcat ttttgtgctg
4D   2461 cccttgtttg ttgaaatacc agctcatctg cagtggcaat gtggagcaat tgctgtttac
     2521 ttctattgga tgaatttctt attgtatctt caaagatttg aaaattgtgg aatttttatt
     2581 gttatgttgg aggtaatttt gaaaactttg ttgaggtcta cagttgtatt tatcttcctt
     2641 cttctggctt ttggactcag cttttacatc ctcctgaatt tacaggatcc cttcagctct
     2701 ccattgcttt ctataatcca gaccttcagc atgatgctag gagatatcaa ttatcgagag
     2761 tccttcctag aaccatatct gagaaatgaa ttggcacatc cagttctgtc ctttgcacaa
     2821 cttgtttcct tcacaatatt tgtcccaatt gtcctcatga atttacttat tggtttggca
     2881 gttggcgaca ttgctgaggt ccagaaacat gcatcattga agaggatagc tatgcaggtg
     2941 gaacttcata ccagcttaga gaagaagctg ccactttggt ttctacgcaa agtggatcag
     3001 aaatccacca tcgtgtatcc caacaaaccc agatctggtg ggatgttatt ccatatattc
     3061 tgtttttat tttgcactgg ggaaataaga caagaaatac caaatgctga taaatcttta
     3121 gaaatggaaa tattaaagca gaaataccgg ctgaaggatc ttacttttct cctggaaaaa
     3181 cagcatgagc tcattaaact gatcattcag aagatggaga tcatctctga gacagaggat
     3241 gatgatagcc attgttcttt tcaagacagg tttaagaaag agcagatgga acaaaggaat
     3301 agcagatgga atactgtgtt gagagcagtc aaggcaaaaa cacaccatct tgagccttag
```

Figure 2.8: *mRNA sequence of hTRPA1. Letters in blue shows the position of primers used in the mutagenesis study, where D denotes down codon (sense), and U denotes up codon (antisense). The yellow highlights are the bases of the residues, C621 (1861, 1862, 1863), F909 (2725, 2726, 2727), Y926 (2776, 2777, 2778) and F944 (2830, 2831, 2832), respectively.*

2.7.3 Generation of stable hTRPA1 transfected HEK293 cells

2.7.3.1 Transfection

HEK293 cells were grown to 50-80 % confluence in a petri-dish (60 × 15 mm, PS Tissue culture dish, Sarstedt) in complete DMEM (supplemented with 2 mM L-glutamine, 100 U ml^{-1} penicillin - 100 U ml^{-1} streptomycin, and 10 % v/v FBS). On the day of transfection, the culture medium was replaced with 2 ml Opti-MEM® (1×) Reduced Serum Medium (Gibco®, Life Technologies™). The transfection reagent was prepared in a polystyrene universal tube (30 ml Universal Container, Scientific Laboratory Supplies) by mixing 40 µl FuGENE® 6 Transfection Reagent (Promega) into 2 ml Opti-MEM at room temperature, and the mixture was incubated for 5 minutes at room temperature. To that, 13.3 µl of 0.3 µg $µl^{-1}$ dsDNA was added, mixed and incubated for a further 15 minutes at room temperature to equilibrate. The transfection reagent FuGENE and DNA were added in 3:1 ratio. The Opti-MEM in the culture dish was replaced with the prepared transfection reaction mixture and incubated at 37 °C for 24 hours in a humidified cell culture incubator with 5 % CO_2.

The reaction mixture was then replaced with 2 ml non-selective (no G418) complete DMEM and incubated in the cell culture incubator for 24 hours. The culture medium was then replaced with 4 ml fresh complete DMEM containing G418 (0.5 mg ml^{-1}) and incubated for another 48 hours to allow selection of G418-resistance cells. The culture medium was changed frequently thereafter to remove dead cells and debris, and to maintain the G418 concentration. Depending on the confluency of the cells, they were transferred to a T25 (Corning) or T75 cell culture flask and maintained in G418 selective DMEM for 7-14 days.

2.7.3.2 Single cell cloning

The transfected cells were single cell cloned by serial dilution in a 96-well cell culture plate (Polystyrene, Flat Bottom, Costar®) as per the Corning's procedure (available from: http://csmedia2.corning.com/LifeSciences/media /pdf/Single_cell_cloning_protocol.pdf). Briefly, 200 µl of cell suspension of concentration 1×10^5 cells ml^{-1} in culture medium (complete DMEM with 0.25 mg ml^{-1} G418) was added to the first well (A1) of 96-well plate containing 100

µl culture medium in all 96 wells, and diluted in 1:2 down the column (A1-H1) from the previous well (i.e. A1-B1, B1-C1, C1-D1). Then fresh 100 µl culture medium was added to the wells in the first column (A1-H1). Using a multichannel pipette, 100 µl of cell suspension from the wells in the first column (A1-H1) was transferred to the wells in the second column (A2-H2), then from second (A2-H2) to the third column (A3-H3), and repeated this 1:2 dilutions across the whole plate, and finally discarded 100 µl from the last column (A8-H8). Fresh culture medium, 100 µl, was added to all the 96 wells to make up the final volume to 200 µl, and the plate was incubated at 37 °C in a humidified cell culture incubator with 5 % CO_2 for 7-10 days.

On the seventh day, all the wells were visualised under an inverted microscope (VWR) and the wells containing single colonies were marked. The colonies were left to expand in the plate for another 3-4 days, and the monoclonal cells were first transferred to a 6-well cell culture plate (Polystyrene, Flat Bottom, Costar® or Greiner Bio-One CELLSTAR®) containing 3 ml culture medium and incubated for another 7 days for expansion before transferring to T75 flasks.

Once the cells reached 80-90 % confluence they were passaged and screened with known agonists and antagonists (standard ligands) by calcium signalling (**Section 2.4.2**) to identify the clones expressing hTRPA1. Unresponsive cells (non-transfected parental HEK293 cells) were discarded and the responses obtained with hTRPA1 mutant expressing cells were compared against the responses obtained with the wild-type hTRPA1. For the flask of cells that showed a diminished response (due to the presence of some parental HEK293 cells), a second round of single cell cloning was carried out.

2.7.4 Gene expression

To determine the level of hTRPA1 gene expressed in the wild-type and mutant hTRPA1 transfected HEK293 cells, the cells were assessed using intracellular flow cytometric analysis. Cells grown in T75 flasks were harvested and diluted in 1× PBS to a density of 5×10^6 cells ml^{-1}. The cell suspension (100 µl) was added to a 96-well plate (Round bottom, Standard TC-Plate, Sarstedt) and centrifuged at 370 × *g* (eppendorf Centrifuge 5810 R) for 5 minutes at 4 °C.

The cells were fixed with 100 µl of 1 % paraformaldehyde (Fluka Chemika, prepared in 1× PBS) by incubating at room temperature for 20 minutes, and washed with 1× PBS (2 × 100 µl) by centrifuging as before. The cells were permeabilised by incubating with 100 µl of 90 % cold methanol (VWR Chemicals) for 30 minutes on ice and washed with PBS as earlier. Before immunostaining, the cells were blocked using 0.5 % cold Bovine Serum Albumin (BSA, Standard Grade Powder, Fisher Scientific, prepared in 1× PBS) blocking buffer for 30 minutes at room temperature.

The cells were first stained with either 10 µg ml^{-1} isotype antibody control (Purified Mouse IgG_1, κ Isotype, BioLegend®) or 10 µg ml^{-1} primary antibody (ANKTM1 (C-5) mouse monoclonal IgG_1, Santa Cruz Biotechnology) in blocking buffer (50 µl) for 30 minutes on ice, and washed with 100 µl fresh blocking buffer. The cells were then stained with 5 µg ml^{-1} secondary antibody (Anti-mouse IgG (Fc specific) FITC Conjugate, Sigma) for 30 minutes on ice in the dark, and washed with blocking buffer and resuspended in 1× PBS (100 µl). The samples were transferred to FACS tubes (Tubes 5 ml, PP, Round bottom, Greiner bio-one) containing 1× PBS (150 µl), and analysed using a Flow Cytometer (Becton Dickinson FACSCalibur™) interfaced to a computer with BD CellQuest Pro™ software. The isotype antibody control was used to set or define the gate level. The data were further analysed using Flowing Software 2.5.1 (http://flowingsoftware.btk.fi/index.php?page=3).

CHAPTER 3: *N*-Cinnamoylanthranilates as modulators of TRPA1

3.1 Introduction

In numerous studies, analogues of *N*-cinnamoylanthranilic acid have shown a wide range of biological activities, including anti-allergic, anti-histaminic, anti-inflammatory, anti-asthmatic,[278,279,311] anti-oxidant,[288,313] anti-fibrotic,[406] anti-proliferative,[306,314] anti-cancer,[310,407] anti-platelet,[408] anti-coagulant[304] and as modulators of B-cells and T-cells,[336,337] and are under investigations for several medicinal applications. The derivative *N*-(3,4-dimethoxycinnamoyl) anthranilic acid (also known as tranilast or Rizaben™) is an anti-inflammatory drug marketed in South Korea and Japan, and has been used for more than twenty years to treat several allergic diseases such as bronchial asthma, allergic rhinitis, hypertrophic scars and scleroderma.[275,278,279,406] It also possesses other biological activities (**Section 1.2** of **Chapter 1**) to those mentioned above. Moreover, *N*-cinnamoylanthranilate derivatives (CADs) have been shown to inhibit TRP channels. For example *N*-(*p*-amylcinnamoyl)anthranilic acid (ACA), which is also a PLA_2 inhibitor,[330] was characterised as a novel TRPM2 (IC_{50} 4.5 μM), TRPM8 (IC_{50} 3.9 μM), TRPC3 (IC 20 μM), TRPC6 (IC_{50} 2.3 μM) and TRPV1 (IC >20 μM) channel blocker.[327] Similarly, *N*-(3-methoxyphenyl)-4-chlorocinnamide (SB366791) has been shown to selectively block TRPV1 (IC_{50} 6 nM)[409] and inactive against TRPM8.[410] The related compounds 5-nitro-2-(phenethylamino)benzoic acid (NPEB, EC_{50} 5.65 μM), 5-nitro-2-(phenethylamino)benzamide (NPBA, EC_{50} >100 μM) and 5-nitro-2-(3-phenylpropylamino)benzoic acid (NPPB, EC_{50} 0.37 μM) selectively activated TRPA1 channels.[411]

Based on the reported evidence, it was anticipated that TRPA1 cation channel specific modulators could be attained by incorporating different substituents and substitution patterns in the *N*-cinnamoylanthranilic acid core structure. Consequently, a series of *N*-cinnamoylanthranilate derivatives (CADs) with different substituents were synthesised to study their structure-activity relationship (SAR) with the non-selective cation channel TRPA1, and thereby the pharmacology of TRPA1 modulators. The chemical structures of the

synthesised CADs are given in **Figure 3.1** and also in the **Appendix**, and the mechanisms of the chemical reactions are shown in **Section 3.2**. All of the synthesised CADs exist in the literature (**Section 3.3**), except *N*-(3-ethoxy-4-hydroxycinnamoyl)anthranilic acid (**AC27**) which is a novel compound. However, this is the first time CADs are being reported as TRPA1 modulators.

Twenty-two derivatives of *N*-cinnamoylanthranilic acid and some of their corresponding methyl ester were screened for agonism and antagonism responses in HEK293 cells stably transfected with hTRPA1, where the transient elevations of $[Ca^{2+}]_i$ were measured using a calcium signalling technique (**Sections 3.4.1** and **3.4.2**). The selectivity of these ligands was determined by evaluating in HEK293 cells stably transfected with pcDNA3 (mock) and hTRPM8 (**Section 3.4.3**). In addition, the reversibility were assessed (**Section 3.4.4**), and the physicochemical properties of all the CADs were considered and correlated with their activities (**Section 3.4.5**). Some of the derivatives were further characterised in Dunkin-Hartley guinea pig vagus nerve preparation (**Section 3.4.6**), and any involvement of CAD in covalent modification of cysteines through conjugate addition were measured using a model thiol (**Section 3.5**). Further to the study undertaken and from the review of biological activities of CADs in the literature (**Section 1.2** of **Chapter 1**), it is anticipated that there could be a correlation between several reported biological activities of CADs and TRP channels (**Section 3.6**).

3.2 Synthetic chemistry

The series of CADs given in **Figure 3.1** were successfully synthesised in good yields by the synthetic approaches given in **Section 2.2** of **Chapter 2**, and the underlying mechanisms of the chemical reactions carried out are shown in **Schemes 3.1** to **3.6**.

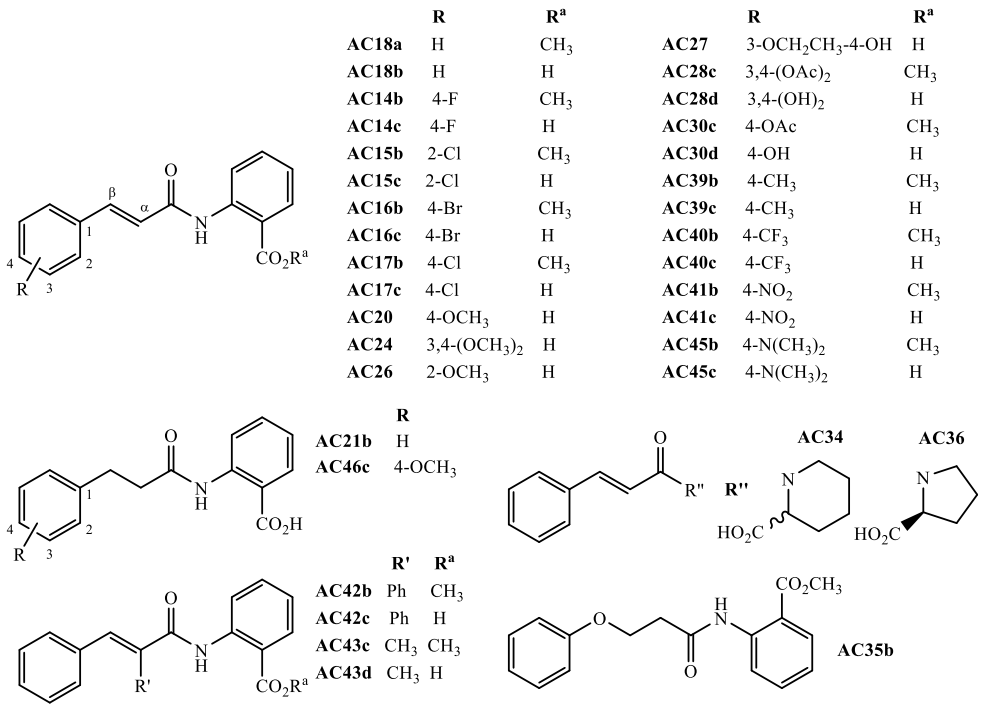

Figure 3.1: *Chemical structures of the synthesised and screened N-cinnamoylanthranilates.*

3.2.1 *N*-Cinnamoylanthranilates from cinnamic acids

N-Cinnamoylanthranilic acid was produced from cinnamic acid through the reaction mechanism shown in **Scheme 3.1**, in which the cinnamic acid first gets converted to its acid chloride by oxalyl chloride and couples to methyl anthranilate in the presence of pyridine to form methyl *N*-cinnamoylanthranilate, and then hydrolyses under a strong basic condition to yield the product. Methyl anthranilate was used instead of anthranilic acid to couple with cinnamoyl chloride, since direct coupling of cinnamoyl chloride with anthranilic acid is known to produce (*E*)-2-styryl-4*H*-benzo[*d*][1,3] oxazin-4-one as a result of intramolecular cyclisation,[378] as shown in **Scheme 3.2**. With the use of methyl anthranilate, the cyclisation is prevented due to the absence of the carboxylic acid group and produces the corresponding methyl *N*-cinnamoylanthranilate. α-Methylcinnamic acid was produced using benzaldehyde and propionic anhydride *via* the Perkin reaction as shown in **Scheme 3.3**.

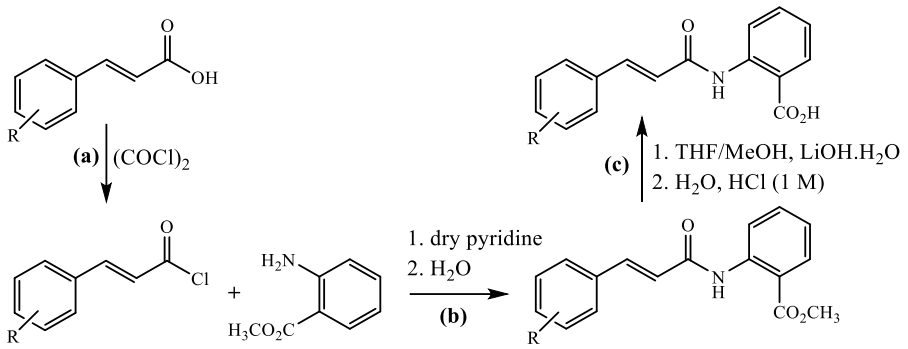

(a) *Acylation of cinnamic acid*

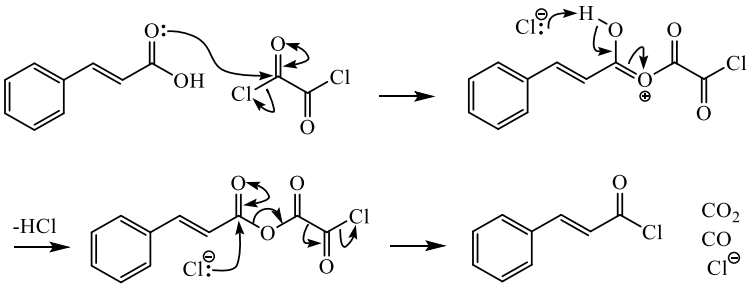

(b) *Coupling of cinnamoyl chloride with methyl anthranilate*

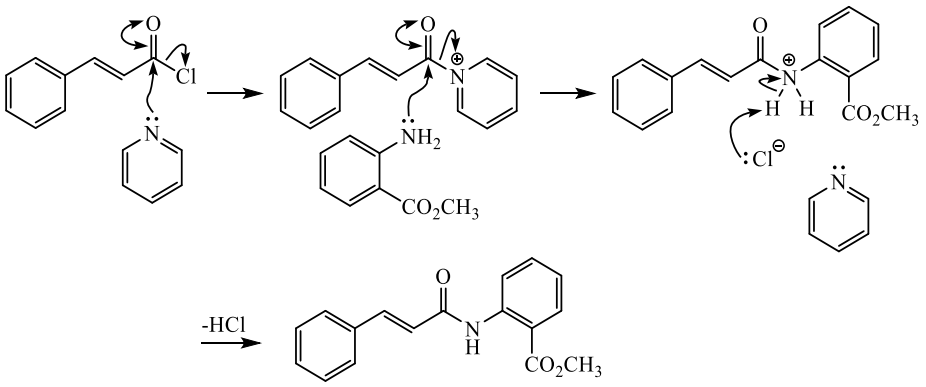

(c) *Hydrolysis of methyl N-cinnamoylanthranilate*

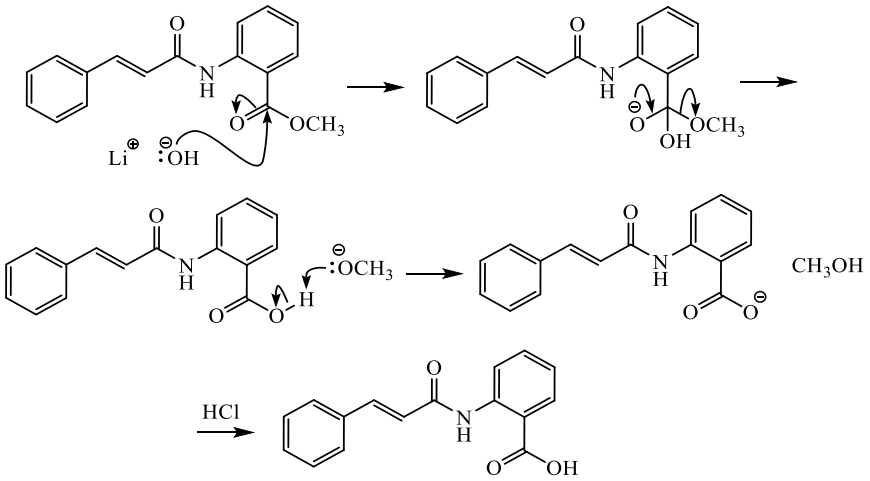

Scheme 3.1: *Reaction mechanism for the formation of N-cinnamoylanthranilate derivatives from cinnamic acid derivatives,* **(a)** *acylation of cinnamic acid,* **(b)** *coupling of cinnamoyl chloride with methyl anthranilate to form methyl N-cinnamoylanthranilate and* **(c)** *hydrolysis of the ester to produce N-cinnamoylanthranilic acid.*

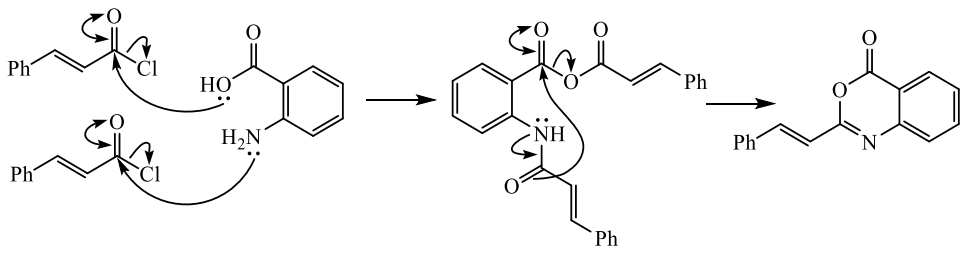

Scheme 3.2: *Reaction mechanism showing that direct coupling of cinnamoyl chloride with anthranilic acid react in 2:1 ratio to produce (E)-2-styryl-4H-benzo[d][1,3]oxazin-4-one via intramolecular cyclisation.*

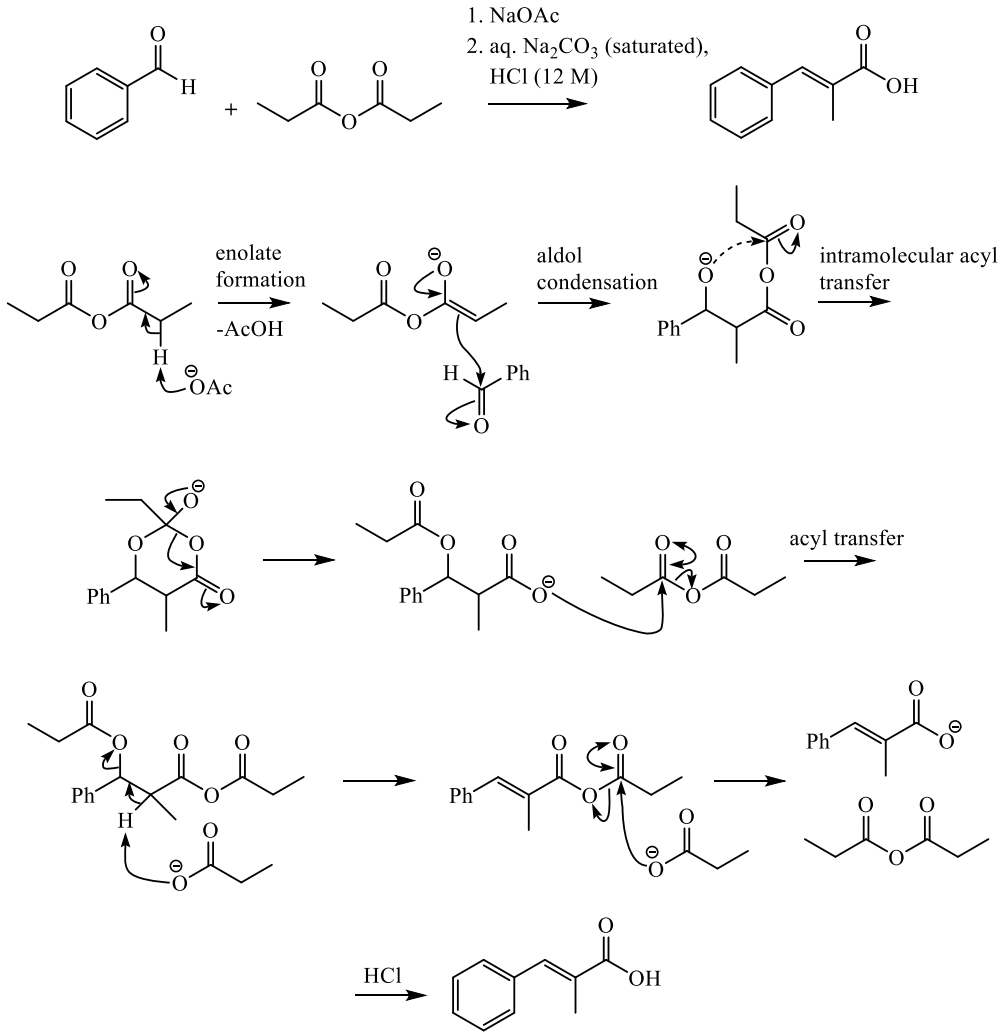

Scheme 3.3: *Reaction mechanism for the formation of α-methylcinnamic acid via Perkin reaction.*

3.2.2 *N*-Cinnamoylanthranilates from aldehydes

The reaction mechanism by which Meldrum's acid is produced from malonic acid, acetic anhydride and acetone is shown in **Scheme 3.4**. To produce *N*-cinnamoylanthranilic acid, Meldrum's acid reacts with anthranilic acid to form 2-[(carboxy)acetyl]aminobenzoic acid, which then condenses with a benzaldehyde derivative *via* a piperidine-catalysed Knoevenagel condensation as shown in **Scheme 3.5**.

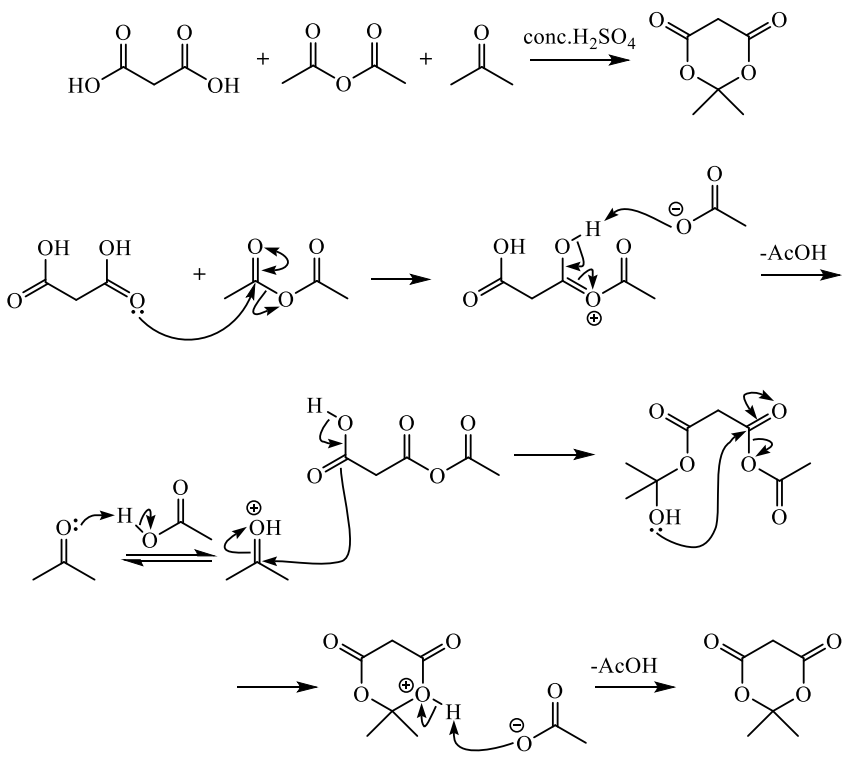

Scheme 3.4: *Reaction mechanism for the formation of Meldrum's acid.*

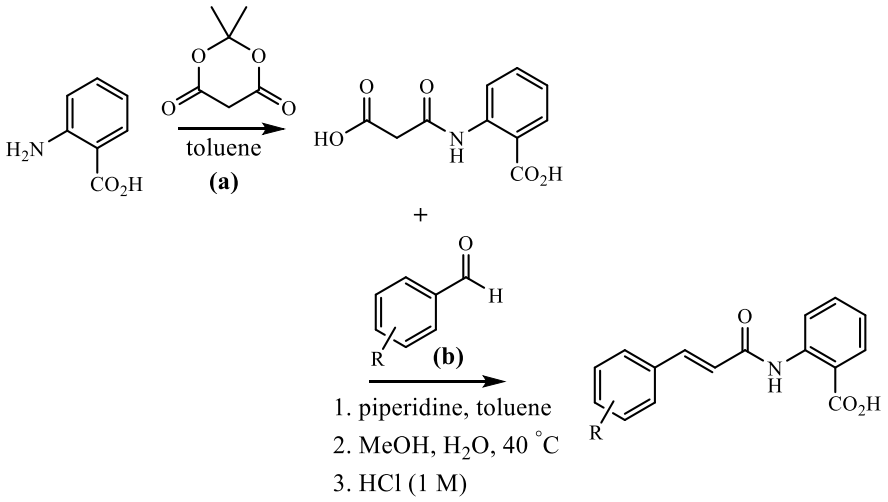

(a) *Formation of 2-[(carboxy)acetyl]aminobenzoic acid*

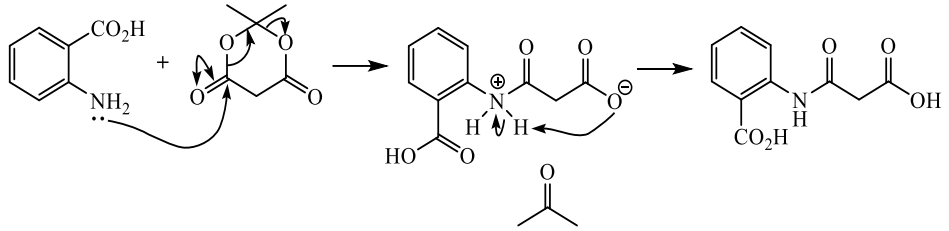

(b) *Knoevenagel condensation*

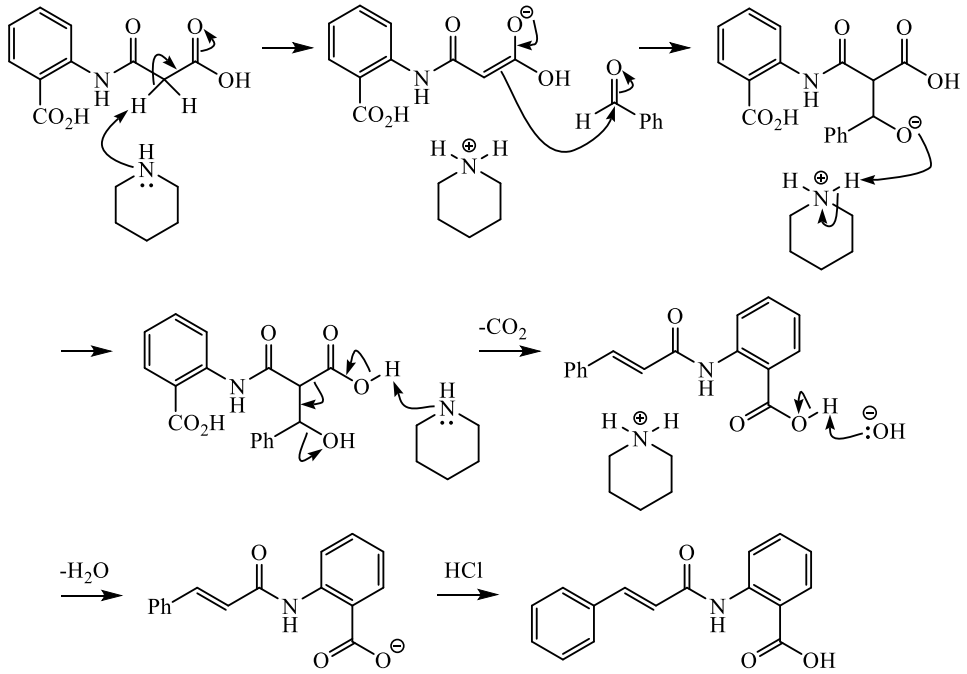

Scheme 3.5: *Reaction mechanism for the formation of N-cinnamoylanthranilate derivatives from aldehyde derivatives,* **(a)** *2-[(carboxyacetyl)amino]benzoic acid is produced by reacting Meldrum's acid with anthranilic acid and* **(b)** *2-[(carboxyacetyl)amino]benzoic acid is condensed with a benzaldehyde via Knoevenagel condensation to produce N-cinnamoylanthranilic acid.*

3.2.3 *N*-Cinnamoyl amino acids

The mechanism by which a cinnamoyl chloride couples to a secondary amino acid under a basic condition is shown in **Scheme 3.6**. The method of this reaction was followed exactly as in the literature,[382] and produced relatively low yield (30-50 %) compared to the other two approaches in **Sections 3.2.1** and **3.2.2**.

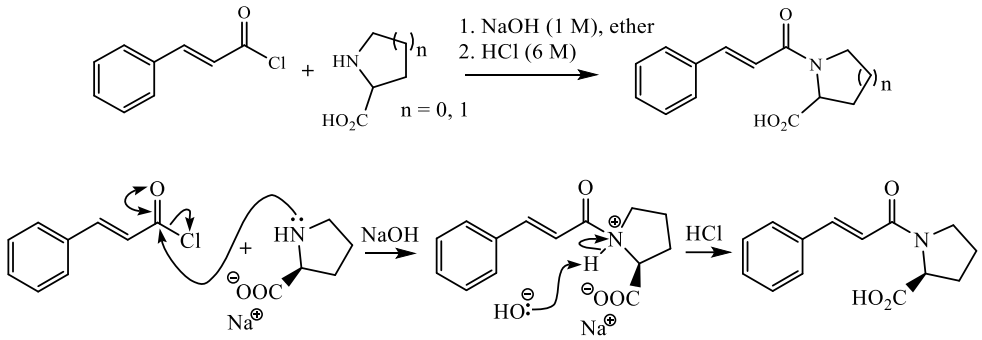

Scheme 3.6: *Reaction mechanism for the formation of N-cinnamoyl amino acids.*

3.3 Chemical information

All the chemical compound characterisation data are given in **Section 2.2.4** of **Chapter 2** along with the synthesis procedures. In ^{1}H NMR, the peaks corresponding to the free carboxylic acid protons were not observed as was the amide proton peak for the compound **AC41** (due to exchangeable NH proton). Due to the presence of rotamers for the compounds **AC34** and **AC36**, and C-F coupling for the compounds **AC14** and **AC40**, doubling or splitting of some carbon signals, respectively, were observed in the ^{13}C NMR. The percentages of the CHN elemental composition found were within ± 0.4 % of the theoretical values. The chemical characterisation results obtained agreed closely with the data of the compounds already reported in the literature (**Table 3.1**). Highly pure compounds as determined by CHN combustion elemental microanalysis, ^{1}H and ^{13}C NMR, and constant melting point were used in the biological activity assays.

Table 3.1: *Chemical data for the synthesised N-cinnamoylanthranilates available in the literature. Abbreviations: nda - no data available, nf - not found.*

Compound name	Code	Reference(s)
Methyl *N*-cinnamoylanthranilate	AC18a	383
N-Cinnamoylanthranilic acid	AC18b	378,381,384
Methyl *N*-(4-fluorocinnamoyl)anthranilate	AC14b	nda
N-(4-Fluorocinnamoyl)anthranilic acid	AC14c	278
Methyl *N*-(2-chlorocinnamoyl)anthranilate	AC15b	nda
N-(2-Chlorocinnamoyl)anthranilic acid	AC15c	384
Methyl *N*-(4-bromocinnamoyl)anthranilate	AC16b	320
N-(4-Bromocinnamoyl)anthranilic acid	AC16c	279,320
Methyl *N*-(4-chlorocinnamoyl)anthranilate	AC17b	nda
N-(4-Chlorocinnamoyl)anthranilic acid	AC17c	384
N-Hydrocinnamoylanthranilic acid	AC21b	385,412
N-(4-Methoxycinnamoyl)anthranilic acid	AC20	276,282,381,384
N-(3,4-Dimethoxycinnamoyl)anthranilic acid	AC24	381,384
N-(2-Methoxycinnamoyl)anthranilic acid	AC26	nda
N-(3-Ethoxy-4-hydroxycinnamoyl)anthranilic acid	AC27	nf
Methyl *N*-(3,4-diacetoxycinnamoyl)anthranilate	AC28c	nda
N-(3,4-Dihydroxycinnamoyl)anthranilic acid	AC28d	276,381,386
Methyl *N*-(4-acetoxycinnamoyl)anthranilate	AC30c	nda
N-(4-Hydroxycinnamoyl)anthranilic acid	AC30d	273,282
N-Cinnamoylpipecolinic acid	AC34	nda
N-Cinnamoylproline	AC36	382
Methyl *N*-(3-phenoxypropionoyl)anthranilate	AC35b	387
Methyl *N*-(4-methylcinnamoyl)anthranilate	AC39b	nda
N-(4-Methylcinnamoyl)anthranilic acid	AC39c	282
Methyl *N*-(4-trifluoromethylcinnamoyl)anthranilate	AC40b	nda
N-(4-Trifluoromethylcinnamoyl)anthranilic acid	AC40c	nda
Methyl *N*-(4-nitrocinnamoyl)anthranilate	AC41b	nda
N-(4-Nitrocinnamoyl)anthranilic acid	AC41c	nda
Methyl *N*-(α-phenylcinnamoyl)anthranilate	AC42b	nda
N-(α-Phenylcinnamoyl)anthranilic acid	AC42c	nda
Methyl *N*-(α-methylcinnamoyl)anthranilate	AC43c	nda
N-(α-Methylcinnamoyl)anthranilic acid	AC43d	nda
Methyl *N*-(4-dimethylaminocinnamoyl)anthranilate	AC45b	nda
N-(4-Dimethylaminocinnamoyl)anthranilic acid	AC45c	413
N-(4-Methoxyhydrocinnamoyl)anthranilic acid	AC46c	nda

3.4 Pharmacology of *N*-cinnamoylanthranilates

3.4.1 Calcium signalling

Agonism of the compounds were measured by assessing the influx of Ca^{2+} in TRPA1-HEK293 cells upon exposure to the test compounds relative to calcimycin, and antagonism of the compounds were measured by the ability of the test compounds to antagonise the agonism of a standard agonist (**Section 2.4.2** of **Chapter 2**). Hence the agonism and antagonism responses ($[Ca^{2+}]_i$ released) of the compounds are presented as the percentage of calcimycin and the standard agonist, respectively. The responses were normalised by subtracting the noise/response obtained for the vehicle control (DMSO). The maximum response in antagonist assays was obtained by normalising the standard agonist-induced response (CA, ACR or WS5) to 100 %, and thus in antagonist assays, a higher percentage value indicates a lower inhibitory effect by the test compound.

3.4.1.1 Solubility of compounds

The compounds containing a free carboxylic acid group were evaluated in the cells as their corresponding carboxylate salt due to deprotonation in the slightly alkaline isotonic assay buffer (pH 7.4). For some derivatives, their insolubility/reprecipitation in the aqueous assay buffer at higher concentrations (300 μM or in some cases greater than 100 μM) was the limiting factor in obtaining a complete dose-response (concentration-effect) curve. Also, most of the methyl esters of CADs were partially soluble or insoluble above 3 μM in the aqueous phase, and hence screening of the esters at higher concentrations was not attainable. Reprecipitation was recorded as spikes in the fluorescence spectrum obtained, due to interruption of the light beam of the spectrophotometer by the solid particles formed once the compound solution prepared in DMSO was added to the assay buffer.

3.4.1.2 Suitability of compounds

As the CADs, **AC28d** ($\lambda_{Ex/Em}$ 393/461) and **AC45c** ($\lambda_{Ex/Em}$ 378/502) were found to autofluoresce (**Figure 3.2**) in the wavelength regions of Fluo-3 ($\lambda_{Ex/Em}$ 506/526 nm) or Fluo-4 ($\lambda_{Ex/Em}$ 494/506 nm) dyes, screening of those two

compounds was not achievable. Due to broad absorption ranges for the two compounds, other long-wavelength calcium dyes such as Calcium Orange ($\lambda_{Ex/Em}$ 549/576 nm) and Calcium Crimson ($\lambda_{Ex/Em}$ 590/615 nm) were also not suitable for screening.

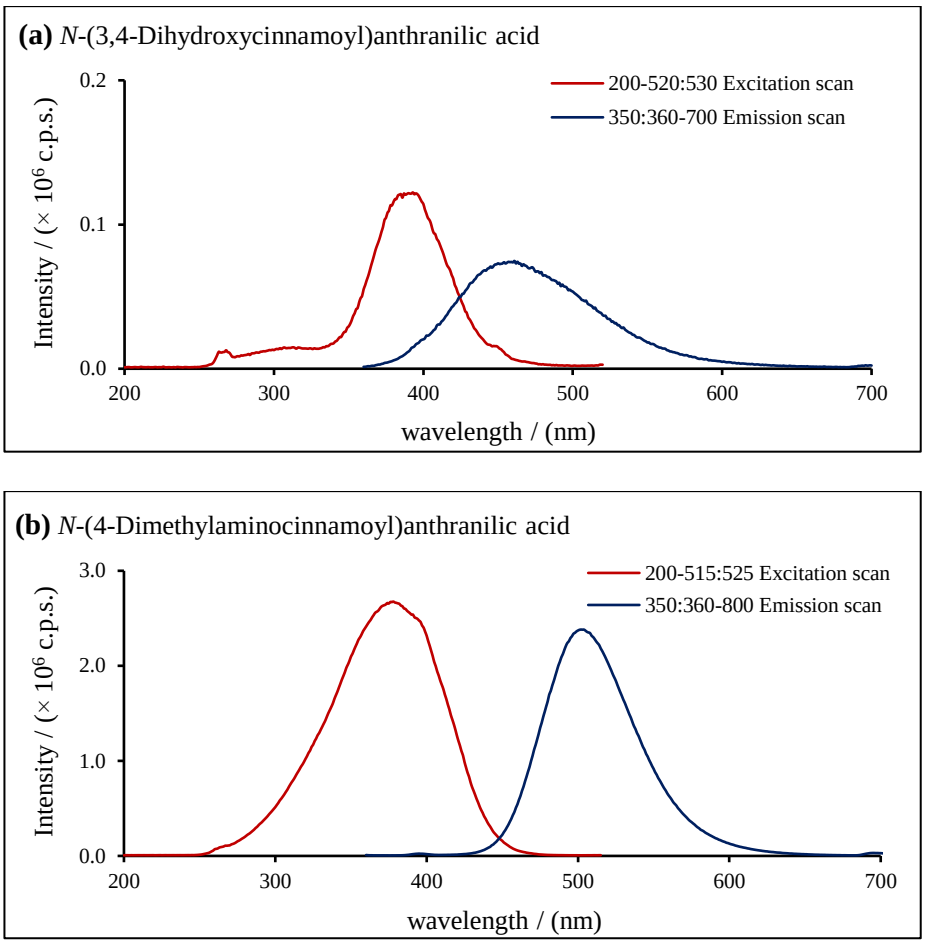

Figure 3.2: *UV-vis absorption and fluorescence spectra of the CAD,* **(a) AC28d** *($\lambda_{Ex/Em}$ 393/461 nm) and* **(b) AC45c** *($\lambda_{Ex/Em}$ 378/502 nm), in isotonic assay buffer.*

3.4.1.3 Variability in responses with different methods

Calcium signalling assays were carried out either in the cuvette-based system using a PTI instrument (**Section 2.4.2.1** of **Chapter 2**) or in the micro-well plate system using a FlexStation (**Section 2.4.2.2** of **Chapter 2**). The only major differences between the two methods were that in the cuvette-based system the cells were in suspension loaded with Fluo-3, whereas in the micro-well plate system the cells loaded with Fluo-4 were adhered to the well surface (native state). However, the estimated EC_{50} values obtained from the fitted

dose-response curves for cinnamaldehyde with Fluo-3 and Fluo-4 (**Figure 3.3**) were 27 and 9 µM, respectively, which is a 0.5 log scale difference that is statistically significant ($p < 0.0001$). This could have been due to the effect of the higher sensitivity of Fluo-4 relative to Fluo-3, as specified in a characterisation study of Fluo-4[414] and in a comparative study of Fluo Ca^{2+} indicators.[415] In addition, different experimental systems might have had an effect, but that needs to be verified.

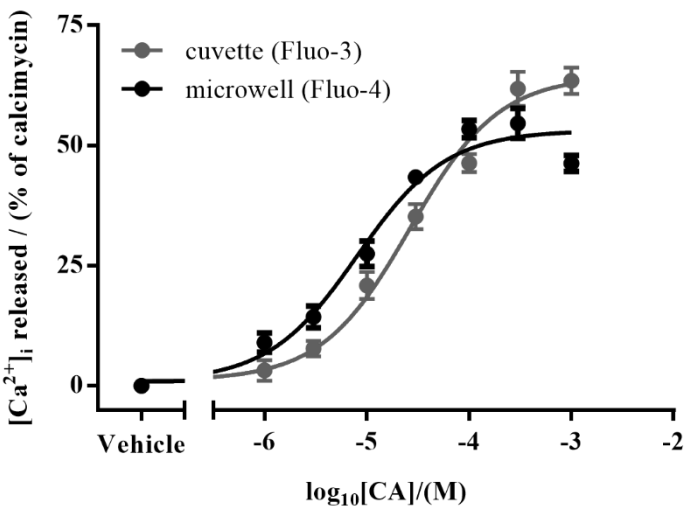

Figure 3.3: *Comparison of the cinnamaldehyde (CA) dose-response curves obtained in two different calcium signalling assay systems with hTRPA1-HEK293 cells either loaded with Fluo-3 or Fluo-4 fluorescent dye, where the obtained EC_{50} values, 27 and 9 µM, respectively, were significantly different ($p < 0.0001$). Each data point on the curve represents the mean of three independent experiments ($N = 3$) in triplicates ($n = 9$) with their SEM, and the statistical significance between the two data sets' $logEC_{50}$ values was determined using the F-test at $p < 0.05$.*

3.4.1.4 Choice of carrier solvent

DMSO and ethanol (EtOH) are the commonly used carrier solvents for water insoluble lipophilic compounds in biochemical studies. These solvents are capable of solubilising both polar and non-polar compounds. However, a significantly different $logEC_{50}$ values ($p < 0.0001$) were obtained when cinnamaldehyde solution prepared in DMSO and EtOH, separately, were evaluated against hTRPA1-HEK293 cells (**Figure 3.4**). The EC_{50} values obtained from the estimated non-linear curve fit for cinnamaldehyde in DMSO was 9 µM, but in EtOH it was 155 µM. The seventeen-fold difference in the values could have been due to membrane permeability issues. DMSO is known

to improve absorbability of drugs that are less water-soluble by increasing permeability across cell membranes,[416] and hence a lower EC_{50} value could have been observed with the use of DMSO compared to ethanol. As a result, DMSO was used as the carrier solvent in the cell-based assays.

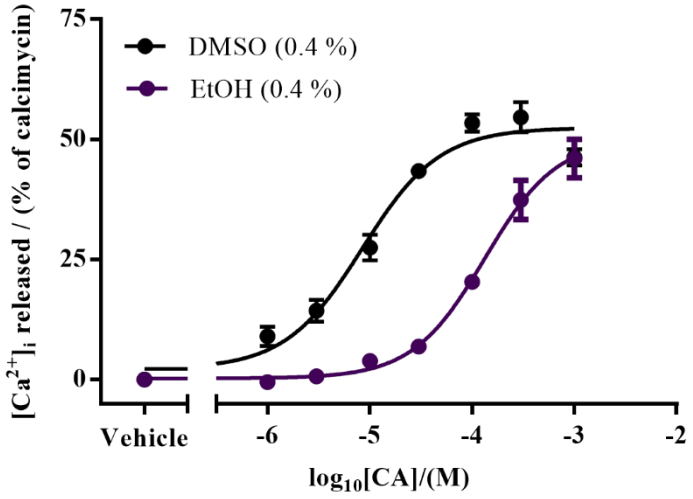

Figure 3.4: *Comparison of the responses obtained in hTRPA1-HEK293 cells for cinnamaldehyde (CA) made in either DMSO or ethanol (0.4 %) solvent, where the obtained EC_{50} values, 9 and 155 µM, respectively, were significantly different ($p < 0.0001$). Each data point represents the mean ± SEM ($N = 3$, $n = 9$), and the statistical significance between the two data sets' $logEC_{50}$ values was determined using the F-test at $p < 0.05$.*

3.4.1.5 Controls

The maximum response control, calcimycin, is an ionophore (mobile-ion carrier) which chelates divalent Ca^{2+} present in the cells, and thereby increases/saturates the intracellular Ca^{2+} concentration, giving a maximum possible response for a given particular amount of cells in a sample. Calcimycin tested at different concentrations (1 to 10 µM), including the concentrations (2 or 8 µM) used in the experiments, did not show any significant difference ($p \geq 0.05$) in the change in relative fluorescence intensity (ΔRFU), that is, in the total amount of $[Ca^{2+}]_i$ released (**Figure 3.5**).

The standard agonists and antagonists for positive controls were chosen based on the ion channel specificity and potency of the ligands. To determine the EC_{50} and IC_{50} values of the standard TRPA1 agonist cinnamaldehyde and antagonist A967079, and TRPM8 agonist WS5 and antagonist AMTB.HCl, in

the experimental system used in the study, dose-response curves were carried out (**Figures 3.6** and **3.7**).

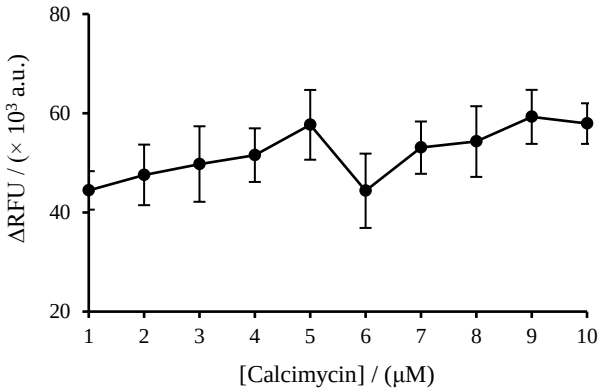

Figure 3.5: *Calcimycin response at different concentrations (1 - 10 μM) in hTRPA1-HEK293 cells. The responses obtained at different concentrations were statistically insignificant ($p \geq 0.05$). Each data point represents the mean ± SD (N = 3), and the statistical significance was determined using one-way ANOVA at $p < 0.05$.*

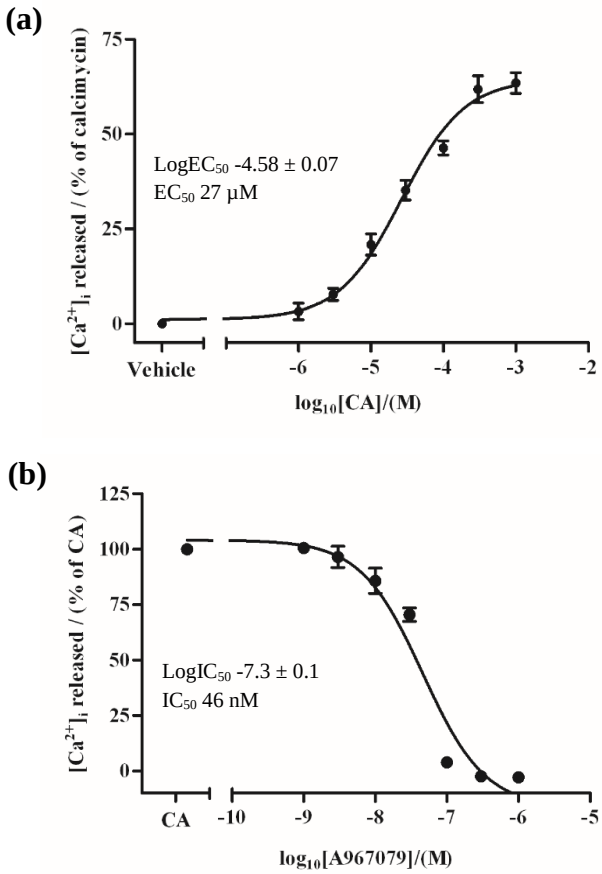

Figure 3.6: *Dose-response curves of the standard TRPA1 agonist and antagonist,* **(a)** *cinnamaldehyde (CA) and* **(b)** *A967079 (against 30 μM CA), respectively, evaluated in hTRPA1-HEK293 cells. Each data point represents the mean ± SEM (N = 3, n = 6).*

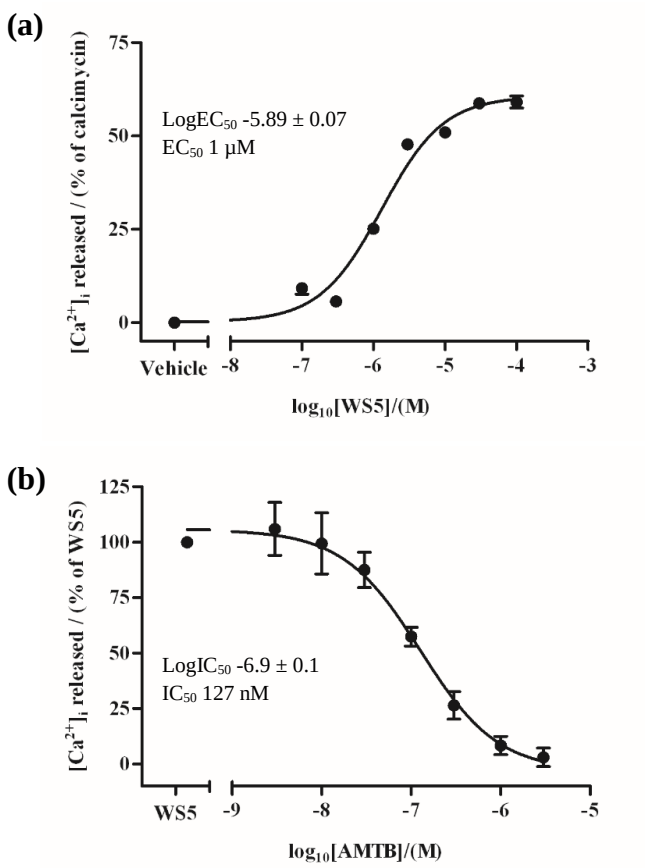

Figure 3.7: *Dose-response curves of the standard TRPM8 agonist and antagonist,* **(a)** *WS5 and* **(b)** *AMTB (against 3 µM WS5), respectively, evaluated in hTRPM8-HEK293 cells. Each data point represents the mean ± SEM (N = 3, n = 6).*

In hTRPA1-HEK293 cells, the agonism of cinnamaldehyde at 30 µM (~EC_{50}) was completely inhibited by the TRPA1 specific standard antagonist A967079 at and above 100 nM. Similarly, in hTRPM8, the agonism by WS5 at 3 µM (closer to EC_{50}) was completely inhibited by the antagonist AMTB.HCl at and above 1 µM, and therefore these concentrations were used in the experiments. On comparing the EC_{50} and IC_{50} values obtained against the original reports for the standard ligands, the IC_{50} of A967079 carried out in a similar system but against different agonist (AITC instead of cinnamaldehyde), closely agreed (**Table 3.2**). This further confirmed the validity of the assay methods utilised. However, perhaps due to use of different species, cell lines and assay methods, a discrepancy in the values for other compounds could have been observed (**Table 3.2**). The vehicle control (0.2 or 0.4 % DMSO) had no considerable activity in hTRPA1 (**Section 3.4.2**) and in mock transfected-HEK293 cells (data not shown), but had a slight antagonising effect in hTRPM8 (**Section 3.4.3.2**).

Table 3.2: *Comparison of the EC_{50} and IC_{50} values of the standard TRPA1 and TRPM8 ligands, obtained in hTRPA1- or hTRPM8-HEK293 cells, against the literature values.*

Ligand	Obtained	Literature value
CA	EC_{50} 27 µM	EC_{50} 61 ± 9 µM in mTRPA1-CHO cells[104]
A967079	IC_{50} 46 nM	IC_{50} 67 nM in hTRPA1-HEK293F cells (against 30 µM AITC)[166]
WS5	EC_{50} 1 µM	EC_{50} 26 ± 7 µM in *Xenopus* oocytes[417]
AMTB	IC_{50} 127 nM	pIC_{50} 6.23 ± 0.02 hTRPM8-HEK293 cells (against icilin EC_{80})[418]

3.4.1.6 Fluorescence spectrum

Examples of traces obtained in assays are shown in **Figure 3.8**. The starting point of the baseline level of each spectrum varied as the internalisation of the fluorescent-dye in cells increased with time during an assay. However, there are other possibilities for the baseline variation, including the use of different cuvettes (**Figure 3.9**) and the variable number of cells in each cuvette or well, but these were considered to have inconsiderable influences in the calcium signalling study undertaken. As can be seen in **Figures 3.8** and **3.9**, the basal fluorescence intensity observed in an assay is 10× higher compared to the intensity with cuvette alone.

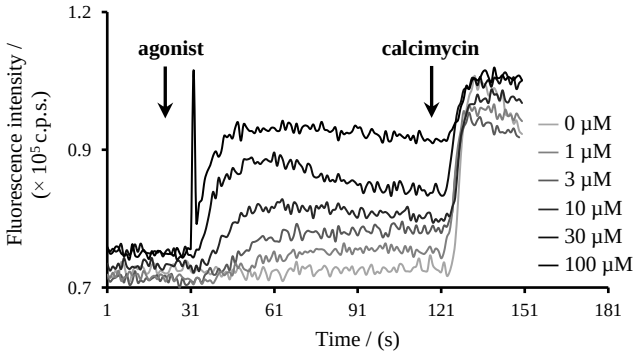

Figure 3.8: *Examples of traces obtained in a calcium signalling assay with a compound at different concentrations.*

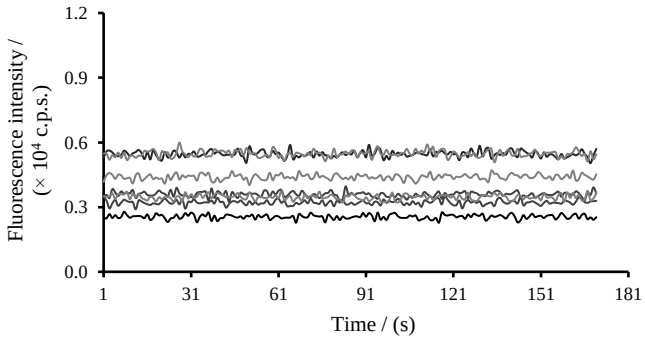

Figure 3.9: *Spectra obtained with seven different cuvettes from the same batch/manufacturer showing the variation in baseline levels with the use of different cuvettes alone.*

3.4.2 Screening of *N*-cinnamoylanthranilates in hTRPA1-HEK293 and structure-activity relationships

The CADs (**Figure 3.1**) were evaluated in hTRPA1-HEK293 cells for agonism and antagonism using fluorescence-based calcium signalling assays. *N*-Cinnamoylanthranilic acids were initially screened for agonism at 30 µM, and those found to be inactive were screened at 100 µM (**Figure 3.10a**), and for antagonism at 100 µM (**Figure 3.10b**). The methyl *N*-cinnamoylanthranilate esters were screened for agonism (**Figure 3.11a**) and antagonism (**Figure 3.11b**), at 3 µM and some at 10 µM based on the solubility of the compounds. As can be seen in **Figures 3.10** and **3.11**, the responses obtained for the positive controls, CA agonist and A967079 antagonist were consistent between assays.

In the initial screening of *N*-cinnamoylanthranilic acids, the CADs **AC41c-**(*p*-NO_2), **AC40c-**(*p*-CF_3), **AC16c-**(*p*-Br), **AC17c-**(*p*-Cl), **AC15c-**(*o*-Cl), **AC14c-**(*p*-F), **AC18b-**(*p*-H), **AC39c-**(*p*-CH_3), **AC20-**(*p*-OCH_3), **AC26-**(*o*-OCH_3), **AC43d-**(α-CH_3) and **AC42c-**(α-Ph) showed ≥25 % agonism at 30 µM (**Figure 3.10a**) and ≥50 % inhibition at 100 µM (**Figure 3.10b**). The CADs **AC24-**(*m*,*p*-$(OCH_3)_2$), **AC27-**(*m*-OCH_2CH_3-*p*-OH), **AC21b-**(*p*-H, α,β-saturated), **AC46c-**(*p*-OCH_3, α,β-saturated), **AC34-**(pipecolinic acid) and **AC36-**(proline) showed weak agonism (<25 %), and the CAD **AC30d-**(*p*-OH) was found to be inactive at both 30 and 100 µM concentrations (**Figure 3.10a**). However, the CADs **AC24-**(*m*,*p*-$(OCH_3)_2$), **AC27-**(*m*-OCH_2CH_3-*p*-OH) and **AC30d-**(*p*-OH) showed ≥40 % inhibition, and the CADs **AC21b-**(*p*-H, α,β-saturated), **AC46c-**(*p*-OCH_3, α,β-saturated), **AC34-**(pipecolinic acid) and **AC36-**(proline) showed weak inhibitory effect (<30 %) as shown in **Figure 3.10b**.

In the initial screening of methyl *N*-cinnamoylanthranilates, all the evaluated esters, including **AC40b-**(*p*-CF_3), **AC16b-**(*p*-Br), **AC17b-**(*p*-Cl), **AC15b-**(*o*-Cl), **AC14b-**(*p*-F), **AC18a-**(*p*-H), **AC39b-**(*p*-CH_3), **AC28c-**(3,4-$(OAc)_2$), **AC30c-**(*p*-OAc), **AC45b-**(*p*-$N(CH_3)_2$), **AC43c-**(α-CH_3), **AC42b-**(α-Ph) and **AC35b-**(phenoxy), showed agonism (**Figure 3.11a**). Most of the methyl *N*-cinnamoylanthranilate esters at 3 µM showed a similar level of agonism to that of their corresponding *N*-cinnamoylanthranilic acid derivatives at 30 µM (**Figure 3.10a**). However, except **AC43c-**(α-CH_3) and **AC42b-**(α-Ph), none of the esters showed antagonism (**Figure 3.11b**).

Based on the activities observed in initial screenings, dose-response curves were carried out for *N*-cinnamoylanthranilic acids that showed higher than 25 % agonism at 30 µM, and for those which had high antagonism and partial agonism. The dose-response curves for the *N*-cinnamoylanthranilic acids with agonism and antagonism responses are presented together in **Figures 3.12** and **3.13**, respectively, to allow cross-comparison between compounds with different substituents. As can be seen from the curves, the effects observed were dose-dependent. Since the methyl *N*-cinnamoylanthranilate esters were insoluble above 3 or 10 µM, a range of concentrations were not testable. The initial screening results and the dose-response results are summarised in **Tables 3.3** and **3.4**, to study the SAR and potency of compounds in the following **Sections 3.4.2.1 - 3.4.2.6**.

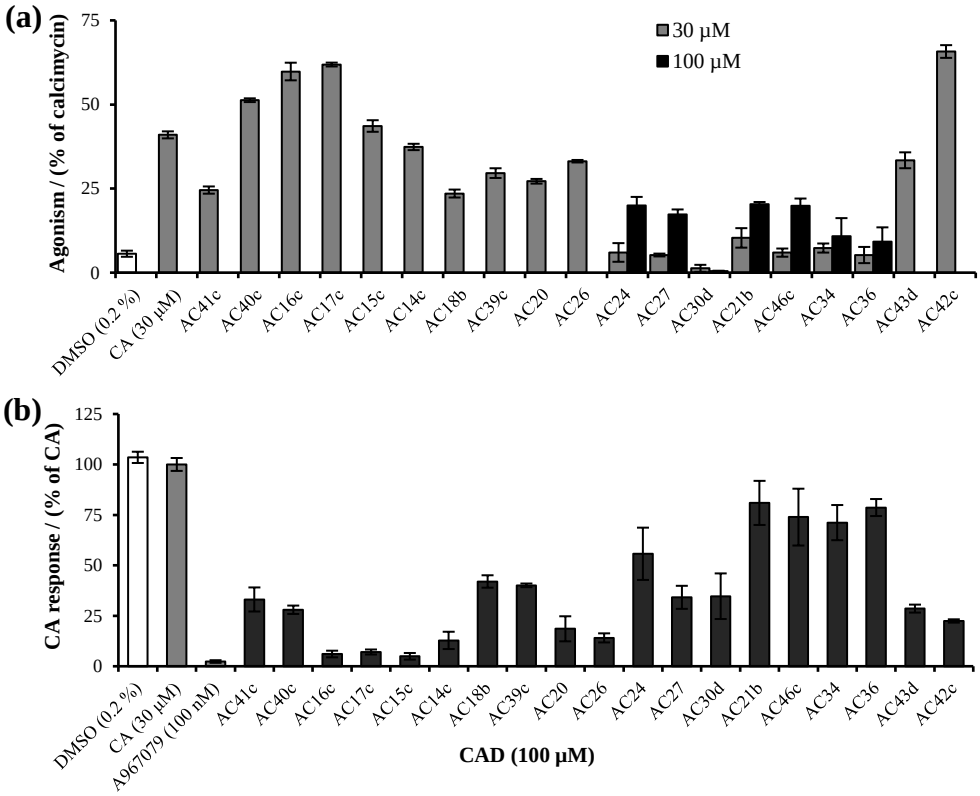

Figure 3.10: *Initial screening results of N-cinnamoylanthranilate derivatives in hTRPA1-HEK293 cells,* **(a)** *agonism and* **(b)** *antagonism. Each bar represents the mean ± SEM (N = 3).*

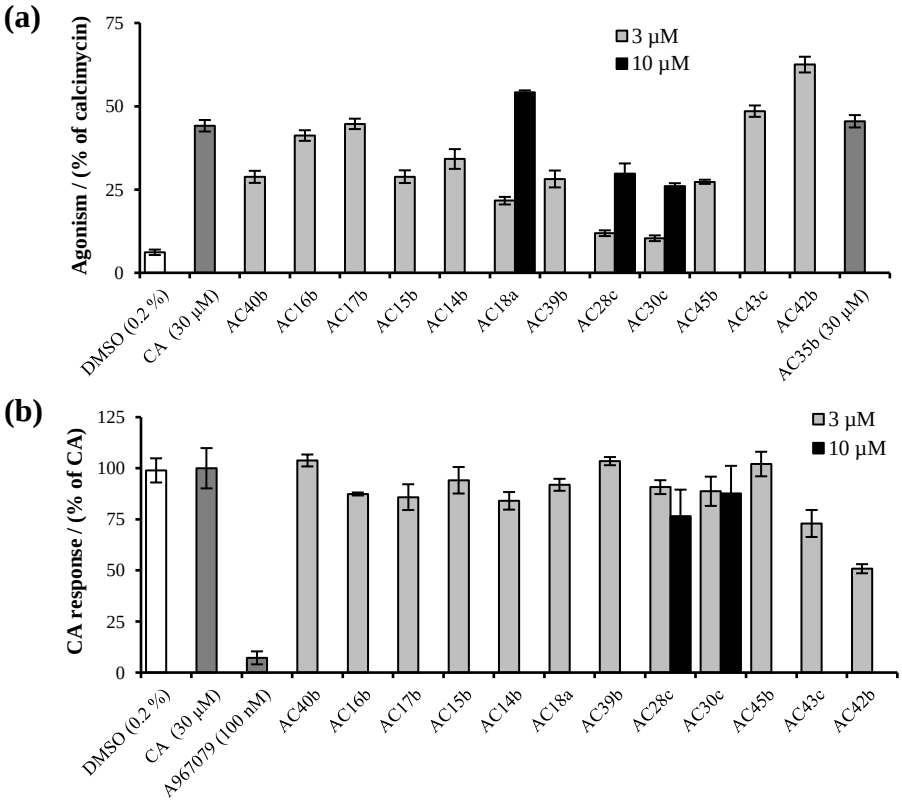

Figure 3.11: *Initial screening results of methyl N-cinnamoylanthranilate derivatives in hTRPA1-HEK293 cells,* **(a)** *agonism and* **(b)** *antagonism. Each bar represents the mean ± SEM (N = 3).*

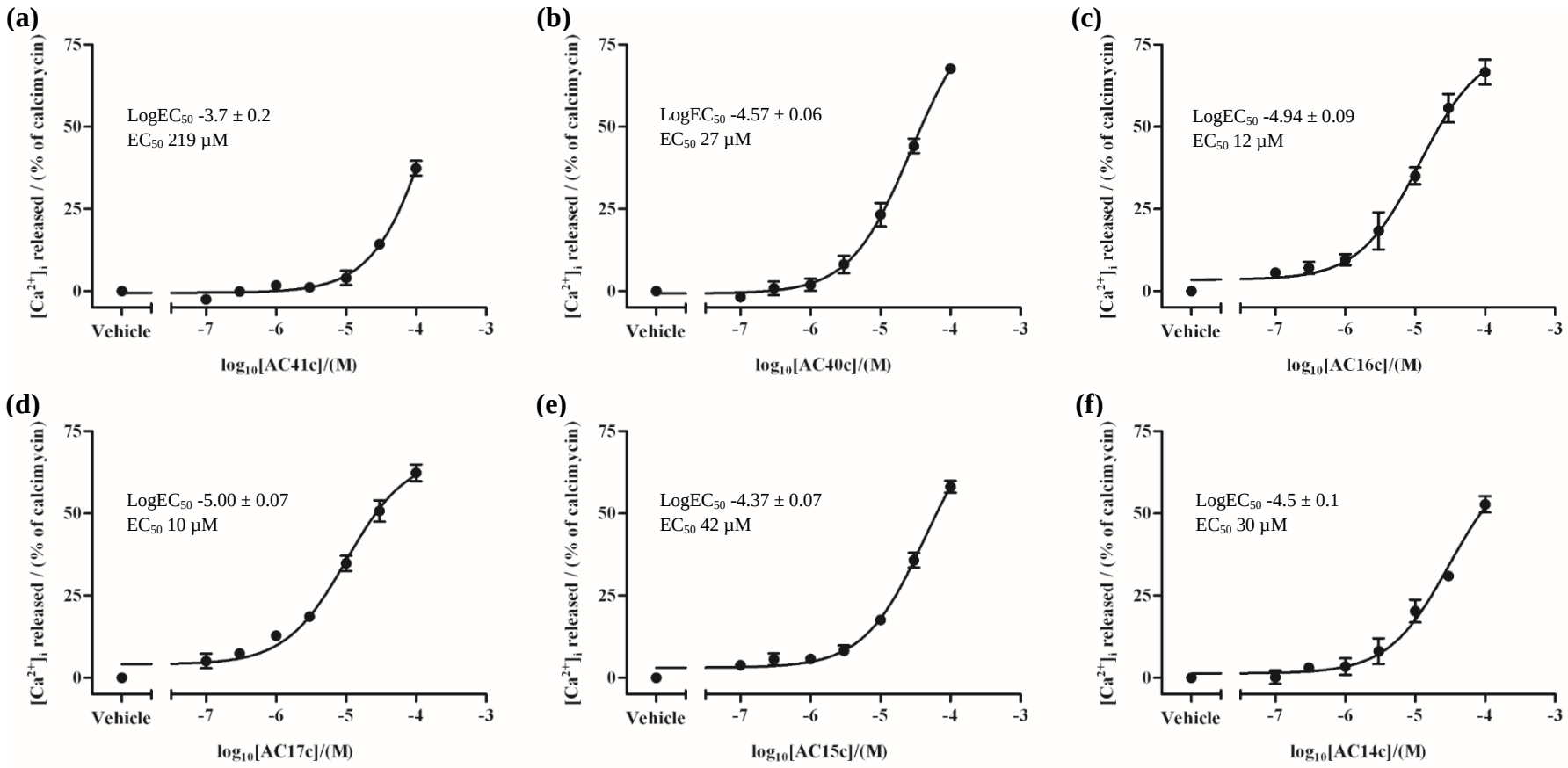

Continued…

Figure 3.12: *Dose-response curves* **(a - k)** *of substituted N-cinnamoylanthranilic acid agonists in hTRPA1-HEK293 cells. Each data point represents the mean ± SEM (N = 3, n = 6).*

Continued…

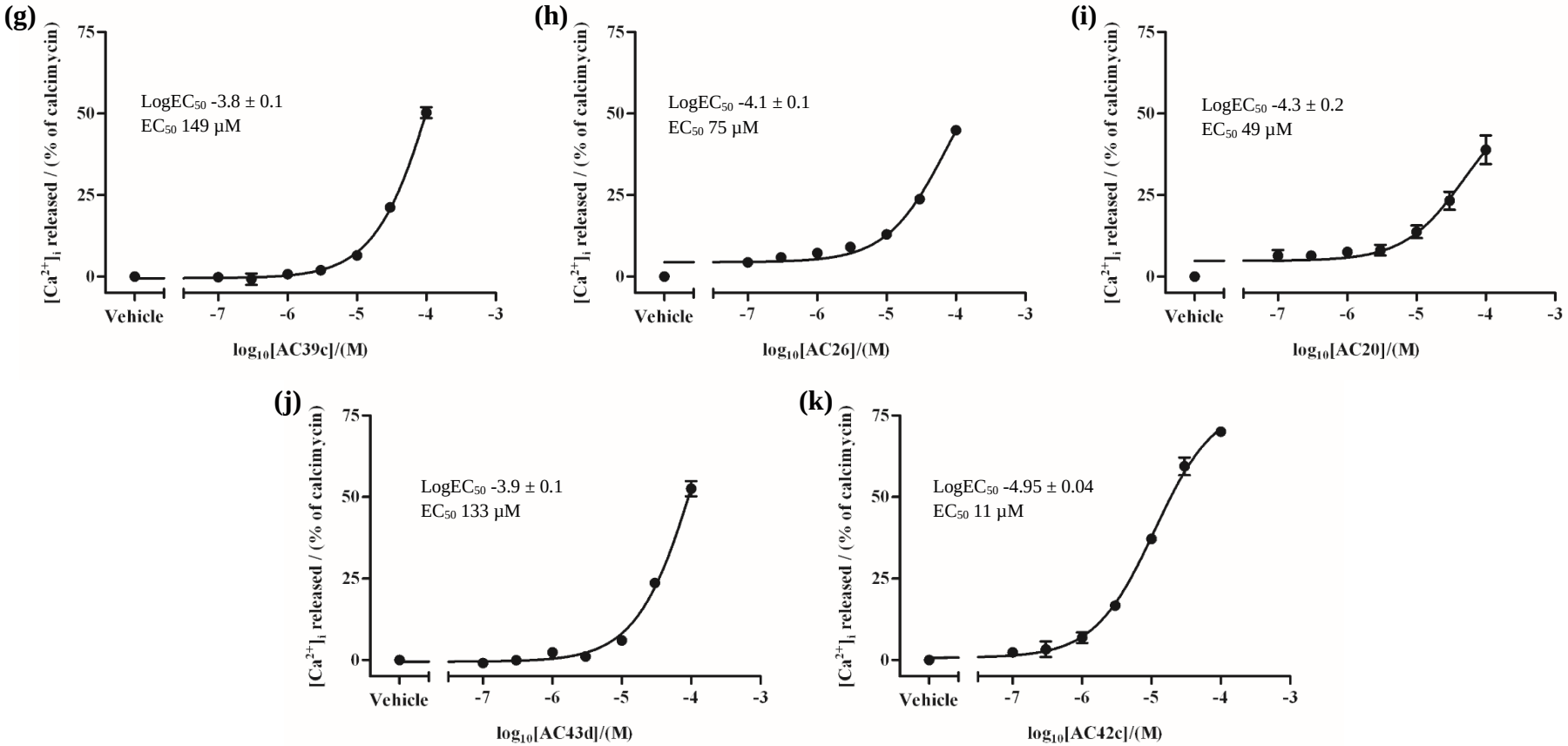

Figure 3.12: *Dose-response curves* **(a - k)** *of substituted N-cinnamoylanthranilic acid agonists in hTRPA1-HEK293 cells. Each data point represents the mean ± SEM (N = 3, n = 6).*

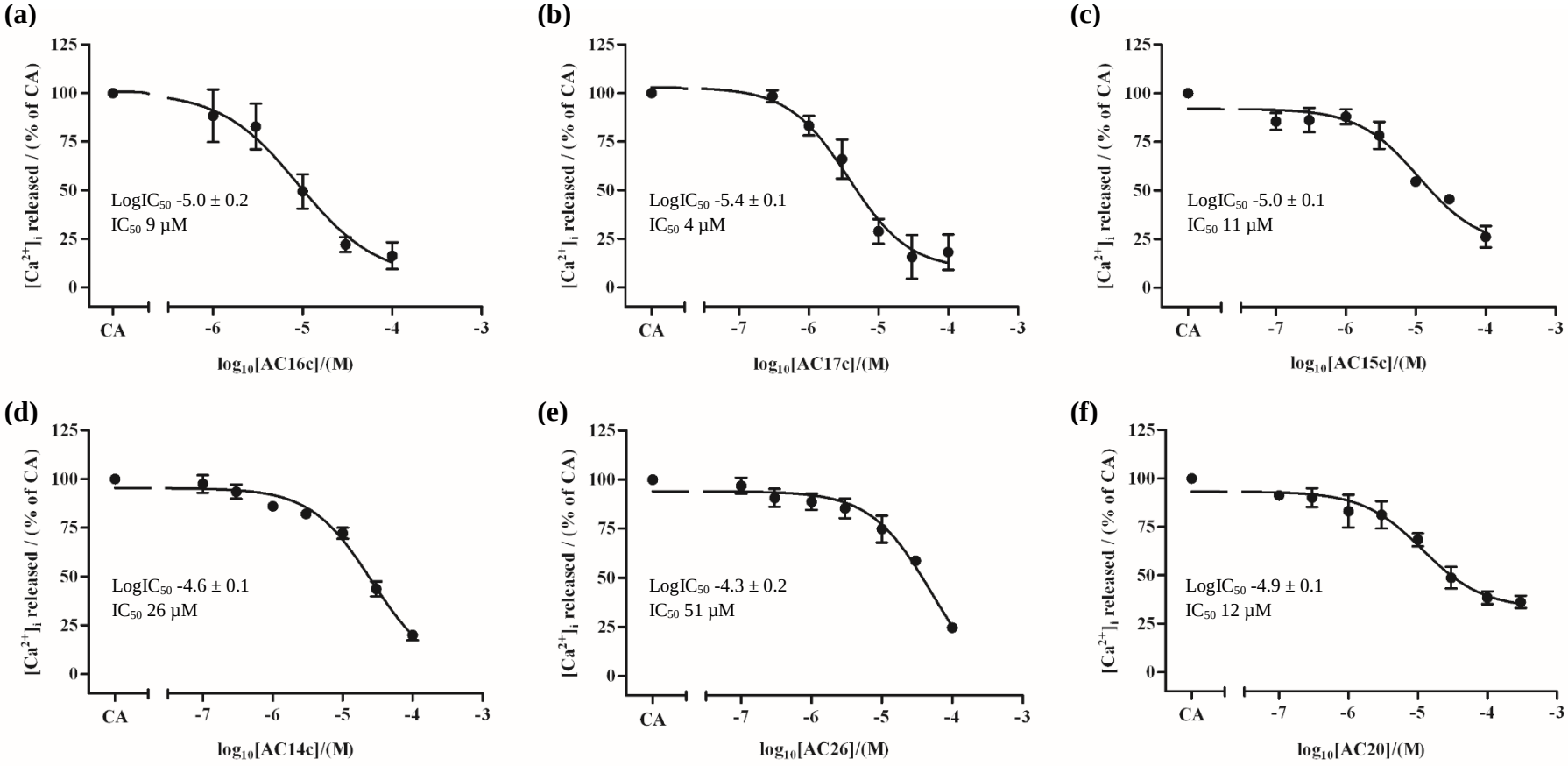

Continued…

Figure 3.13: *Dose-response curves* **(a - i)** *of substituted N-cinnamoylanthranilic acid antagonists in hTRPA1-HEK293 cells. Each data point represents the mean ± SEM (N = 3, n = 6).*

Continued…

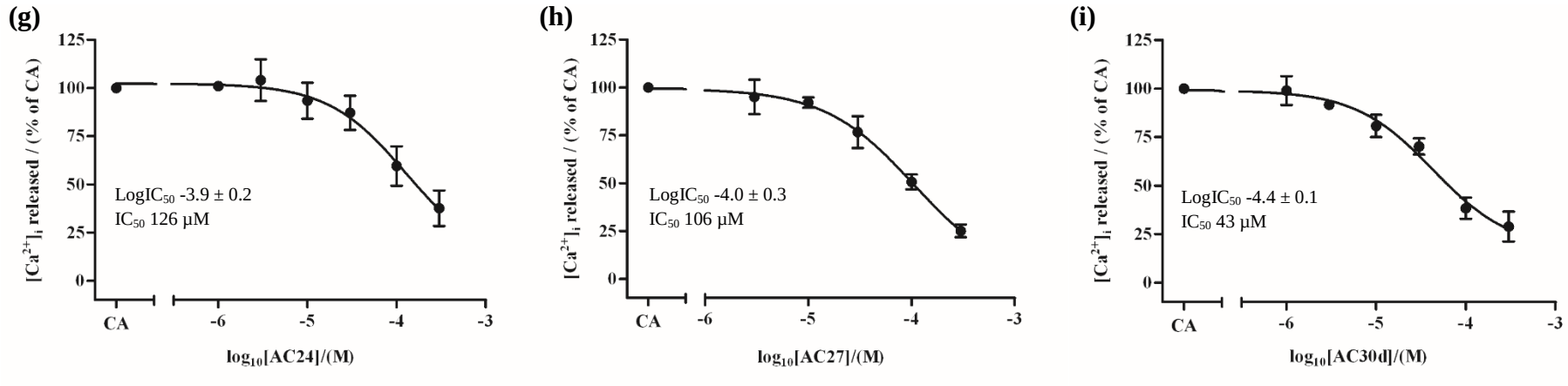

Figure 3.13: *Dose-response curves* **(a - i)** *of substituted N-cinnamoylanthranilic acid antagonists in hTRPA1-HEK293 cells. Each data point represents the mean ± SEM (N = 3, n = 6).*

Table 3.3: *Screening results of the synthesised N-cinnamoylanthranilic acids in hTRPA1-HEK293 cells. The concentrations at which the compounds were tested are specified in the corresponding column title. Dose-response curves were carried out for the compounds which showed >25 % agonist activity at 30 µM, and that had partial agonism and high antagonism, in the initial screening. Each value represents the mean ± SEM (N = 3).*

Compound	**Substituents**	**hTRPA1-HEK293 cells**			
		Agonism / (% calcimycin) 30 µM *N* = 3 ± SEM	**Antagonism, CA response / (% CA) 100 µM *N* = 3 ± SEM**	**EC_{50} /(µM) *n* = 6, *N* = 3**	**IC_{50} /(µM) *n* = 6, *N* = 3**
AC18b	-	24 ± 1	42 ± 3	-	-
AC41c	4-NO_2	25 ± 1	33 ± 6	219	-
AC40c	4-CF_3	51 ± 1	28 ± 2	27	-
AC16c	4-Br	60 ± 3	6 ± 2	12	9
AC17c	4-Cl	62 ± 1	7 ± 1	10	4
AC15c	2-Cl	44 ± 2	5 ± 2	42	11
AC14c	4-F	37 ± 1	13 ± 4	30	26
AC39c	4-CH_3	30 ± 1	40 ± 1	149	-
AC26	2-OCH_3	33 ± 1	14 ± 2	75	51
AC20	4-OCH_3	27 ± 1	19 ± 6	49	12
AC24	3,4-$(OCH_3)_2$	6 ± 3	56 ± 13	-	126
AC27	3-OEt-4-OH	5 ± 1	34 ± 6	-	106
AC30d	4-OH	1 ± 1	35 ± 11	-	43
AC28d	3,4-$(OH)_2$	Fluorescing compounds			
AC45c	4-$N(CH_3)_2$				
AC21b	α,β-saturated	10 ± 3	81 ± 11	-	-
AC46c	α,β-saturated, 4-OCH_3	6 ± 1	74 ± 14	-	-
AC34	Pipecolinic acid	7 ± 1	71 ± 9	-	-
AC36	Proline	5 ± 2	79 ± 4	-	-
AC43d	α-CH_3	33 ± 2	29 ± 2	133	-
AC42c	α-Ph	66 ± 2	22 ± 1	11	-

Table 3.4: *Screening results of the methyl N-cinnamoylanthranilates (3 µM) in hTRPA1-HEK293 cells. As* **AC41b** *(4-NO_2) was insoluble in DMSO at room temperature, it was not evaluated. Each value represents the mean ± SEM (N = 3).*

Compound	**Substituents**	**hTRPA1-HEK293 cells**	
		Agonism / (% calcimycin) 3 µM *N* = 3 ± SEM	**Antagonism, CA response / (% CA) 3 µM *N* = 3 ± SEM**
AC18a	-	22 ± 1	No inhibitory effects.
AC40b	4-CF_3	29 ± 2	
AC16b	4-Br	41 ± 2	
AC17b	4-Cl	45 ± 2	
AC15b	2-Cl	29 ± 2	
AC14b	4-F	34 ± 3	
AC39b	4-CH_3	28 ± 3	
AC30c	4-OAc	10 ± 1	
AC28c	3,4-$(OAc)_2$	12 ± 1	
AC45b	4-$N(CH_3)_2$	27 ± 1	
AC43c	α-CH_3	49 ± 2	73 ± 7
AC42b	α-Ph	63 ± 2	51 ± 2
AC35b	Phenoxy	45 ± 2 (at 30 µM)	No inhibitory effect.

3.4.2.1 Ring substituted and unsubstituted derivatives

On comparing the SAR of the CADs in hTRPA1 (**Figure 3.1** and **Table 3.3**), among the CADs containing the COOH group, the unsubstituted *N*-cinnamoylanthranilic aicd [**AC18b-**(*p*-H)] had a moderate agonistic effect, and the electron withdrawing group (EWG)-substituted CADs [**AC41c-**(*p*-NO_2) and **AC40c-**(*p*-CF_3)] were agonists. The halogenated CADs [**AC16c-**(*p*-Br), **AC17c-**(*p*-Cl), **AC15c-**(*o*-Cl) and **AC14c-**(*p*-F)] with inductive electron withdrawing but lone pair donating properties showed potent agonism with desensitising effect, and the CADs [**AC39c-**(*p*-CH_3), **AC26-**(*o*-OCH_3) and **AC20-**(*p*-OCH_3)] with a weak/moderate electron donating group (EDG) showed bimodal activity, that is, they possessed partial agonism and antagonism. As the electron donating nature of the EDG becomes stronger (**Figure 3.14**) the agonism of the compounds decreased and became antagonists [**AC24-**(*m*,*p*-$(OCH_3)_2$), **AC27-**(*m*-OCH_2CH_3-*p*-OH) and **AC30d-**(*p*-OH)].

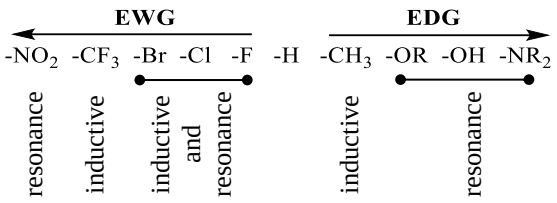

Figure 3.14: *Electronic effects of the substituents, EWG - electron withdrawing group and EDG - electron donating group.*

The derivatives with strong EWGs, -NO_2 (EC_{50} 219 µM) and -CF_3 (EC_{50} 27 µM), showed a slight deviation from the trend in the potency of agonism in comparison to the halogenated CADs (**Table 3.3** and **Figure 3.12a-f**), which could have been due to different electronic effects (**Figure 3.14**) or due to the presence of large polar -NO_2 group (**Figure 3.15**) and steric effects of the bulky groups. The halogenated CADs with bromo or chloro substituent at the *para*-position (**AC16c** and **AC17c**) had similar potency with EC_{50} values of 12 and 10 µM, and IC_{50} of 9 and 4 µM (**Figures 3.12c**,**d** and **3.13a**,**b**), respectively, whereas the fluorinated CAD (**AC14c**) showed slightly varying response, with EC_{50} 30 µM and IC_{50} 26 µM (**Figure 3.12f** and **3.13d**), relative to other halogens in the series. The observed trend appeared to be related to the strength of the electronegativity (χ) of the halogen atoms [F (χ 4.0) > Cl

(χ 3.0) > Br (χ 2.8)], with highest electronegative atom substituted CAD being least potent. However, the small difference in the EC_{50} and IC_{50} values between the CADs with bromo and chloro substituent could be due to the balance between the steric effect and electronegativity difference, in which Cl with smaller atomic radius [Br (114 pm) > Cl (99 pm)] and lower electronegativity being more potent. As the halogenated CADs [**AC16c**-(*p*-Br), **AC17c**-(*p*-Cl), **AC15c**-(*o*-Cl) and **AC14c**-(*p*-F)] showed potent agonism and antagonism (**Table 3.3**), it was thought that they possess desensitising effects after activation of the channel. Therefore, the desensitising effects of the halogenated CADs were studied by recording real-time spectra for 10 minutes, that is, for the length of the pre-incubation period in an antagonist assay and by observing the changes in the spectrum during that time (**Figure 3.16**). Since cinnamaldehyde and flufenamic acid are known to have desensitising effects,[146,154] they were evaluated (**Figure 3.16a**,**b**) along with the CADs and other fenamate analogues, mefenamic acid and diclofenac, under the same conditions for comparison (**Figure 3.16c-h**). It was observed that at the concentration eliciting a maximum response, the elevated Ca^{2+} level caused by the agonism was sustained (**Figure 3.16b**). However, at a submaximal concentration the effect dropped over a few seconds (200-300 s) and on continuous exposure to an agonist (CA) a diminished response was obtained (**Figure 3.16c-h**), which is due to desensitisation of the channel as reported in a study.[146] At the lower tested concentration of the CADs (10 µM), the agonism response dropped back nearer to the spectral baseline within 10 minutes of administration and desensitised the agonism of the standard agonist cinnamaldehyde (30 µM) added to it (**Figure 3.16e-h**).

The CADs with an electron donating methyl (**AC39c**, *p*-CH_3, 30 ± 1 % agonism) or methoxy (**AC20**, *p*-OCH_3, 27 ± 1 % agonism) group possessed similar agonist activity at 30 µM in the initial screening (**Figure 3.10a**). However, on comparing the EC_{50} of **AC39c** (*p*-CH_3, 149 µM, **Figure 3.12g**) and **AC20** (*p*-OCH_3, 49 µM, **Figure 3.12i**), **AC39c**-(*p*-CH_3) appeared to be less potent, perhaps due to different electronic effects (inductive/resonance) exerted by the substituents (**Figure 3.14**), and/or the hydrophobic/hydrophilic nature of the substituents (**Figure 3.15**).

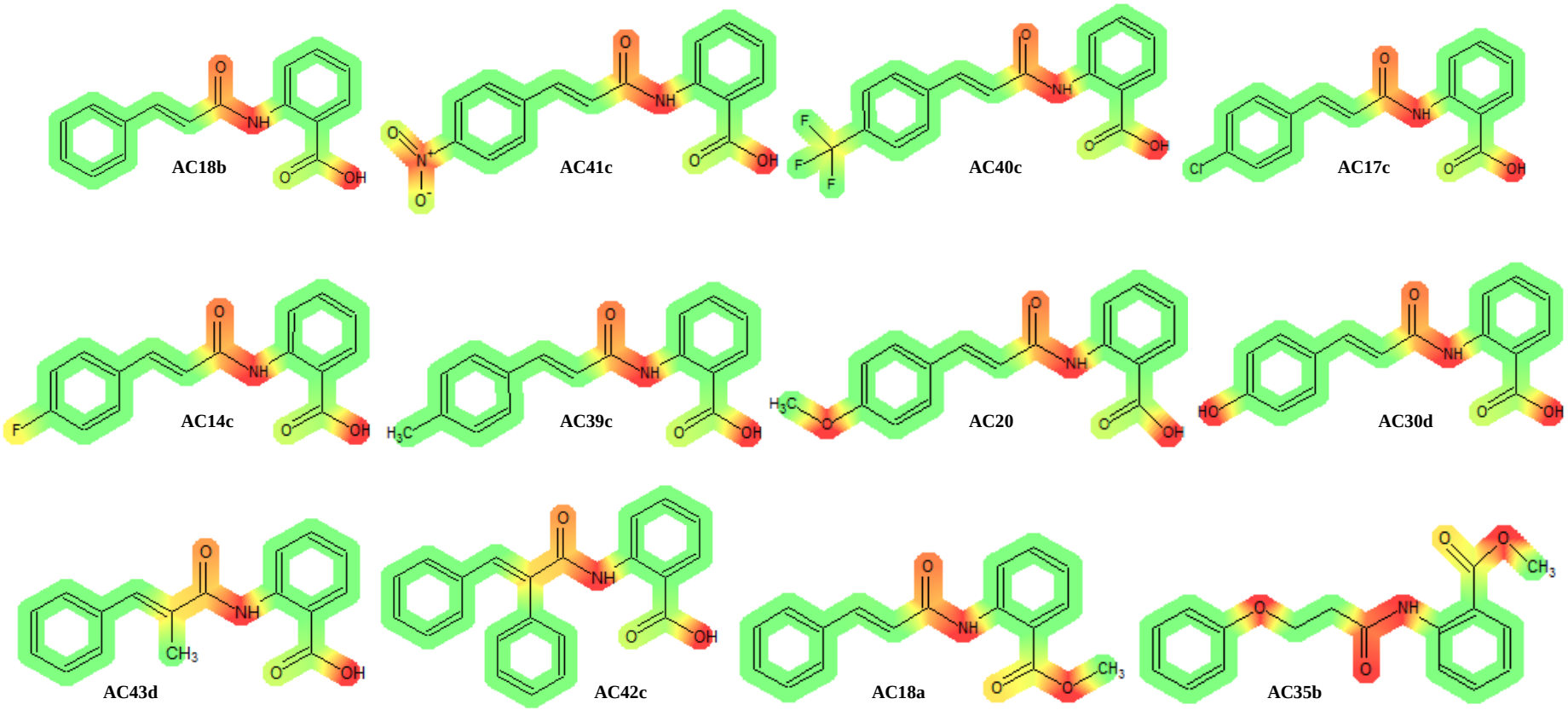

Figure 3.15: *Colour coded mapping of some analogues of N-cinnamoylanthranilic acid structures highlighting the lipophilicity/hydrophilicity nature of an atom/functional group/substructure. Green colour indicates the lipophilic (non-polar) parts, red indicates the hydrophilic (polar) groups, and the colour gradient represents the degree of lipophilicity/hydrophilicity.*

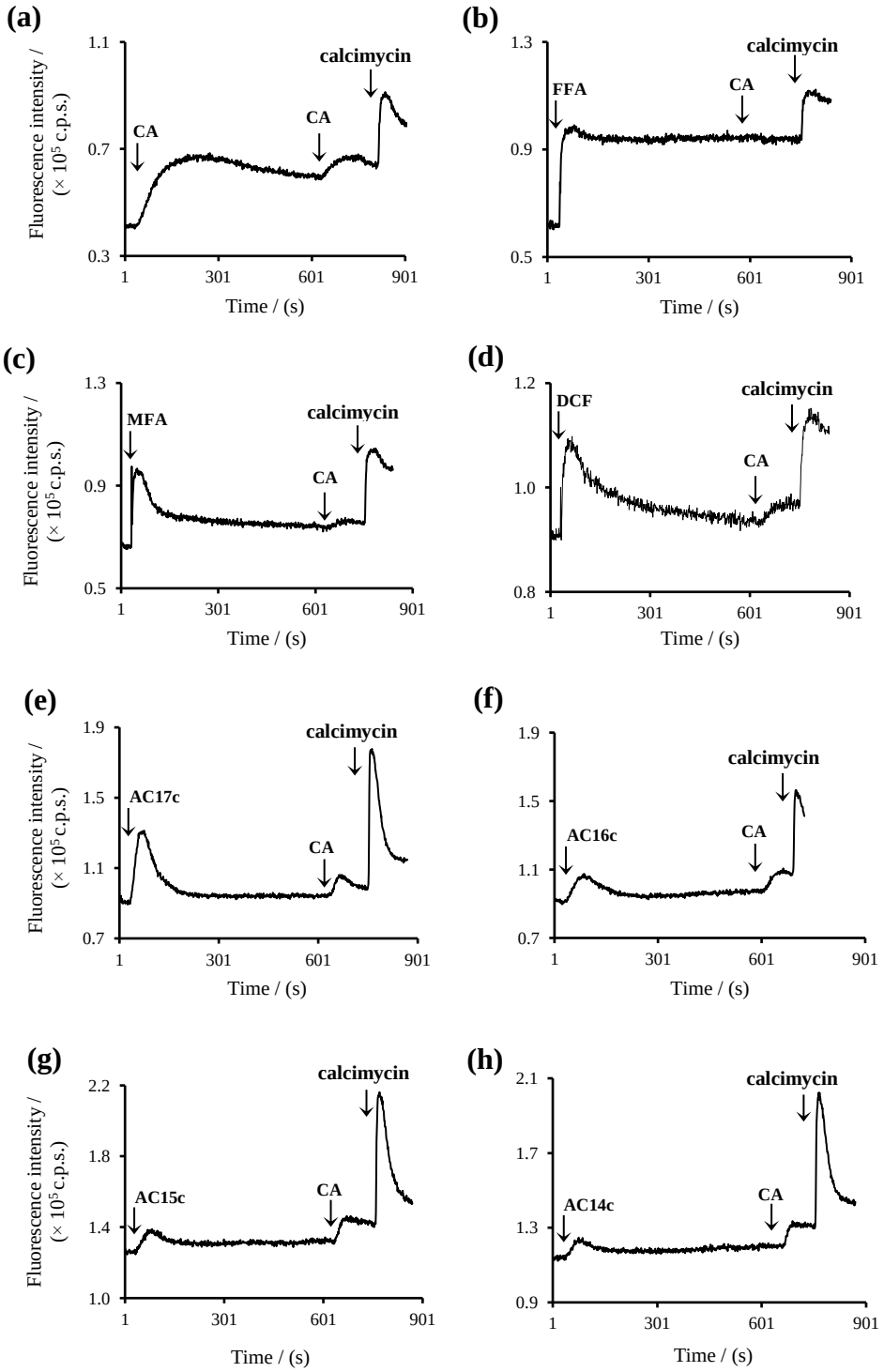

Figure 3.16: *Real-time spectrum recorded for 10 minutes (incubation period) for the compounds with bimodal activity (potent agonism and desensitisation) in hTRPA1-HEK293 cells,* **(a)** *cinnamaldehyde (CA, 30 µM),* **(b)** *flufenamic acid (FFA, 100 µM),* **(c)** *mefenamic acid (MFA, 10 µM),* **(d)** *diclofenac (DCF, 10 µM),* **(e)** *p-Cl CAD-***AC17c** *(10 µM),* **(f)** *p-Br CAD-***AC16c** *(10 µM),* **(g)** *o-Cl CAD-***AC15c** *(10 µM) and* **(h)** *p-F CAD-***AC14c** *(10 µM). The concentration of CA in the second addition was 30 µM.*

Stronger EDG disubstituted CADs [**AC24**-(*m*,*p*-$(OCH_3)_2$) and **AC27**-(*m*-OCH_2CH_3-*p*-OH)] exhibited partial agonist and antagonist activities, whilst **AC30d**-(*p*-OH) showed only an antagonistic effect and no agonism below 100 µM (**Figure 3.10**). Nevertheless, the CADs **AC24**-(*m*,*p*-$(OCH_3)_2$) and **AC27**-(*m*-OCH_2CH_3-*p*-OH), disubstituted with EDGs, were less potent with IC_{50} 126 and 106 µM (**Figure 3.13g**,**h**) respectively, whereas the IC_{50} of the monosubstituted CAD **AC30d**-(*p*-OH) was 43 µM (**Figure 3.13i**). The latter suggests that the bulkiness of the methoxy and ethoxy groups in **AC24** and **AC27** could have led to steric effects compared to the CAD **AC30d** with a hydroxy group. Additionally, the hydroxy group could have interacted with the receptor *via* hydrogen bonding. It was also found that **AC30d**-(*p*-OH) exhibit competitive insurmountable antagonism[419,420] from the right-downward shift observed in the cinnamaldehyde dose-response curve on pre-incubation with **AC30d** (**Figure 3.17**). However, on comparing the obtained EC_{50} values, 27 µM (no inhibitor) and 37 µM (with 100 µM inhibitor **AC30d**), the difference was statistically insignificant. The reversibility of the compound is discussed in **Section 3.4.4**.

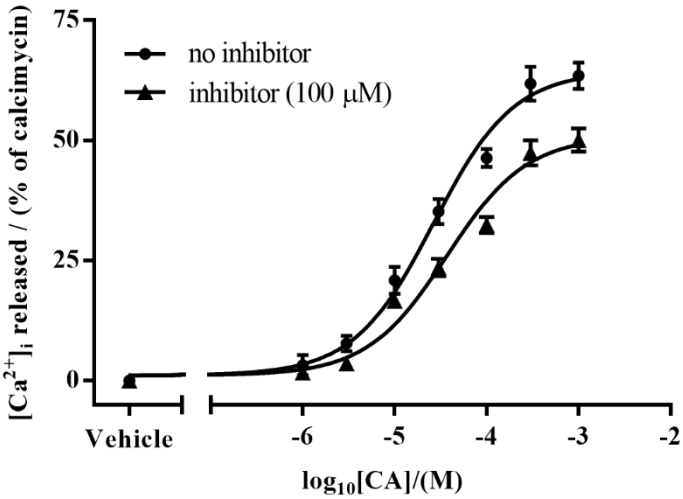

Figure 3.17: *Dose-response curves of cinnamaldehyde (CA) against hTRPA1-HEK293 cells untreated and pre-treated with the inhibitor (p-OH)CAD-***AC30d** *(100 µM). The competitive insurmountable antagonism by* **AC30d** *can be seen by the right-downward shift of the CA curve. The EC_{50} of CA obtained without the inhibitor (27 µM, N = 3, n = 9) and in the presence of inhibitor (37 µM, N = 3, n = 6) were not significantly different. Each data point represents the mean ± SEM, and the statistical significance between the two data sets' $logEC_{50}$ values was determined using the F-test at $p < 0.05$.*

In general, the EDG substituted compounds with a higher number of hydrogen bond donors and acceptors had greater antagonistic effect in hTRPA1 channels. This perhaps suggests that the ligands which can bind to amino acid residues through greater hydrogen bonding are involved in blocking of the channels more effectively. Additionally, the agonism of structurally related compounds in the literature, including ACA an inhibitor of TRPM2 (IC_{50} 4.5 μM), TRPM8 (IC_{50} 3.9 μM), TRPC3 (IC 20 μM), TRPC6 (IC_{50} 2.3 μM) and TRPV1 (IC >20 μM),[327] and SB366791 a selective TRPV1 (IC_{50} 6 nM) antagonist[409,410] were evaluated against hTRPA1-HEK293 cells for comparison (**Figure 3.18**).

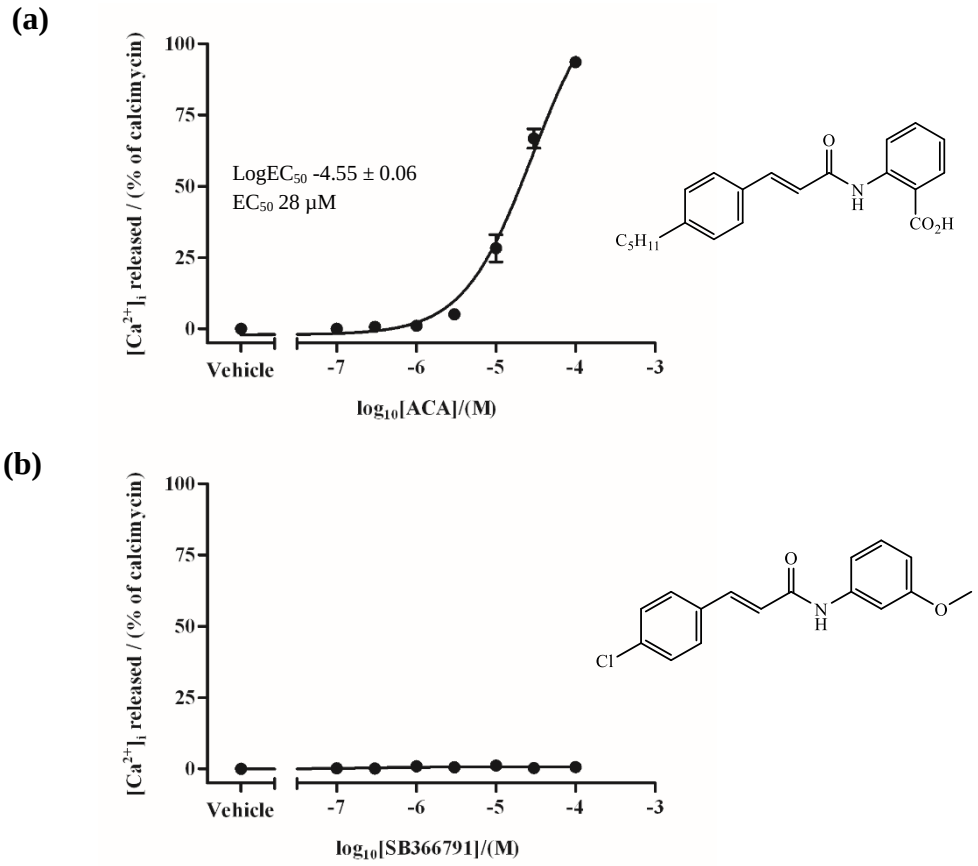

Figure 3.18: *Dose-response curves of the N-cinnamoylanthranilate analogues* **(a)** *ACA and* **(b)** *SB366791 in hTRPA1-HEK293 cells. Each data point represents the mean ± SEM (N = 3, n = 9).*

Though ACA with a *para n*-pentyl group was reported to inhibit different TRP channels,[327] in this study it was found to activate hTRPA1 (EC_{50} 28 μM, **Figure 3.18a**) potently relative to the methyl substituted CAD **AC39c** (EC_{50} 149 μM). The TRPV1 inhibitor, SB366791 had no agonism in hTRPA1 at

any of the tested concentrations (0.1 - 300 µM, **Figure 3.18b**). The structure of SB366791 was similar to **AC17c-**(*p*-Cl), but had an additional methoxy substituent *meta* to the amide linker in the anthranilate moiety that was lacking COOH group, which resulted in inactiveness.

The trend observed with the EWG and EDG substituents in this study was also observed in another study which measured the activity of benzylidenemalononitriles (BMN) against hTRPA1.[421] By comparing the agonism of selected *para* substituted BMN irritants at 3 µM, the following activities were observed: 4-NO_2 10 %; 4-CF_3 43 %; 4-Br 87 %; 4-Cl 67 %; 4-F 87 %; 4-OMe 9 %; 3,4-$(OMe)_2$ 9 %; 4-OH 2 % of maximum mean fluorescence.[421] The order of potency of the measured responses was similar to the trend found in this study.

3.4.2.2 *Ortho*- and *para*-substituted derivatives

Ortho-substituted CADs, **AC15c** (*o*-Cl, EC_{50} 42 µM and IC_{50} 11 µM, **Figures 3.12e** and **3.13c**) and **AC26** (*o*-OCH_3, EC_{50} 75 µM and IC_{50} 51 µM, **Figures 3.12h** and **3.13e**) were less efficacious, relative to their corresponding *para*-substituted analogues **AC17c** (*p*-Cl, EC_{50} 10 µM and IC_{50} 4 µM, **Figures 3.12d** and **3.13b**) and **AC20** (*p*-OCH_3, EC_{50} 49 µM and IC_{50} 12 µM, **Figures 3.12i** and **3.13f**). The steric effects of the *ortho* substituents and the non-planarity of the molecule resulting from steric strain could have led to less interaction with the channel.

3.4.2.3 α,β-Unsaturated and α,β-saturated derivatives

In hTRPA1, α,β-saturated CADs [**AC21b-**(*p*-H) and **AC46c-**(*p*-OCH_3)] showed poor activity (**AC21b** 10 ± 3 and **AC46c** 6 ± 1 % agonism at 30 µM) compared to the CADs [**AC18b-**(*p*-H) and **AC20-**(*p*-OCH_3)]with an α,β-unsaturated (alkene) group (**AC18b** 24 ± 1 and **AC20** 27 ± 1 % agonism at 30 µM), as seen in **Figure 3.10a**. This signified that the presence of non-rotatable α,β-unsaturated bond enhances the activity of the compound distinctly, presumably by providing a more fixed molecular conformation to bind to the receptor. The presence of freely rotatable sp^3 C-C single bonds, and the tetrahedral arrangement around the sp^3 carbon centres results in non-

planar structures with variable spatial arrangements, which in turn decreases the interactions between the compounds and the receptor sites, that is, the ligand binding affinity. As a consequence, poorer activities could have been observed.

3.4.2.4 α-Substituted and α-unsubstituted derivatives

The α-substituted CADs either with a methyl or a phenyl group were more potent agonists (**AC43d** 33 ± 2 and **AC42c** 66 ± 2 % agonism) relative to the unsubstituted CAD (**AC18b** 24 ± 1 % agonism), as shown in **Figure 3.10a**. Among the α-substituted and unsubstituted compounds, the derivative **AC42c-**(α-Ph) showed pronounced agonist potency (EC_{50} 11 μM, **Figure 3.12k**), suggesting that a unique π-π interaction may have a role in the activity of the compound.

3.4.2.5 Planar and non-planar derivatives

The compounds [**AC34-**(pipecolinic acid) and **AC36-**(proline)] with a non-planar tertiary amide group showed weak responses (7 ± 1 and 5 ± 2 % agonism, and 29 ± 9 and 21 ± 4 % inhibition, respectively, **Figure 3.10**) relative to the planar secondary amide group containing parent compound (**AC18b** 24 ± 1 % agonism and 58 ± 3 % inhibition). This revealed that the presence of a secondary amide (-CONH) and the anthranilate moiety plays an important role in the activity of CADs. Similarly, in the literature[2,8] most of the compounds reported as agonists or antagonists contained at least a secondary amine or an amide group. Also from the observed very weak responses for the non-planar compounds, **AC34-**(pipecolinic acid) and **AC36-**(proline), it is thought that π-stacking interactions of the aromatic anthranilate ring and conformation of the compound structure (**Figure 3.19**) could contribute an effect on modulating the channel.

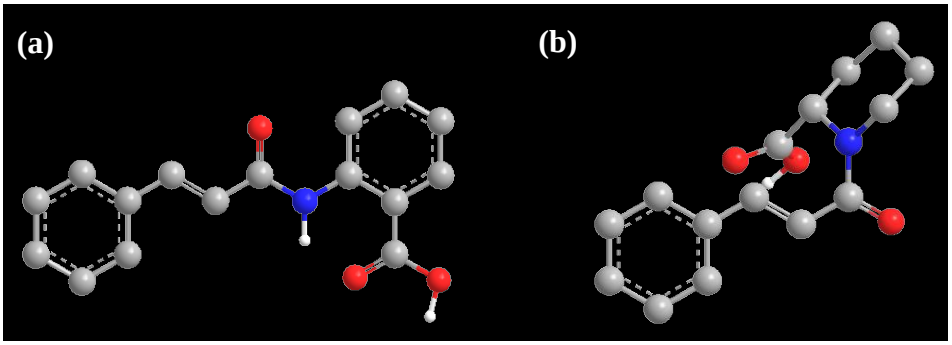

Figure 3.19: *Optimised geometry of the compounds,* **(a)** *planar N-cinnamoylanthranilic acid* (**AC18b**)*, and* **(b)** *non-planar N-cinnamoyl pipecolinic acid* (**AC34**)*, determined using the energy minimisation molecular mechanics force-field MM2.*

3.4.2.6 Carboxylic acid and carboxylate ester derivatives

The methyl *N*-cinnamoylanthranilate esters evaluated in hTRPA1 at 3 µM (**Figure 3.11a**) showed a similar level of agonism to that of their corresponding *N*-cinnamoylanthranilic acid derivatives at 30 µM (**Figure 3.10a**), but there were no considerable antagonism shown by the esters, except **AC43c-**(α-CH_3) and **AC42b-**(α-Ph) with desensitising effects (**Figure 3.11b**). Therefore, the methyl ester derivatives were potent agonists relative to their free carboxylic acids. However, the esters were less soluble in the assay buffer relative to the acid group containing compounds.

3.4.3 Channel specificity

3.4.3.1 Screening of *N*-cinnamoylanthranilates in mock-HEK293

The derivatives of *N*-cinnamoylanthranilates, evaluated at 30 and 100 µM, and methyl *N*-cinnamoylanthranilates at 3 µM, did not show any response in the negative control pcDNA3 mock-transfected HEK293 cells (N = 3, data not shown). An example of the fluorescence spectrum obtained in mock-transfected HEK293 cells is shown in **Figure 3.20**. This proved that in TRPA1 transfected HEK293 cells, the compounds were selective to TRPA1, and had no effect, with regard to triggering calcium flux, on other components of the cells, including endogenously expressed channels/receptors. HEK293 cells endogenously express a number of ion channel receptors, including purinoceptors ($P2Y_1$[422] and $P2Y_2$[422]), voltage-gated potassium channels,[423,424] sodium channels (β1A[425] and $Na_v1.7$[426]), sphingosine-1-phosphate receptors

(Edg-1, Edg-3 and Edg-5),[427] calcium channels[428] including TRPC channels (TRPC1, TRPC3, TRPC4, TRPC6 and TRPC7),[429,430] and M_3 muscarinic acetylcholine receptor.[431]

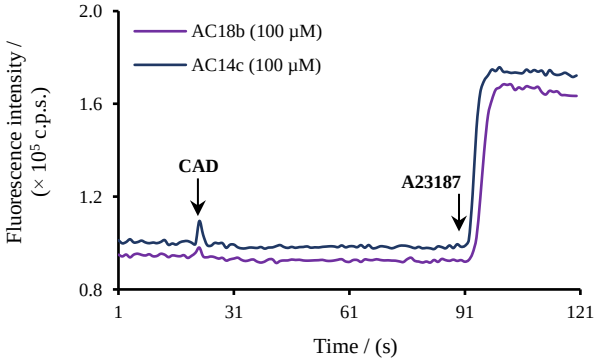

Figure 3.20: *An example of the fluorescence spectrum obtained for the compounds* **AC18b-**(*p*-H) *and* **AC14c-**(*p*-F)*, when screened in mock-transfected HEK293 cells. Similar responses were obtained for all the tested compounds. The CAD and A23187 arrows indicate the time points at which a test compound and the calcimycin were added.*

3.4.3.2 Screening of *N*-cinnamoylanthranilates in hTRPM8-HEK293

TRPM8 is a cold-sensitive channel like TRPA1[260,432] and stimulated by a number of ligands that could modulate TRPA1,[127,433] and hence the compounds were evaluated against stably transfected hTRPM8-HEK293 cells for relative selectivity. There were no agonism seen for all the CADs screened in hTRPM8-transfected HEK293 at the concentrations 30 and 100 μM of *N*-cinnamoylanthranilates, and 3 μM of methyl *N*-cinnamoyl anthranilates (data not shown), where **AC42c** and **AC42b** with an α-phenyl substituent were exceptions exhibiting weak agonism (**Figure 3.21a**). The majority of the compounds that had an agonistic effect in hTRPA1 (**Figures 3.10a** and **3.11a**) showed a relatively weak inhibitory effect in hTRPM8 evaluated at the high concentrations (**Figure 3.21b**). The vehicle control also had a slight antagonising effect in hTRPM8 (inhibits ~20 % of WS5 response, **Figure 3.21b**).

Dose-response curves were carried out for the compounds [**AC40c-**(*p*-CF_3), **AC16c-**(*p*-Br), **AC15c-**(*o*-Cl), **AC26-**(*o*-OCH_3), **AC43d-**(α-CH_3) and **AC35b-**(phenoxy)] that showed high antagonism (**Figure 3.22**), and among which **AC35b** (methyl 3-phenoxypropionoylanthranilate) was found to be a

most potent hTRPM8 antagonist (IC_{50} 10 µM, **Figure 3.22f**). In addition, it was observed from the IC_{50} values that the CAD **AC16c-**(*p*-Br) which showed antagonism in both hTRPA1 (IC_{50} 9 µM, **Figure 3.13a**) and hTRPM8 (IC_{50} 59 µM, **Figure 3.22b**) had more selectivity for TRPA1 as the compound was more potent in hTRPA1. However, the CAD **AC15c-**(*o*-Cl) and **AC26-**(*o*-OCH_3) had only a 10 µM difference in the IC_{50} values obtained against hTRPA1 (**AC15c** 11 and **AC26** 51 µM, **Figure 3.13c**,**e**) and hTRPM8 (**AC15c** 21 and **AC26** 41 µM, **Figure 3.22c**,**d**).

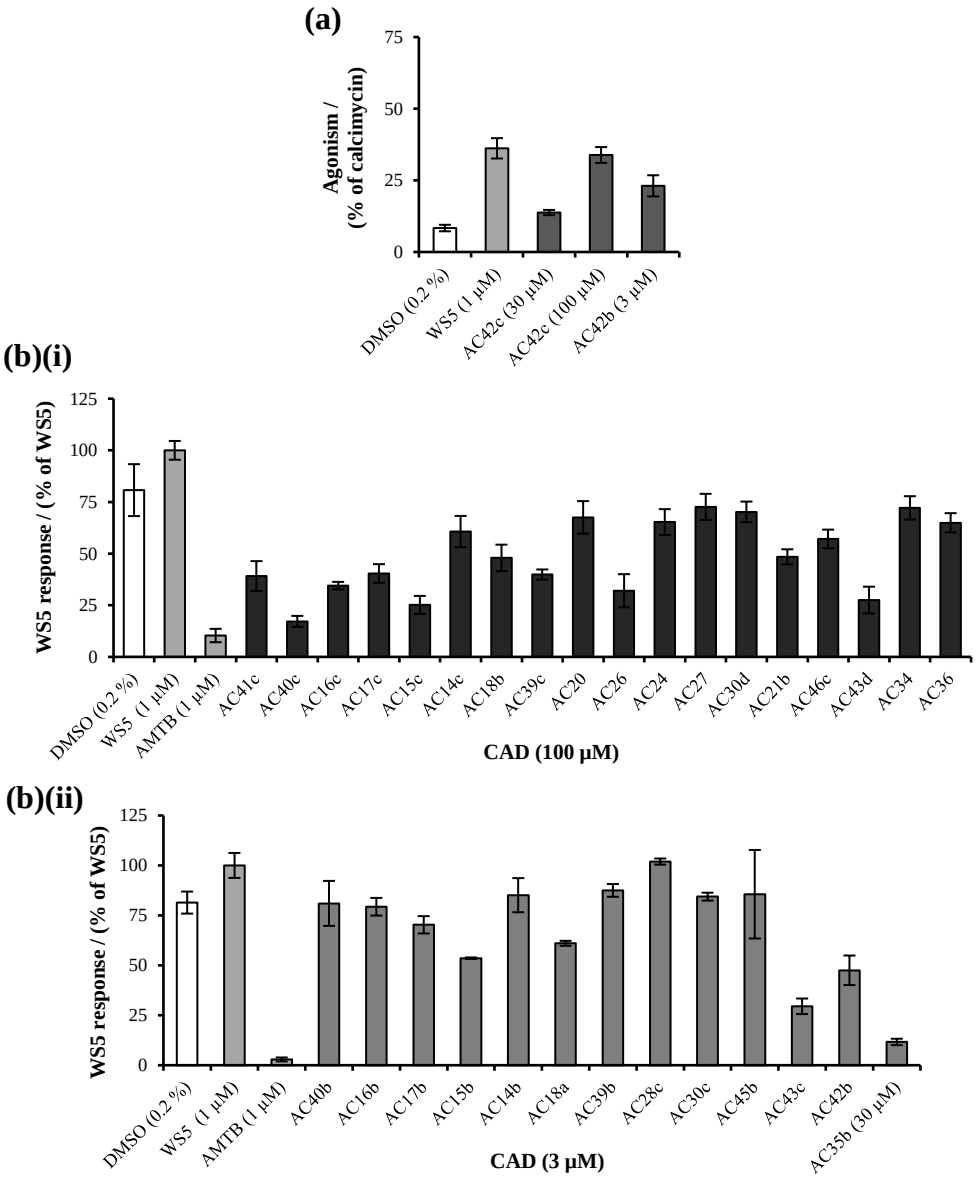

Figure 3.21: *Initial screening results of N-cinnamoylanthranilate derivatives in hTRPM8-HEK293 cells,* **(a)** *agonism, and* **(b)(i)** *antagonism of N-cinnamoylanthranilic acids and* **(b)(ii)** *antagonism of methyl N-cinnamoylanthranilates. Each bar represents the mean ± SEM (N = 3).*

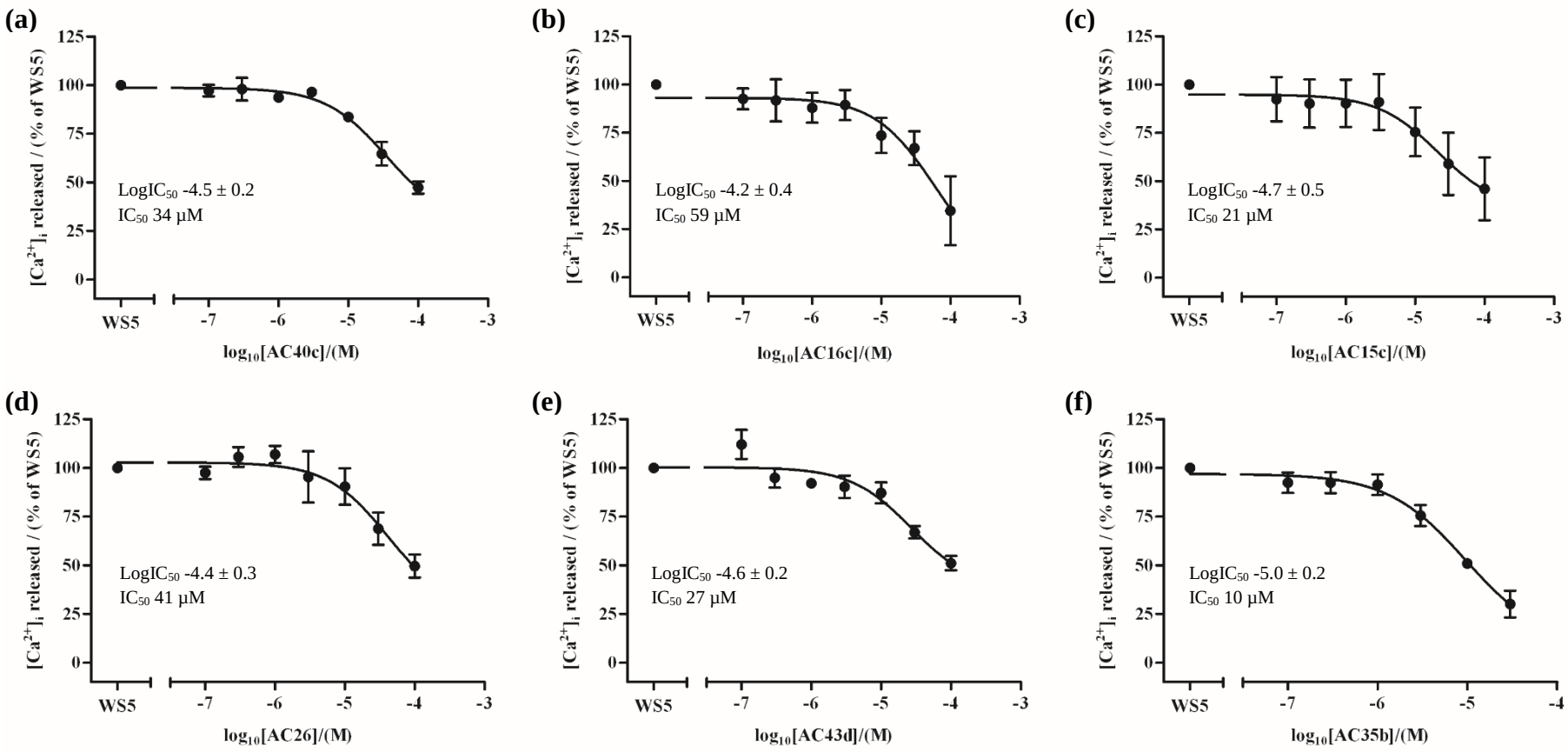

Figure 3.22: *Dose-response curves* **(a - f)** *of N-cinnamoylanthranilate antagonists in hTRPM8-HEK293 cells. Each data point represents the mean ± SEM (N =3, n = 6).*

Table 3.5: *Screening results of the synthesised N-cinnamoylanthranilic acids in hTRPM8-HEK293 cells. The concentrations at which the compounds were tested are specified in the corresponding column title. Dose-response curves were carried out for the compounds which showed >60 % inhibitory effect. Each value represents the mean ± SEM (N = 3).*

Compound	**Substituents**	**hTRPM8-HEK293 cells**			
		Agonism / (% calcimycin) 30 and 100 µM *N* = 3 ± SEM	**Antagonism, WS5 response / (% WS5) 100 µM *N* = 3 ± SEM**	**LogIC$_{50}$ *n* = 6, *N* = 3 ± SEM**	**IC$_{50}$ /(µM)**
AC18b	-	No agonism response was obtained for any of these compounds, and hence the effects of the compounds were specific to hTRPA1.	48 ± 6	-	-
AC41c	4-NO_2		39 ± 7	-	-
AC40c	4-CF_3		17 ± 3	-4.5 ± 0.2	34
AC16c	4-Br		35 ± 2	-4.2 ± 0.4	59
AC17c	4-Cl		40 ± 5	-	-
AC15c	2-Cl		25 ± 4	-4.7 ± 0.5	21
AC14c	4-F		61 ± 8	-	-
AC39c	4-CH_3		48 ± 3	-	-
AC26	2-OCH_3		32 ± 8	-4.4 ± 0.3	41
AC20	4-OCH_3		68 ± 8	-	-
AC24	3,4-$(OCH_3)_2$		65 ± 6	-	-
AC27	3-OEt-4-OH		73 ± 6	-	-
AC30d	4-OH		70 ± 5	-	-
AC28d	3,4-$(OH)_2$		Fluorescing compounds		
AC45c	4-$N(CH_3)_2$				
AC21b	α,β-saturated		48 ± 4	-	-
AC46c	α,β-saturated, 4-OCH_3		57 ± 5	-	-
AC34	Pipecolinic acid		72 ± 6	-	-
AC36	Proline		65 ± 5	-	-
AC43d	α-CH_3		28 ± 7	-4.6 ± 0.2	27
AC42c	α-Ph	14 ± 1, 34 ± 3	not measured	-	-

Table 3.6: *Screening results of the methyl N-cinnamoylanthranilates (3 µM) in hTRPM8-HEK293 cells. As* **AC41b** *(4-NO_2) was insoluble in DMSO at room temperature, it was not evaluated. Each value represents the mean ± SEM (N = 3).*

Compound	**Substituents**	**hTRPM8-HEK293 cells**	
		Agonism / (% calcimycin) 3 µM *N* = 3 ± SEM	**Antagonism, WS5 response / (% WS5) 3 µM *N* = 3 ± SEM**
AC18a	-	No agonism response obtained for any of these compounds.	61 ± 1
AC40b	4-CF_3		81 ± 11
AC16b	4-Br		79 ± 4
AC17b	4-Cl		70 ± 4
AC15b	2-Cl		53 ± 1
AC14b	4-F		85 ± 9
AC39b	4-CH_3		88 ± 3
AC30c	4-OAc		84 ± 2
AC28c	3,4-$(OAc)_2$		102 ± 2
AC45b	4-$N(CH_3)_2$		86 ± 22
AC43c	α-CH_3		30 ± 4
AC42b	α-Ph	23 ± 4	48 ± 7
AC35b	Phenoxy	No agonism	12 ± 2 (at 30 µM)

Overall, the CADs that were active in hTRPM8 contained a halogen substituent, or an *ortho*- or α-position substitutions, and mostly the agonists of hTRPA1 showed antagonism in hTRPM8 at a higher concentration, and other compounds were selective to hTRPA1 over hTRPM8. The results are further summarised in **Tables 3.5** and **3.6** for clarity. However, to conclude on the specificity, further selectivity assays against other ion channels are necessary.

3.4.4 Reversibility

Further to the competitive insurmountable antagonism observed with *p*-OH CAD-**AC30d** (**Figure 3.17**), its irreversibility nature was revealed in a washout experiment (**Figure 3.23**) performed as described in **Section 2.4.2** of **Chapter 2**. Irreversible competitive antagonists are referred to as insurmountable, because binding of such ligands results in a permanent reduction in the number of available receptors. Consequently, agonists are unable to bind to all the receptors and cannot exert the same level of response as with the untreated cells.[419]

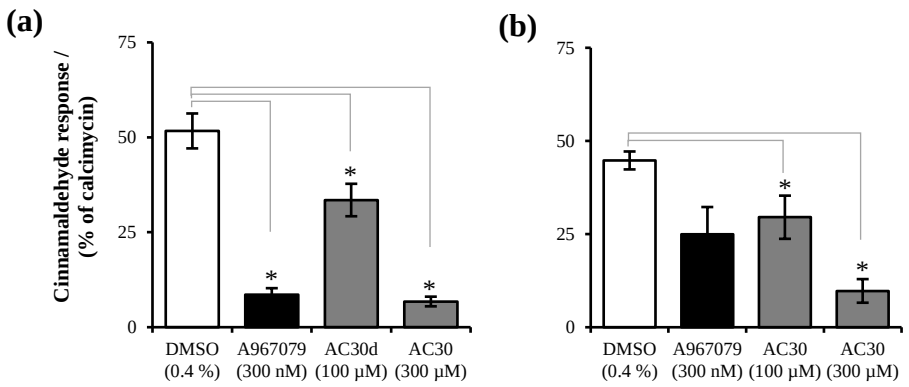

Figure 3.23: (a) *Inhibitory effect shown in cells pre-treated with the compunds and* **(b)** *irreversibility of N-(4-hydroxycinnamoyl)anthranilic acid* (**AC30d**) *on hTRPA1-HEK293 cells. Each bar represents the mean ± SEM (N = 3, n = 6), and the statistical significance was determined using one-way ANOVA at *p < 0.05.*

The reversibility of halogenated CADs with bimodal activity in hTRPA1 was also verified by a washout experiment. The desensitising effect shown by the halogenated CADs [**AC16c**-(*p*-Br), **AC17c**-(*p*-Cl), **AC15c**-(*o*-Cl) and **AC14c**-(*p*-F)] on hTRPA1 was found to be reversible up to 10 µM for

AC16c-(*p*-Br) and **AC17c**-(*p*-Cl), and up to 30 µM for **AC15c**-(*o*-Cl) and **AC14c**-(*p*-F), and were irreversible at higher concentrations (**Figure 3.24**). As the compounds were reversible at lower concentrations, the irreversibility at higher concentrations could have possibly been due to, but not limited to, slow dissociation of the ligand from the receptor.[419]

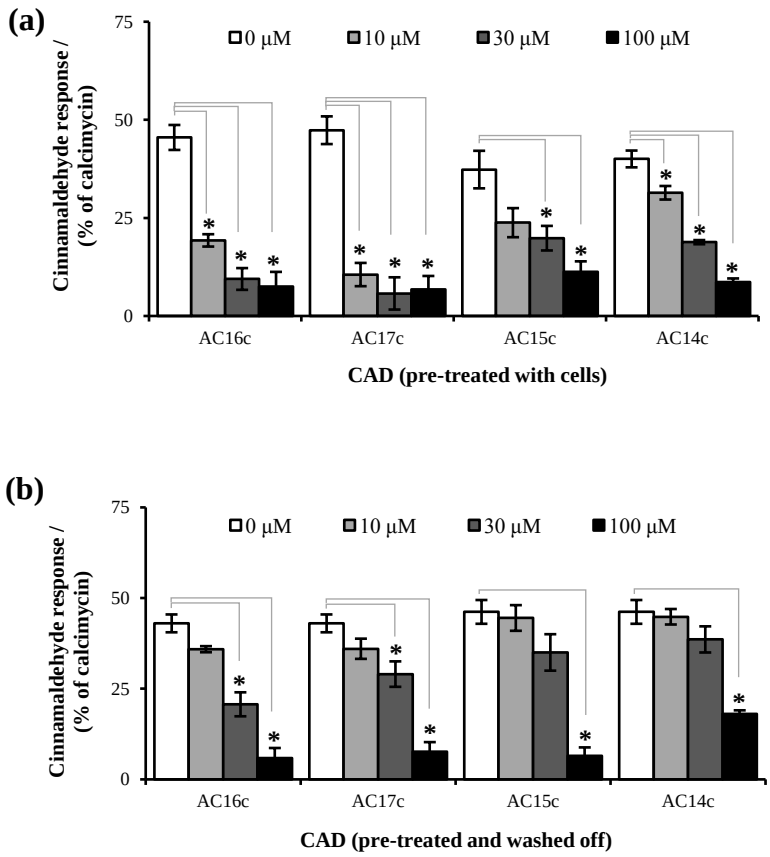

Figure 3.24: (a) *Desensitising effect and* **(b)** *reversibility of halogenated N-cinnamoylanthranilic acids [***AC16b**-*(p-Br),* **AC17b**-*(p-Cl),* **AC15b**-*(o-Cl) and* **AC14b**-*(p-F)] on hTRPA1-HEK293 cells. Each bar represents the mean ± SEM (N = 3, n = 6), and the statistical significance was determined using one-way ANOVA at *p < 0.05.*

3.4.5 Physicochemical property-activity relationships

With respect to the physicochemical properties, it was observed that among similar analogues, the compounds possessing higher n-octanol/water (calculated) partition coefficient (clogP) were the most potent agonists, and the agonism decreased with a decrease in clogP value (**Tables 3.7** and **3.8**), which was also in agreement with compounds in the literature.[128,411] For

example, the EC_{50} of NPEB (5.65 μM)[411] with clogP 4.7 is much lower than for NPBA (>100 μM)[411] with clogP 3.3. The logP [$\log(c_{n\text{-octanol}}/c_{water})$] is a measure of a compound's lipophilicity (hydrophobicity/hydrophilicity). Larger values indicate that the compound is less hydrophilic and could result in poor absorption or increased permeation. As logP increases, binding to serum albumin also increases due to the increased hydrophobicity. To check the reliability of the values calculated by different softwares, the clogP values obtained in ACD/I-Lab software were compared to the values calculated by ChemBioOffice 2014, and was found to tally within the limit of uncertainty stated by ACD/I-Lab. Distribution coefficient [$\log D = \log(c_{n\text{-octanol}}/c_{water})$] is also a measure of the lipophilicity, and is pH dependent. As the CADs with free carboxylic acid are ionised to carboxylate ion in the buffer at pH 7.4, their logD were compared and the observed trend in the activity was similar to that of logP. The CADs with small clogD values were more soluble, which was consistent with the corresponding high calculated solubility (clogS) values (**Tables 3.7** and **3.8**).

Generally, the CADs with a higher number of hydrogen bond donors, hydrogen bond acceptors, larger topological polar surface area and logS, and lower logP had greater inhibitory effects with poorer or absence of agonism in hTRPA1. In addition, with the exception of **AC42c-**(α-Ph, COOH) and **AC42b-**(α-Ph, $COOCH_3$) with clogP > 5, all the CADs assessed were consistent with Lipinski's rule-of-five[434] [physicochemical parameter ranges: MW ≤ 500, logP ≤ 5, H-bond donors (sum of OHs and NHs) ≤ 5 and H-bond acceptors (sum of Os and Ns) ≤ 10], and Veber's rule[435] [no. of rotatable bonds ≤ 10 (ligand affinity decreases by 0.5 kcal on average for every two rotatable bonds) and polar surface area ≤ 140 $Å^2$] of lead-likeness and oral bioavailability (**Tables 3.7** and **3.8**).

Table 3.7: *Physicochemical properties of N-cinnamoylanthranilic acids showing that the compounds obeyed the Lipinski's rule-of-five and the Veber's rules of lead-likeness / oral bioavailability, except* AC42c. *Lipophilicity [partition coefficient (clogP) and distribution coefficient, (clogD)], solubility (clogS) and acid dissociation constant (pK_a) parameters are given for comparison. Abbreviations: MW - molecular weight, H-bond - hydrogen bond, TPSA - topological polar surface area.*

Compound	Substituent	MW (≤ 500)	H-bond donors (≤ 5)	H-bond acceptors (≤ 10)	Rotatable bonds (≤ 10)	TPSA/(Å^2) (≤ 140 Å^2)	clogP (≤ 5)	clogD at pH 7.4	pK_a at pH 7.4	clogS at pH 7.4
AC41c	4-NO_2	312.28	2	7	5	115.23	4.3 ± 0.4	-0.42	3.4 ± 0.8	-2.42
AC40c	4-CF_3	335.28	2	4	5	66.4	5.5 ± 0.6	0.77	3.4 ± 0.8	-2.66
AC16c	4-Br	346.17	2	4	4	66.4	5.4 ± 0.5	0.53	3.4 ± 0.8	-2.47
AC17c	4-Cl	301.72	2	4	4	66.4	5.1 ± 0.4	0.19	3.4 ± 0.8	-2.52
AC15c	2-Cl	301.72	2	4	4	66.4	4.9 ± 0.4	0.18	3.4 ± 0.8	-2.47
AC14c	4-F	285.27	2	4	4	66.4	4.5 ± 0.5	-0.38	3.4 ± 0.8	-2.36
AC39c	4-CH_3	281.31	2	4	4	66.4	5.0 ± 0.4	0	3.5 ± 0.8	-2.08
AC26	2-OCH_3	297.30	2	5	5	75.63	4.5 ± 0.4	-0.14	3.4 ± 0.8	-2.02
AC20	4-OCH_3	297.30	2	5	5	75.63	4.5 ± 0.4	-0.14	3.5 ± 0.8	-1.88
AC24	3,4-$(OCH_3)_2$	327.33	2	6	6	84.86	4.4 ± 0.4	-0.74	3.5 ± 0.8	-1.89
AC27	3-OCH_2CH_3-4-OH	327.33	3	6	6	95.86	4.3 ± 0.4	-0.45	3.5 ± 0.8	-1.97
AC30d	4-OH	283.28	3	5	4	86.63	4.0 ± 0.4	-0.66	3.5 ± 0.8	-1.50
AC28d	3,4-$(OH)_2$	299.28	4	6	4	106.86	3.5 ± 0.4	-1.10	3.5 ± 0.8	-1.21
AC45c	4-$N(CH_3)_2$	310.35	2	5	5	69.64	5.0 ± 0.5	-0.19	3.5 ± 0.8	-2.58
AC18b	-	267.28	2	4	4	66.4	4.5 ± 0.4	-0.21	3.5 ± 0.8	-1.73
AC21b	α,β saturated	269.29	2	4	5	66.4	4.1 ± 0.3	-0.46	3.5 ± 0.4	-0.68
AC46c	α,β saturated, 4-OCH_3	299.32	2	5	6	75.63	4.0 ± 0.3	-0.37	3.5 ± 0.4	-0.77
AC34	Pipecolinic acid	259.30	1	4	3	57.61	1.8 ± 0.4	-2.38	3.3 ± 0.8	0.57
AC36	Proline	245.27	1	4	3	57.61	1.2 ± 0.4	-2.41	3.2 ± 0.9	0.61
AC43d	α-CH_3	281.31	2	4	4	66.4	5.1 ± 0.4	0	3.5 ± 0.8	-1.96
AC42c	α-Ph	343.37	2	4	5	66.4	6.7 ± 0.8	1.00	3.4 ± 0.8	-3.43

Table 3.8: *Physicochemical properties of methyl N-cinnamoylanthranilates showing that the compounds obeyed the Lipinski's rule-of-five and the Veber's rules of lead-likeness / oral bioavailability, except* AC42b. *Lipophilicity [partition coefficient (clogP) and distribution coefficient, (clogD)], solubility (clogS) and acid dissociation constant (pK_a) parameters are given for comparison. Abbreviations: MW - molecular weight, H-bond - hydrogen bond, TPSA - topological polar surface area.*

Compound	Substituent	MW (≤ 500)	H-bond donors (≤ 5)	H-bond acceptors (≤ 10)	Rotatable bonds (≤ 10)	TPSA/(Å^2) (≤ 140 Å^2)	clogP (≤ 5)	clogD at pH 7.4	pK_a at pH 7.4	clogS at pH 7.4
AC41b	4-NO_2	326.31	1	7	6	104.23	4.6 ± 0.4	3.48	13.6 ± 0.9	-5.78
AC40b	4-CF_3	349.31	1	4	6	55.4	5.8 ± 0.6	4.73	13.7 ± 0.9	-6.01
AC16b	4-Br	360.21	1	4	5	55.4	5.7 ± 0.5	4.50	13.8 ± 0.9	-5.82
AC17b	4-Cl	315.75	1	4	5	55.4	5.4 ± 0.4	4.51	13.8 ± 0.9	-5.87
AC15b	2-Cl	315.75	1	4	5	55.4	5.2 ± 0.4	4.51	13.7 ± 0.9	-5.83
AC14b	4-F	299.30	1	4	5	55.4	4.8 ± 0.5	3.87	13.9 ± 0.9	-5.73
AC39b	4-CH_3	295.34	1	4	5	55.4	5.3 ± 0.4	3.87	13.9 ± 0.9	-5.44
AC30c	4-OAc	339.35	1	6	7	81.7	4.3 ± 0.4	3.70	13.8 ± 0.9	-5.46
AC28c	3,4-$(OAc)_2$	397.38	1	8	9	108	3.3 ± 0.4	3.43	13.6 ± 0.9	-5.77
AC45b	4-$N(CH_3)_2$	324.38	1	5	6	58.64	5.3 ± 0.5	4.15	4.8 ± 0.8	-5.90
AC18a	-	281.31	1	4	5	55.4	4.8 ± 0.4	3.79	13.9 ± 0.9	-5.09
AC43c	α-CH_3	295.34	1	4	5	55.4	5.4 ± 0.4	4.14	13.9 ± 0.9	-5.31
AC42b	α-Ph	357.41	1	4	6	55.4	7.0 ± 0.8	5.31	13.9 ± 0.9	-6.76
AC35b	Phenoxy	299.32	1	5	7	64.63	3.6 ± 0.3	3.55	11.9 ± 0.5	-3.87

3.4.6 Electrophysiology

The agonistic and antagonistic effects of the compounds, **AC40c-**(*p*-CF_3) and **AC17c-**(*p*-Cl) at 100 µM and **AC30d-**(*p*-OH) at 300 µM, were tested on fully characterised isolated guinea pig vagus nerve preparations as described in **Section 2.5** of **Chapter 2**. The compounds showed a small degree of activation of the vagus nerve (**Figure 3.25a-c**) with **AC40c-**(*p*-CF_3) having the largest effect as in the HEK293 cells exogenously expressing hTRPA1 (**Figure 3.12b**,**d**). However, the potency of the responses obtained in a tissue (nerves) could not be compared to those obtained in HEK293 cells overexpressing hTRPA1, primarily due to variations in the expression level of TRPA1, the type of assay and species difference.

Acrolein was used as the TRPA1 standard agonist to determine the inhibitory effects of the compounds, as desensitisation of responses were observed with the use of cinnamaldehyde in depolarisation measurements.[154,436] As a positive control, incubation with the TRPA1 standard antagonist HC030031 (10 µM) inhibited the depolarisation induced by 300 µM acrolein (**Figure 3.25d**). However, contrary to the antagonistic effects observed in hTRPA1-HEK293 cells (**Figure 3.26b**), neither of the compounds **AC17c-**(*p*-Cl) nor **AC30d-**(*p*-OH) exhibited any antagonism against depolarisation of the guinea pig vagus nerve by acrolein. This discrepancy in results could possibly be due to, but not limited to, a consequence of species difference, and a higher concentration would have been required to elicit the response in the vagus nerve tissue. Comparing the TRPA1 amino acid sequences of *Homo sapiens* (human) and *Cavia porcellus* (guinea pig rodent), it was found that there is only 79 % identity (**Figure 3.27**). The low sequence homology with 21 % variation could have led to differences in responses.

It has been reported that several ligands, including caffeine, menthol and thioaminals (e.g. 4-methyl-*N*-[2,2,2-trichloro-1-(4-nitro-phenylsulfanyl)-ethyl]-benzamide), with potent antagonistic effects in hTRPA1 showed reduced potency, agonism or inactivity in rodent TRPA1.[255,256,264] Similarly, it was also reported that rodent TRPA1 is activated by cold, whereas human and rhesus monkey TRPA1 are not stimulated.[170] The menthol and cold

species difference were attributed to just a single residue, V875 in primates and G878 in rodents.[170]

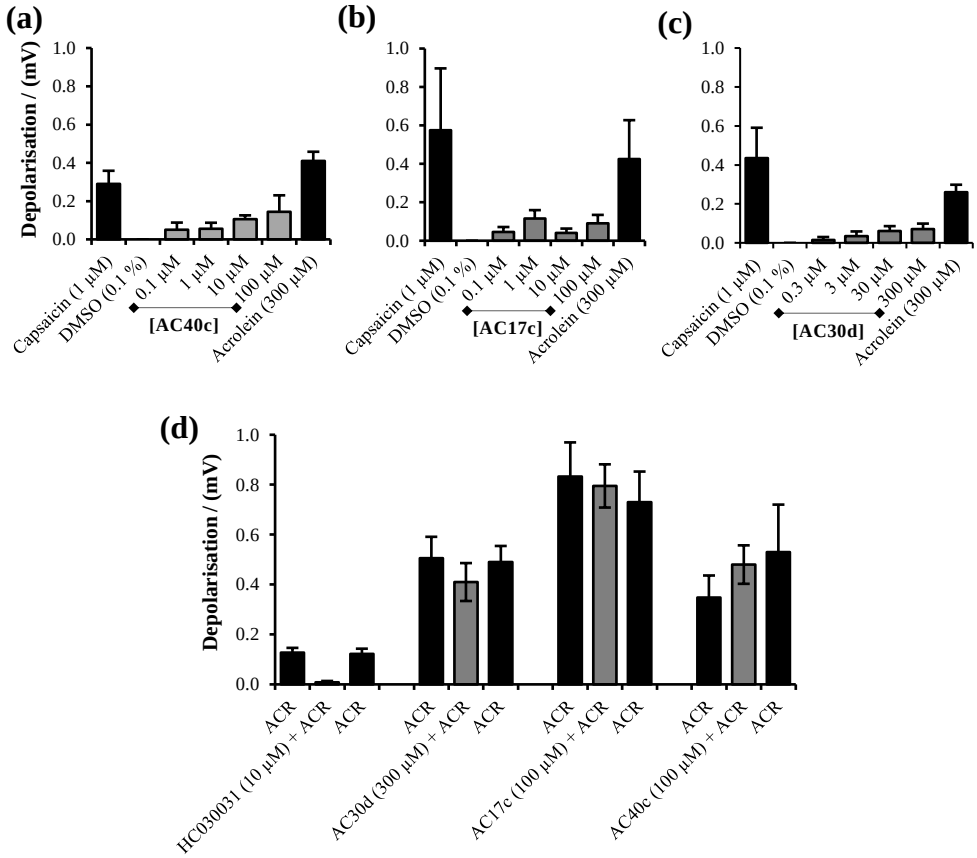

Figure 3.25: (a - c) *Agonism and* **(d)** *antagonism against acrolein (ACR, 300 µM) induced depolarisation of CADs* **AC40c-***(p-CF$_3$),* **AC17c-***(p-Cl) and* **AC30d-***(p-OH), on isolated guinea pig vagus nerve preparations. Each bar represents the mean ± SEM (N = 4).*

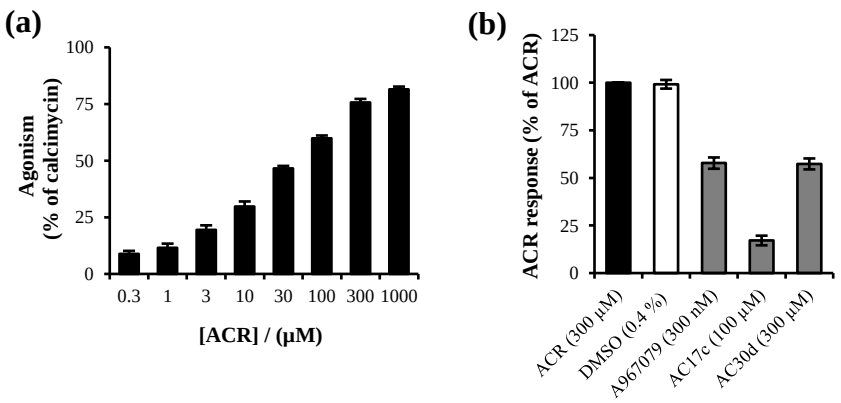

Figure 3.26: (a) *Dose-response of acrolein (ACR) and* **(b)** *antagonism of* **AC17c-***(p-Cl) and* **AC30d-***(p-OH) against acrolein (300 µM), in hTRPA1-HEK293 cells. Each data point represents the mean ± SEM (N = 3, n = 9).*

Identities	Positives	Gaps
882/1117 (79%)	995/1117 (89%)	8/1117 (0%)

```
HUMAN  1     MKRSLRKMWRPGEKKEPQGVVYEDVPDDTEDFKESLKVVFEGSAYGLQNFNKQK-KLKRC  59
             MKRSLRK+ R GE  EPQG VY+ V D   D K+  KVVFEG+   LQ+  K + KL +
CAVPO  1     MKRSLRKLLRSGET-EPQGAVYQGVDDSMPDSKD-FKVVFEGNECRLQHIIKNRWKLNKY  58

HUMAN  60    DDMDTFFLHYAAAEGQIELMEKITRDSSLEVLHEMDDYGNTPLHCAVEKNQIESVKFLLS  119
             ++ +   LH+AA EGQ+ELM+ I   SS EVL+ MD+YGNTP+H A E NQ+ESVKFLL
CAVPO  59    EEENVSALHHAAGEGQLELMKMIISGSSCEVLNLMDNYGNTPMHWAAENNQVESVKFLLI  118

HUMAN  120   RGANPNLRNFNMMAPLHIAVQGMNNEVMKVLLEHRTIDVNLEGENGNTAVIIACTTNNSE  179
              GANPNLRN NMMAPLHIAVQGM+NE+ KVL+EH + ++NLEGENGNTAV+I CT +NSE
CAVPO  119   HGANPNLRNNNMMAPLHIAVQGMHNEMAKVLIEHSSTNINLEGENGNTAVMITCTKDNSE  178

HUMAN  180   ALQILLKKGAKPCKSNKWGCFPIHQAAFSGSKECMEIILRFGEEHGYSRQLHINFMNNGK  239
              L+ILLKKGAK CKSNKWG FP+HQAAFSG+K+CME+IL+FGEE GYSRQ HINF+NN +
CAVPO  179   ILEILLKKGAKLCKSNKWGDFPVHQAAFSGAKKCMELILKFGEEDGYSRQCHINFVNNKQ  238

HUMAN  240   ATPLHLAVQNGDLEMIKMCLDNGAQIDPVEKGRCTAIHFAATQGATEIVKLMISSYSGSV  299
              +PLHLAVQ+G+LEMIKMCLDNGA I+ +E G+C A+HFAATQGATEIVKLM+SSYSG+
CAVPO  239   VSPLHLAVQSGNLEMIKMCLDNGAHIEKIENGKCMALHFAATQGATEIVKLMLSSYSGNS  298

HUMAN  300   DIVNTTDGCHETMLHRASLFDHHELADYLISVGADINKIDSEGRSPLILATASASWNIVN  359
             +I+N  DG HET+LHRASLFDHHELADYLISVGADIN  DSEGR+PL+LATASASWNIVN
CAVPO  299   NIINAVDGNHETLLHRASLFDHHELADYLISVGADINITDSEGRTPLVLATASASWNIVN  358

HUMAN  360   LLLSKGAQVDIKDNFGRNFLHLTVQQPYGLKNLRPEFMQMQQIKELVMDEDNDGCTPLHY  419
             LLLSKGA+VDIKD  GRNFLH TVQQPYGLKNLRPEFMQMQ+IK LVMDEDNDGCTPLHY
CAVPO  359   LLLSKGARVDIKDYLGRNFLHFTVQQPYGLKNLRPEFMQMQEIKALVMDEDNDGCTPLHY  418

HUMAN  420   ACRQGGPGSVNNLLGFNVSIHSKSKDKKSPLHFAASYGRINTCQRLLQDISDTRLLNEGD  479
             AC+QG   SVNNLLGFNVSI+SKSKDKKSPLHFAASYGRINTCQRLLQDISDTRLLNEGD
CAVPO  419   ACKQGVHVSVNNLLGFNVSIYSKSKDKKSPLHFAASYGRINTCQRLLQDISDTRLLNEGD  478

HUMAN  480   LHGMTPLHLAAKNGHDKVVQLLLKKGALFLSDHNGWTALHHASMGGYTQTMKVILDTNLK  539
             LHGMTPLHLAAKNGHDKVVQLLLKKGALFLSDHNGWTALHHASMGGYTQTMKVILDTN+K
CAVPO  479   LHGMTPLHLAAKNGHDKVVQLLLKKGALFLSDHNGWTALHHASMGGYTQTMKVILDTNMK  538

HUMAN  540   CTDRLDEDGNTALHFAAREGHAKAVALLLSHNADIVLNKQQASFLHLALHNKRKEVVLTI  599
             CTDRLDE+GNTALHFAAREGHAKAVALLL+H+ADIVLNKQQASFLH+ALHNKRKEVV+T
CAVPO  539   CTDRLDEEGNTALHFAAREGHAKAVALLLNHDADIVLNKQQASFLHIALHNKRKEVVITT  598

HUMAN  600   IRSKRWDECLKIFSHNSPGNKCPITEMIEYLPECMKVLLDFCMLHSTEDKSCRDYYIEYN  659
             IR+KRWDECLK+F+H SP N+CPITEMIEYLPECMK+LLDFCM+ STEDKSC+DY+IEYN
CAVPO  599   IRNKRWDECLKVFTHCSPSNRCPITEMIEYLPECMKILLDFCMIPSTEDKSCQDYHIEYN  658

HUMAN  660   FKYLQCPLEFTKKTPT-QDVIYEPLTALNAMVQNNRIELLNHPVCKEYLLMKWLAYGFRA  718
             F+YLQCPL+FT+K P  Q+V YEPL+ LN MVQ+NRIELLNHPVCKEYLLMKW AYGFRA
CAVPO  659   FRYLQCPLQFTRKLPAEQEVHYEPLSTLNVMVQHNRIELLNHPVCKEYLLMKWCAYGFRA  718

HUMAN  719   HMMNLGSYCLGLIPMTILVVNIKPGMAFNSTGIINETSDHSEILDTTNSYLIKTCMILVF  778
             HMMNLGSYCLGLIPMT+LV+NIKPG AFNSTGIINET + +   DTTNSY IK CMILVF
CAVPO  719   HMMNLGSYCLGLIPMTLLVINIKPGTAFNSTGIINETHNQT---DTTNSYPIKVCMILVF  775

HUMAN  779   LSSIFGYCKEAGQIFQQKRNYFMDISNVLEWIIYTTGIIFVLPLFVEIPAHLQWQCGAIA  838
             LSSIFGYCKE  QIFQQKRNYF+D +N LEW+IYT  IIFVLPLFV IPA++QWQCGAIA
CAVPO  776   LSSIFGYCKEVIQIFQQKRNYFLDYNNALEWVIYTKSIIFVLPLFVSIPAYVQWQCGAIA  835

HUMAN  839   VYFYWMNFLLYLQRFENCGIFIVMLEVILKTLLRSTVVFIFLLLAFGLSFYILLNLQDPF  898
             ++ YWMNFL+YLQRFEN GIFIVMLEVI +TLLRST VFIFLLLAFGLSFY+LLN QD F
CAVPO  836   IFLYWMNFLMYLQRFENWGIFIVMLEVIFRTLLRSTGVFIFLLLAFGLSFYVLLNAQDAF  895

HUMAN  899   SSPLLSIIQTFSMMLGDINYRESFLEPYLRNELAHPVLSFAQLVSFTIFVPIVLMNLLIG  958
              SPLLS++QTF+MMLGD+NYR+++L+P+L+NEL +PVLSF QL++FT+FVPIVLMNLLIG
CAVPO  896   RSPLLSLVQTFTMMLGDVNYRDTYLQPFLKNELTYPVLSFVQLIAFTMFVPIVLMNLLIG  955

HUMAN  959   LAVGDIAEVQKHASLKRIAMQVELHTSLEKKLPLWFLRKVDQKSTIVYPNKPRSGGMLFH  1018
             LAVGDIAEVQKHASLKRIAMQVELHTSLEKKLP+WFLR+VDQKSTIVYPN+PR G +L
CAVPO  956   LAVGDIAEVQKHASLKRIAMQVELHTSLEKKLPIWFLRRVDQKSTIVYPNRPRYGPVL-R  1014

HUMAN  1019  IFCFLFCTGEIRQEIPNADKSLEMEILKQKYRLKDLTFLLEKQHELIKLIIQKMEIISET  1078
             +F + F   E RQE+PN D  LE+E+LKQKYRLKDLT LLEKQHELIKLIIQKMEIISET
CAVPO  1015  LFHYFFGVQETRQELPNTDTCLELEMLKQKYRLKDLTSLLEKQHELIKLIIQKMEIISET  1074

HUMAN  1079  EDDDSHCSFQDRFKKEQMEQRNSRWNTVLRAVKAKTH  1115
             ED+D+H SFQDRFKKE++EQ NS+WN VLRAVK K H
CAVPO  1075  EDEDNHSSFQDRFKKERLEQMNSKWNFVLRAVKTKPH  1111
```

Figure 3.27: *The sequence alignment of human (Homo sapiens) and guinea pig (Cavia porcellus) TRPA1, aligned using NCBI BLAST, showing 79 % identity. Terms: identities, number of amino acids that are identical; positives* (+)*, number of amino acids that are identical plus the number of different amino acids that have similar chemical properties; gaps* (-)*, denotes a gap in the alignment; space* ( )*, amino acids that are completely different.*

3.5 Indirect measure of covalent modification of cysteines

It was considered that the CADs may conceivably undergo covalent modification due to the presence of α,β-unsaturated carboxamide function (Michael acceptor). In previous work, the rates of NMR scale model reactions as a proxy for monitoring covalent modification of TRPA1 cysteine residues has been correlated with agonism levels observed *in vitro*.[123] Hence the propensity of CADs to undergo covalent modification through conjugate addition of the thiol group in cysteine (*N*-acetyl- L-cysteine methyl ester or *N*-acetyl-L-cysteine) to the α,β-unsaturated double bond was evaluated for a representative CAD **AC18a** (**Scheme 3.7**), using a proton NMR time study.[123] This revealed that the CAD had no reactivity with the thiol group of cysteine in d_6-DMSO (**Figure 3.28**), as there were no differences in the intensity of the peaks for the protons at δ 6.64 (d, $1H^5$) and 7.77 (d, $1H^6$), nor appearance of any new peaks over the time intervals monitored (10 minutes, 1, 3.5 and 6 hours). Other potential non-covalent ligand binding sites for the CADs are discussed in **Chapter 5**.

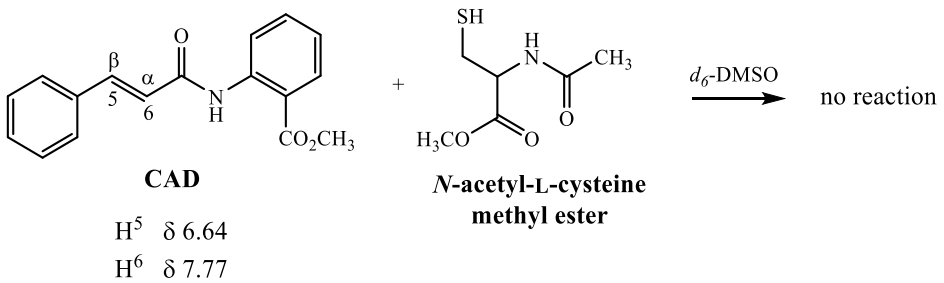

Scheme 3.7: *Example of a ^1H NMR reaction carried out to assess the possibility of covalent modification of cysteine residues by CADs.*

(a) Methyl *N*-cinnamoylanthranilate (AC18a)

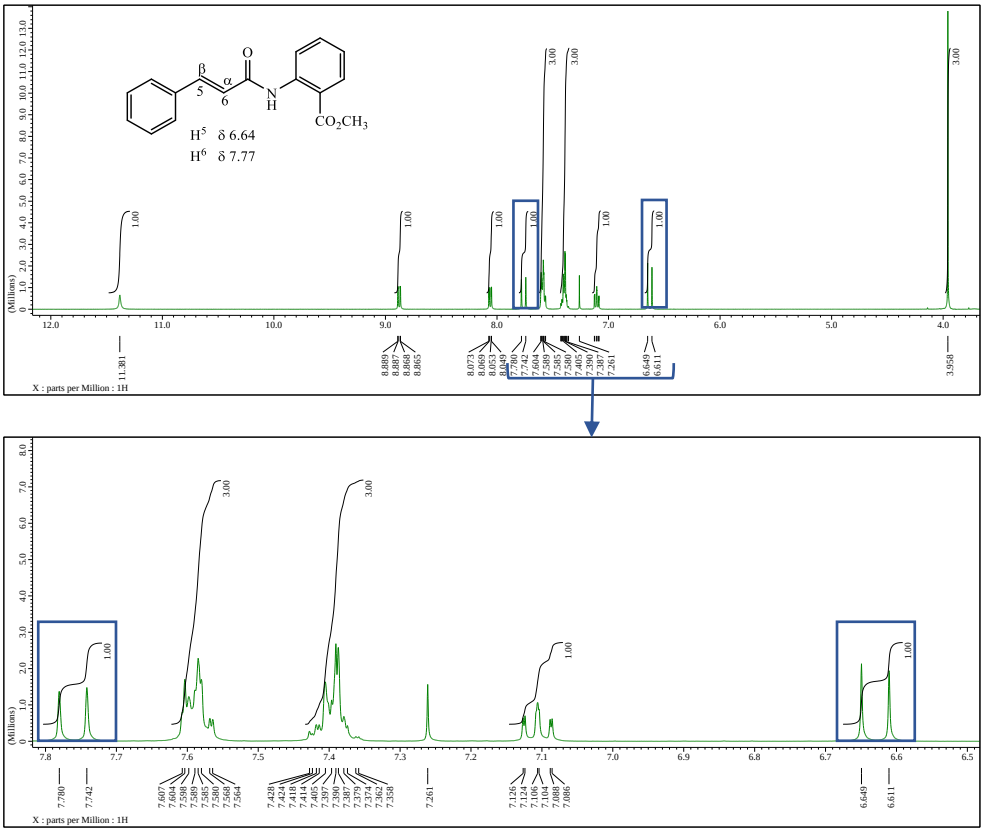

Continued…

Figure 3.28: *^{1}H NMR spectra of the reactions carried out to assess, if any, covalent modification of cysteine residues,* **(a)** CAD **AC18a** *in $CDCl_3$,* **(b)** *the CAD with N-acetyl-L-cysteine methyl ester, and* **(c)** *CAD with N-acetyl-L-cysteine, in d_6-DMSO at time intervals* **(i)** *10 minutes,* **(ii)** *1 hour,* **(iii)** *3.5 hours and* **(iv)** *6 hours.*

Continued…

(b) AC18a + *N*-acetyl-L-cysteine methyl ester

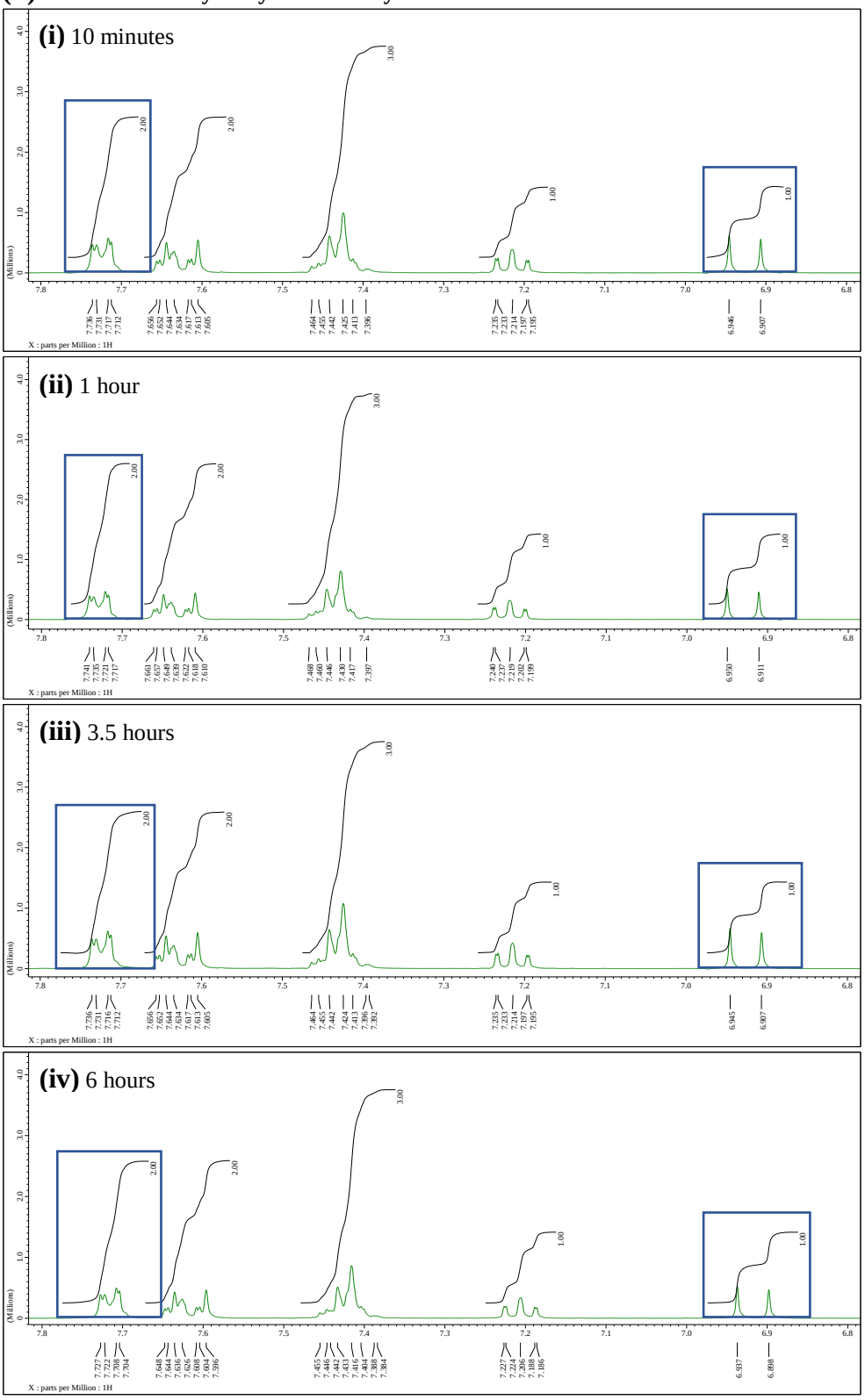

Continued…

Figure 3.28: *^{1}H NMR spectra of the reactions carried out to assess, if any, covalent modification of cysteine residues,* **(a)** CAD **AC18a** *in $CDCl_3$,* **(b)** *the CAD with N-acetyl-L-cysteine methyl ester, and* **(c)** *CAD with N-acetyl-L-cysteine, in d_6-DMSO at time intervals* **(i)** *10 minutes,* **(ii)** *1 hour,* **(iii)** *3.5 hours and* **(iv)** *6 hours.*

Continued…

(c) AC18a + *N*-acetyl-L-cysteine

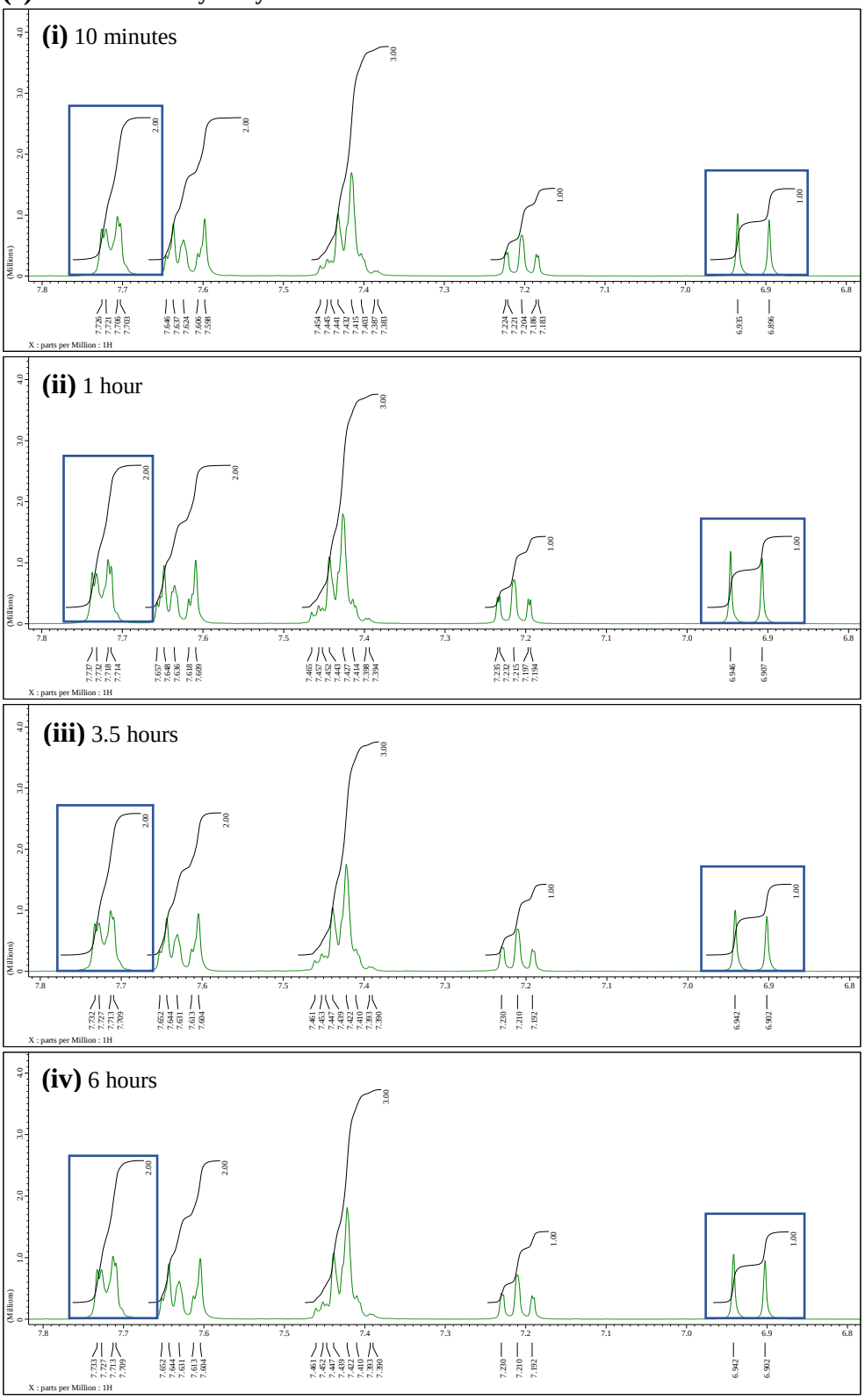

Figure 3.28: *^{1}H NMR spectra of the reactions carried out to assess, if any, covalent modification of cysteine residues,* **(a)** CAD **AC18a** *in $CDCl_3$,* **(b)** *the CAD with N-acetyl-L-cysteine methyl ester, and* **(c)** *CAD with N-acetyl-L-cysteine, in d_6-DMSO at time intervals* **(i)** *10 minutes,* **(ii)** *1 hour,* **(iii)** *3.5 hours and* **(iv)** *6 hours.*

3.6 TRP channels could be the reason behind numerous activities of *N*-cinnamoylanthranilates in the literature

In addition to the overall findings, it is postulated that there could be a correlation between the several biological activities of CADs reported in the literature (**Section 1.2** of **Chapter 1**) and TRP channels. This is plausible due to the known participation of TRP channels in a wide range of cellular functions.[3] Key to this suggestion is a recent study,[437] which reports that TRPA1 is necessary for TGF-β signalling. Loss of the receptor significantly suppresses the mRNA expression of the inflammatory cytokines, interleukin-6 (IL-6), α-smooth muscle actin (α-SMA) involved in fibrosis, substance P involved in inflammation, vascular endothelial growth factor (VEGF), collagen Iα1 and the phosphorylation of kinases induced by TGF-β, and thereby results in attenuation of fibrogenic and inflammatory reactions. Likewise, in the literature, the anti-allergic, anti-inflammatory,[278,279,311] anti-oxidant,[288,313] anti-fibrotic,[406] anti-proliferative,[306,314] and anti-cancer[310,407] properties of CADs were related to inhibition of cytokines, chemokines and growth factors. Hence it is summarised that the fundamental reason behind attenuation of cytokines and growth factors shown by CADs, might be the consequence of effects imposed by CADs on TRP channels.

3.7 Conclusions

The series of *N*-cinnamoylanthranilates with electron-withdrawing and/or electron-donating substituents evaluated were found to possess various activities ranging from agonism, partial agonism, antagonism and desensitising effect in hTRPA1, in a concentration-dependent manner and with a trend in the SAR. From the overall observations and information, it was deduced that hydrogen bonding from the amide and the carboxylic acid groups, and hydrophobic π-π stacking interactions of the aromatic rings contribute to the channel modulation. Screening of compounds in hTRPM8 and pcDNA3 mock cells verified that the majority of the CADs were selective to hTRPA1. Moreover, the structurally related compound in the literature, ACA, an inhibitor of TRPM2, TRPM8, TRPC3, TRPC6 and TRPV1[327]

channels was found to activate hTRPA1 (EC_{50} 28 µM) with similar potency to those of other CADs evaluated in the study.

Different substituents and substitution patterns on the derivatives have shown differences in biological activities, which agree with the hypothesis, that is, the functional groups present on the compounds triggers the action of TRPA1 channels. The CAD **AC30d** (*p*-OH, IC_{50} 43 µM) with strong EDG-substituent and CAD **AC42c** (α-Ph, EC_{50} 11 µM) with an α-phenyl substituent show promise as selective hTRPA1 antagonist and agonist for further study. Using the key SARs found in the study, the structures of the compounds could be optimised to make the CADs more potent modulators of TRPA1. Moreover, owing to the fact that the CAD, tranilast is a clinically accepted anti-allergic drug with reduced side effects,[291] CADs could have the potential in clinical development in general. However, the functional characterisation of some of the CADs in guinea pig vagus nerve showed poor activity, and was thought to be due to species difference and/or limitations with tested concentrations, as discussed in **Section 3.4.6**. In addition to this study, it is predicted that the diverse activities of CADs reported in the literature could possibly be due to existence of some correlation between TRP channels and cytokines and growth factors, which warrants further study.

CHAPTER 4: Aryl sulfonamides as modulators of TRPA1

4.1 Introduction

Probenecid [*p*-(dipropylsulfamyl)benzoic acid, **M1**, **Figure 4.1**], a competitive inhibitor of organic anion transporters, is commonly used to prevent leakage of Ca^{2+} sensitive fluorescent dyes from cells.[348,349,354] However, in a recent study,[354] it was found that TRPA1 is activated (EC_{50} 4.2 mM) by probenecid, and prolonged incubation with probenecid during dye-loading process leads to desensitisation of the channel and consequently decreases the potency of the agonists evaluated. For instance, when hTRPA1 expressing CHO cells were dye-loaded with probenecid (2 mM), the EC_{50} obtained for the TRPA1 agonist AITC significantly ($p < 0.01$) increased from 1.5 to 7.3 μM.[354] In addition, different pharmaceutical companies have claimed analogues of aryl sulfonamides as potent TRPA1 antagonists.[372-376]

It was observed that most of the compounds claimed as TRPA1 antagonists by the companies, Janssen Pharmaceuticals,[372] Orion Corporation,[373] Pharmeste[374] and Hoffmann-La Roche,[375,376] possessed a 4-fluorobenzenesulfonamide motif (**A1**, **Figure 4.1**), as shown in **Figure 1.34** (**Section 1.3.2** of **Chapter 1**). As probenecid with the structure 4-carboxybenzenesulfonamide activates, and aryl sulfonamides with 4-fluorobenzenesulfonamide inhibit the channel, it was hypothesised that the carboxylic acid group on the probenecid leads to activation and fluoro group on the antagonists are important for the antagonistic effect on TRPA1 channel modulation.

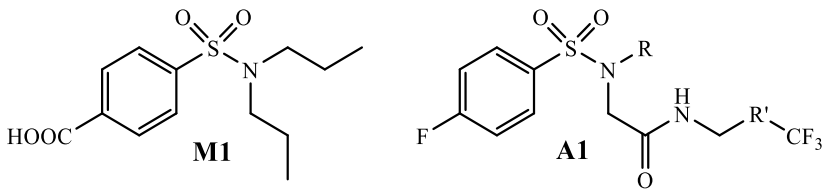

Figure 4.1: *The chemical structure of probenecid* (**M1**), *and observed core structure of the TRPA1 antagonists* (**A1**).

Consequently, derivatives of aryl sulfonamide derivatives (ASDs) were synthesised to study their structure-activity relationship (SAR) with the non-

selective cation channel TRPA1. The chemical structures of the synthesised ASDs are given in **Figure 4.2** and also in the **Appendix**, and the mechanisms of the chemical reactions and some of the compound information are given in **Sections 4.2** and **4.3**, respectively. Though aryl sulfonamides have been reported as potent TRPA1 antagonists in previous studies,[372-376] this is the first approach to study their SAR in hTRPA1 by assessing small and extended structures of sulfonamide derivatives.

Twenty-two aryl sulfonamides were screened for agonism and antagonism responses in HEK293 cells stably transfected with hTRPA1, where the transient elevations of $[Ca^{2+}]_i$ were characterised by performing calcium signalling using a FlexStation (**Sections 4.4.1** and **4.4.2**). The selectivity of the compounds was determined by evaluating in HEK293 cells stably transfected with either pcDNA3 (mock) or hTRPM8 (**Section 4.4.3**). Furthermore, the physicochemical properties of the ASDs were assessed and correlated with their activities (**Section 4.4.4**).

4.2 Synthetic chemistry

A series of ASDs (**Figure 4.2**) were successfully synthesised using the classical methodologies described in **Section 2.3** of **Chapter 2**. The mechanisms of the chemical reactions carried out to synthesise ASDs are shown in **Schemes 4.1** and **4.2**.

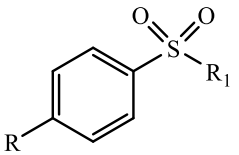

	R	R_1
M1	COOH	dipropylamine
M2	H	diethylamine
M3	OCH_3	diethylamine
M4	OCH_3	pyrrolidine
M5	F	diethylamine
M6	F	pyrrolidine
M7	F	piperidine
M8	F	morpholine
M9	F	indoline
M10	NHAc	diethylamine
M11	COOH	diethylamine
M12	COOH	pyrrolidine
M13	COOH	piperidine
M14	COOH	morpholine

Continued…

Figure 4.2: *Chemical structures of the synthesised and screened aryl sulfonamides*.

Continued…

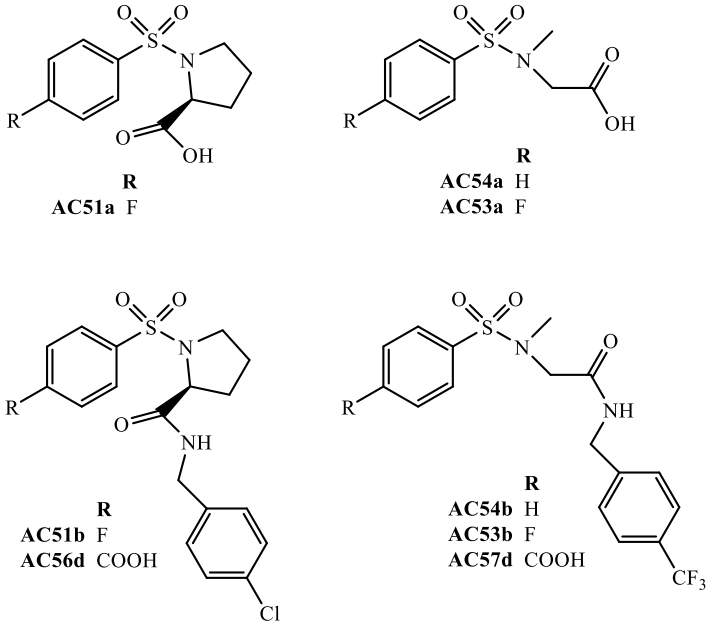

Figure 4.2: *Chemical structures of the synthesised and screened aryl sulfonamides*.

4.2.1 Aryl sulfonamides

The reaction mechanism by which a secondary amine couples to a sulfonyl chloride *via* sulfonylation to form a small aryl sulfonamide followed by formation of the amide on further coupling to a benzylamine to produce an extended aryl sulfonamide is shown in **Scheme 4.1**. When 4-(chlorosulfonyl)benzoic acid was used in the reaction, an alternative reaction path was followed as shown in **Scheme 4.2**, otherwise it would lead to two carboxylic acid groups on reacting with an amino acid (sulfonylation) that can react with benzylamine in the following step. As shown in **Scheme 4.2**, first the secondary amine was protected using Boc_2O and was coupled to benzylamine, followed by deprotection using TFA and sulfonylation to 4-(chlorosulfonyl)benzoic acid to produce the extended aryl sulfonamide.

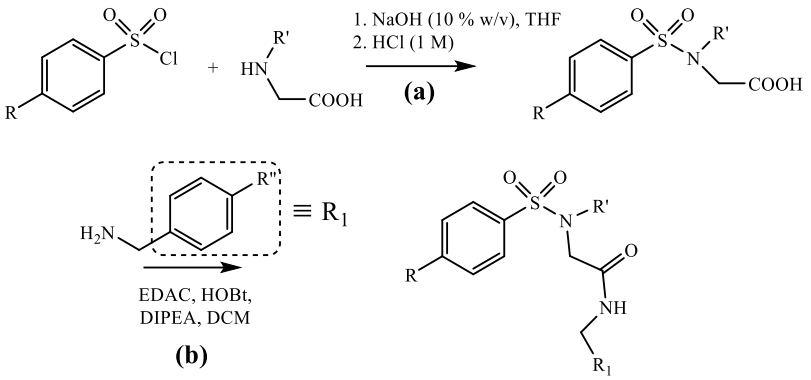

(a) *Sulfonylation*

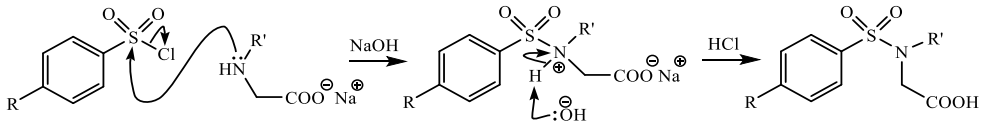

(b) *Coupling of aryl sulfonamide with benzylamine*

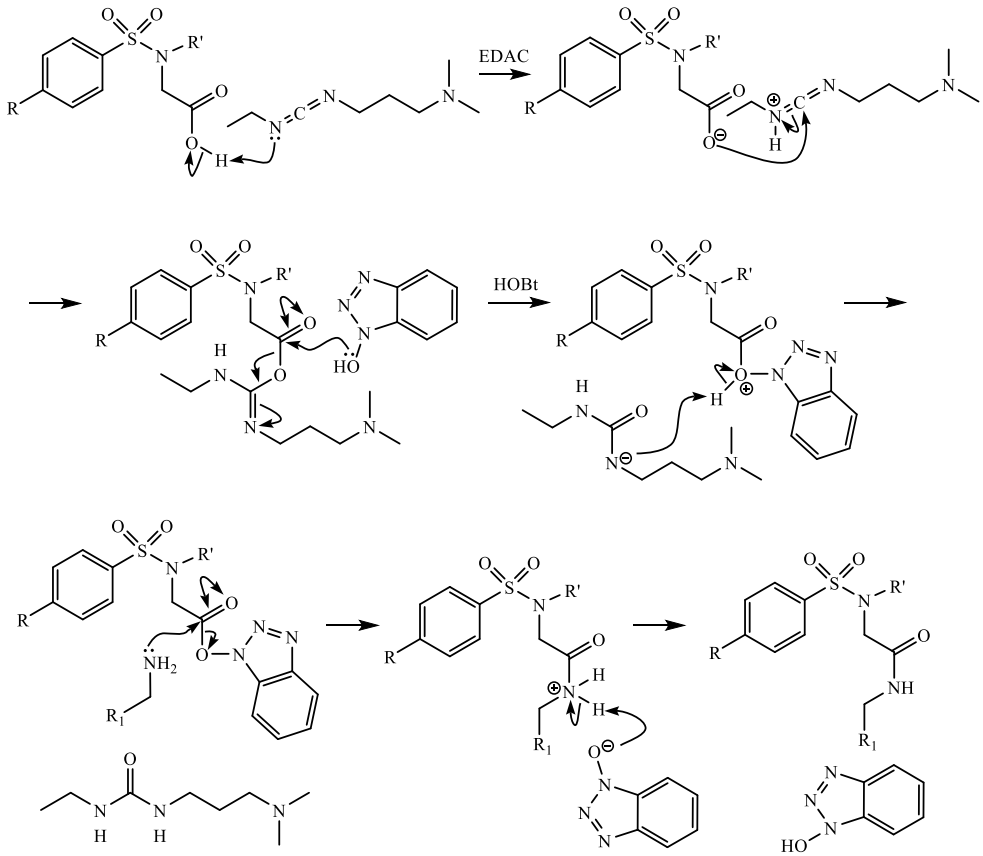

Scheme 4.1: *Reaction mechanism for the formation of aryl sulfonamides,* **(a)** *sulfonylation, and* **(b)** *amide formation.*

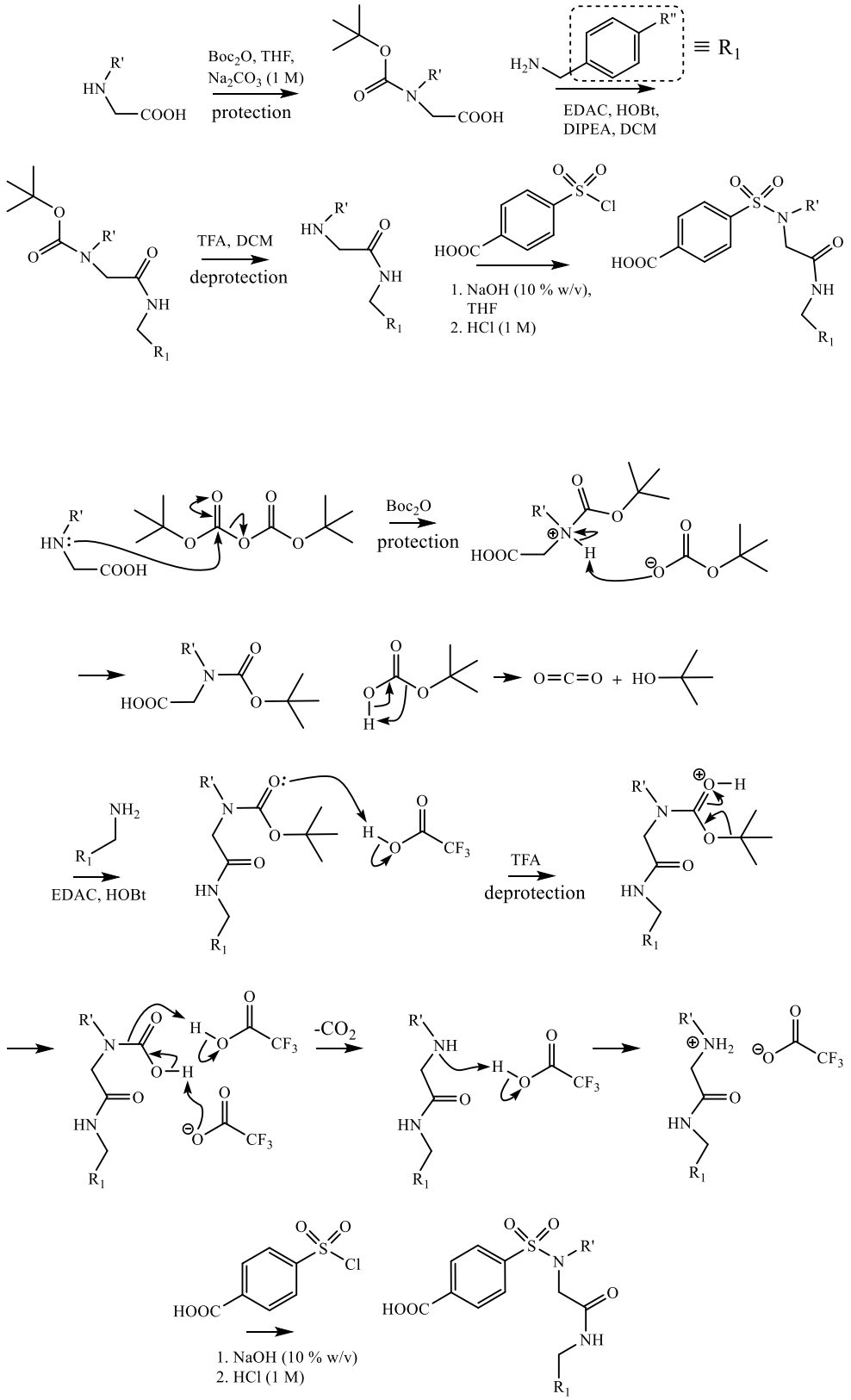

Scheme 4.2: *Reaction mechanism for the formation of aryl sulfonamides with protection and deprotection steps.*

4.2.2 4-(Chlorosulfonyl)benzoic acid

4-(Chlorosulfonyl)benzoic acid was produced *via* modified Sandmeyer reaction through the mechanism shown in **Scheme 4.3**. The nitrous acid produced *in situ* from sodium nitrite in the presence of hydrochloric acid undergoes protonation to form the nitrosonium ion. The electrophilic nitrosonium ion reacts with 4-aminobenzoic acid and forms the diazonium salt *via* a nitrosamine intermediate. The aromatic diazo group is then replaced *via* an aryl radical addition to sulfur dioxide, catalysed by copper(I) chloride, to form the aryl sulfonyl chloride.

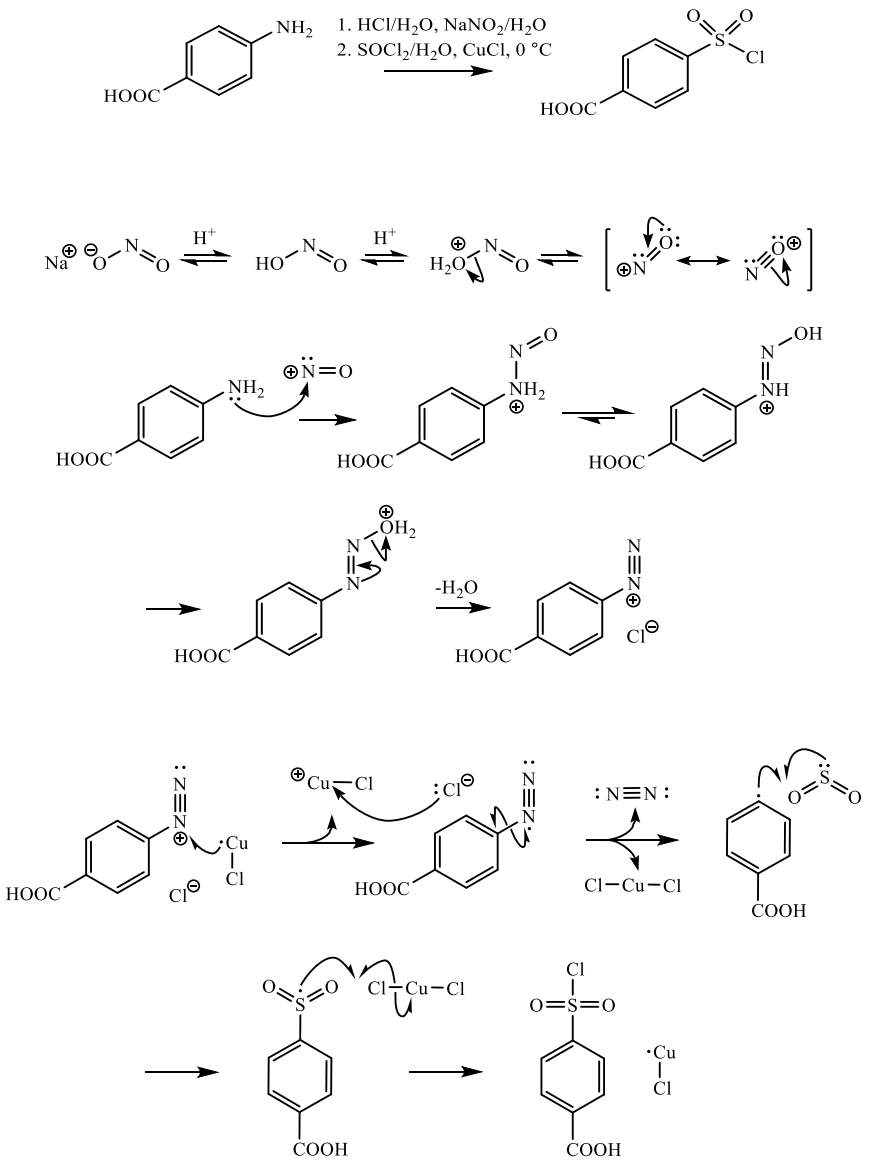

Scheme 4.3: *Reaction mechanism for the formation of 4-(chlorosulfonyl)benzoic acid via modified Sandmeyer reaction.*

4.3 Chemical information

All the chemical compound characterisation data are given in **Sections 2.3.1** and **2.3.2** of **Chapter 2** along with the synthesis procedures. Due to C-F couplings, doubling of some carbon signals were observed in the ^{13}C NMR spectra of the compounds **AC51** and **AC53**. The percentages of the CHN elemental composition found were within ± 0.4 % of the theoretical values. The chemical characterisation results obtained agreed closely with the data of the compounds already reported in the literature (**Table 4.1**). Among the synthesised ASDs, **AC53b**, **AC54b**, **AC56d** and **AC57d** were found to be novel compounds. Highly pure compounds as determined by CHN combustion elemental microanalysis, ^{1}H and ^{13}C NMR, and constant melting point were used in the biological activity assays.

Table 4.1: *Chemical data for the synthesised aryl sulfonamides available in the literature. Abbreviations: nda - no data available, nf - not found.*

Compound name	Code	Reference(s)
N,*N*-Diethylbenzenesulfonamide	M2	393,398,438
N,*N*-Diethyl-4-methoxybenzenesulfonamide	M3	394,395
1-((4-Methoxyphenyl)sulfonyl)pyrrolidine	M4	395
N,*N*-Diethyl-4-fluorobenzenesulfonamide	M5	396
1-((4-Fluorophenyl)sulfonyl)pyrrolidine	M6	439
1-((4-Fluorophenyl)sulfonyl)piperidine	M7	397
4-((4-Fluorophenyl)sulfonyl)morpholine	M8	398
1-((4-Fluorophenyl)sulfonyl)indoline	M9	nda
N-(4-(*N*,*N*-Diethylsulfamoyl)phenyl)acetamide	M10	399,440
4-(*N*,*N*-Diethylsulfamoyl)benzoic acid	M11	400,441
4-(Pyrrolidin-1-ylsulfonyl)benzoic acid	M12	442
4-(Piperidin-1-ylsulfonyl)benzoic acid	M13	400,443
4-(Morpholinosulfonyl)benzoic acid	M14	400
((4-Fluorophenyl)sulfonyl)-L-proline	AC51a	372
(*S*)-*N*-(4-Chlorobenzyl)-1-((4-fluorophenyl)sulfonyl) pyrrolidine-2-carboxamide	AC51b	373
N-((4-Fluorophenyl)sulfonyl)-*N*-methylglycine	AC53a	376
2-((4-Fluoro-*N*-methylphenyl)sulfonamido)-*N*-(4-(trifluoromethyl)benzyl)acetamide	AC53b	nf
N-Methyl-*N*-(phenylsulfonyl)glycine	AC54a	401,444
2-(*N*-Methylphenylsulfonamido)-*N*-(4-(trifluoromethyl) benzyl)acetamide	AC54b	nf
(*S*)-4-((2-((4-Chlorobenzyl)carbamoyl)pyrrolidin-1-yl) sulfonyl)benzoic acid	AC56d	nf
4-(*N*-Methyl-*N*-(2-oxo-2-((4-(trifluoromethyl)benzyl) amino)ethyl)sulfamoyl)benzoic acid	AC57d	nf

4.4 Pharmacology of aryl sulfonamides

4.4.1 Calcium signalling

Agonism of the compounds were measured by assessing the influx of Ca^{2+} in TRPA1-HEK293 cells upon exposure to the test compounds relative to calcimycin, and antagonism of the compounds were measured by the ability of the test compounds to antagonise the agonism of a standard agonist (**Section 2.4.2** of **Chapter 2**). Hence the agonism and antagonism responses ($[Ca^{2+}]_i$ released) of the compounds are presented as the percentage of calcimycin and the standard agonist, respectively. The responses were normalised by subtracting the noise/response obtained for the vehicle control (DMSO). The maximum response in antagonist assays was obtained by normalising the standard agonist-induced response (AITC) to 100 %, and thus in antagonist assays, a higher percentage value indicates a lower inhibitory effect by the test compound.

4.4.1.1 Solubility of compounds

The compounds containing a free carboxylic acid group were evaluated in the cells as their corresponding carboxylate salt due to deprotonation in the slightly alkaline isotonic assay buffer (pH 7.4). However, higher concentrations of ASDs made in DMSO precipitated in the assay buffer, and hence the maximum concentration evaluated was limited to 300 or 1000 μM.

4.4.1.2 Controls

Calcimycin (8 μM) was used as the maximum response control. The standard agonists AITC and WS12, and antagonists A967079 and AMTB, used as the positive controls in hTRPA1 and hTRPM8, respectively, were chosen based on the ion channel specificity and potency of the ligands. Dose-response curves carried out for the positive controls to determine the EC_{50} and IC_{50} values are given in **Figures 4.3** and **4.4**.

The EC_{50} and IC_{50} values obtained for these standard ligands were broadly consistent with the values found in the original reports[104,166,417,418] as can be seen in **Table 4.2**. Perhaps, variations in the assay methods, conditions, species and/or cell lines between the studies could have contributed to the

differences in the results (**Table 4.2**). In hTRPA1-HEK293 cells, the agonism of AITC at 10 µM (~EC_{50}) was completely inhibited by the TRPA1 specific standard antagonist A967079 at and above 300 nM. Similarly, in hTRPM8, the agonism by WS12 at 100 nM (~EC_{50}) was completely inhibited by the antagonist AMTB.HCl at 3 µM. The vehicle control (0.4 % DMSO) had no activity in hTRPA1 and in mock transfected-HEK293 cells, but had antagonising effect in hTRPM8.

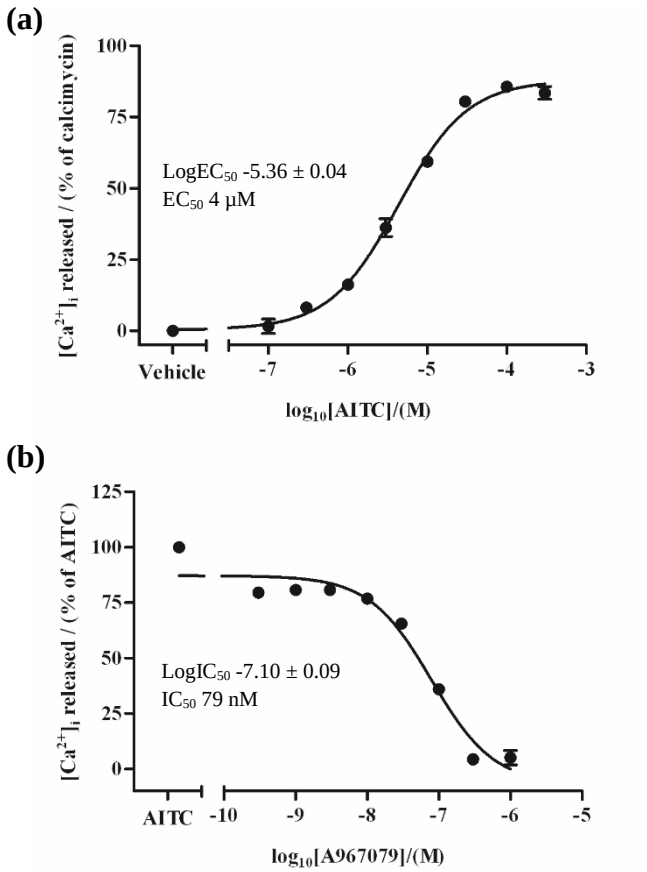

Figure 4.3: *Dose-response curves of the standard TRPA1 agonist and antagonist,* **(a)** *AITC and* **(b)** *A967079 (against 10 µM AITC), respectively, evaluated in hTRPA1-HEK293 cells. Each data point represents the mean ± SEM (N = 3, n = 9).*

Table 4.2: *Comparison of the EC_{50} and IC_{50} values of the standard TRPA1 and TRPM8 ligands, obtained in hTRPA1- or hTRPM8-HEK293 cells, against the literature values.*

Ligand	Obtained	Literature value
AITC	EC_{50} 4 µM	EC_{50} 22 ± 3 µM in mTRPA1-CHO cells[104]
A967079	IC_{50} 79 nM	IC_{50} 67 nM in hTRPA1-HEK293F cells (against 30 µM AITC)[166]
WS12	EC_{50} 80 nM	EC_{50} 12 ± 5 µM in *Xenopus* oocytes[417]
AMTB	IC_{50} 0.5 µM	pIC_{50} 6.23 ± 0.02 hTRPM8-HEK293 cells (against icilin EC_{80})[418]

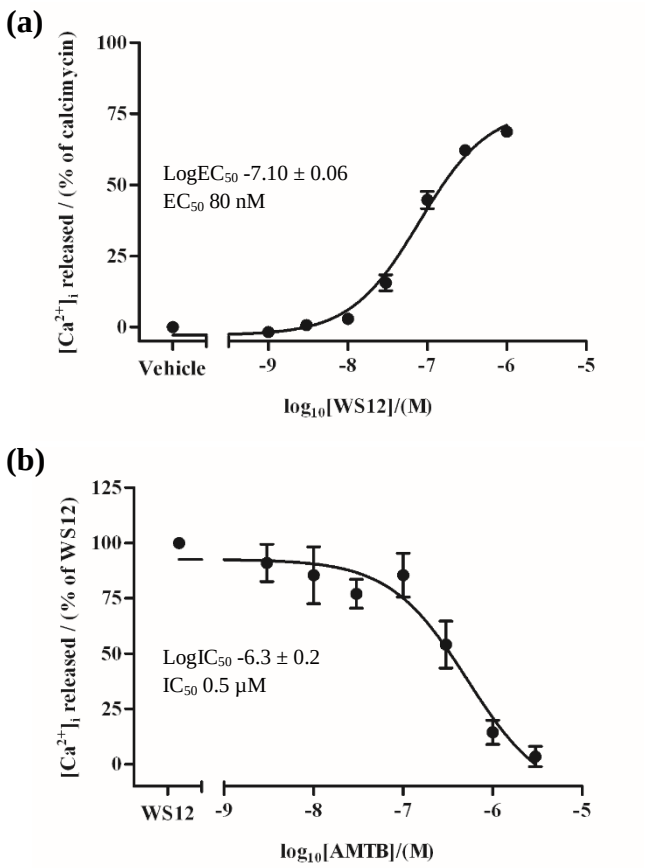

Figure 4.4: *Dose-response curves of the standard TRPM8 agonist and antagonist,* **(a)** *WS12 and* **(b)** *AMTB (against 100 nM WS12), respectively, evaluated in hTRPM8-HEK293 cells. Each data point represents the mean ± SEM (N = 3, n = 9).*

4.4.2 Screening of aryl sulfonamides in hTRPA1-HEK293 and structure-activity relationships

A dose-response curve for probenecid (**M1**) was carried out on hTRPA1-HEK293 cells to determine the active concentration range of the compound in the fluorescence-based calcium signalling assay method utilised (**Figure 4.5**). However, a complete dose-response curve was not attainable due to insolubility of the compound at higher concentrations as mentioned earlier, and a considerable amount of activity was observed only at the high concentrations, 100, 300 and 1000 µM, tested (**Figure 4.5**). The activity of **M1** obtained at the maximum concentration (1000 µM) in hTRPA1-HEK293 cells was approximately 50 % higher than that reported[354] in hTRPA1-CHO cells, with an EC_{50} value of 4.2 mM, using a FlexStation calcium-imaging assay.[354]

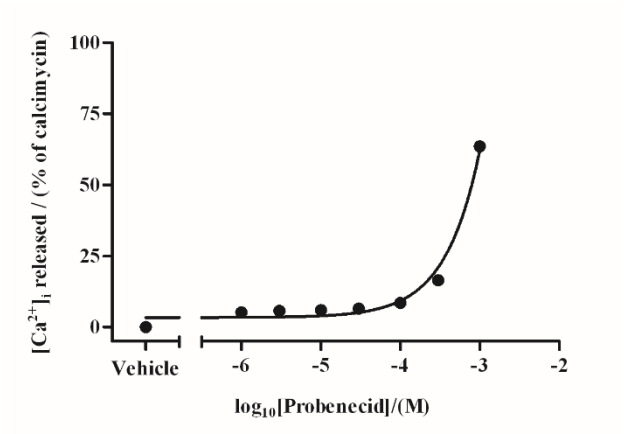

Figure 4.5: *Dose-response curve of probenecid* (**M1**) *obtained against hTRPA1-HEK293 cells. Each data point represents the mean ± SEM (N = 3, n = 9).*

The aryl sulfonamides **M2 - M14** (**Figure 4.2**) along with **M1** were screened against hTRPA1-HEK293 cells for agonism and antagonism at the concentrations 100, 300 and 1000 µM (**Figure 4.6**). Among the derivatives tested for agonism (**Figure 4.6a**), **M1**, **M3**, **M4** and **M9 - M14** showed activity, in a concentration-dependent manner, whereas **M2** and **M5 - M8** were inactive at any of the concentrations tested. The active derivatives **M3**, **M4** and **M9 - M11** showed only <20 % of calcimycin response at the concentrations 100 and 300 µM, as observed with **M1**, and differences in potency of the compounds were observed only at 1000 µM (**Figure 4.6a**). Among the derivatives **M1 - M14** screened for antagonism, except **M5** with weak antagonism (inhibited 26 ± 5 % of AITC agonism) other derivatives had no antagonistic effect (**Figure 4.6b**).

On comparing the SAR of the active ASDs **M2 - M14** on hTRPA1 (**Figures 4.2** and **4.6a**), irrespective of the amine attached to the aryl sulfonyl group, the derivatives **M3** and **M4** with -OCH_3 as their R substituent showed similar weak agonism (10 ± 5 and 13 ± 4 % of calcimycin, respectively, at 1000 µM). The -COOH group containing derivatives **M11 - M14**, and acetanilide (CH_3CONH-) containing derivative **M10** also showed agonism, with **M13** being the most potent (50 ± 4 % of calcimycin) among them. The derivatives, **M10** with CH_3CONH- and **M11** with -COOH as the R group, and having the same R_1 diethylamide group attached to the sulfonyl group, showed similar agonism (23 ± 1 and 21 ± 6 % of calcimycin, at 1000 µM, respectively).

However, the derivatives with H or F atom as the R substituent, **M2** and **M5 - M8**, had no agonism. A drop in the activity of **M9** with an increase in concentration was observed due to high insoluble nature of the compound relative to other derivatives. The observed trend was that the derivatives with hydrophilic substituents *para* to the sulfonyl group showed agonism. Colour coded mapping of the aryl sulfonamide structures (**M1 - M14**) highlighting the lipophilicity/hydrophilicity nature of the functional groups are shown in **Figure 4.7**.

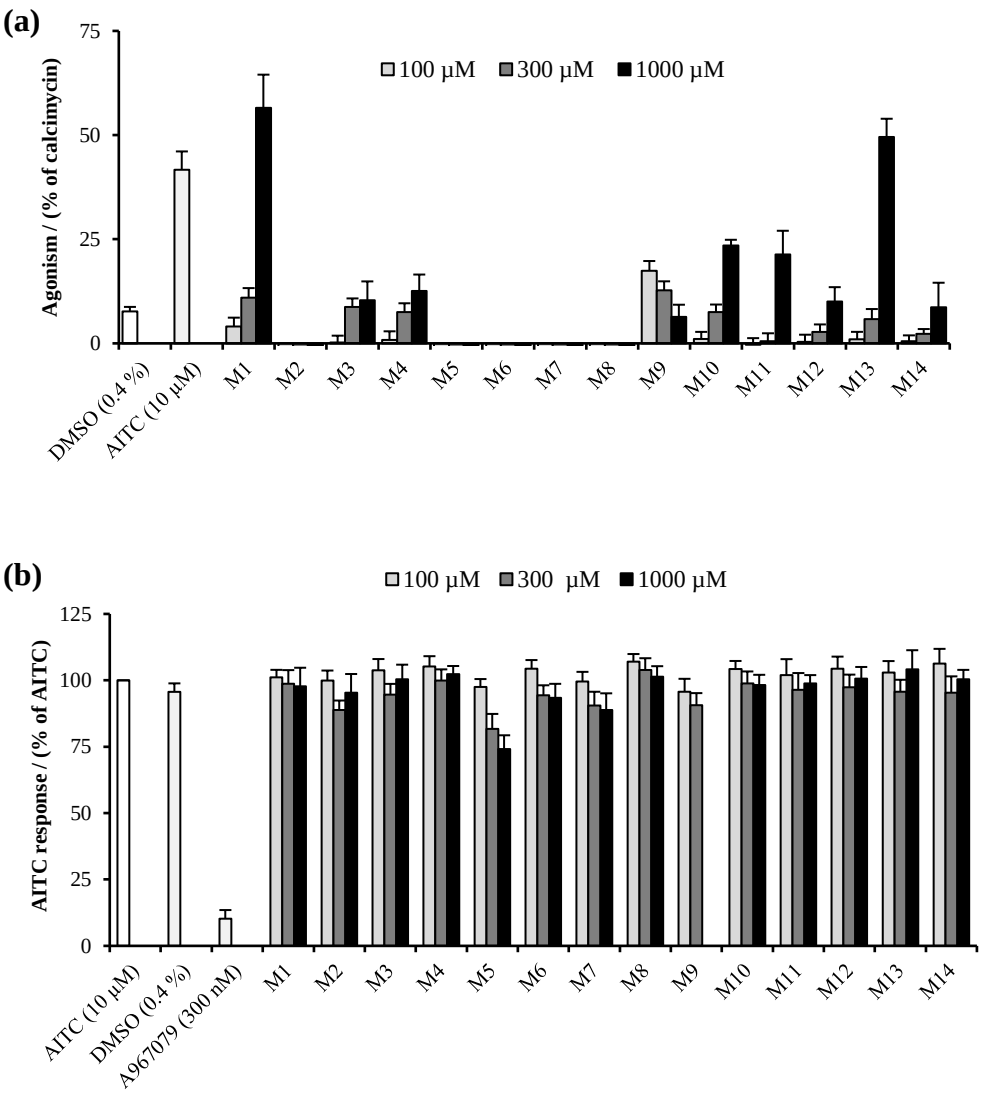

Figure 4.6: *Screening results of probenecid derivatives in hTRPA1-HEK293 cells,* **(a)** *agonism and* **(b)** *antagonism. As* **M9** *was partially soluble at 1000 µM, its antagonism was not tested. Each bar represents the mean ± SEM (N = 3, n = 9).*

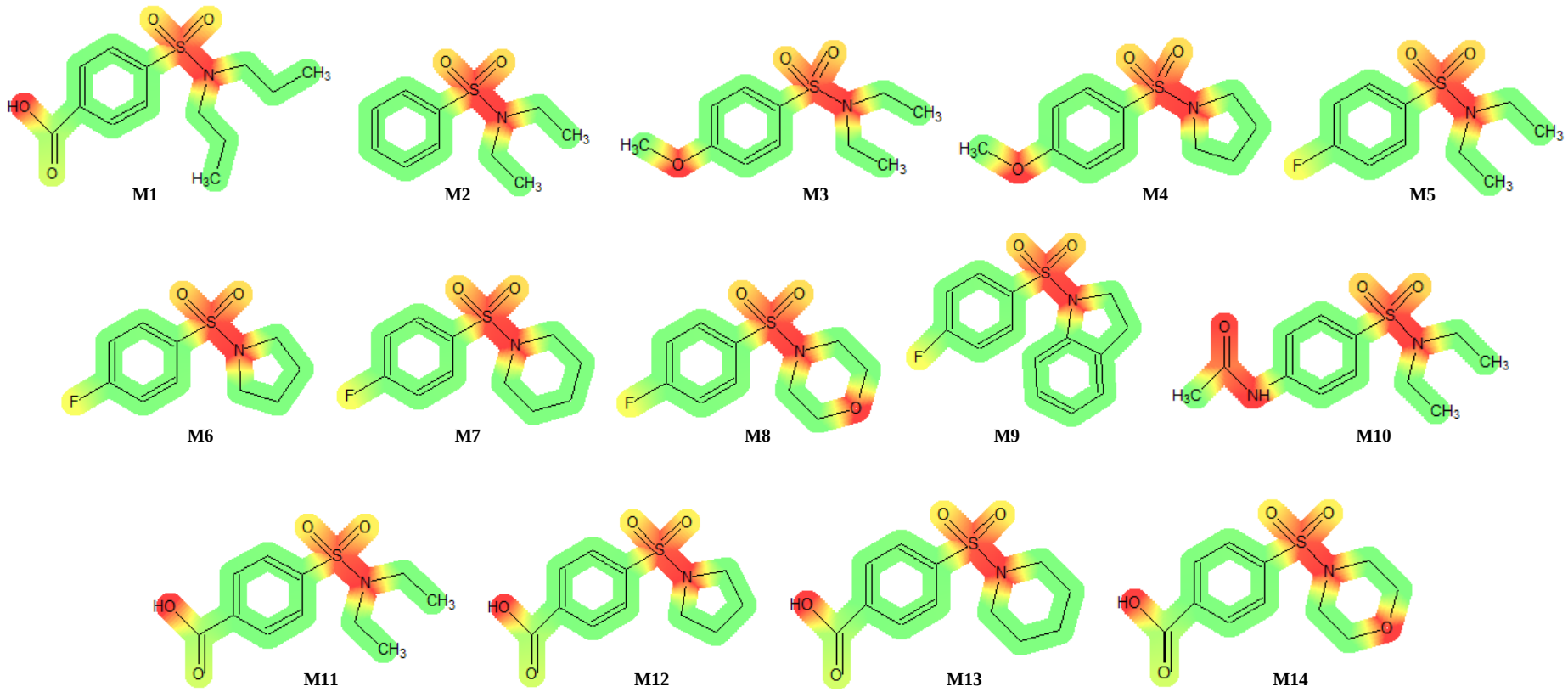

Figure 4.7: *Colour coded mapping of small aryl sulfonamide derivative structures highlighting the lipophilicity/hydrophilicity nature of an atom/functional group/substructure. Green colour indicates the lipophilic parts, red indicates the hydrophilic groups, and the colour gradient represents the degree of lipophilicity/hydrophilicity.*

Further to the acquired SAR, the ASD **AC51b** (**Figures 4.2** and **4.8**) reported as a TRPA1 antagonist by the Orion Corporation company,[373] and an analogue of **AC51b** (**AC56d**) with COOH substituent were synthesised and screened (**Figure 4.9**) to determine if the antagonistic effect of **AC51b** shifts to an agonist with the COOH group, as observed with **M1 - M14** small aryl sulfonamides (**Figure 4.6**). Moreover, by identifying the common core structures of the aryl sulfonamides those have been claimed as TRPA1 antagonists by the pharmaceutical companies, including Janssen Pharmaceuticals,[372] Orion Corporation,[373] Pharmeste[374] and Hoffmann-La Roche,[375,376] the ASD **AC53b** and its analogues with R substituent H (**AC54b**) or COOH (**AC57d**) were also synthesised, screened (**Figure 4.9**) and compared to identify any changes in the activity. In addition, some of their sub-structures (**AC51a**, **AC53a** and **AC54a**) were also screened (**Figure 4.9**). The IC_{50} obtained for **AC51b** (10 µM, **Figure 4.8**) closely agreed with the reported value (12.5 µM evaluated against 5 µM AITC agonist in hTRPA1-HEK293 cells using FlexStation).[247,373] Along with **AC51b**, the ASDs **AC51a**, **AC53a**, **AC54a**, **AC53b**, **AC54b**, **AC56d** and **AC57d** were screened for agonism at 30, 100, 300 and 1000 µM (**Figure 4.9a**), and for antagonism at 100 and 300 µM (**Figure 4.9b**).

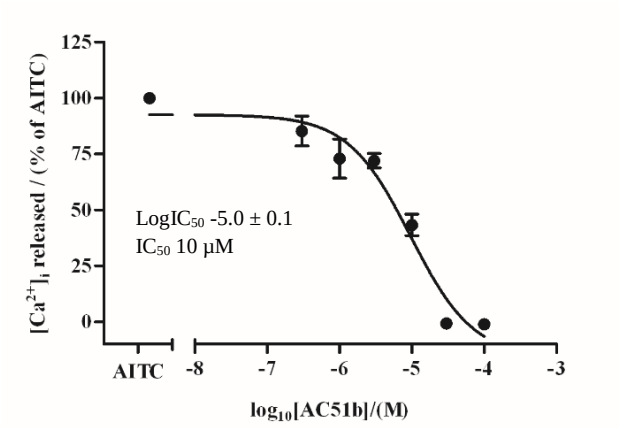

Figure 4.8: *Dose-response curve of* **AC51b** *obtained against hTRPA1-HEK293 cells. Each data point represents the mean ± SEM (N = 3, n = 9).*

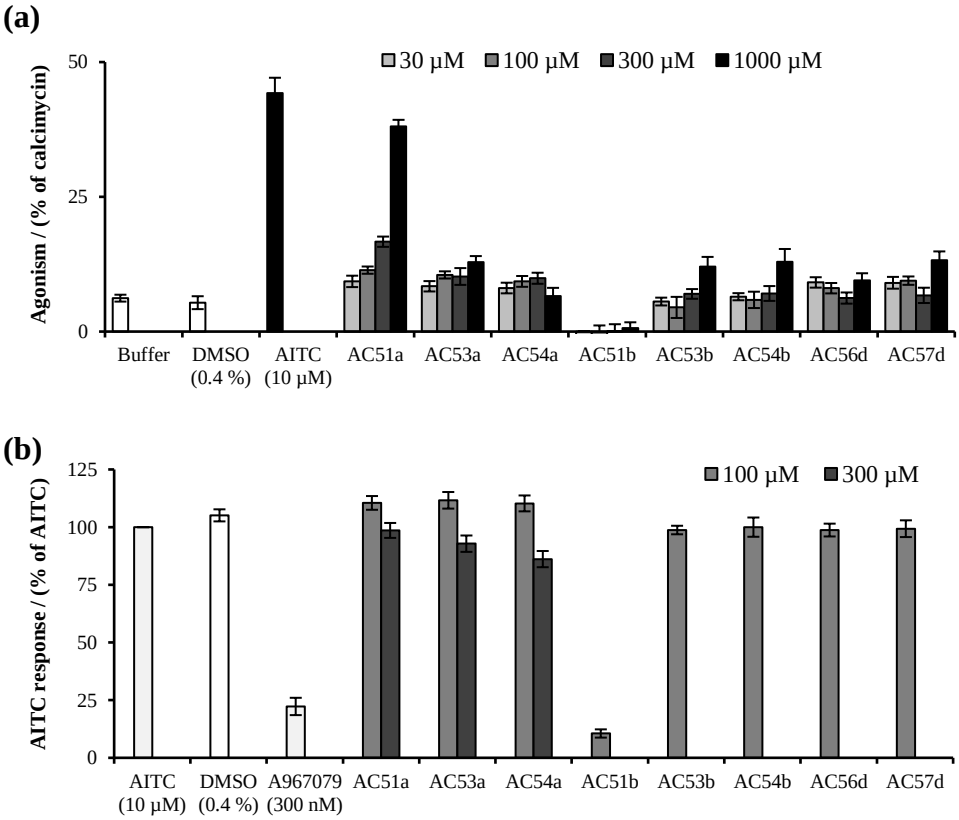

Figure 4.9: *Screening results of aryl sulfonamide derivatives in hTRPA1-HEK293 cells,* **(a)** *agonism and* **(b)** *antagonism. As* **AC51b**, **AC53b**, **AC54b**, **AC56d** *and* **AC57d** *were partially soluble at 300 µM, their antagonism were not tested above 100 µM. Each bar represents the mean ± SEM (N = 3, n = 9).*

The derivatives, **AC51a**, **AC53a**, **AC54a**, **AC53b**, **AC54b**, **AC56d** and **AC57d**, except **AC51b** with no agonism, showed a similar level of weak agonism (<15 % of calcimycin) at different concentrations tested (**Figure 4.9a**). However, only **AC51a** at 1000 µM showed 38 ± 1 % of calcimycin response, which is the highest observed agonism response among the latter ASDs screened. In the antagonist assay, the reference compound **AC51b** at 100 µM had antagonistic effect (inhibited 89 ± 2 % of AITC agonism) as reported in the literature,[373] and **AC54a** showed poor antagonism (inhibits 14 ± 4 % of AITC agonism) at 300 µM, but other derivatives did not have any inhibitory effects (**Figure 4.9b**).

With respect to the SAR, strikingly, replacement of the fluoro group in **AC51b** with a carboxylic acid (**AC56d**) led to complete elimination of the antagonism response. This could have been due to different electronic effects

of the substituents, and moreover, the size of the COOH group could have limited site accessibility and thereby interaction with the same binding site(s) as of **AC51b** in the receptor. However, the proposed structure, **AC53b**, and its analogues, **AC54b** and **AC57d**, with few variations relative to **AC51b**, showed weak agonism. This might be due to different structural conformations/spatial arrangements at their minimum energy level that could have led to different interactions with the TRPA1 protein. For comparison, the optimised geometry of the compounds, **AC51b** and **AC53b**, determined using the energy minimisation molecular mechanics force-field MM2 is shown in **Figure 4.10**.

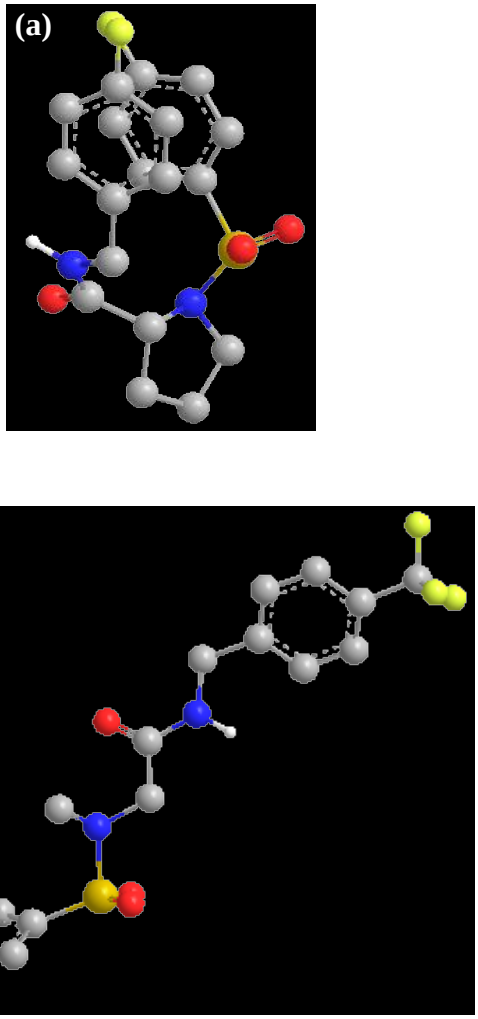

Figure 4.10: *Optimised geometry of the compounds* **(a) AC51b** *and* **(b) AC53b**, *determined using the energy minimisation molecular mechanics force-field MM2.*

4.4.3 Channel specificity

The ASDs were evaluated against pcDNA3 mock-transfected HEK293 cells (N = 3) as a negative control, and against hTRPM8-HEK293 cells (N = 3) for relative selectivity as TRPM8 is a cold-sensitive channel like TRPA1 and stimulated by a number of ligands that could modulate TRPA1. All the ASDs tested at 300 µM were inactive on pcDNA3 mock-HEK293 cells, and neither showed agonism nor antagonism on hTRPM8-HEK293 cells (data not shown). Hence it was revealed that the ASDs were selective for TRPA1 over TRPM8 and endogenously expressed ion channels/receptors in HEK293 cells as described in **Section 3.4.3.1** of **Chapter 3**.

4.4.4 Physicochemical property-activity relationships

The derivatives with a higher total number of hydrogen acceptors and donors, and large topological polar surface area (**Table 4.3**) have shown activity in TRPA1. However, as the structures of the aryl sulfonamide derivatives varied substantially, a clear trend between the activity and clogP was not observable.

Table 4.3: *Physicochemical properties of aryl sulfonamides showing that the compounds obeyed the Lipinski's rule-of-five and the Veber's rules of lead-likeness / oral bioavailability. Lipophilicity [partition coefficient (clogP) and distribution coefficient, (clogD)], solubility (clogS) and acid dissociation constant (pK_a) parameters are given for comparison. Abbreviations: MW - molecular weight, H-bond - hydrogen bond, TPSA - topological polar surface area.*

Compound	MW (≤ 500)	H-bond donors (≤ 5)	H-bond acceptors (≤ 10)	Rotatable bonds (≤ 10)	TPSA/(Å^2) (≤ 140 Å^2)	clogP (≤ 5)	clogD at pH 7.4	pK_a at pH 7.4	clogS at pH 7.4
M1	285.36	1	5	7	83.06	3.3 ± 0.3	-0.69	3.6 ± 0.4	-0.01
M2	213.30	0	3	4	45.76	2.4 ± 0.3	1.87	-	-2.89
M3	243.32	0	4	5	54.99	2.9 ± 0.3	1.76	-	-3.07
M4	241.31	0	4	3	54.99	2.3 ± 0.3	1.56	-	-2.36
M5	231.29	0	3	4	45.76	2.7 ± 0.4	1.73	-	-2.80
M6	229.27	0	3	2	45.76	2.1 ± 0.4	1.50	-	-2.56
M7	243.30	0	3	2	45.76	2.7 ± 0.4	2.14	-	-2.80
M8	245.27	0	4	2	54.99	1.4 ± 0.5	0.80	-	-2.19
M9	277.31	0	3	2	45.76	2.5 ± 0.4	3.20	-	0
M10	270.35	1	5	5	74.86	2.0 ± 0.3	1.17	-	-3.17
M11	257.31	1	5	5	83.06	2.2 ± 0.3	-1.48	3.6 ± 0.4	0.59
M12	255.29	1	5	3	83.06	1.6 ± 0.3	-1.72	3.6 ± 0.4	0.59
M13	269.32	1	5	3	83.06	2.2 ± 0.3	-1.30	3.6 ± 0.4	0.57
M14	271.29	1	6	3	92.29	0.9 ± 0.4	-2.57	3.6 ± 0.4	0.57
AC51a	273.28	1	5	3	83.06	1.4 ± 0.5	-3.38	3.4 ± 0.4	0.56
AC53a	247.24	1	5	4	83.06	1.6 ± 0.5	-3.13	3.4 ± 0.4	0.61
AC54a	229.25	1	5	4	83.06	1.3 ± 0.4	-3.20	3.4 ± 0.4	0.64
AC51b	396.86	1	5	5	74.86	3.0 ± 0.6	2.50	-	-4.84
AC53b	404.38	1	5	7	74.86	3.4 ± 0.6	3.31	-	-4.57
AC54b	386.39	1	5	7	74.86	3.0 ± 0.6	3.30	-	-4.80
AC56d	422.88	2	7	6	112.16	2.6 ± 0.5	-0.82	3.6 ± 0.4	-1.19
AC57d	430.40	2	7	8	112.16	2.9 ± 0.6	-0.63	3.6 ± 0.4	-1.22

4.5 Conclusions

The aryl sulfonamides evaluated were found to be weakly active on hTRPA1. As hypothesised, substitution of the fluoro group in an aryl sulfonamide hTRPA1 antagonist (**AC51b**) to a carboxylic acid group (**AC56d**), led to complete elimination of the antagonism response and shifted to an agonist as observed with -COOH group containing small aryl sulfonamides in the study. A minor alteration in the structure showed a substantial change in the activity. Screening of the compounds in hTRPM8 and pcDNA3 mock cells showed that the sulfonamides evaluated in the study were relatively selective to hTRPA1. Determining the binding site of the reference derivative **AC51b** would further lead to better understanding of the compound interactions in TRPA1, and thus aid in optimising the sulfonamide structure for potent and selective hTRPA1 modulators. Hence binding site studies were carried out and the results are discussed in the following **Chapter 5**.

CHAPTER 5: Ligand binding sites in TRPA1

5.1 Introduction

The mechanism by which electrophilic compounds activate TRPA1 had been described systematically in previous studies.[118,119,123] However, the non-covalent mechanism(s) of TRPA1 modulation (activation or inhibition) by non-reactive compounds have not yet been completely resolved. The lack of complete understanding of the mechanism hinders the development of drug-like antagonists for TRPA1 channel. Hence additional pharmacological studies on the non-reactive activators against TRPA1 are essential for the better understanding of the channel function. Moreover, the understanding of the mechanism could potentially aid in the development of novel TRPA1 specific modulators.

In the literature, targeted gene mutation studies revealed three cysteine residues (C621, C641 and C665 in human) located at the *N*-terminus of TRPA1 to be crucial for the activation of TRPA1 by electrophilic compounds such as cinnamaldehyde (CA), allyl isothiocyanate (AITC) and acrolein (ACR).[118,119] However, among the three cysteines, C621 was shown to be the most important residue for electrophilic activation.[119,377] Mutagenesis studies had also demonstrated that non-electrophilic activators such as menthol interact directly with TRPA1 residues S873 and T874 located within the transmembrane S5.[150] Whereas, multiple binding sites including S873, T874, F909, F944, T945, V948 and I950 residues in the pore loop of S5 and S6 linker (**Figure 5.1**) have been reported for the potent TRPA1 specific antagonist A967079.[103,151,152] Amongst those residues, the greatest reduction in antagonism was seen when the phenylalanine (F944 or F909) was substituted with a residue (alanine or threonine) without the phenyl ring.[103,152]

In this study, to identify the molecular binding sites of *N*-cinnamoylanthranilate derivatives (CADs, **Figure 3.1**), aryl sulfonamides (ASDs, **Figure 4.1**) and some known TRPA1 ligands (**Figure 5.2**), selected amino acid residues within the TRPA1 putative pore region S5-S6 (F909, Y926 and F944, **Figure 5.1**) and at the *N*-terminus (C621) were mutated separately using site-directed mutagenesis, and studied. The S873/T874

double mutant previously made in-house at the University of Hull (unpublished work) was also incorporated in this study.

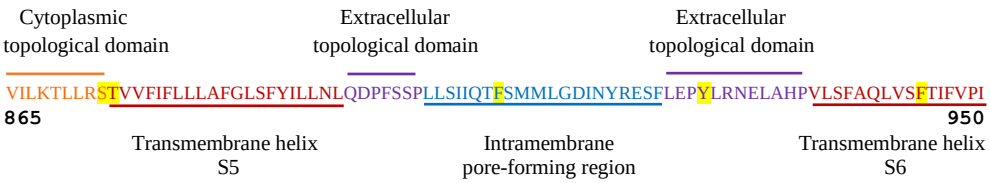

Figure 5.1: *Locations of hTRPA1 residues (V865 - I950) within segments 5 (S5) and 6 (S6), determined using a single-particle cryo-electron microscopy.*[103] *The highlighted residues were mutated in this study.*

The residues S873/T874, F909, F944 and C621 were chosen from four different studies in the literature.[103,150,152,377] The selection of the residues were based on the functional groups on the ligands and the residues that could participate in either non-covalent interactions, such as hydrogen bonding (S873/T874[150]) or π-π stacking (F909[103] and F944[152]), or covalent modification (C621[377]). The Y926 residue was proposed in this study as it is capable of participating in both hydrogen bonding and π-π stacking non-covalent interactions, and is also located between the reported F909 and F944 residues.

The hTRPA1 mutants were stably transfected into HEK293 cells and were characterised with known TRPA1 ligands using calcium signalling assays, as described in **Section 2.4** of **Chapter 2**, and compared against the wild-type (WT)-hTRPA1 responses (**Section 5.2.1**). Calcium signalling assays were performed using a PTI fluorescence spectrophotometer for the mutant S873V/T874L (**Section 5.2.2**), whereas the other three mutants including F909A, F944A and C621A were assayed using a FlexStation (**Sections 5.2.3 - 5.2.5**).

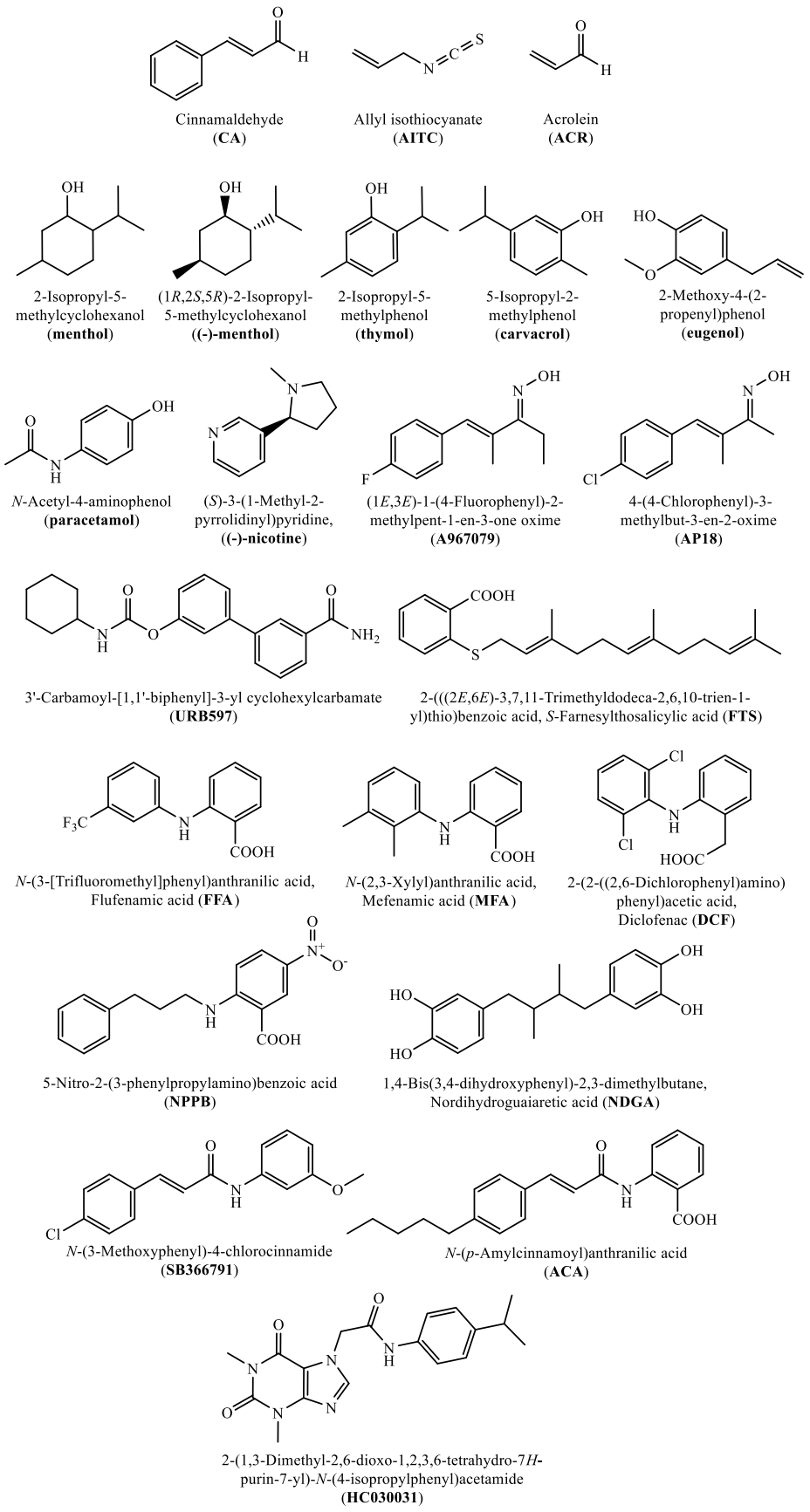

Figure 5.2: *Chemical structures, names and codes of the known TRPA1 ligands characterised in wild-type and mutant hTRPA1.*

5.2 Site-directed mutagenesis

DNA constructs of the hTRPA1 mutants, C621A, F909A, Y926S and F944A, were successfully prepared as described in **Section 2.7** of **Chapter 2**. The details of the designed mutagenic primer sequences are provided in **Table 5.1**. Existence of a band similar to the WT-hTRPA1 positive control in gel electrophoresis analysis confirmed the presence of hTRPA1 DNA constructs in the samples from transformed bacterial colonies (**Figure 5.3**).

Table 5.1: *Information about the designed primer sequences and oligonucleotides containing the mutants C621A, F909A, Y926S and F944A.*

C621A

Primer sequences:

Primer Name	Primer Sequence (5′ to 3′)
	5′-attctatcatttctgtaattggagctttattgcctggagaattatgactgaaaatc-3′
t1861g_g1862c	5′-gattttcagtcataattctccaggcaataaagctccaattacagaaatgatagaat-3′

Oligonucleotide information:

Length / (nucleotides)	Primer melting temperature / (°C)	Duplex Energy at 68 °C / (kcal mol^{-1})	Energy Cost of Mismatches / (%)
56	78.32	-46.72	6.54
56	78.32	-51.73	1.41

Primer-template duplexes:

```
5′-gattttcagtcataattctccaggcaataaatgtccaattacagaaatgatagaat-3′
   |||||||||||||||||||||||||||||||||   |||||||||||||||||||||||
3′-ctaaaagtcagtattaagaggtccgttatttcgaggttaatgtctttactatctta-5′

5′-gattttcagtcataattctccaggcaataaagctccaattacagaaatgatagaat-3′
   |||||||||||||||||||||||||||||||||   |||||||||||||||||||||||
3′-ctaaaagtcagtattaagaggtccgttatttacaggttaatgtctttactatctta-5′
```

F909A

Primer sequences:

Primer Name	Primer Sequence (5′ to 3′)
	5′-gatatctcctagcatcatgctggcggtctggattatagaaagcaat-3′
t2725g_t2726c	5′-attgctttctataatccagaccgccagcatgatgctaggagatatc-3′

Oligonucleotide information:

Length / (nucleotides)	Primer melting temperature / (°C)	Duplex Energy at 68 °C / (kcal mol^{-1})	Energy Cost of Mismatches / (%)
46	78.52	-50.24	3.41
46	78.52	-50.11	1.02

Primer-template duplexes:

```
5′-attgctttctataatccagacctttcagcatgatgctaggagatatc-3′
   ||||||||||||||||||||||||   ||||||||||||||||||||||||
3′-taacgaaagatattaggtctggcggtcgtactacgatcctctatag-5′
5′-attgctttctataatccagaccgccagcatgatgctaggagatatc-3′
   ||||||||||||||||||||||||   ||||||||||||||||||||||||
3′-taacgaaagatattaggtctggaagtcgtactacgatcctctatag-5′
```

Continued…

Continued…

Table 5.1: *Information about the designed primer sequences and oligonucleotides containing the mutants C621A, F909A, Y926S and F944A.*

Y926S

Primer sequences:

Primer Name	Primer Sequence (5′ to 3′)
	5′-caattcatttctcagagatggttctaggaaggactctcga-3′
a2777c	5′-tcgagagtccttcctagaaccatctctgagaaatgaattg-3′

Oligonucleotide information:

Length / (nucleotides)	Primer melting temperature / (°C)	Duplex Energy at 68 °C / (kcal mol^{-1})	Energy Cost of Mismatches / (%)
40	78.52	-46.48	4.64
40	78.52	-44.41	0.32

Primer-template duplexes:

```
5′-tcgagagtccttcctagaaccatatctgagaaatgaattg-3′
   ||||||||||||||||||||||||||  ||||||||||||||||||
3′-agctctcaggaaggatcttggtagagactctttacttaac-5′
5′-tcgagagtccttcctagaaccatctctgagaaatgaattg-3′
   ||||||||||||||||||||||||||  ||||||||||||||||||
3′-agctctcaggaaggatcttggtatagactctttacttaac-5′
```

F944A

Primer sequences:

Primer Name	Primer Sequence (5′ to 3′)
	5′-gacaattgggacaaatattgtggcggaaacaagttgtgcaaaggac-3′
t2830g t2831c	5′-gtcctttgcacaacttgtttccgccacaatatttgtcccaattgtc-3′

Oligonucleotide information:

Length / (nucleotides)	Primer melting temperature / (°C)	Duplex Energy at 68 °C / (kcal mol^{-1})	Energy Cost of Mismatches / (%)
46	78.52	-50.21	3.41
46	78.52	-45.77	1.12

Primer-template duplexes:

```
5′-gtcctttgcacaacttgtttcctt cacaatatttgtcccaattgtc-3′
   ||||||||||||||||||||||||   ||||||||||||||||||||||||||
3′-caggaaacgtgttgaacaaaggcggtgttataaacagggttaacag-5′
5′-gtcctttgcacaacttgtttccgc cacaatatttgtcccaattgtc-3′
   ||||||||||||||||||||||||   ||||||||||||||||||||||||||
3′-caggaaacgtgttgaacaaaggaagtgttataaacagggttaacag-5′
```

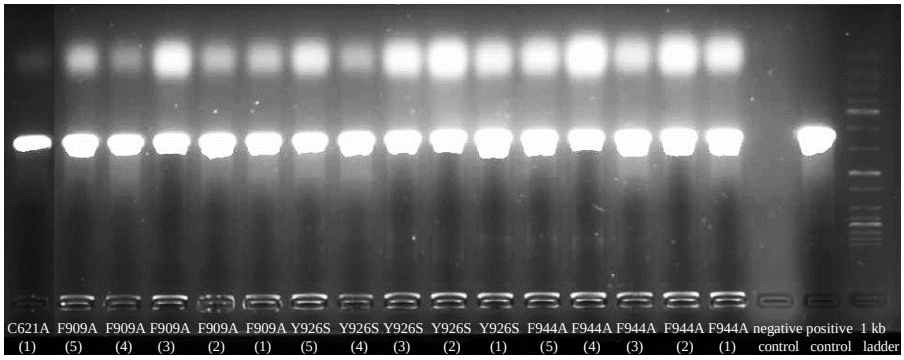

Figure 5.3: *UV illumination of the bands obtained in a gel electrophoresis analysis (performed on a 1.3 % agarose gel containing Midori green DNA stain) of the samples from transformed bacterial colonies. Wherever possible, in each type of mutant, five different bacterial colonies were picked, and the wells are labelled accordingly.*

DNA sequencing results of the synthesised hTRPA1 DNA constructs, confirmed the presence of the mutants C621A, F909A, Y926S and F944A (**Figure 5.4**) in the extracted bacterial clone samples [C621A (1), F909A (5), Y926S (1) and F944A (1), **Figure 5.3**]. Alignment of the DNA sequenced results with the parent hTRPA1 FASTA using the nucleotide BLAST tool on PubMed showed that the sequences in the sequenced regions, 1740-2646 for C621A, 2516-3357 for F909A, 2517-3357 for Y926S and 2518-3357 for F944A, matched exactly with that of the primary hTRPA1 sequence, excluding the substituted nucleotides those highlighted in yellow in **Figure 5.4**. As the mutants were present in the analysed samples, other bacterial clone samples were not DNA sequenced.

However, only three (C621A, F909A and F944A) out of four mutants were stably transfected into HEK293 cells and single cell cloned. To produce the Y926S mutant cell line, another transfection or few more repeats of single cell cloning would be required, but due to time constrains this could not be accomplished in this study. The mutant, S873V/T874L-hTRPA1 DNA was constructed and transfected into HEK293 cells previously in-house at the University of Hull.

C621A (1)

GGCCTCCTTTTTGCACCTTGCACTTCACAATAAGAGGAAGGAGGTTGTTCTTACGATCATCAGGAGCAAAAGATGGG
ATGAATGTCTTAAGATTTTCAGTCATAATTCTCCAGGCAATAAAGCTCCAATTACAGAAATGATAGAATACCTCCCT
GAATGCATGAAGGTACTTTTAGATTTCTGCATGTTGCATTCCACAGAAGACAAGTCCTGCCGAGACTATTATATCGA
GTATAATTCAAATATCTTCAATGTCCATTAGAATTCACCAAAAAAACACCTACACAGGATGTTATATATGAACCGCT
TACAGCCCTCAACGCAATGGTACAAAATAACCGCATAGAGCTTCTCAATCATCCTGTGTGTAAAGAATATTTACTCA
TGAAATGGTTGGCTTATGGATTTAGAGCTCATATGATGAATTTAGGATCTTACTGTCTTGGTCTCATACCTATGACCA
TTCTCGTTGTCAATATAAAACCAGGAATGGCTTTCAACTCAACTGGCATCATCAATGAAACTAGTGATCATTCAGAA
ATACTAGATACCACGAATTCATATCTAATAAAAACTTGTATGATTTTAGTGTTTTTATCAAGTATATTTGGGTATTGC
AAAGAAGCGGGGCAAATTTTCCAACAGAAAAGGAATTATTTTATGGATATAAGCAATGTTCTTGAATGGATTATCTA
CACGACGGGCATCATTTTTGTGCTGCCCTTGTTTGTTGAAATACCAGCTCATCTGCAGTGGCAATGTGGAGCAATTG
CTGTTTACTTCTATTGGATGAATTTCTTATTGTATCTTCAAAGATTTGAAAATTGTGGAATTTTTATTGTTATGTTGGA
GGTAATTTTGAAAACTTTGTTGAGGTCTACAGTTGTATTTATCTTCCTTCTTCTG

F909A (5)

TTTACTTCTATTGGATGAATTTCTTATTGTATCTTCAAAGATTTGAAAATTGTGGAATTTTTATTGTTATGTTGGAGGT
AATTTTGAAAACTTTGTTGAGGTCTACAGTTGTATTTATCTTCCTTCTTCTGGCTTTTGGACTCAGCTTTTACATCCTC
CTGAATTTACAGGATCCCTTCAGCTCTCCATTGCTTTCTATAATCCAGACCGCCAGCATGATGCTAGGAGATATCAAT
TATCGAGAGTCCTTCCTAGAACCATATCTGAGAAATGAATTGGCACATCCAGTTCTGTCCTTTGCACAACTTGTTTCC
TTCACAATATTTGTCCCAATTGTCCTCATGAATTTACTTATTGGTTTGGCAGTTGGCGACATTGCTGAGGTCCAGAAA
CATGCATCATTGAAGAGGATAGCTATGCAGGTGGAACTTCATACCAGCTTAGAGAAGAAGCTGCCACTTTGGTTTCT
ACGCAAAGTGGATCAGAAATCCACCATCGTGTATCCCAACAAACCCAGATCTGGTGGGATGTTATTCCATATATTCT
GTTTTTTATTTTGCACTGGGGAAATAAGACAAGAAATACCAAATGCTGATAAATCTTTAGAAATGGAAATATTAAAG
CAGAAATACCGGCTGAAGGATCTTACTTTTCTCCTGGAAAAACAGCATGAGCTCATTAAACTGATCATTCAGAAGAT
GGAGATCATCTCTGAGACAGAGGATGATGATAGCCATTGTTCTTTTCAAGACAGGTTTAAGAAAGAGCAGATGGAA
CAAAGGAATAGCAGATGGAATACTGTGTTGAGAGCAGTCAAGGCAAAAACACACCATCTTGAGCCTGAACAAAAA
CTTATTTCTGAAGATCTGTAGCTCGAGCATGCATCTAGAGGGCCCTATTCTATAGTGTCACCTAAATGCTAGAGCTC
GCTGATCAGCCTCGACTGTGCCTTCTAGTTGCCAGCCATCTGTTGTTTGCC

Y926S (1)

TTACTTCTATTGGATGATTTCTTATTGTATCTTCAAAGATTTGAAAATTGTGGAATTTTTATTGTTATGTTGGAGGTAA
TTTTGAAAACTTTGTTGAGGTCTACAGTTGTATTTATCTTCCTTCTTCTGGCTTTTGGACTCAGCTTTTACATCCTCCT
GAATTTACAGGATCCCTTCAGCTCTCCATTGCTTTCTATAATCCAGACCTTCAGCATGATGCTAGGAGATATCAATTA
TCGAGAGTCCTTCCTAGAACCATCTCTGAGAAATGAATTGGCACATCCAGTTCTGTCCTTTGCACAACTTGTTTCCTT
CACAATATTTGTCCCAATTGTCCTCATGAATTTACTTATTGGTTTGGCAGTTGGCGACATTGCTGAGGTCCAGAAACA
TGCATCATTGAAGAGGATAGCTATGCAGGTGGAACTTCATACCAGCTTAGAGAAGAAGCTGCCACTTTGGTTTCTAC
GCAAAGTGGATCAGAAATCCACCATCGTGTATCCCAACAAACCCAGATCTGGTGGGATGTTATTCCATATATTCTGT
TTTTTATTTTGCACTGGGGAAATAAGACAAGAAATACCAAATGCTGATAAATCTTTAGAAATGGAAATATTAAAGCA
GAAATACCGGCTGAAGGATCTTACTTTTCTCCTGGAAAAACAGCATGAGCTCATTAAACTGATCATTCAGAAGATGG
AGATCATCTCTGAGACAGAGGATGATGATAGCCATTGTTCTTTTCAAGACAGGTTTAAGAAAGAGCAGATGGAACA
AAGGAATAGCAGATGGAATACTGTGTTGAGAGCAGTCAAGGCAAAAACACACCATCTTGAGCCTGAACAAAAACTT
ATTTCTGAAGATCTGTAGCTCGAGCATGCATCTAGAGGGCCCTATTCTATAGTGTCACCTAAATGCTAGAGCTCGCT
GATCAGCCTCGACTGTGCCTTCTAGTTGCCAGCCATCTGTTGTTTGCCCCTCCCCCGTGCCTTCCTTGACCCTGGAAG
GG

F944A (1)

TACTTCTATTGGATGATTTCTTATTGTATCTTCAAAGATTTGAAAATTGTGGAATTTTTATTGTTATGTTGGAGGTAAT
TTTGAAAACTTTGTTGAGGTCTACAGTTGTATTTATCTTCCTTCTTCTGGCTTTTGGACTCAGCTTTTACATCCTCCTG
AATTTACAGGATCCCTTCAGCTCTCCATTGCTTTCTATAATCCAGACCTTCAGCATGATGCTAGGAGATATCAATTAT
CGAGAGTCCTTCCTAGAACCATATCTGAGAAATGAATTGGCACATCCAGTTCTGTCCTTTGCACAACTTGTTTCCGCC
ACAATATTTGTCCCAATTGTCCTCATGAATTTACTTATTGGTTTGGCAGTTGGCGACATTGCTGAGGTCCAGAAACAT
GCATCATTGAAGAGGATAGCTATGCAGGTGGAACTTCATACCAGCTTAGAGAAGAAGCTGCCACTTTGGTTTCTACG
CAAAGTGGATCAGAAATCCACCATCGTGTATCCCAACAAACCCAGATCTGGTGGGATGTTATTCCATATATTCTGTT
TTTTATTTTGCACTGGGGAAATAAGACAAGAAATACCAAATGCTGATAAATCTTTAGAAATGGAAATATTAAAGCA
GAAATACCGGCTGAAGGATCTTACTTTTCTCCTGGAAAAACAGCATGAGCTCATTAAACTGATCATTCAGAAGATGG
AGATCATCTCTGAGACAGAGGATGATGATAGCCATTGTTCTTTTCAAGACAGGTTTAAGAAAGAGCAGATGGAACA
AAGGAATAGCAGATGGAATACTGTGTTGAGAGCAGTCAAGGCAAAAACACACCATCTTGAGCCTGAACAAAAACTT
ATTTCTGAAGATCTGTAGCTCGAGCATGCATCTAGAGGGCCCTATTCTATAGTGTCACCTAAATGCTAGAGCTCGCT
GATCAGCCTCGACTGTGCCTTCTAGTTGCCAGCCATCTGTTGTTTGCCCCTCCCCCG

Figure 5.4: *DNA sequencing results of the hTRPA1 DNA constructs extracted from the bacterial clone samples, C621A (1), F909A (5), Y926S (1) and F944A (1). As the mutants were present in these samples, other bacterial clone samples were not DNA sequenced.*

Using flow cytometry, attempts were made to determine the levels of TRPA1 expressed in the cloned cells. However, a positive response for the negative control, pcDNA3 mock-transfected HEK293 cells, was observed. Thus, the positive responses obtained for the mutants were thought to be unreliable (**Figure 5.5**). This could have been observed due to the non-specificity of the chosen TRPA1 monoclonal IgG_1 antibody, ANKTM1 (C-5).

ANKTM1 (C-4) is another available TRPA1 monoclonal antibody that could have been utilised, but its specificity is also not known. The difference between the two antibodies is that the antibody, ANKTM1 (C-5) is used for mapping amino acids 965-1119, and ANKTM1 (C-4) for epitope mapping of amino acids 1088-1112, at the *C*-terminus region of human origin ANKTM1. At present, other than these two antibodies, there is no other suitable monoclonal TRPA1 antibody available.[89] Another possible protein quantification experiment that is suitable is a tag-based assay that could possibly be performed as described in the literature,[103] but this remains as a further work.

On the other hand, the mutants were characterised using known TRPA1 activators by calcium signalling assays and were compared against the wild-type responses. The chemical structures of the ligands screened in wild-type and mutant (S873V/T874L, F909A, F944A and C621A) hTRPA1 stably transfected HEK293 cells are given in **Figures 3.1**, **4.1** and **5.2** (all the chemical structures of the ligands are also given in the **Appendix**), and the characterisation results are provided in **Sections 5.2.1 - 5.2.5**.

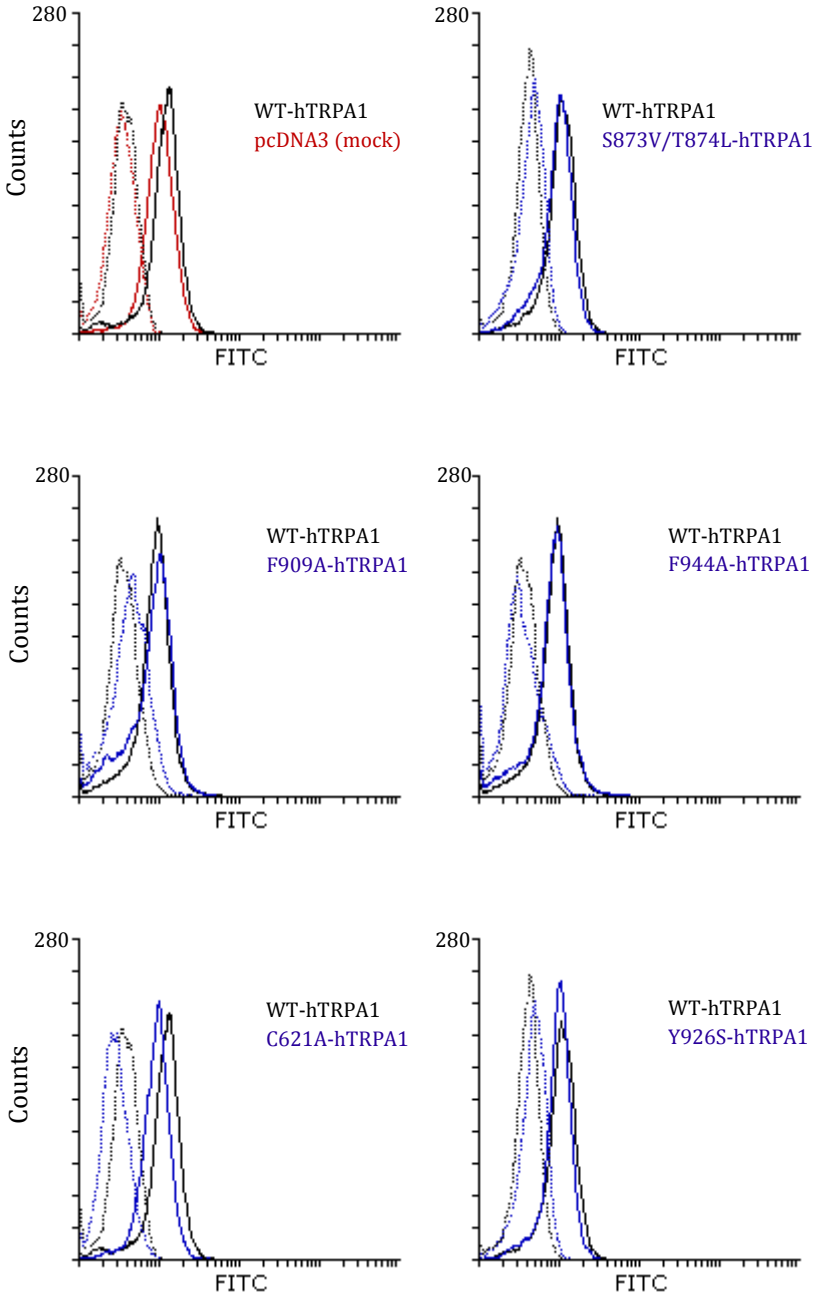

Figure 5.5: *Spectra obtained from intracellular flow cytometric analysis, to determine the expression levels of hTRPA1 gene in the hTRPA1 mutants. As a positive and a negative control, wild-type (WT)-hTRPA1 and pcDNA3 (mock) were used, respectively. Isotype antibody was used to define the gates. The dotted-lines indicate pre-incubation with an isotype antibody and the solid-lines indicate primary antibody (ANKTM1).*

5.2.1 Screening of TRPA1 ligands in WT-hTRPA1

To choose the concentration of the ligands to test in hTRPA1 mutants, dose-response curves were first carried out for all the ligands in WT-hTRPA1 HEK293 cells (**Figures 5.2** and **5.6 - 5.10**). The EC_{50} and IC_{50} values obtained were broadly consistent with the values found in the original reports (**Table 5.2**). Perhaps, variations in the assay methods, conditions, species and/or cell lines between the studies could have contributed to the differences in the results (**Table 5.2**).

Dose-response curves of the electrophilic compounds, CA,[104] ACR[109] and AITC,[104] which covalently modify the cysteine residues at the *N*-termini,[118,119] are grouped together in **Figure 5.6**. The observed order of agonising potency was AITC (EC_{50} 4 µM) > CA (EC_{50} 9 µM) > ACR (EC_{50} 27 µM), and CA was less efficacious relative to AITC and ACR with the latter two displaying similar efficacy.

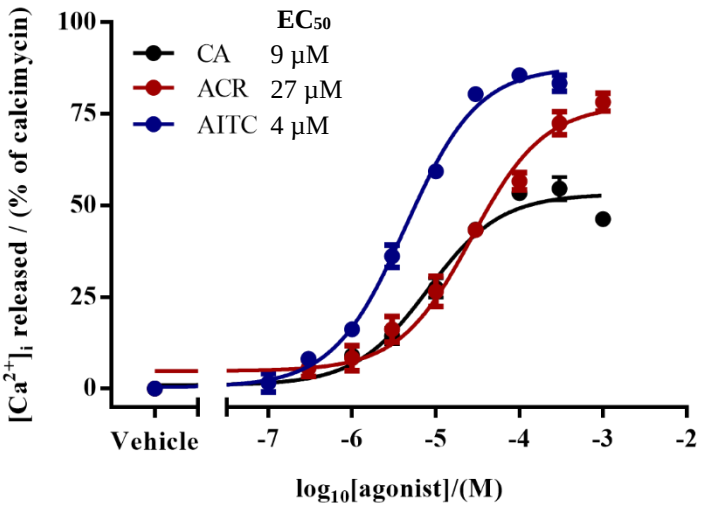

Figure 5.6: *Dose-response curves of the electrophilic compounds, CA, ACR and AITC, in WT-hTRPA1 HEK293 cells. Each data point represents the mean ± SEM of N = 3 (n = 9).*

Similarly, dose-response curves of non-electrophilic activators, including menthol[127] that has been shown to interact directly with the hTRPA1 residues S873 and T874 in the S5,[150] and other structurally related compounds, thymol,[127,128] carvacrol,[129] eugenol[104,445] and paracetamol,[145] are presented together in **Figure 5.7**. Among those, the most potent compound was carvacrol with an observed order of potency, carvacrol (EC_{50} 17 µM) >

menthol (EC_{50} 30 µM) > thymol (EC_{50} 60 µM) > eugenol (EC_{50} 168 µM). Of those, thymol was found to be most efficacious and menthol the least. Paracetamol was found to be essentially inactive in hTRPA1, which was consistent with the earlier finding.[145]

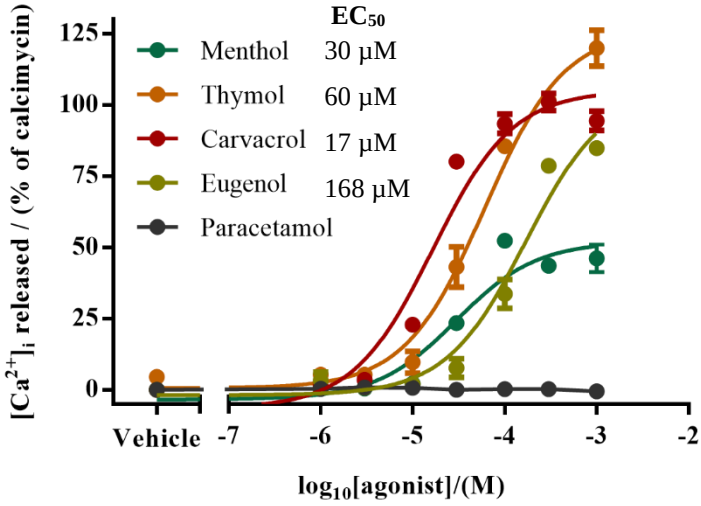

Figure 5.7: *Dose-response curves of the non-electrophilic compounds, menthol, thymol, carvacrol, eugenol and paracetamol, in WT-hTRPA1 HEK293 cells. Each data point represents the mean ± SEM of N = 3 (n = 9).*

Dose-response curves of hTRPA1 active non-steroidal anti-inflammatory drugs (NSAIDs), FFA, MFA and DCF fenamates,[146] are shown in **Figure 5.8a**. The observed order of potency, FFA (EC_{50} 7 µM) > MFA (EC_{50} 16 µM) > DCF (EC_{50} 56 µM), was consistent with the original report[146] (**Table 5.2**), and the three fenamates had similar efficacy. The dose-response curves of structurally related anthranilate derivatives, NPPB, ACA and SB366791 are given in **Figure 5.8b**. As found in the literature, NPPB was found to be a potent hTRPA1 agonist with EC_{50} 0.6 µM, which was very close to the reported value 0.32 µM[411] (**Table 5.2**). Interestingly, ACA, a TRPM2, TRPM8, TRPC3, TRPC6 and TRPV1[327] channels blocker, was found to activate hTRPA1 with EC_{50} 28 µM, whereas structurally related SB366791, a TRPV1 antagonist,[409,410] was ineffective in hTRPA1.

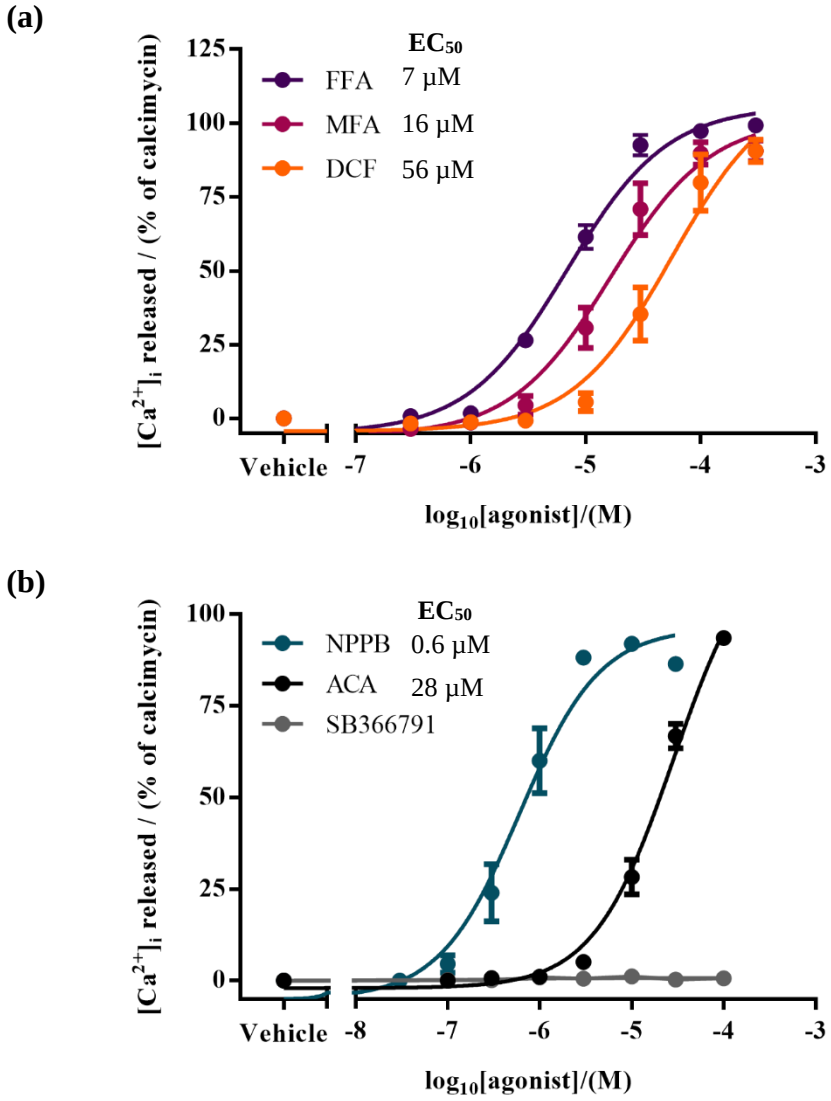

Figure 5.8: *Dose-response curves of the anthranilic acid derivatives,* **(a)** *FFA, MFA and DCF (NSAIDs) and* **(b)** *NPPB, ACA and SB366791, in WT-hTRPA1 HEK293 cells. Each data point represents the mean ± SEM of N = 3 (n = 9).*

The dose-response curves of structurally diverse TRPA1 activators, NDGA[446] (EC_{50} 35 µM), FTS[447] (EC_{50} 0.8 µM), URB597[448] (EC_{50} 0.1 µM) and (-)-nicotine[156] (EC_{50} 2 M), are presented in **Figure 5.9**. With respect to the EC_{50} values of the ligands evaluated, URB597 (EC_{50} 0.1 µM) was found to be the most potent hTRPA1 activator. Though a response of 87 % of calcimycin at 100 µM was reached, the curve of URB597 did not form a sigmoidal curve (**Figure 5.9c**) as seen for other compounds in **Figures 5.6 - 5.10**. (-)-Nicotine was found to activate mouse TRPA1 with EC_{50} ~10 µM in electrophysiological measurements,[156] and the estimated EC_{50} obtained in hTRPA1 using the fluorescence-based assay was 2 M. Since a complete

sigmoidal curve was not attainable (**Figure 5.9d**) within the range of concentrations tested (1 - 1000 µM), and as it is only effective (25 % of calcimycin) at the highest concentration tested (1000 µM), the compound could have shown a non-specific effect.

(a)

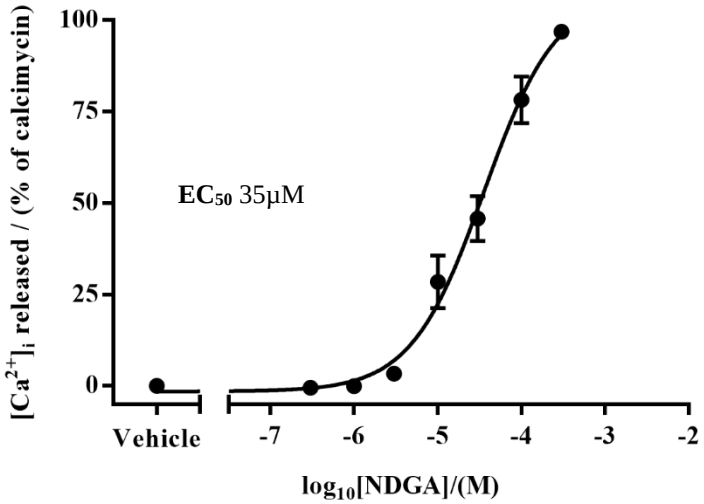

(b)

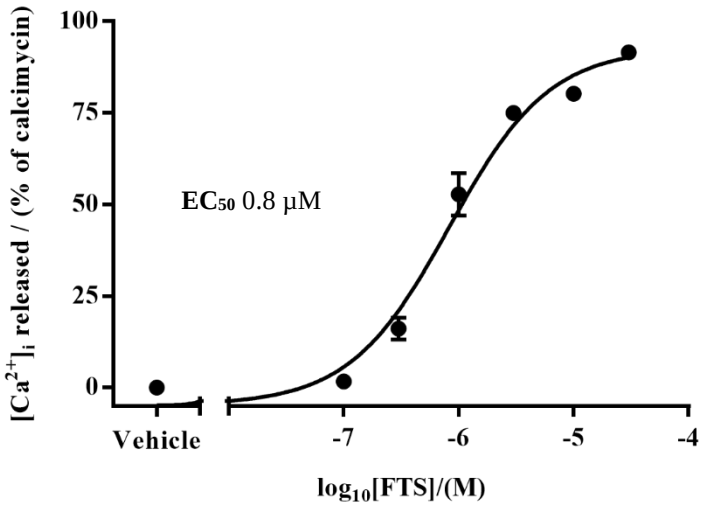

Continued…

Figure 5.9: *Dose-response curves of the TRPA1 activators,* **(a)** *NDGA,* **(b)** *FTS,* **(c)** *URB597 and* **(d)** *(-)-nicotine, in WT-hTRPA1 HEK293 cells. Each data point represents the mean ± SEM of N = 3 (n = 9).*

Continued…

(c)

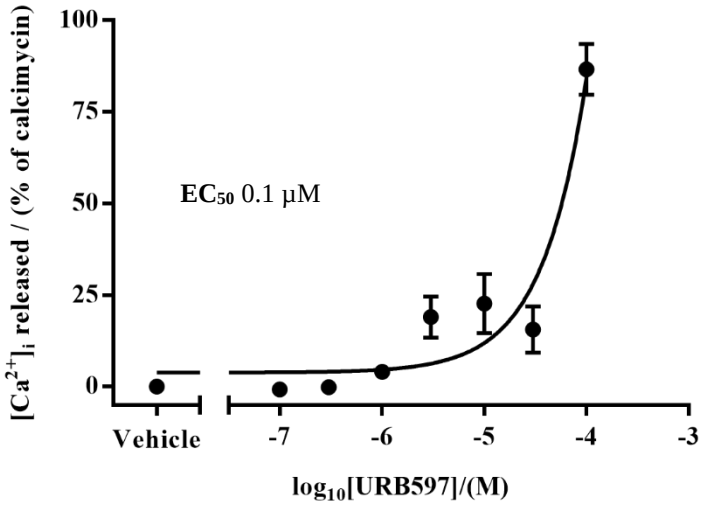

(d)

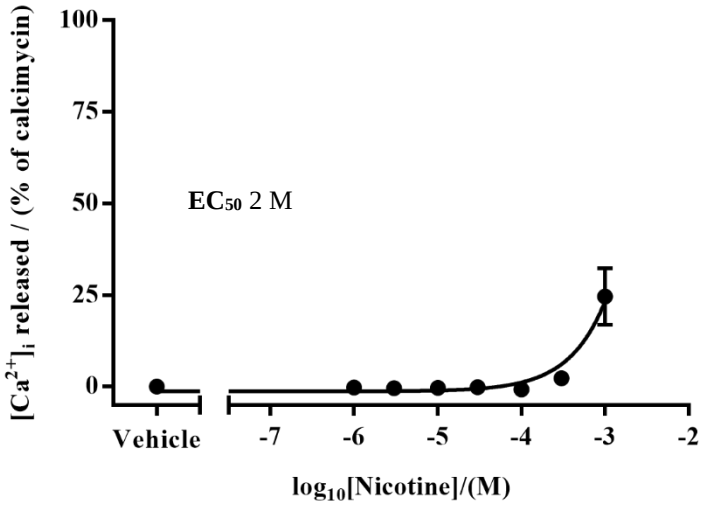

Figure 5.9: *Dose-response curves of the TRPA1 activators,* **(a)** *NDGA,* **(b)** *FTS,* **(c)** *URB597 and* **(d)** *(-)-nicotine, in WT-hTRPA1 HEK293 cells. Each data point represents the mean ± SEM of N = 3 (n = 9).*

The antagonism of well-known hTRPA1 inhibitors A967079,[166] AP18,[449] and HC030031[253] were evaluated against 10 µM AITC elicited agonism, and the obtained dose-response curves are shown in **Figure 5.10**. Among the antagonists tested, the oxime compound A967079 was highly potent (IC_{50} 79 nM, **Figure 5.10a**) compared to its derivative AP18 (IC_{50} 4 µM, **Figure 5.10b**) and HC030031 (IC_{50} 18 µM, **Figure 5.10c**), which was consistent with other reports as given in **Table 5.2**.

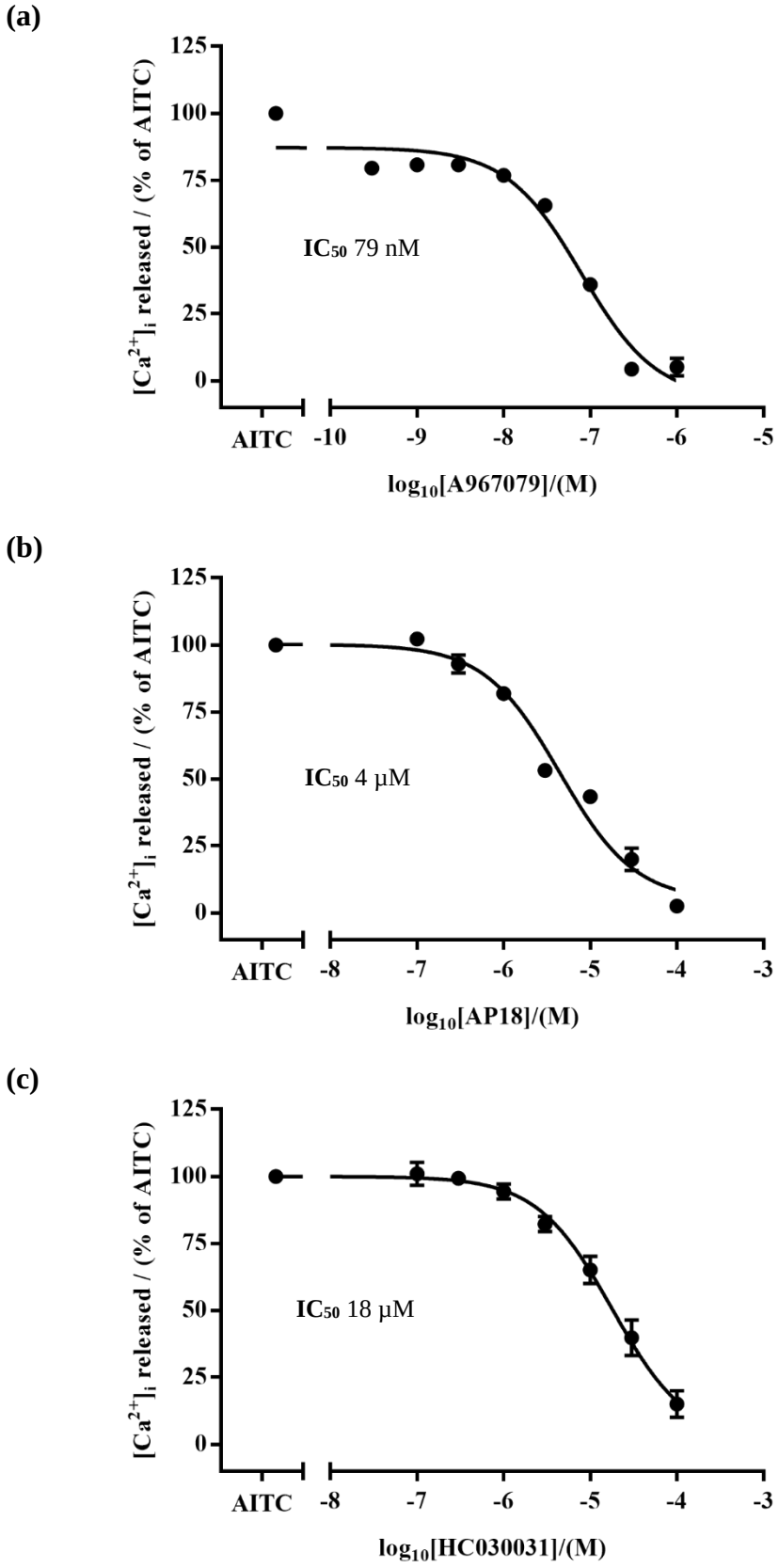

Figure 5.10: *Dose-response curves of the TRPA1 antagonists,* **(a)** *A967079,* **(b)** *AP18 and* **(c)** *HC030031, in WT-hTRPA1 HEK293 cells. Each data point represents the mean ± SEM of N = 3 (n = 9).*

Table 5.2: *The EC_{50} and IC_{50} values of the known ligands obtained in hTRPA1-HEK293 cells using a FlexStation are compared with the literature values of the original findings. Abbreviations: FLIPR, fluorometric imaging plate reader assay; EP, electrophysiology; FS, FlexStation ND, not determined.*

	Obtained value		**Literature value**
Ligand	**LogEC_{50} ± SEM**	**EC_{50}**	**EC_{50}, species, assay**
CA[104]	-5.07 ± 0.09	9 µM	61 ± 9 µM, mouse TRPA1-CHO cells, FLIPR.[104]
ACR[109]	-4.57 ± 0.07	27 µM	5 ± 1 µM, human TRPA1-*Xenopus oocytes*, EP.[109]
AITC[104]	-5.36 ± 0.04	4 µM	22 ± 3 µM, mouse TRPA1-CHO cells, FLIPR.[104]
Menthol[127]	-4.5 ± 0.1	30 µM	95 ± 15 µM, mouse TRPA1-CHO cells, EP.[127]
Thymol[127,128]	-4.22 ± 0.06	60 µM	20 µM, human TRPA1-HEK293 cells, FLIPR.[128]
Carvacrol[129]	-4.78 ± 0.09	17 µM	ND
Eugenol[104,445]	-3.77 ± 0.09	168 µM	261 ± 9 µM, human TRPA1-HEK293 cells, EP.[445]
Paracetamol[145]	inactive	-	ND
FFA[146]	-5.16 ± 0.06	7 µM	24 ± 3 µM, WI-38 cells (human fibroblast), FS.[146] 57 ± 5 µM, human TRPA1-HEK293 cells, FS.[146]
MFA[146]	-4.78 ± 0.09	16 µM	61 ± 5 µM, WI-38 cells (human fibroblast), FS.[146]
DCF[146]	-4.2 ± 0.1	56 µM	210 ± 22 µM, WI-38 cells (human fibroblast), FS.[146]
NPPB[411]	-6.22 ± 0.09	0.6 µM	0.32 µM, human TRPA1-HEK293 cells, FLIPR.[411]
ACA	-4.55 ± 0.06	28 µM	ND
SB366791	inactive	-	ND
NDGA[446]	-4.45 ± 0.08	35 µM	4.9 ± 1.7 µM, human TRPA1-HEK293 cells, FS.[446]
FTS[447]	-6.08 ± 0.07	0.8 µM	7 ± 4 µM, human TRPA1-HEK293 cells, FLIPR.[447]
URB597[448]	-0.87	0.1 µM	24.5 ± 3.2 µM, human TRPA1-HEK293F cells, FLIPR.[448]
Nicotine[156]	0.34	2 M	~10 µM, mouse TRPA1-CHO cells, EP.[156]
Ligand	**LogIC_{50} ± SEM**	**IC_{50}**	**IC_{50}, species, assay**
A967079[166]	-7.10 ± 0.09	79 nM	67 nM against AITC (30 µM), human TRPA1-HEK293F cells, FLIPR[166]
AP18[449]	-5.35 ± 0.08	4 µM	3.1 µM against CA (50 µM), human TRPA1-CHO cells, FLIPR.[449]
HC030031[253]	-4.75 ± 0.09	18 µM	6.2 ± 0.2 µM against AITC (5 µM), human TRPA1-HEK293 cells, fluorescence-based plate reader.[253]

The dose-response curves of the CADs and the ASDs were presented and discussed in **Chapters 3** (**Figures 3.12** and **3.13**, **Section 3.4.2**) and **4** (**Figures 4.5** and **4.8**, **Section 4.4.2**). The concentration of the ligand corresponding to the maximum response or closer to EC_{50} or IC_{50} were chosen and screened in the mutant-hTRPA1.

5.2.2 Screening of TRPA1 ligands in S873V/T874L-hTRPA1

The S873V/T874L-hTRPA1 HEK293 cells were characterised with known TRPA1 agonists (**Figure 5.2**), including electrophilic compounds and ligands which can potentially form hydrogen bonding to the S873 and/or S874 residues (**Figure 5.11**). As can be seen in **Figure 5.11a**, an unexpected reduction in response was observed with the electrophilic compound CA, relative to WT-hTRPA1, and therefore it was suspected that non-transfected parental HEK293 cells were present. Hence the mutant cell line made previously in-house was single cell cloned to isolate the transfected cells from the parental HEK293 cells, and the re-isolated cell-line was characterised again with TRPA1 active ligands (**Figure 5.11b**).

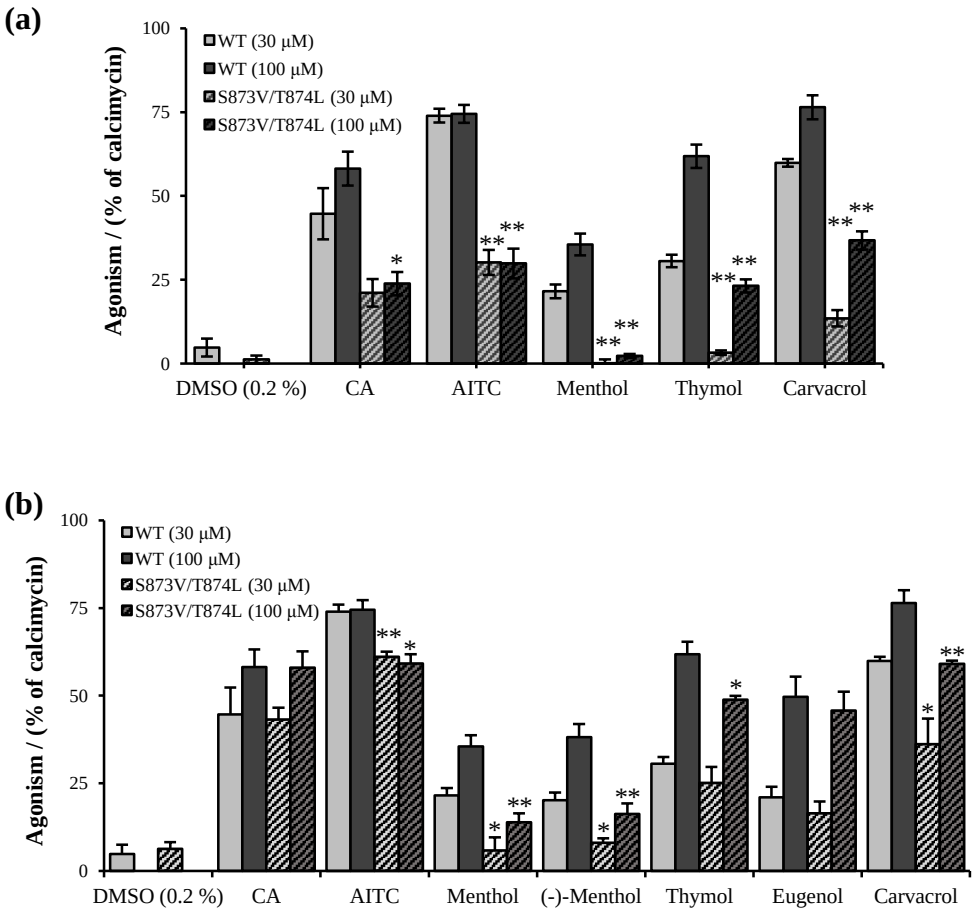

Figure 5.11: *Characterisation of hTRPA1 mutant S873V/T874L with known agonists,* **(a)** *before and* **(b)** *after single cell isolation, and compared against the responses obtained in WT-hTRPA1 HEK293 cells. Each bar represents the mean ± SEM of N = 3, and statistical significance was compared relative to WT at *p < 0.05 and **p < 0.01, using one-way ANOVA.*

As expected from the literature reports, significantly diminished responses ($p < 0.05$ or 0.01) were obtained for menthol,[150] thymol[150] and AITC[450] (**Figure 5.11b**). Since CA undergoes covalent modification at cysteine residues at the *N*-termini and does not bind to the mutated site, no significant differences in responses were, as expected, observed at the concentrations tested (30 and 100 µM) relative to WT-hTRPA1 (**Figure 5.11b**). Similarly, it was found that the eugenol response was not affected by the mutation as no significant differences were observed at the tested concentrations (**Figure 5.11b**). In the mutant hTRPA1, agonism of carvacrol and antagonism of A967079 were also significantly reduced ($p < 0.05$ or 0.01, **Figures 5.11b** and **5.12b**).

In the original finding[150] of the double mutant S873V/T874L, as determinants of menthol and thymol sensitivity in hTRPA1, it was reported that the response shown by mustard oil (active compound AITC) was unaffected in the mutant. Whereas in another study,[450] it was observed that the AITC induced response was substantially reduced with the single mutant of either S873A or T874A residues of hTRPA1, where it is worth noting that the substituted residues in the two studies were different. In this study, however, it was found that the AITC response was significantly reduced with the double mutant S873V/T874L (**Figure 5.11b**). As described in another finding,[150] thymol showed reduced activity in the mutant, but a significant reduction was observed only at 100 µM and not at 30 µM (**Figure 5.11b**). Unsurprisingly in this study, carvacrol, a structural analogue of thymol (**Figure 5.2**), showed significantly reduced responses at both 30 and 100 µM concentrations (**Figure 5.11b**).

It was reported that the hTRPA1 antagonist AP18 failed to inhibit the mustard oil-elicited agonism in the mutant S873V/T874L-hTRPA1.[150] Whereas, it was identified in the mutant S873I/T874V-hTRPA1, that the residues S873 and T874 are essential for the antagonistic effect of A967079 (an analogue of AP18) against CA elicited response.[151] Similarly, it was found that the antagonism of A967079 against CA was significantly diminished in the double mutant S873V/T874L (**Figure 5.12b**). However, as the responses were only reduced and not completely abolished, the ligands are only partially

dependent on these two residues, and thus other exploitable sites on hTRPA1 have to be considered.

In order to determine the binding site(s) of the CADs (**Figure 3.1**), they were screened in the S873V/T874L mutant for agonism at 100 µM (**Figure 5.12a**) and for antagonism at different concentrations (**Figure 5.12b**). However, the CADs did not show any significant changes in responses relative to WT-hTRPA1. Thus, it was revealed that the CADs do not bind at the menthol binding site.

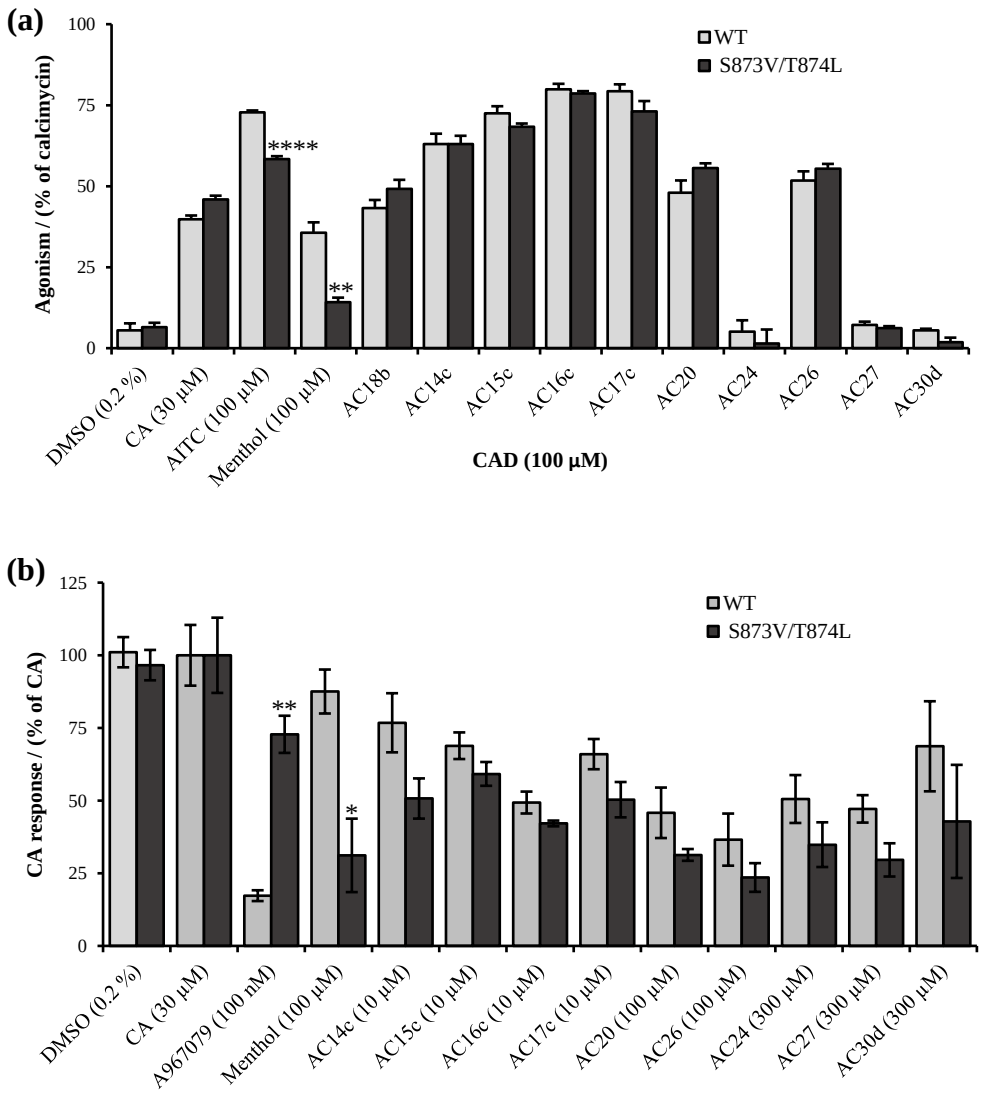

Figure 5.12: *Evaluation of CADs for* **(a)** *agonism and* **(b)** *antagonism, in S873V/T874L-hTRPA1 HEK293 cells, and compared against the responses obtained in WT-hTRPA1 HEK293 cells. Each bar represents the mean ± SEM of N = 3, and statistical significance was compared relative to WT at *p < 0.05, **p < 0.01 and ****p < 0.0001, using one-way ANOVA.*

5.2.3 Screening of TRPA1 ligands in C621A-hTRPA1

The chemical structures of the ligands characterised in the mutant C621A-hTRPA1 are given in **Figures 5.2**, **3.1** and **4.1**. As reported in the literature, significantly reduced agonism responses were obtained for the electrophilic compounds, CA ($p < 0.01$), AITC ($p < 0.01$) and ACR ($p < 0.0001$), in the mutant C621A-hTRPA1 relative to the responses obtained in WT-hTRPA1 HEK293 cells (**Figure 5.13a**).[118,119] In the literature, a complete abolition of CA agonism was observed with the triple mutant C621S/C641S/C665S of hTRPA1.[118,451] Whereas, it was found that CA and AITC responses are partially reduced in the single mutant C621A-hTRPA1, as observed in other studies.[119,411] However, the ACR response was almost fully eradicated in the C621A mutant, and this signified the importance of the particular cysteine residue in TRPA1 activation by electrophilic compounds. The TRPA1 antagonists could not be evaluated in the mutant, since the standard agonists (CA, AITC and ACR) of hTRPA1 bind to the mutated site.

Intriguingly, significantly diminished agonism responses were obtained with non-reactive compounds, including menthol ($p < 0.05$), carvacrol ($p < 0.01$) (**Figure 5.13b**), FFA ($p < 0.01$), DCF ($p < 0.05$), NPPB ($p < 0.05$) (**Figure 5.13c**), FTS ($p < 0.05$, **Figure 5.13d**), AC35b ($p < 0.01$, **Figure 5.14a**), and probenecid ($p < 0.01$, **Figure 5.15a**). A similar type of effect with non-reactive compounds had been previously described for menthol, NPPB and FTS.[411] Though the reduced effects observed with NPPB and FTS in the mutant C621A were not statistically significant in their study, a significant reduction in agonism were observed with the mutations of different cysteine residues at the *N*-terminus. FTS was reported to show significantly reduced response in C641A and C665A single mutants,[411] and NPPB in C641A single mutant[411] and C621S/C641S/C665S triple mutant[451]. In another study, single mutations of the two cysteine residues C641A and C665A, have shown to significantly decrease and increase the responses of menthol activity, respectively, relative to wild-type.[411]

Menthol is known to have its determinants in the S5 (S873/S874),[150] and these cysteine residues are located within the *N*-termini topological domain proximate to S1. The influence on the activity of menthol by the cysteine

mutants, suggests that S5 might closely interact with the *N*-termini cysteines. In addition, the electrophilic compound AITC is known to activate TRPA1 *via* covalent modification at the *N*-termini cysteines (C621, C641 and C665).[118,119] However, in the double mutant of the S5 residues S873/S874, AITC was found to show significantly reduced agonism (**Figure 5.11b**, **Section 5.2.2**). Therefore, it seems to be that the interaction between these two domains/regions could possibly have a critical impact on the modulation of TRPA1.

According to the above observations, the cysteine residues not only serve as determinants of reactive electrophilic compounds, but also have a substantial effect on the modulation of non-reactive compounds. Hence the cysteine residues at the *N*-terminus play a general role in the function of TRPA1 channel. The disruption to the disulfide bridges between and within the *N*-termini cysteine monomers, including between C621 and C645, and other cysteines[97] could perhaps resulted in reduced activities of non-reactive compounds due to changes in the conformation of TRPA1 rather than covalent modification at the cysteines.

Due to the presence of an α,β-unsaturated carbonyl unit (Michael acceptor) in CADs, it was considered that these compounds may undergo covalent modification through conjugate addition. However, except for AC35b with a more divergent structure to the parent CAD (AC18b), other CADs did not show any reduced responses, but led to increased responses relative to that observed in the WT-hTRPA1 (**Figure 5.14a**).

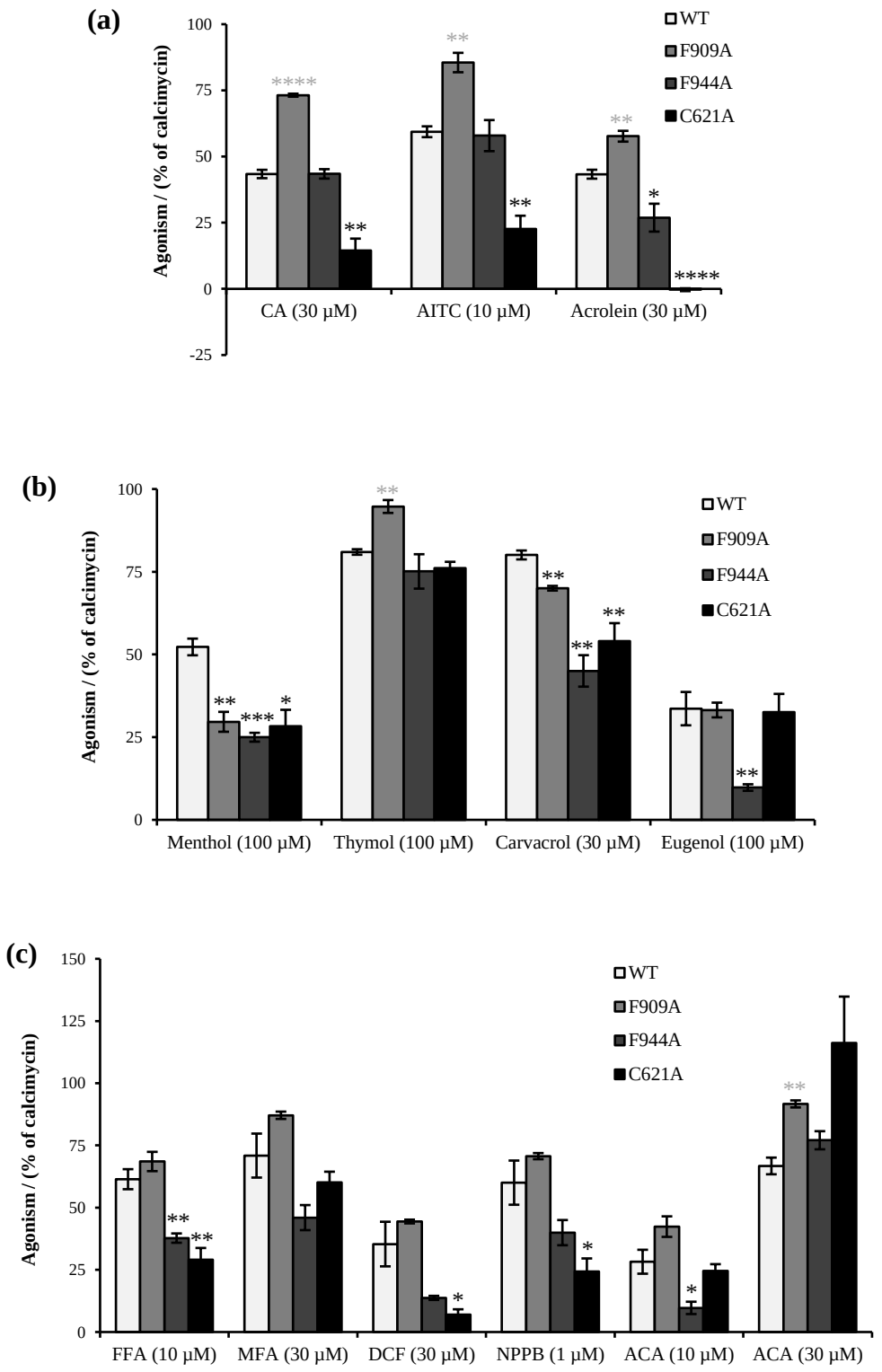

Continued…

Figure 5.13: *Screening results of TRPA1 ligands in the hTRPA1 mutants, F909A, F944A and C621A, and comparison of the responses against WT-hTRPA1 HEK293 cells* **(a - e)**. *Each bar represents the mean ± SEM of N = 3 (n = 6), and statistical significance was compared relative to WT at *p < 0.05, **p < 0.01, ***p < 0.001 and ****p < 0.0001, using one-way ANOVA; black stars indicate significant reduction and grey stars indicate significant increase in response relative to WT.*

Continued…

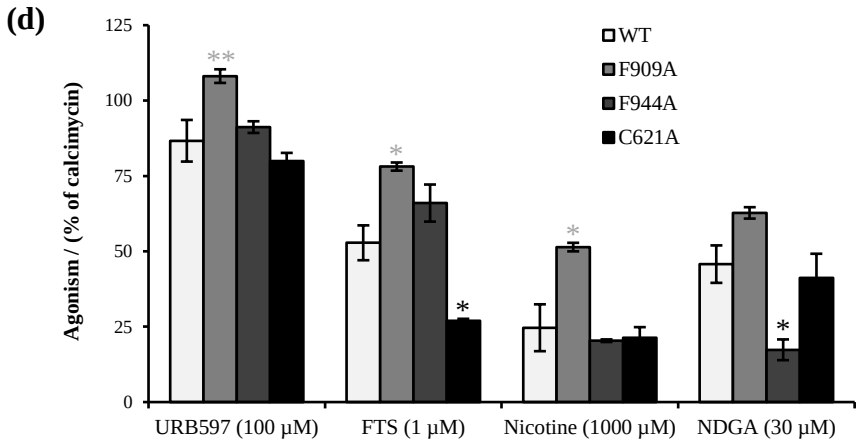

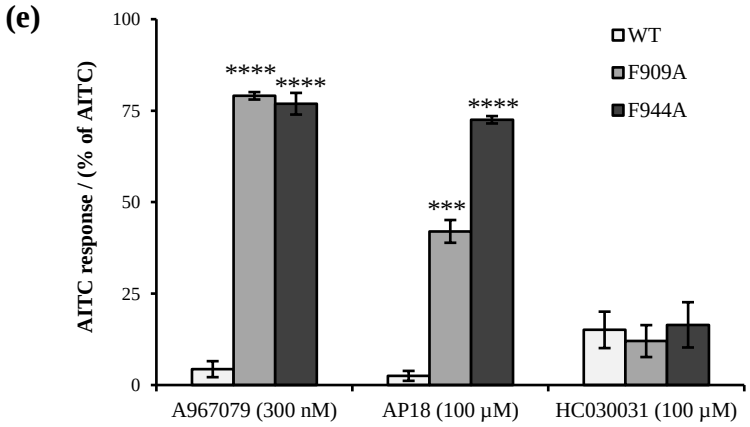

Figure 5.13: *Screening results of TRPA1 ligands in the hTRPA1 mutants, F909A, F944A and C621A, and comparison of the responses against WT-hTRPA1 HEK293 cells* **(a - e)**. *Each bar represents the mean ± SEM of N = 3 (n = 6), and statistical significance was compared relative to WT at *p < 0.05, **p < 0.01, ***p < 0.001 and ****p < 0.0001, using one-way ANOVA; black stars indicate significant reduction and grey stars indicate significant increase in response relative to WT.*

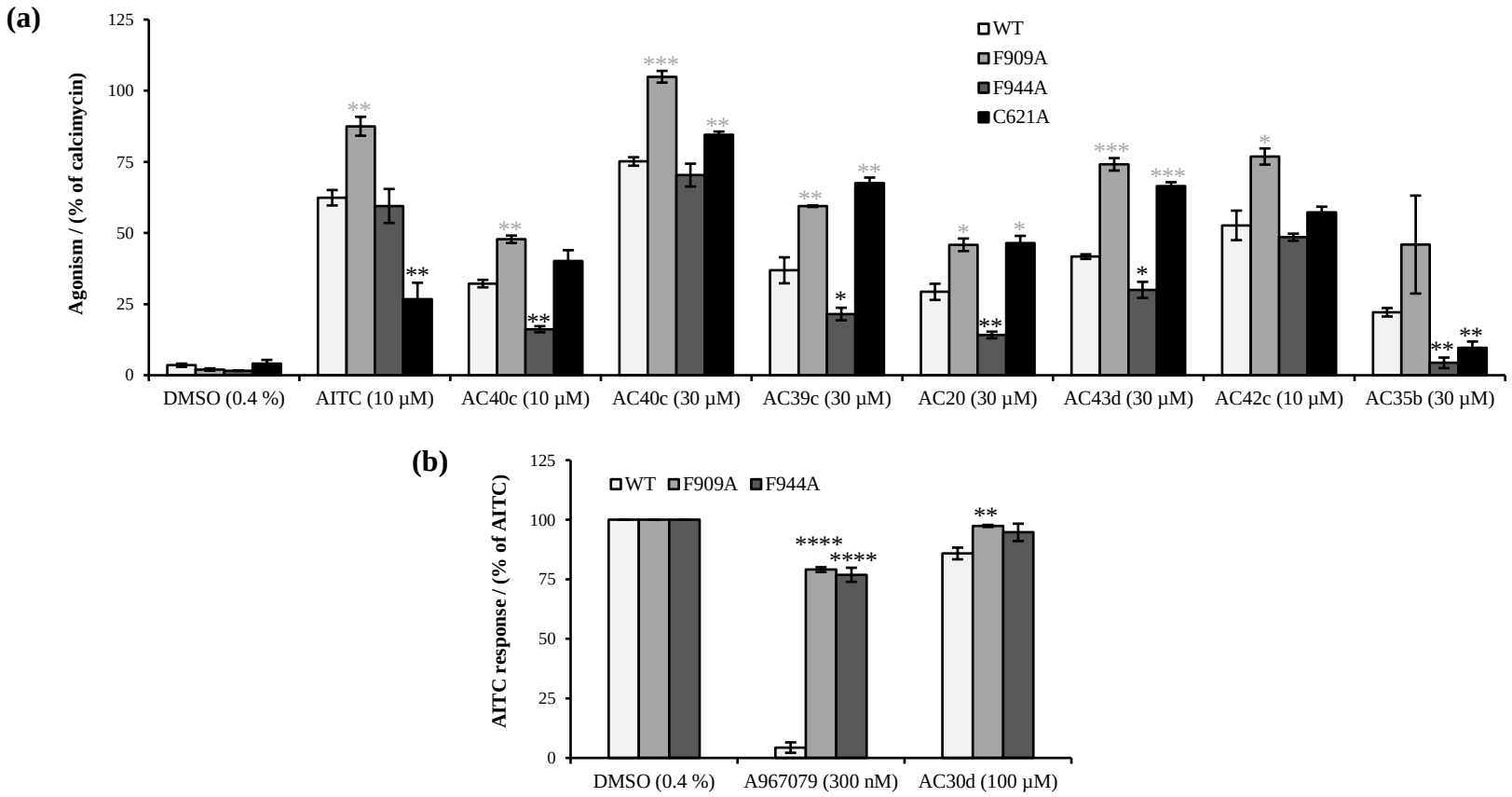

Figure 5.14: *Screening results of CADs in the hTRPA1 mutants, F909A, F944A and C621A, and comparison of the responses against WT-hTRPA1 HEK293 cells,* **(a)** *agonism and* **(b)** *antagonism. Each bar represents the mean ± SEM of N = 3 (n = 6), and statistical significance was compared relative to WT at *p < 0.05, **p < 0.01, ***p < 0.001 and ****p < 0.0001, using one-way ANOVA; black stars indicate significant reduction and grey stars indicate significant increase in response relative to WT.*

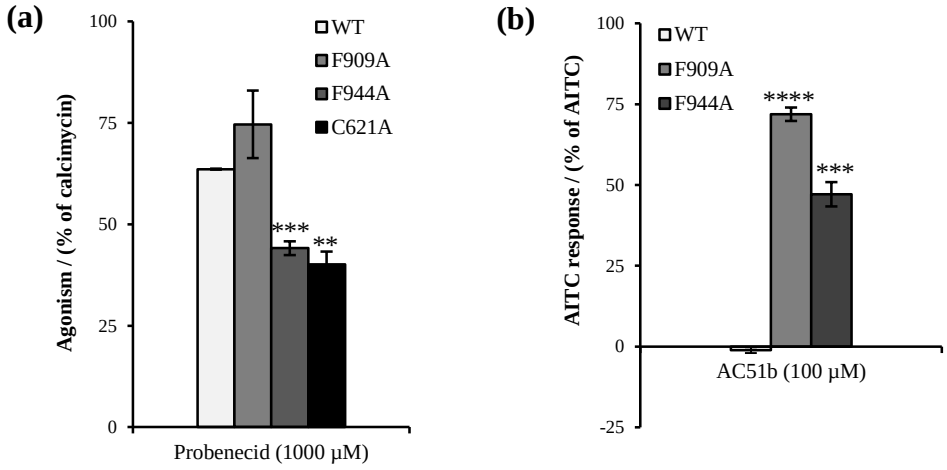

Figure 5.15: *Screening results of ASDs in the hTRPA1 mutants, F909A, F944A and C621A, and comparison of the responses against WT-hTRPA1 HEK293 cells,* **(a)** *agonism and* **(b)** *antagonism. Each bar represents the mean ± SEM of N = 3 (n = 6), and statistical significance was compared relative to WT at **p < 0.01, ***p < 0.001 and ****p < 0.0001, using one-way ANOVA.*

5.2.4 Screening of TRPA1 ligands in F909A-hTRPA1

Among the ligands (**Figures 5.2**, **3.1** and **4.1**) evaluated in the mutant F909A-hTRPA1 HEK293 cells (**Figures 5.13 - 5.15**), a significantly ($p < 0.0001$) reduced inhibitory effect was observed for the antagonist A967079 relative to the responses obtained in WT-hTRPA1 (**Figure 5.13e**), as was expected from a literature report.[103] As predicted, significantly ($p < 0.001$) reduced antagonism was obtained with the oxime derivative AP18 antagonist (**Figure 5.13e**), which is structurally similar to A967079. Reduced antagonistic responses were also obtained for the CAD, AC30d ($p < 0.01$, **Figure 5.14b**), and the ASD, AC51b[373,452] ($p < 0.0001$, **Figure 5.15b**) antagonists. Since all the tested antagonists with distinct structures, except HC030031 (**Figure 5.13e**), have shown significant differences in this mutant (**Figures 5.13e**, **5.14b** and **5.15b**), F909 residue seems to be a key residue for antagonism in hTRPA1.

In addition to the antagonists, there was a drop in the agonism of menthol and carvacrol in the absence of the F909 residue ($p < 0.01$, **Figure 5.13b**). As menthol lacks aromaticity and cannot participate in π-π interactions, it seems to be that menthol interacts with the residue through hydrophobic interactions. In addition, for most of the other compounds, the responses were

significantly higher than that observed in WT-hTRPA1 as shown in **Figures 5.13a-d** and **5.14a**, in which the level of significance is indicated with grey stars. This could have been observed due to changes in the structural conformation of hTRPA1 as a result of the substitution of the aromatic residue F909 to alanine. Though it had been already reported that the antagonists, A967079 bind to the F909 residue and HC030031 does not show any significant change in response relative to wild-type,[103] this is the first time the other compounds were evaluated and studied at this site.

5.2.5 Screening of TRPA1 ligands in F944A-hTRPA1

A significant drop in activity was found for many of the ligands (**Figures 5.2**, **3.1** and **4.1**) evaluated in the mutant F944A-hTRPA1 HEK293 cells, which includes ACR ($p < 0.05$, **Figure 5.13a**), menthol, carvacrol and eugenol ($p < 0.01$, **Figure 5.13b**), FFA ($p < 0.01$, **Figure 5.13c**) and ACA ($p < 0.05$, **Figure 5.13c**), NDGA ($p < 0.05$, **Figure 5.13d**), A967079 and AP18 ($p < 0.0001$, **Figure 5.13e**), AC40c and AC35b ($p < 0.01$, **Figure 5.14a**), AC39c and AC43d ($p < 0.05$, **Figure 5.14a**), probenecid ($p < 0.001$, **Figure 5.15a**), and AC51b ($p < 0.001$, **Figure 5.15b**), relative to the responses obtained in WT-hTRPA1. Though it had been already reported that the antagonists, A967079 binds to the F944 residue, and HC030031 does not show any significant differences in response relative to the wild-type,[152] this is the first time the other compounds were evaluated and studied at this site.

The reduced responses obtained for the non-aromatic compounds, ACR and menthol that cannot participate in π-π stacking interactions, suggest that the compounds interact with the residue through hydrophobic interactions. In the case of ACA and AC40c, reduced responses were obtained only at a lower concentration (10 µM) and not at a higher concentration (30 µM), as shown in **Figures 5.13c** and **5.14a**, respectively. Also, the deviation in the response of thymol compared to its analogue carvacrol could be due to testing of the compound at a high concentration (**Figure 5.13b**). It has been stated in a report, that testing a ligand only at a supramaximal concentration does not show the actual effect.[83] Hence a complete dose-response curve of the

compounds against the mutant is required to demonstrate the effect more clearly and reliably.

The responses obtained for A967079 in both F909 and F944 mutants were equal ($p < 0.0001$) as shown in **Figure 5.13e**. However, the analogue AP18 had significant difference in response (**Figure 5.13e**), in which the inhibition was nearly abolished in the mutant F944A ($p < 0.0001$), but not in F909A ($p < 0.001$). On the other hand, the ASD AC51b preferentially binds to F909 ($p < 0.0001$) compared to F944 ($p < 0.001$) as can be seen in **Figure 5.15**, which could be due to the ligand size, site accessibility and location of the amino acid residue in the TRPA1 channel structure. The F909 residue is located in the upper region of the pore, and the ligands have to pass this residue before reaching the inner region of the pore containing F944 residue. Thus, the larger size ligand like AC51b could have interacted with the first available F909A residue. As most of the ligands with different functional groups and structures have shown significant reductions in responses in the mutant F944A, the F944 residue might serve as a general determinant in the modulation of hTRPA1 channel.

5.3 Conclusions

In addition to the ^{1}H NMR studies carried out with a CAD (**Section 3.5** of **Chapter 3**), the findings with the C621A mutant (**Section 5.2.3**) further suggest that the CADs do not undergo covalent modification at the *N*-terminal cysteine. The drop in activities of the TRPA1 modulators in the mutants F909A and F944A demonstrated that the corresponding compounds may possibly bind to the aromatic phenylalanine in the hTRPA1 putative pore region non-covalently *via* π-π stacking and/or hydrophobic interactions. Of the two residues, F944 was found to be the priority site for many TRPA1 active ligands, including derivatives with hydroxy groups (menthol analogues), NSAIDs (fenamates), anthranilic acid derivatives, CADs and ASDs, suggesting that this is a key residue vital for the modulation of TRPA1 channel in general. Whereas, the oxime derivatives preferably bound to the F909 residue. Since a complete elimination of the responses were not observed with most of the ligands, it seems to be that the ligands might

additionally interact with other nearby residues, which remains to be verified. Moreover, complete dose-response curves for the compounds those have shown different effects in the mutants will demonstrate the difference in potency of the ligands relative to wild-type.

Overall, the residues within the S5-S6 putative pore region were found to be crucial for the chemosensation role of TRPA1. Moreover, a possible interaction between *N*-termini cysteines (proximate to S1) and putative pore (S5-S6) was deduced, as a result of the electrophilic compounds those activate TRPA1 channels *via* covalent modification showed a significant effect on the TRPA1 mutants within the pore region and *vice versa*. These interesting findings on the binding site(s) of various structurally distinct TRPA1 ligands will certainly lead to a better understanding of the modulation of TRPA1 channels, and potentially contribute in the development of TRPA1 specific modulators.

CHAPTER 6: Summary

6.1 Calcium signalling

Fluorescence-based calcium signalling assays were utilised throughout the study to measure the $[Ca^{2+}]_i$ on activation of the cation channel, TRPA1 or TRPM8, by chemical modulators. This was a suitable approach to screen a large number of compounds at different concentrations in a population of cells either in suspension or in the adherent form. The use of a high wavelength fluorescent probe [Fluo-3 ($\lambda_{Ex/Em}$ 506/526 nm) or Fluo-4 ($\lambda_{Ex/Em}$ 494/506 nm)] ensured that the spectral properties of the test compounds did not interfere with the assay and thereby lead to false positives. Variations in responses were observed when the assays were carried out using slightly altered methods (**Section 3.4.1.3** of **Chapter 3**). For example, the EC_{50} obtained for cinnamaldehyde in the cuvette-based system with cells in suspension loaded with Fluo-3 was 27 µM, whereas in the micro-well plate system with cells adhered to the surface loaded with Fluo-4 was 9 µM, which is significantly different ($p < 0.0001$). Also, with the use of different carrier solvents, such as DMSO or ethanol, significantly varied compound potency ($p < 0.0001$) was observed (**Section 3.4.1.4** of **Chapter 3**). The EC_{50} obtained for cinnamaldehyde in DMSO was 9 µM, but in EtOH it was 155 µM. As a small variability between assays can lead to different results, these were considered when comparing any results against the literature findings.

6.2 *N*-Cinnamoylanthranilates as modulators of TRPA1

As TRPA1 modulators, a series of *N*-cinnamoylanthranilate derivatives (CADs) with different substituents were successfully synthesised in good yields (**Section 2.2.4** of **Chapter 2**). Among the CADs synthesised, *N*-(3-ethoxy-4-hydroxycinnamoyl)anthranilic acid (**AC27**) was found to be a novel compound. Though all other CADs exist in the literature, this was the first time CADs were found as TRPA1 modulators. The series of twenty-two *N*-cinnamoylanthranilic acid derivatives with electron-withdrawing and/or electron-donating substituents, and some of their corresponding methyl ester, screened using calcium signalling assays for agonism and antagonism responses in HEK293 cells stably transfected with hTRPA1 were found to

possess various activities ranging from agonism, partial agonism, antagonism and desensitising effects in hTRPA1 (**Section 3.4.2** of **Chapter 3**). The effects observed were concentration-dependent, and interestingly, a clear trend in the structure-activity relationship (SAR) was observed with different functional groups.

Among the CADs containing the COOH group, the unsubstituted *N*-cinnamoylanthranilic acid (**AC18b**) had a moderate agonistic effect, and the electron withdrawing group (EWG) substituted CADs were agonists. The halogenated CADs, with inductive electron withdrawing but lone pair donating properties, showed potent agonism with a desensitising effect, and the CADs with weak/moderate electron donating group (EDG) showed bimodal activity, that is, they possessed partial agonism and antagonism. As the electron donating nature of the EDG becomes stronger, the agonism of the compounds decreased and became antagonists. The trend observed with the EWG and EDG substituents in this study was also observable in another study in the literature, which measured the potency of benzylidenemalononitriles with different substituents in hTRPA1.[421]

In general, the EDG substituted compounds with a higher number of hydrogen bond donors and acceptors had greater antagonistic effect in hTRPA1 channels. This perhaps suggested that the ligands which can bind to amino acid residues through greater hydrogen bonding are involved in blocking of the channels more effectively. Moreover, it was found that the *ortho*-substituted CADs were less efficacious relative to their corresponding *para*-substituted analogues, and the presence of a non-rotatable α,β-unsaturated bond enhanced the activity of the compound distinctly. The α-substituted CADs were found to be more potent agonists relative to the unsubstituted CAD. The non-planar compounds with a tertiary amide group showed weak responses relative to the planar, secondary amide group containing parent compound (**AC18b**). This revealed that the presence of a secondary amide (-CONH) and the anthranilate moiety plays an important role in the activity of CADs. All the methyl ester CADs evaluated in hTRPA1 were potent agonists with no considerable antagonism compared to their corresponding free carboxylic acid derivative, but esters had solubility

limitations. Additionally, the structurally related compounds in the literature, including ACA, an inhibitor of TRPM2, TRPM8, TRPC3, TRPC6 and TRPV1[327] channels was found to activate hTRPA1, and SB366791, an inhibitor of TRPV1[409] was inactive in hTRPA1. From the overall observations and information, it was deduced that hydrogen bonding from the amide and the carboxylic acid groups, and hydrophobic π-π stacking interactions of the aromatic rings are key contributors to the channel modulation.

All the CADs evaluated in pcDNA3 mock-transfected HEK293 cells as a negative control (**Section 3.4.3.1** of **Chapter 3**) did not show any response, which demonstrated that in the transfected HEK293 cells, with regard to triggering calcium flux, the compounds were selective to TRPA1 and/or TRPM8 channels, and had no effect on other components of the cells including endogenously expressed channels/receptors: $P2Y_1$,[422] $P2Y_2$,[422] voltage-gated potassium channels,[423,424] sodium channels (β1A[425] and $Na_v1.7$[426]), sphingosine-1-phosphate receptors (Edg-1, Edg-3 and Edg-5),[427] calcium channels[428] including TRPC (TRPC1, TRPC3, TRPC4, TRPC6 and TRPC7),[429,430] and M_3 muscarinic acetylcholine receptor.[431]

Moreover, all the compounds evaluated in HEK293 cells stably transfected with hTRPM8 for selectivity (**Section 3.4.3.2** of **Chapter 3**) did not show any agonism, except α-phenyl substituted CAD **AC42c** with weak agonism. However, the majority of the compounds that had an agonistic effect in hTRPA1 showed a relatively weak inhibitory effect in hTRPM8 at a high concentration (100 μM). Nevertheless, to conclude on the specificity, further selectivity assays against other ion channels are necessary.

With respect to the physicochemical properties of CADs (**Section 3.4.5** of **Chapter 3**), it was observed that among similar analogues, the compounds possessing higher clogP values were the most potent agonists and the agonism decreased with a decrease in clogP value, which was also in agreement with compounds in the literature.[128,411] Furthermore, the CADs with a higher number of hydrogen bond donors, hydrogen bond acceptors, larger topological polar surface area and logS, and lower logP had greater inhibitory

effects with poorer or absence of agonism in hTRPA1. Moreover, all the CADs, except α-phenyl substituted CAD **AC42c**, were consistent with Lipinski's rule-of-five and Veber's rules of lead-likeness and oral bioavailability, and hence show promise as potential leads in drug discovery. In addition, owing to the fact that the CAD, tranilast (**AC24**) is a clinically accepted anti-allergic drug with reduced side effects,[291] CADs possibly have the potential to be utilised in clinical development in general. The functional characterisation of some of the CADs in Dunkin-Hartley guinea pig vagus nerve (**Section 3.4.6** of **Chapter 3**) showed poor activities, and was thought to be due to species difference and/or limitations with the tested compound concentrations.

In addition to the study undertaken and from the review of several biological activities of CADs in the literature (**Section 1.2** of **Chapter 1**), it was postulated that there could be a correlation between the several biological activities of CADs and TRP channels (**Section 3.6** of **Chapter 3**), as these channels are involved in a wide range of cellular functions.[3]

6.3 Aryl sulfonamides as modulators of TRPA1

To study the SAR of probenecid derivatives in TRPA1 after observation of its agonism and desensitising effect in a reported study,[354] a series of aryl sulfonamide derivatives (ASDs) based on the probenecid core structure (small aryl sulfonamides) and TRPA1 antagonists in the literature[372-376] (extended aryl sulfonamides) were successfully synthesised (**Section 2.3** of **Chapter 2**). Among the synthesised ASDs, **AC53b**, **AC54b**, **AC56d** and **AC57d** were found to be novel compounds. The series of twenty-two ASDs screened using calcium signalling assays for agonism and antagonism responses in HEK293 cells stably transfected with hTRPA1 were mostly found to have weak agonism or were inactive on hTRPA1 (**Section 4.4.2** of **Chapter 4**).

On comparing the SAR of small ASDs on hTRPA1, irrespective of amine attached to the aryl sulfonyl group, the derivatives with $-OCH_3$, -COOH and CH_3CONH- group as their substituent showed weak agonism in a concentration-dependent manner. However, the derivatives with H or F atom

as the substituent had no agonism. The observed trend was that the derivatives with hydrophilic substituents *para* to the sulfonyl group showed agonism. As the structures of the derivatives had different substituents on both sides of the sulfonyl group, a general trend in the SAR could not be clearly concluded. However, interestingly, substitution of the fluoro group in an aryl sulfonamide hTRPA1 antagonist [**AC51b**, (*S*)-*N*-(4-chlorobenzyl)-1-((4-fluorophenyl)sulfonyl)pyrrolidine-2-carboxamide[373]] to a carboxylic acid group (**AC56d**), led to complete elimination of the antagonistic effect and shifted to an agonist as observed in small aryl sulfonamides with a COOH group in the study. All the ASDs were found to be inactive on both pcDNA3 mock- and hTRPM8-HEK293 cells, which revealed that the ASDs were selective for TRPA1 over TRPM8 and other endogenously expressed ion channels/receptors in HEK293 cells.

6.4 Ligand binding sites in TRPA1

To identify the binding sites of CADs, ASDs and some known TRPA1 ligands, the compounds were screened in HEK293 cells stably transfected with hTRPA1 mutants (**Sections 5.2.2 - 5.2.5** of **Chapter 5**), which were successfully produced using site-directed mutagenesis (**Section 5.2** of **Chapter 5**) of selected amino acid residues within the hTRPA1 putative pore region S5-S6 (S873V/T874L, F909A and F944A) and at the *N*-terminus (C621A).

When characterising the menthol binding site[150] mutant S873V/S874L-hTRPA1, it was found that in addition to menthol,[150] thymol,[150] AITC[450] and A967079,[151] as reported in the literature, carvacrol also interacts with these residues. Moreover, screening of the CADs and eugenol in the mutant S873V/S874L did not show any significantly reduced responses relative to the WT-hTRPA1, indicating that their binding site is elsewhere.

In the A967079 binding site[103] mutant F909A-hTRPA1, relative to the responses obtained in WT-hTRPA1, significantly reduced inhibitory effects were observed for the antagonists AP18, CAD-AC30d and ASD-AC51b. Since all the tested antagonists, except HC030031, showed significant effects in the mutant, F909 seems to be a key residue responsible for antagonism in

hTRPA1. In addition to the antagonists, there was a significant drop in the agonism of menthol and carvacrol. As menthol lacks aromaticity and cannot participate in π-π interactions, it seems that menthol interacts with the residue through hydrophobic interactions. The responses for most of the other compounds were significantly higher than that observed in WT-hTRPA1, which could be due to changes in the structural conformation of hTRPA1 as a result of substituting the aromatic residue F909 to alanine.

In another A967079 binding site[152] mutant F944A-hTRPA1, a significant drop in activity was found for many ligands including ACR, menthol, carvacrol, eugenol, FFA, NDGA, AP18, CADs (AC40c, AC35b, AC39c, AC43d and ACA) and ASDs (probenecid and AC51b), relative to the responses obtained in WT-hTRPA1. Similar responses were obtained for A967079 in both F909 and F944 mutants. However, the analogue AP18 had significant differences in response in the two mutants, in which the inhibitory effect was nearly abolished in the mutant F944A, but not in F909A. The ASD-AC51b was found to preferentially bind to F909 compared to F944, perhaps due to the size of the ligand and site accessibility.

The C621 single residue that is crucial for the TRPA1 activation by reactive electrophilic compounds, including CA, ACR and AITC,[118,119] was found to be involved in the modulation of hTRPA1 by the non-reactive compounds, menthol, carvacrol, FFA, DCF, NPPB, FTS, AC35b and probenecid, where significant attenuation in the agonism was observed with the mutant C621A-hTRPA1. A similar type of effect has been previously described in different cysteine residues at the *N*-terminus for the compounds menthol and FTS (C641A and C665A single mutants),[411] and NPPB (C641A single mutant[411] and C621S/C641S/C665S triple mutant[451]). The findings together suggested that the cysteine residues not only serve as determinants of reactive electrophilic compounds, but also have a substantial effect on the modulation of non-reactive compounds, and thus the cysteine residues at the *N*-terminus play a general role in the function of the channel. As mentioned in the literature,[411] it seems to be that the S5 domain might closely interact with the *N*-termini cysteines and could possibly have a critical impact on the modulation of TRPA1. For instance, menthol is known to have its

determinants in the S5 (S873/S874),[150] and the cysteine residues are located within the *N*-termini topological domain proximate to S1. Moreover, the electrophilic compound AITC is known to activate TRPA1 *via* covalent modification at the *N*-termini cysteines (C621, C641 and C665).[118,119] However, in the double mutant of the S5 residues S873/S874, AITC was found to show significantly reduced agonism. However, other structurally related ligands, including thymol, eugenol, MFA, URB597, ACA, (-)-nicotine, NDGA and CADs did not show any significantly reduced responses in this mutant relative to the WT-hTRPA1. In addition to the ^{1}H NMR studies carried out with a thiol model (**Section 3.5** of **Chapter 3**) to determine any involvement of CAD in covalent modification of cysteines through conjugate addition, the findings in the C621A mutant confirmed that the CADs do not undergo covalent modification at the *N*-terminal cysteine.

CHAPTER 7: Conclusions and further work

It was explicitly found from the studies undertaken that different substituents and substitution patterns on compounds show differences in TRPA1 receptor activities, which agrees with the hypothesis made, that is, the functional groups present on the chemical compounds trigger the action of TRPA1 channels. Moreover, the CADs with different pharmacological activities, including agonism, partial agonism, antagonism and desensitising effects, show promise as useful TRPA1 modulators for further study, as both TRPA1 agonists and antagonists have hope in the treatment of TRPA1 related disorders as described in **Chapter 1** (**Section 1.1.6.1**). However, to conclude on the specificity of the CADs activity, further selectivity assays against other TRP channels are necessary. Further supporting the hypothesis, a minor alteration in a known TRPA1 antagonist structure showed a substantial change in the activity, for example, Orion Corporation disclosed fluorinated aryl sulfonamide derivative **AC51b** lost its antagonism when the fluoro group was replaced with a carboxylic acid group and shifted to an agonist. Overall, it was found that strong SAR exist between analogues of compounds and the activity of TRP channels. Using the key findings of the SARs in **Chapters 3** and **4**, which are summarised in **Chapter 6**, potent and selective TRPA1 modulators could be developed as drugs for TRPA1 related disorders and/or diseases.

Moreover, the residues within the S5-S6 putative pore region were found to be crucial for the chemosensation role of TRPA1. Of the residues tested, F944 was found to be the priority site for many TRPA1 active ligands with different functional groups and structures, including derivatives with hydroxy groups (menthol analogues), NSAIDs (fenamates) and other anthranilic acid derivatives, CADs and ASDs, suggesting that this is an important residue for the modulation of TRPA1 channel in general. The overall interesting findings on the binding site(s) of the structurally distinct classes of TRPA1 ligands in **Chapter 5** (summarised in **Chapter 6**) will certainly lead to a better understanding of the modulation of TRPA1 channels and potentially aid in the development of TRPA1 specific modulators. Since complete elimination of the responses were not observed with most of the ligands, it seems that the

ligands might additionally interact with other nearby residues, which remains to be verified. In addition, complete dose-response curves for the compounds that have shown different effects in the mutants will show the difference in potency of the ligands relative to wild-type. Determination of other exploitable binding sites by TRPA1 ligands would further lead to better understanding of the compound interactions in TRPA1, and thus assist in the development of potent and selective hTRPA1 modulators.

In the calcium signalling assays utilised, the changes in $[Ca^{2+}]_i$ levels were measured. However, to identify if the effects shown by a test compound is due to direct binding to TRPA1 or TRPM8 channel, or an indirect effect through other mechanisms such as activation of GPCR that results in modulation of the TRP channels through phosphorylation signalling pathways, other assays like electrophysiological measurements, ideally a patch clamp, could be used together with the fluorescence-based calcium signalling assays to enhance the understanding of the effects shown by the compounds.

References

1. Minke B. Drosophila mutant with a transducer defect. *Biophys Struct Mech*. 1977;3(1):59-64.
2. Montell C, Jones K, Hafen E, Rubin G. Rescue of the Drosophila phototransduction mutation trp by germline transformation. *Science*. 1985;230(4729):1040-3.
3. Dadon D, Minke B. Cellular functions of transient receptor potential channels. *Int J Biochem Cell Biol*. 2010;42(9):1430-45.
4. Nilius B. TRP channels in disease. *Biochim Biophys Acta*. 2007;1772(8):805-12.
5. Clapham DE. TRP channels as cellular sensors. *Nature*. 2003;426(6966):517-24.
6. Corey DP. New TRP channels in hearing and mechanosensation. *Neuron*. 2003;39(4):585-8.
7. Moran MM, Xu H, Clapham DE. TRP ion channels in the nervous system. *Curr Opin Neurobiol*. 2004;14(3):362-9.
8. Pedersen SF, Owsianik G, Nilius B. TRP channels: an overview. *Cell Calcium*. 2005;38(3-4):233-52.
9. Minke B. TRP channels and Ca^{2+} signaling. *Cell Calcium*. 2006;40(3):261-75.
10. Montell C, Birnbaumer L, Flockerzi V. The TRP channels, a remarkably functional family. *Cell*. 2002;108(5):595-8.
11. Montell C, Birnbaumer L, Flockerzi V, Bindels RJ, Bruford EA, Caterina MJ, Clapham DE, Harteneck C, Heller S, Julius D, Kojima I, Mori Y, Penner R, Prawitt D, Scharenberg AM, Schultz G, Shimizu N, Zhu MX. A unified nomenclature for the superfamily of TRP cation channels. *Mol Cell*. 2002;9(2):229-31.
12. Walker RG, Willingham AT, Zuker CS. A Drosophila mechanosensory transduction channel. *Science*. 2000;287(5461):2229-34.
13. Sidi S, Friedrich RW, Nicolson T. NompC TRP channel required for vertebrate sensory hair cell mechanotransduction. *Science*. 2003;301(5629):96-9.
14. Levine JD, Alessandri-Haber N. TRP channels: Targets for the relief of pain. *Biochim Biophys Acta*. 2007;1772(8):989-1003.
15. Takahashi N, Kozai D, Mori Y. TRP channels: sensors and transducers of gasotransmitter signals. *Front Physiol*. 2012;3(324).
16. Bach G. Mucolipin 1: endocytosis and cation channel - a review. *Pflügers Arch*. 2005;451(1):313-7.
17. Philipp S, Cavalie A, Freichel M, Wissenbach U, Zimmer S, Trost C, Marquart A, Murakami M, Flockerzi V. A mammalian capacitative calcium entry channel homologous to Drosophila TRP and TRPL. *EMBO J*. 1996;15(22):6166-71.
18. Philipp S, Wissenbach U, Flockerzi V. Molecular biology of calcium channels. In: Putney J, editor. *Calcium Signaling*. Boca Raton: CRC Press; 2000. p. 321–42.
19. Okada T, Shimizu S, Wakamori M, Maeda A, Kurosaki T, Takada N, Imoto K, Mori Y. Molecular cloning and functional characterization of a novel receptor-activated TRP Ca^{2+} channel from mouse brain. *J Biol Chem*. 1998;273(17):10279-87.
20. Schaefer M, Plant TD, Obukhov AG, Hofmann T, Gudermann T, Schultz G. Receptor-mediated regulation of the nonselective cation channels TRPC4 and TRPC5. *J Biol Chem*. 2000;275(23):17517-26.
21. Ma HT, Patterson RL, van Rossum DB, Birnbaumer L, Mikoshiba K, Gill DL. Requirement of the inositol trisphosphate receptor for activation of store-operated Ca^{2+} channels. *Science*. 2000;287(5458):1647-51.
22. Ma HT, Venkatachalam K, Parys JB, Gill DL. Modification of store-operated channel coupling and inositol trisphosphate receptor function by 2-aminoethoxydiphenyl borate in DT40 lymphocytes. *J Biol Chem*. 2002;277(9):6915-22.
23. Venkatachalam K, van Rossum DB, Patterson RL, Ma HT, Gill DL. The cellular and molecular basis of store-operated calcium entry. *Nat Cell Biol*. 2002;4(11):e263-72.
24. Maroto R, Raso A, Wood TG, Kurosky A, Martinac B, Hamill OP. TRPC1 forms the stretch-activated cation channel in vertebrate cells. *Nat Cell Biol*. 2005;7(2):179-85.
25. Kim J, Chung YD, Park DY, Choi S, Shin DW, Soh H, Lee HW, Son W, Yim J, Park CS, Kernan MJ, Kim C. A TRPV family ion channel required for hearing in Drosophila. *Nature*. 2003;424(6944):81-4.
26. Colbert HA, Smith TL, Bargmann CI. OSM-9, a novel protein with structural similarity to channels, is required for olfaction, mechanosensation, and olfactory adaptation in Caenorhabditis elegans. *J Neurosci*. 1997;17(21):8259-69.

27. Kanzaki M, Zhang YQ, Mashima H, Li L, Shibata H, Kojima I. Translocation of a calcium-permeable cation channel induced by insulin-like growth factor-I. *Nat Cell Biol*. 1999;1(3):165-70.
28. Vriens J, Watanabe H, Janssens A, Droogmans G, Voets T, Nilius B. Cell swelling, heat, and chemical agonists use distinct pathways for the activation of the cation channel TRPV4. *Proc Natl Acad Sci U S A*. 2004;101(1):396-401.
29. Chung MK, Lee H, Mizuno A, Suzuki M, Caterina MJ. 2-Aminoethoxydiphenyl borate activates and sensitizes the heat-gated ion channel TRPV3. *J Neurosci*. 2004;24(22):5177-82.
30. Van Der Stelt M, Di Marzo V. Endovanilloids. Putative endogenous ligands of transient receptor potential vanilloid 1 channels. *Eur J Biochem*. 2004;271(10):1827-34.
31. Chung MK, Guler AD, Caterina MJ. Biphasic currents evoked by chemical or thermal activation of the heat-gated ion channel, TRPV3. *J Biol Chem*. 2005;280(16):15928-41.
32. McNamara FN, Randall A, Gunthorpe MJ. Effects of piperine, the pungent component of black pepper, at the human vanilloid receptor (TRPV1). *Br J Pharmacol*. 2005;144(6):781-90.
33. Moqrich A, Hwang SW, Earley TJ, Petrus MJ, Murray AN, Spencer KS, Andahazy M, Story GM, Patapoutian A. Impaired thermosensation in mice lacking TRPV3, a heat and camphor sensor in the skin. *Science*. 2005;307(5714):1468-72.
34. Vriens J, Owsianik G, Fisslthaler B, Suzuki M, Janssens A, Voets T, Morisseau C, Hammock BD, Fleming I, Busse R, Nilius B. Modulation of the Ca^2 permeable cation channel TRPV4 by cytochrome P450 epoxygenases in vascular endothelium. *Circ Res*. 2005;97(9):908-15.
35. Xu H, Blair NT, Clapham DE. Camphor activates and strongly desensitizes the transient receptor potential vanilloid subtype 1 channel in a vanilloid-independent mechanism. *J Neurosci*. 2005;25(39):8924-37.
36. Ahern GP, Wang X, Miyares RL. Polyamines are potent ligands for the capsaicin receptor TRPV1. *J Biol Chem*. 2006;281(13):8991-5.
37. Vennekens R, Hoenderop J, Prenen J, Stuiver M, Willems P, Droogmans G, Nilius B, Bindels R. Permeation and gating properties of the novel epithelial Ca^{2+} channel. *J Biol Chem*. 2000;275:3963–69.
38. Vennekens R, Prenen J, Hoenderop JGJ, Bindels RJM, Droogmans G, Nilius B. Pore properties and ionic block of the rabbit epithelial calcium channel expressed in HEK 293 cells. *J Physiol*. 2001;530(Pt 2):183-91.
39. Yue L, Peng J-B, Hediger MA, Clapham DE. CaT1 manifests the pore properties of the calcium-release-activated calcium channel. *Nature*. 2001;410(6829):705-9.
40. den Dekker E, Hoenderop JG, Nilius B, Bindels RJ. The epithelial calcium channels, TRPV5 & TRPV6: from identification towards regulation. *Cell Calcium*. 2003;33(5-6):497-507.
41. Nijenhuis T, Hoenderop JG, Nilius B, Bindels RJ. (Patho)physiological implications of the novel epithelial Ca^{2+} channels TRPV5 and TRPV6. *Pflügers Arch*. 2003;446(4):401-9.
42. Kuhn FJ, Luckhoff A. Sites of the NUDT9-H domain critical for ADP-ribose activation of the cation channel TRPM2. *J Biol Chem*. 2004;279(45):46431-7.
43. Perraud AL, Fleig A, Dunn CA, Bagley LA, Launay P, Schmitz C, Stokes AJ, Zhu Q, Bessman MJ, Penner R, Kinet JP, Scharenberg AM. ADP-ribose gating of the calcium-permeable LTRPC2 channel revealed by Nudix motif homology. *Nature*. 2001;411(6837):595-9.
44. Runnels LW, Yue L, Clapham DE. TRP-PLIK, a bifunctional protein with kinase and ion channel activities. *Science*. 2001;291(5506):1043-7.
45. Schmitz C, Perraud AL, Johnson CO, Inabe K, Smith MK, Penner R, Kurosaki T, Fleig A, Scharenberg AM. Regulation of vertebrate cellular Mg^{2+} homeostasis by TRPM7. *Cell*. 2003;114(2):191-200.
46. Launay P, Fleig A, Perraud AL, Scharenberg AM, Penner R, Kinet JP. TRPM4 is a Ca^{2+}-activated nonselective cation channel mediating cell membrane depolarization. *Cell*. 2002;109(3):397-407.
47. McHugh D, Flemming R, Xu S, Perraud A, Beech D. Critical intracellular Ca^{2+} dependence of transient receptor potential melastatin 2 (TRPM2) cation channel activation. *J Biol Chem*. 2003;278:11002–6.

48. Lee N, Chen J, Sun L, Wu S, Gray KR, Rich A, Huang M, Lin JH, Feder JN, Janovitz EB, Levesque PC, Blanar MA. Expression and characterization of human transient receptor potential melastatin 3 (hTRPM3). *J Biol Chem*. 2003;278(23):20890-7.
49. Grimm C, Kraft R, Sauerbruch S, Schultz G, Harteneck C. Molecular and functional characterization of the melastatin-related cation channel TRPM3. *J Biol Chem*. 2003;278(24):21493-501.
50. Hofmann T, Chubanov V, Gudermann T, Montell C. TRPM5 is a voltage-modulated and Ca^{2+}-activated monovalent selective cation channel. *Curr Biol*. 2003;13(13):1153-8.
51. Monteilh-Zoller MK, Hermosura MC, Nadler MJ, Scharenberg AM, Penner R, Fleig A. TRPM7 provides an ion channel mechanism for cellular entry of trace metal ions. *J Gen Physiol*. 2003;121(1):49-60.
52. Oberwinkler J, Lis A, Giehl KM, Flockerzi V, Philipp SE. Alternative splicing switches the divalent cation selectivity of TRPM3 channels. *J Biol Chem*. 2005;280(23):22540-8.
53. Perraud AL, Schmitz C, Scharenberg AM. TRPM2 Ca^{2+} permeable cation channels: from gene to biological function. *Cell Calcium*. 2003;33(5-6):519-31.
54. Voets T, Nilius B, Hoefs S, van der Kemp AW, Droogmans G, Bindels RJ, Hoenderop JG. TRPM6 forms the Mg^{2+} influx channel involved in intestinal and renal Mg^{2+} absorption. *J Biol Chem*. 2004;279(1):19-25.
55. Kuhn FJ, Heiner I, Luckhoff A. TRPM2: a calcium influx pathway regulated by oxidative stress and the novel second messenger ADP-ribose. *Pflügers Arch*. 2005;451(1):212-9.
56. Grimm C, Kraft R, Schultz G, Harteneck C. Activation of the melastatin-related cation channel TRPM3 by D-*erythro*-sphingosine. *Mol Pharmacol*. 2005;67(3):798-805.
57. Nilius B, Prenen J, Droogmans G, Voets T, Vennekens R, Freichel M, Wissenbach U, Flockerzi V. Voltage dependence of the Ca^{2+}-activated cation channel TRPM4. *J Biol Chem*. 2003;278(33):30813-20.
58. Ullrich ND, Voets T, Prenen J, Vennekens R, Talavera K, Droogmans G, Nilius B. Comparison of functional properties of the Ca^{2+}-activated cation channels TRPM4 and TRPM5 from mice. *Cell Calcium*. 2005;37(3):267-78.
59. McKemy DD, Neuhausser WM, Julius D. Identification of a cold receptor reveals a general role for TRP channels in thermosensation. *Nature*. 2002;416(6876):52-8.
60. Talavera K, Yasumatsu K, Voets T, Droogmans G, Shigemura N, Ninomiya Y, Margolskee RF, Nilius B. Heat activation of TRPM5 underlies thermal sensitivity of sweet taste. *Nature*. 2005;438(7070):1022-5.
61. Peier AM, Moqrich A, Hergarden AC, Reeve AJ, Andersson DA, Story GM, Earley TJ, Dragoni I, McIntyre P, Bevan S, Patapoutian A. A TRP channel that senses cold stimuli and menthol. *Cell*. 2002;108(5):705-15.
62. Bharate SS, Bharate SB. Modulation of Thermoreceptor TRPM8 by Cooling Compounds. *ACS Chem Neurosci*. 2012;3(4):248-67.
63. Qian F, Germino FJ, Cai Y, Zhang X, Somlo S, Germino GG. PKD1 interacts with PKD2 through a probable coiled-coil domain. *Nat Genet*. 1997;16(2):179-83.
64. Tsiokas L, Kim E, Arnould T, Sukhatme VP, Walz G. Homo- and heterodimeric interactions between the gene products of PKD1 and PKD2. *Proc Natl Acad Sci U S A*. 1997;94(13):6965-70.
65. Wu G, Somlo S. Molecular genetics and mechanism of autosomal dominant polycystic kidney disease. *Mol Genet Metab*. 2000;69(1):1-15.
66. Delmas P. Polycystins: from mechanosensation to gene regulation. *Cell*. 2004;118(2):145-8.
67. Delmas P, Padilla F, Osorio N, Coste B, Raoux M, Crest M. Polycystins, calcium signaling, and human diseases. *Biochem Biophys Res Commun*. 2004;322(4):1374-83.
68. Delmas P. Polycystins: polymodal receptor/ion-channel cellular sensors. *Pflügers Arch*. 2005;451(1):264-76.
69. Qian F, Noben-Trauth K. Cellular and molecular function of mucolipins (TRPML) and polycystin 2 (TRPP2). *Pflügers Arch*. 2005;451(1):277-85.
70. Delmas P, Nauli SM, Li X, Coste B, Osorio N, Crest M, Brown DA, Zhou J. Gating of the polycystin ion channel signaling complex in neurons and kidney cells. *FASEB J*. 2004;18(6):740-2.
71. Hanaoka K, Qian F, Boletta A, Bhunia AK, Piontek K, Tsiokas L, Sukhatme VP, Guggino WB, Germino GG. Co-assembly of polycystin-1 and -2 produces unique cation-permeable currents. *Nature*. 2000;408(6815):990-4.

72. Huang AL, Chen X, Hoon MA, Chandrashekar J, Guo W, Trankner D, Ryba NJ, Zuker CS. The cells and logic for mammalian sour taste detection. *Nature*. 2006;442(7105):934-8.
73. Ishimaru Y, Inada H, Kubota M, Zhuang H, Tominaga M, Matsunami H. Transient receptor potential family members PKD1L3 and PKD2L1 form a candidate sour taste receptor. *Proc Natl Acad Sci U S A*. 2006;103(33):12569-74.
74. LaPlante JM, Falardeau J, Sun M, Kanazirska M, Brown EM, Slaugenhaupt SA, Vassilev PM. Identification and characterization of the single channel function of human mucolipin-1 implicated in mucolipidosis type IV, a disorder affecting the lysosomal pathway. *FEBS Lett*. 2002;532(1-2):183-7.
75. LaPlante JM, Ye CP, Quinn SJ, Goldin E, Brown EM, Slaugenhaupt SA, Vassilev PM. Functional links between mucolipin-1 and Ca^{2+}-dependent membrane trafficking in mucolipidosis IV. *Biochem Biophys Res Commun*. 2004;322(4):1384-91.
76. Kiselyov K, Chen J, Rbaibi Y, Oberdick D, Tjon-Kon-Sang S, Shcheynikov N, Muallem S, Soyombo A. TRP-ML1 is a lysosomal monovalent cation channel that undergoes proteolytic cleavage. *J Biol Chem*. 2005;280(52):43218-23.
77. Soyombo AA, Tjon-Kon-Sang S, Rbaibi Y, Bashllari E, Bisceglia J, Muallem S, Kiselyov K. TRP-ML1 regulates lysosomal pH and acidic lysosomal lipid hydrolytic activity. *J Biol Chem*. 2006;281(11):7294-301.
78. Jaquemar D, Schenker T, Trueb B. An ankyrin-like protein with transmembrane domains is specifically lost after oncogenic transformation of human fibroblasts. *J Biol Chem*. 1999;274(11):7325-33.
79. Story GM, Peier AM, Reeve AJ, Eid SR, Mosbacher J, Hricik TR, Earley TJ, Hergarden AC, Andersson DA, Hwang SW, McIntyre P, Jegla T, Bevan S, Patapoutian A. ANKTM1, a TRP-like channel expressed in nociceptive neurons, is activated by cold temperatures. *Cell*. 2003;112(6):819-29.
80. Salas MM, Hargreaves KM, Akopian AN. TRPA1-mediated responses in trigeminal sensory neurons: interaction between TRPA1 and TRPV1. *Eur J Neurosci*. 2009;29(8):1568-78.
81. Hjerling-Leffler J, Alqatari M, Ernfors P, Koltzenburg M. Emergence of functional sensory subtypes as defined by transient receptor potential channel expression. *J Neurosci*. 2007;27(10):2435-43.
82. Brozmanova M, Ru F, Surdenikova L, Mazurova L, Taylor-Clark T, Kollarik M. Preferential activation of the vagal nodose nociceptive subtype by TRPA1 agonists in the guinea pig esophagus. *Neurogastroenterol Motil*. 2011;23(10):e437-45.
83. Zygmunt PM, Högestätt ED. Mammalian transient receptor potential (TRP) cation channels. In: Nilius B, Flockerzi V, (eds.) *Handb Exp Pharmacol*. 1. 1 ed. Berlin Heidelberg: Springer-Verlag; 2014. p. 583-630.
84. Earley S. TRPA1 channels in the vasculature. *Br J Pharmacol*. 2012;167(1):13-22.
85. Prasad P, Yanagihara AA, Small-Howard AL, Turner H, Stokes AJ. Secretogranin III directs secretory vesicle biogenesis in mast cells in a manner dependent upon interaction with chromogranin A. *J Immunol*. 2008;181(7):5024-34.
86. Baraldi PG, Preti D, Materazzi S, Geppetti P. Transient receptor potential ankyrin 1 (TRPA1) channel as emerging target for novel analgesics and anti-inflammatory agents. *J Med Chem*. 2010;53(14):5085-107.
87. Andrade EL, Meotti FC, Calixto JB. TRPA1 antagonists as potential analgesic drugs. *Pharmacol Ther*. 2012;133(2):189-204.
88. Nilius B, Appendino G, Owsianik G. The transient receptor potential channel TRPA1: from gene to pathophysiology. *Pflügers Arch*. 2012;464(5):425-58.
89. Fernandes ES, Vong CT, Quek S, Cheong J, Awal S, Gentry C, Aubdool AA, Liang L, Bodkin JV, Bevan S, Heads R, Brain SD. Superoxide generation and leukocyte accumulation: key elements in the mediation of leukotriene B_4-induced itch by transient receptor potential ankyrin 1 and transient receptor potential vanilloid 1. *FASEB J*. 2013;27(4):1664-73.
90. Oh M-H, Oh SY, Lu J, Lou H, Myers A, Zhu Z, Zheng T. TRPA1-dependent pruritus in IL-13-induced chronic atopic dermatitis. *J Immunol*. 2013;191(11):5371-82.
91. Bellono NW, Kammel LG, Zimmerman AL, Oancea E. UV light phototransduction activates transient receptor potential A1 ion channels in human melanocytes. *Proc Natl Acad Sci U S A*. 2013;110(6):2383-8.
92. Buch TR, Schafer EA, Demmel MT, Boekhoff I, Thiermann H, Gudermann T, Steinritz D, Schmidt A. Functional expression of the transient receptor potential channel TRPA1, a

sensor for toxic lung inhalants, in pulmonary epithelial cells. *Chem Biol Interact*. 2013;206(3):462-71.
93. Vennekens R, Menigoz A, Nilius B. TRPs in the brain. *Rev Physiol Biochem Pharmacol*. 2012;163:27-64.
94. Gaudet R. A primer on ankyrin repeat function in TRP channels and beyond. *Mol Biosyst*. 2008;4(5):372-9.
95. Nilius B, Prenen J, Owsianik G. Irritating channels: the case of TRPA1. *J Physiol*. 2011;589(Pt 7):1543-9.
96. Cvetkov TL, Huynh KW, Cohen MR, Moiseenkova-Bell VY. Molecular architecture and subunit organization of TRPA1 ion channel revealed by electron microscopy. *J Biol Chem*. 2011;286(44):38168-76.
97. Wang L, Cvetkov TL, Chance MR, Moiseenkova-Bell VY. Identification of in vivo disulfide conformation of TRPA1 ion channel. *J Biol Chem*. 2012;287(9):6169-76.
98. Jordt SE, Bautista DM, Chuang HH, McKemy DD, Zygmunt PM, Hogestatt ED, Meng ID, Julius D. Mustard oils and cannabinoids excite sensory nerve fibres through the TRP channel ANKTM1. *Nature*. 2004;427(6971):260-5.
99. Doerner JF, Gisselmann G, Hatt H, Wetzel CH. Transient receptor potential channel A1 is directly gated by calcium ions. *J Biol Chem*. 2007;282(18):13180-9.
100. Zurborg S, Yurgionas B, Jira JA, Caspani O, Heppenstall PA. Direct activation of the ion channel TRPA1 by Ca^{2+}. *Nat Neurosci*. 2007;10(3):277-9.
101. Wang YY, Chang RB, Waters HN, McKemy DD, Liman ER. The nociceptor ion channel TRPA1 is potentiated and inactivated by permeating calcium ions. *J Biol Chem*. 2008;283(47):32691-703.
102. Sura L, Zima V, Marsakova L, Hynkova A, Barvik I, Vlachova V. C-terminal acidic cluster is involved in Ca^{2+}-induced regulation of human transient receptor potential ankyrin 1 channel. *J Biol Chem*. 2012;287(22):18067-77.
103. Paulsen CE, Armache J-P, Gao Y, Cheng Y, Julius D. Structure of the TRPA1 ion channel suggests regulatory mechanisms. *Nature*. 2015;520(7548):511-7.
104. Bandell M, Story GM, Hwang SW, Viswanath V, Eid SR, Petrus MJ, Earley TJ, Patapoutian A. Noxious cold ion channel TRPA1 is activated by pungent compounds and bradykinin. *Neuron*. 2004;41(6):849-57.
105. Kang K, Pulver SR, Panzano VC, Chang EC, Griffith LC, Theobald DL, Garrity PA. Analysis of Drosophila TRPA1 reveals an ancient origin for human chemical nociception. *Nature*. 2010;464(7288):597-600.
106. Corey DP, Garcia-Anoveros J, Holt JR, Kwan KY, Lin SY, Vollrath MA, Amalfitano A, Cheung EL, Derfler BH, Duggan A, Geleoc GS, Gray PA, Hoffman MP, Rehm HL, Tamasauskas D, Zhang DS. TRPA1 is a candidate for the mechanosensitive transduction channel of vertebrate hair cells. *Nature*. 2004;432(7018):723-30.
107. Fajardo O, Meseguer V, Belmonte C, Viana F. TRPA1 channels mediate cold temperature sensing in mammalian vagal sensory neurons: pharmacological and genetic evidence. *J Neurosci*. 2008;28(31):7863-75.
108. Karashima Y, Talavera K, Everaerts W, Janssens A, Kwan KY, Vennekens R, Nilius B, Voets T. TRPA1 acts as a cold sensor in vitro and in vivo. *Proc Natl Acad Sci U S A*. 2009;106(4):1273-8.
109. Bautista DM, Jordt SE, Nikai T, Tsuruda PR, Read AJ, Poblete J, Yamoah EN, Basbaum AI, Julius D. TRPA1 mediates the inflammatory actions of environmental irritants and proalgesic agents. *Cell*. 2006;124(6):1269-82.
110. Liu B, Escalera J, Balakrishna S, Fan L, Caceres AI, Robinson E, Sui A, McKay MC, McAlexander MA, Herrick CA, Jordt SE. TRPA1 controls inflammation and pruritogen responses in allergic contact dermatitis. *FASEB J*. 2013;27(9):3549-63.
111. Horvath A, Tekus V, Boros M, Pozsgai G, Botz B, Borbely E, Szolcsanyi J, Pinter E, Helyes Z. Transient receptor potential ankyrin 1 (TRPA1) receptor is involved in chronic arthritis: in vivo study using TRPA1-deficient mice. *Arthritis Res Ther*. 2016;18:6.
112. Bessac BF, Jordt SE. Breathtaking TRP channels: TRPA1 and TRPV1 in airway chemosensation and reflex control. *Physiology*. 2008;23:360-70.
113. Mukhopadhyay I, Gomes P, Aranake S, Shetty M, Karnik P, Damle M, Kuruganti S, Thorat S, Khairatkar-Joshi N. Expression of functional TRPA1 receptor on human lung fibroblast and epithelial cells. *J Recept Signal Transduct Res*. 2011;31(5):350-8.
114. Belvisi MG, Dubuis E, Birrell MA. Transient receptor potential A1 channels: insights into cough and airway inflammatory disease. *Chest*. 2011;140(4):1040-7.

115. Zygmunt PM, Andersson DA, Hogestatt ED. Δ^9-Tetrahydrocannabinol and cannabinol activate capsaicin-sensitive sensory nerves via a CB_1 and CB_2 cannabinoid receptor-independent mechanism. *J Neurosci*. 2002;22(11):4720-7.
116. Bautista DM, Movahed P, Hinman A, Axelsson HE, Sterner O, Hogestatt ED, Julius D, Jordt SE, Zygmunt PM. Pungent products from garlic activate the sensory ion channel TRPA1. *Proc Natl Acad Sci U S A*. 2005;102(34):12248-52.
117. Macpherson LJ, Geierstanger BH, Viswanath V, Bandell M, Eid SR, Hwang S, Patapoutian A. The pungency of garlic: activation of TRPA1 and TRPV1 in response to allicin. *Curr Biol*. 2005;15(10):929-34.
118. Hinman A, Chuang HH, Bautista DM, Julius D. TRP channel activation by reversible covalent modification. *Proc Natl Acad Sci U S A*. 2006;103(51):19564-8.
119. Macpherson LJ, Dubin AE, Evans MJ, Marr F, Schultz PG, Cravatt BF, Patapoutian A. Noxious compounds activate TRPA1 ion channels through covalent modification of cysteines. *Nature*. 2007;445(7127):541-5.
120. Macpherson LJ, Xiao B, Kwan KY, Petrus MJ, Dubin AE, Hwang S, Cravatt B, Corey DP, Patapoutian A. An ion channel essential for sensing chemical damage. *J Neurosci*. 2007;27(42):11412.
121. Takahashi N, Kuwaki T, Kiyonaka S, Numata T, Kozai D, Mizuno Y, Yamamoto S, Naito S, Knevels E, Carmeliet P, Oga T, Kaneko S, Suga S, Nokami T, Yoshida J, Mori Y. TRPA1 underlies a sensing mechanism for O_2. *Nat Chem Biol*. 2011;7(10):701-11.
122. Bessac BF, Sivula M, von Hehn CA, Caceres AI, Escalera J, Jordt SE. Transient receptor potential ankyrin 1 antagonists block the noxious effects of toxic industrial isocyanates and tear gases. *FASEB J*. 2009;23(4):1102-14.
123. Sadofsky LR, Boa AN, Maher SA, Birrell MA, Belvisi MG, Morice AH. TRPA1 is activated by direct addition of cysteine residues to the *N*-hydroxysuccinyl esters of acrylic and cinnamic acids. *Pharmacol Res*. 2011;63(1):30-6.
124. Ibarra Y, Blair NT. Benzoquinone reveals a cysteine-dependent desensitization mechanism of TRPA1. *Mol Pharmacol*. 2013;83(5):1120-32.
125. Eberhardt MJ, Filipovic MR, Leffler A, de la Roche J, Kistner K, Fischer MJ, Fleming T, Zimmermann K, Ivanovic-Burmazovic I, Nawroth PP, Bierhaus A, Reeh PW, Sauer SK. Methylglyoxal activates nociceptors through transient receptor potential channel A1 (TRPA1): a possible mechanism of metabolic neuropathies. *J Biol Chem*. 2012;287(34):28291-306.
126. Zhong J, Minassi A, Prenen J, Taglialatela-Scafati O, Appendino G, Nilius B. Umbellulone modulates TRP channels. *Pflügers Arch*. 2011;462(6):861-70.
127. Karashima Y, Damann N, Prenen J, Talavera K, Segal A, Voets T, Nilius B. Bimodal action of menthol on the transient receptor potential channel TRPA1. *J Neurosci*. 2007;27(37):9874-84.
128. Lee SP, Buber MT, Yang Q, Cerne R, Cortes RY, Sprous DG, Bryant RW. Thymol and related alkyl phenols activate the hTRPA1 channel. *Br J Pharmacol*. 2008;153(8):1739-49.
129. Xu H, Delling M, Jun JC, Clapham DE. Oregano, thyme and clove-derived flavors and skin sensitizers activate specific TRP channels. *Nat Neurosci*. 2006;9(5):628-35.
130. Moilanen LJ, Laavola M, Kukkonen M, Korhonen R, Leppanen T, Hogestatt ED, Zygmunt PM, Nieminen RM, Moilanen E. TRPA1 contributes to the acute inflammatory response and mediates carrageenan-induced paw edema in the mouse. *Sci Rep*. 2012;2:380.
131. Bautista DM, Pellegrino M, Tsunozaki M. TRPA1: A gatekeeper for inflammation. *Annu Rev Physiol*. 2013;75:181-200.
132. Cavanaugh EJ, Simkin D, Kim D. Activation of transient receptor potential A1 channels by mustard oil, tetrahydrocannabinol and Ca^{2+} reveals different functional channel states. *Neuroscience*. 2008;154(4):1467-76.
133. Huang J, Liu CH, Hughes SA, Postma M, Schwiening CJ, Hardie RC. Activation of TRP channels by protons and phosphoinositide depletion in Drosophila photoreceptors. *Curr Biol*. 2010;20(3):189-97.
134. Andersson DA, Gentry C, Moss S, Bevan S. Clioquinol and pyrithione activate TRPA1 by increasing intracellular Zn^{2+}. *Proc Natl Acad Sci U S A*. 2009;106(20):8374-9.
135. Hu H, Bandell M, Petrus MJ, Zhu MX, Patapoutian A. Zinc activates damage-sensing TRPA1 ion channels. *Nat Chem Biol*. 2009;5(3):183-90.
136. Streng T, Axelsson HE, Hedlund P, Andersson DA, Jordt SE, Bevan S, Andersson KE, Hogestatt ED, Zygmunt PM. Distribution and function of the hydrogen sulfide-sensitive TRPA1 ion channel in rat urinary bladder. *Eur Urol*. 2008;53(2):391-9.

137. Li L, Rose P, Moore PK. Hydrogen sulfide and cell signaling. *Annu Rev Pharmacol Toxicol*. 2011;51:169-87.
138. Andersson DA, Gentry C, Bevan S. TRPA1 has a key role in the somatic pro-nociceptive actions of hydrogen sulfide. *PLoS ONE*. 2012;7(10):e46917.
139. Zhang D, Macinkovic I, Devarie-Baez NO, Pan J, Park CM, Carroll KS, Filipovic MR, Xian M. Detection of protein S-sulfhydration by a tag-switch technique. *Angew Chem Int Ed Engl*. 2014;53(2):575-81.
140. Takahashi N, Mizuno Y, Kozai D, Yamamoto S, Kiyonaka S, Shibata T, Uchida K, Mori Y. Molecular characterization of TRPA1 channel activation by cysteine-reactive inflammatory mediators. *Channels*. 2008;2(4):287-98.
141. de la Roche J, Eberhardt MJ, Klinger AB, Stanslowsky N, Wegner F, Koppert W, Reeh PW, Lampert A, Fischer MJ, Leffler A. The molecular basis for species-specific activation of human TRPA1 protein by protons involves poorly conserved residues within transmembrane domains 5 and 6. *J Biol Chem*. 2013;288(28):20280-92.
142. Fujita F, Uchida K, Moriyama T, Shima A, Shibasaki K, Inada H, Sokabe T, Tominaga M. Intracellular alkalization causes pain sensation through activation of TRPA1 in mice. *J Clin Invest*. 2008;118(12):4049-57.
143. Wang YY, Chang RB, Liman ER. TRPA1 is a component of the nociceptive response to CO_2. *J Neurosci*. 2010;30(39):12958-63.
144. Wang YY, Chang RB, Allgood SD, Silver WL, Liman ER. A TRPA1-dependent mechanism for the pungent sensation of weak acids. *J Gen Physiol*. 2011;137(6):493-505.
145. Andersson DA, Gentry C, Alenmyr L, Killander D, Lewis SE, Andersson A, Bucher B, Galzi J-L, Sterner O, Bevan S, Högestätt ED, Zygmunt PM. TRPA1 mediates spinal antinociception induced by acetaminophen and the cannabinoid Δ^9-tetrahydrocannabiorcol. *Nat Commun*. 2011;2:551-62.
146. Hu H, Tian J, Zhu Y, Wang C, Xiao R, Herz JM, Wood JD, Zhu MX. Activation of TRPA1 channels by fenamate nonsteroidal anti-inflammatory drugs. *Pflügers Arch*. 2010;459(4):579-92.
147. Peyrot des Gachons C, Uchida K, Bryant B, Shima A, Sperry JB, Dankulich-Nagrudny L, Tominaga M, Smith AB, Beauchamp GK, Breslin PA. Unusual pungency from extra-virgin olive oil is attributable to restricted spatial expression of the receptor of oleocanthal. *J Neurosci*. 2011;31(3):999-1009.
148. Fajardo O, Meseguer V, Belmonte C, Viana F. TRPA1 channels: Novel targets of 1,4-dihydropyridines. *Channels*. 2008;2(6):429-38.
149. Meseguer V, Karashima Y, Talavera K, D'Hoedt D, Donovan-Rodriguez T, Viana F, Nilius B, Voets T. Transient receptor potential channels in sensory neurons are targets of the antimycotic agent clotrimazole. *J Neurosci*. 2008;28(3):576-86.
150. Xiao B, Dubin AE, Bursulaya B, Viswanath V, Jegla TJ, Patapoutian A. Identification of transmembrane domain 5 as a critical molecular determinant of menthol sensitivity in mammalian TRPA1 channels. *J Neurosci*. 2008;28(39):9640-51.
151. Nakatsuka K, Gupta R, Saito S, Banzawa N, Takahashi K, Tominaga M, Ohta T. Identification of molecular determinants for a potent mammalian TRPA1 antagonist by utilizing species differences. *J Mol Neurosci*. 2013;51(3):754-62.
152. Klement G, Eisele L, Malinowsky D, Nolting A, Svensson M, Terp G, Weigelt D, Dabrowski M. Characterization of a ligand binding site in the human transient receptor potential ankyrin 1 pore. *Biophys J*. 2013;104(4):798-806.
153. Kim D, Cavanaugh EJ. Requirement of a soluble intracellular factor for activation of transient receptor potential A1 by pungent chemicals: role of inorganic polyphosphates. *J Neurosci*. 2007;27(24):6500-9.
154. Alpizar YA, Gees M, Sanchez A, Apetrei A, Voets T, Nilius B, Talavera K. Bimodal effects of cinnamaldehyde and camphor on mouse TRPA1. *Pflügers Arch*. 2013;465(6):853-64.
155. Schulze A, Oehler B, Urban N, Schaefer M, Hill K. Apomorphine is a bimodal modulator of TRPA1 channels. *Mol Pharmacol*. 2013;83(2):542-51.
156. Talavera K, Gees M, Karashima Y, Meseguer VM, Vanoirbeek JA, Damann N, Everaerts W, Benoit M, Janssens A, Vennekens R, Viana F, Nemery B, Nilius B, Voets T. Nicotine activates the chemosensory cation channel TRPA1. *Nat Neurosci*. 2009;12(10):1293-9.
157. Zhong J, Pollastro F, Prenen J, Zhu Z, Appendino G, Nilius B. Ligustilide: a novel TRPA1 modulator. *Pflügers Arch*. 2011;462(6):841-9.

158. Bang S, Yoo S, Oh U, Hwang SW. Endogenous lipid-derived ligands for sensory TRP ion channels and their pain modulation. *Arch Pharm Res*. 2010;33(10):1509-20.
159. Bang S, Yoo S, Yang TJ, Cho H, Hwang SW. Isopentenyl pyrophosphate is a novel antinociceptive substance that inhibits TRPV3 and TRPA1 ion channels. *Pain*. 2011;152(5):1156-64.
160. Park CK, Xu ZZ, Liu T, Lu N, Serhan CN, Ji RR. Resolvin D2 is a potent endogenous inhibitor for transient receptor potential subtype V1/A1, inflammatory pain, and spinal cord synaptic plasticity in mice: distinct roles of resolvin D1, D2, and E1. *J Neurosci*. 2011;31(50):18433-8.
161. Takaishi M, Uchida K, Fujita F, Tominaga M. Inhibitory effects of monoterpenes on human TRPA1 and the structural basis of their activity. *J Physiol Sci*. 2014;64(1):47-57.
162. Holzer P. Transient receptor potential (TRP) channels as drug targets for diseases of the digestive system. *Pharmacol Ther*. 2011;131(1):142-70.
163. Kichko TI, Lennerz J, Eberhardt M, Babes RM, Neuhuber W, Kobal G, Reeh PW. Bimodal concentration-response of nicotine involves the nicotinic acetylcholine receptor, transient receptor potential vanilloid type 1, and transient receptor potential ankyrin 1 channels in mouse trachea and sensory neurons. *J Pharmacol Exp Ther*. 2013;347(2):529-39.
164. Kwan KY, Allchorne AJ, Vollrath MA, Christensen AP, Zhang DS, Woolf CJ, Corey DP. TRPA1 contributes to cold, mechanical, and chemical nociception but is not essential for hair-cell transduction. *Neuron*. 2006;50(2):277-89.
165. da Costa DS, Meotti FC, Andrade EL, Leal PC, Motta EM, Calixto JB. The involvement of the transient receptor potential A1 (TRPA1) in the maintenance of mechanical and cold hyperalgesia in persistent inflammation. *Pain*. 2010;148(3):431-7.
166. Chen J, Joshi SK, DiDomenico S, Perner RJ, Mikusa JP, Gauvin DM, Segreti JA, Han P, Zhang XF, Niforatos W, Bianchi BR, Baker SJ, Zhong C, Simler GH, McDonald HA, Schmidt RG, McGaraughty SP, Chu KL, Faltynek CR, Kort ME, Reilly RM, Kym PR. Selective blockade of TRPA1 channel attenuates pathological pain without altering noxious cold sensation or body temperature regulation. *Pain*. 2011;152(5):1165-72.
167. Nassini R, Gees M, Harrison S, De Siena G, Materazzi S, Moretto N, Failli P, Preti D, Marchetti N, Cavazzini A, Mancini F, Pedretti P, Nilius B, Patacchini R, Geppetti P. Oxaliplatin elicits mechanical and cold allodynia in rodents via TRPA1 receptor stimulation. *Pain*. 2011;152(7):1621-31.
168. Andersson DA, Gentry C, Light E, Vastani N, Vallortigara J, Bierhaus A, Fleming T, Bevan S. Methylglyoxal evokes pain by stimulating TRPA1. *PLoS ONE*. 2013;8(10):e77986.
169. May D, Baastrup J, Nientit MR, Binder A, Schunke M, Baron R, Cascorbi I. Differential expression and functionality of TRPA1 protein genetic variants in conditions of thermal stimulation. *J Biol Chem*. 2012;287(32):27087-94.
170. Chen J, Kang D, Xu J, Lake M, Hogan JO, Sun C, Walter K, Yao B, Kim D. Species differences and molecular determinant of TRPA1 cold sensitivity. *Nat Commun*. 2013;4:2501.
171. Kindt KS, Viswanath V, Macpherson L, Quast K, Hu H, Patapoutian A, Schafer WR. *Caenorhabditis elegans* TRPA-1 functions in mechanosensation. *Nat Neurosci*. 2007;10(5):568-77.
172. Wei H, Hamalainen MM, Saarnilehto M, Koivisto A, Pertovaara A. Attenuation of mechanical hypersensitivity by an antagonist of the TRPA1 ion channel in diabetic animals. *Anesthesiology*. 2009;111(1):147-54.
173. Kwan KY, Glazer JM, Corey DP, Rice FL, Stucky CL. TRPA1 modulates mechanotransduction in cutaneous sensory neurons. *J Neurosci*. 2009;29(15):4808-19.
174. Kerstein PC, del Camino D, Moran MM, Stucky CL. Pharmacological blockade of TRPA1 inhibits mechanical firing in nociceptors. *Mol Pain*. 2009;5:19.
175. Fernandes ES, Russell FA, Spina D, McDougall JJ, Graepel R, Gentry C, Staniland AA, Mountford DM, Keeble JE, Malcangio M, Bevan S, Brain SD. A distinct role for transient receptor potential ankyrin 1, in addition to transient receptor potential vanilloid 1, in tumor necrosis factor α-induced inflammatory hyperalgesia and Freund's complete adjuvant-induced monarthritis. *Arthritis Rheum*. 2011;63(3):819-29.
176. Schmelz M, Schmidt R, Bickel A, Handwerker HO, Torebjork HE. Specific C-receptors for itch in human skin. *J Neurosci*. 1997;17(20):8003-8.
177. Ross SE. Pain and itch: insights into the neural circuits of aversive somatosensation in health and disease. *Curr Opin Neurobiol*. 2011;21(6):880-7.

178. Namer B, Carr R, Johanek LM, Schmelz M, Handwerker HO, Ringkamp M. Separate peripheral pathways for pruritus in man. *J Neurophysiol*. 2008;100(4):2062-9.
179. Roberson DP, Gudes S, Sprague JM, Patoski HA, Robson VK, Blasl F, Duan B, Oh SB, Bean BP, Ma Q, Binshtok AM, Woolf CJ. Activity-dependent silencing reveals functionally distinct itch-generating sensory neurons. *Nat Neurosci*. 2013;16(7):910-8.
180. Liu T, Ji RR. Oxidative stress induces itch via activation of transient receptor potential subtype ankyrin 1 in mice. *Neurosci Bull*. 2012;28(2):145-54.
181. Wilson SR, Gerhold KA, Bifolck-Fisher A, Liu Q, Patel KN, Dong X, Bautista DM. TRPA1 is required for histamine-independent, Mas-related G protein-coupled receptor-mediated itch. *Nat Neurosci*. 2011;14(5):595-602.
182. Akiyama T, Carstens MI, Carstens E. Facial injections of pruritogens and algogens excite partly overlapping populations of primary and second-order trigeminal neurons in mice. *J Neurophysiol*. 2010;104(5):2442-50.
183. Alenmyr L, Hogestatt ED, Zygmunt PM, Greiff L. TRPV1-mediated itch in seasonal allergic rhinitis. *Allergy*. 2009;64(5):807-10.
184. Namer B, Seifert F, Handwerker HO, Maihofner C. TRPA1 and TRPM8 activation in humans: effects of cinnamaldehyde and menthol. *Neuroreport*. 2005;16(9):955-9.
185. Wilson SR, Nelson AM, Batia L, Morita T, Estandian D, Owens DM, Lumpkin EA, Bautista DM. The ion channel TRPA1 is required for chronic itch. *J Neurosci*. 2013;33(22):9283-94.
186. Cevikbas F, Wang X, Akiyama T, Kempkes C, Savinko T, Antal A, Kukova G, Buhl T, Ikoma A, Buddenkotte J, Soumelis V, Feld M, Alenius H, Dillon SR, Carstens E, Homey B, Basbaum A, Steinhoff M. A sensory neuron-expressed IL-31 receptor mediates T helper cell-dependent itch: Involvement of TRPV1 and TRPA1. *J Allergy Clin Immunol*. 2014;133(2):448-60.
187. Hoffmann T, Kistner K, Miermeister F, Winkelmann R, Wittmann J, Fischer M, Weidner C, Reeh P. TRPA1 and TRPV1 are differentially involved in heat nociception of mice. *Eur J Pain*. 2013;17(10):1472-82.
188. Obata K, Katsura H, Mizushima T, Yamanaka H, Kobayashi K, Dai Y, Fukuoka T, Tokunaga A, Tominaga M, Noguchi K. TRPA1 induced in sensory neurons contributes to cold hyperalgesia after inflammation and nerve injury. *J Clin Invest*. 2005;115(9):2393-401.
189. Katsura H, Obata K, Mizushima T, Yamanaka H, Kobayashi K, Dai Y, Fukuoka T, Tokunaga A, Sakagami M, Noguchi K. Antisense knock down of TRPA1, but not TRPM8, alleviates cold hyperalgesia after spinal nerve ligation in rats. *Exp Neurol*. 2006;200(1):112-23.
190. Diogenes A, Akopian AN, Hargreaves KM. NGF up-regulates TRPA1: implications for orofacial pain. *J Dent Res*. 2007;86(6):550-5.
191. Dai Y, Wang S, Tominaga M, Yamamoto S, Fukuoka T, Higashi T, Kobayashi K, Obata K, Yamanaka H, Noguchi K. Sensitization of TRPA1 by PAR2 contributes to the sensation of inflammatory pain. *J Clin Invest*. 2007;117(7):1979-87.
192. Ji G, Zhou S, Carlton SM. Intact Aδ-fibers up-regulate transient receptor potential A1 and contribute to cold hypersensitivity in neuropathic rats. *Neuroscience*. 2008;154(3):1054-66.
193. Wang S, Dai Y, Fukuoka T, Yamanaka H, Kobayashi K, Obata K, Cui X, Tominaga M, Noguchi K. Phospholipase C and protein kinase A mediate bradykinin sensitization of TRPA1: a molecular mechanism of inflammatory pain. *Brain*. 2008;131(Pt 5):1241-51.
194. Schwartz ES, Christianson JA, Chen X, La JH, Davis BM, Albers KM, Gebhart GF. Synergistic role of TRPV1 and TRPA1 in pancreatic pain and inflammation. *Gastroenterology*. 2011;140(4):1283-91.e1-2.
195. Taylor-Clark TE, Undem BJ. Sensing pulmonary oxidative stress by lung vagal afferents. *Respir Physiol Neurobiol*. 2011;178(3):406-13.
196. Kaneko Y, Szallasi A. Transient receptor potential (TRP) channels: a clinical perspective. *Br J Pharmacol*. 2014;171(10):2474-507.
197. Meotti FC, Forner S, Lima-Garcia JF, Viana AF, Calixto JB. Antagonism of the transient receptor potential ankyrin 1 (TRPA1) attenuates hyperalgesia and urinary bladder overactivity in cyclophosphamide-induced haemorrhagic cystitis. *Chem Biol Interact*. 2013;203(2):440-7.
198. Andre E, Campi B, Materazzi S, Trevisani M, Amadesi S, Massi D, Creminon C, Vaksman N, Nassini R, Civelli M, Baraldi PG, Poole DP, Bunnett NW, Geppetti P, Patacchini R. Cigarette smoke-induced neurogenic inflammation is mediated by α,β-

unsaturated aldehydes and the TRPA1 receptor in rodents. *J Clin Invest*. 2008;118(7):2574-82.
199. Bessac BF, Sivula M, von Hehn CA, Escalera J, Cohn L, Jordt SE. TRPA1 is a major oxidant sensor in murine airway sensory neurons. *J Clin Invest*. 2008;118(5):1899-910.
200. Nassenstein C, Kwong K, Taylor-Clark T, Kollarik M, Macglashan DM, Braun A, Undem BJ. Expression and function of the ion channel TRPA1 in vagal afferent nerves innervating mouse lungs. *J Physiol*. 2008;586(6):1595-604.
201. Taylor-Clark TE, McAlexander MA, Nassenstein C, Sheardown SA, Wilson S, Thornton J, Carr MJ, Undem BJ. Relative contributions of TRPA1 and TRPV1 channels in the activation of vagal bronchopulmonary C-fibres by the endogenous autacoid 4-oxononenal. *J Physiol*. 2008;586(14):3447-59.
202. Birrell MA, Belvisi MG, Grace M, Sadofsky L, Faruqi S, Hele DJ, Maher SA, Freund-Michel V, Morice AH. TRPA1 agonists evoke coughing in guinea pig and human volunteers. *Am J Respir Crit Care Med*. 2009;180(11):1042-7.
203. Andre E, Gatti R, Trevisani M, Preti D, Baraldi PG, Patacchini R, Geppetti P. Transient receptor potential ankyrin receptor 1 is a novel target for pro-tussive agents. *Br J Pharmacol*. 2009;158(6):1621-8.
204. Taylor-Clark TE, Kiros F, Carr MJ, McAlexander MA. Transient receptor potential ankyrin 1 mediates toluene diisocyanate-evoked respiratory irritation. *Am J Respir Cell Mol Biol*. 2009;40(6):756-62.
205. Taylor-Clark TE, Undem BJ. Ozone activates airway nerves via the selective stimulation of TRPA1 ion channels. *J Physiol*. 2010;588(Pt 3):423-33.
206. Moller DR, McKay RT, Bernstein IL, Brooks SM. Persistent airways disease caused by toluene diisocyanate. *Am Rev Respir Dis*. 1986;134(1):175-6.
207. Coffey MJ, Wheeler CS, Gross KB, Eschenbacher WL, Sporn PH, Peters-Golden M. Increased 5-lipoxygenase metabolism in the lungs of human subjects exposed to ozone. *Toxicology*. 1996;114(3):187-97.
208. Brooks SM, Weiss MA, Bernstein IL. Reactive airways dysfunction syndrome (RADS): Persistent asthma syndrome after high level irritant exposures. *Chest*. 1985;88(3):376-84.
209. Prezant DJ, Levin S, Kelly KJ, Aldrich TK. Upper and lower respiratory diseases after occupational and environmental disasters. *Mt Sinai J Med*. 2008;75(2):89-100.
210. Shakeri MS, Dick FD, Ayres JG. Which agents cause reactive airways dysfunction syndrome (RADS)? A systematic review. *Occup Med (Lond)*. 2008;58(3):205-11.
211. Caceres AI, Brackmann M, Elia MD, Bessac BF, del Camino D, D'Amours M, Witek JS, Fanger CM, Chong JA, Hayward NJ, Homer RJ, Cohn L, Huang X, Moran MM, Jordt SE. A sensory neuronal ion channel essential for airway inflammation and hyperreactivity in asthma. *Proc Natl Acad Sci U S A*. 2009;106(22):9099-104.
212. Moran MM, McAlexander MA, Biro T, Szallasi A. Transient receptor potential channels as therapeutic targets. *Nat Rev Drug Discov*. 2011;10(8):601-20.
213. Ye Y, Dang D, Zhang J, Viet CT, Lam DK, Dolan JC, Gibbs JL, Schmidt BL. Nerve growth factor links oral cancer progression, pain, and cachexia. *Mol Cancer Ther*. 2011;10(9):1667-76.
214. Lozano-Ondoua AN, Symons-Liguori AM, Vanderah TW. Cancer-induced bone pain: Mechanisms and models. *Neurosci Lett*. 2013;557(Pt A):52-9.
215. Materazzi S, Fusi C, Benemei S, Pedretti P, Patacchini R, Nilius B, Prenen J, Creminon C, Geppetti P, Nassini R. TRPA1 and TRPV4 mediate paclitaxel-induced peripheral neuropathy in mice via a glutathione-sensitive mechanism. *Pflügers Arch*. 2012;463(4):561-9.
216. Barriere DA, Rieusset J, Chanteranne D, Busserolles J, Chauvin MA, Chapuis L, Salles J, Dubray C, Morio B. Paclitaxel therapy potentiates cold hyperalgesia in streptozotocin-induced diabetic rats through enhanced mitochondrial reactive oxygen species production and TRPA1 sensitization. *Pain*. 2012;153(3):553-61.
217. Trevisan G, Materazzi S, Fusi C, Altomare A, Aldini G, Lodovici M, Patacchini R, Geppetti P, Nassini R. Novel therapeutic strategy to prevent chemotherapy-induced persistent sensory neuropathy by TRPA1 blockade. *Cancer Res*. 2013;73(10):3120-31.
218. Andersson KE, Gratzke C, Hedlund P. The role of the transient receptor potential (TRP) superfamily of cation-selective channels in the management of the overactive bladder. *BJU Int*. 2010;106(8):1114-27.
219. Kanai AJ. Afferent mechanism in the urinary tract. *Handb Exp Pharmacol*. 2011(202):171-205.

220. Birder LA. Nervous network for lower urinary tract function. *Int J Urol*. 2013;20(1):4-12.
221. Du S, Araki I, Yoshiyama M, Nomura T, Takeda M. Transient receptor potential channel A1 involved in sensory transduction of rat urinary bladder through C-fiber pathway. *Urology*. 2007;70(4):826-31.
222. Andrade EL, Forner S, Bento AF, Leite DF, Dias MA, Leal PC, Koepp J, Calixto JB. TRPA1 receptor modulation attenuates bladder overactivity induced by spinal cord injury. *Am J Physiol Renal Physiol*. 2011;300(5):F1223-34.
223. Yu YB, Yang J, Zuo XL, Gao LJ, Wang P, Li YQ. Transient receptor potential vanilloid-1 (TRPV1) and ankyrin-1 (TRPA1) participate in visceral hyperalgesia in chronic water avoidance stress rat model. *Neurochem Res*. 2010;35(5):797-803.
224. Hughes PA, Harrington AM, Castro J, Liebregts T, Adam B, Grasby DJ, Isaacs NJ, Maldeniya L, Martin CM, Persson J, Andrews JM, Holtmann G, Blackshaw LA, Brierley SM. Sensory neuro-immune interactions differ between irritable bowel syndrome subtypes. *Gut*. 2013;62(10):1456-65.
225. Kojima R, Nozawa K, Doihara H, Keto Y, Kaku H, Yokoyama T, Itou H. Effects of novel TRPA1 receptor agonist ASP7663 in models of drug-induced constipation and visceral pain. *Eur J Pharmacol*. 2014;723:288-93.
226. Lee I, Kim HK, Kim JH, Chung K, Chung JM. The role of reactive oxygen species in capsaicin-induced mechanical hyperalgesia and in the activities of dorsal horn neurons. *Pain*. 2007;133(1-3):9-17.
227. Sisignano M, Park CK, Angioni C, Zhang DD, von Hehn C, Cobos EJ, Ghasemlou N, Xu ZZ, Kumaran V, Lu R, Grant A, Fischer MJ, Schmidtko A, Reeh P, Ji RR, Woolf CJ, Geisslinger G, Scholich K, Brenneis C. 5,6-EET is released upon neuronal activity and induces mechanical pain hypersensitivity via TRPA1 on central afferent terminals. *J Neurosci*. 2012;32(18):6364-72.
228. Gregus AM, Doolen S, Dumlao DS, Buczynski MW, Takasusuki T, Fitzsimmons BL, Hua X-Y, Taylor BK, Dennis EA, Yaksh TL. Spinal 12-lipoxygenase-derived hepoxilin A_3 contributes to inflammatory hyperalgesia via activation of TRPV1 and TRPA1 receptors. *Proc Natl Acad Sci U S A*. 2012;109(17):6721-6.
229. Due MR, Park J, Zheng L, Walls M, Allette YM, White FA, Shi R. Acrolein involvement in sensory and behavioral hypersensitivity following spinal cord injury in the rat. *J Neurochem*. 2014;128(5):776-86.
230. Kim YS, Son JY, Kim TH, Paik SK, Dai Y, Noguchi K, Ahn DK, Bae YC. Expression of transient receptor potential ankyrin 1 (TRPA1) in the rat trigeminal sensory afferents and spinal dorsal horn. *J Comp Neurol*. 2010;518(5):687-98.
231. Stokes A, Wakano C, Koblan-Huberson M, Adra CN, Fleig A, Turner H. TRPA1 is a substrate for de-ubiquitination by the tumor suppressor CYLD. *Cell Signal*. 2006;18(10):1584-94.
232. Yokoyama T, Ohbuchi T, Saito T, Sudo Y, Fujihara H, Minami K, Nagatomo T, Uezono Y, Ueta Y. Allyl isothiocyanates and cinnamaldehyde potentiate miniature excitatory postsynaptic inputs in the supraoptic nucleus in rats. *Eur J Pharmacol*. 2011;655(1-3):31-7.
233. Lee SM, Cho YS, Kim TH, Jin MU, Ahn DK, Noguchi K, Bae YC. An ultrastructural evidence for the expression of transient receptor potential ankyrin 1 (TRPA1) in astrocytes in the rat trigeminal caudal nucleus. *J Chem Neuroanat*. 2012;45(1-2):45-9.
234. Koch M, Kreutz S, Bottger C, Grabiec U, Ghadban C, Korf HW, Dehghani F. The cannabinoid WIN 55,212-2-mediated protection of dentate gyrus granule cells is driven by CB_1 receptors and modulated by TRPA1 and $Ca_v2.2$ channels. *Hippocampus*. 2011;21(5):554-64.
235. Shigetomi E, Tong X, Kwan KY, Corey DP, Khakh BS. TRPA1 channels regulate astrocyte resting calcium and inhibitory synapse efficacy through GAT-3. *Nat Neurosci*. 2011;15(1):70-80.
236. Kosugi M, Nakatsuka T, Fujita T, Kuroda Y, Kumamoto E. Activation of TRPA1 channel facilitates excitatory synaptic transmission in substantia gelatinosa neurons of the adult rat spinal cord. *J Neurosci*. 2007;27(16):4443-51.
237. Wrigley PJ, Jeong HJ, Vaughan CW. Primary afferents with TRPM8 and TRPA1 profiles target distinct subpopulations of rat superficial dorsal horn neurones. *Br J Pharmacol*. 2009;157(3):371-80.
238. Uta D, Furue H, Pickering AE, Rashid MH, Mizuguchi-Takase H, Katafuchi T, Imoto K, Yoshimura M. TRPA1-expressing primary afferents synapse with a morphologically

identified subclass of substantia gelatinosa neurons in the adult rat spinal cord. *Eur J Neurosci*. 2010;31(11):1960-73.
239. Cho J-H, Jeong M-Y, Choi I-S, Lee H-J, Jang I-S. TRPA1-like channels enhance glycinergic transmission in medullary dorsal horn neurons. *J Neurochem*. 2012;122(4):691-701.
240. Proudfoot CJ, Garry EM, Cottrell DF, Rosie R, Anderson H, Robertson DC, Fleetwood-Walker SM, Mitchell R. Analgesia mediated by the TRPM8 cold receptor in chronic neuropathic pain. *Curr Biol*. 2006;16(16):1591-605.
241. Raisinghani M, Zhong L, Jeffry JA, Bishnoi M, Pabbidi RM, Pimentel F, Cao DS, Evans MS, Premkumar LS. Activation characteristics of transient receptor potential ankyrin 1 and its role in nociception. *Am J Physiol Cell Physiol*. 2011;301(3):C587-600.
242. Wei H, Saarnilehto M, Falck L, Viisanen H, Lasierra M, Koivisto A, Pertovaara A. Spinal transient receptor potential ankyrin 1 channel induces mechanical hypersensitivity, increases cutaneous blood flow, and mediates the pronociceptive action of dynorphin A. *J Physiol Pharmacol*. 2013;64(3):331-40.
243. Jeffry JA, Yu S-Q, Sikand P, Parihar A, Evans MS, Premkumar LS. Selective targeting of TRPV1 expressing sensory nerve terminals in the spinal cord for long lasting analgesia. *PLoS ONE*. 2009;4(9):e7021.
244. Yue HY, Jiang CY, Fujita T, Kumamoto E. Zingerone enhances glutamatergic spontaneous excitatory transmission by activating TRPA1 but not TRPV1 channels in the adult rat substantia gelatinosa. *J Neurophysiol*. 2013;110(3):658-71.
245. Wei H, Chapman H, Saarnilehto M, Kuokkanen K, Koivisto A, Pertovaara A. Roles of cutaneous versus spinal TRPA1 channels in mechanical hypersensitivity in the diabetic or mustard oil-treated non-diabetic rat. *Neuropharmacology*. 2010;58(3):578-84.
246. Wei H, Koivisto A, Pertovaara A. Spinal TRPA1 ion channels contribute to cutaneous neurogenic inflammation in the rat. *Neurosci Lett*. 2010;479(3):253-6.
247. Wei H, Koivisto A, Saarnilehto M, Chapman H, Kuokkanen K, Hao B, Huang J-L, Wang Y-X, Pertovaara A. Spinal transient receptor potential ankyrin 1 channel contributes to central pain hypersensitivity in various pathophysiological conditions in the rat. *Pain*. 2011;152(3):582-91.
248. Koltzenburg M, Lundberg LE, Torebjork HE. Dynamic and static components of mechanical hyperalgesia in human hairy skin. *Pain*. 1992;51(2):207-19.
249. Olausson B. Recordings of polymodal single C-fiber nociceptive afferents following mechanical and argon-laser heat stimulation of human skin. *Exp Brain Res*. 1998;122(1):44-54.
250. Kremeyer B, Lopera F, Cox JJ, Momin A, Rugiero F, Marsh S, Woods CG, Jones NG, Paterson KJ, Fricker FR, Villegas A, Acosta N, Pineda-Trujillo NG, Ramirez JD, Zea J, Burley MW, Bedoya G, Bennett DL, Wood JN, Ruiz-Linares A. A gain-of-function mutation in TRPA1 causes familial episodic pain syndrome. *Neuron*. 2010;66(5):671-80.
251. Binder A, May D, Baron R, Maier C, Tolle TR, Treede RD, Berthele A, Faltraco F, Flor H, Gierthmuhlen J, Haenisch S, Huge V, Magerl W, Maihofner C, Richter H, Rolke R, Scherens A, Uceyler N, Ufer M, Wasner G, Zhu J, Cascorbi I. Transient receptor potential channel polymorphisms are associated with the somatosensory function in neuropathic pain patients. *PLoS ONE*. 2011;6(3):e17387.
252. Patapoutian A, Tate S, Woolf CJ. Transient receptor potential channels: targeting pain at the source. *Nat Rev Drug Discov*. 2009;8(1):55-68.
253. McNamara CR, Mandel-Brehm J, Bautista DM, Siemens J, Deranian KL, Zhao M, Hayward NJ, Chong JA, Julius D, Moran MM, Fanger CM. TRPA1 mediates formalin-induced pain. *Proc Natl Acad Sci U S A*. 2007;104(33):13525-30.
254. Fischer MJ, Leffler A, Niedermirtl F, Kistner K, Eberhardt M, Reeh PW, Nau C. The general anesthetic propofol excites nociceptors by activating TRPV1 and TRPA1 rather than $GABA_A$ receptors. *J Biol Chem*. 2010;285(45):34781-92.
255. Bianchi BR, Zhang XF, Reilly RM, Kym PR, Yao BB, Chen J. Species comparison and pharmacological characterization of human, monkey, rat, and mouse TRPA1 channels. *J Pharmacol Exp Ther*. 2012;341(2):360-8.
256. Klionsky L, Tamir R, Gao B, Wang W, Immke DC, Nishimura N, Gavva NR. Species-specific pharmacology of trichloro(sulfanyl)ethyl benzamides as transient receptor potential ankyrin 1 (TRPA1) antagonists. *Mol Pain*. 2007;3:39.
257. Chen J, Zhang X-F, Kort ME, Huth JR, Sun C, Miesbauer LJ, Cassar SC, Neelands T, Scott VE, Moreland RB, Reilly RM, Hajduk PJ, Kym PR, Hutchins CW, Faltynek CR.

Molecular determinants of species-specific activation or blockade of TRPA1 channels. *J Neurosci*. 2008;28(19):5063.
258. Nagatomo K, Kubo Y. Caffeine activates mouse TRPA1 channels but suppresses human TRPA1 channels. *Proc Natl Acad Sci U S A*. 2008;105(45):17373-8.
259. Bang S, Hwang SW. Polymodal ligand sensitivity of TRPA1 and its modes of interactions. *J Gen Physiol*. 2009;133(3):257.
260. Caspani O, Heppenstall PA. TRPA1 and cold transduction: an unresolved issue? *J Gen Physiol*. 2009;133(3):245-9.
261. Kwan KY, Corey DP. Burning cold: involvement of TRPA1 in noxious cold sensation. *J Gen Physiol*. 2009;133(3):251-6.
262. Latorre R. Perspectives on TRP channel structure and the TRPA1 puzzle. *J Gen Physiol*. 2009;133(3):227-9.
263. Sawada Y, Hosokawa H, Hori A, Matsumura K, Kobayashi S. Cold sensitivity of recombinant TRPA1 channels. *Brain Res*. 2007;1160:39-46.
264. Chen J, Kym PR. TRPA1: the species difference. *J Gen Physiol*. 2009;133(6):623-25.
265. Viswanath V, Story GM, Peier AM, Petrus MJ, Lee VM, Hwang SW, Patapoutian A, Jegla T. Opposite thermosensor in fruitfly and mouse. *Nature*. 2003;423(6942):822-3.
266. Clapham DE. Calcium signaling. *Cell*. 2007;131(6):1047-58.
267. Paredes RM, Etzler JC, Watts LT, Zheng W, Lechleiter JD. Chemical calcium indicators. *Methods*. 2008;46(3):143-51.
268. Bianchi BR, Moreland RB, Faltynek CR, Chen J. Application of large-scale transiently transfected cells to functional assays of ion channels: different targets and assay formats. *Assay Drug Dev Technol*. 2007;5(3):417-24.
269. Chen J, Lake MR, Sabet RS, Niforatos W, Pratt SD, Cassar SC, Xu J, Gopalakrishnan S, Pereda-Lopez A, Gopalakrishnan M, Holzman TF, Moreland RB, Walter KA, Faltynek CR, Warrior U, Scott VE. Utility of large-scale transiently transfected cells for cell-based high-throughput screens to identify transient receptor potential channel A1 (TRPA1) antagonists. *J Biomol Screen*. 2007;12(1):61-9.
270. Luo J, Zhu Y, Zhu MX, Hu H. Cell-based calcium assay for medium to high throughput screening of TRP channel functions using FlexStation 3. *J Vis Exp*. 2011(54).
271. Reed PW, Lardy HA. A23187: a divalent cation ionophore. *J Biol Chem*. 1972;247(21):6970-7.
272. Schmaus G, Joppe H, Herrmann M, Luntzel CS, Vossing T. Symrise GmbH & Co KG. *Anthranilic acid amides and derivatives thereof as cosmetic and pharmaceutical agents*. Patent US2006/0089413A1. 2006.
273. Collins FW. Oat phenolics: avenanthramides, novel substituted N-cinnamoylanthranilate alkaloids from oat groats and hulls. *J Agri Food Chem*. 1989;37(1):60-6.
274. Kelly DJ, Williams SJ, Zammit S. Fibrotech Therapeutics Pty Ltd. *Halogenated analogues of anti-fibrotic agents*. Patent US8624056B2. 2014.
275. Occleston NL, O'Kane S, Goldspink N, Ferguson MW. New therapeutics for the prevention and reduction of scarring. *Drug Discov Today*. 2008;13(21-22):973-81.
276. Zammit SC, Cox AJ, Gow RM, Zhang Y, Gilbert RE, Krum H, Kelly DJ, Williams SJ. Evaluation and optimization of antifibrotic activity of cinnamoyl anthranilates. *Bioorg Med Chem Lett*. 2009;19(24):7003-6.
277. John WS, David S, Steven Z, James KD, Ernest GR, Henry K. Fibrotech Therapeutics Pty Ltd. *Therapeutic compounds*. Patent WO2008/003141A1. 2008.
278. Harita K, Ajisawa Y, Iizuka K, Kinoshita Y, Kamijo T, Kobayashi M. Kissei Yakuhin Kogyo Kabushiki Kaisha. *Aromatic carboxylic amide derivatives*. Patent US3940422A. 1976.
279. Harita K, Ajisawa Y, Iizuka K, Toda M, Kinoshita Y, Kamijo T, Kobayashi M. Kissei Yakuhin Kogyo Kabushiki Kaisha. *Aromatic amidocarboxylic acids and pharmaceutical compositions thereof*. Patent US4026896A. 1977.
280. Noda K, Nakagawa A, Motomura T, Tsuji M, Amano H, Ide H. Hisamitsu Pharmaceutical Co Inc. *Novel anthranilic acid derivatives*. Patent US4337270A. 1982.
281. Schmaus G, Joppe H, Herrmann M, Luntzel CS, Vössing T. Symrise AG. *Anthranillic acid amides and derivatives thereof as cosmetic and pharmaceutical active compounds*. Patent US8409552B2. 2013.

282. Kozaburo H, Yukiyoshi A, Kinji I, Yukihiko K, Tetsuhide K, Michihiro K. Kissei Pharmaceutical Co., Ltd. *Antiallergic composition containing aromatic carboxylic amide derivatives and method of using the same*. Patent 4070484. 1978.
283. Li Y, Liu FY, Peng YM, Li J, Chen J. Mast cell, a promising therapeutic target in tubulointerstitial fibrosis. *Med Hypotheses*. 2007;69(1):99-103.
284. Zhang J, Shi GP. Mast cells and metabolic syndrome. *Biochim Biophys Acta*. 2012;1822(1):14-20.
285. Ma J-J, Si L-F, Lin Z-B. Effects of *N*-(3', 4', 5'-trimethoxycinnamoyl) ortho-aminobenzoic acid on antigen-induced contraction of guinea-pig ileum and the degranulation of and histamine release from mast cells. *J Chinese Pharm Sci*. 1992;1(1):41-5.
286. Herzberg U, Wadsworth S, Cooper K. *Compositions and methods for preventing or reducing postoperative ileus and gastric stasis in mammals*. Patent US2007/0286892A1. 2007.
287. Yamamoto T, Shibazaki T, Ajisawa Y, Yamamoto R, Kinoshita Y. Kissei Pharmaceutical Co Ltd Nitten Ophthalmic Research Institute Company. *Pharmaceutical compositions containing N-(3,4-dimethoxycinnamoyl) anthranilic acid*. Patent US5356620A. 1994.
288. Schneider A, Moraru A, Krüger C, Laage R, Pitzer C. *Use of tranilast and derivatives thereof for the therapy of neurological conditions*. Patent US2011/0112187A1. 2011.
289. Bernardon JM. Centre International de Recherches Dermatologiques. *Bi-aromatic compounds, composition containing them and uses*. Patent US6326510B1. 2001.
290. Schmaus G, Röding J. Symrise GmbH & Co KG. *Mixtures comprising anthranilic acid amides and antidandruff agents as cosmetic and pharmaceutical compositions for alleviating itching*. Patent US2009/0226537A1. 2009.
291. Yamada H, Tajima S, Nishikawa T, Murad S, Pinnell SR. Tranilast, a selective inhibitor of collagen synthesis in human skin fibroblasts. *J Biochem*. 1994;116(4):892-7.
292. Yamada H, Tajima S, Nishikawa T. Tranilast inhibits collagen synthesis in normal, scleroderma and keloid fibroblasts at a late passage culture but not at an early passage culture. *J Dermatol Sci*. 1995;9(1):45-7.
293. Pinto YM, Pinto-Sietsma SJ, Philipp T, Engler S, Kossamehl P, Hocher B, Marquardt H, Sethmann S, Lauster R, Merker HJ, Paul M. Reduction in left ventricular messenger RNA for transforming growth factor β_1 attenuates left ventricular fibrosis and improves survival without lowering blood pressure in the hypertensive TGR(mRen2)27 rat. *Hypertension*. 2000;36(5):747-54.
294. Suzawa H, Kikuchi S, Ichikawa K, Koda A. Inhibitory action of tranilast, an anti-allergic drug, on the release of cytokines and PGE_2 from human monocytes-macrophages. *Jpn J Pharmacol*. 1992;60(2):85-90.
295. Hattori T, Wang PL. Inhibition by tranilast of nifedipine-induced proliferation of cultured human gingival fibroblasts. *Eur J Pharmacol*. 2004;498(1-3):79-81.
296. Bonnet F, Cao Z, Cooper ME, Cox AJ, Kelly DJ, Gilbert RE. Tranilast attenuates vascular hypertrophy, matrix accumulation and growth factor overexpression in experimental diabetes. *Diabetes Metab*. 2003;29(4 Pt 1):386-92.
297. Jones SE, Gilbert RE, Kelly DJ. Tranilast reduces mesenteric vascular collagen deposition and chymase-positive mast cells in experimental diabetes. *J Diabetes Complications*. 2004;18(5):309-15.
298. Soma J, Sato K, Saito H, Tsuchiya Y. Effect of tranilast in early-stage diabetic nephropathy. *Nephrol Dial Transplant*. 2006;21(10):2795-9.
299. Chikaraishi A, Hirahashi J, Takase O, Marumo T, Hishikawa K, Hayashi M, Saruta T. Tranilast inhibits interleukin-1β-induced monocyte chemoattractant protein-1 expression in rat mesangial cells. *Eur J Pharmacol*. 2001;427(2):151-8.
300. Saiura A, Sata M, Hirata Y, Nagai R, Makuuchi M. Tranilast inhibits transplant-associated coronary arteriosclerosis in a murine model of cardiac transplantation. *Eur J Pharmacol*. 2001;433(2-3):163-8.
301. Bossi I, Klersy C, Black AJ, Cortina R, Choussat R, Cassagneau B, Jordan C, Laborde J-C, Laurent J-P, Bernies M, Fajadet J, Marco J. In-stent restenosis: long-term outcome and predictors of subsequent target lesion revascularization after repeat balloon angioplasty. *J Am Coll Cardiol*. 2000;35(6):1569-76.
302. Holmes DR, Savage M, LaBlanche JM, Grip L, Serruys PW, Fitzgerald P, Fischman D, Goldberg S, Brinker JA, Zeiher AM, Shapiro LM, Willerson J, Davis BR, Ferguson JJ, Popma J, King SB, Lincoff AM, Tcheng JE, Chan R, Granett JR, Poland M. Results of

Prevention of REStenosis with Tranilast and its Outcomes (PRESTO) trial. *Circulation*. 2002;106(10):1243-50.
303. Miyazawa K, Kikuchi S, Fukuyama J, Hamano S, Ujiie A. Inhibition of PDGF- and TGF-β1-induced collagen synthesis, migration and proliferation by tranilast in vascular smooth muscle cells from spontaneously hypertensive rats. *Atherosclerosis*. 1995;118(2):213-21.
304. Miyazawa K, Fukuyama J, Misawa K, Hamano S, Ujiie A. Tranilast antagonizes angiotensin II and inhibits its biological effects in vascular smooth muscle cells. *Atherosclerosis*. 1996;121(2):167-73.
305. Ward MR, Sasahara T, Agrotis A, Dilley RJ, Jennings GL, Bobik A. Inhibitory effects of tranilast on expression of transforming growth factor-β isoforms and receptors in injured arteries. *Atherosclerosis*. 1998;137(2):267-75.
306. Ogita H, Isobe Y, Takaku H, Sekine R, Goto Y, Misawa S, Hayashi H. Synthesis and structure-activity relationship of diarylamide derivatives as selective inhibitors of the proliferation of human coronary artery smooth muscle cells. *Bioorg Med Chem Lett*. 2001;11(4):549-51.
307. Platten M, Wick W, Wischhusen J, Weller M. *N*-[3,4-dimethoxycinnamoyl]-anthranilic acid (tranilast) suppresses microglial inducible nitric oxide synthase (iNOS) expression and activity induced by interferon-γ (IFN-γ). *Br J Pharmacol*. 2001;134(6):1279-84.
308. Kemp B, Nandurkar H, Gilbert R. The University of Melbourne, St Vincent's Institute of Medical Research. *Methods of modulating FLT3 activity*. Patent WO2005110392A1. 2005.
309. Raffa D, Maggio B, Plescia F, Cascioferro S, Plescia S, Raimondi MV, Daidone G, Tolomeo M, Grimaudo S, Di Cristina A, Pipitone RM, Bai R, Hamel E. Synthesis, antiproliferative activity, and mechanism of action of a series of 2-{[(2*E*)-3-phenylprop-2-enoyl]amino}benzamides. *Eur J Med Chem*. 2011;46(7):2786-96.
310. Raffa D, Maggio B, Raimondi MV, Cusimano MG, Amico G, Carollo A, Conaldi PG, Bai R, Hamel E, Daidone G. 2-Cinnamamido, 2-(3-phenylpropiolamido), and 2-(3-phenylpropanamido)benzamides: synthesis, antiproliferative activity, and mechanism of action. *Eur J Med Chem*. 2013;65:427-35.
311. Spiecker M, Lorenz I, Marx N, Darius H. Tranilast inhibits cytokine-induced nuclear factor κB activation in vascular endothelial cells. *Mol Pharmacol*. 2002;62(4):856-63.
312. Cooper K, Young J, Wadsworth S, Cui H, diZerega GS, Rodgers KE. Reduction of post-surgical adhesion formation with tranilast. *J Surg Res*. 2007;141(2):153-61.
313. Miyachi Y, Imamura S, Niwa Y. The effect of tranilast of the generation of reactive oxygen species. *J Pharmacobiodyn*. 1987;10(6):255-9.
314. Ogita H, Isobe Y, Takaku H, Sekine R, Goto Y, Misawa S, Hayashi H. Synthesis and structure-activity relationship of diarylamide derivatives as selective inhibitors of the proliferation of human endothelial cells. *Bioorg Med Chem*. 2002;10(11):3473-80.
315. Isaji M, Miyata H, Ajisawa Y, Yoshimura N. Inhibition by tranilast of vascular endothelial growth factor (VEGF)/vascular permeability factor (VPF)-induced increase in vascular permeability in rats. *Life Sci*. 1998;63(4):PL71-4.
316. Rabenhorst J, Machinek A, Schmaus G, Herrmann M, Vielhaber G, Pillai R. Symrise GmbH & Co KG. *Antimicrobially active compounds for treating bad breath*. Patent US2008/0008660A1. 2008.
317. Konrad RJ, Jolly YC, Major C, Wolf BA. Inhibition of phospholipase A_2 and insulin secretion in pancreatic islets. *Biochim Biophys Acta*. 1992;1135(2):215-20.
318. Thams P, Capito K. Inhibition of glucose-induced insulin secretion by the diacylglycerol lipase inhibitor RHC 80267 and the phospholipase A_2 inhibitor ACA through stimulation of K^+ permeability without diminution by exogenous arachidonic acid. *Biochem Pharmacol*. 1997;53(8):1077-86.
319. Namazi MR, Soma J. Tranilast: a novel weapon against insulin resistance. *Med Hypotheses*. 2005;64(6):1135-7.
320. Lennox JR, Antane SA, Butera JA. American Home Products Corporation. *Anthranilic acid analogs*. Patent US6046239A. 2000.
321. Ishibashi S, Ikeda U, Ihara T, Shimada K. Tranilast inhibits contraction and Ca^{2+} movement of porcine coronary arteries. *Atherosclerosis*. 1997;130(1-2):113-9.
322. Ihara T, Ikeda U, Ishibashi S, Shimada K. Tranilast inhibits contraction of rat aortic smooth muscle. *Eur J Pharmacol*. 1997;329(1):43-8.

323. Mizuno K, Okamoto H, Horio T. Inhibitory influences of tranilast on multinucleated giant cell formation from monocytes by supernatant of concanavalin A-stimulated mononuclear cells. *J Dermatol Sci*. 2000;24(3):166-70.
324. Hauel N, Priepke H, Damm K, Schnapp A. *Carboxylic acid amides, pharmaceutical compositions containing these compounds, their use and preparation*. Patent US2002/0099089A1. 2002.
325. Junichi Y, Yoichi T, Eiji H, Hitoshi A, Yukie T. Toyama Chemical Co Ltd. *Novel Anthranilic acid derivative or salt thereof*. Patent EP1820795A1. 2007.
326. Banga HS, Simons ER, Brass LF, Rittenhouse SE. Activation of phospholipases A and C in human platelets exposed to epinephrine: role of glycoproteins IIb/IIIa and dual role of epinephrine. *Proc Natl Acad Sci U S A*. 1986;83(23):9197-201.
327. Harteneck C, Frenzel H, Kraft R. *N*-(*p*-Amylcinnamoyl)anthranilic acid (ACA): a phospholipase A_2 inhibitor and TRP channel blocker. *Cardiovasc Drug Rev*. 2007;25(1):61-75.
328. Kurosawa M, Hisada T, Ishizuka T. Effect of phospholipase A_2 inhibitor ONO-RS-082 on substance P-induced histamine release from rat peritoneal mast cells. *Int Arch Allergy Immunol*. 1992;97(3):226-8.
329. Fukunaga M, Fujiwara Y, Ochi S, Yokoyama K, Shoji T, Fukuhara Y, Orita Y, Kamada T, Badr KF, Ueda N. Mechanism of induction of prostaglandin E_2 production by endothelin 1 in cultured rat mesangial cells. *Exp Nephrol*. 1996;4(6):340-9.
330. Liu L. Regulation of lung surfactant secretion by phospholipase A_2. *J Cell Biochem*. 1999;72(1):103-10.
331. Zhu J, Wang X, Ognyanov VI, Norman MH, Liu Q, Kelly MG, Han N, Fotsch CH, Doherty EM, Chen N, Chakrabarti PP, Bo YY. Amgen Inc. *Vanilloid receptor ligands and their use in treatments*. Patent WO2003/049702A2. 2003.
332. Campbell M, Hatley RJ, Heer JP, Mason AM, Pinto IL, Rahman SS, Smith IED. Smithkline Beecham Corporation. *Anthranilic acid derivatives and their use as activators of the HM74A receptor*. Patent US2007/0191378A1. 2007.
333. Colletti SL, Beresis RT, Chen W, Tata JR, Shen HC, Marley DM, Deng Q, Frie JL, Ding FX. *Niacin receptor agonists, compositions containing such compounds and methods of treatment*. Patent US2007/0299101A1. 2007.
334. Colletti SL, Tata JR, Shen HC, Ding FX, Frie JL, Imbriglio JE, Chen W. *Niacin receptor agonists, compositions containing such compounds and methods of treatment*. Patent US2007/0281969A1. 2007.
335. Yamamori T, Nagata K, Ishizuka N, Sakai K. Shionogi & Co Ltd. *Utilities of amide compounds*. Patent US8106051B2. 2012.
336. Lionel SM, Jane IJ, Owen WR. Angiogen Pharmaceuticals Pty Ltd. *A method of modulating B cell functioning*. Patent WO2006/053390A1. 2006.
337. Steinman L, Platten M, Ho PP-K, Selley ML. *Tranilast as modulator of T cell functioning for use in the treatment of autoimmune diseases*. Patent EP2253313A1. 2010.
338. Lin LFH. *Neuroprotective small organic molecules, compositions and uses related thereto*. Patent US2006/0014807A1. 2006.
339. Eudes A, Baidoo EE, Yang F, Burd H, Hadi MZ, Collins FW, Keasling JD, Loque D. Production of tranilast [*N*-(3',4'-dimethoxycinnamoyl)-anthranilic acid] and its analogs in yeast Saccharomyces cerevisiae. *Appl Microbiol Biotechnol*. 2011;89(4):989-1000.
340. Eudes A, Juminaga D, Baidoo EE, Collins FW, Keasling JD, Loque D. Production of hydroxycinnamoyl anthranilates from glucose in Escherichia coli. *Microb Cell Fact*. 2013;12:62.
341. Loque D, Eudes AG. The Regents of the University of California. *Host cells and methods for producing cinnamoyl anthranilate and analogs thereof*. Patent US2013/0078683A1. 2013.
342. Eudes A, Benites VT, Wang G, Baidoo EEK, Lee TS, Keasling JD, Loqué D. Precursor-directed combinatorial biosynthesis of cinnamoyl, dihydrocinnamoyl, and benzoyl anthranilates in Saccharomyces cerevisiae. *PLoS ONE*. 2015;10(10):e0138972.
343. McKinney SE, Peck HM, Bochey JM, Byham BB, Schuchardt GS, Beyer KH. Benemid *p*-(di-*n*-sulfyaml)-benzoid acid; toxicologic properties. *J Pharmacol Exp Ther*. 1951;102(3):208-14.
344. Beyer KH, Miller KA, Russo HF, Patch EA, Verwey WF. The inhibitory effect of Carinamide on renal elimination of penicillin. *Am J Physiol*. 1947;149:355–68.

345. Beyer RH, Wiebelhaus VD, Russe HF, Peck HM, McKinney SE. Benemid: An anticatabolite; its pharmacological properties. *Fed Proc*. 1950 9:258.
346. Boger WP, Pitts FW, Gallagher ME. Benemid and carinamide: comparison of effect on para-aminosalicylic acid (PAS) plasma concentrations. *J Lab Clin Med*. 1950;36(2):276-82.
347. Cunningham RF, Israili ZH, Dayton PG. Clinical pharmacokinetics of probenecid. *Clin Pharmacokinet*. 1981;6(2):135-51.
348. Di Virgilio F, Steinberg TH, Swanson JA, Silverstein SC. Fura-2 secretion and sequestration in macrophages. A blocker of organic anion transport reveals that these processes occur via a membrane transport system for organic anions. *J Immunol*. 1988;140(3):915-20.
349. McDonough PM, Button DC. Measurement of cytoplasmic calcium concentration in cell suspensions: correction for extracellular Fura-2 through use of Mn^{2+} and probenecid. *Cell Calcium*. 1989;10(3):171-80.
350. Neff NH, Tozer TN, Brodie BB. Application of steady-state kinetics to studies of the transfer of 5-hydroxyindoleacetic acid from brain to plasma. *J Pharmacol Exp Ther*. 1967;158(2):214.
351. van Praag HM, Korf J, Schut D. Cerebral monoamines and depression. An investigation with the Probenecid technique. *Arch Gen Psychiatry*. 1973;28(6):827-31.
352. Bang S, Kim KY, Yoo S, Lee SH, Hwang SW. Transient receptor potential V2 expressed in sensory neurons is activated by probenecid. *Neurosci Lett*. 2007;425(2):120-5.
353. Silverman W, Locovei S, Dahl G. Probenecid, a gout remedy, inhibits pannexin 1 channels. *Am J Physiol, Cell Physiol*. 2008;295(3):C761-7.
354. McClenaghan C, Zeng F, Verkuyl JM. TRPA1 agonist activity of probenecid desensitizes channel responses: consequences for screening. *Assay Drug Dev Technol*. 2012;10(6):533-41.
355. Gutman AB. Uric acid metabolism and gout. *Am J Med*. 1950;9(6):799-817.
356. Gutman AB, Yu TF. Benemid (*p*-di-*n*-propylsulfamyl)-benzoic acid) as uricosuric agent in chronic gouty arthritis. *Trans Assoc Am Physicians*. 1951;64:279-88.
357. Roch-Ramel F, Guisan B. Renal transport of urate in humans. *News Physiol Sci*. 1999;14:80-84.
358. Boger WP, Strickland SC. Probenecid (benemid); its uses and side-effects in 2,502 patients. *AMA Arch Intern Med*. 1955;95(1):83-92.
359. Robbins N, Koch SE, Tranter M, Rubinstein J. The history and future of probenecid. *Cardiovasc Toxicol*. 2012;12(1):1-9.
360. Guldberg HC, Ashcroft GW, Crawford TBB. Concentration of 5-hydroxyindolyacetic acid and homovanillic acid in the cerebrospinal fluid of the dog before and during treatment with Probenecid. *Life Sci*. 1966;5:1571–5.
361. Lake CR, Wood JH, Ziegler MG, Ebert MH, Kopin IJ. Probenecid-induced norepinephrine elevations in plasma and CSF. *Arch Gen Psychiatry*. 1978;35(2):237-40.
362. van Praag HM, Flentge F, Korf J, Dols LC, Schut T. The influence of probenecid on the metabolism of serotonin, dopamine and their precursors in man. *Psychopharmacologia*. 1973;33(2):141-51.
363. Silva-Adaya D, Pérez-De La Cruz V, Villeda-Hernández J, Carrillo-Mora P, González-Herrera IG, García E, Colín-Barenque L, Pedraza-Chaverrí J, Santamaría A. Protective effect of L-kynurenine and probenecid on 6-hydroxydopamine-induced striatal toxicity in rats: Implications of modulating kynurenate as a protective strategy. *Neurotoxicol Teratol*. 2011;33(2):303-12.
364. Grynkiewicz G, Poenie M, Tsien RY. A new generation of Ca^{2+} indicators with greatly improved fluorescence properties. *J Biol Chem*. 1985;260(6):3440-50.
365. Tsien RY, Rink TJ, Poenie M. Measurement of cytosolic free Ca^{2+} in individual small cells using fluorescence microscopy with dual excitation wavelengths. *Cell Calcium*. 1985;6(1):145-57.
366. Kahn AM, Weinman EJ. Urate transport in the proximal tubule: in vivo and in vesicle studies. *Am J Physiol*. 1985;249:789–98.
367. Malgaroli A, Milani D, Meldolesi J, Pozzan T. Fura-2 measurement of cytosolic free Ca^{2+} in monolayers and suspensions of various types of animal cells. *J Cell Biol*. 1987;105(5):2145-55.
368. Mitsui M, Abe A, Tajimi M, Karaki H. Leakage of the fluorescent Ca^{2+} indicator fura-2 in smooth muscle. *Jpn J Pharmacol*. 1993;61(3):165-70.

369. Hu HZ, Gu Q, Wang C, Colton CK, Tang J, Kinoshita-Kawada M, Lee LY, Wood JD, Zhu MX. 2-Aminoethoxydiphenyl borate is a common activator of TRPV1, TRPV2, and TRPV3. *J Biol Chem*. 2004;279(34):35741-8.
370. Juvin V, Penna A, Chemin J, Lin YL, Rassendren FA. Pharmacological characterization and molecular determinants of the activation of transient receptor potential V2 channel orthologs by 2-aminoethoxydiphenyl borate. *Mol Pharmacol*. 2007;72(5):1258-68.
371. Qin N, Neeper MP, Liu Y, Hutchinson TL, Lubin ML, Flores CM. TRPV2 is activated by cannabidiol and mediates CGRP release in cultured rat dorsal root ganglion neurons. *J Neurosci*. 2008;28(24):6231-8.
372. Berthelot DJC, Gijsen HJM, Zaja M, Rech J, Lebsack A, Xiao W, Breitenbucher JG, Branstetter B. *Heterocyclic amides as modulators of TRPA1*. Patent WO2010141805A1. 2010.
373. Orion Corporation. *New pharmaceutical compounds*. Patent EP2520566A1. 2012.
374. Fruttarolo F, Pavani MG, Bencivenni S, Gatti R, Napoletano M. Pharmeste S R L In Liquidation. *Novel sulfonamide trpa1 receptor antagonists*. Patent WO2014135617A1. 2014.
375. Brotherton-Pleiss CE, Chen H, Chen S, Chen Z, Erickson SD, Estrada A, Kim K, Li H, Lovey AJ, Lyssikatos JP, Qian Y, So S-S, Wovkulich PM, Yi L. Hoffmann-La Roche. *Substituted sulfonamide compounds*. Patent WO2014049047A1. 2014.
376. Brotherton-Pleiss CE, Chen Z, Erickson SD, Qian Y. Hoffmann-La Roche. *Novel acetamide derivatives as trp channel antagonists*. Patent WO2014076038A1. 2014.
377. Bahia PK, Parks TA, Stanford KR, Mitchell DA, Varma S, Stevens SM, Taylor-Clark TE. The exceptionally high reactivity of Cys 621 is critical for electrophilic activation of the sensory nerve ion channel TRPA1. *J Gen Physiol*. 2016;147(6):451-65.
378. Bain DI, Smalley RK. Synthesis of 2-substituted-4*H*-3,1-benzoxazin-4-ones. *J Chem Soc C*. 1968(0):1593-7.
379. Kick E, Lawrence R, Fink B, Misra R, Vite G. *Anthranilic acid derivatives as inhibitors of 17beta-hydroxysteroid dehydrogenase 3*. Patent US2006/0135619A1. 2006.
380. Nesterova IN, Shanazarov AK, Poznyak AM, Lakoza MI, Shemeryankin BV, Granik VG. Improved method of synthesizing 2,2-dimethyl-4,6-dioxo-1,3-dioxane (Meldrum's Acid). *Pharm Chem J*. 1994;28(8):583-5.
381. Williams SJ, Stapleton D, Zammit S, Kelly DJ, Gilbert RE, Krum H. Fibrotech Therapeutics Pty Ltd. *Therapeutic compounds*. Patent WO2008/003141A1. 2008.
382. Soai K, Ookawa A. Asymmetric conjugate addition of organometallic reagents in the presence of tertiary amines to chiral α,β-unsaturated amido carboxylic acids. Addition order of reagents as an unprecedented factor in the determination of the sense of asymmetric induction. *J Chem Soc Perkin Trans 1*. 1986:759-64.
383. Stephen H, Wadge G. Syntheses in the quinazolone series. Part IV. The conversion of *N*-aroylorthanilamides into 2-arylquinazol-4-ones. *J Chem Soc*. 1956(0):4420-1.
384. Kamat SP, Parab SJ. A simple two-step synthesis of avenanthramides, constituents of oats (Avena sativa L). *Indian J Chem B*. 2007;46(12):2074-8.
385. Marr EB, Bogert MT. Researches on quinazolines. XXXIX. The synthesis of quinazoline derivatives structurally analogous to the angostura alkaloids galiopine and galipine. *J Am Chem Soc*. 1935;57(4):729-32.
386. Bratt K, Sunnerheim K, Bryngelsson S, Fagerlund A, Engman L, Andersson RE, Dimberg LH. Avenanthramides in oats (Avena sativa L.) and structure-antioxidant activity relationships. *J Agric Food Chem*. 2003;51(3):594-600.
387. Kim S, Shin BS, Ma E. Synthesis and Caco-2 cell permeability of *N*-substituted anthranilamide esters as ADP inhibitor in platelets. *Arch Pharm Res*. 2015;38(6):1147-56.
388. Verma KR, Singla R, Punniyakoti VT. A facile synthesis of 2-benzyloxy/2-(4-isopropylbenzyloxy)-2-methyl-3-(4-substituted phenyl)propanoic acid based insulin sensitizing agents: RSR13-15 and PKR13-15. *Med Chem Res*. 2004;13(8):660-76.
389. Remaut H, Lo A, Waksman G, Selwood D, Gane P. Vib Vzw, Vrije Universiteit Brussel, Ucl Business Plc. *Compounds having antibacterial activity*. Patent WO2014173904A1. 2014.
390. Hogan PJ, Cox BG. Aqueous process chemistry: The preparation of aryl sulfonyl chlorides. *Org Process Res Dev*. 2009;13(5):875-9.
391. Zhang Z, Aerschot AV, Hendrix C, Busson R, David F, Sandra P, Herdewijn P. Synthesis of alanine and proline amino acids with amino or guanidinium substitution on the side chain. *Tetrahedron*. 2000;56(16):2513-22.

392. Hartwig S, Nguyen MM, Hecht S. Exponential growth of functional poly(glutamic acid)dendrimers with variable stereochemistry. *Polym Chem*. 2010;1(1):69-71.
393. Gupta SK. New reactions and reagents; VI. A simple synthesis of *N,N*-dialkylsulfonamides via the reaction of dialkylsulfamyl chlorides with aromatic hydrocarbons. *Synthesis*. 1977;1977(1):39-41.
394. Lube A, Neumann WP, Niestroj M. Tin for organic synthesis, 13. A new and regioselective method for the synthesis of aromatic, heteroaromatic, and olefinic sulfonamides by electrophilic destannylation. *Chem Ber*. 1995;128(12):1195-8.
395. Ruano JLG, Parra A, Marzo L, Yuste F, Mastranzo VM. One-pot synthesis of sulfonamides from methyl sulfinates using ultrasound. *Tetrahedron*. 2011;67(16):2905-10.
396. Badetti E, Moreno-Mañas M, Pleixats R, Sebastián RM, Serra A, Soler R, Vallribera A. Nucleophilic aromatic substitution on 4-fluorophenylsulfonamides: nitrogen, oxygen, and sulfur nucleophiles. *Synlett*. 2005;2005(3):449-52.
397. Zhang W, Luo M. Iron-catalyzed synthesis of arylsulfinates through radical coupling reaction. *ChemComm*. 2016;52(14):2980-3.
398. Zhu H, Shen Y, Deng Q, Tu T. Copper-catalyzed electrophilic amination of sodium sulfinates at room temperature. *ChemComm*. 2015;51(92):16573-6.
399. Gray WH, Buttle GAH, Stephenson D. Derivatives of *p*-aminobenzenesulphonamide in the treatment of streptococcal infection in mice. *Biochem J*. 1937;31(5):724-7.
400. Itaya M, Takai Y, Kaiya T. Synthetic studies in benzimidazole series. IV. Synthesis of 2-[*p*-(substituted sulfamoyl)phenyl]benzimidazoles. *Yakugaku Zasshi*. 1966;86(7):600-8.
401. Mikhalev VA, Dorokhova MI, Smolina NE. Mechanism of transformation of α-acylamino-β-hydroxypropiophenones into corresponding benzoylacetyls. I. Synthesis and cleavage of α-benzenesulfonamido- and α-benzenesulfonomethylamido-β-hydroxypropiophenones. *Zh Obshch Khim*. 1959;29:3488-92.
402. Thomas P, Smart TG. HEK293 cell line: A vehicle for the expression of recombinant proteins. *J Pharmacol Toxicol Methods*. 2005;51(3):187-200.
403. Sadofsky LR, Campi B, Trevisani M, Compton SJ, Morice AH. Transient receptor potential vanilloid-1-mediated calcium responses are inhibited by the alkylamine antihistamines dexbrompheniramine and chlorpheniramine. *Exp Lung Res*. 2008;34(10):681-93.
404. Morgan K, Sadofsky LR, Crow C, Morice AH. Human TRPM8 and TRPA1 pain channels, including a gene variant with increased sensitivity to agonists (TRPA1 R797T), exhibit differential regulation by SRC-tyrosine kinase inhibitor. *Biosci Rep*. 2014;34(4).
405. Maher SA, Birrell MA, Belvisi MG. Prostaglandin E_2 mediates cough via the EP_3 receptor: implications for future disease therapy. *Am J Respir Crit Care Med*. 2009;180(10):923-8.
406. James KD, John WS, Steven Z. Fibrotech Therapeutics Pty Ltd, The University of Melbourne. *Halogenated analogues of anti-fibrotic agents*. Patent WO2009/079692A1. 2009.
407. Raffa D, Maggio B, Plescia F, Cascioferro S, Plescia S, Raimondi MV, Daidone G, Tolomeo M, Grimaudo S, Di Cristina A, Pipitone RM, Bai R, Hamel E. Synthesis, antiproliferative activity, and mechanism of action of a series of 2-{[(2*E*)-3-phenylprop-2-enoyl]amino}benzamides. *Eur J Med Chem*. 2011;46(7):2786-96.
408. Iwasa Y, Iwasa T, Matsui K, Yoshimura T, Tanaka N, Miyazaki K. Anti-platelet action of an anti-allergic agent, N-(3',4'-dimethoxycinnamoyl)anthranilic acid (tranilast). *Eur J Pharmacol*. 1986;120(2):231-4.
409. Gunthorpe MJ, Rami HK, Jerman JC, Smart D, Gill CH, Soffin EM, Luis Hannan S, Lappin SC, Egerton J, Smith GD, Worby A, Howett L, Owen D, Nasir S, Davies CH, Thompson M, Wyman PA, Randall AD, Davis JB. Identification and characterisation of SB-366791, a potent and selective vanilloid receptor (VR1/TRPV1) antagonist. *Neuropharmacology*. 2004;46(1):133-49.
410. Weil A, Moore SE, Waite NJ, Randall A, Gunthorpe MJ. Conservation of functional and pharmacological properties in the distantly related temperature sensors TRPV1 and TRPM8. *Mol Pharmacol*. 2005;68(2):518-27.
411. Liu K, Samuel M, Ho M, Harrison RK, Paslay JW. NPPB structure-specifically activates TRPA1 channels. *Biochem Pharmacol*. 2010;80(1):113-21.
412. Biabani MAF, Baake M, Lovisetto B, Laatsch H, Helmke E, Weyland H. Marine bacteria. X. Anthranilamides: New antimicroalgal active substances from a marine Streptomyces sp. *J Antibiot*. 1998;51(3):333-40.

413. Rani P, Srivastava VK, Kumar A. Isoxazolinyl derivatives of anthranilic acid as antiinflammatory agents. *Indian J Chem B*. 2003;42(7):1729-33.
414. Gee KR, Brown KA, Chen WNU, Bishop-Stewart J, Gray D, Johnson I. Chemical and physiological characterization of fluo-4 Ca^{2+}-indicator dyes. *Cell Calcium*. 2000;27(2):97-106.
415. Hagen BM, Boyman L, Kao JPY, Lederer WJ. A comparative assessment of fluo Ca^{2+} indicators in rat ventricular myocytes. *Cell Calcium*. 2012;52(2):170-81.
416. Wood DC, Wood J. Pharmacologic and biochemical considerations of dimethyl sulfoxide. *Ann N Y Acad Sci*. 1975;243:7-19.
417. Sherkheli MA, Vogt-Eisele AK, Bura D, Beltran Marques LR, Gisselmann G, Hatt H. Characterization of selective TRPM8 ligands and their structure activity response (S.A.R) relationship. *J Pharm Pharm Sci*. 2010;13(2):242-53.
418. Lashinger ESR, Steiginga MS, Hieble JP, Leon LA, Gardner SD, Nagilla R, Davenport EA, Hoffman BE, Laping NJ, Su X. AMTB, a TRPM8 channel blocker: evidence in rats for activity in overactive bladder and painful bladder syndrome. *Am J Physiol Renal Physiol*. 2008;295(3):F803.
419. Vauquelin G, Van Liefde I, Birzbier BB, Vanderheyden PM. New insights in insurmountable antagonism. *Fundam Clin Pharmacol*. 2002;16(4):263-72.
420. Vauquelin G, Van Liefde I, Vanderheyden P. Models and methods for studying insurmountable antagonism. *Trends Pharmacol Sci*. 2002;23(11):514-8.
421. Lindsay CD, Green C, Bird M, Jones JTA, Riches JR, McKee KK, Sandford MS, Wakefield DA, Timperley CM. Potency of irritation by benzylidenemalononitriles in humans correlates with TRPA1 ion channel activation. *R Soc Open Sci*. 2015;2(1):140160-77.
422. Schachter JB, Sromek SM, Nicholas RA, Harden TK. HEK293 human embryonic kidney cells endogenously express the $P2Y_1$ and $P2Y_2$ receptors. *Neuropharmacology*. 1997;36(9):1181-7.
423. Yu SP, Kerchner GA. Endogenous voltage-gated potassium channels in human embryonic kidney (HEK293) cells. *J Neurosci Res*. 1998;52(5):612-7.
424. Jiang B, Sun X, Cao K, Wang R. Endogenous Kv channels in human embryonic kidney (HEK-293) cells. *Mol Cell Biochem*. 2002;238(1):69-79.
425. Moran O, Nizzari M, Conti F. Endogenous expression of the β1A sodium channel subunit in HEK-293 cells. *FEBS Lett*. 2000;473(2):132-4.
426. He B, Soderlund DM. Human embryonic kidney (HEK293) cells express endogenous voltage-gated sodium currents and $Na_v1.7$ sodium channels. *Neurosci Lett*. 2010;469(2):268-72.
427. Meyer zu Heringdorf D, Lass H, Kuchar I, Lipinski M, Alemany R, Rumenapp U, Jakobs KH. Stimulation of intracellular sphingosine-1-phosphate production by G-protein-coupled sphingosine-1-phosphate receptors. *Eur J Pharmacol*. 2001;414(2-3):145-54.
428. Berjukow S, Doring F, Froschmayr M, Grabner M, Glossmann H, Hering S. Endogenous calcium channels in human embryonic kidney (HEK293) cells. *Br J Pharmacol*. 1996;118(3):748-54.
429. Bugaj V, Alexeenko V, Zubov A, Glushankova L, Nikolaev A, Wang Z, Kaznacheyeva E, Bezprozvanny I, Mozhayeva GN. Functional properties of endogenous receptor- and store-operated calcium influx channels in HEK293 cells. *J Biol Chem*. 2005;280(17):16790-7.
430. Zagranichnaya TK, Wu X, Villereal ML. Endogenous TRPC1, TRPC3, and TRPC7 proteins combine to form native store-operated channels in HEK-293 cells. *J Biol Chem*. 2005;280(33):29559-69.
431. Luo J, Busillo JM, Benovic JL. M_3 muscarinic acetylcholine receptor-mediated signaling is regulated by distinct mechanisms. *Mol Pharmacol*. 2008;74(2):338-47.
432. McKemy DD. How cold is it? TRPM8 and TRPA1 in the molecular logic of cold sensation. *Mol Pain*. 2005;1:16.
433. Takaishi M, Fujita F, Uchida K, Yamamoto S, Sawada Shimizu M, Hatai Uotsu C, Shimizu M, Tominaga M. 1,8-Cineole, a TRPM8 agonist, is a novel natural antagonist of human TRPA1. *Mol Pain*. 2012;8:86.
434. Lipinski CA. Lead- and drug-like compounds: the rule-of-five revolution. *Drug Discov Today Technol*. 2004;1(4):337-41.
435. Veber DF, Johnson SR, Cheng HY, Smith BR, Ward KW, Kopple KD. Molecular properties that influence the oral bioavailability of drug candidates. *J Med Chem*. 2002;45(12):2615-23.

436. Anand U, Otto WR, Facer P, Zebda N, Selmer I, Gunthorpe MJ, Chessell IP, Sinisi M, Birch R, Anand P. TRPA1 receptor localisation in the human peripheral nervous system and functional studies in cultured human and rat sensory neurons. *Neurosci Lett*. 2008;438(2):221-7.
437. Okada Y, Shirai K, Reinach PS, Kitano-Izutani A, Miyajima M, Flanders KC, Jester JV, Tominaga M, Saika S. TRPA1 is required for TGF-β signaling and its loss blocks inflammatory fibrosis in mouse corneal stroma. *Lab Invest*. 2014;94(9):1030-41.
438. Schneider C, Broda E, Snieckus V. Directed ortho-metalation-cross-coupling strategies. One-pot Suzuki reaction to biaryl and heterobiaryl sulfonamides. *Org Lett*. 2011;13(14):3588-91.
439. Narayanam MK, Ma G, Champagne PA, Houk KN, Murphy JM. Synthesis of [^{18}F]fluoroarenes by nucleophilic radiofluorination of *N*-arylsydnones. *Angew Chem Int Ed*. 2017;56(42):13006-10.
440. Barbosa MLdC, Melo GMdA, Cupertino da Silva YK, Lopes RdO, Tenorio de Souza E, Cavalcanti de Queiroz A, Smaniotto S, Alexandre-Moreira MS, Barreiro EJ, Lima LM. Synthesis and pharmacological evaluation of *N*-phenyl-acetamide sulfonamides designed as novel non-hepatotoxic analgesic candidates. *Eur J Med Chem*. 2009;44(9):3612-20.
441. Ashnagar A, Naseri NG, Naderi M. Synthesis of a series of dialkylsulphamylbenzoic acids. *Biosci Biotechnol Res Asia*. 2007;4(1):217-20.
442. Muehle H, Schiller I, Prijs B. Chemische Fabrik Schweizerhall. *Derivatives of 4-sulfamoylbenzoic acid*. Patent CH444846. 1968.
443. Khodarahmi GA, Chen CS, Hakimelahi GH, Tseng CT, Chern JW. Design, synthesis, and cytotoxicity of 4-sulfonamide substituted benzamidobenzimidazolones and an acyl benzimidazolone. *J Iran Chem Soc*. 2005;2(2):124-34.
444. Nikolenko LM. Preparation of arylsulfonyl derivatives of amino acids. *Zh Obshch Khim*. 1956;26:806-8.
445. Chung G, Im ST, Kim YH, Jung SJ, Rhyu MR, Oh SB. Activation of transient receptor potential ankyrin 1 by eugenol. *Neuroscience*. 2014;261:153-60.
446. Redmond WJ, Camo M, Mitchell V, Vaughan CW, Connor M. Nordihydroguaiaretic acid activates hTRPA1 and modulates behavioral responses to noxious cold in mice. *Pharmacol Res Perspect*. 2014;2(6):e00079.
447. Maher M, Ao H, Banke T, Nasser N, Wu NT, Breitenbucher JG, Chaplan SR, Wickenden AD. Activation of TRPA1 by farnesyl thiosalicylic acid. *Mol Pharmacol*. 2008;73(4):1225-34.
448. Niforatos W, Zhang X-F, Lake MR, Walter KA, Neelands T, Holzman TF, Scott VE, Faltynek CR, Moreland RB, Chen J. Activation of TRPA1 channels by the fatty acid amide hydrolase inhibitor 3′-carbamoylbiphenyl-3-yl cyclohexylcarbamate (URB597). *Mol Pharmacol*. 2007;71(5):1209.
449. Petrus M, Peier AM, Bandell M, Hwang SW, Huynh T, Olney N, Jegla T, Patapoutian A. A role of TRPA1 in mechanical hyperalgesia is revealed by pharmacological inhibition. *Mol Pain*. 2007;3:40.
450. Ohara K, Fukuda T, Okada H, Kitao S, Ishida Y, Kato K, Takahashi C, Katayama M, Uchida K, Tominaga M. Identification of significant amino acids in multiple transmembrane domains of human transient receptor potential ankyrin 1 (TRPA1) for activation by eudesmol, an oxygenized sesquiterpene in hop essential oil. *J Biol Chem*. 2015;290(5):3161-71.
451. Redmond WJ, Gu L, Camo M, McIntyre P, Connor M. Ligand determinants of fatty acid activation of the pronociceptive ion channel TRPA1. *PeerJ*. 2014;2:e248.
452. Preti D, Saponaro G, Szallasi A. Transient receptor potential ankyrin 1 (TRPA1) antagonists. *Pharm Pat Anal*. 2015;4(2):75-94.

Appendix

Chemical structures and codes of synthesised *N*-cinnamoylanthranilate derivatives (CADs)

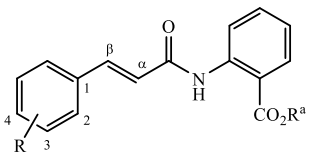

	R	R^a		R	R^a
AC18a	H	CH_3	**AC27**	$3\text{-}OCH_2CH_3\text{-}4\text{-}OH$	H
AC18b	H	H	**AC28c**	$3,4\text{-}(OAc)_2$	CH_3
AC14b	4-F	CH_3	**AC28d**	$3,4\text{-}(OH)_2$	H
AC14c	4-F	H	**AC30c**	4-OAc	CH_3
AC15b	2-Cl	CH_3	**AC30d**	4-OH	H
AC15c	2-Cl	H	**AC39b**	$4\text{-}CH_3$	CH_3
AC16b	4-Br	CH_3	**AC39c**	$4\text{-}CH_3$	H
AC16c	4-Br	H	**AC40b**	$4\text{-}CF_3$	CH_3
AC17b	4-Cl	CH_3	**AC40c**	$4\text{-}CF_3$	H
AC17c	4-Cl	H	**AC41b**	$4\text{-}NO_2$	CH_3
AC20	$4\text{-}OCH_3$	H	**AC41c**	$4\text{-}NO_2$	H
AC24	$3,4\text{-}(OCH_3)_2$	H	**AC45b**	$4\text{-}N(CH_3)_2$	CH_3
AC26	$2\text{-}OCH_3$	H	**AC45c**	$4\text{-}N(CH_3)_2$	H

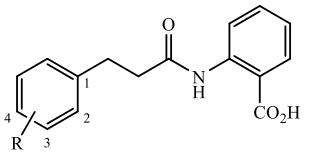

	R
AC21b	H
AC46c	$4\text{-}OCH_3$

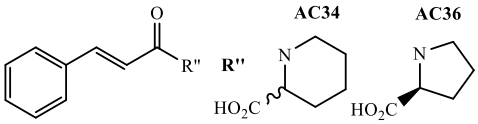

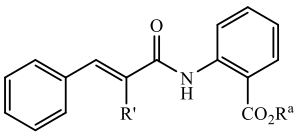

	R'	R^a
AC42b	Ph	CH_3
AC42c	Ph	H
AC43c	CH_3	CH_3
AC43d	CH_3	H

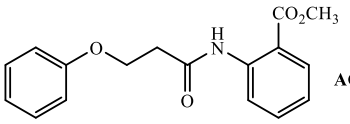

Chemical structures and codes of synthesised aryl sulfonamide derivatives (ASDs)

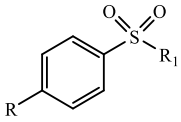

	R	R_1
M1	COOH	dipropylamine
M2	H	diethylamine
M3	OCH_3	diethylamine
M4	OCH_3	pyrrolidine
M5	F	diethylamine
M6	F	pyrrolidine
M7	F	piperidine
M8	F	morpholine
M9	F	indoline
M10	NHAc	diethylamine
M11	COOH	diethylamine
M12	COOH	pyrrolidine
M13	COOH	piperidine
M14	COOH	morpholine

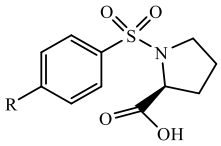

	R
AC51a	F

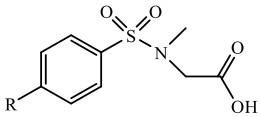

	R
AC54a	H
AC53a	F

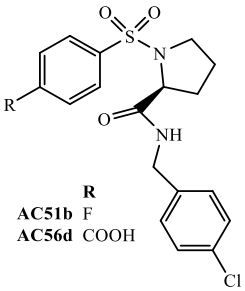

	R
AC51b	F
AC56d	COOH

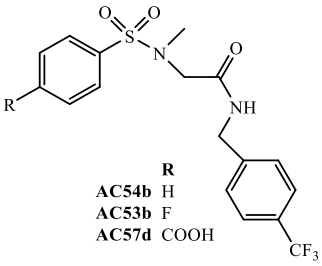

	R
AC54b	H
AC53b	F
AC57d	COOH

Chemical structures, names and codes of known ligands characterised in hTRPA1

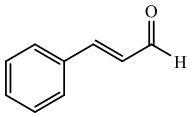

Cinnamaldehyde
(**CA**)

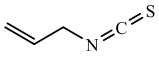

Allyl isothiocyanate
(**AITC**)

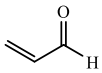

Acrolein
(**ACR**)

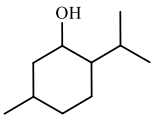

2-Isopropyl-5-methylcyclohexanol
(**menthol**)

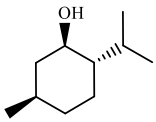

(1*R*,2*S*,5*R*)-2-Isopropyl-5-methylcyclohexanol
(**(-)-menthol**)

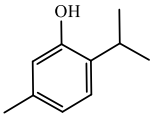

2-Isopropyl-5-methylphenol
(**thymol**)

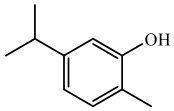

5-Isopropyl-2-methylphenol
(**carvacrol**)

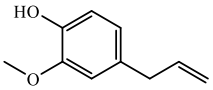

2-Methoxy-4-(2-propenyl)phenol
(**eugenol**)

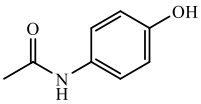

N-Acetyl-4-aminophenol
(**paracetamol**)

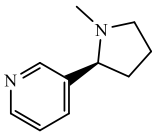

(*S*)-3-(1-Methyl-2-pyrrolidinyl)pyridine,
(**(-)-nicotine**)

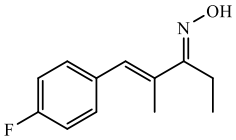

(1*E*,3*E*)-1-(4-Fluorophenyl)-2-methylpent-1-en-3-one oxime
(**A967079**)

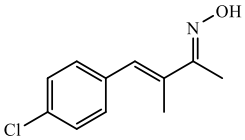

4-(4-Chlorophenyl)-3-methylbut-3-en-2-oxime
(**AP18**)

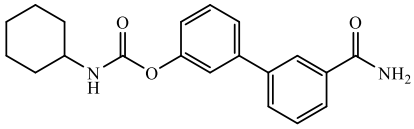

3'-Carbamoyl-[1,1'-biphenyl]-3-yl cyclohexylcarbamate
(**URB597**)

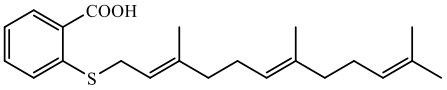

2-(((2*E*,6*E*)-3,7,11-Trimethyldodeca-2,6,10-trien-1-yl)thio)benzoic acid, *S*-Farnesylthosalicylic acid (**FTS**)

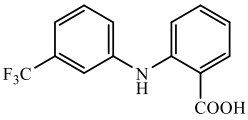

N-(3-[Trifluoromethyl]phenyl)anthranilic acid,
Flufenamic acid (**FFA**)

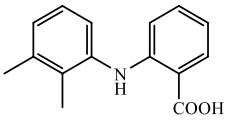

N-(2,3-Xylyl)anthranilic acid,
Mefenamic acid (**MFA**)

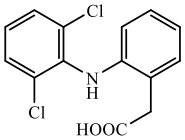

2-(2-((2,6-Dichlorophenyl)amino)phenyl)acetic acid,
Diclofenac (**DCF**)

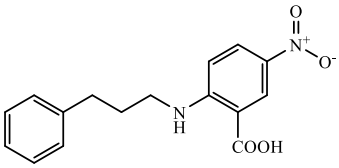

5-Nitro-2-(3-phenylpropylamino)benzoic acid
(**NPPB**)

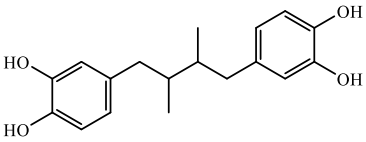

1,4-Bis(3,4-dihydroxyphenyl)-2,3-dimethylbutane,
Nordihydroguaiaretic acid (**NDGA**)

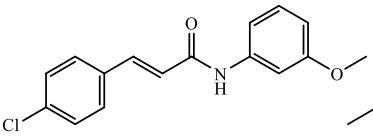

N-(3-Methoxyphenyl)-4-chlorocinnamide
(**SB366791**)

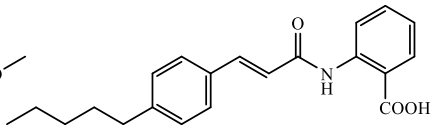

N-(*p*-Amylcinnamoyl)anthranilic acid
(**ACA**)

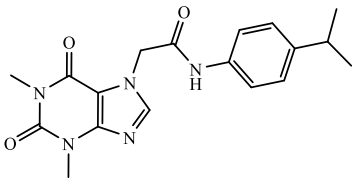

2-(1,3-Dimethyl-2,6-dioxo-1,2,3,6-tetrahydro-7*H*-purin-7-yl)-*N*-(4-isopropylphenyl)acetamide
(**HC030031**)